THE DESIGN AND BEHAVIOUR OF CRUSH PILLARS ON THE MERENSKY REEF

MICHAEL DU PLESSIS

Presented as fullfilment for the degree

Doctor of Philosophy: PhD (Mining Engineering)

IN THE FACULTY OF ENGINEERING, BUILT ENVIRONMENT AND INFORMATION TECHNOLOGY

DEPARTMENT OF MINING ENGINEERING

UNIVERSITY OF PRETORIA

PRETORIA

2015

DECLARATION

I hereby declare that this thesis is my own unaided work. It is being submitted for the degree of Doctor of Philosophy (Mining Engineering) to the University of Pretoria, Pretoria. It has not been submitted before for any degree or examination to any other University. This thesis represents my own opinion and interpretation of information received from the mining industry or people in the mining industry. The thesis has been compiled whilst employed by Lonmin Platinum.

_____

Michael du Plessis

Dated this ___ day of _____ 2015

ABSTRACT

THE DESIGN AND BEHAVIOUR OF CRUSH PILLARS ON THE MERENSKY REEF

MICHAEL DU PLESSIS

Supervisor: Prof. Francois Malan

Department: Mining Engineering

University: University of Pretoria

Degree: PhD (Mining Engineering)

Crush pillars are used as part of the stope support in intermediate depth tabular mining stopes. Crush pillar design should ensure that the pillars crush when formed at the mining face. This behaviour of the pillars is typically achieved when the pillars have a width to height ratio of approximately 2:1. Once crushed, the residual stress state of the pillars provides a local support function.

Crush pillars are extensively used in the platinum mines of South Africa. In most cases effective pillar crushing is not achieved, resulting in pillar seismicity. The objective of the research was to determine the parameters which influence crush pillar behaviour. A limit equilibrium model was identified as being able to simulate the behaviour of the pillars. The model implemented in a displacement discontinuity boundary element code provided insights into the stress evolution of a pillar depending on its position relative to the mining face, the effect of over-sized pillars, the impact of geological structures, layout and rock mass parameters as well as mining depth.

An underground mining trial was conducted at Lonmin Platinum to measure and visually observe the behaviour of crush pillars. This was the most comprehensive monitoring of these pillars ever conducted in the platinum industry. The visually observed behaviour of the pillars agreed well with the findings of the measurements and the pillar fracturing profiles obtained at various stages of the pillar

forming cycle. A sequence and mode of pillar failure could be identified. The results indicated that a pillar reaches a residual stress state when separated from the mining face. The pillar experiences secondary, subsequent reductions in stress when new pillars are formed. This unloading phase, has in the past, typically only been referred to as continued strain softening behaviour. However, it was found that at some point the pillars experienced no further reduction in stress whilst the pillars continued to deform. This observation was verified by convergence measurements. After all mining stopped, continued convergence was recorded.

A numerical model was used to back analyse the behaviour of the underground trial site which consisted of an approximately 22 000 m^2 of mined area and 55 crush pillars. To date, no numerical modelling of a mine-wide tabular layout, which explicitly included a large number of crush pillars, had been reported in South Africa. This work is therefore considered a major novel contribution to this field of research. After model calibration, both the observed and measured behaviour of the crush pillars in the trial site could be replicated. This was especially useful in evaluating the stress conditions measured above the pillars as well as the total amount of convergence experienced adjacent to the pillars and at the panel mid-spans. The findings validated the use of the limit equilibrium model implemented in a displacement discontinuity boundary element code to simulate the behaviour of crush pillars on a large scale.

ACKNOWLEDGEMENTS

I wish to express my appreciation to the following organisations and persons who made this study possible:

1 The contribution of Prof. John Napier with regards to the implementation of the limit equilibrium model in boundary elements as well as the development of the TEXAN code is greatly appreciated.

2 Prof. Francois Malan, my supervisor, for his guidance and support.

3 Lonmin Platinum: The research project was scoped as part of the long term mining strategy for Lonmin Platinum. The company supported the proposal to research the pillar system to ensure a reduction in risk and an optimised extraction strategy. The allocation of financial support, resources and time to conduct the study is greatly appreciated.

4 The following persons are gratefully acknowledged for the support and assistance with the study and underground trial on Lonmin Platinum:

a. Mr. Mark Munroe (Former Executive Vice President of Lonmin Platinum)

b. Mr. Mike Da Costa (Previous Vice President Karee Mine)

c. Mr. Jurgens Visser (Head of Technical Services)

d. The K3 Rock Engineering team, namely: Mr. Otto van der Merwe (Rock Engineering Manager – Karee), Mr. Marius Pretorius (Rock Engineer – K3#), Mrs. Goitsimang Ramaboa (Learner Rock Engineer – K3#) who assisted in managing the mining cycle, instrumentation and data collection processes.

e. Mr. Fanie Viljoen (Mine Overseer – K3#) for his support in allocating a trial site and a dedicated crew to mine the area according to the prescribed requirements.

TABLE OF CONTENTS

LIST OF FIGURES

LIST OF TABLES

LIST OF SYMBOLS AND ABBREVIATIONS

APS	Average pillar stress (MPa).
E	Young's modulus (GPa), Stress-strain relationship.
FOS	Factor of safety
MPa	Mega Pascal
GPa	Giga Pascal
m	Metre
m^2	Square metre
mbs	Metre below surface
g	Gravitational acceleration (m/s^2)
ρ	Density (kg/m^3)
deg	Degrees
t	Thickness of beam (m)
k-ratio	Ratio of horizontal to vertical stress
ν	Poisson's ratio
σ_1, σ_2, σ_3	Major, intermediate and minor principal stresses
τ	Shear stress (MPa)
SR	Support resistance (kN/m^2)
σ_c	Unconfined peak strength of rock (MPa), also referred to as UCS
UCS	Uniaxial compressive strength (MPa); equivalent to C_0
UCS_b	Crushed material residual strength; equivalent to C_b
w:h	Width to height ratio
l:w	Length to width ratio
φ	Friction angle
k	Strata stiffness (GN/m)
λ	Post peak pillar stiffness (GN/m)
λ_c	Critical pillar stiffness (GN/m)
PFI	Pillar fracture index
MIF	Mining induced fractures
RQD	Rock quality designation
C	Cohesion (MPa)
C_r	Residual cohesion (MPa)
m_0	Strengthening parameter (intact)
m_b	Strengthening parameter (residual)
φ_0	Intact friction angle (degrees)
φ_b	Residual friction angle (degrees)

CHAPTER 1

MOTIVATION FOR THIS STUDY

The design and behaviour of crush pillars for the Merensky Reef stopes

1. INTRODUCTION

Mining aims to maximise the extraction ratio of a particular orebody. Mine stability is a key consideration and the type of layout (i.e. pillar type and mining span) must be suitable for the geotechnical environment. Safe mining practices therefore need to ensure mine stability, but also minimise the amount of ore left *in-situ* as pillars.

To understand the stability methods applied in shallow hard rock tabular mines (< 1000 m below surface), Ozbay et al (1995) conducted a survey of the strategies and criteria applied to stabilise the stoping environment using pillars. A comprehensive review of the current practices at the time identified four types of pillars being used. This will be discussed in detail below. The key findings were that each mine developed their pillar design methods based on practical experience. This resulted in very different pillar layouts, even between neighbouring mines with similar geotechnical conditions. The main aim of these pillar systems were to support the overburden and cater for large tensile zones and geological weaknesses in the hangingwall. Figure 1.1 details the different pillar behaviour associated with various pillar width to height (w:h) ratios.

Pillar types:

- **Non yield or Rigid pillars:** These in-stope pillars support the overburden to surface and are intended to remain intact and in the elastic portion of the load deformation curve during the life of the mine.
- **Crush pillars:** These slender in-stope pillars are intended to crush at the mining face. The pillars act as local stope support and are reliant on residual pillar strength to support to the height of the highest potentially unstable parting. A crush pillar system must be used in conjunction with a regional pillar system.
- **Yield pillars:** These in-stope pillars are larger than crush pillars and are intended to reach their peak and residual strength only when the pillars are in the back area of a stope. The pillars have the same function as a crush pillar system; act as local support whereby the delayed residual pillar strength must support to the height of the highest potentially unstable parting. This pillar system must also be used in conjunction with a regional pillar system.
- **Regional pillars:** These pillars are used in conjunction with either crush or yield pillars and are required to support the overburden rock mass to surface. These pillars must be spaced to take cognisance of the rock mass behaviour (i.e. convergence). The pillars are required to be indestructible and to some extent control seismicity. Where sufficient geological losses exist, these losses can be incorporated as part of the regional pillar layout and design. These pillars are also used

to compartmentalize a mine to ensure that pillar runs, fires or floods are prevented from affecting the entire mine, in which case the pillars also act as barrier pillars.

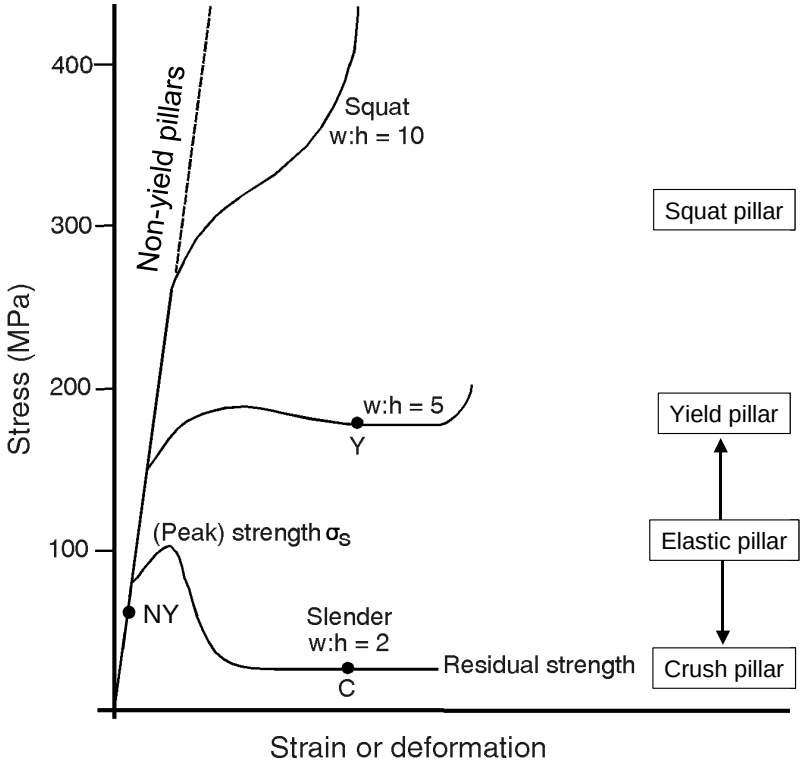

Figure 1.1: Typical stress-strain behaviour of hard rock pillars of different w:h ratios (after Jager and Ryder, 1999). Operating points: NY = Non yield pillars, Y = Yield pillars, C = Crush pillars.

Figure 1.2 is an illustration of the stress-strain relationship of a pillar. The initial straight line relationship of the curve to the yield point corresponds to the elastic response of the pillar. The yield point indicates the onset of inelastic behaviour whereafter the pillar exhibits strain hardening until it reaches its peak strength. Load shedding follows until the pillar reaches its residual strength.

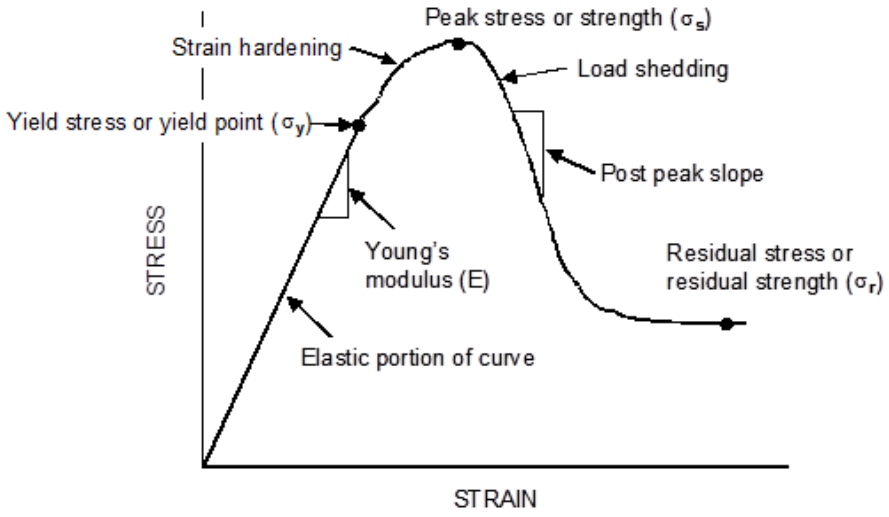

Figure 1.2: Diagram indicating the complete stress-strain curve of a pillar (after Ryder and Jager, 2002).

A typical mining configuration for an in-stope pillar layout on a hard rock narrow tabular mine (stoping width = 0.9 – 2 m) consists of pillars being positioned either adjacent to raises or winzes (dip mining) or strike gullies (breast mining). The pillars are separated in the direction of mining by a holing to allow for either ventilation (vent holing) or to increase extraction (pillar holing). These holings are commonly mined between 2 – 4 m wide. Where crush or yield pillars are used, a siding (1 – 2.5 m wide) is mined adjacent to the raise or gully to ensure that the failed rock do not fall into this travelling way. These sidings are carried a maximum of either 3 m or 6 m behind the panel face (depending on the standard applied by the respective mining company). Inter-pillar spans vary between 20 m and 35 m. Figure 1.3 is an example of a typical up-dip layout. Here an off-reef haulage links to the reef horizon via a cross-cut and travelling way.

The type of pillar system required is depth dependent. Mining with non-yield pillars should only be considered to the depth where crush pillar mining should be employed. The limitations of using non-yield or yield pillar systems implies that beyond some critical depth a crush pillar system is ideally required, unless backfill is used. Ozbay and Roberts (1988) suggested that crush pillars be implemented at a depth of approximately 400 m below surface based on the assumption that the average face abutment stress at this depth is greater than the strength of the pillars. In the case of crush pillars, failure of the pillars is expected, but must occur in a controlled manner. Pillar failure and the resulting load shedding should ideally be continuous to prevent accumulation of elastic strain energy. Once the residual strength of a crush pillar is reached, the post-peak behaviour is assumed to result in an increasing strength of the pillar in reaction to continuous elastic and inelastic stope convergence.

Crush pillar mining appears to be a method unique to South African tabular hard rock mines. This pillar system is applied to relatively shallow and intermediate depth gold and platinum orebodies. As the main objective is to investigate Merensky Reef crush pillars, the pillar behaviour of other reef types is considered beyond the scope of this study. The objective of the research is to gain an improved understanding of the behaviour of crush pillars and the factors influencing this behaviour.

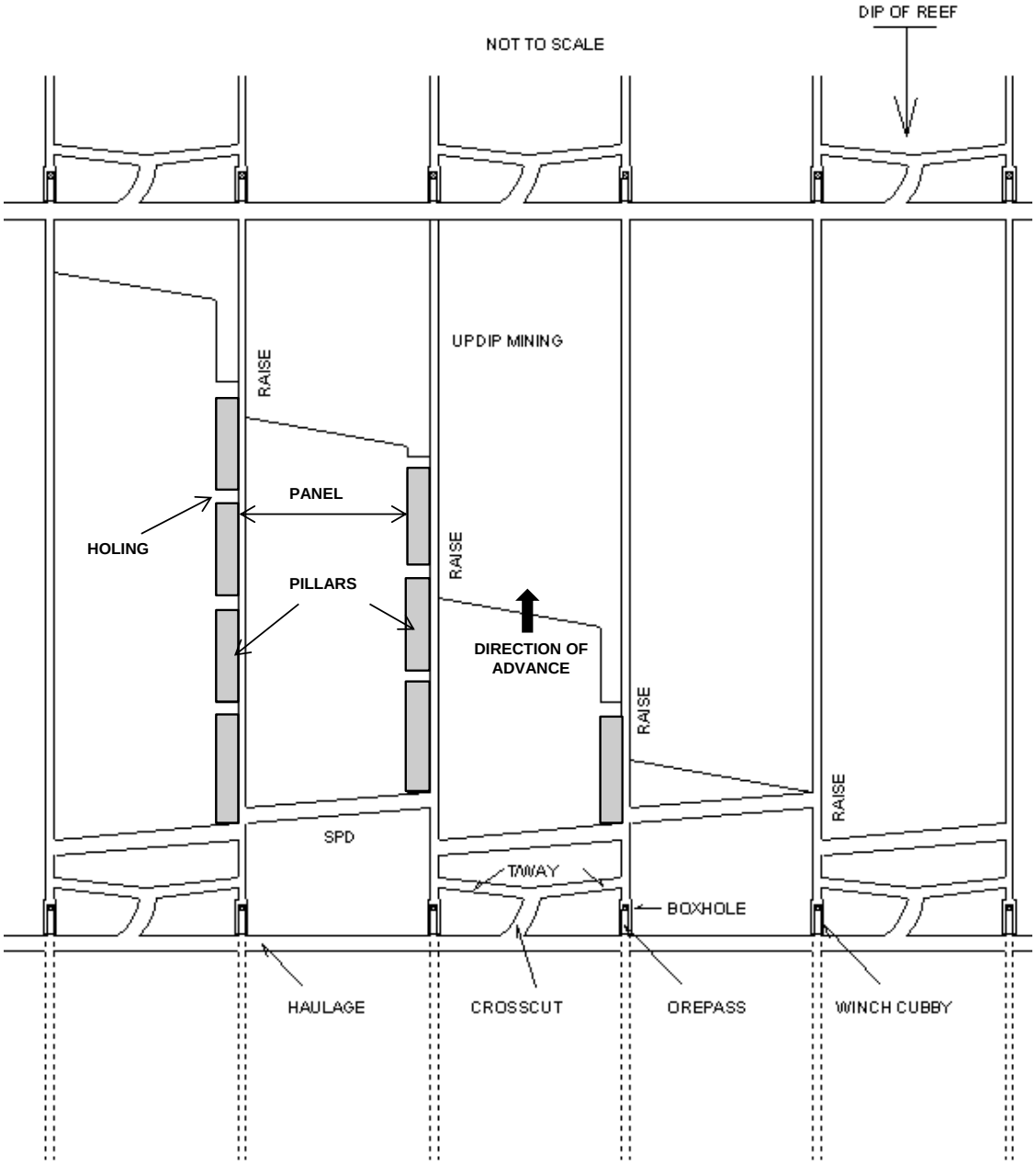

Figure 1.3: General in-stope pillar layout (plan view) for narrow tabular reef mining. The mining direction represents an up-dip mining configuration.

Figure 1.4: Photograph of a crush pillar from a trial site on Lonmin Platinum.

1.1. Geotechnical environment associated with the Merensky Reef

The Merensky Reef forms part of the Critical Zone of the Rustenburg Layered Suite (Ryder et al, 2002). It has been traced for 300 km around the entire outcrop of the eastern and western limbs of the Bushveld Complex and to depths of 5 km (refer to Figure 1.5). The UG2 Reef is found below the Merensky Reef. This middling ranges from as little as 20 m (Thabazimbi area) to approximately 210 m (Brits area) and extends to 400 m in other areas. The Merensky Reef has a very thin chromitite layer (millimetre thickness) overlain by a feldspathic pyroxenite. A second chromitite layer may occur at the top. The average Merensky channel width can vary, although a practical and economical stoping width of approximately 1.1 m is typically applied. The Merensky Reef dips between 9 and 22 degrees along the western and north-western limbs of the Bushveld Complex, but can dip as steep as 45 and 60 degrees along certain portions of the Eastern Limb. Both reef horizons are disrupted by faults, dykes, potholes and Iron-Rich Ultramafic Pegmatite (IRUPs).

The Merensky Reef is characterised by two distinct and consistent steeply-dipping joint sets (J1 and J2). The Merensky Reef is overlain by Norite and Anorthosite. This middling to the top of the Bastard Merensky Reef varies between 5 m and 45 m. Results from geotechnical logged drillcore indicate good ground

conditions exist in the immediate hangingwall of the Merensky Reef. Instabilities are mostly limited to the presence of doming features, flat dipping joints and shear zones. Rock strengths vary from approximately 90 - 140 MPa for Pyroxenite to 160 – 220 MPa for Norite, Spotted and Mottled Anorthosite. The stress state is characterised by residual stress along the NNW-SSE trending fault planes and pockets of anomalous stress. The k-ratio (horizontal stress to vertical stress ratio) obtained from stress measurements indicate a k-ratio of approximately 2.

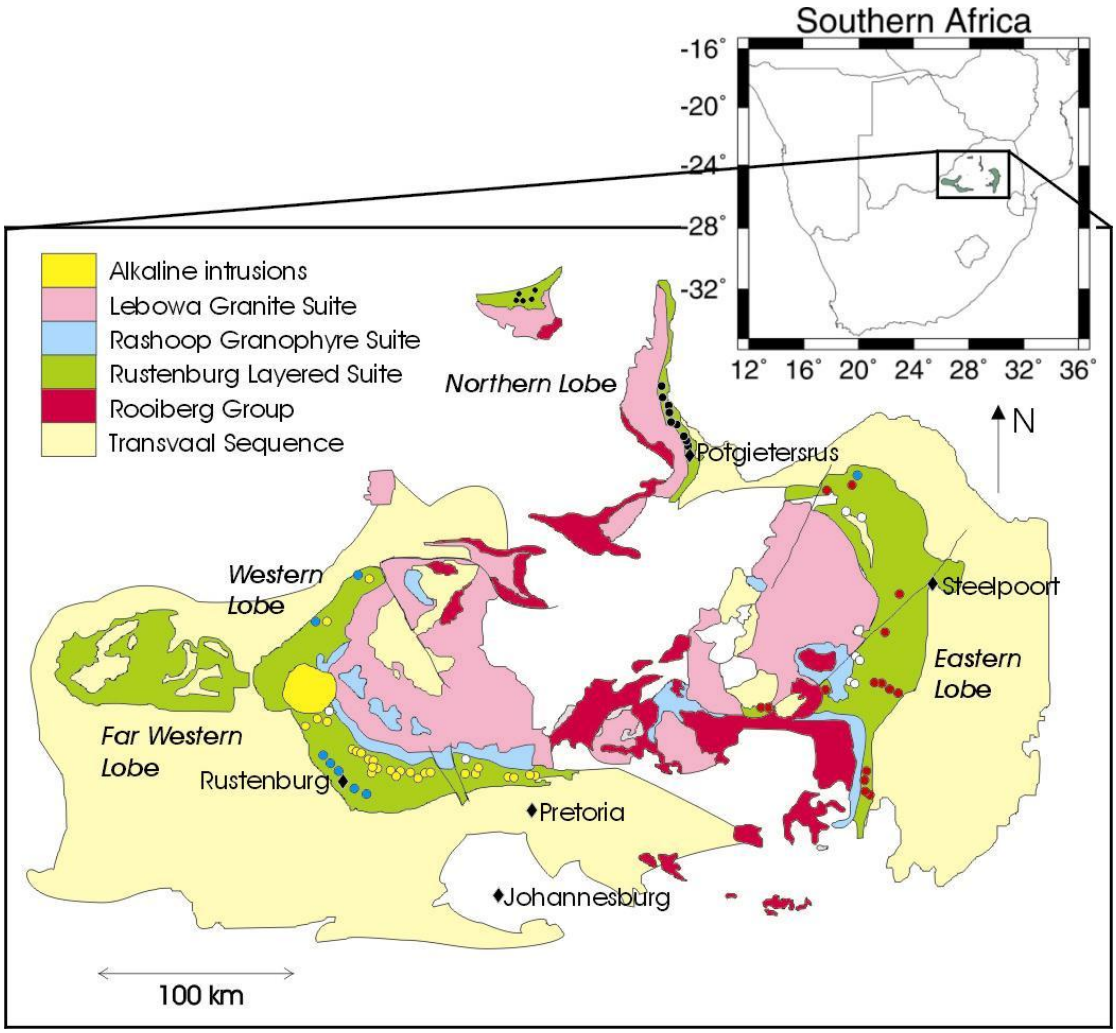

Figure 1.5: Geological map of the Bushveld Complex.

1.2. Project background

Ozbay et al (1995) described that the main purpose of the crush pillars was to provide enough resistance to support the rock up to the highest known parting plane (Bastard Reef contact, 5 – 45 m) and not support the full overburden to surface. The survey conducted by Ozbay et al (1995) indicated that layouts in shallow hard rock tabular mines consisted of approximately 30 - 33 m panel spans (inter-pillar) with relatively slender pillars 3, 4, 6 m (length) by 2, 2.5, 3, 4 m (width) positioned along strike gullies (some with a 1 m siding). The pillars were separated by 0.5 – 3 m holings (refer to Table 1.1).

It was found that the design of crush pillar layouts were initially conducted using dimensions which were successful in other areas with similar geotechnical conditions. The pillar dimensions and spacing in the new layouts were then adjusted until the pillars provided the required behaviour. The typical range of width to height (w:h) ratios of the crush pillars varied between 1.5 – 2.5. This accommodated the varying stoping widths (0.9 – 2 m), the weak footwall rock in some areas and structural weaknesses in the rock. An alternative design approach was to cut the pillars at a w:h ratio of 2 and then increase or decrease the pillar width until crushing was achieved.

RPM (Rustenburg Section) was the first platinum mine reported to have used crush pillars (Ozbay et al, 1995). It was implemented as early as 1974 on Frank Shaft (now Khomanani Mine) and RPM (Union Section) in 1977 (Korf, 1978). The pillar system was introduced to prevent backbreaks as a result of large spans created when changing the support method from initially stonewalls (1927) to stonepacks to crush pillars (1974) as mining progressed deeper (Frank Shaft 19 level is at approximately 500 m below surface). Interestingly, none of the platinum crush pillar sites investigated by Ozbay et al (1995) were at the time making use of regional pillars in conjunction with the crush pillars. *Backbreaks in platinum mines are defined as the collapse of an entire stoping area when mining spans exceed the critical span permissible by the hangingwall beams.*

At Randfontein Estate Gold mine, at a depth of approximately 700 m below surface, crush pillars were used with w:h ratios of 1.65. It was reported that pillars with larger w:h ratios were burst prone. Similarly, Durban Roodepoort Deep employed yield pillars at a depth of 800 – 1000 m below surface. These pillars yielded in a stable manner 20 – 30 m behind the face when cut at a w:h ratio of 1.7. Both mines employed regional pillars in conjunction with the crush or yield pillars to control the behaviour of the rock mass and alleviate backbreaks.

Table 1.1: A summary of crush pillars used on the Merensky Reef horizon (after Ozbay et al, 1995).

	Depth (mbs)	Reef dip (deg)	Pillar length (m)	Pillar width (m)	Stoping width (m)	Panel span (m)	Holing width (m)	w:h	Extraction (%)
RPM (Rustenburg)	400	9	6	2	1.1	34	3	1.82	96
RPM (Rustenburg)	650	9	4	2.5	1.1	33.5	4	2.27	97
RPM (Rustenburg)	650	9	4	3	1.3	33	4	2.31	96
RPM (Union)	650	18	4	2	0.9	33	2	2.22	96
RPM (Union)	1000	18	4	2	0.9	33	2	2.22	96
RPM (Union)	200	18	4	2	1.3	33	2	1.54	96
RPM (Amandelbult)	400	9	3	4	1.3	32	2	3.08	93

Currently, crush pillars are used as local support between regional pillars and must support the hangingwall to the height of the highest known instability plane (i.e. tensile zone between regional pillars or deadweight potential to the upper-most weak horizon or marker) to prevent the occurrence of backbreaks. Closely spaced support elements are typically used between adjacent rows of pillars to provide additional in-panel support. The stope support within a crush pillar environment must accommodate the required yielding characteristics and if required, energy absorption capabilities (if seismicity is anticipated). A crush pillar system is dependent on regional pillars to either support the overburden rock mass to surface Ryder et al (2002), or compartmentalise mining blocks, or control rock mass stiffness by managing the regional closure.

Although crush pillars (crush or yield mechanism) has extensively been applied on the Merensky Reef horizon since the late 1970's, little is known about their behaviour and no design methodology exists. The design of crush pillars and the assumed behaviour is still predominantly limited to specifying a width to height ratio (w:h) of approximately 2:1, a factor of safety (FOS) less that unity (<1) and the assumption that pillars should be crushing close to the face whilst the pillar is being cut.

On most mining operations, the design of the crush pillars is based on trial and error. As the pillar strength is unknown, the pillar sizes are adjusted to obtain the correct behaviour. Several factors affect the behaviour of the crush pillars and in many cases satisfactory pillar crushing is not achieved. This results in a seismic risk in many of the mines using crush pillars. If pillar crushing is not initiated whilst the pillar is being formed at the mining face, as the mining face advances and the pillars move to the back area of a stope, smaller pillars may burst while oversized pillars may punch into the footwall (Figure 1.6 and 1.7).

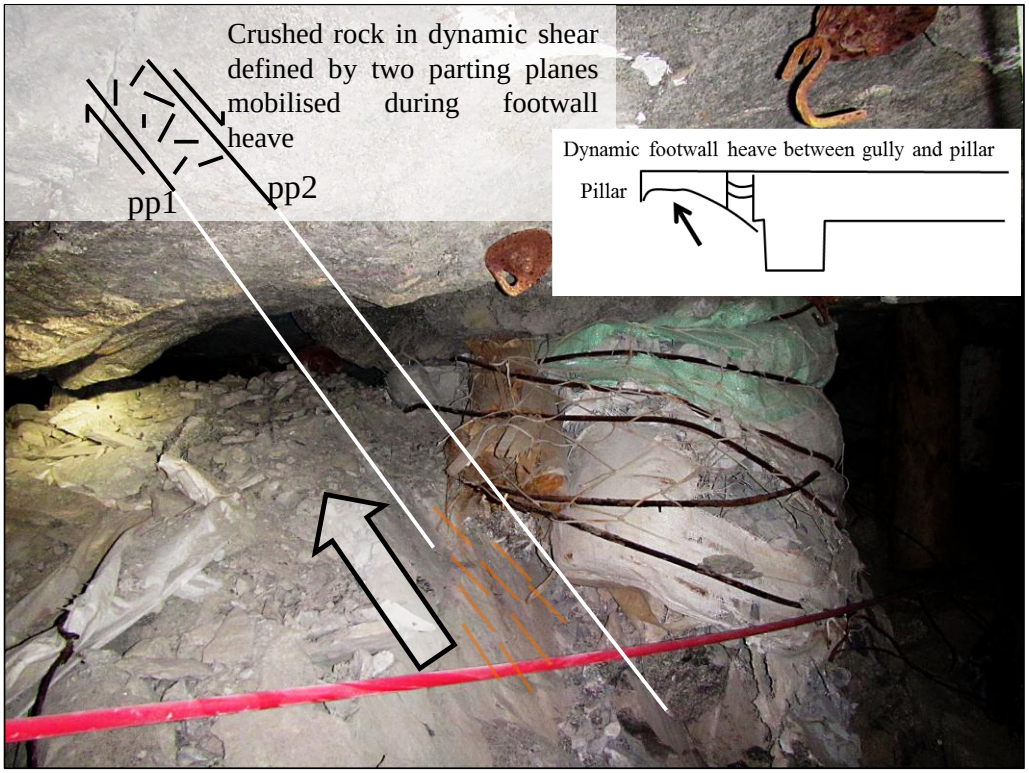

Figure 1.6: Example of pillar foundation failure. The crushed rock is contained in the siding between the pillar (not visible on far left) and the pack. The rings around the grout pack snapped during the event. The shattered timber elongate is an indication of the magnitude of this behaviour.

Figure 1.7: Example of pillar bursting. The scattered pillar material was ejected into the siding. The white lines indicate the scatter relative to the stoping width. Timber elongates indicate dynamic loading as a result of the event.

If pillars are designed in a manner that they are fractured during cutting by the face abutment stresses, the pillars will already have yielded and reached their residual strength. Further compression of the pillars will be associated with an increase in load and stability will be insured (Ozbay and Roberts, 1988). The stiffness of the strata must therefore be greater than the post-peak stiffness of the pillar (Figure 1.8) or violent pillar failure and hangingwall instability will occur.

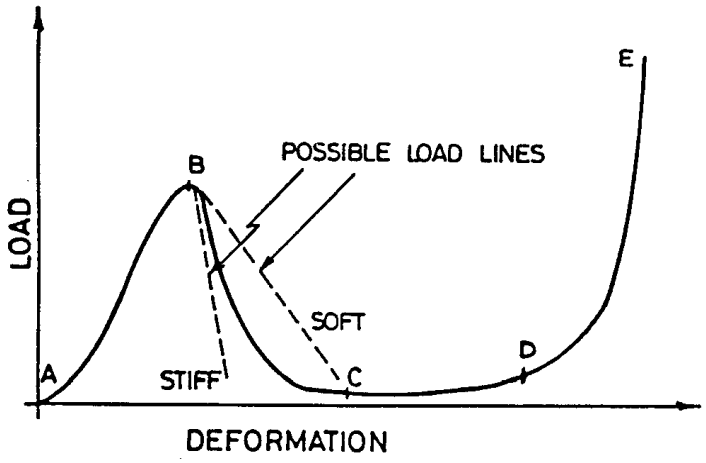

Figure 1.8: Stable (line stiff) and unstable (line soft) loading of a rock specimen along its complete-load deformation curve. Regions A-B, B-C, C-D and D-E represents pre-peak, post-peak, residual strength and strain hardening respectively (after Ozbay and Roberts, 1988).

There are many factors influencing the behaviour of crush pillars. These factors impact on the ability of the pillar to crush as well as the reaction of the strata in response to the pillar entering a post-peak state. Some of the contributing factors are highlighted below:

- mining depth (stress),
- stope layouts (position of the pillar and presence of a siding),
- mining height, panel span, pillar size,
- rock mass stiffness and the influence of extraction ratio (i.e. potholes or unmined ground) or regional pillars,
- behaviour of the pillar foundation relative to the pillar strength and load being applied,
- peak and residual pillar strength,
- pillar stress and how it is dissipated,
- impact of surrounding geological features (i.e. potholes) and the influence on rock strength or composition,
- mining discipline resulting in oversized pillars.

During the past 40 years several of these parameters have been researched using visual observations, *in-situ* measurements, laboratory testing and numerical simulations. Based on the work conducted, critical parameters have been identified, although there are still many contradicting findings between researchers.

In most cases, the above mentioned factors are ignored by Geotechnical Engineers and crush pillar layouts remained virtually unchanged over the last number of years. The simple design guidelines have nevertheless been used relatively successful on many of the gold and platinum mines in South Africa.

1.3. Problem statement and scope of the study

"The design and behaviour of crush pillars on the Merensky Reef"

The objective of this study is to address many of the shortcomings regarding the understanding of crush pillar behaviour. It is necessary to understand how the pillars behave and investigate the parameters which will affect the pillar performance and influence pillar crushing. On most operations where crush pillars are utilised, pillar crushing is not achieved. Crush pillars are implemented at relatively shallow depth, the pillar dimensions have remained essentially unchanged over many years and the impact of regional pillars and geological losses contributing to the regional behaviour of the rock mass are overlooked. Furthermore, in many cases the pillar system is the source of seismicity.

At the end of Chapter 2, various parameters are identified from the literature review which is believed to effect the performance of crush pillars. The parameters considered for this study will focus on:

1. Design criteria: Pillar size and stress.
2. Risk: Pillar instability.

These parameters have guided the scope of this study and are listed below.

1.1 Effect of pillar width: Pillar width and mining height influences pillar behaviour (refer to Figure 1.1). Various crush pillar widths (i.e. 2, 2.5 and 3 m) and mining heights (i.e. 1 m and 1.5 m) are applied on the Merensky Reef horizon. The impact of pillar width and width to height ratio must be determined to establish the affect it has on the overall performance of the pillar system. This will assist in determining if pillar dimensions can be standardised (width to height ratio or standard pillar width).

1.2 The impact of mining depth on pillar crushing: Guidelines are required regarding the implementation of crush pillars at different depths to ensure pillar crushing can be achieved safely.

1.3 Determining the peak crush pillar strength: The residual pillar strength was previously estimated using instrumentation and back analyses. The peak pillar strength is unknown, however, accurate

measurements will provide great insight with respect to the behaviour of the pillar system relating to the complete stress cycle. This could also provide detail regarding when and where relative to the mining face the peak and residual states are reached.

1.4 ***Determining the residual crush pillar strength:*** Although the residual crush pillar strength has previously been estimated, accurate measurements will confirm this and provide insight into the behaviour of the pillar system.

1.5 ***Determining if and how convergence is related to pillar crushing:*** Various factors can affect the amount of convergence experienced at a pillar position at different distances from the face. The behaviour of the pillar and the relation to the convergence experienced at the site should be investigated. Also, the effect of elastic convergence experienced in a panel on pillar crushing should be investigated.

2.1 ***The effect of oversized pillars:*** On many operations pillar crushing is not achieved as a result of pillars being cut too big. These pillars typically do not crush when formed at the face and can be a major source of seismicity in the back areas.

2.2 ***The impact of geological losses (e.g. potholes) and mining losses on pillar crushing:*** On many operations, pillar crushing is not achieved as a result of unmined blocks of ground left *in-situ*. Although these unmined blocks provide regional stability, it influences the behaviour of the pillars in the area surrounding them.

1.4. Methodology

The implementation of a crush pillar system on many mines is problematic owing to the difficulty of controlling pillar sizes with poor drilling and blasting practices. A comprehensive literature survey was conducted to establish the current criteria, based on past research, on the implementation of a crush pillar system.

The application of a limit equilibrium model was investigated to represent the pillar failure. Crushing of the outer portions of a pillar and the stress transfer to the pillar core can be replicated by the model. At the start of the study there was a need for a tool to investigate both the micro parameters affecting crush pillar performance as well as being capable of back analysing crush pillars on a mine wide scale. Non-linear continuum plasticity finite element or finite difference models are typically used to analyse local failure and deformation mechanisms. These methods are, however, difficult to apply and are not suited to the large-scale analysis of tabular stopes which include a large number of small pillars. The limit equilibrium model implemented in the TEXAN displacement discontinuity boundary element (DDM) code (Napier and Malan, 2007) provided a numerical modelling approach that could fulfil these requirements. A simple idealised crush pillar layout was used to investigate the effect of various parameters on crush pillar behaviour. The impact of the rock and pillar properties, layout parameters, mining sequence and the effect of off-reef structures in a layout could be investigated. The numerical model provided a method to investigate when pillars would crush, where they would crush relative to the mining face and why some pillars could potentially burst.

An analytical solution was derived by the author to estimate the average residual pillar stress for a completely failed two-dimensional (2D) pillar. The purpose of applying an analytical solution was to provide an appropriate tool which can be used to guide on crush pillar dimensions. The results of the numerical modelling were compared to the results obtained from the analytical solution. This provided a better understanding of pillar stress and stress change as a function of mining. The results improved the confidence in the limit equilibrium model as a suitable tool to assess crush pillar behaviour. It was found that the output of the analytical solution is nevertheless very sensitive to the choice of input parameter and is only suited to pillars with low w:h ratios.

In an attempt to calibrate the model, the properties of the Merensky Reef had to be quantified using laboratory rock specimen testing. The objective of the tests was to determine the elastic and post-peak properties of the rock contained in the pillar and pillar foundations. The performance of the pillars depends on the composition of the pillars. If a pillar comprises of a larger percentage Anorthosite, the pillar fractures more readily. However, the presence of Anorthositic rock in a pillar poses a higher seismic risk. Post failure rock testing is typically not conducted on specimens from most South African hard rock mines. Almost no record could be found of any post-failure rock testing on Merensky samples. It was, however, important to

have insight to the post-failure properties of the pillar material to assist with the calibration of the model. Both elastic and post-failure laboratory tests were therefore conducted. It should be noted that in many cases the parameters derived from laboratory testing may not be directly related to the parameters controlling the failure mechanism in an underground crush pillar.

An underground trial mining site was identified and established on Lonmin Platinum. The unknowns highlighted by the literature review or determined from the preliminary numerical analyses were used to guide the experimental trial. The objective of the trial was to mine a sufficiently large area using a crush pillar system to quantify the pillar behaviour by:

- Considering the behaviour of the pillars throughout the trial section,
- Targeting random pillars and measuring the individual pillar behaviour using instrumentation,
- Planning various pillar dimensions to validate the preliminary research findings,
- Instrumenting the trial area to such an extent that the behaviour of the pillars could be interpreted through measurement and observation.

The trial area was situated between potholes and therefore typical of what would be found on any platinum mine. The layout opted for ensured that the pillar behaviour would not be influenced by excavations such as gullies or sidings. The pillar dimension was selected to give a w:h ratio < 2:1 (2 m x 4 m pillars). Also, due to the small pillar dimensions required, it was expected that the trial area would consist of pillars having various final pillar dimensions resulting in a range of width to height ratios ($1 \leq w{:}h \leq 3$). The influence of pillar dimensions, geological structures (potholes) and different rock composition could therefore be assessed. The key parameters recorded were:

- Pillar dimensions,
- Pillar stress (absolute),
- Change in pillar stress through continuous strain change measurements,
- Convergence using closure-ride stations and continuous closure loggers,
- Pillar dilation using borehole extensometers,
- External pillar fracturing using photogrammetry and visual observations,
- Internal pillar fracturing through borehole camera surveys and micro seismic measurements.

The intent was to determine how the pillars behave prior to being formed, whilst being cut at the mining face and as the face advanced. All measurements could be compared to visual observations and photogrammetry. Trends could therefore be determined based on a pillar's behaviour relative to the face position.

The trial area comprising a mined area of approximately 22 000 m^2 was back analysed using the numerical model. Initially, it was attempted to use the actual rock properties obtained from the laboratory testing as the

input parameters representing the pillar material. However, the intact and crushed material residual strength are mostly responsible for the onset of pillar failure and the residual stress state achieved. Through successive cycles of parameter testing, the modelling parameters selected provided simulated results which closely resembled the observed underground pillar behaviour. Once the model was calibrated, both the observed and measured behaviour of the crush pillars in the trial site could be replicated. This was especially useful in evaluating the stress condition measured above the pillars as well as the total amount of convergence experienced adjacent to the pillars and at the panel mid-spans. The results validate the use of the limit equilibrium model implemented in a displacement discontinuity boundary element code to simulate the behaviour of crush pillars on a large scale. No record exists of any prior successful attempts in South Africa of back analysing the behaviour of crush pillars on such a large scale.

The objective of the study was to quantify and model the behaviour of Merensky crush pillars. This was achieved by both the results of the underground trial and the numerical simulations.

1.5. Novel contributions made by the author

In this study, various new methods to examine the behaviour of crush pillars were investigated. This resulted in an improved understanding of crush pillar behaviour. The novel contributions by the author included:

- The application of a limit equilibrium model to represent the behaviour of crush pillars.
- From the study, a set of design criteria could be derived by the author to guide on the safe implementation of a crush pillar system. For the first time, parameters contributing to pillar instability could be investigated. The presence of unmined blocks of ground (i.e. potholes) or inconsistencies in the mining layout contributing to the formation of oversized pillars (i.e. lagging siding) has, up to now, not been considered in any form of analyses to evaluate crush pillar behaviour.
- The author derived an analytical solution to estimate the average pillar stress of a completely failed crush pillar to investigate the behaviour of crush pillars. The results identified trends in terms of pillar behaviour as well as limitations regarding the application of analytical solutions.
- Almost no historic records of any post failure rock testing on Merensky samples could be found. Therefore, post failure rock testing of Merensky Reef samples was conducted to have some insight to the post failure properties of the pillar material.
- An underground crush pillar trial site was established and managed by the author. From the observations the failure mode of the crush pillars could be recorded and interpreted to provide a guide on the behaviour of the pillar system. This has not been systematically recorded for crush pillars before.
- The instrumentation programme during the trial site was one of the most comprehensive monitoring exercises ever conducted at a crush pillar site in South Africa. The measured performance could also

be related to the pillar condition as observed during the pillar forming cycle. The results have revealed new information regarding the behaviour of crush pillars. Secondary unloading cycles, ongoing pillar dilation and continued convergence as a result of pillar deformation could be identified. Also, the internal condition of pillars could be verified with a new seismic velocity process developed and tested on the crush pillars in the trial site to verify external observations and measurements. The residual state of a crush pillar could therefore be validated and related to events in the pillar forming cycle. The behaviour of the crush pillars in the trial site provide parameters to benchmark the performance of the pillar system against and can therefore be used as a guide to understand how to identify acceptable pillar behaviour.

- The back analyses of the underground trial site by the author validated the use of the limit equilibrium model implemented in the TEXAN code to simulate the behaviour of crush pillars on a large scale. To date, no numerical modelling of a mine-wide tabular layout, which explicitly included a large number of crush pillars, had been reported in South Africa. Once the model was calibrated, both the observed and measured behaviour of the crush pillars in the trial site could be replicated.

During the period of the study various papers were published by the author to share the research findings. The publications are listed below. Two of these papers were refereed journal publications.

Du Plessis, M., Malan, D.F. and Napier, J.A.L. (2011). Evaluation of a limit equilibrium model to simulate crush pillar behaviour. *J. South. Afr. Inst. Min. Metall.*, vol. 111, no. 12, pp. 875-885.

Du Plessis, M. and Malan, D.F. (2011). A new approach to simulate crush pillar behaviour in a tabular layout. *Proc. 12th ISRM congress*, Beijing, China.

- Area of study: Chapter 2 (Literature review) and Chapter 3 (Model formulation).

Du Plessis, M. and Malan, D.F. (2012). The simulation of crush pillar behaviour in the tabular layouts of the Bushveld Complex. *Proc. EuRock 2012*, Stockholm, Sweden.

- Area of study: Chapter 3 (Model formulation) and Chapter 4 (Simulation of crush pillar behaviour).

Du Plessis, M. and Malan, D.F. (2014). Evaluation of pillar width on crush pillar behaviour using a limit equilibrium solution. *Proc. EuRock 2014*, Vigo, Spain.

- Area of study: Chapter 3 (Model formulation), Chapter 4 (Simulation of crush pillar behaviour) and Chapter 6 (Assessment of an analytical solution).

Du Plessis, M. and Malan, D.F. (2014). Designing controlled pillar failure – crush pillar support. *Proc. 6th International Platinum conference*. Sun City, South Africa, pp. 339-346.

Du Plessis, M. and Malan, D.F. (2015). Designing controlled pillar failure – crush pillar support. *J. South. Afr. Inst. Min. Metall.*, vol. 115, pp. 481-488.

- Area of study: Chapter 2 (Literature review), Chapter 3 (Model formulation), Chapter 4 (Simulation of crush pillar behaviour) and Chapter 6 (Assessment of an analytical solution).

Du Plessis, M. and Malan, D.F. (2015). Assessing the behaviour of Merensky Reef crush pillars. *Proc. 13th ISRM congress*, Montreal, Canada.

- Area of study: Chapter 8 (Underground trial observations) and Chapter 10 (Back analyses of the underground trial).

Du Plessis, M. and Malan, D.F. (2016). The behaviour of Merensky crush pillars as measured at a trial mining site. *EuRock 2016*, Turkey. Paper submitted for publication.

- Area of study: Chapter 8 (Underground trial observations), Chapter 9 (Underground trial measurements) and Chapter 10 (Back analyses of the underground trial).

1.6. References

Jager, A.J. and Ryder, J.A. (1999). *A handbook on Rock Engineering Practice for Tabular Hard Rock mines*. SIMRAC, Johannesburg.

Korf, C.W. (1978). Stick and pillar support on Union Section, Rustenburg Platinum Mines, *Ass. Min. Mngrs. S.Afr.*, pp. 71-82

Napier, J.A.L. and Malan, D.F. (2007). The computational analysis of shallow depth tabular mining problems. *J. South. Afr. Inst. Min. Metall.*, vol. 107, Nov 2007, pp. 725-742.

Ozbay, M.U., and Roberts, M.K.C. (1988). Yield pillars in stope support. *Proceedings SANGORM Symposium in Africa*, Swaziland, pp. 317-326.

Ozbay, M.U., Ryder, J.A. and A.J. Jager (1995). The design of pillar systems as practiced in shallow hard-rock tabular mines in South Africa. *J. South. Afr. Inst. Min. Metall*.

Ryder, J.A. and Jager, A.J. (2002). *A textbook on Rock Mechanics for Tabular Hard Rock mines*. SIMRAC, Johannesburg.

CHAPTER 2

LITERATURE SURVEY

Existing design criteria and assumed behaviour of crush pillars

2. LITERATURE SURVEY

This section focusses on past research conducted. It also provides guidance with respect to further research requirements.

2.1. Crush pillar behaviour and available design criteria

The various parameters which influence the behaviour of crush pillars are described in the following sections. It is necessary to understand the effect of each parameter on the pillar performance to obtain a better holistic understanding regarding the behaviour of the pillar system.

2.1.1. Effect of pillar geometry on crush pillar behaviour

Crush pillars typically have a width to height (w:h) ratio of 2:0 – 3:0 for the lower (residual) and upper (yield point) boundaries respectively (Figure 1.2) and a factor of safety of less than one as it is reliant on guaranteed pillar crushing (failure) occurring behind the face (Ryder et al, 2002). Given general mining constraints, a minimum practical pillar dimension of 2 m wide is recommended in a narrow stoping width environment (i.e. 1 - 1.5 m) to account for out of line mining. The crush pillar dimensions (width) are dependent on the stoping width. Owing to the function of crush pillars, being to support either to the height of the tensile zone or to the height of the highest known separation plane, a regional pillar system is required to support the overburden rock mass to surface.

The load requirement of a crush pillar to function as local support can be determined from the support resistance required (equation 2.1). This is dictated by the height of the most prominent parting in the hangingwall. Support resistance in the order of 1 MPa was determined by Roberts et al (2005a) based on the back analysis of backbreaks which occurred at Randfontein Estates and Northam where the failures took place at 40 m and 30 m in the hangingwall respectively. Parting heights of 10 m and 20 m would result in a support resistance requirement of approximately 0.3 MPa and 0.6 MPa respectively.

$$SR = (\rho \cdot t) \cdot g \qquad (2.1)$$

With

SR = Support resistance (kN/m^2)

ρ = Density of hangingwall (kg/m^3)

t = Height or thickness of beam to support (m)

g = Gravitational acceleration (m/s^2)

Roberts et al (2002) indicated that pillar compression may be used as a parameter to estimate the extent of yielding and failure within a pillar. From analysis utilising a finite element code (ELFEN), it was determined that a rib pillar with a length to width (l:w) ratio of 2, 3 and 5 display a peak pillar strength reduction of 13.6 %, 6.5 % and 2 % respectively compared to a two-dimensional pillar of infinite length.

Furthermore, rectangular pillars typically display an increase in strength of 1.4 times that of square pillars with the same w:h ratio. This agreed with the finding of Ryder and Ozbay (1990). They suggested strength increases of 1.1, 1.2 and 1.3 for l:w ratios of 2, 3 and 4 respectively. For this reason, a practical l:w ratio should be considered. It was found that the pillar peak and residual strength will be obtained at between 8 - 12 and a further 6 - 8.5 millistrains for pillars with a l:w ratio of 2 and 3 respectively (i.e. a pillar with a w:h = 2:0; stoping width = 1 m). Roberts et al (2005b) determined, based on laboratory, underground measurements and observations that pillar peak strength is achieved at between 3 - 10 millistrains and residual strength is achieved at 8 - 15 millistrains. This agrees well with the behaviour modelled by Roberts et al (2002).

A crush pillar will be subjected to yield and failure at various distances from the face which should correspond to the above mentioned strain rates. This essentially entails that the pillars reach their residual strength at approximately 9 m behind the face. At mining depths less than 600 m below surface, this point will be reached much further from the face (if at all) due to the pillar stress to strength ratio and lack of convergence.

Canbulat et al (2006) conducted a detailed survey on three shafts along the western limb of the Bushveld Complex which had pillar bursting problems and associated injuries and fatalities. The aim of the survey was to determine the quality of pillar cutting. The findings are shown in Table 2.1 and Figure 2.1. It can be seen that only a small portion of the surveyed pillars fall within the initial w:h design range of between 2 and 3. Pillar cutting is therefore a critical parameter in controlling pillar behaviour.

Table 2.1: Summary of survey on quality of pillar cutting at three different shafts (after Canbulat et al, 2006).

		Deviation from design (%)	
		Pillar width (m)	**Pillar length (m)**
Shaft A			
241 pillars surveyed	**Undersize**	30.3	6.6
Pillar dimensions:	**Correct size**	17.8	6.6
3 m x 3 m and 4 m x 4 m	**Oversize**	51.9	86.7
Shaft B			
516 pillars surveyed	**Undersize**	38.6	18.4
Pillar dimensions:	**Correct size**	33.1	22.3
4 m x 3 m and 4 m x 4 m	**Oversize**	28.3	59.3
Shaft C			
178 pillars surveyed	**Undersize**	30.3	9.0
Pillar dimensions:	**Correct size**	32.6	19.7
4 m x 4 m and 4 m x 3 m	**Oversize**	37.1	71.4

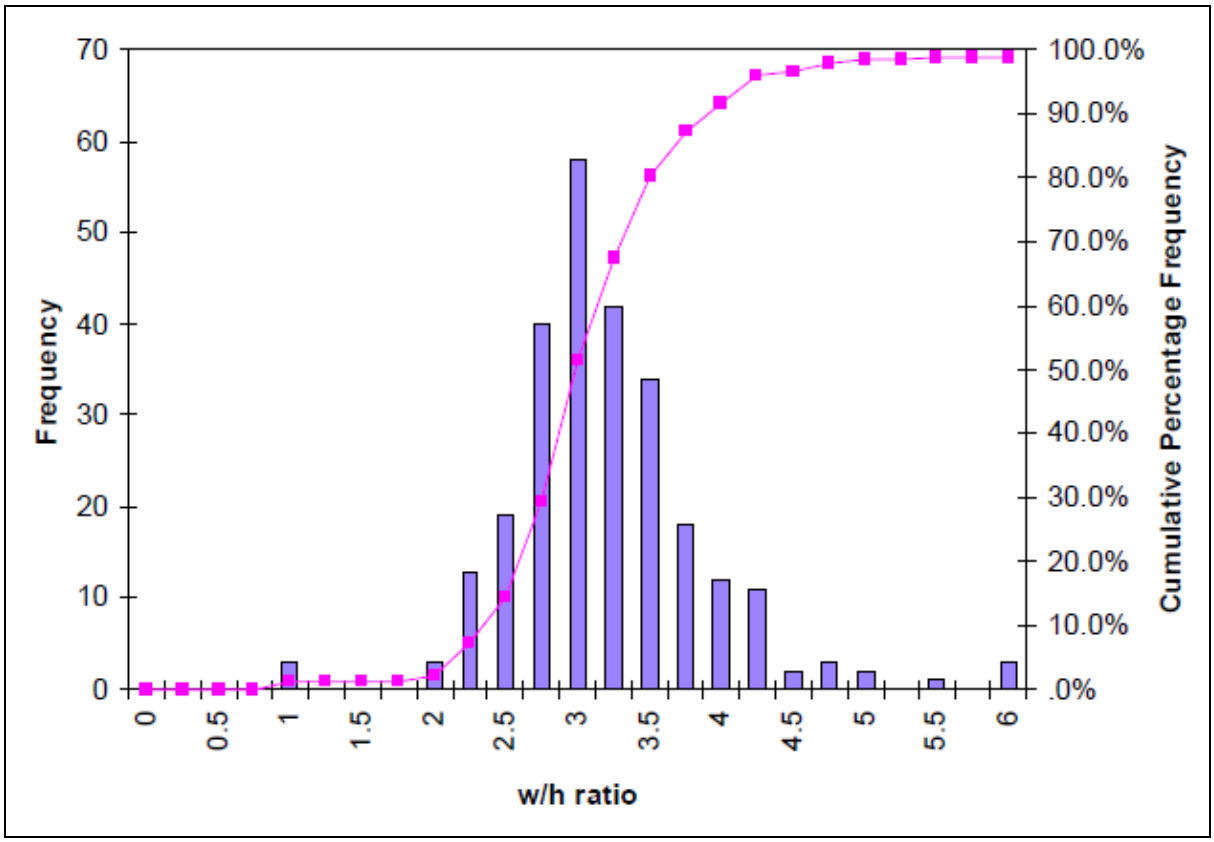

Figure 2.1: Crush pillar w:h ratio at shafts A and C (after Canbulat et al, 2006).

2.1.2. Pillar-system stiffness

The behaviour of the rock mass in response to mining must be taken into consideration. Various factors such as depth of mining, stress regime and mining strategy (extraction ratio) can cause mine instability, whilst factors such as advance rate and volume of mining can induce a shift in the loading condition.

It is still believed that the conditions for instability arise in the post-peak range of the stress-strain behaviour of the rock mass. Cook (1965) recognised that rock bursts is a problem in global stability in mines and subsequently, Cook (1967) discussed the significance of the post-peak behaviour of rock in compression. Specimens do not only display strain softening behaviour at a microscopic level. In fact, much of the macroscopic softening effects observed in compression tests can be accounted for by geometric effects associated by the distinct zones of rigid and plastic behaviour which exist in a non-homogeneous medium in a post-peak state (Drescher and Vardoulakis, 1982)

Rock mass stability has been expressed by means of stiffness (Salamon, 1970) where the rock mass behaviour (macro) is related to the load-displacement performance characteristic (micro) of a specimen in a testing machine and represented by a spring.

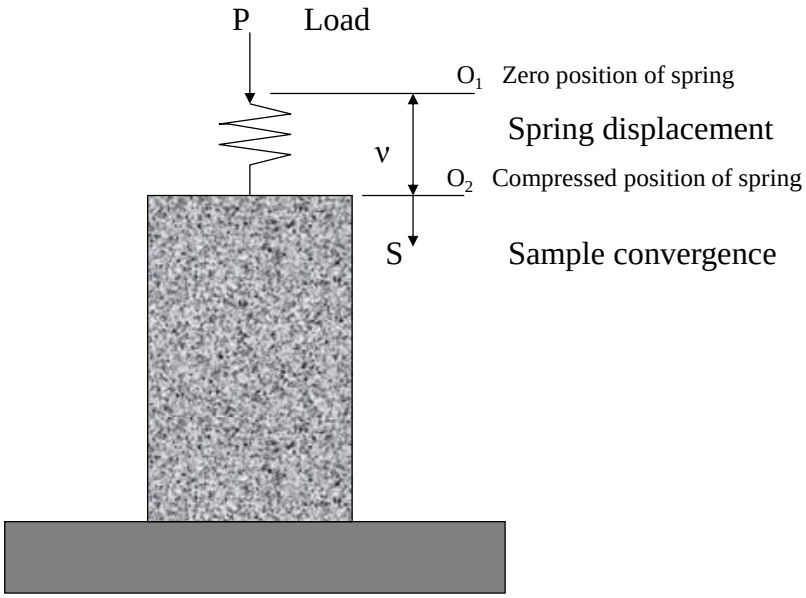

Figure 2.2: Diagram indicating a rock specimen being loaded in a testing machine.

The load-convergence characteristic of the rock specimen and the spring can be expressed by:

$$P_r = f(S) \tag{2.2}$$

$$P_s = k \cdot (\nu - S) \tag{2.3}$$

With

P = Load (kN). Subscripts r = rock and s = spring

k = Spring stiffness

ν = Displacement of spring

S = Convergence characteristic of rock specimen

For equilibrium to exist at some stage when loading the specimen through the spring, the net forces at the rock-spring interface should be zero *($P_r - P_s$)*. A disturbance in the state of equilibrium, i.e. applying a small external force at point O_2 (Figure 2.2) will cause an incremental change in the force in the rock and spring and incremental change in convergence *ΔS*. From equations (2.2) and (2.3) the incremental change in force in the rock and the spring is given by:

$$P_r = f'(S)\Delta S = \lambda \Delta S$$

and

$$P_s = -k\Delta S$$

Therefore the net probing force causing an incremental displacement *ΔS* is given by:

$$\begin{aligned} \Delta P &= \Delta P_r - \Delta P_s \\ &= (k + \lambda) \cdot \Delta S \end{aligned} \tag{2.4}$$

With *$(k + \lambda)$* interpreted as the spring-specimen stiffness and λ the slope of the specimen force-displacement characteristic. The condition for global stability is assured if stable equilibrium is guaranteed. The global work term must be greater than zero ($\ddot{W} > 0$) where $\ddot{W}$ represents the second order variation of the total potential energy of the system:

$$\begin{aligned} \ddot{W} &= \frac{1}{2}\Delta P \Delta S \\ &= \frac{1}{2}(k + \lambda)\Delta S^2 \end{aligned} \tag{2.5}$$

Equilibrium of the spring – specimen is assured if:

$$(k + \lambda) > 0 \qquad (2.6)$$

During laboratory uniaxial compression strength (UCS) testing, the stability of the equilibrium between the testing machine load and the specimen resistance in the specimen's post-peak regime depends on the relationship between the stiffness of the testing machine and the post-peak stiffness of the test specimen. If the stiffness of the testing machine (slope of B in Figure 2.3) is less than the slope of the post-peak load-deformation relation of the specimen, the test results in violent failure of the specimen. Failure will, however, not occur if the stiffness of the machine (slope of line A in Figure 2.3) is greater than the slope of the post-peak load-deformation relationship of the specimen.

By applying the correlation between uniaxial rock testing and loading of an isolated pillar, Salamon (1970) showed that the equilibrium between a pillar being loaded and the post-peak behaviour is stable irrespective of the convergence experienced by the pillar if:

$$(k + \lambda) > 0 \qquad (2.6)$$

With
k = Stiffness of loading strata
λ = Post-peak pillar stiffness

If pillars are designed to be intact when cut at the face and only fail later, λ can become negative once the pillar reaches peak strength and instability will occur ($k + \lambda < 0$). If pillars are designed in such a way that they are fractured during cutting by the face abutment stresses so that the pillars will already have yielded and reached their residual strength, further compression of the pillars will be associated with an increase in load (λ becomes positive) and stability will be insured (Ozbay and Roberts, 1988).

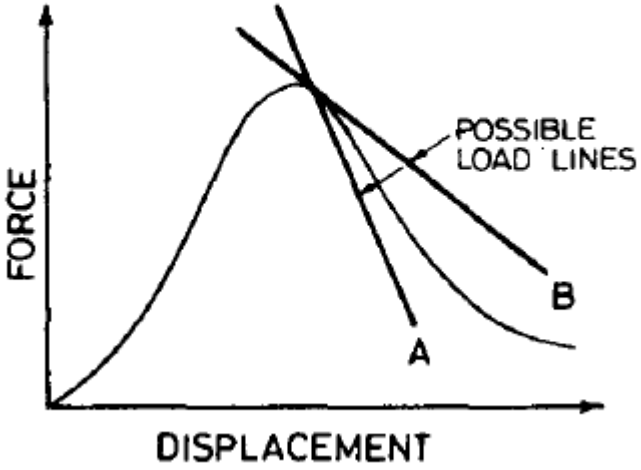

Figure 2.3: Rock specimen loading under uniaxial compression; stiffness characteristic (after Ozbay, 1988). Line A: Stable specimen loading, Line B: Unstable specimen loading.

The stiffness of the strata must therefore be greater than the post-peak stiffness of the pillar or violent pillar failure and hangingwall instability will occur. The potential for unstable pillar behaviour is therefore governed by the stiffness of the loading system and load shedding modulus of the material. The pillar design should be aimed at determining pillar dimensions for which the post-peak curve of the pillar levels off (is as flat as possible).

Where the gradient of the post-failure specimen (pillar) is greater than the gradient of the test machine (rock mass) stiffness, instability will occur (Salamon and Oravecz, 1976). Salamon predicted that the softest loading system (strata stiffness) will present the greatest danger to uncontrolled failure.

The slope of the post-peak load deformation relationship becomes flatter with increasing w:h ratios. Samples consisting of jointed or fractured material have a flatter post-peak modulus than samples made up of initially competent specimens. Pillar layouts must therefore be designed to satisfy equation (2.6) where pillars continue to carry load in their post-peak state (this holds for crush and yield type pillars).

Starfield and Fairhurst (1968) suggested that equation (2.6) be used to evaluate the stability of individual pillars in a stratiform orebody. Accordingly it can be used to assess the stability of the entire mine structure as mining induced displacements as a result of volumetric changes in the rock mass are resisted by the pillars. The behaviour of the rock mass is therefore representative of the spring and the pillar, that of the

specimen. Pillar instability is likely to occur when λ_i (for individual pillar stiffness) is negative in the post-peak range and therefore:

$$|\lambda_i| > k_{li} \qquad (2.7)$$

With

λ_i = Individual pillar post-peak stiffness

k_{li} = Local rock mass stiffness

i = 1, 2, …N

N = Number of pillars in the layout

Both Salamon (1970) and Brady and Brown (1981) discussed the state of stability for pillars whereby the information required consisted of the post-peak stiffness of the pillar and the mine local stiffness at the various positions within the layout. For convenience, the post-peak deformation of a pillar can be described by a characteristic stiffness (λ').

The post-peak pillar stiffness (λ') can be determined from the elastic pillar stiffness (λ) and the pillar geometry. From laboratory results (e.g. Figure 2.4) it was found that the ratio of (λ / λ') decreases as the diameter to length ratio (d:l) of the specimens increases (specimen length decreases for a constant specimen diameter) corresponding in a change from steep to flat post-peak behaviour (the slope of the post-peak pillar relationship becomes flatter with increasing width to height ratios).

The pillar stability index $(k_l + \lambda')$ can be determined by calculating mine local (k_l) and pillar elastic (λ) stiffness to estimate the post-failure (λ') stiffness.

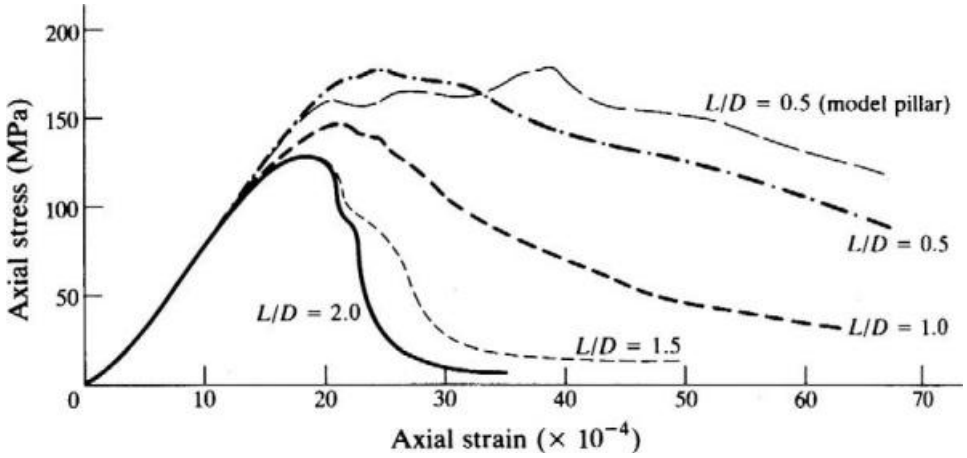

Figure 2.4: Uniaxial compression test results on a marble with different length:diameter (L/D) ratios (after Starfield and Wawersik, 1972).

Brady and Brown (1981) used a direct formulation of the boundary element method. This was also demonstrated by Ozbay (1988) using MINSIM-D (Napier and Stephansen, 1987) and MINAP (Crouch, 1976) to determine mine local stiffness and pillar stiffness in the elastic range. The various ratios of elastic / post-peak stiffness for corresponding width to height (w:h) ratios were estimated from published data on laboratory specimens. The available laboratory and *in-situ* data was subsequently reworked as presented in Figure 2.5 (Ozbay, 1988).

The figure suggests that pillar failure at any pillar width to height ratio may result in instability. This is as a result of mine local stiffness increasing relatively slow with a decrease in stope span. The country rock is therefore always readily deformable in comparison to the pillar. The stiffness ratios of jointed specimens are very different from non-jointed specimens. Stable pillar post-peak behaviour can be assured from higher width to height ratios. The discontinuities in a rock mass have a dominant effect on the post-peak deformation properties of the medium and may control the potential for mine global stability. Joint sets and other features orientated to favour slip during the development of new fractures in a pillar can be expected to lead to stable yield of the pillar.

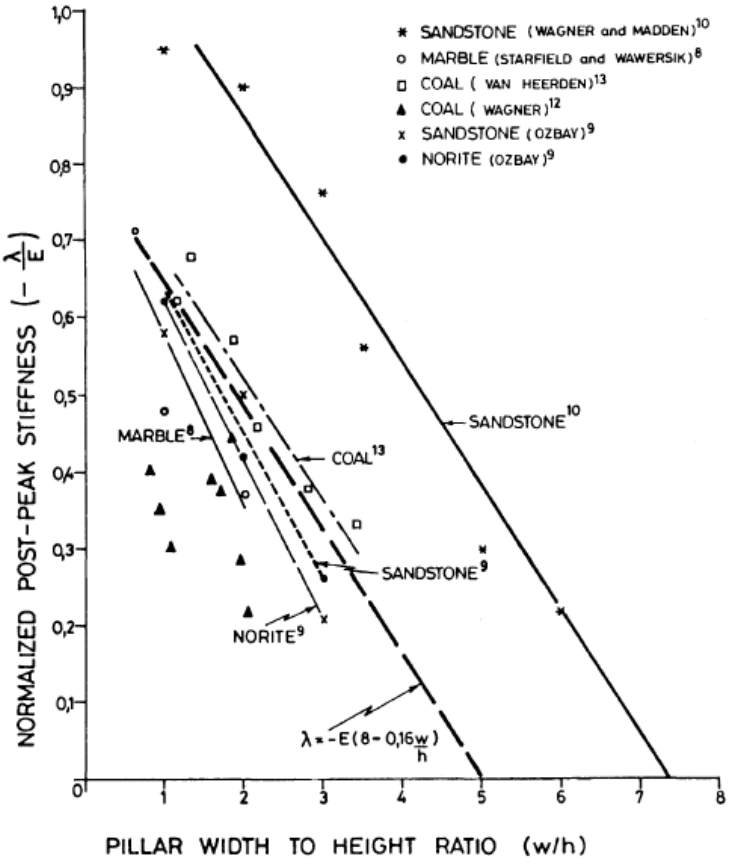

Figure 2.5: Post-peak stiffness $|-\lambda|$ normalised with respect to elastic modulus E as a function of w:h ratio (after Ozbay, 1988).

A more accurate description is therefore required for the post-peak behaviour of a pillar to describe its deformation mode, including:

- Changes in macroscopic response associate with fracture development,
- Effects arising from slip on these induced features,
- Time dependence of deformation.

Ozbay (1988) proposed, as part of the design methodology to design yield pillars, methods to determine the various stiffness parameters which must be taken into consideration to satisfy equation (2.6). These include:

- **Local stiffness (k_{li})** which is the stiffness of the strata at a specific pillar location assuming all pillars in a layout are in their pre-failure regime,
- **Critical stiffness ($-\lambda_c$)** is the steepest slope bounding the load-deformation curve of the pillars and hence the worst-case option assuming that all the pillars in the system are at a post-peak state (failed state) and implies that pillar layouts are stable if ($\lambda > \lambda_c$),
- **Post-peak pillar stiffness ($-\lambda$).**

Ryder and Ozbay (1990) differentiated between local and regional strata stiffness.

- **Local stiffness (k_{li})**, defined above as the stiffness of the strata at a specific pillar location with all pillars being in a pre-failure regime,
- **Regional stiffness (k_r)** which is also equivalent to **Critical stiffness ($-\lambda_c$)** thus $k_r = -\lambda_c$. where all pillars are in a post failure state (negative stiffness) of which the pillars can have the same stiffness values (after Salamon, 1974) or varied negative stiffness's as a result in varied pillar dimensions (after Ryder and Napier, 1987).

Pillar failure will be stable if the pillar post-failure stiffness ($-\lambda$) is less than the effective stiffness of the strata (k), thus ($k > -\lambda$).

The local strata stiffness is understood as the force required to cause a unit increment in closure (displacement) between the hanging-and footwall at the position of the pillar and is therefore positive by definition. Where λ is negative (failing pillars), stability depends on the relative stiffness of the strata and the pillars in the post-peak regime.

Ozbay (1988) proposed the use of numerical analyses (boundary element modelling) to obtain both the Local and Regional, or Critical stiffness. The local stiffness is obtained by determining the load on a pillar (F) and convergence (s_1) for the pillar of interest. A second convergence (s_2) is determined when the pillar is removed from the layout and can be expressed by:

$$k = F / (s_2 - s_1) \quad (2.8)$$

Ryder and Napier (1987) determined that, by modelling a pillar layout directly in which the pillars are assigned negative stiffness (λ), and the value of λ is decreased in successive runs until the solution process fails to converge, the critical pillar stiffness ($-\lambda_c$) where ($-\lambda_c = k_r$) is approached. Typically no more than two or three runs are necessary to pinpoint the value of k_r with satisfactory precision.

For large mined out areas with no regional pillars, the regional strata stiffness (k_r) approaches zero. The effect of reducing regional stability (opening spans or mining pillars) does have an effect on stiffness, but more so on the increase in convergence which will be experienced and in turn will result in increased loading of the in-stope pillars.

Ozbay (1988) assumed the relationship between post-peak stiffness (λ) and width to height ratios of pillars (Figure 2.5) within the range of 0.7 < w:h < 5 to be:

$$\lambda / E = 0.16 \cdot (w/h) - 0.8 \quad (2.9)$$

With
E =Elastic modulus of the pillar material (GPa)

Equation 2.9 can be used to estimate the post-peak pillar stiffness (-λ) based on the field data used to compile Figure 2.5. The critical stiffness ($-\lambda_c$) will have a lower value and is dependent on factors such as:

- Extraction
- Mining depth
- Maximum regional pillar span
- Pillar height
- Crush pillar width
- Elastic modulus of the rock mass (E)
- Poissons ratio

Furthermore, accurate rock mass parameters (E, ν) and specimen load-deformation information is required to make accurate estimations regarding the pillar system's state of stiffness (Figure 2.5).

Crush pillars, by definition should already have crushed and therefore be yielding when cut at the face. Further compression of the pillars is associated with increase in load and λ should become positive which

meets the stability requirements of equation 2.6. It was also postulated Ozbay and Roberts (1988) that a pillar which is already in a crushed state when cut, is in a residual state and therefore λ can never be negative along the load deformation path; "Instability is not possible".

2.1.3. Pillar foundations

A pillar system is dependent on the behaviour of the foundations comprising of the hanging-and footwall and pillar material. The damage to pillar foundations increase with an increase in contact friction angle along the hangingwall, footwall or both interfaces. This corresponds to predictions made from laboratory punch tests, Spencer and York (1999). Finite discrete element analysis (ELFEN), Roberts et al (2002) indicated that at low contact friction angles the damage is concentrated above and below the centre of the pillar, the magnitude of the deformations being small with the pillar being crushed. As the contact friction angle increases so also does the damage to the foundations and as a result, reduced pillar crushing.

- At a contact friction angle of 20 degrees the damage is concentrated above the edges of the pillar.
- At 40 degrees the damage and failure is heavily concentrated around the corners of the pillars.

It was also found that the post failure modulus of the pillar increases with an increase in contact friction angle and w:h ratio.

Designs to avoid foundation failure along non-yield (rigid) pillars has traditionally been based on:

$$APS = f \cdot \sigma_c \qquad (2.10)$$

f = Multiplying factor. Traditional design assumed f = 2.5 (COMRO, 1988)
σ_c = UCS of the foundation rock

This traditional assumption was, however, found to be exaggerated and that values of much lower (f) resulted in foundation failure. An alternative approach to estimate the value of (f) is to quantify the yield stress (σ_y) of the pillar foundation. A change from pure elastic behaviour occurs at the yield point which allows for stress regeneration as a result of regional convergence (York, 1998). This yield point can therefore be incorporated as a design limit, above which the onset of more severe foundation damage begins (Prandtl wedge). York noted that the ultimate strength of the pillar system is strongly influenced by the stiffness and degree of horizontal confinement provided by the loading environment. Yield stress can therefore be used as a parameter to indicate foundation stability (pillar punching potential).

2.1.4. Residual pillar strength

Once a crush pillar has failed, it must be capable of supporting the potential deadweight resulting from hangingwall separation. The residual strength of an instrumented quartzite crush pillar at 700 m below

surface was estimated to be approximately 8% of its peak value (10 MPa – 13 MPa), (Ozbay and Roberts, 1988). Instrumented pillars on the Merensky Reef at RPM at approximately 1100 m below surface estimated the residual strength of a crush pillar (w:h = 2:1) to be 19 MPa following approximately 90 millistrains of deformation (Roberts et al, 2005b). Back analyses of the pillar performance indicated that the range of residual strength for the pillars could vary between 13 – 25 MPa. It is estimated that the pillar of which the residual strength was measured had a post-peak stiffness (λ) of 12 GN / m. This post-peak pillar stiffness was determined by applying the principles of Ozbay and Roberts (1988) for a stress drop of 75 MPa - 19 MPa over 5 millistrains of deformation.

2.1.5. Pillar strength performance characteristic

Roberts et al (2002) found that the correlation between width to height ratio and pillar strength follows a power law relationship for which the nature of the relationship is controlled by the contact friction angle of the pillar-foundation. This contradicts the theory proposed by York et al (1998) that the relationship between pillar shape and strength is linear.

York pursued the concept that rock strength decreases with an increase in sample size and that beyond a critical sample size there will be no further strength reduction (Bieniawski and Van Heerden, 1975). Following York's interpretation of laboratory UCS test results, it was tentatively concluded that hard rocks (Bushveld igneous rocks) have a critical size much smaller than those of soft rocks (Coal) which would remove the need for large scale *in-situ* tests. Laboratory test results are therefore representative of the *in-situ* performance, taking to account the boundary conditions in the centre of a pillar as well as loading rates (following van Heerden's test analogy of large *in-situ* specimens). Furthermore, *in-situ* hard rock pillars are larger than the defined critical size and therefore it was interpreted that volume should not be a variable in pillar design.

The two well-known pillar formulae used to determine the peak pillar strength of pillars are the Power formula Salamon and Munro (1967) and Hedley Grant (1972) and the Linear formula Bieniawski and Van Heerden (1975). The generalised forms of these equations are given below.

Power formula:

$$P_{strength} = K \cdot {w^{\alpha}}/{h^{\beta}} \qquad (2.11)$$

Linear formula:

$$P_{strength} = K \cdot \left(b + (1-b) \cdot \frac{w}{h} \right) \qquad (2.12)$$

Where:

$P_{strength}$ = Pillar strength (MPa)

h = Pillar height (m)

w = Pillar width (m)

b = Slope parameter describing the effect of w:h on rock strength

K = Actual *in-situ* strength of 1 m^3 of rock (MPa). Also referred to as design rock mass strength (DRMS). De-ratings are applied to the rock strength (UCS) and rock mass condition to obtain an estimate of K.

α, β = Empirical constants

According to York et al (1998) the power formula takes volume into account (can be used for all ranges of specimen diameters) whereas the linear formulae only accounts for the geometric effect of increasing width to height ratio (must be adjusted for varying specimen diameters). As York removed the volume effect from the pillar system, it was concluded that the linear formula performs almost as well as the power formula for low width to height ranges.

The contact friction angle at the pillar interfaces effectively determines the exponents of the power law equation. The exponents increase as the contact friction angle increases. It was found that the contact friction angle of steel platens (laboratory test) is approximately 10 – 20 degrees. York et al (1998) determined it to be only approximately 13 degrees for which the results appeared to follow a linear trend as a result of the low exponents of the power law relationship. At a contact friction angle smaller than 20 degrees the behaviour can be approximated as a linear function. Furthermore, laboratory test results always produce a scatter to which a curve can be fitted with comparative confidence. Modelling conducted by Roberts et al (2002) indicated that the linear law does not apply at contact friction angles greater than 10 degrees. It is believed that the friction angle over the contact area of a pillar exceeds 20 degrees and could be as high as 40 degrees and for this reason the pillar strength relationship is assumed to be exponential rather than linear.

Watson et al (2008) applied a maximum likelihood back-analyses study (similar to Salamon-Munro) on failed and stable pillars in an attempt to develop a strength formula for Merensky pillars. Preliminary strength parameters were derived for both the standard linear and power formula. Due to difficulties in establishing realistic pillar loads through MINSIM modelling and variable parameters such as rock strengths, effect of sidings and stoping widths the analyses was mainly conducted on the pillars of Impala Platinum and the results biased towards the Impala pillars. Other sites discarded in the final analyses for the formulation of the strength parameters included RPM Rustenburg, Amandelbult and Lonmin Karee section. The observational study ranked pillars based on their visual condition (failed or burst pillars, presumed failed pillars, damaged pillars, scaling visible or no-damage) to ensure that pillars which are in a post-peak state could be assessed (failed pillars were simulated by giving them a stress of 20 MPa). Adjustments were

accounted for by accommodating an increase in pillar height due to the influence of gullies (after Roberts et al, 2002) and pillar length (after Wagner, 1974).

The findings from the study were that the linear equation appeared to have provided a slightly better evaluation of the Impala data than the power formula. A significantly greater standard deviation was obtained if the entire data base including all the sites were considered (compare Figure 2.6 and Figure 2.7). The available data was re-evaluated by the author to determine the applicability thereof on crush pillars. The findings are summarised in Tables 2.2 – 2.5 which indicates that:

- The majority of the assessed pillars had a w:h ratio greater than 2,
- Approximately 45% of all the assessed pillars were categorised as failed or presumed failed,
- Approximately 14% of these categorised "failed or presumed failed" pillars were in fact failed and 86% presumed failed,
- The same percentages apply for pillars having a w:h ratio less and greater than 2,
- Approximately 63% of the database consisted of Impala pillars of which 18% of the Impala pillars were classified as being in a post-peak state,
- Only 24% of the Impala pillars had a w:h ratio < 2 whilst approximately 76% had a w:h ratio >2,
- Table 2.4 details the variance in true w:h versus effective w:h ratio as a result of the influences of sidings, gullies and pillar length which seems to effect the overall ratio by between ± (5 – 30)%.

Based on this assessment, the assumption by Watson et al (2008) that the linear formula provides a better estimate of the pillar strength is biased towards the Impala pillars and pillars with a w:h ratio greater than 2. The Impala pillars are typically classified as yield pillars and are intended to only reach their post-peak state once the pillars are in the back area and not when cut on the face (crush pillars). Figure 2.6 and Figure 2.7 also provides a good indication of the modelled pillar stresses (APS) versus the calculated pillar strengths (linear formula) based on the strength parameters determined from the assessment of the Impala pillars. Comparative analysis using both the linear and power formula with the Watson strength parameters yield similar results with regard to pillar dimensions versus factor of safety (FOS).

Table 2.2: Assessed w:h ratios of failed pillars (data from PlatMine report after Watson et al, 2007).

Total	Number	%	w:h ≤ 2	w:h 2 - 3	w:h ≥ 3
All pillars assessed	194	100%			
Failed and presumed failed pillars (class 3 /4)	87	45%	14%	49%	37%

Table 2.3: Breakdown per area of assessed pillars being in their post-peak state (data from PlatMine report after Watson et al, 2007).

	Total	Amblt	Imp 4#	Imp 8#	Imp 10#	Turf 18 Lvl	Turf 31 Lvl
Failed pillars (Class 3)	12	6	2	1	2	0	1
Presumed failed pillars (Class 4)	75	22	0	0	31	7	17
w:h ≤ 2	12	0	1	0	7	3	1
w:h 2 - 3	**43**	**26**	1	1	**8**	3	4
w:h ≥ 3	**32**	2	0	0	**16**	1	**13**

Table 2.4: Summary detailing failed pillar sites and pillar dimensions (data from PlatMine report after Watson et al, 2007).

	Depth (m below surface)	Pillar length (m)	Pillar width (m)	Stoping width (m)	True w:h	(w:h)eff
RPM (Amandelbult)	650	6	4	1.4	2.9	2.7
RPM (Amandelbult)	650	6	3	1.4	2.1	2.2
RPM (Amandelbult)	650	4.2	3.6	1.4	2.4	2.1
RPM (Amandelbult)	650	4	4	1.4	2.9	2.2
RPM (Amandelbult)	650	4	3	1.4	2.1	1.9
RPM (Amandelbult)	650	10	4.6	1.4	3.3	3.5
Impala 4#	160	4	3.8	1.5	2.5	2
Impala 4#	160	5	3	1.5	2	1.9
Impala 8#	320	9	3	1.2	2.5	1.9
Impala 10#	890	6	5	1.2	4.2	4.5
Impala 10#	890	7	6	1.2	5	5.4
RPM (Turfontein)	1350	26	5	0.9	5.6	6.9

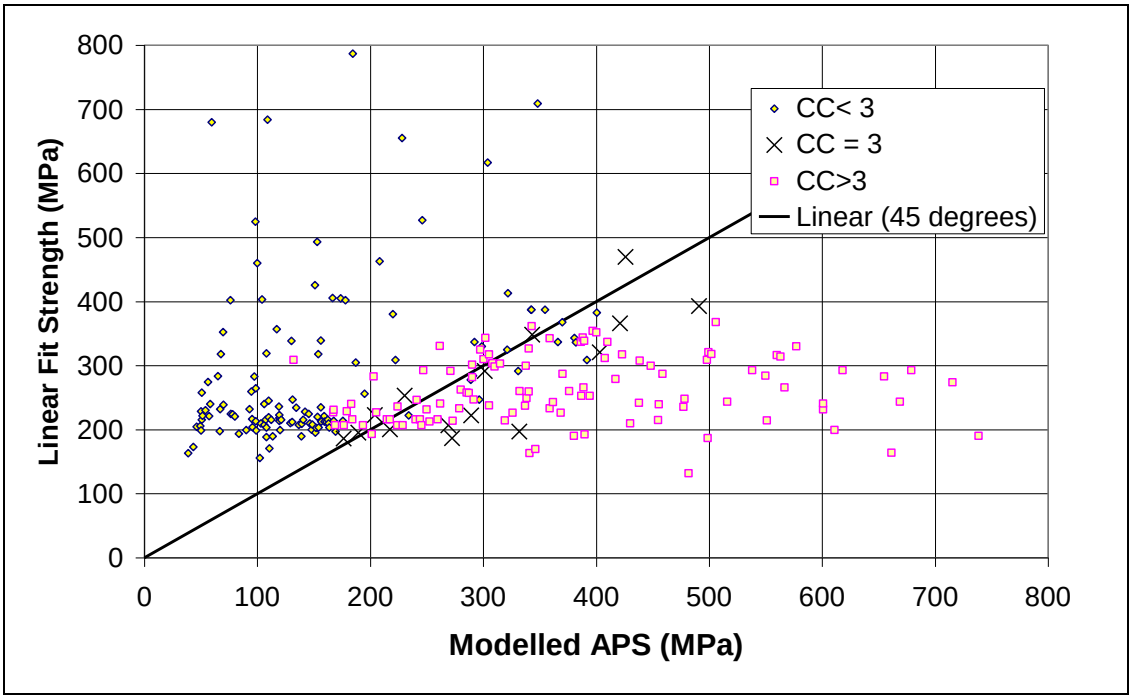

Figure 2.6: Back fit strengths for the entire database, using the linear pillar strength formula (after Watson et al, 2007). CC refers to "condition code" 0 (pillar with no visible damage) to 5 (pillar heavily damaged).

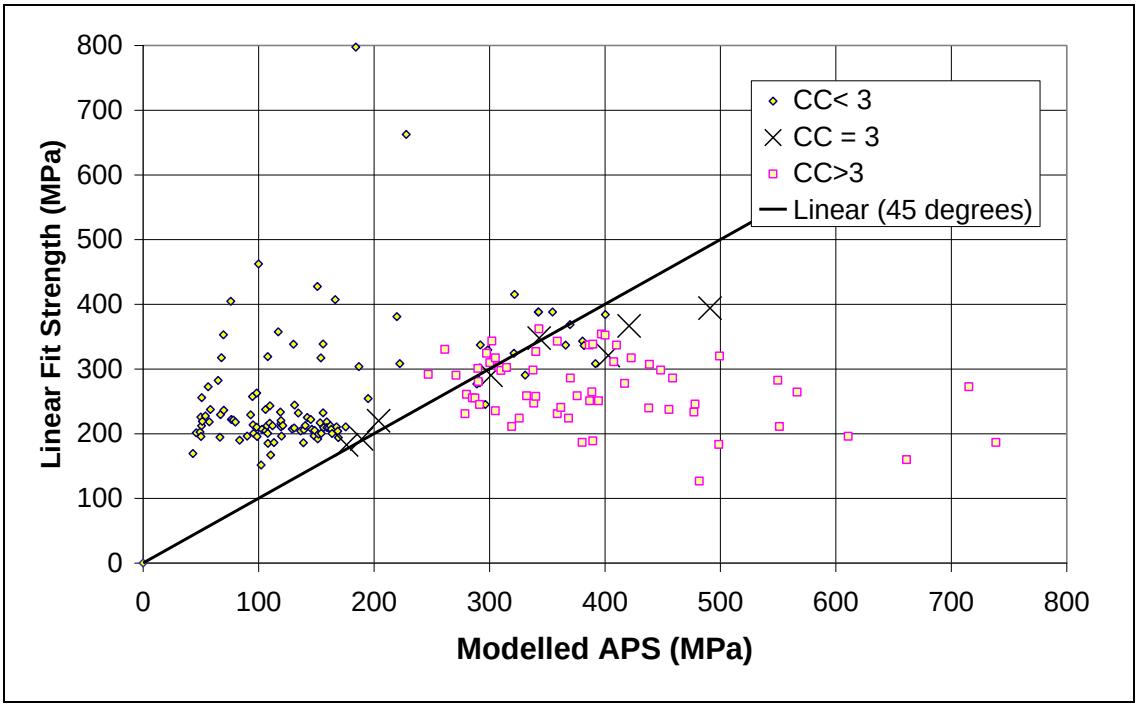

Figure 2.7: Back fit strengths for the Impala Platinum pillars only, using the linear pillar strength formula (after Watson et al, 2007). CC refers to "condition code" 0 (pillar with no visible damage) to 5 (pillar heavily damaged).

2.2. Monitoring of crush pillar behaviour

The mechanisms driving pillar failure is complex as various factors in different environments influence pillar behaviour. To quantify all these parameters for design purposes can be costly. It is, however, necessary to understand the rock mass response and pillar behaviour as accurately as possible, as generalised behavioural assumptions might not be valid for all cases.

This section will give an overview of the historic insights obtained from instrumented Merensky crush pillar sites. Most of this previous research was conducted in an attempt to understand the behaviour of crush pillars using actual measurements. The results of both crush and yield pillars are included in this assessment.

2.2.1. Behaviour of a 2:1 crush pillar

The measured and observed behaviour of a 2:1 Merensky crush pillar is shown in Figure 2.8 and Table 2.5. Based on stress measurements Roberts et al (2005b) determined that a crush pillar reaches its peak strength at between 3 – 10 millistrain, then fails following a further compression of approximately 5 millistrain along an estimated negative post-peak stiffness slope of 12 GN / m. Following further compression to the extent of 50 – 90 millistrain, it is assumed that footwall heave occurs as a result of the lateral confinement of the foundation. At this point it is assumed that the yielding or crushing of the foundation restricts the pillar's loading capacity as the pillar is reliant on the foundations, which is the limiting load bearing component. Further compression could result in an increase in the contact friction angle. This could results in strain hardening behaviour with the slope of the stress-strain curve becoming positive. This is assumed to occur when the vertical strain is > 0.4.

Of significance is the high residual crush pillar strength of 13 - 25 MPa (Table 2.5). The fact that failed pillars with a relatively small width to height ratio (2:1) do maintain such large residual strength is not always appreciated. The function of crush pillars is to support the tensile zone between regional support or to provide support up to any potential separation plane in the hangingwall. It would not have been able to fulfil this function if it did not maintain these large residual strength values. The value of the peak pillar strength is unknown. The values quoted in Table 2.5 are based on estimates as described by Ryder and Ozbay (1990).

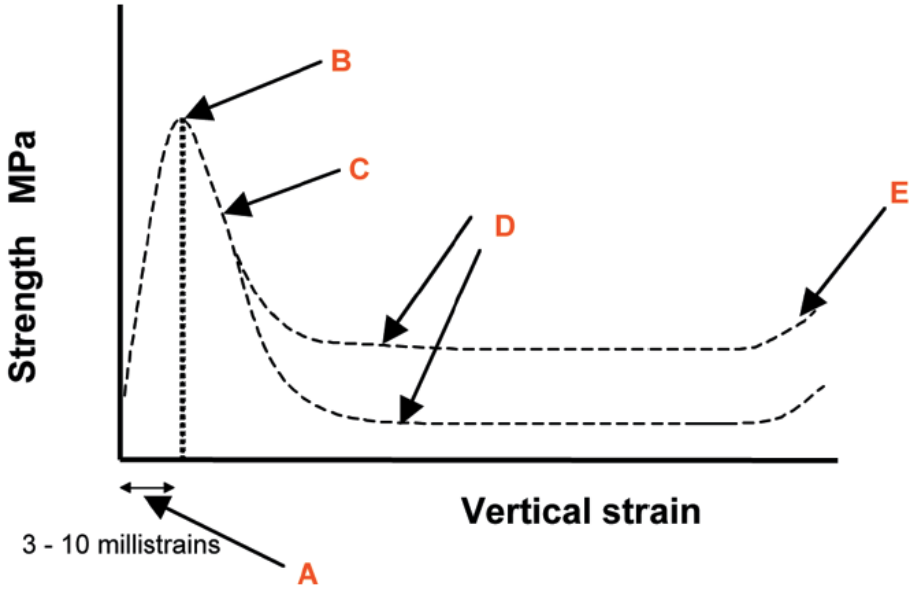

Figure 2.8: Stress-strain curve of a 2:1 crush pillar (after Roberts et al, 2005b).

Table 2.5: Estimated behaviour of a crush pillar with a w:h ratio of 2:1 (after Roberts et al, 2005b).

Position	Behaviour	Value	Unit
A	Stope convergence	3 - 10	Millistrain
B	Peak strength	75 - 150	MPa
C	Post failure slope	12	GN / m
D	Residual pillar strength	13 -25	MPa
E	Strain hardening	50 - 90	Millistrain

2.2.2. Behaviour of yielding pillars

Lougher (1994) conducted experimental work in an attempt to understand the complete load-deformation characteristics of the Impala Merensky yield pillars. At the time of the study, Impala was already using yield pillars for a period of approximately 20 years. Owing to the inconsistent failure mode of the pillars, which was ascribed to the variation in rock mass or reef type properties, pillar cutting discipline and jointing, several researchers (Dunham 1976, Lear 1980, Spencer and Kotze 1980, Spencer 1993) attempted to understand and predict the actual behaviour of the yield pillars. Although the general behaviour of the pillars was described as being stable, pillar bursts and pillar punching did occur in the back areas. The general pillar design on Impala consisted of a grid of 5 m x 5 m in-panel pillars laid out between dip regional pillars, which limited the mining span and controlled the regional rock mass behaviour (stiffness).

The instrumented pillars dimensions were:

- Site 1: 4 m x 5.5 m. The pillar dimension was reduced to 3.2 m x 5.5 m (w:h = 3.2),
- Site 2: 2.4 m x 8.3 m (w:h = 2.4)
- Nominal size of pillars in instrumented area: 3 m x 6 m.

From the measured pillar stress and rock mass convergence, it was determined that the stress change was small up to a convergence of 2 mm, followed by an almost linear increase in stress to a peak of 95.3 MPa (refer to Figure 2.9). The measured convergence of 9 mm agreed well with the back analysed MINSIM-D results for the areas where the behaviour was elastic (no footwall heave). *Note:* The convergence measured was approximately 4 m away from the pillar in the adjacent mined-out panel (to prevent the impact of footwall heave on the measurement). It therefore did not account for the initial convergence experienced when this adjacent panel was being mined. The slope of the curve implies a pillar modulus of 14.8 GPa. This might, however, not be the actual pillar modulus as the measured convergence was much higher than the vertical displacements experienced by the pillar.

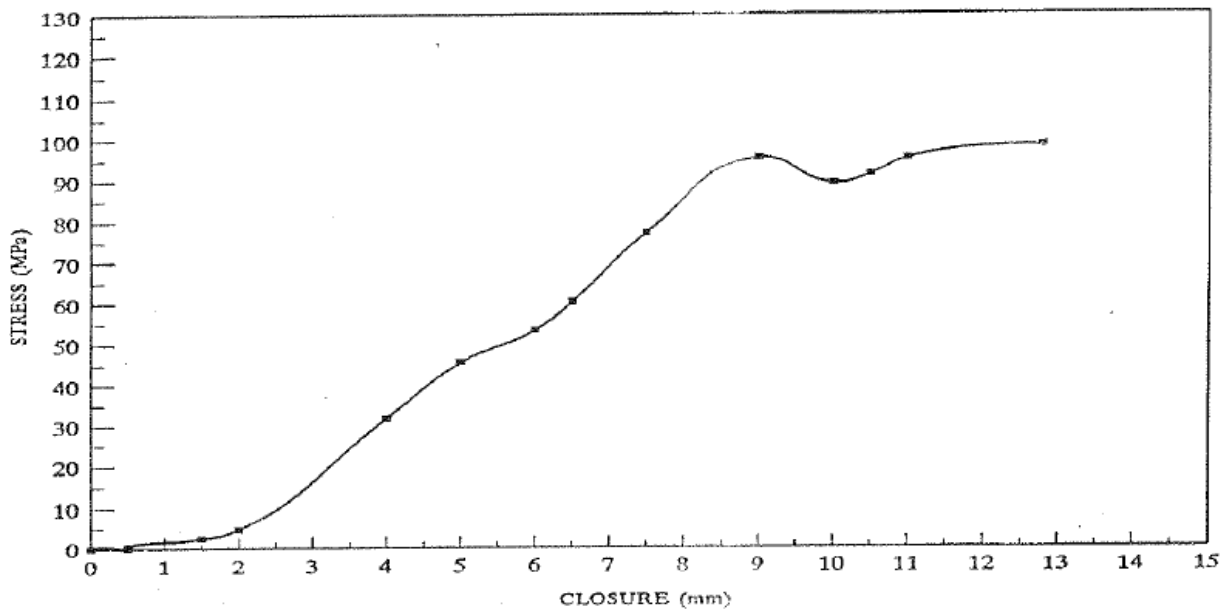

Figure 2.9: *In-situ* stress-convergence measurement results (after Lougher, 1994).

Petroscope observations determined that intense slabbing occurs at the pillar edge, which does not propagate deeper into the pillar as the pillar stress increases, suggesting the pillar core is intact even at a distance of 30 m behind the mining face. Furthermore, the hangingwall remained stable with most of the failure observed as footwall heave. This also agreed well with the observed behaviour of a 3 m x 6 m pillar cut at

1000 m below surface at another site where intense fracturing was observed around the pillar although the core was still intact (failure is reported as a pillar burst or foundation failure).

For the pillar evaluated, the pre-peak modulus and peak stress values were estimated to be 68 GPa (MINSIM-D back analyses) and 206 MPa (from measurements) respectively. The *in-situ* stress change of 95 MPa was adjusted to account for the initial state of stress at the time the instruments were installed (111 MPa), the abutment stress as determined by MINSIM-D resulting in the peak value of 206 MPa. The far off-reef field displacements were best approximated by using a pillar moduli of 68 MPa, which also compared well with the measured and modelled convergence and stress values.

From the study conducted, the post-peak pillar behaviour was described as yielding without shedding load (plastic). The behavioural mechanism was attributed to pillar punching into the footwall.

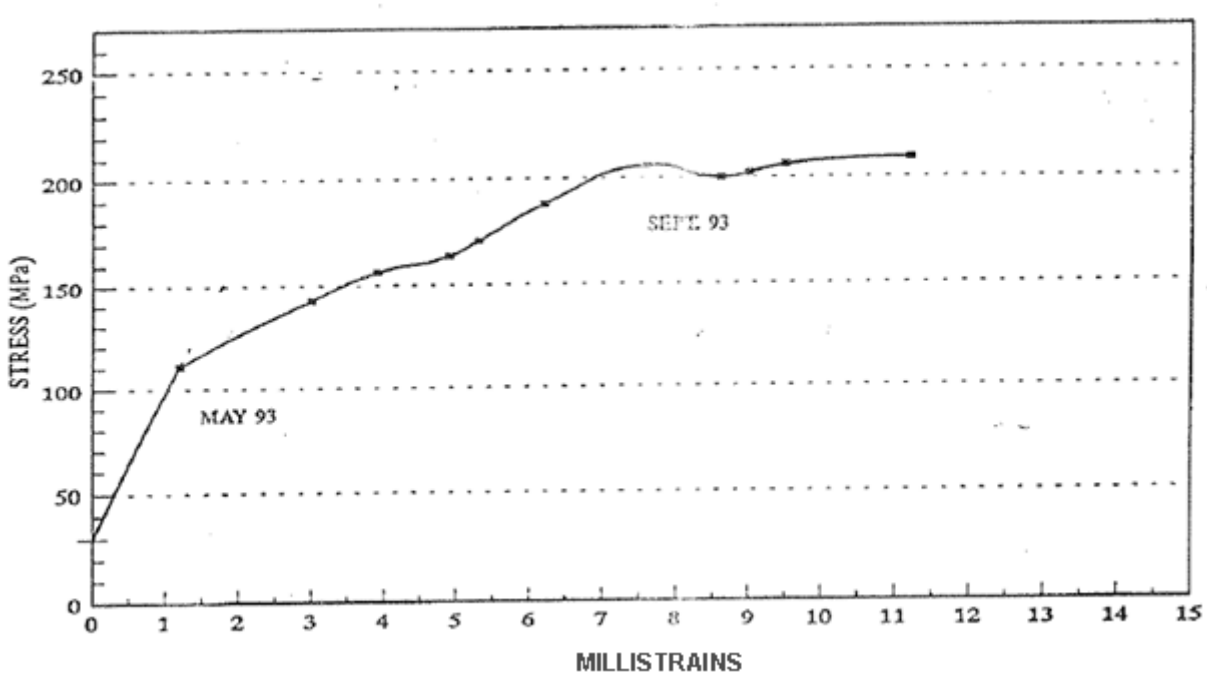

Figure 2.10: *In-situ* pillar stress-strain behaviour (strain from convergence measurements, Lougher 1994).

Piper et al (2005) conducted an extensive monitoring program on the performance of the Impala yielding pillars. The monitored grid pillars had w:h ratios ranging between 0.9 – 2.6, stoping width of approximately 2 m and were positioned within a limited span (60 m x 120 m) between large dip and strike pillars which influenced the overall rock mass behaviour (extraction ratio ≈ 77%). The results illustrated that a pillar with a width of 2.3 m (w:h = 1.3) was not completely fractured, even 50 m from the face. Pillars less

than 3 m wide (w:h = 1.7) still had an unfractured core width of 1.5 m. It was determined that the pillar width will have to be less than 2 m (w:h = 1.1) in order to be completely fractured for this particular layout.

From convergence measurements it was established that the rate of convergence was only slightly higher at the face than in the back area (30 m from face) and therefore it appeared as if the pillars were not yielding. The average convergence rate was 0.38 mm / m of face advance suggesting that the average convergence would be 38 mm / 100 m face advance (approximately 2 millistrains). The maximum measured convergence was 33 mm (0.87 mm / m) and the minimum 3 mm (0.07 mm / m).

From the various results it was concluded that either the full overburden load was not transferred to the pillars due to the limited span or the hangingwall strata was very stiff and therefore the load was primarily carried by the regional pillars.

2.2.3. Effect of pillar fracturing as an indicator of pillar performance and associated pillar behaviour

Canbulat et al (2006) conducted an extensive assessment of the rock mass conditions and monitored the behaviour of crush pillars using closure-ride stations, extensometers, borehole camera surveys, geological and geotechnical mapping and seismic monitoring at sites where crush pillar mining was conducted. Some of these sites included Merensky pillars.

To assess the behaviour of different crush pillars under different mining and geotechnical conditions, the fracturing of pillars, expressed as a pillar fracturing index (PFI) was determined as a quantitative indication of the pillar condition. UDEC modelling was used to investigate the behaviour of a crush pillar. The PFI measurements allowed for a comparison with the numerical analyses. Grodner and Canbulat (2005) developed the concept of determining an index correlating pillar fracturing based on the underground monitoring to pillar behaviour (type).

The PFI ranges (%) were determined to be:

- Rigid pillars: PFI > 90
- Yield pillars: PFI 45 – 90
- Crush pillars: PFI < 45

PFI is simply an adaption of the Rock Quality Designation (RQD) where PFI is determined by borehole camera observations in a drill hole. As a drill hole is used for the assessment, the effect of time can be determined by repeat measurements. PFI is determined from:

$$PFI = \frac{\Sigma(lenghts\ of\ hole\ with\ fractures > 10cm\ apart)}{Total\ length\ of\ hole} \times 100 \qquad (2.13)$$

PFI takes account of possible factors which impact on pillar behaviour as it is merely a measure of the rock mass response and not an attempt to quantify individual components. It allows for the comparison of different sites by quantifying the fracture pattern within any pillar.

It was found that all crush pillars had PFI's of less than 45. The PFI range was determined and verified to be similar in different mines and on different reefs where the age of the pillars were similar. Pillars which initially had a PFI of a yield pillar would drop to the PFI of a crush pillar after several weeks. Poorly cut pillars can therefore be presumed to act as crush pillars over time.

PFI has been established as a useful indicator and can be used for:

- With time the PFI of a pillar degrades and therefore it is anticipated that the PFI can be used as an estimate of where a pillar is within the pillar's stress-strain state.
- The rate of change in PFI reduces over time. Crush and yield pillars might reduce to similar PFI values at various positions from the face (estimated at more than 60 m). The time period over which this value is reached will, however, vary.
- The rate of change in PFI might also be an indicator of the rate of change in convergence in different geotechnical areas. This indicator can be useful to design pillars for different reef types.

The Merensky pillar sites instrumented included crush pillars (Mine A and D) and yield pillars (Mine B) of which the spacing of the regional pillars varied between 60 m and 120 m. Table 2.6 details the pillar dimensions and w:h ratio of the pillars at the various sites.

Table 2.6: Pillar parameters at Merensky monitoring sites (after Canbulat et al, 2006).

		Mining depth (m below surface)	Panel span (m)	Pillar length (m)	Pillar width (m)	Stope width (m)	w:h ratio
Mine A	Site 1	1030	30	7.5	2	1	2.00
Mine B	Site 1	1100	30	10	3	1.4	2.14
	Site 2	1306	28	stub	3.5	1.8	1.94
	Site 3	1200	30	15	4.5	1.9	2.37
	Site 4	1240	32	stub	3	1.7	1.76
Mine D	Various						

With regular blasting, time dependent convergence rates at the crush pillar site **(Mine A)** at a distance of 15 m - 20 m from the face was found to be approximately 2 mm / day, Malan et al (2005). The steady-state convergence rates were estimated to vary between 2.2 mm / day and 0.14 mm / day.

At the site at **Mine B** using yield pillars, a total convergence of 23 mm was measured during the instrumentation period. The steady-state convergence was approximately 0.65 mm / day. The pillar dilation, which was measured with extensometers anchored at the centre of the pillar, indicated a maximum pillar dilation of 54 mm. This corresponded well with the measured collar movement of 46 mm. It was found that the PFI showed a decrease in rate of change as mining moved away from the pillar. The rate of change in PFI might therefore be an indicator of how the pillar is behaving. The dilation appears to be controlled by the amount of fractures as the change in dilation compared well with the change in PFI. It was concluded that pillar dilation is equal to approximately twice the convergence at a specific site.

At **Mine D,** areas with poor ground conditions were investigated in an attempt to relate crush pillar and rock mass behaviour to the critical parameters governing the overall pillar system behaviour. It was found that in areas where no sidings were cut, pillar sidewalls were failing much later and only when the gullies were cleaned at the end of stoping. It was found that sidewall slabbing in this instance was more dependent on the mining phase (gully cleaning) than geotechnical conditions. In the areas where poor ground conditions were experienced, it appeared that the major contributors were larger pillars or increased spans. If pillar failure occurs, it is focussed on the weakest portion of the system and therefore poorly mined pillars could result in pillar, hanging or footwall failure.

From the underground studies the following conclusions were made:

- There is no correlation found between the micro-seismicity of a crushing pillar and larger distant events.
- Crush pillars are not completely formed ahead of the face as pillar fracturing continues several metres behind the face. This was also confirmed by seismic monitoring, detailed mapping, monitoring and results from the PFI.
- The orientation and position of mining induced fractures (MIF) forms parallel to the long axis of the pillar with the density increasing as the pillar moves further away the intact reef. Additional MIF forms parallel to the free face as the pillar faces are developed.
- Where low cohesive contacts are present at the reef contacts, the pillar fails by axial splitting rather than regular hour-glassing (similar to a sample compressed uniaxially with frictionless platens).
- If a weak hangingwall is present, fallout can change the w:h ratio of the pillar, affecting the performance of the pillar.

- Weak footwall can result in gully sidewall failure. This could mobilise the pillar fractures and cause increased dilation of the fractures.

Preliminary MINSIM modelling was conducted in an attempt to better understand the crush pillar behaviour under different loading conditions by estimating the changes in pillar loading after being cut in the face and as it moves into the back area. MINSIM does not take inelastic behaviour into account and therefore the pillar stress increases steadily as the distance to the face increases.

To overcome the limitations of a linear elastic model, UDEC was used to determine the following:

- Can fractures in a pillar heal with time?
- Can the core of a crush pillar fracture?

Findings were that both of these situations are possible given the correct set of circumstances. During the life cycle of a pillar, fractures form, open, and at a later stage is forced closed again due to the dilation of either existing or new fractures forming. Pillar fracturing, although initiated at the pillar edges, can propagate through the core of the pillar. The pillar-system comprising of hanging, footwall and reef often has an overriding effect on the pillar condition. Rock mass parameters, as well as discontinuities, influence the way in which a pillar behaves.

2.2.4. Measured and assessed rock behaviour of the Bushveld Merensky Reef

A comprehensive research program was conducted by the CSIR in conjunction with PlatMine (Watson, 2010). Measurement and analysis was carried out on instrumented underground pillars in three mines along the Western Limb of the Bushveld Complex. This work was conducted to obtain an improved understanding of the behaviour of “crush type” pillars on the Merensky Reef horizon. The work consisted of extensive underground field measurements and observations of the rock mass and pillars as mining continued at depths ranging between 600 m and 1400 m below surface. The results of the *in-situ* measurements were compared to the behaviour of laboratory rock specimens. Numerical models (FLAC and MINSIM) were used to simulate the various behaviours (Watson, 2010).

Watson et al (2007) concluded that the linear formula, (after Bieniawski and van Heerden, 1975) provided a slightly better approximation of the peak pillar strength than the power formula. Some anomalies were found when comparing measured to calculated peak pillar strengths, but these were attributed to the difference in foundation rock.

Watson’s Merensky formula parameters are based only on the data collected at Impala Mine as it provided a lower standard deviation and improved correlation to failed versus unfailed cases compared to the entire Merensky database. Approximately 40% of the calculated results compared well with the actual measured

results, although pillar dimensions were adjusted during the calculations to find a best fit correlation (variations of pillar width, height, effective width and effective height).

The derived parameters are therefore only applicable to areas with similar geotechnical conditions as Impala Mine and for pillars with a width to height ratio greater than 3 (yielding pillars). Table 2.7 compares the measured versus calculated peak and residual pillar strengths. However, in all instances, the measured pillar stresses were significantly adjusted (upward) to be comparable to the back analysed elastic numerical modelling results. The peak pillar strength formula was derived based on elastic modelling results for unfailed pillars on Impala. Similarly, the residual pillar strengths were estimated based on the results of an analytical solution (equation 2.14) derived by Salamon (1992). The adjusted results are displayed in Figures 2.12 – 2.14.

Table 2.7: Comparison of measured versus calculated pillar peak strength using the linear formula (after Watson, 2010).

Site	Pillar no.	Peak strength (MPa) measured	Linear formula peak strength (MPa)	Accuracy of formula as a percentage (%)	Residual strength (MPa) measured	w:h (actual)
Amandelbult	P1	320	215	67	20	2.3
Amandelbult	P2a	276	213	77	14	2.7
Amandelbult	P2b	265	213	80	17	2.7
Impala	P1	295	290	98	32	4.7
Impala	P2a	320	288	90	32	2.9
Impala	P2b	327	288	88	32	2.9
Impala	P3	263	260	99	28	2.1
Impala	S1	353	363	103	33	6.7
Union	P1	191	207	108	16	2.0

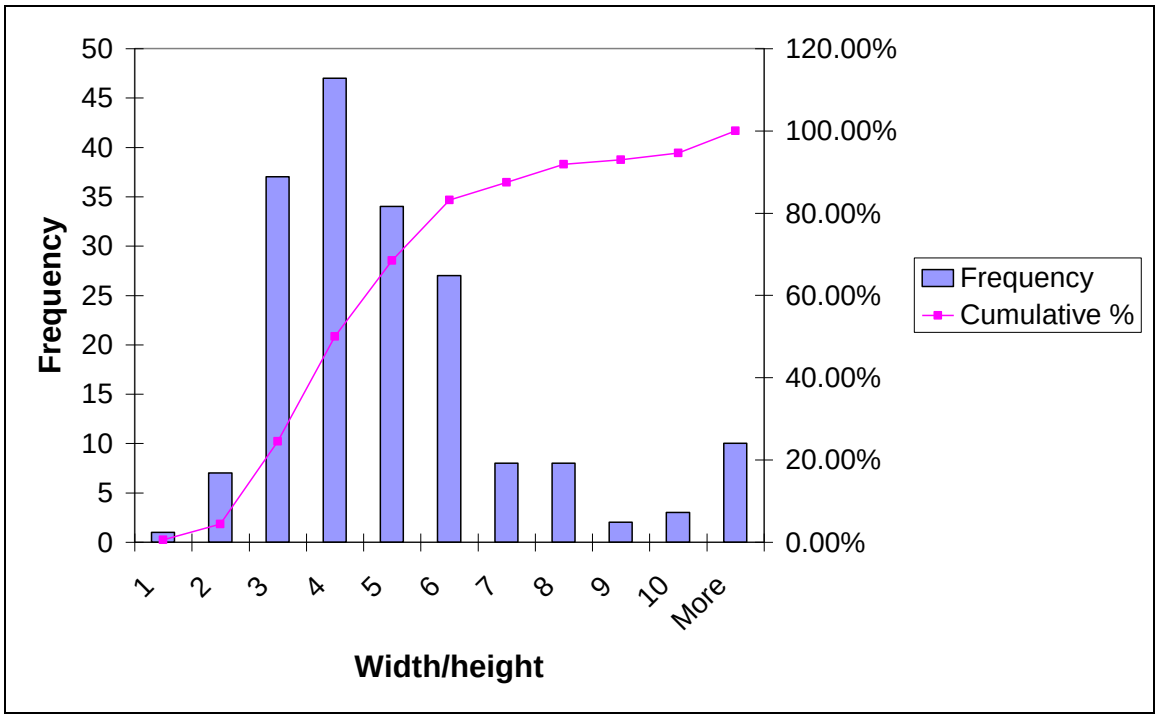

Figure 2.11: Distribution of pillar w:h ratios in the Merensky database (the formula parameters were derived based on the findings of Watson, 2010).

Seven pillars were monitored at three instrumentation sites where stress changes were recorded with strain cells installed in the hangingwall above the pillars. MINSIM models and Boussinesq equations were used to back analyse the measured pillar behaviour, as well as to validate the peak and residual strengths measured at the underground sites. The peak pillar strength was checked against the proposed linear equation. Rough estimates of pillar performance profiles were created from an adjusted best fit solution. Assumptions were made to overcome the effects which discontinuities could have had on the measurements. Furthermore, adjustments were also made to account for the influence of the advance strike gully (ASG) on the width to height of some pillars.

At the Amandelbult site, two pillars were monitored at approximately 600 m below surface. The results indicated a relatively rapid drop in stress after failure, followed by a relatively large stress regeneration. This is assumed to be linked to the effect of the confinement added by the broken rock in the gully. The effect of the strong footwall might have contributed to the high pillar loads as minimal damage was observed on the pillars foundations.

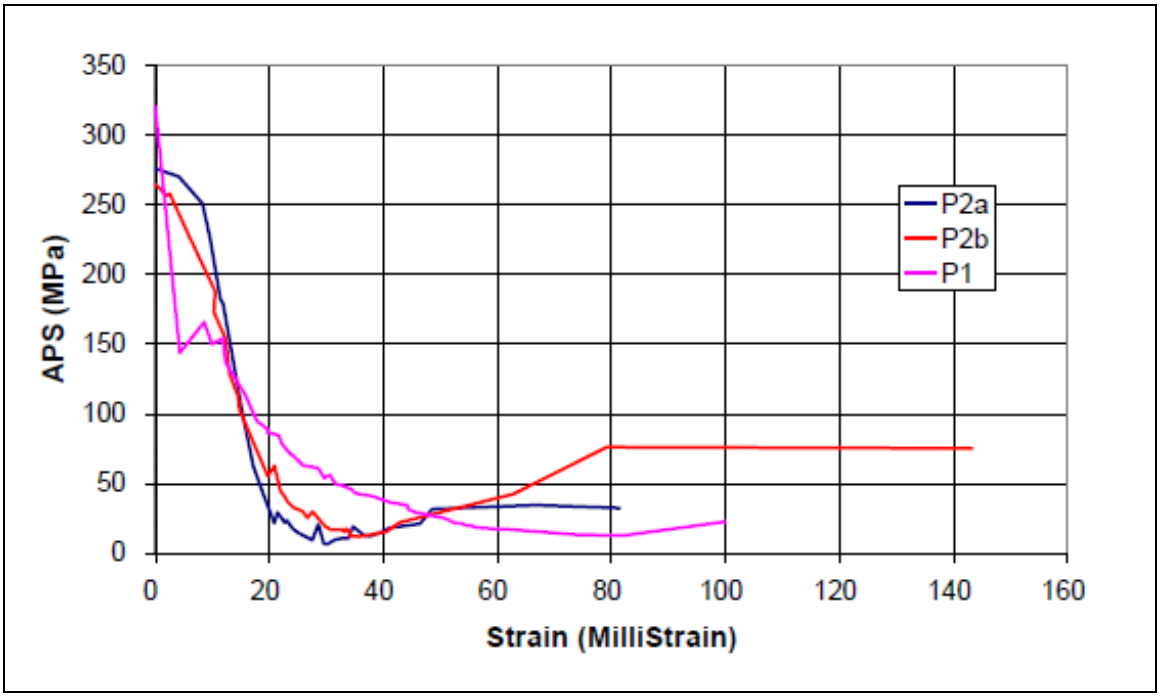

Figure 2.12: Stress-strain curve for the Amandelbult pillars (after Watson, 2010).

At the Impala site, three yield and one stability pillar (8 m wide) was instrumented at approximately 1100 m below surface. In contrast to the behaviour of the Amandelbult pillars, no further stress reduction or stress regeneration was observed once the residual strength of the pillar was reached, even though the final convergence measurements were similar. Monitoring continued for several months after mining was completed. From the measurements it was concluded that there were no difference in the residual strengths of the crush and stability pillar indicating that the fractured foundations had reached their maximum loading capacity.

Although the smallest crush pillar was approximately the same size as the Amandelbult pillars, the residual strength was almost double. Another interesting finding was that the strains measured were significantly less than the convergence indicating that the strata was potentially behaving inelastic (bending over pillars). The post-peak (strain softening) behaviour of all the instrumented pillars was very similar, even though the pillars were of a different size.

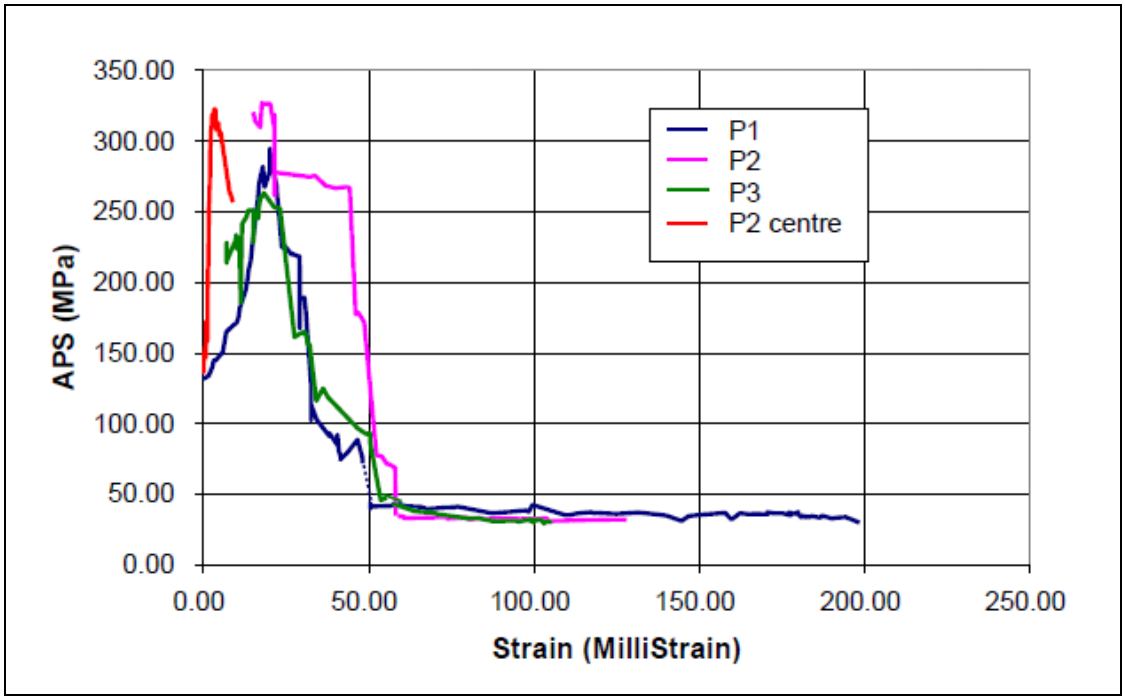

Figure 2.13: Stress-strain curve for the Impala pillars (after Watson, 2010).

At the Union site, a pillar was cut in the middle of a panel at approximately 1400 m below surface, away from the influence of any other abutments (isolated). The pillar, however, failed prematurely and the peak stress estimated with the aid of a numerical model. The post-peak behaviour of the pillar was similar to the Amandelbult pillars.

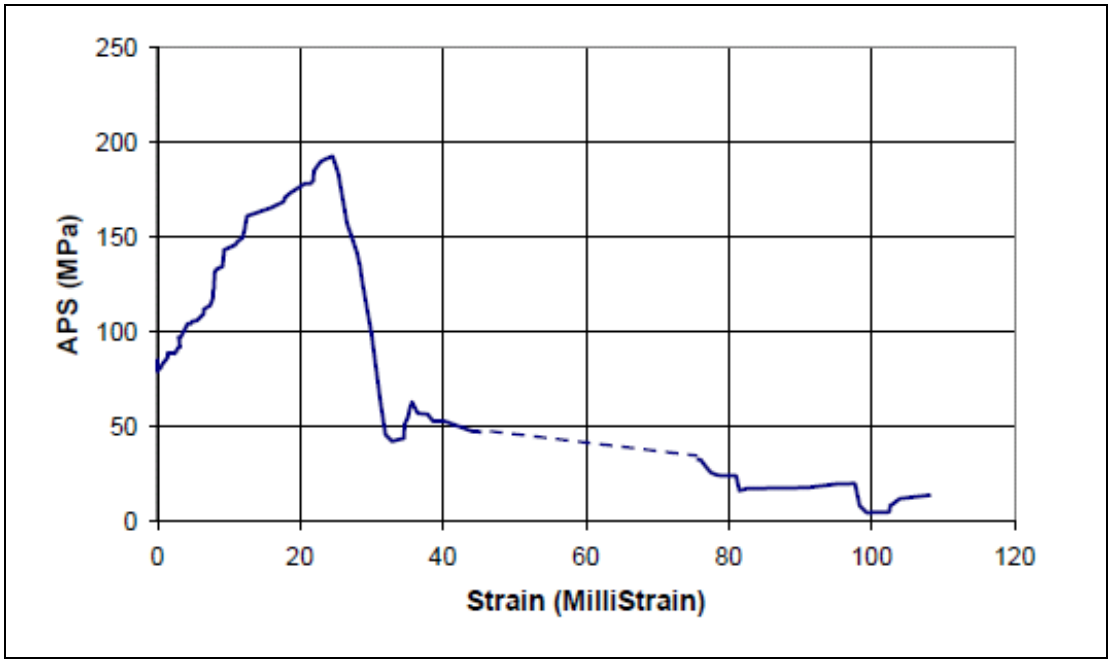

Figure 2.14: Stress-strain curve for the Union pillar (after Watson, 2010).

Two dimensional FLAC models were used to verify the peak pillar strength formula. The results were compared to the underground measurements as well as laboratory testing conducted by Spencer and York (1999). The results compared well with the Impala measurements (w:h > 3). Although non-linear behaviour of rock specimens were identified in the laboratory, non-linear behaviour of the rock did not appear to have affected the pillar behaviour observed underground. The results from the extensometer monitoring indicated that prior to pillar failure, the behaviour of the hanging-and footwall above and below the pillar were elastic with elastic constants similar to the laboratory values. The models indicated that the yield capacity of the pillar foundations were exceeded at a w:h ratio of approximately 3.

The models showed good agreement with the underground residual stress measurements for the lower width to height ratio pillars (w:h < 3) when high contact friction angles (40 degrees) were assumed in the model.

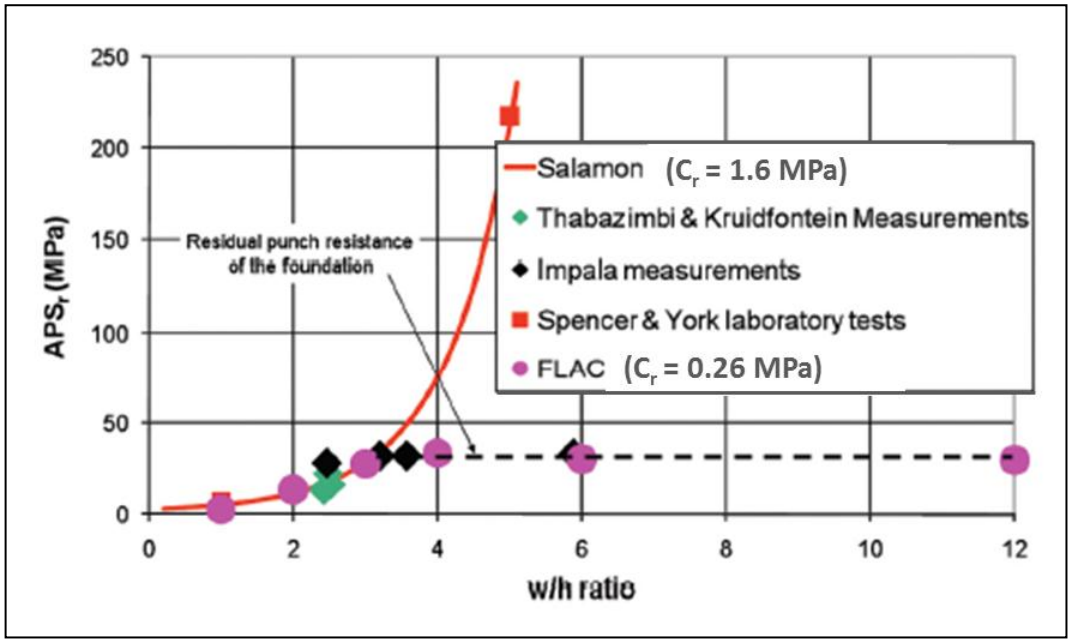

Figure 2.15: The strengthening effect of pillar w:h ratio on residual APS (after Watson, 2010).

Watson (2010) identified three mechanisms during pillar failure:

- **Fracturing and crushing of the pillar** (note that footwall and hangingwall fracturing is not synonymous with foundation failure),
- **Wedge formation:** This occurs in the form of shear fractures which affect the punch resistance,
- **Punching:** This is accommodated by the formation of Prandtl wedge failure, which would add to the inelastic closure observed in the panel.

The FLAC modelling indicated that punching could initiate at width to height ratios of 1.2 for ductile material. For brittle materials, larger width to height ratios would be required. At low width to height ratios, pillars were prone to crushing and at larger ratios, the hanging-and footwall were susceptible to failure. The elastic model indicated that the horizontal stress change measured at the various sites was due to the formation of additional compressive stress orientated perpendicular to the pillars which result in vertical fracture development and dilation above the pillars.

At most sites, the measured inelastic convergence was as a result of inelastic deformation of the footwall. The final pillar residual strength appeared to be controlled by the fracturing of the footwall. The effect of pillar scaling on pillar width to height ratio was confirmed by the observed versus measured pillar behaviour.

The post-peak strain softening behaviour of all the pillars were similar as the initial unloading portion of the curves suggested that little inelastic strain occurs. The convergence measurements appear to provide reasonable estimates of the pillar behaviour in the strain softening period. The pillars at the Impala site had a slightly different post-peak behaviour and were attributed to the presence of a persistent shallow dipping discontinuity in the footwall (≈ 1 m in the footwall).

From the site investigations it appeared that the footwall foundations were much more fractured and damaged than the hangingwall foundations with persistent footwall punching observed. It was found that foundation damage could have a serious impact on pillar peak strength and will possibly also affect the residual pillar strength. The Impala measurements further suggested that at higher width to height ratios, the pillar residual strength reaches a sustained peak value. This could imply that the bearing capacity of the footwall foundation limits the pillar performance once it is exceeded; there is little strength increase above a pillar width to height ratio of 3.2.

Salamon (1992) indicated that a cohesion (post failure) of approximately 1.6 MPa is required to simulate the magnitude of the measured residual strengths of coal pillars. Various values were assumed by Watson (2010) for the residual cohesion (0.011 MPa, 1.1 MPa, 0.4 MPa, 0.26 MPa) and an internal angle of friction (30˚, 40˚) for the Merensky pillars to simulate the measured behaviour of the pillars. Indications are that Salamon's estimated parameter values provide the most appropriate fit for the analytical solution derived by Salamon (equation 2.14) which is based on a limit equilibrium material loaded between two platens. This result compared well with laboratory punch tests allowing for foundation damage, performed on Impala Merensky specimens (Spencer and York, 1999). The application of the limit equilibrium model cannot, however, model foundation failure. Furthermore the underground data is limited to a small range of width to height ratios and difficult to compare accurately (Figure 2.16).

$$APS_P = \frac{2h \times 0.8 \cdot \left(\frac{C_r}{0.5}\right)}{2.5w} \cdot \left[e^{2.5\left(\frac{w}{2h}\right)} - 1 \right] \quad (2.14)$$

With

APS_p = APS peak value

h = Half pillar height

w = Half pillar width

C_r = Residual cohesion

The effect of failed rock material against the edge of a pillar is difficult to quantify. The modelling results indicated high values of post failure cohesion which show that the broken material might possibly not have been completely crushed.

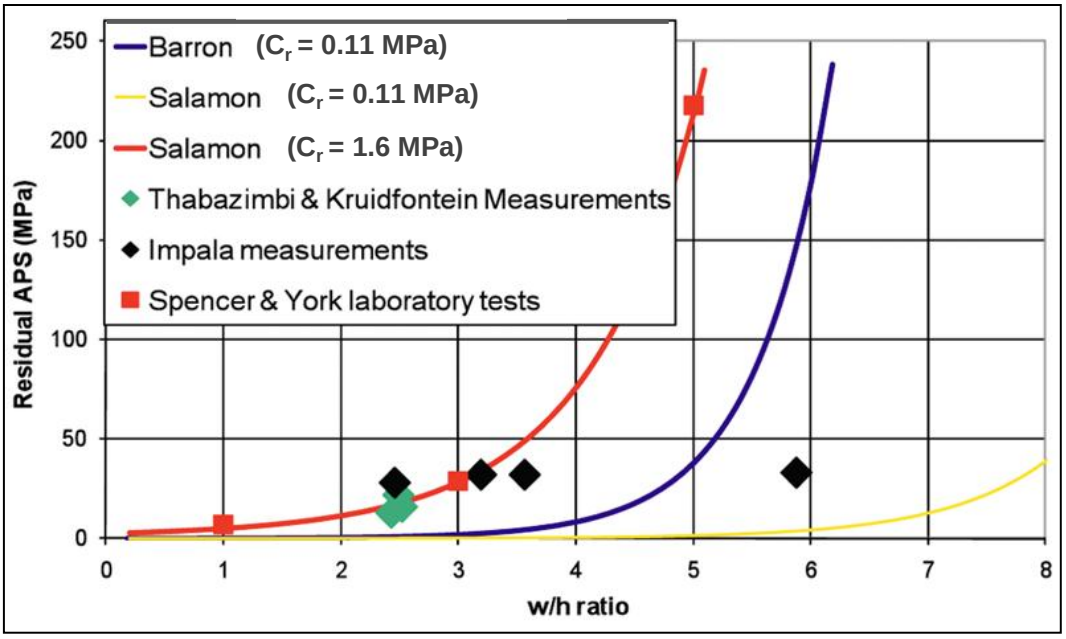

Figure 2.16: Pillar w:h strengthening effect on residual APS (after Watson, 2010).

Salamon's analytical solution provided a good estimate for the residual stress measurements of the Amandelbult and Union pillars (w:h < 3). The output of the solution is, however, controlled by the choice of input parameters (cohesion = 1.6 MPa; internal friction angle = 30 degrees). The results indicate an exponential increase in residual strength with increasing width to height ratio (w:h < 3.2).

Pillar bursts were investigated at Amandelbult (600 m below surface) which occurred approximately 10 m behind the face. These were assessed using elastic modelling to determine the loading conditions. A crush pillar system which is properly designed should allow pillar failure close to the face where the loading

environment (rock mass) is stiff. Softer loading conditions further from the face might result in violent failure. Evidence from the pillar bursts suggested that unfailed pillars located 10 m or more from the face are in a soft loading environment which could result in violent pillar bursting. A slope of the loading (5 mm / GN) was determined from the back analysis of the failed pillars. The instrumented pillars which did not burst, failed at a post failure loading stiffness of approximately 3.2 mm / GN.

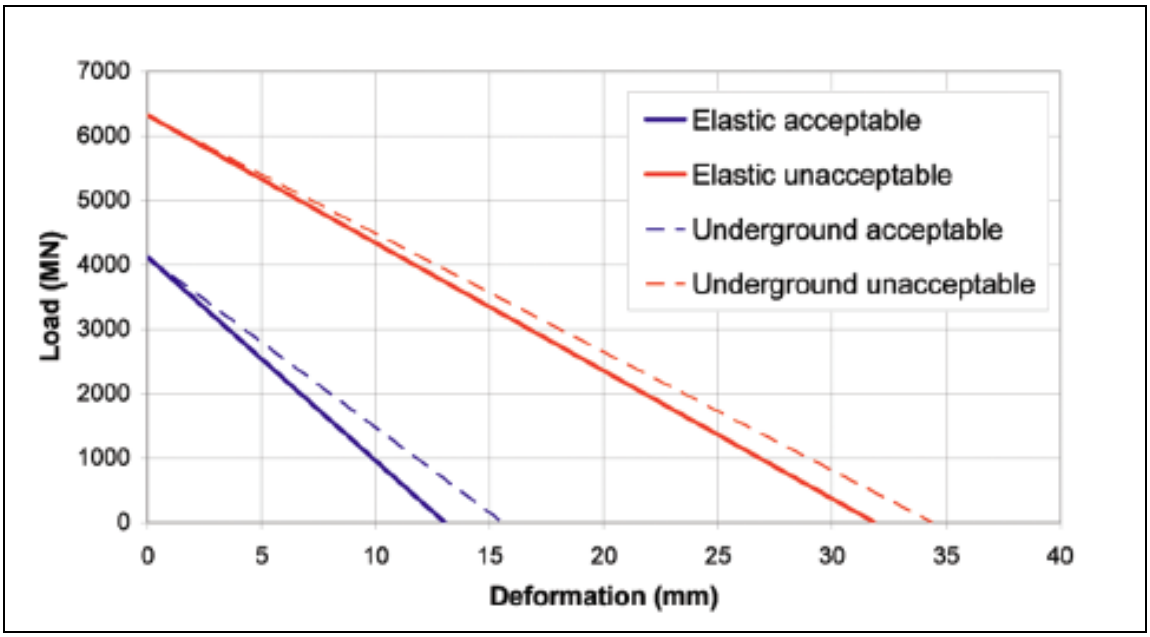

Figure 2.17: Effect of rock mass stiffness on crush pillar behaviour (after Watson, 2010).

From the various results, Watson (2010) established a correlation between peak and residual pillar strength and width to height ratio. It is hypothesised that pillars can be designed to fail close to the face in a sufficiently stiff loading environment by matching the pillar strength to the loading capacity of the strata close to the advancing face. At shallow depth it will be more difficult and it is anticipated that the layout will have to be modified to ensure effective pillar crushing, but with sufficient residual pillar strength to prevent backbreaks. Watson further suggested that if pillar widths have to be reduced, insufficient residual strength can be accounted for by reducing panel spans to ensure that the required residual strength is sufficient for the spans.

Watson proposed a design strategy whereby a crush pillar system can be designed by:

- Determining the pillar residual strength based on the support resistance requirement to the height of the most prominent parting,
- Apply a width to height ratio from a back analysed design chart to ensure that the residual strength is achieved (Figure 2.18),
- Calculate peak pillar strength from the proposed Merensky linear pillar formula,
- Determine the available pillar stress using an elastic model.

The pillar stress to strength ratio will determine if the pillars will fail at the face. Changes in panel span or preconditioning are proposed as methods to ensure crushing if the system does not behave as expected.

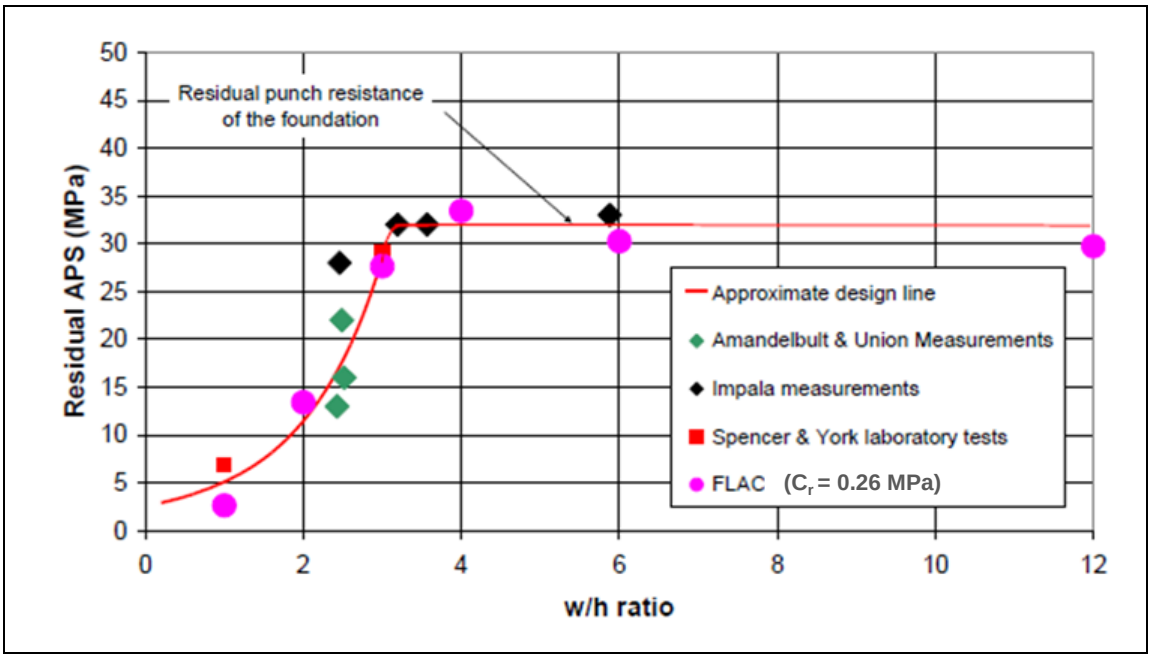

Figure 2.18: Pillar residual strength as a function of w:h ratio (after Watson, 2010).

2.3. Summary of current knowledge regarding crush pillars

This section provides a summary of the content outlined in this chapter. Design guidelines, parameters, and past learning provide benchmarks against which further research can be compared to. It also provides guidance with respect to further research requirements.

Crush pillar design is typically limited to a pillar width to height range between 1.5 and 2.5. The implementation of actual pillar layouts on mines have essentially developed from the adoption of pillar sizes from other mines and pillar sizes being adjusted over time to obtain the desired behaviour. As the function of crush pillars are to support the immediate hangingwall between pillar lines to the height of the highest unstable parting, a regional pillar system is required to support the overburden rock mass to surface and control the overall rock mass behaviour. Various factors such as depth of mining, stress regime, stability strategy (extraction ratio) can cause mine instability, whilst factors such as advance rate and volume of mining can affect the loading conditions.

From the findings of the earlier research it is clear that crush pillars are affected by the following parameters:

- Rock mass stiffness: Regional pillar size, spacing and layout vary in different mines. This affects the overall rock mass stiffness and the resulting crush pillar behaviour.
- Poor pillar cutting accounts for most of the variations in width to height ratio. This results in a deviation from the design requirements and affects the pillar performance. Approximately 30% of pillars are cut to the required width and 20% to the required length.
- The effect of stoping width, gullies, sidings and mining sequence affect the pillar performance as it impacts on pillar height and confinement.

Most of the Merensky crush-type pillars monitored in previous experimental sites had width to height ratios between 1.5 and 4.7. Various design criteria were formulated based on the behaviour of these pillars. Rectangular rib pillars typically display an increase in pillar strength of 1.4 times that of square pillars for the same width to height ratio. A strength increase of 1.1, 1.2 and 1.3 for pillar length to width ratios of 2, 3 and 4 respectively is typically assumed. The assumption that a crush pillar should provide a support resistance of 1 MPa across a stope was adopted based on instances where the parting, up to the height that needed to be supported, was in excess of 30 m above the reef. The actual instability height above a typical Merensky stope varies based on layout and geological location (i.e. parting height of 10 m – 40 m corresponds to a support resistance of 0.3 MPa – 1 MPa).

The behaviour of both crush and yield pillars studied, comprised of a large range of width to height ratios. By definition crush pillars (crush at face) or yield pillars (crush in back area) are classified as having w:h ratios of 1.5 – 2.5 and approximately 3 respectively.

The monitoring of instrumented crush pillars (w:h ≈ 2:1) illustrated that the peak pillar strength was obtained at between 3 – 10 millistrains and the residual strength at between 8 – 15 millistrains. This agreed well with modelling conducted, which indicated ranges of 8 – 12 millistrains and 14 – 20 millistrains for the peak and residual pillar strengths respectively. The pillar behaviour is very reliant on the stiffness of the strata. For controlled pillar crushing to occur, the stiffness of the strata must be greater than the stiffness of the pillar. The post-peak failure slope of a 2:1 Merensky crush pillar was estimated at approximately 12 GN / m. A study conducted on pillars that failed violently illustrated that uncrushed pillars, which are situated 10 m or more from the face, are in a soft loading environment. This can contribute to pillar bursting.

From rock mass monitoring, it was established that the convergence in a crush pillar panel is time dependent and predominantly associated with the blast (≈ 2.2 mm / day up to 30 m from face). Steady-state convergence was found to vary between 0.14 – 2.2 mm / day. Research on yield pillars indicated that in most cases pillars situated at between 30 – 60 m from the face were not crushing. These panels were subjected to approximately 2 millistrains of deformation at these locations (average convergence of 0.38 mm / m of advance). The major contributors to the pillar behaviour (not crushing) were attributed to the size of the yield pillars and the spacing of the regional pillars (stiff rock mass). In areas where the pillars were yielding, detailed fracture mapping and the interpretation of measured yield pillar performance ascribed the mode of failure to yielding foundations. It was also established that once the foundations were yielding, the pillars displayed no further increase in load. It was therefore a limiting factor to the load bearing capability of these crush type pillars.

Fracture mapping across various reef types and geotechnical domains revealed that similar pillar types (rigid, crush or yield pillars) behaved in a similar manner, even if the geotechnical and geological components were different. As a quantitative tool, a pillar fracture index (PFI) was defined which indicated that crush pillars have a fracture index of less than 45 whereas yield pillars had a fracture index of 45 – 90. The rate of change in PFI reduces over time and therefore crush and yield pillars might reduce to similar PFI values at various positions from the face (estimated at more than 60 m from the face).

The residual strength of an instrumented Merensky crush pillar (2:1 pillar) was determined to be 19 MPa, but could vary between 13 – 25 MPa. The damage to pillar foundations increases with an increase in friction angle over the contact area of a pillar. The pillar system is reliant on the behaviour of the hangingwall, footwall and reef material. High contact friction angles (i.e. 40 degrees) could induce punching. An increase in contact friction angle or width to height ratio could affect the post failure modulus of the pillar.

The peak strength of the pillars can be determined by applying either the linear or the power formula with the power formula taking volume into account (can be used for all ranges of specimen diameters). The linear formulae only accounts for the geometric effect of increasing width to height ratio (must be adjusted for

varying specimen diameters). If the volume effect is removed from the pillar system, it can be concluded that the linear formula performs almost as well as the power formula for low width to height ranges. The contact friction angle effectively determines the exponent of the power law equation. The exponent increases as the contact friction angle at the pillar interface increases. It was found that the contact friction angle of steel platens (laboratory test) is approximately 10 - 20 degrees for which the results appeared to follow a linear trend as a result of the low exponents of the power law relationship.

The findings of a more recent study, for which a Merensky pillar strength formula was derived, indicated that the linear equation appeared to have provided a slightly better performance compared to the power formula. The formula was, however, based only on a study of pillars at Impala Mine. Based on this assessment, the assumption that the linear formula provides a better estimate of the pillar strength is biased towards the Impala pillars and pillars with a width to height ratio greater than 2 (approximately 3). The Impala pillars are typically classified as yield pillars and are intended to only reach their post-peak state once the pillars are in the back area and not when cut on the face (crush pillars). The models showed good agreement with the underground residual stress measurements for the lower width to height ratio pillars (w:h < 3) when high contact friction angles (40 degrees) were assumed in the model. The results of an analytical solution provided a good estimate of the residual stress measurements indicating an exponential increase in residual strength with increasing width to height ratio (w:h < 3.2).

As pillar scaling is expected, it is recommended that a siding equal to at least 1 m is cut adjacent to the raises or gullies, positioned adjacent to the pillars. It was found that a 1 m siding (minimum practical dimension) will result in a pillar strength reduction of approximately 7%, whereas a siding in excess of 2 m has no impact on the strength of the pillar. A siding will reduce the risk of failed rock falling from the pillar sidewalls into the travelling ways. Alternatively, the pillars should be placed at the panel mid-spans where there will be no additional height effect. It was, however, also found that in some areas where no sidings were cut, pillar sidewalls were failing much later and only when the gullies were cleaned at the end of stoping. It was established that sidewall slabbing in this instance was more dependent on the mining phase (gully cleaning) than geotechnical conditions.

The following uncertainties are highlighted below as a guide to focus the research. This is based on the findings from the literature review. Furthermore, various impractical recommendations were presented by previous researchers.

Crush pillars are defined as slender in-stope pillars which attain the post-peak failure state whilst being cut at the face.

1. Various ***crush pillars have been instrumented*** in recent years with the behaviour of the pillars being ascribed as crush pillars although the pillars had ***w:h ratios > 2*** and as high as 4.7. In most cases, the pillars did not crush at the face, yet conclusions were drawn regarding the behaviour of the pillars based on stress measurements and parameters such as foundation failure. In most cases, these pillars should never have been classified as crush pillars. It is imperative that only the pillars which meet the criteria of crushing at the face and width to height ratio's less than 2.5 be investigated to determine their behaviour. A minimum pillar dimension (width and length) should be established to ensure crush pillars will crush in a stable manner at the face.

2. ***A minimum crush pillar width of 2 m is suggested*** to cater for factors such as out-of line mining (Ryder and Jager, 2002). Roberts et al (2002) suggested, based on numerical modelling, a pillar length to width ratio of at least 2, but preferably 3 be applied. This corresponds to a strength increase of 10 and 20 percent respectively compared to that of square pillars. Pillar width is stoping width dependent. The results of an instrumented crush pillar (Roberts et al, 2005b) with a width to height ratio of 2 and width to length ratio of 3, provided similar results to that obtained from modelling (after Roberts et al, 2002). This confirmed that the pillar peak strength is reached at between 8 - 12 millistrains and residual strength between 14 – 20 millistrains. Several factors can affect the amount of convergence experienced at the pillar position at different distances from the face. The main contributors are depth of mining, pillar dimension, strata stiffness and the ability of the pillar to crush. Watson (2010) determined from instrumented sites that residual pillar strength increases exponentially with increasing width to height ratios (w:h < 3.2). At higher width to height ratios the pillar residual strength appeared to reach a peak value which is sustained. Based on the study, this could imply that the strength of the pillar foundation limits the pillar performance. On-going monitoring indicated that there was no further increase in residual pillar strength, even months later. It should be investigated if crush pillars should have width to height ratios greater than 2 or be cut wider than 2 m. Furthermore, the effect of convergence or the relation to pillar crushing or the residual stress state of a pillar needs to be investigated.

3. If ***crush pillars are to fail whilst being formed at the face*** the pillars should already be in a post failure state (residual state) once cut and should ideally have a positive post-peak stiffness (Ryder

and Ozbay, 1990). It should therefore be investigated why unstable and unexpected pillar behaviour is still observed.

4. The ***post-peak stiffness of a pillar determines if the pillar will fail in a stable or unstable manner.*** To determine the post-peak stiffness of a pillar, accurate rock mass parameters are required. Ozbay (1988) provided guidelines to determine the post-peak pillar stiffness, but the parameters were based on various rock and reef types. The design of a crush pillar system should be aimed at achieving pillar crushing close to the stiff face abutment. The stiffness of the strata must be greater than the post-peak stiffness of the pillar to ensure that violent pillar failure does not occur. The post-peak behaviour of a crush pillar formed at the mining face should be investigated to establish the effect on pillar stiffness.

5. ***Pillar cutting is a major problem***. Canbulat et al (2006) reported on the quality of pillar cutting following the investigation of hundreds of pillars at various sites. The findings were that only approximately 30% of the pillar widths and 20% of the pillar lengths conformed to the required design. The quality of pillar cutting has a significant impact on the pillar design and behaviour.

6. ***Various factors affect the behaviour of pillars***. These include parameters such as stoping width, presence of sidings and pillar stress. The effects of these parameters have been researched and can be taken into account by means of adjustments such as effective pillar widths, heights, pillar performance or confinement. In most cases the layout or mining discipline influences the presence of these factors which add to the unpredictability of the pillar behaviour. Layouts should be kept simple and basic principles must be applied (e.g. cutting of a siding). Adjustments or assumptions should ideally not be applied.

7. ***Pillar strength formula*** has been established to determine peak pillar strength. These formulas were developed based on the back analysis of failed pillar cases on various reef types. Two versions are currently available namely the power formula after Salamon and Munro (1967), Hedley Grant (1972) and the linear formula, Bieniawski and Van Heerden (1975). Much debate exist regarding the most applicable formula to use in the platinum mines. York et al (1998) and Roberts et al (2002) determined that the power formula takes consideration of the high contact friction angle present at the pillar interface and the volume effect of varying sample sizes. Watson et al (2008) derived new parameters applicable to the Merensky Reef for both the power and linear formula which provide similar results and factors of safety for back analysed pillar dimensions. The parameters are, however, biased towards Impala Mine case studies and pillars where the w:h > 3.

8. ***Factors of Safety*** are applied for stable pillars to ensure that the pillar stress does not exceed the pillar strength. Pillar failure is assumed for a factor of safety of less than 1. Stacey (2001) used a factor of safety of 0.7 and 1 for the determination of the pillar peak strength for crush and yield pillars respectively, ensuring the assumed post-peak behaviour. To date, the peak strength of crush pillars are unknown. Watson (2010) instrumented pillars in the Bushveld of which the peak and residual pillar strengths were estimated using MINSIM modelling and Boussinesq equations, of which the validity itself is still questionable. The peak pillar strengths were verified against the newly developed "Watson" linear equation (Watson et al, 2008) which is biased towards the Impala yield pillars with a width to height ratio > 3. The application of a factor of safety is therefore very difficult to apply as the peak strength of a crush pillar is unknown.

9. Canbulat et al (2006) established a ***Pillar Fracture Index (PFI)*** which indicated that, over time, the PFI of crush pillars will decrease and that the PFI of crush and yield pillars might converge to a similar value at a certain position from the face. The study concluded that the behaviour of crush pillars in various geotechnical environments is similar. It is therefore important to obtain the required behaviour by matching the correct pillar dimension and loading environment. This characteristic could be more important than establishing the peak strength of a crush pillar or applying a FOS.

10. ***At what depth should crush pillars be employed?*** Although Ozbay and Roberts (1988) indicated that crush pillars should be implemented from approximately 400 m below surface, more recent indications are that pillars at 600 m below surface are not crushing as expected due to the different geotechnical environments.

11. ***Ensuring pillar crushing and accurate crush pillar behaviour*** has been a major challenge to date. Since the introduction of crush pillars on various mines, pillar sizes have been adjusted to ensure pillars behave as expected. As this is not always possible, other techniques such as preconditioning or changes in panel spans have been recommended. This is not always a practical solution as on many mines the reef drives are pre-developed and therefore spans or pillar sizes cannot be adjusted. Pre-conditioning is a technique which is difficult to implement. Rock mass parameters vary between geotechnical environments and therefore it might never be possible to apply standard pillar dimensions to all mines. Simple design principles are therefore required to guide the Geotechnical Engineer regarding the implementation of a crush pillar system.

12. ***Deformation of the rock mass as a function of pillar crushing*** has only been quantified in terms of measured convergence inside the panels. Stress-strain curves are approximated as the actual pillar compression could not be measured. No relationship has been established between convergence in

the panel and pillar compression, although convergence measurements conducted by Watson (2010) were conducted 1 m from the pillar edge to obtain a realistic estimate. Canbulat et al (2006) determined that the pillar dilation is equal to approximately twice the amount of convergence at that site. This must still be substantiated. The dependence of convergence on pillar compression must be quantified as these parameters may be independent.

13. The residual strength of Merensky crush pillars were determined to be approximately 19 MPa (ranging between 13 MPa – 25 MPa). ***The function of the pillar in a residual state*** is to provide a support function to the height of the uppermost parting or weakness plane. This was determined to be approximately 1 MPa for a 30 m parting height (Roberts et al, 2005b). The Bastard Merensky varies between 5 m and 45 m in height, which implies a much lower support resistance requirement (10 m – 0.3 MPa). This needs to be verified.

14. ***Regional pillars control the strata stiffness*** and with increased spans or absence of regional pillars the regional stiffness approaches zero Ryder and Ozbay (1990). Mining of regional or barrier pillars or increased spans do influence the strata regional (k_r) or pillar critical ($-\lambda_c$) stiffness. This effects the convergence experienced in a stope and the rate of loading pillars are subjected to. It may be important to understand and define the regional stiffness to ensure that sufficient pillar crushing will occur close to the face. Factors such as a high percentage geological loss could impact on this parameter and influence the pillar behaviour. Cases where instrumented pillars with low width to height ratios did not crush in a generally stiff environment as a result of limited mining span has been recorded (Piper et al, 2005).

The scope of this study is to investigate some of these aspects. At the end of Chapter 1, the problem statement defined to study the most prominent contributors leading to the unpredictable behaviour of crush pillars on the Merensky Reef. This unpredictability is a major hazard for platinum mines utilising crush pillars on the Merensky Reef horizon. This study will therefore investigate the critical parameters which define crush pillar behaviour on the Merensky Reef horizon.

2.4. References

Bieniawski, Z.T. and Van Heerden, W.L. (1975). The significance of *in-situ* tests on large rock specimens. *Int. J. Rock Mech. Min. Sci. and Geomech. Abstr*., Vol. 12 no.4, pp. 101-113.

Brady, B.H.G. and Brown, E.T. (1981). Energy changes and stability in mine structures: design applications of boundary element methods. *Trans. Inst. Min. Metall., 90: A61–8.*

Canbulat, I., Grodner, N., Lightfoot, N., Ryder, J., Essrich, F., Dlokweni, A., Wilkinson, C., Krog, G. and Prohaska, G. (2006). The determination of loading conditions for crush pillars and the performance of crush pillars under dynamic loading. SIMRAC project SIM040302, Johannesburg.

COMRO, (1988). *Industry Guide to Methods of Ameliorating the Hazards of Rockfall and Rockbursts*. Ch. Of Mines, Johannesburg.

Cook, N.G.W. (1965). A note on rockburst consideration as a problem of stability. *J. South. Afr. Inst. Min. Metall*., vol. 65, pp. 437–446.

Cook, N.G.W. (1967). Contribution to discussion on pillar stability. *J. South. Afr. Inst. Min. Metall.*

Crouch, S.L. (1976). Analysis of stresses and displacements around underground excavations: An application of the displacement discontinuity method. University of Minnesota Geomechanics Report, pp. 268.

Dresher, A. and Vardoulakis, I. (1982). Geometric softening in triaxial tests on granular material. Geotechnique 32, pp. 291–303.

Grodner, M.W. and Canbulat, I. (2005). A methodology for quantification of hard rock pillar behaviour. *3rd Southern African Rock Engineering Symposium.* South African Institute of Mining and Metallurgy Symposium Series 41, pp. 121-130.

Hedley, D.G.F. and Grant, F. (1972). Stope pillar design for the Elliot Lake uranium mines. *Bull. Can. Inst. Min. Metal*., pp. 65.

Lougher, D.R. (1994). An *in-situ* Investigation into the Behaviour of the Surrounding Rock Mass in a Hard Rock Pillar Mining Environment. M.Sc theses, University of the Witwatersrand, Johannesburg.

Malan, D.F., Janse van Rensburg, A.L. and D.P. Roberts (2005). Closure monitoring as a design and risk assessment tool in platinum mines. *3rd Southern African Rock Engineering Symposium.* South African Institute of Mining and Metallurgy Symposium Series 41, pp. 231-243.

Napier, J.A.L and Stephansen, S.J. (1987). Analysis of deep-level mine design problems using the MINSIM-D boundary element program. *Proceedings of the Twentieth International Symposium on the Application of Computers and Mathematics in the mineral industries.* Volume 1: *Mining*. Johannesburg, SAIMM, pp. 3-19.

Ozbay, M.U. (1988). The stability and design of yield pillars located at shallow and moderate depths. *J. South. Afr. Inst. Min. Metall*. Volume 89, No 3, pp. 73–79.

Ozbay, M.U., and Roberts, M.K.C. (1988). Yield pillars in stope support. *Proceedings SANGORM Symposium in Africa,* Swaziland. pp. 317-326.

Piper, P.S. and Flanagan, F.W. (2005). The *in-situ* performance of yielding pillars at Impala 12 shaft. *3rd Southern African Rock Engineering Symposium*. South African Institute of Mining and Metallurgy Symposium Series 41.

Roberts, D.P., Canbulat, I. and Jager, J.A. (2002). Design parameters for mine pillars: strength of pillars adjacent to gullies; design of stable pillars with w:h ratio greater than 6; optimum depth for crush pillars. SIMRAC final report, GAP617, SIMRAC, Johannesburg.

Roberts, D.P., Roberts, M.K.C. and Jager, A.J. (2005a). Alternative support systems for mechanised stopes. PlatMine project report 2004-0189, CSIR, Division of Miningtek, Johannesburg, RSA.

Roberts, D.P., Roberts, M.K.C., Jager, A.J. and Coetzer, S. (2005b). The determination of the residual strength of hard rock crush pillars with a width to height ratio of 2:1. *J. South. Afr. Inst. Min. Metall*. vol. 105, pp. 401–408.

Ryder, J.A. and Napier, J.A.L. (1987). Unpublished material, quoted. Reference after Ryder and Ozbay (1990).

Ryder, J.A. and Ozbay, M.U. (1990). A methodology for designing pillar layouts for shallow mining. *Int. Symp. on static and Dyn. considerations in Rock Engineering,* Swaziland, ISRM.

Ryder, J.A. and Jager, A.J. (2002). *A textbook on Rock Mechanics for Tabular Hard Rock mines*. SIMRAC, Johannesburg.

Salamon, M.D.G. and Munro, A.H. (1967). A study of the strength of coal pillars. *J. South. Afr. Inst. Min. Metall*., vol. 68. 1967.

Salamon, M.D.G (1970). Stability, instability and design of pillar workings. *Int. J. Rock Mech*. Min. Sci., vol. 7, 1970, pp. 613-631.

Salamon, M.D.G. (1974). Rock Mechanics of Underground Excavations. *Proc. 3rd Congr. ISRM.*, Denver. Vol 2, pp. 951-1099.

Salamon, M.D.G. and Oravecz, K.I. (1976). Rock Mechanics in Coal Mining. Coal Mining Research Controlling Council. Chamber of Mines.

Salamon, M.D.G. (1992). Strength and stability of coal pillars, *Workshop on coal pillar mechanics and design, US Bureau of the Interior*. US Bureau of Mines, Santa Fe, USA.

Spencer, D. and York, G. (1999). Back-analysis of yielding pillar system behaviour at Impala Platinum Mine. *Proc. SARES99,* Johannesburg, RSA, pp 44-52.

Stacey, T.R. and Swart, A.H. (2001). *Booklet Practical Rock Engineering Practice for Shallow and Opencast Mines*. SIMRAC, Johannesburg.

Starfield, A.M. and Fairhurst, C. (1968). How high speed computers advanced design of practical mine pillar systems. *Eng. Min. J*., May 1968, pp 78-84.

Starfield, A. M. and Wawersik, W. (1972). Pillars as structural components in room-and-pillar design. *Basic and Applied Rock Mechanics, Proc. 10th U. S. Symp. Rock Mech.,* Austin (ed. K. E. Gray), 793–809. Soc. Min. Engrs, AIME: New York.

Wagner, H. (1974). Determination of the complete load-deformation characteristics of coal pillars. *Proceedings of the 3rd International Congress on Rock Mechanics*, ISRM, Denver, Vol. 2B, pp 1076-1082.

Watson, B.P., Ryder, J.A., Kataka, M.O., Kuijpers, J.S. and Leteane, F.P, (2007). Merensky and UG2 pillar strengths back-analyses. PlatMine report 1.2, CSIR, Johannesburg.

Watson, B.P., Ryder, J.A., Kataka, M.O., Kuijpers, J.S. and Leteane, F.P. (2008). Merensky pillar strength formulae based on back analysis of pillar failures at Impala Platinum, *J. South. Afr. Inst. Min. Metall*. pp.108:449-461.

Watson, B.P. (2010). Rock Behaviour of the Bushveld Merensky Reef and the Design of Crush Pillars. PhD thesis, School of Mining Engineering, University of the Witwatersrand, Johannesburg, South Africa.

York, G. Canbulat, I., Kabeya, K.K., Le Bron, K., Watson, B.P. and Wiliams, S.B. (1998). Develop guidelines for the design of pillar systems for shallow and intermediate depth, tabular, hard rock mines and provide a methodology and support requirements for the panels between pillars. SIMRAC final report, GAP334, SIMRAC, Johannesburg.

York, G. (1998). Numerical modelling of the yielding of stabilising pillar foundation system and new design consideration of stabilising pillar foundations. *J. South. Afr. Inst. Min. Metall*. pp. 281-297.

CHAPTER 3

FORMULATION OF A MODEL TO ASSESS CRUSH PILLAR BEHAVIOUR

Assessment of a limit equilibrium model to represent crush pillar behaviour

3. MODEL FORMULATION

As described by Malan and Napier (2006), a major challenge in the design of pillar layouts is to integrate an appropriate representation of the pillar failure behaviour with the overall analysis of the tabular mining stress distribution. As crush pillars consist of crushed reef material, the detailed inelastic analysis of seam or reef crushing behaviour is most appropriately conducted by means of non-linear finite element or finite difference models. However, for tabular excavation layouts, stress interactions in three dimensions can be efficiently represented using a boundary element model based on displacement discontinuity elements.

Some simplification to the problem is possible if the fractured seam or reef material is known to be concentrated within or close to the mining horizon and does not extend appreciably into the hangingwall or footwall regions. This will often be the case when considering the design of crush pillars in shallow mining layouts. Various strategies have been suggested to represent non-linear seam behaviour using limit equilibrium methods (e.g. Brummer, 1987) or the so-called "enhanced" displacement discontinuity method (Yacoub and Curran, 1999) in which reef-parallel strain components are included in the set of unknown variables that are evaluated on the reef horizon. In this study an analytic limit equilibrium model, similar to coal seam deformation models introduced by Barron (1984), is employed to represent the behaviour of the reef material in pillars. Malan and Napier (2006) did a preliminary evaluation of a similar model and demonstrated that it is feasible to model pillar crushing.

The objective of this chapter is to extend this original evaluation of the model. It should be noted that Salamon (1992) introduced a refinement of the Barron model which he called the "enhanced confined core concept" of pillar strength. The focus of the study will be to illustrate the value of these limit equilibrium models when implemented in boundary element codes, such as TEXAN, to represent the behaviour of the reef material in the pillars (Malan and Napier, 2006) and (Napier and Malan, 2007).

3.1. An overview of the TEXAN code

In the displacement discontinuity boundary element method (DDM), mine layouts are approximated as irregular shaped planar cracks (or slits) where the 'width' of the crack, corresponding to the excavation height, is assumed to be negligible compared to the in-plane, lateral dimensions. The TEXAN (Tabular EXcavation ANalyser) code (Napier and Malan, 2007) utilises a general revision of this approach in which triangular or quadrilateral element shapes are introduced in conjunction with higher order variations of the displacement discontinuity shape functions. This facilitates an accurate evaluation of detailed stress and displacement components close to excavation surfaces and allow for the assessment of tabular layouts which includes a large number of pillars.

3.2. Formulation of the limit equilibrium model

A pillar can be divided in a large number of vertical slices (Barron, 1984). The elastic stresses acting on the pillar can be analysed and compared to an appropriate failure criterion. Once a slice has failed, its residual stress is calculated. This is compared to the initial elastic stress of which the difference is transferred to the remaining unfailed slices. The successive analysis of each slice determines the depth of the failed zone, the final stress distribution, the pillar strength and for the case of failed pillars, the residual strength.

Malan and Napier (2006) illustrated the force equilibrium of a material "slice" of a fractured pillar as shown in Figure 3.1. The slice of fractured material has a mining height *H* at a distance *x* from the stope face. The slice is confined by reef-parallel and reef-normal stress components σ_s and σ_n respectively as well as by shear tractions τ .

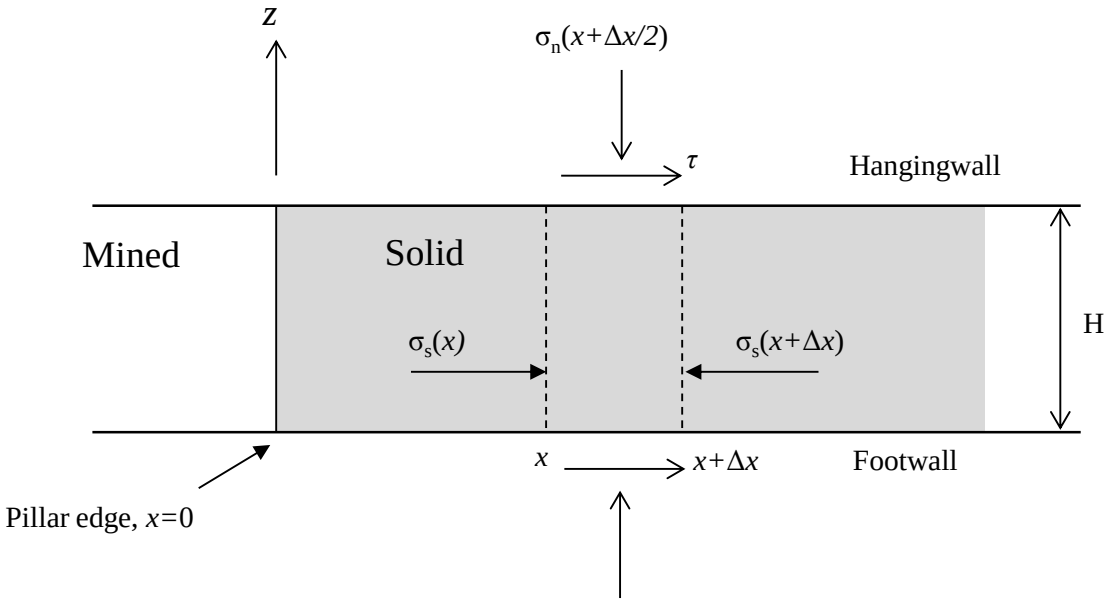

Figure 3.1: Force equilibrium of an elementary material slice between two bounding surfaces (after Malan and Napier, 2006).

It is assumed that the edge of the pillar is at x = 0 and that the seam-parallel stress component σ_s is uniform over the height of the pillar and increases as *x* increases. From Figure 3.1 it can be inferred that the equilibrium force balance acting on the slice of height *H* and unit out of plane width requires that;

$$H\sigma_s(x+\Delta x) = H\sigma_s(x) + 2\tau\Delta x \qquad (3.1)$$

Taking the limit Δx → 0 equation (3.1) can be written in the form of the differential equation;

$$\frac{d\sigma_s}{dx} = \frac{2\tau}{H} \tag{3.2}$$

Equation (3.2) can be solved for σ_s if a relationship exists between τ and σ_s. This can be established by making the following assumptions:

(a) Assume that τ is related to the surface-normal stress σ_n by a frictional slip condition of the form:

$\tau = \mu\sigma_n$; where μ is the friction coefficient. (3.3)

(b) Assume that σ_n is related to the average stress σ_s by a failure relationship of the form:

$\sigma_n = C + m\sigma_s$; where C and m are specified constants. (3.4)

Substituting equations (3.4) and (3.3) into equation (3.2) yields the required differential equation as follows:

$$\frac{d\sigma_s}{dx} = \frac{2\mu}{H}(C + m\sigma_s) \tag{3.5}$$

Equation (3.5) can be integrated directly if it is written in the separable form;

$$\int \frac{d\sigma_s}{C + m\sigma_s} = \int \frac{2\mu}{H} dx \tag{3.6}$$

Integrating equation (3.6) yields the solution to equation (3.5) in the form;

$$\ln(C + m\sigma_s) = \frac{2\mu m x}{H} + A \tag{3.7}$$

where A is a constant that can be determined by applying the boundary condition that the average horizontal stress σ_s is equal to an edge constraint stress p when x = 0. Hence, substituting $\sigma_s = p$ and x = 0 in equation (3.7) yields;

$$A = \ln(C + mp)$$

The average horizontal stress is then recovered from equation (3.7) as a function of the distance *x* from the edge of the pillar in the form;

$$\sigma_s = (C/m + p)\exp(2\mu mx/H) - C/m \qquad (3.8)$$

The seam-normal stress component σ_n can be obtained by substituting the expression for σ_s given by equation (3.8) into equation (3.4) to yield;

$$\sigma_n = (C + mp)\exp(2\mu mx/H) \qquad (3.9)$$

It is apparent from an examination of equations (3.8) and (3.9) that the solutions for σ_s and σ_n become degenerate (have zero values) if both *C* and *p* are equal to zero. In order to proceed further with the application of the simple limit equilibrium model some explicit assumptions has to be made concerning the choice of suitable values for *C* and *p*. In the present approach, it is assumed that p = 0 and that the average unconfined strength of the material *C*, at the edge of the pillar in the failed state is equal to C_b. The parameter C_b is therefore equivalent to the residual unconfined strength of the crushed material (UCS_b). This assumption is tenable if the pillar is able to bear some vertical load at the unsupported edge x = 0. Specifically, from equation (3.9), the vertical load is $\sigma_n = C_b$ when x = 0. If the pillar edge is, in fact, free-standing then this must be the case. However, it is apparent that the depth of the failed edge zone will be very sensitive to the exact choice of C_b.

Setting p = 0 in equations (3.8) and (3.9) and defining:

$$\alpha = 2\mu m/H$$

yields the following expressions for the horizontal and vertical stress values in the edge region:

$$\sigma_s = C_b(e^{\alpha x} - 1)/m \qquad (3.10)$$

$$\sigma_n = C_b e^{\alpha x} \qquad (3.11)$$

The simple stress model depicted in Figure 3.1 has been extended by Salamon (1992) to allow for an explicit variation of the stress components σ_{xx}, σ_{yy} and σ_{xz} as functions of both the edge distance coordinate *x* and the vertical coordinate *z* between the floor and roof of the pillar region. It is assumed that the material

satisfies a limit equilibrium relationship between the maximum and minimum local principal stress components σ_1 and σ_3 at each point (x,z) in the failed region that is of the form;

$$\sigma_1(x,z) = m\sigma_3(x,z) \tag{3.12}$$

The values of the principal stress components σ_1 and σ_3 can be expressed as functions of the individual stress components σ_{xx}, σ_{yy} and σ_{xz} which are, in turn, defined in terms of the derivatives of an Airy stress function, $\Phi(x,z)$ that is assumed to have the form;

$$\Phi(x,s) = \exp[ax + f(z)] \tag{3.13}$$

Substituting these expressions into equation (3.12) allows the stress components to be solved in a closed but rather complicated form (Salamon 1992). From the assumed relationship (3.12), it is noted that this model assumes that the cohesive strength, C = 0, and requires the specification of a non-zero confining stress, *p*, at the edge of the pillar. No allowance is made for roof or floor foundation failure processes and all stress components increase exponentially from the pillar edge. The added complexity of this extended limit equilibrium model is not explored in the present approach.

As pointed out by Salamon et al (2003), a Mohr-Coulomb plasticity model without strain softening behaviour is inadequate for simulating actual pillar behaviour where rapid load shedding or "bursting" may occur. To address this shortcoming, it is assumed that initial failure in the seam or reef is controlled by the additional relationship:

$$\sigma_n \leq C_0 + m_0\sigma_s \tag{3.14}$$

where C_0 and m_0 represent the intact strength of the pillar material. Equation (3.14) is used as well to determine implicitly the boundaries between the pillar intact core and the failed edge regions.

3.3. Analytical solution for the APS of a failed 2D pillar

Equation (3.11) predicts an exponential increase in the pillar stress away from the edge towards the centre of the pillar (Malan and Napier, 2006). In this section this model is further explored by the author to determine the stress state of a completely failed two-dimensional pillar. This model will further on be referred to as the ***Du Plessis model*** in this study.

If the pillar width is *w* and if the pillar is completely failed then, assuming that the stress profile is symmetric about the centre of the pillar, the average stress in the pillar is given by:

$$APS = \frac{2\int_0^{\frac{w}{2}} \sigma_n dx}{w} \tag{3.15}$$

By substituting equation (3.11) into (3.15), it follows that:

$$APS = \frac{2C_b\int_0^{\frac{w}{2}} e^{\alpha x} dx}{w} = \frac{2C_b}{\alpha w}\left[e^{\alpha w/2} - 1\right] \tag{3.16}$$

Substituting $\alpha = 2\mu m / H$ into equation (3.16), the average pillar stress can be expressed as;

$$APS = \frac{C_b H}{\mu m w}\left[e^{\frac{\mu m w}{H}} - 1\right] \tag{3.17}$$

The form of equation (3.17) suggests that the average stress can be written compactly in the following dimensionless form;

$$\frac{APS}{C_b} = \frac{e^{\eta} - 1}{\eta} \tag{3.18}$$

where the constant $\eta = \mu m w / H$ represents a non-dimensional parameter that is proportional to the width to height ratio. In the limiting case when the width *w* becomes very small, $\eta \to 0$ and $APS \to C_b$. This clearly indicates that some caution should be exercised in using the simple limit equilibrium model for very slender failed pillars where $w < H$.

The behaviour of the model derived above can be illustrated using a specific choice of the basic parameters. The following constants were assumed for the initial comparison:

- C_b = 5 MPa
- m = 2
- $\mu = \tan\phi = \tan 30°$
- w = 10 m
- H = 5 m

If these values are inserted into equation (3.17), it is found that the APS = 19.63 MPa. This value was compared with the numerical modelling example described in Section 3.5. As mentioned above, it should be noted that the residual APS value for a failed pillar predicted by equation (3.17) is very sensitive to the width to height ratio of the pillar. To illustrate this, equation (3.17) is plotted for different width to height ratios.

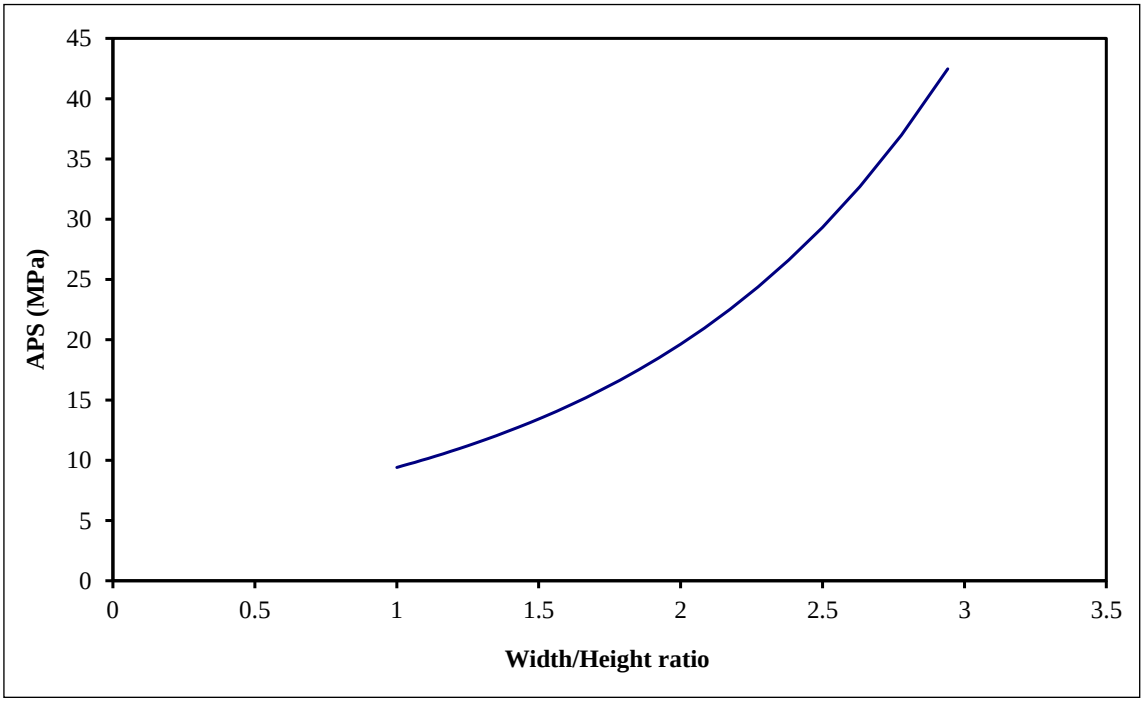

Figure 3.2: Simulated residual APS values for a failed pillar at different width to height ratios.

To illustrate the effect of different friction angles, equation (3.17) is plotted for friction angles from 5 to 45 degrees. The other parameters used remained constant as described above. Note that as the friction angle approaches zero, the residual APS tends to C_b (residual strength of the crushed material).

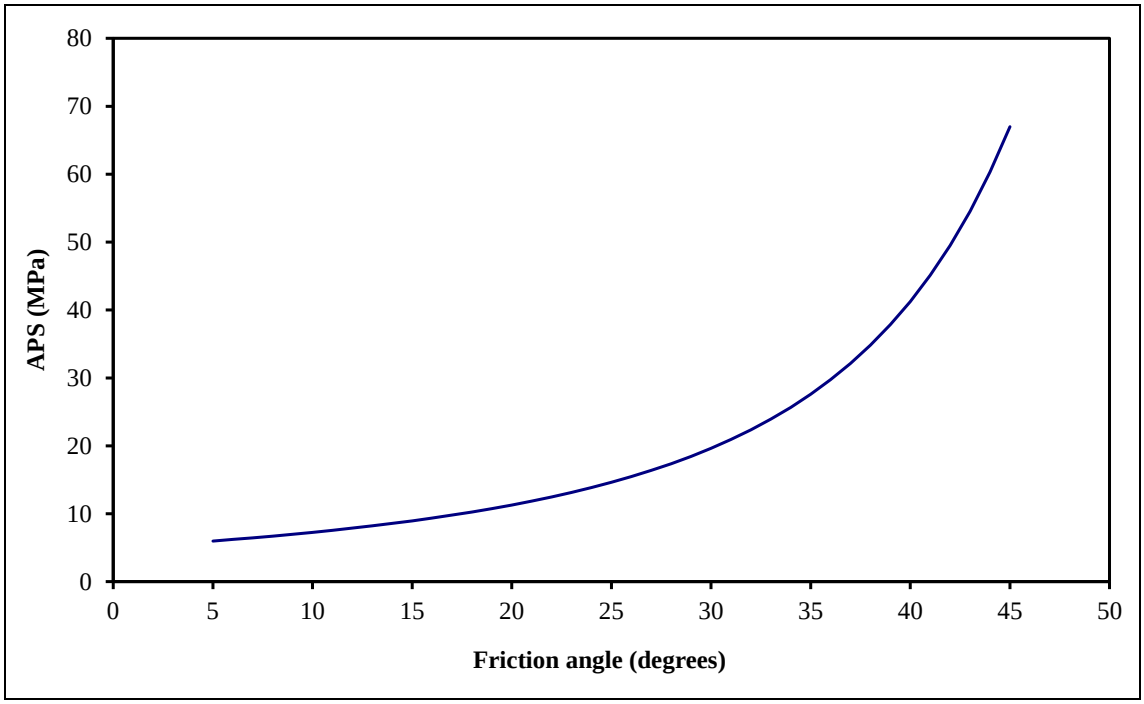

Figure 3.3: Simulated residual APS values for a failed pillar as a function of assumed friction angle.

3.4. Implementation of the crush pillar model in TEXAN

An overview of the TEXAN tabular excavation computer program is given by Napier and Malan (2007). The code can currently solve both 2D and 3D problems with multiple interacting tabular reef planes and planar fault planes. These planes are tessellated with displacement discontinuity elements to represent stope ride and convergence movements or to model slip movements on fault planes. Elements can be in an "infinite" space or in a "semi-infinite" space with a flat, stress-free surface. The medium is assumed to be elastic and isotropic. Analytical kernel expressions are used to compute half-space influence functions in 3D. Elements can be 2D line segments, 3D triangles or 3D convex quadrilaterals. In particular, square elements can be used if required. Both in-plane and anti-plane components are allowed in 2D analyses.

Each element can have one or more internal collocation points giving constant or higher order variation discontinuity densities. Triangular elements can be defined to have 1, 10 or 15 internal collocation points giving constant, cubic (third order) or quartic (fourth order) discontinuity variations respectively. Quadrilateral elements can be defined with 1 or 9 internal collocation points. A quadrilateral element with 9 internal collocation points is assigned a bi-quadratic shape function (degenerate fourth order).

Stress and displacement field values (so-called "benchmark" values) close to excavation surfaces are accurately computed with higher order elements if the normal projection of the field point falls within the element perimeter. Stress singularities can nevertheless arise close to element boundaries (approximately within 0.1 of the element "diameter"). Field values cannot be computed accurately within a distance of approximately two to three element "diameters" normal to the element plane when using constant elements. Additional attributes of the TEXAN code include the ability to specify mixed displacement and stress component boundary conditions on specific elements, the inclusion of backfill regions in mined areas and the ability to simulate fault slip processes by activating pre-defined element tessellations in sequential mining steps.

Regarding the limit equilibrium model, the examples given in Section 3.3 are relevant to plane strain layout configurations and, therefore, are of limited use in application to tabular layout pillar design. It will be very difficult to extend the simple differential relationship embodied in equation (3.5) to the case of a pillar having an irregular, two-dimensional plan shape. In particular, it is apparent that the slip field orientation in the pillar should depend on the relative magnitude and direction of the in-seam principal stress components and the detailed pillar shape. In order to maintain the appealing features of the simple model, it is assumed that equations (3.10) and (3.11) can still be applied at each internal pillar element collocation point where stress conditions are evaluated. The crucial assumption is made that the distance that is used at each such point is interpreted as the closest distance from the point to the relevant polygonal edge defining the pillar shape. It is straightforward to compute this distance for all pillar and abutment element collocation points.

This simple strategy then permits the limit equilibrium model to be extended to general tabular layout problems with irregular shaped pillars.

3.5. Numerical modelling of the APS of a failed pillar

A specific model geometry simulated with the TEXAN code is shown in Figure 3.4. It was attempted to simulate a "rib" pillar to approximate the 2D solution of APS given in the previous section. The pillar was simulated at a depth of a 1000 mbs and the vertical stress gradient was 0.031 MPa / m.

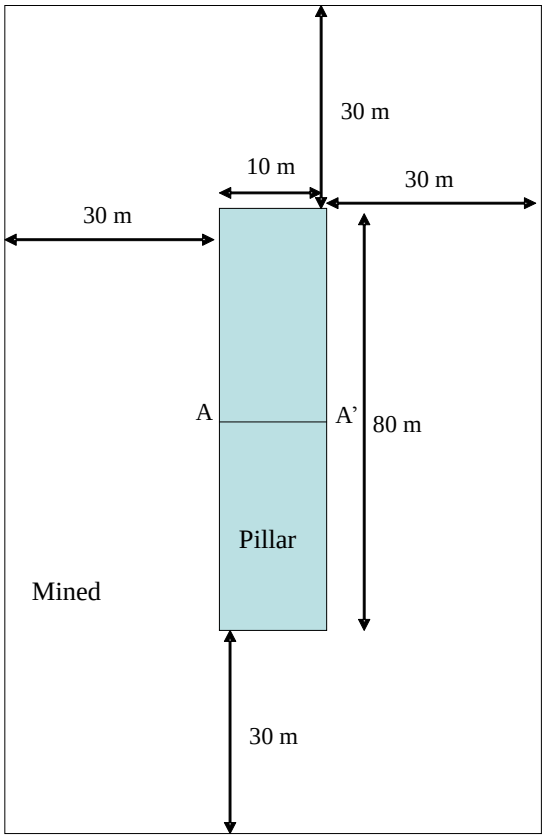

Figure 3.4: Layout simulated: Square elements of 1 m size were used for the initial simulation. The stress profile along Section A - A' was plotted. The pillar was simulated as a rigid pillar and then allowed to crush in a second simulation.

Figure 3.5 illustrates the stress distribution along Section A - A' for the rigid pillar. Note the classical stress profile for a simulation in which the pillars are assumed to be rigid (incompressible). The simulated APS value for the pillar (average of all 800 collation points) was 110.56 MPa. In comparison, Figure 3.6 illustrate the stress profile along Section A - A' if a limit equilibrium model is assumed and the parameters given in Section 3.3 are assumed (C_b = 5 MPa, m = 2, $\mu = \tan\phi = \tan 30°$ and H = 5 m; the peak and residual values are assumed to be similar). The behaviour predicted by equation (3.11) is also plotted in the figure.

The average of the 10 simulated values across Section A - A' is 19.48 MPa. This is in close agreement with the analytical value of 19.63 MPa calculated in Section 3.3 using equation (3.17). The average APS for the entire pillar is 18.65 MPa. This is slightly lower owing to the effects at the two ends of the pillar (an infinite long rib pillar was only approximated, but not simulated).

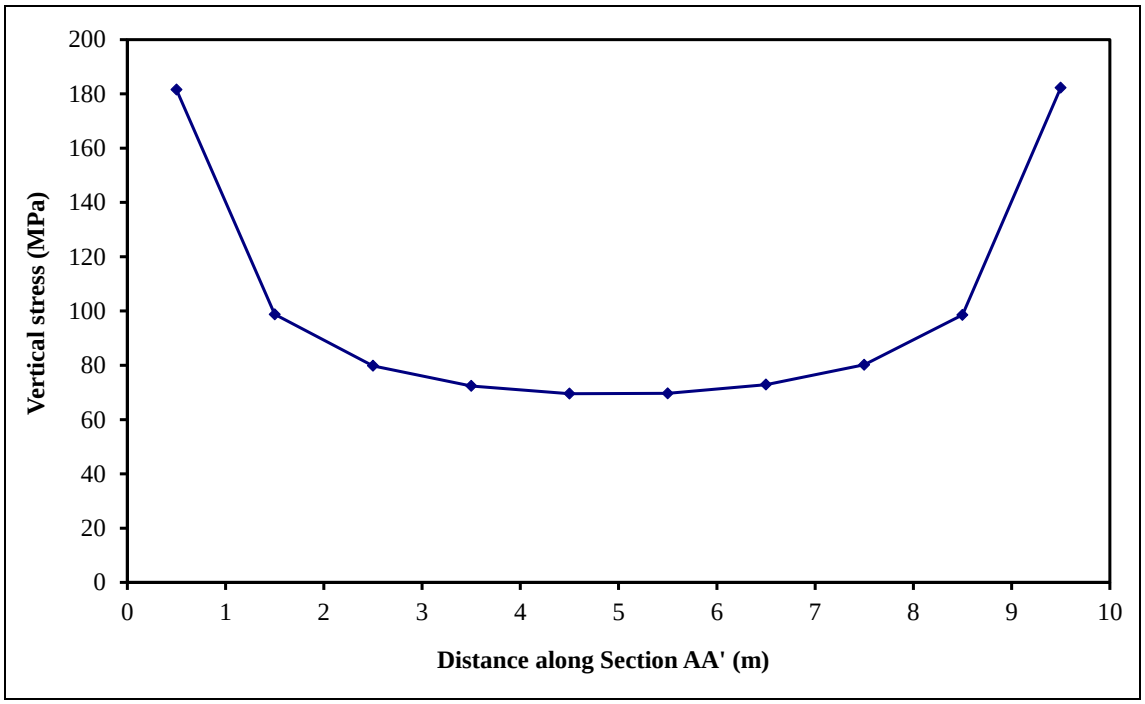

Figure 3.5: Simulated vertical stress along Section A - A' for a rigid pillar.

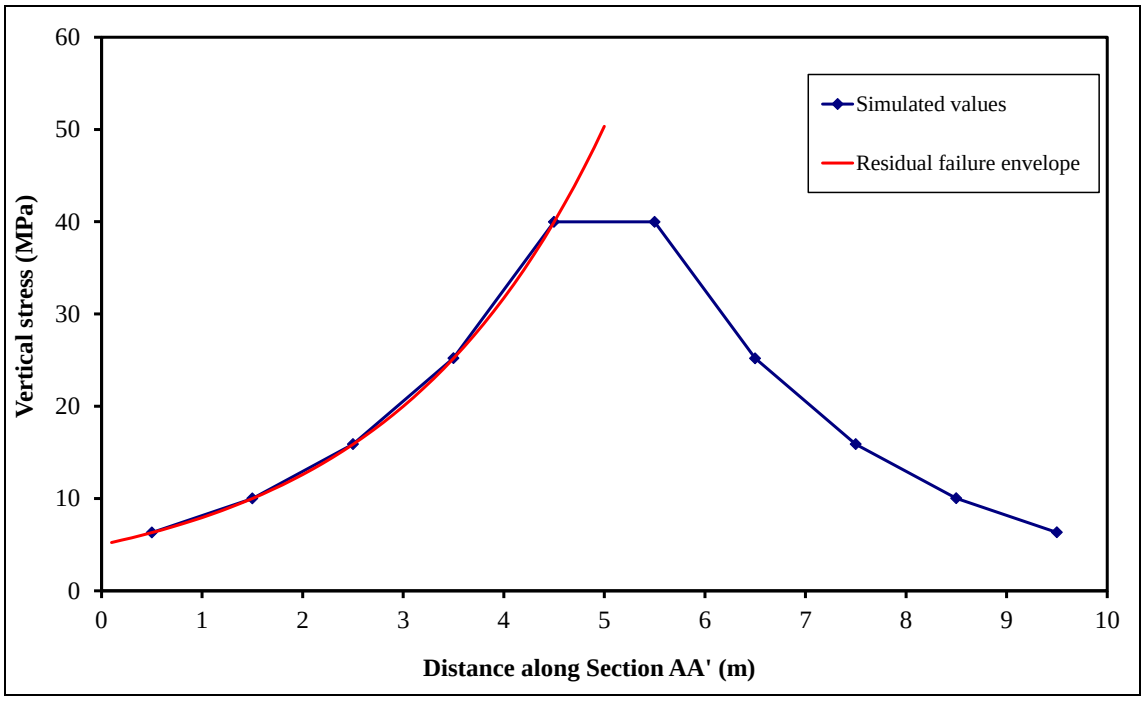

Figure 3.6: Simulated vertical stress along Section A - A' for a limit equilibrium model.

From Figure 3.6, a key attribute of the limit equilibrium model is clearly visible: The stresses increase in an exponential fashion towards the centre of the pillar. Salamon (1992) identified this as a potential problem as it may lead to the formation of unduly high stresses in the core of wide pillars. The magnitude of these stresses may become sufficiently high to cause failure in the hangingwall or footwall. The current model as implemented in TEXAN can allow this off reef failure to be evaluated in restricted cases by allowing shear failure planes to grow from the pillar edges. This off reef failure was not considered in this current study, however.

3.5.1. Effect of element size

Regarding APS calculations using displacement discontinuity boundary element programs, Napier and Malan (2011) have illustrated that the simulated average pillar stress (APS) can depend on the chosen mesh size. Regarding the limit equilibrium model, it is expected that the mesh size will also play a role. This is of particular importance when simulating a large scale crush pillar layout as the pillar width may be as small as 2 – 3 m. In TEXAN, the limit equilibrium equation is applied at each internal pillar point where stress conditions are evaluated. The distance that is used at each such point is interpreted as the closest distance from the point to the relevant polygonal edge defining the pillar shape. This closest distance will be dependent on the element tessellation covering the pillar and care should be taken that the average element size is much smaller than the width of the pillar.

To investigate this effect, the geometry shown in Figure 3.4 was simulated using the same modelling parameters but with different element sizes. Figure 3.7 illustrates the effect of element size when using square constant strength (single collocation point) elements. As expected, very coarse element sizes (5 m) will underestimate the residual strength of the failed pillar. The few element collocation points present fall outside the higher stresses of the central core of the failed pillar and therefore the average stress is underestimated. Note that the data point for the 2 m element size is considered as an “outlier” as this is the only size where an uneven number of elements were required to cover the width of the 10 m pillar. This resulted in the collocation point of the centre row of elements capturing the high stress value in the centre of the pillar (see Figure 3.7).

The effect of using an irregular mesh of triangular elements was also investigated. An example of such a mesh covering the pillar is shown in Figure 3.9. Simulations with various average element sizes were conducted. The results are shown in Figure 3.8.

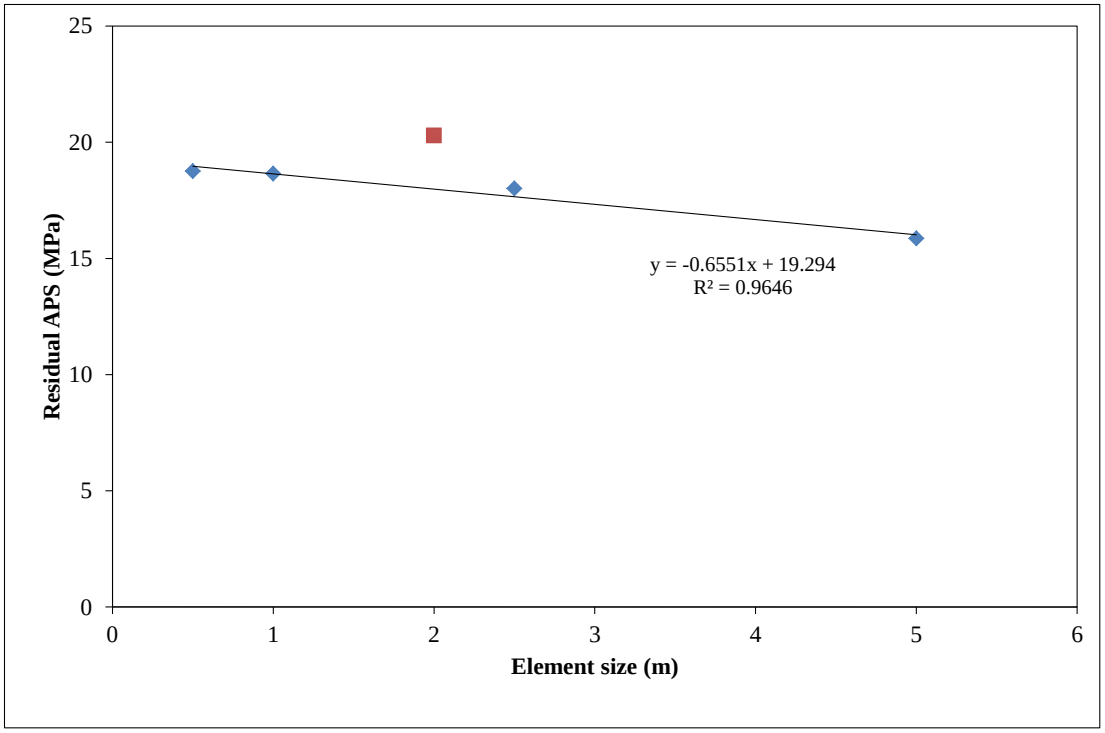

Figure 3.7: Effect of element size (square single collocation point elements) on simulated residual APS of a 10 m wide pillar (Figure 3.4). The 2 m element size (red square) was excluded from the trend line calculation (see discussion in text).

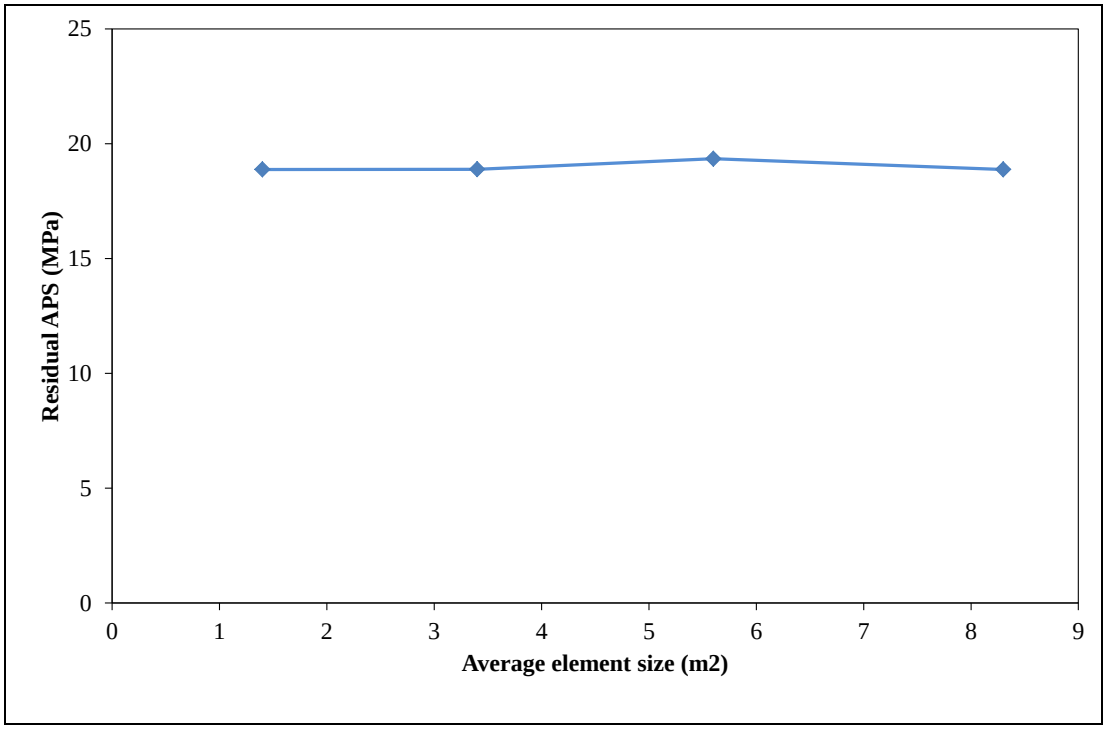

Figure 3.8: Effect of element size (triangular single collocation point elements) on the simulated residual APS of a 10 m wide pillar (Figure 3.4).

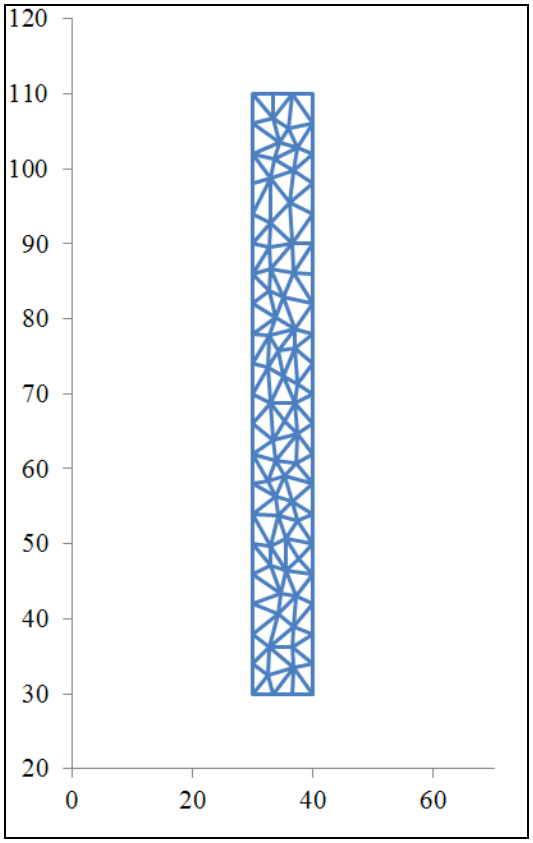

Figure 3.9: Example of the tessellation of triangular elements used for the pillar shown in Figure 3.4.

3.6. Summary

This chapter described the evaluation of a simple limit equilibrium model to simulate the behaviour of crush pillars in platinum mines. The model is currently available as a constitutive code in the TEXAN boundary element program. For the evaluation, an analytical model was used to calculate the residual APS values of the crush pillars. The values predicted by this model were compared to the numerical values obtained from the TEXAN simulations. Good agreement was obtained between the two models and this serves as a useful validation of the model implemented in the numerical code. In general, the limit equilibrium model appears to be very attractive to simulate pillar failure as the gradual crushing of the outside of the pillar and the transfer of stress to the intact core can be replicated.

3.7. References

Barron, K. (1984). An analytical approach to the design of coal pillars. *CIM Bulletin*, vol. 77, no 868, pp. 37–44.

Brummer, R.K. (1987). Modelling the non-linear behaviour of fractured seams in deep gold mines, In: APCOM 87. *Proceedings of the Twentieth International Symposium on the Applications of Computers and Mathematics in the Mineral Industries*. Volume 1: Mining, Johannesburg, SAIMM, pp. 21-32.

Malan, D.F. and Napier, J.A.L. (2006). Practical application of the TEXAN code to solve pillar design problems in tabular excavations. *SANIRE 2006 Symposium - Facing the Challenges*, Rustenburg, pp. 55-74.

Napier, J.A.L. and Malan, D.F. (2007). The computational analysis of shallow depth tabular mining problems. *J. South. Afr. Inst. Min. Metall.*, vol. 107, Nov 2007, pp. 725-742.

Napier, J.A.L. and Malan, D.F. (2011). Numerical computation of average pillar stress and implications for pillar design, *J. South. Afr. Inst. Min. Metall.*, vol. 111, no. 12, pp. 837-846.

Salamon, M.D.G. (1992). Strength and stability of coal pillars, *Workshop on coal pillar mechanics and design, US Bureau of the Interior*. US Bureau of Mines, Santa Fe, USA.

Salamon, M.D.G., Badr, S., Mendoza, R. and Ozbay, M.U. (2003). Pillar Failure in deep coal seams: numerical simulation. *In Proceedings of the 10th Congress of the International Society for Rock Mechanics*. published by the South African Institute for Mining and Metallurgy, Johannesburg, pp. 1011-1018.

Yacoub, T.E. and Curran, J.H. (1999). Analysis of post-peak pillar behaviour using the enhanced displacement discontinuity method. *In Proceedings of the 37th U.S. Rock Mechanics Symposium*, Balkema, pp. 169-176.

CHAPTER 4

SIMULATION OF CRUSH PILLAR BEHAVIOUR

4. SIMULATION OF CRUSH PILLAR BEHAVIOUR

During the past four decades, several parameters governing the behaviour of crush pillars were studied in an attempt to better understand and predict the behaviour of these pillars. Crush pillar layouts have, however, remained essentially unchanged over this period. The examples presented in the previous section illustrate the potential of a simple limit equilibrium model to simulate the behaviour of crush pillars. In this chapter, the behaviour of crush pillars will be investigated using the limit equilibrium model implemented in a boundary element code.

The objective is to use a simple representative model as an investigation tool of the behaviour of crush pillars in a representative layout. The purpose is to understand when pillars will crush, where they will crush relative to the mining face and why some pillars can potentially burst. Various parameters will be assessed to establish the factors governing crush pillar behaviour. These include rock mass parameters, mining depth (stress) and pillar geometric effects such as, pillar width, pillar height and pillar length.

4.1. Simulating a crush pillar layout

The TEXAN code was used to simulate an idealised crush pillar layout. The simulated layout is shown in Figure 4.1. It consists of a 30 m x 70 m stope panel with a second panel being mined in a sequential fashion adjacent to this first panel. The layout was simulated as eight mining steps with 7 crush pillars being formed in this process. For the second panel, the size of each mining step was 10 m and the sizes of the crush pillars were 4 m x 6 m. A 2 m mining height was used, resulting in these 4 m wide pillars having a width to height ratio of two. These pillar dimensions may not necessarily be realistic when compared to actual layouts, but were assumed in order to illustrate the behaviour of the crush pillar model. The element sizes used were 0.5 m.

The parameters used for the simulations are shown in Table 4.1. Note that these values were chosen arbitrarily. The intent was to establish trends regarding the pillar behaviour even though the parameters used may not fully represent the actual environment. A better calibration of this model based on underground measurements is described in the following chapters.

For the first simulation, the pillars were not allowed to crush and were simulated as “rigid” pillars in an elastic rock mass. Figure 4.2 illustrates the expected increase in pillar stress as the pillars move into the back area. The simulation was repeated using the crush pillar model. Figure 4.3 illustrates the APS values on three of the pillars (D, E and F) as a function of mining step. Note that the pillar stresses gradually increases as the mining face approaches. For the chosen parameters, the peak APS value is achieved during the mining step when the pillars are formed. The pillars then crush completely during the next mining step whereafter

the residual APS is maintained. For the crush pillar model, the peak stress on the pillars (≈ 56 MPa) is far less than for the pillars which are not allowed to fail (≈ 130 MPa).

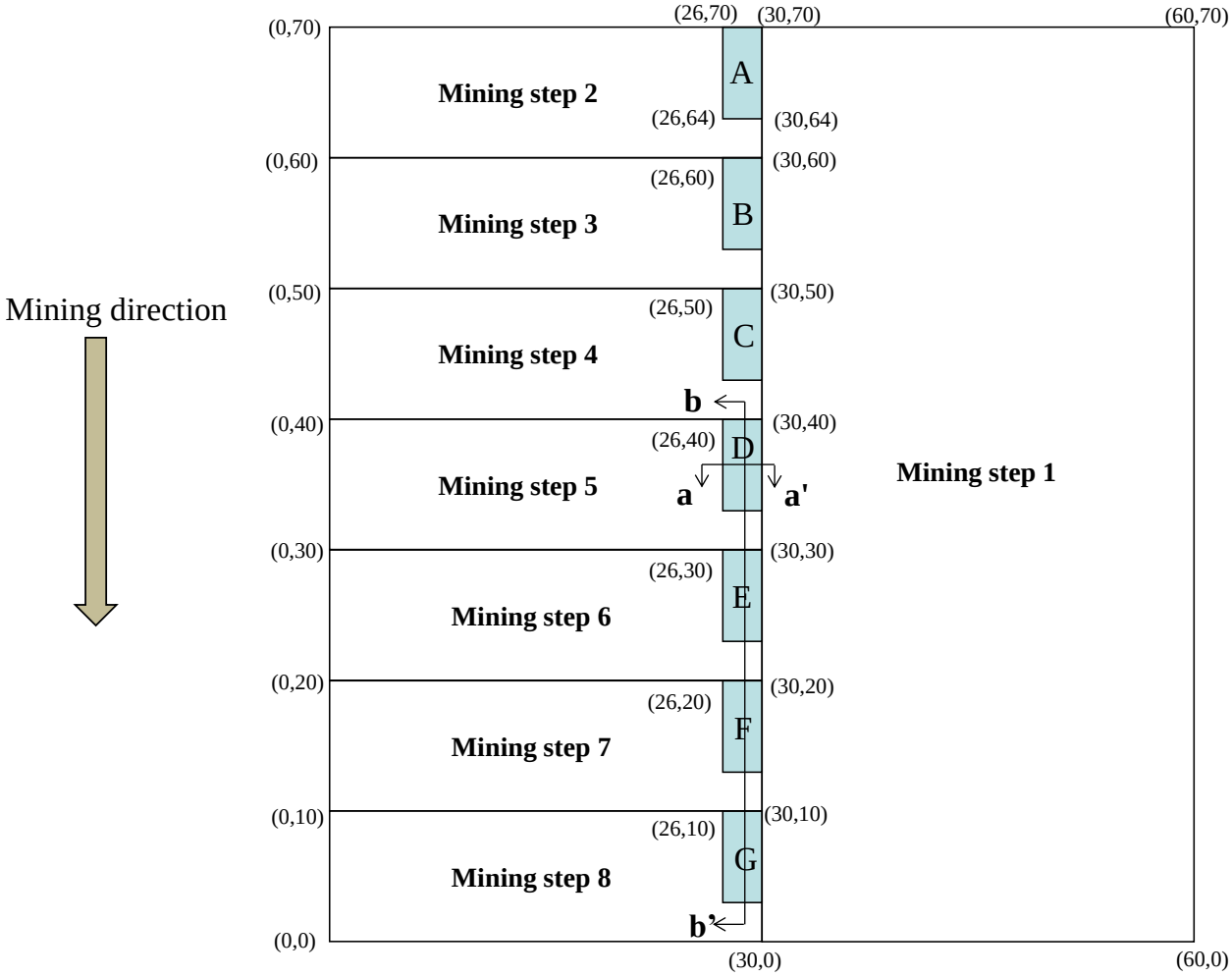

Figure 4.1: Idealised crush pillar layout simulated in the TEXAN code.

Table 4.1: Parameters used for the crush pillar simulations.

General Parameters	Value
Young's modulus	70 GPa
Poisson's ratio	0.25
Stress gradient	0.03 MPa/m
Depth	600 m
Reef dip	0°
Crush model parameters	**Value**
Intact material strength C_0	5 MPa
Crushed material strength C_b	5 MPa
Intact slope m_0	5
Residual slope m_b	3
Bounding friction angle φ	35°
Seam height	2 m
Seam stiffness modulus	10^6 MPa/m

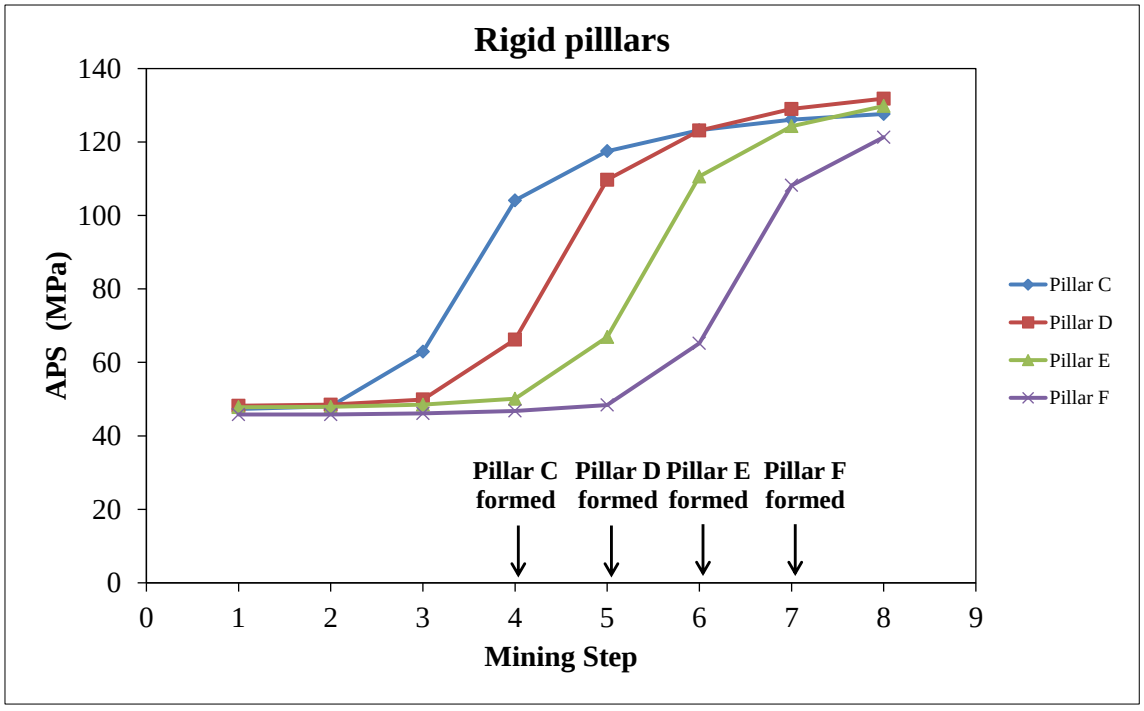

Figure 4.2: Simulated pillar stress if the pillars are not allowed to crush ("rigid" pillars).

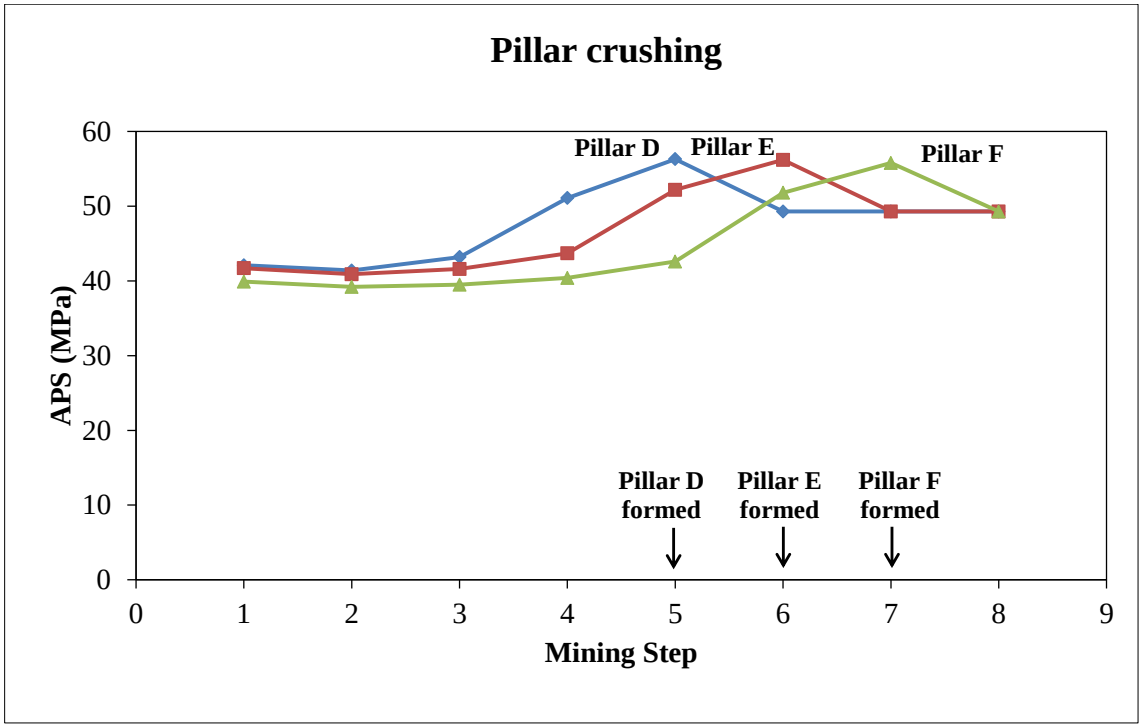

Figure 4.3: Simulated pillar stress if the pillars are allowed to crush (limit equilibrium model).

If the pillars did not crush, the pillars would be at a higher stress (see Figure 4.2). Once these pillars move into the back area, the change in stress caused by a mining increment is lower compared to a pillar in close proximity to the face. The pillars might therefore either not crush at all (especially when oversized) or fail violently as the stresses on the pillars are much higher and the loading environment (rock mass) has become much softer as it is no longer close to the face abutment.

Figure 4.4 illustrates the stress profile along Section a - a' (Figure 4.1) for pillar D. After Step 1, the pillar is still part of the abutment of the first panel. It can be seen from the stress profile that some crushing of this abutment has already occurred and the peak stress value is located approximately 2.5 m inside the rock. This stress peak gradually moves deeper into the rock as can be seen for the profile of Step 4. During Step 5 the pillar is formed and the profile becomes nearly symmetrical. During the next step, the stress increase causes complete failure of the core and the residual stress profile is assumed (also refer to Section 4.1.1).

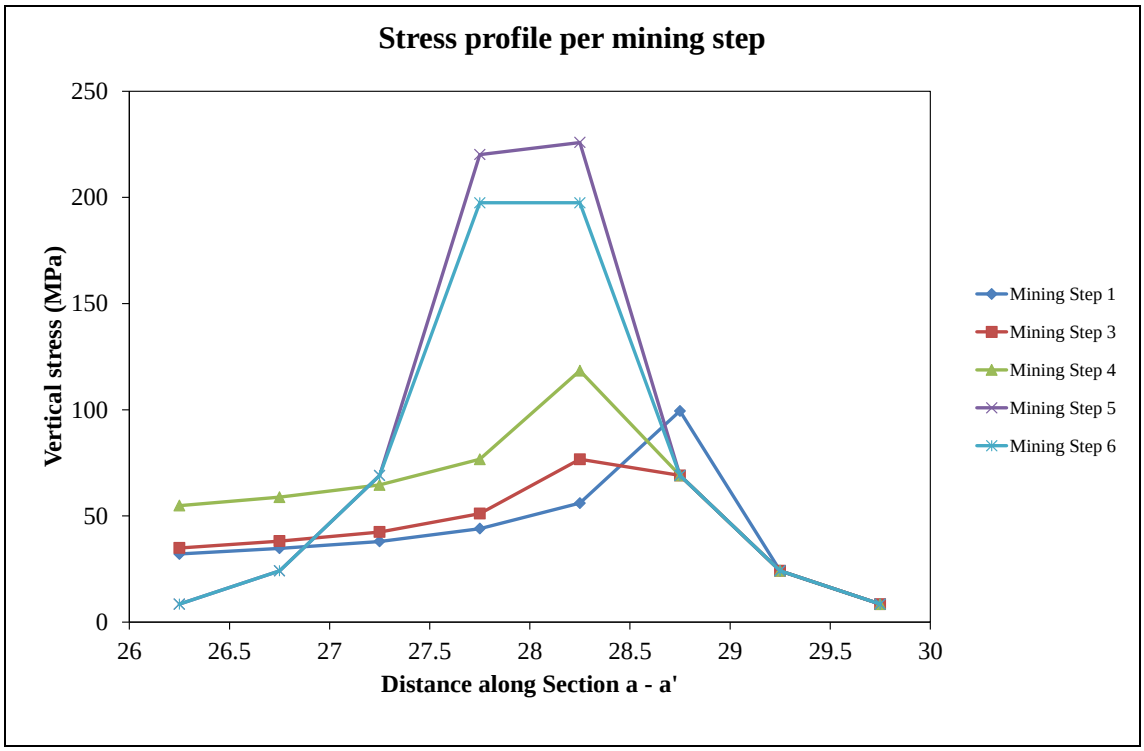

Figure 4.4: Simulated stress profile for pillar D along section a - a' (see Figure 4.1) for the different mining steps.

4.1.1. Effect of oversized pillars

A problem endemic to crush pillar layouts is the poor cutting of the pillars (Canbulat et al 2006). This frequently results in oversized pillars being present in these layouts. The larger pillars do not always crush in a stable manner and may fail violently in the back area of a stope. The idealised crush pillar layout simulated above was used to investigate the effect of an oversized crush pillar present in a layout. The geometry simulated was identical to that shown in Figure 4.1 except that pillar D was increased in size to a 6 m x 6 m pillar (w:h = 3:1). The modified geometry is shown in Figure 4.5.

The simulated stress values for pillar D (6 m x 6 m) are shown in Figure 4.6 and compared to the smaller pillar (4 m x 6 m) of the first simulation. Note that the APS value of the larger pillar is 73 MPa after Step 8. This is much higher than the 49 MPa simulated for the 4 m x 6 m pillar. Figure 4.7 illustrates the stress profile along Section a - a' (see Figure 4.5) for Pillar D. Note that the core of the pillar is still intact. As previously mentioned, these pillars, in the back area of a stope are at a higher stress. The change in stress is lower compared to the pillar being formed at the face and might as a result not crush. This may lead to violent failure in the back area if the pillar becomes more highly stressed.

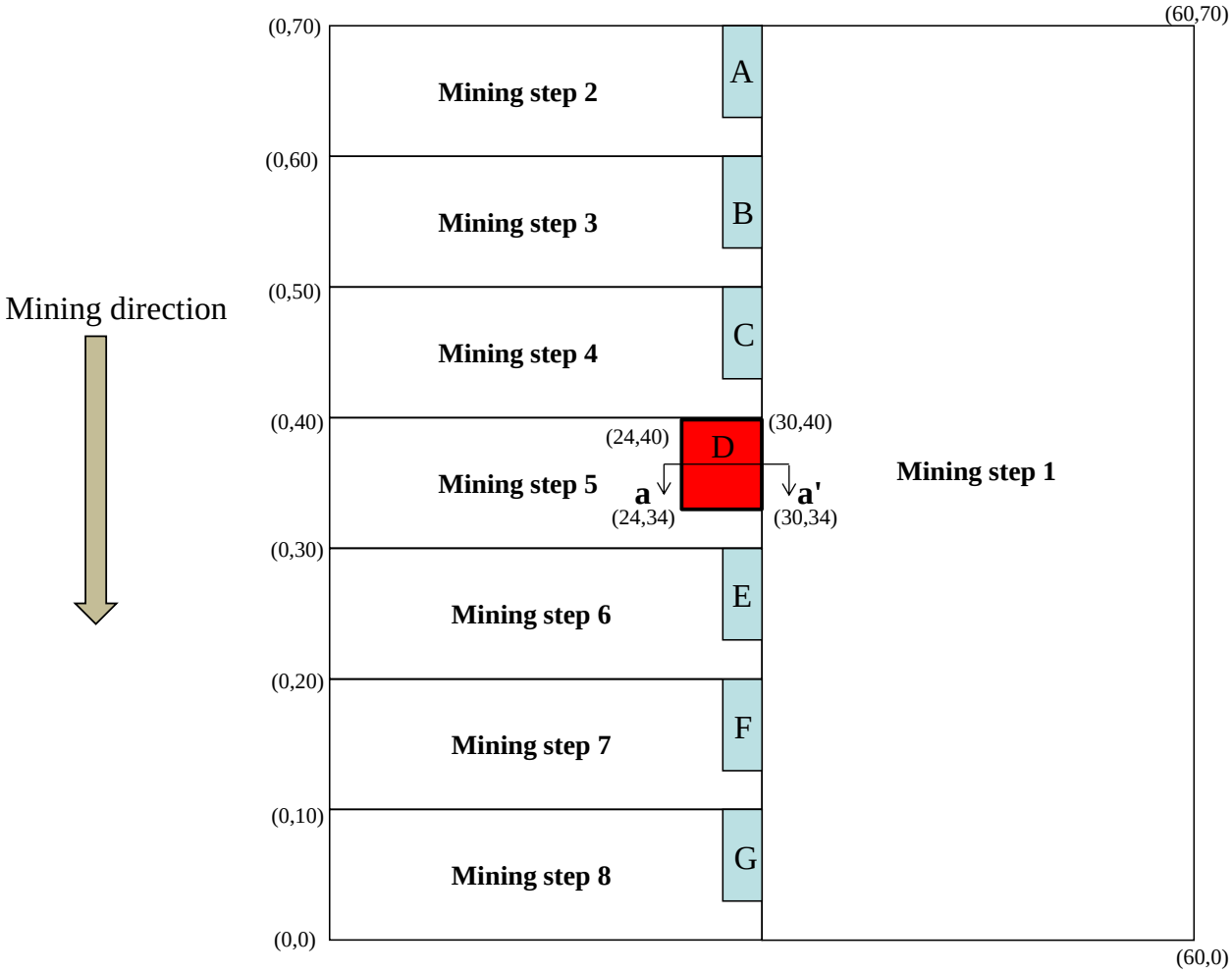

Figure 4.5: Geometry used to simulate the effect of an oversized crush pillar (D).

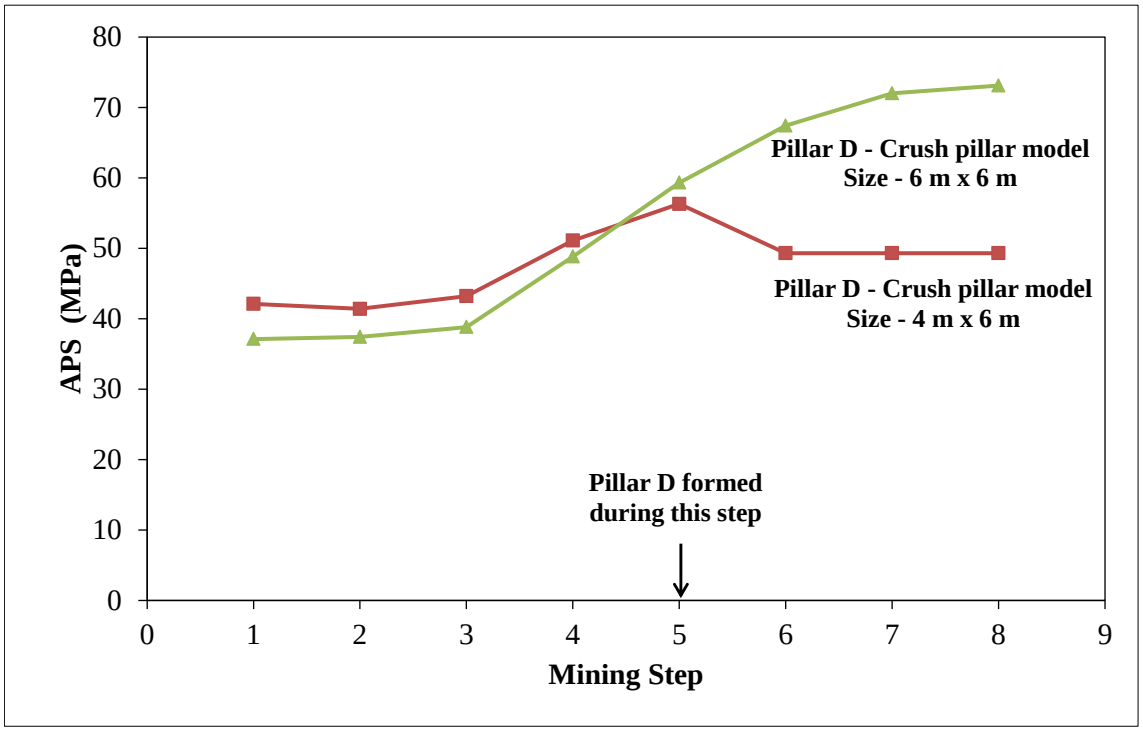

Figure 4.6: Comparison of the APS value on pillar D for the two pillar sizes. Except for this difference in size, all other model parameters were identical. Note that 6 m x 6 m (w:h = 3:1) pillar does not crush to the same extent as the 4 m x 6 m (w:h = 2:1) pillar; (stoping width = 2 m).

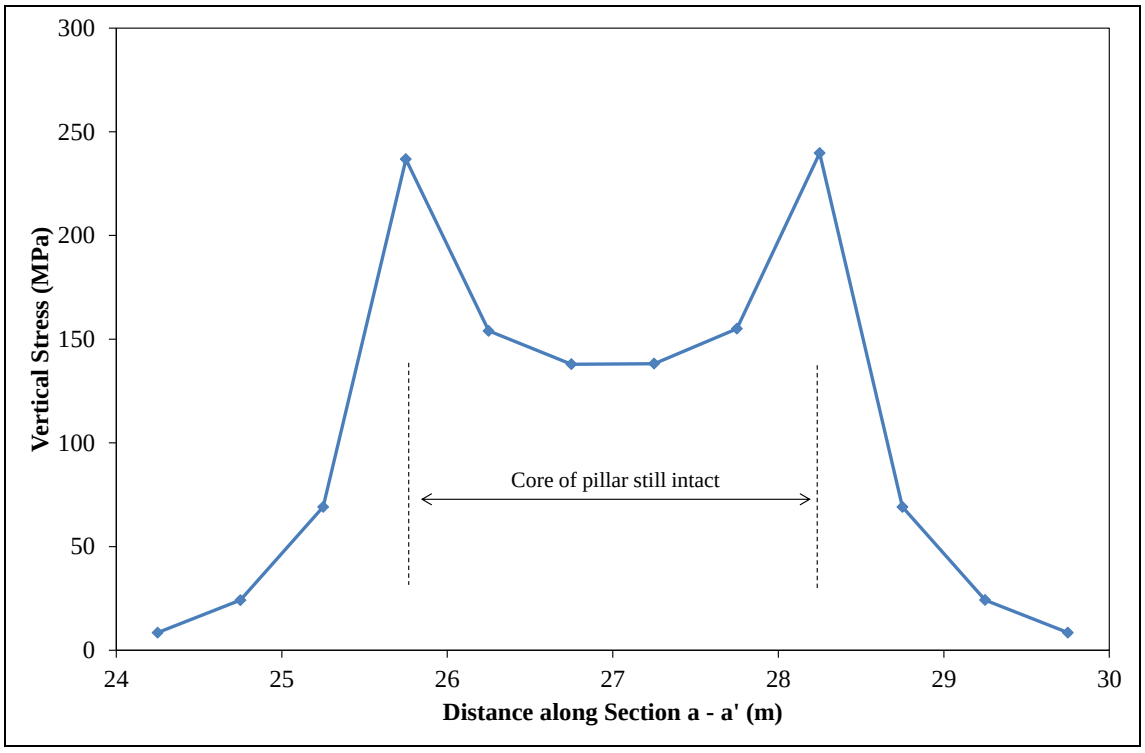

Figure 4.7: Stress profile along Section a - a' (Figure 4.5) for the oversized pillar D after mining step 8.

4.1.2. Effect of rock mass parameters on simulated pillar behaviour

Simulations were conducted to establish the impact of the various rock mass parameters governing the pillar behaviour. Table 4.2 details the various parameters tested for a 4 m x 6 m crush pillar. All of the simulations were compared to the original runs where the parameters used are detailed in Table 4.1. For these simulations, the general parameters were kept constant with only the parameter of interest modified. The results indicate that the simulated pillar behaviour is very sensitive to the parameters used (refer to Figure 4.9). Figure 4.8 illustrates this effect for sets of parameters where pillars can either behave as an elastic non yield pillar, crush in the face or crush in the back area of a stope depending on the combination of rock mass parameters used.

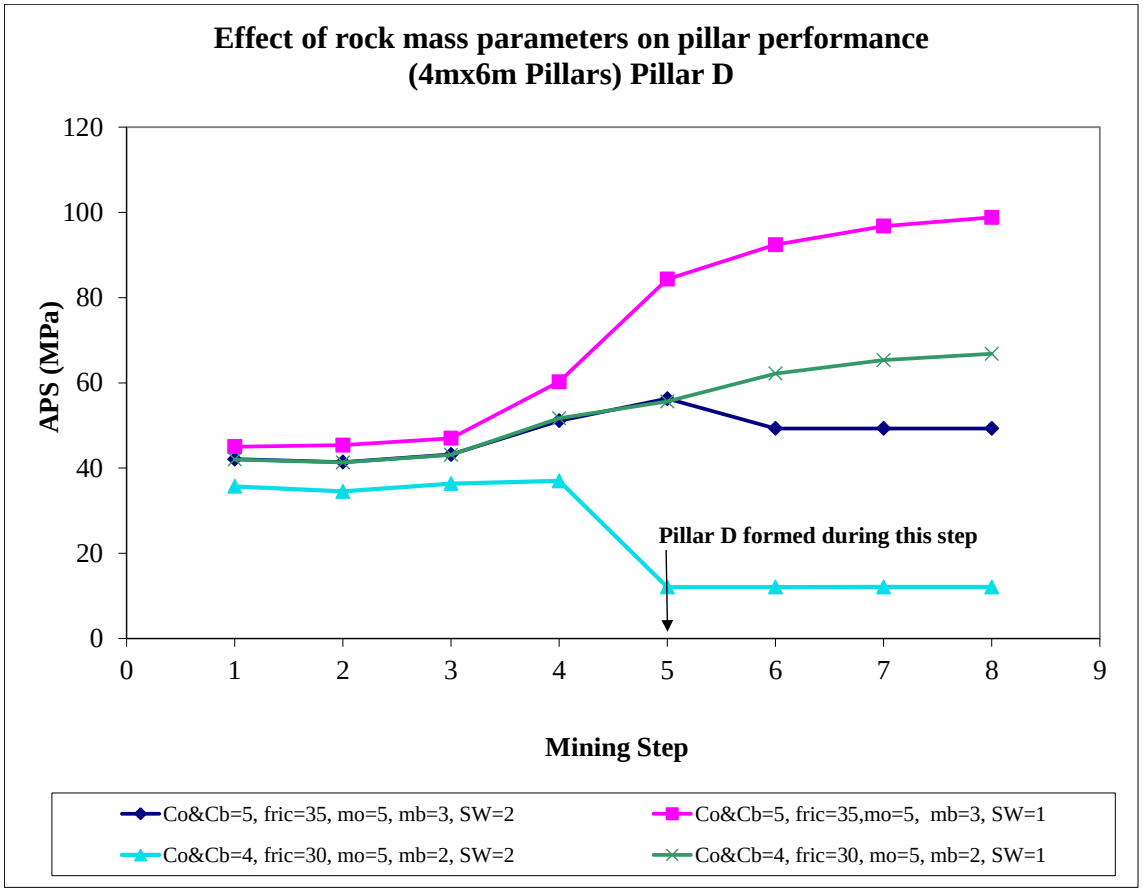

Figure 4.8: Pillar behaviour for different pillar parameters (stoping width (SW) referred to in legend was varied between 1 m and 2 m as indicated).

Table 4.2: Parameters used for comparative analysis to determine the effect on the simulated pillar behaviour. The table details the range of parameters and not necessarily the combination of parameters used.

Combination of Parameters used in simulations										
Friction angle										
φ (degrees)	35	33	30	27						
Material strength										
C_0 Intact (MPa)	5	5	5	4	3					
C_b Crushed (MPa)	5	4	3	4	3					
Slope parameter (m)										
m_0 Intact slope	5	5	5	5	5	2	2	3	4	4
m_b Residual slope	5	4	3	2	1	2	3	3	3	4

Figure 4.9 is a combined graph indicating the impact of the various parameters for a layout consisting of 4 m x 6 m crush pillars (w:h = 2). It appears as if the original parameters used to test the simulation of pillar crushing with a limit equilibrium model are at the upper limit of the simulations carried out in terms of residual APS. All of the results displayed are for pillar D which is formed in mining step 5 (refer to Figure 4.1 for the simulated layout).

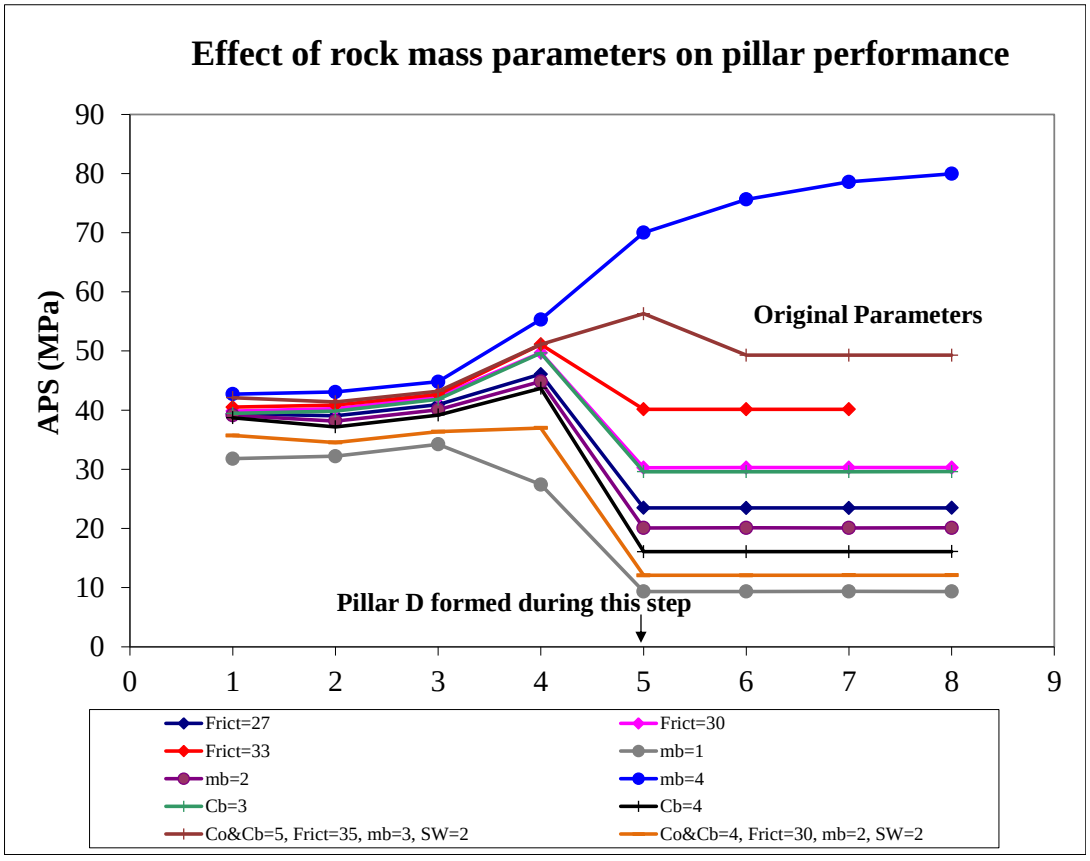

Figure 4.9: Effect of rock mass parameters on pillar behaviour (4 m x 6 m pillar – w:h = 2:1).

Effect of material strength

The material strength parameter allows for the free standing face condition. At the pillar edge, the unconfined strength of the material (failed state) is equal to C_b, assuming that there is no horizontal stress present at the pillar edge along the reef plane. At this point, $C_b = \sigma_n$ implying that the pillar can withstand some vertical load at the unsupported edge.

The effect of both intact (C_0) and the crushed material residual strength (C_b) was investigated. From Figure 4.10 and Figure 4.11 it can be seen that the combinations of inputs affect the overall pillar behaviour (early versus late pillar crushing) and the residual APS achieved.

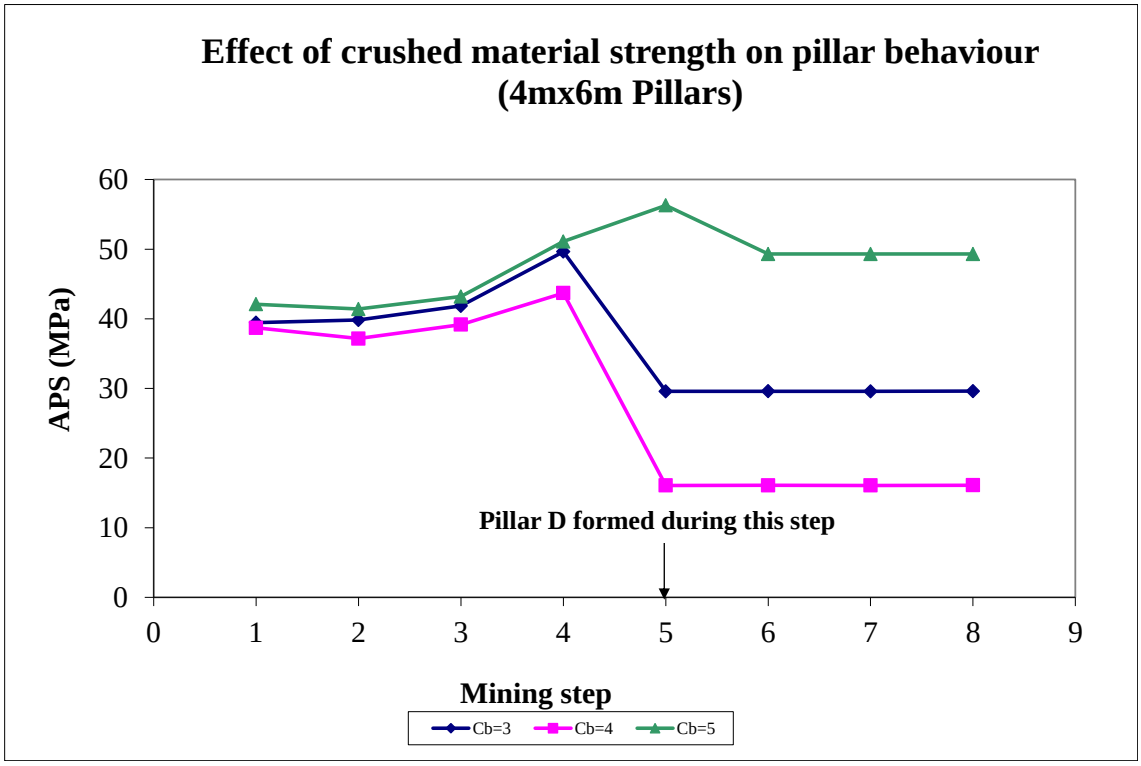

Figure 4.10: Effect of crushed material residual strength on pillar performance (Co: Intact = 5).

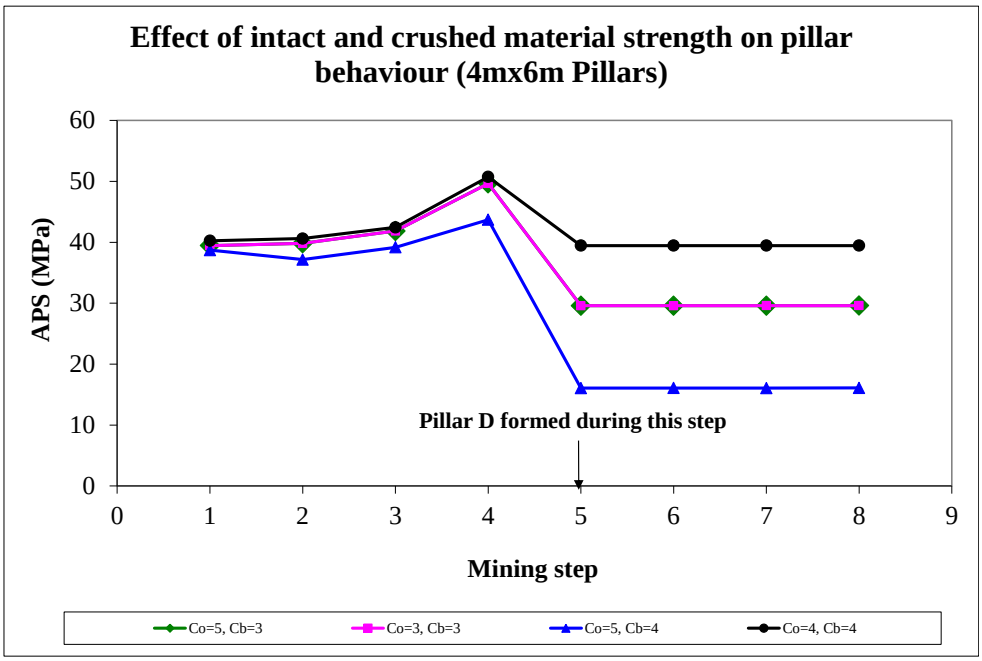

Figure 4.11: Effect of intact and crushed material strength on pillar performance.

Effect of friction angle

The friction angle is the parameter governing the frictional coefficient along the pillar contacts which represents the force resisting the displacement of a slice of material. Figure 4.12 illustrates that higher friction angles result in higher residual pillar stress. In the simulation, a friction angle of 35 degrees prevents the pillar from crushing when formed in the face. This simulation is, however, dependent on the effect of the other input parameters used as well.

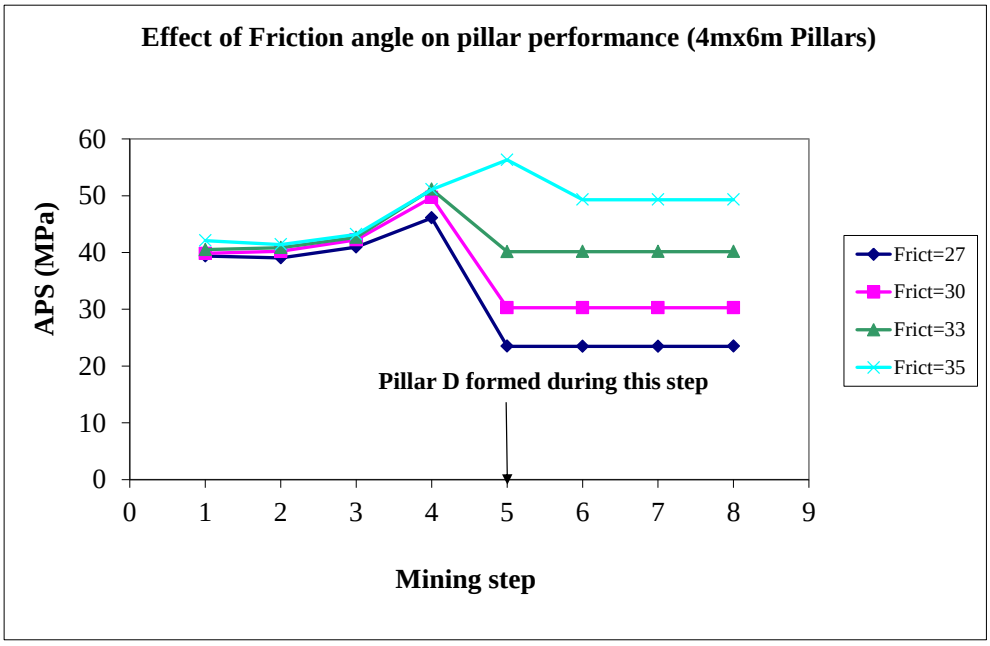

Figure 4.12: Effect of friction angle on pillar performance.

Effect of strengthening parameter (m)

The strengthening parameter (*m*) is the tangent of the failure envelope used in the limit equilibrium model. The intact slope parameter effects the pillar's peak strength and ability to crush. Higher values result in stronger pillars. Figure 4.13 indicates that for higher values of m_0 (intact) a higher pillar stress is required to result in pillar crushing (e.g. $m_0 = 5$). Although, once the peak strength of the pillar has been reached and the pillar fails, the pillar moves to a residual state (e.g. $m_0 = 5$). Late or no pillar crushing can however occur depending on the value of the parameter.

The residual slope parameter (m_b) effects the post failure behaviour and the post-peak response of the pillar. Figure 4.14 illustrates that for higher residual values of m_b, the lower the probability of achieving pillar crushing in the face (also influenced by choice of other parameters).

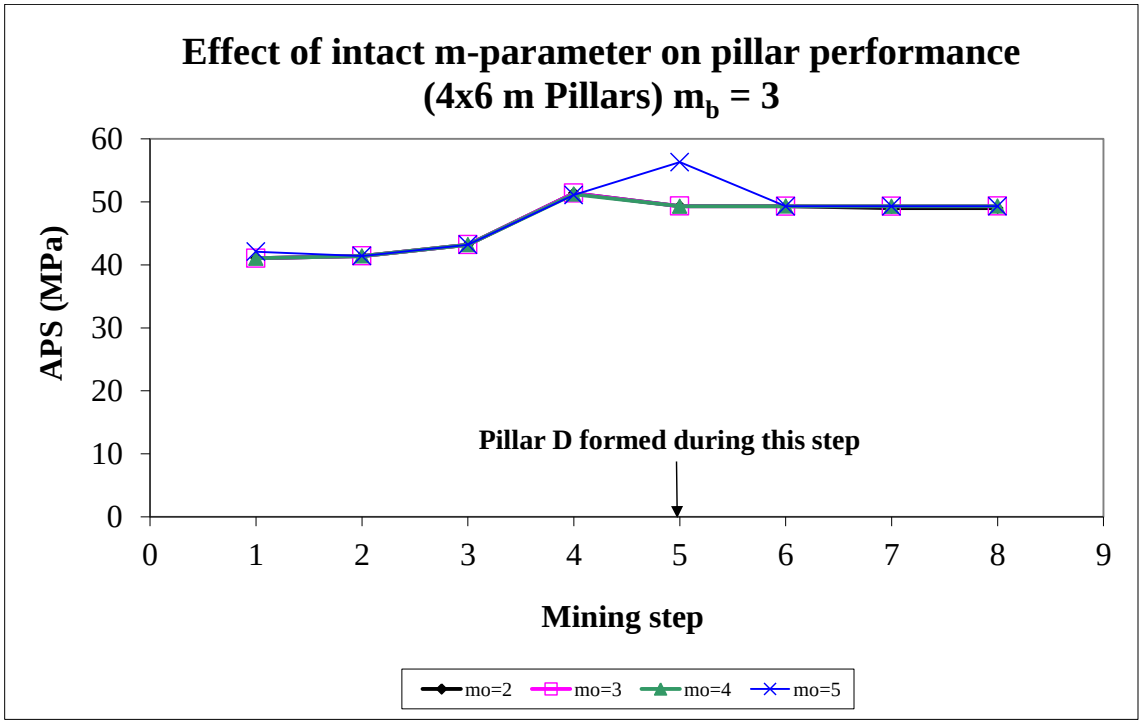

Figure 4.13: Effect of the intact slope parameter on pillar performance ($m_b = 3$).

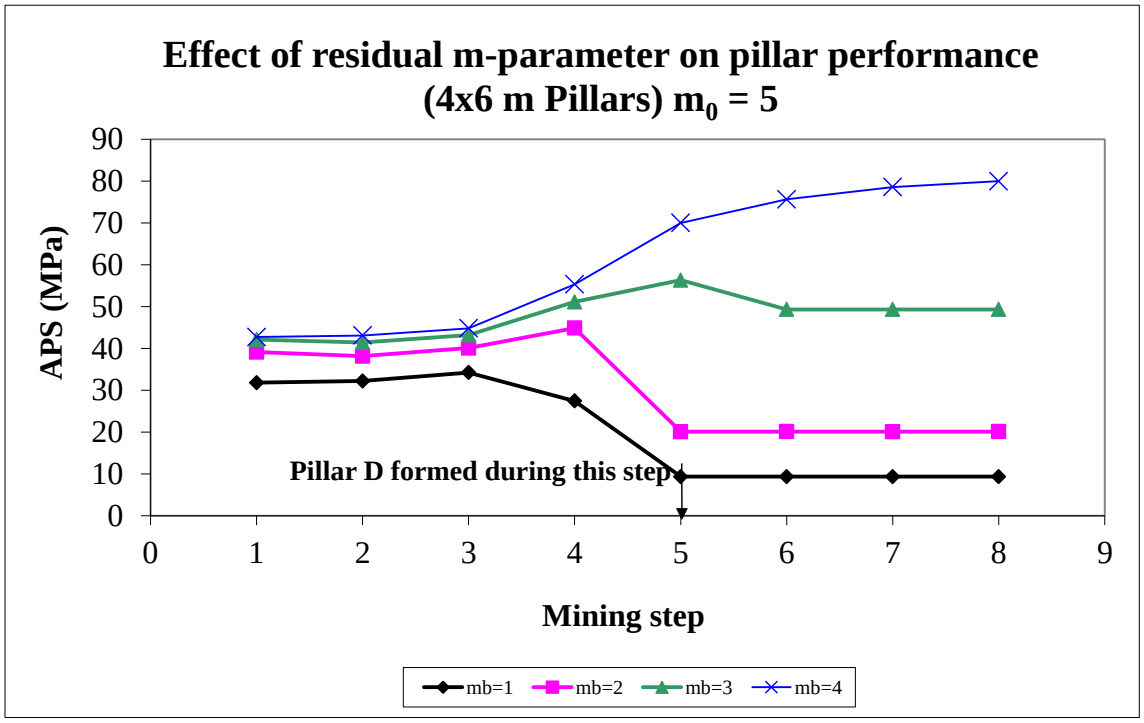

Figure 4.14: Effect of residual slope parameter on pillar performance (m_0 = 5).

4.1.3. Effect of mining parameters on simulated pillar behaviour

In addition to the rock mass properties governing the pillar behaviour, the layout parameters will also greatly influence the stress state and the behaviour of a pillar. These parameters are investigated below.

Effect of pillar size

Various pillar sizes were simulated using the original set of parameters (Table 4.1). All of the conclusions in this section are therefore based on the values assumed for these parameters. The effect of pillar width is illustrated in Figure 4.15. Pillars with a width to height ratio greater than two will most likely not crush and result in "unsatisfactory" behaviour (Jager and Ryder, 1999). The wider pillars will either result in pillar crushing occurring in the back area, or not crushing at all. Figure 4.16 compares the results of three different pillar layouts, each having a different pillar width. The results are for section a – a' through pillar D as indicated in Figure 4.1. The figure indicates the exponential stress increase towards the centre of the pillar. As indicated in the previous chapter, this could however lead to excessively high stresses in the core of wide pillars where a crushed state is not achieved. Note that the stress profile for the w:h = 2:1 pillar is for step 5 and just before the pillar completely crushes and moves to a residual state in step 6 (compare results to Figure 4.15 indicating the stress development as a result of mining). At this point the pillar has completely crushed from the outside towards the centre of the pillar. The pillar core also reaches a maximum stress limit whereafter complete failure of the pillar is reached and the pillar moves to a residual state (as can be seen for w:h = 1.5 pillar). As mentioned, the core of an over-sized pillar does not reach this maximum stress limit

and remains intact. These pillars could potentially burst when fully loaded or punch into the footwall resulting in excessive footwall heave (Jager and Ryder, 1999).

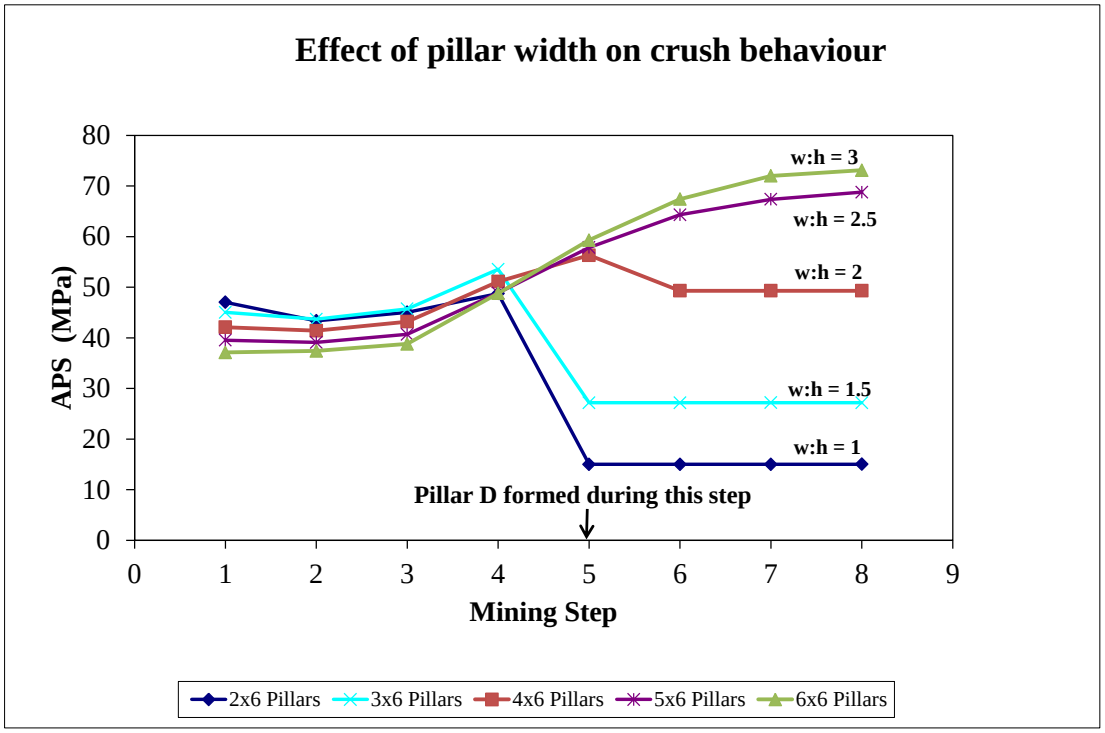

Figure 4.15: Effect of pillar width on pillar performance (600 m below surface).

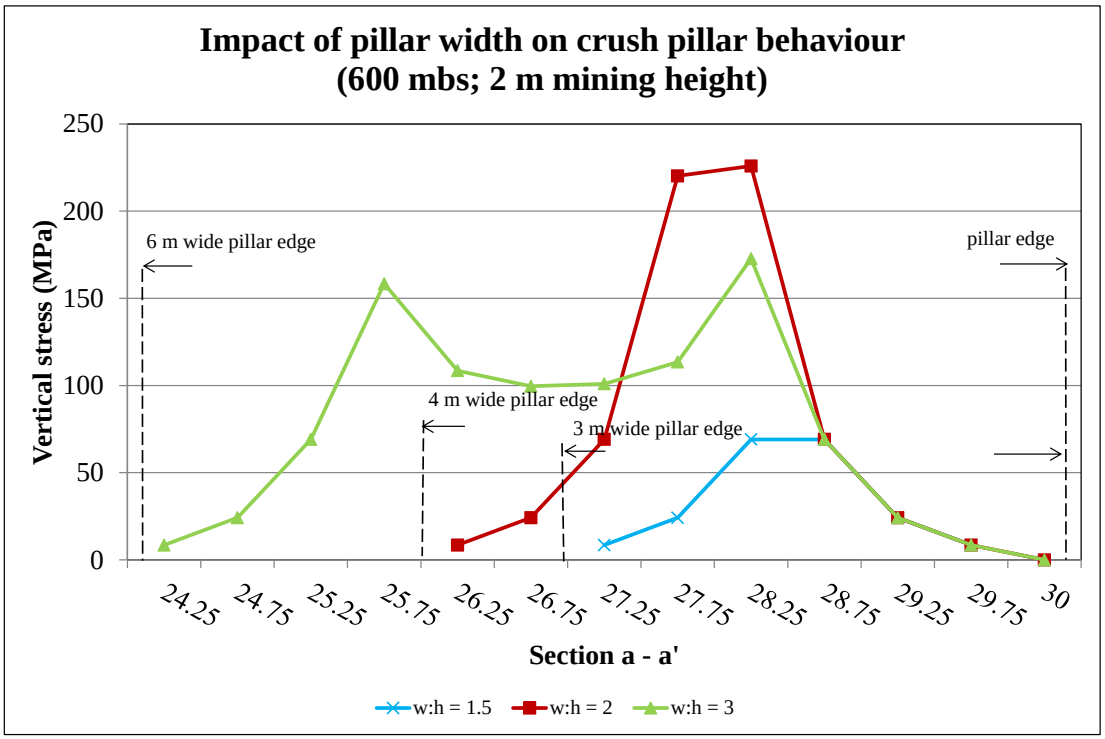

Figure 4.16: Simulated vertical stress along section a – a' for pillars with different w:h ratios.

In addition to pillar width, the effect of pillar length was investigated as a function of pillar performance and pillar crushing. The simulated layouts indicated that almost no increase in pillar stress or behaviour was achieved for crush pillars (w:h = 2) with a width to length ratio of 2, 3 or 4 (refer to Figure 4.17). The smaller pillars had a slightly higher peak stress (≈ 5 MPa or 7% higher) whereas the 8 m long pillars had a higher residual stress (≈ 7 MPa or 12% higher). Nevertheless, all the pillars crushed in the step where they were formed (step 5). Pillar width therefore appears to be the major contributor to the performance of crush pillars.

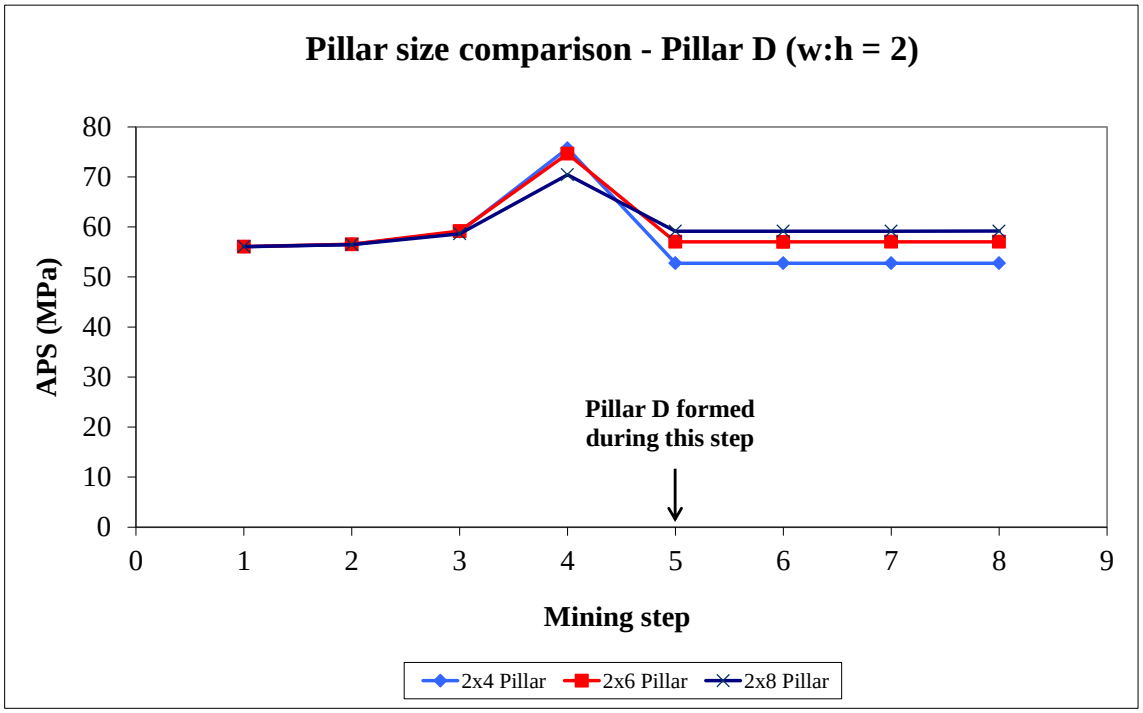

Figure 4.17: Effect of pillar length on pillar performance (600 m below surface; stoping width = 1 m).

Effect of mining depth

Four mining depths were simulated to compare the effect of crush pillar loading and behaviour as a result of mining depth. As expected, the results indicated that the average pillar stress experienced by a pillar before crushing is higher with increased mining depth. The residual pillar stress, which is governed by the modeling parameters (material properties) and pillar width, resulted in the same residual APS. Figure 4.18 highlights the importance of mining depth on crush pillar behaviour. In the figure it can be seen that a crush pillar with a width to height ratio of two (w:h = 2) will not crush at 400 metres below surface (for the assumed model parameters).

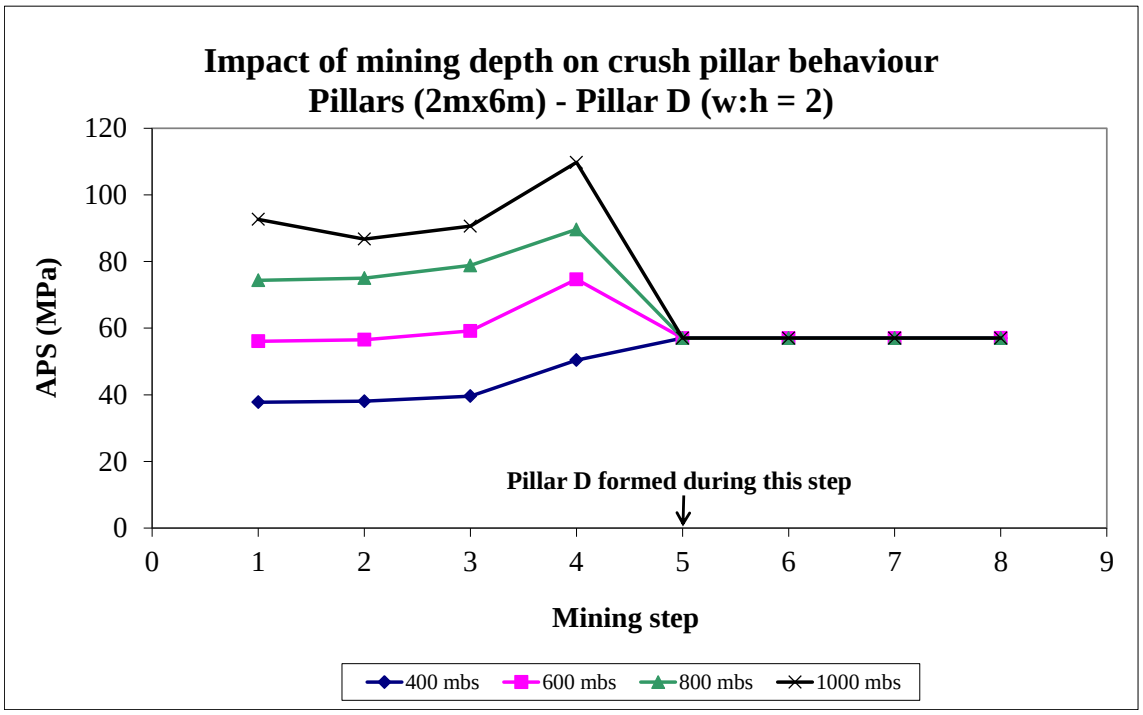

Figure 4.18: Effect of mining depth on behaviour of a 2:1 crush pillar (stoping width = 1 m).

Ozbay and Roberts (1988) suggested that crush pillars should be implemented at a depth greater than 400 m below surface. This was based on the assumption that the average face stress at this depth is large enough to enable crushing of the pillars. On many operations where crush pillars are implemented at relatively shallow depths (i.e. 400 m below surface) pillar crushing is not achieved. At this shallow depth very slender pillars will be required to achieve pillar crushing. Figure 4.19 compares the pillar behaviour of various pillar widths at 400 m below surface. A minimum width to height ratio of 1.5 will be required to ensure that the pillar crushes on the face when it is formed (for the assumed model parameters). This will, however, be very impractical to apply and will be very difficult to achieve (1.5 m wide pillar in a 1 m stoping width) as a result of pillar cutting discipline as well as drilling and blasting practices. Also, there might still be other factors, such as potholes present in a layout, which could further influence the pillar behaviour.

Various pillar widths resulting in various width to height ratios were also simulated for a crush pillar at 600 metres below surface (Figure 4.20). For the entire range of pillar widths simulated, pillar crushing does occur at 600 m below surface whilst the pillar is being cut in the face. The pillar with a w:h = 2 did, however, in comparison to the other pillars result in a relatively high peak stress and residual stress.

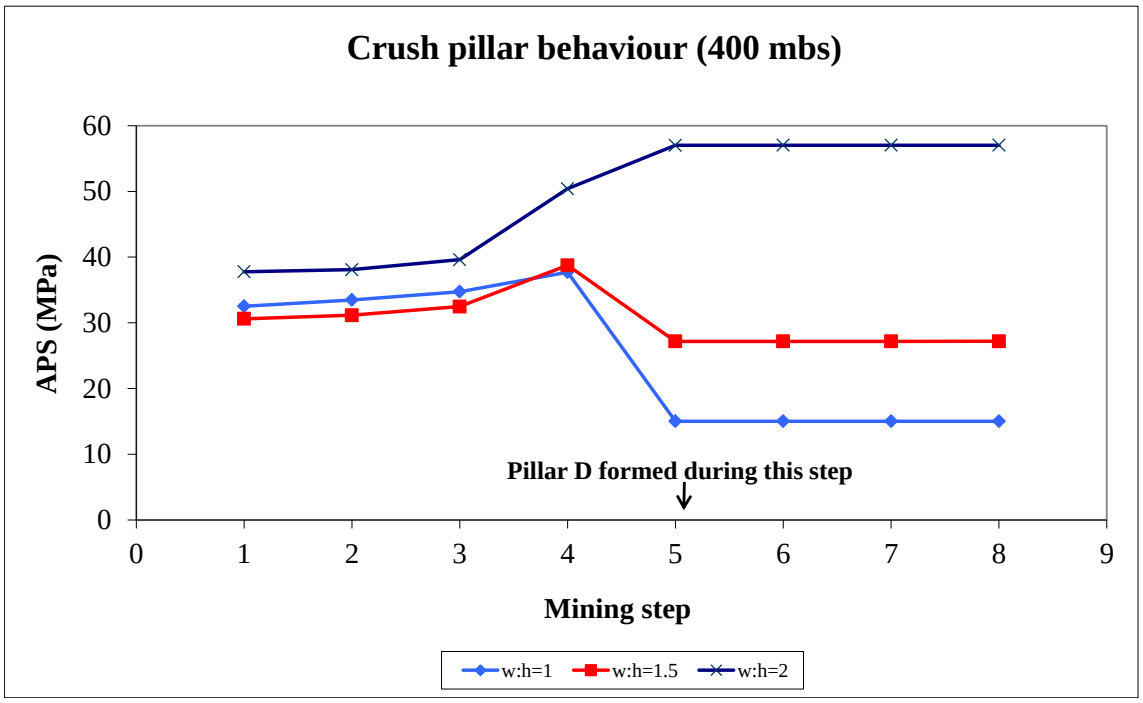

Figure 4.19: Effect of width to height ratio on crush pillar performance at 400 m below surface.

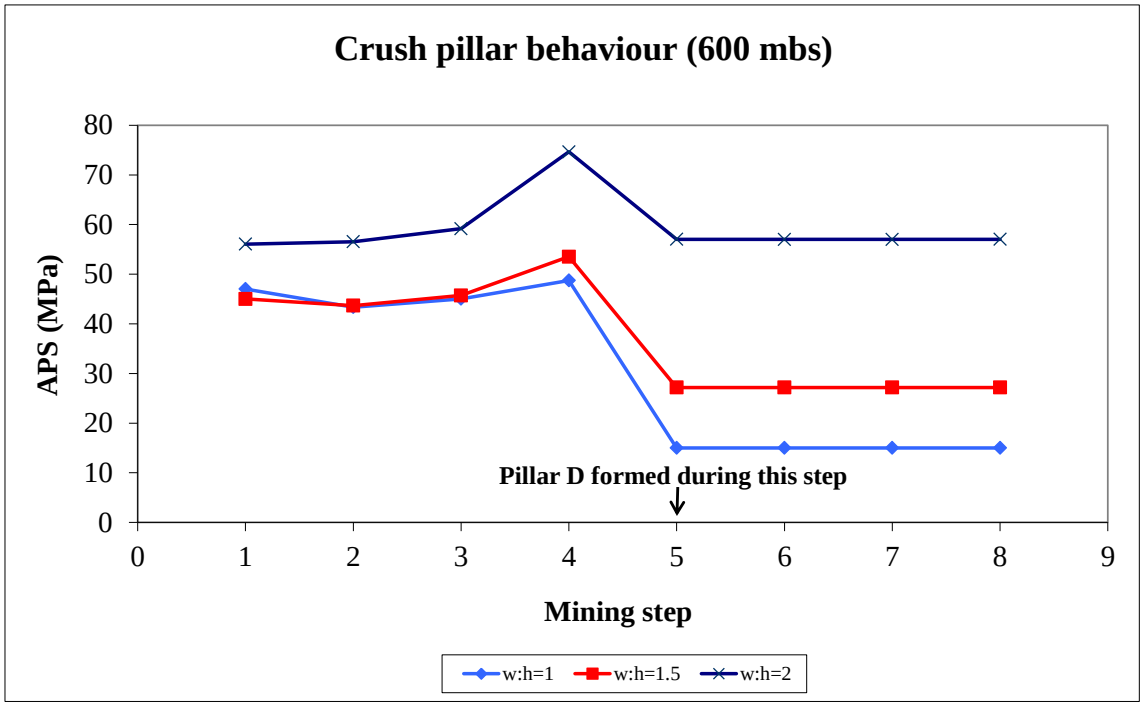

Figure 4.20: Effect of width to height ratio on crush pillar performance at 600 m below surface.

Simulations were conducted for a pillar height of 1 m and 2 m for two layouts having the same width to height ratio (w:h = 2). The pillars at the lower stoping width (2 m wide pillar, 1 m high stoping width), had higher initial, peak and residual stress levels. At 600 m below surface the larger pillars (4 m wide pillar, 2 m high stoping width) crushed slightly later (step 6) as it achieved its peak stress whilst being cut and then only moved to the residual state (Figure 4.21). Figure 4.22 indicates the stress profile along section a - a' through pillar D for these two layouts (mining step 5). Similarly Figure 4.23 compares the stress profile from the edge of pillar D, over the pillar holing and ahead of the solid mining face (long axis of the pillar line; section b – b') for both a 1 m and 2 m mining height (for mining step 5). The 2 m wide pillar (1 m stoping height; SW = 1) did experience pillar crushing whilst the pillar was being formed at the mining face. In both cases, significantly high face stresses are achieved in the first approximately 2 m ahead of the mining face. This is sufficiently high to initiate early pillar crushing whilst the pillar is being formed at the face. This is, however, not achieved for larger pillars with w:h > 2:1. Lower pillar edge stress is achieved for the pillars with larger w:h ratios (110 MPa for a pillar with w:h = 3:0 compared to 189 MPa for a pillar with w:h = 2:0).

These results illustrate the importance of stoping width on the overall performance of crush pillars at this depth. The wider pillars are at a lower initial stress and do need more time to crush, even if at the same width to height ratio. When simulated at increased depth, the pillar stress for both scenarios (pillar height of 1 m and 2 m) were sufficient to induce pillar crushing. Here again the narrower pillars experienced higher stress levels (compare Figure 4.18 and Figure 4.24).

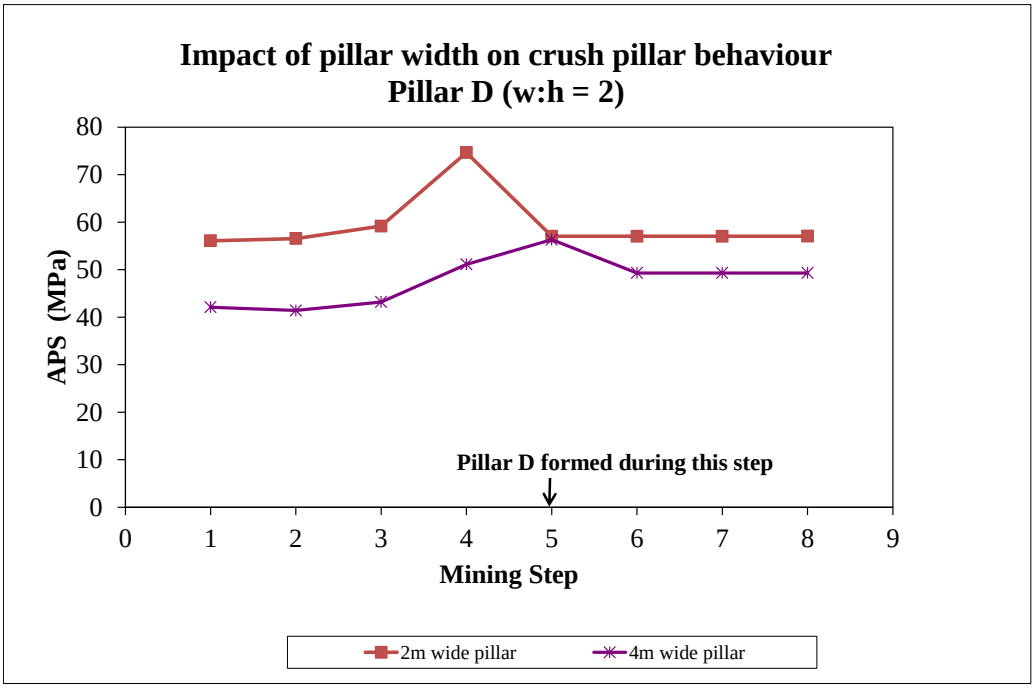

Figure 4.21: Effect of pillar width on pillar behaviour for w:h = 2:1 pillar (mining height: 1 m versus 2 m).

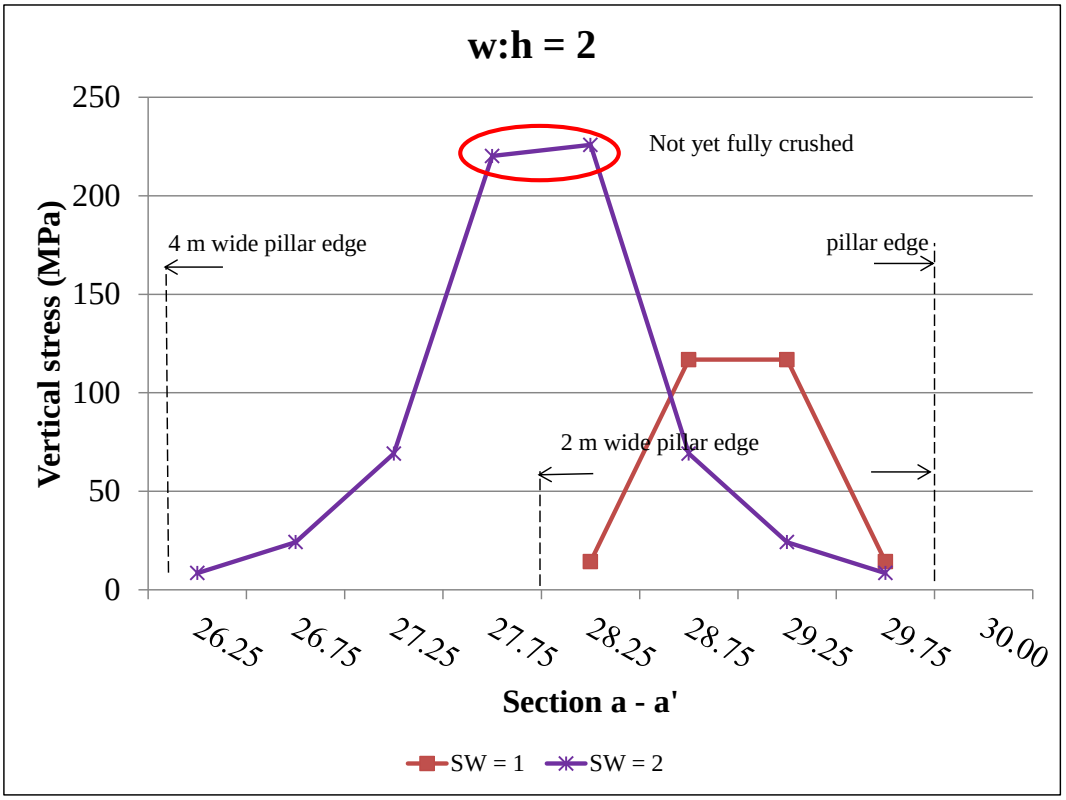

Figure 4.22: Effect of stoping width (SW) on pillar behaviour for pillar w:h = 2:1 along section a – a' through pillar D.

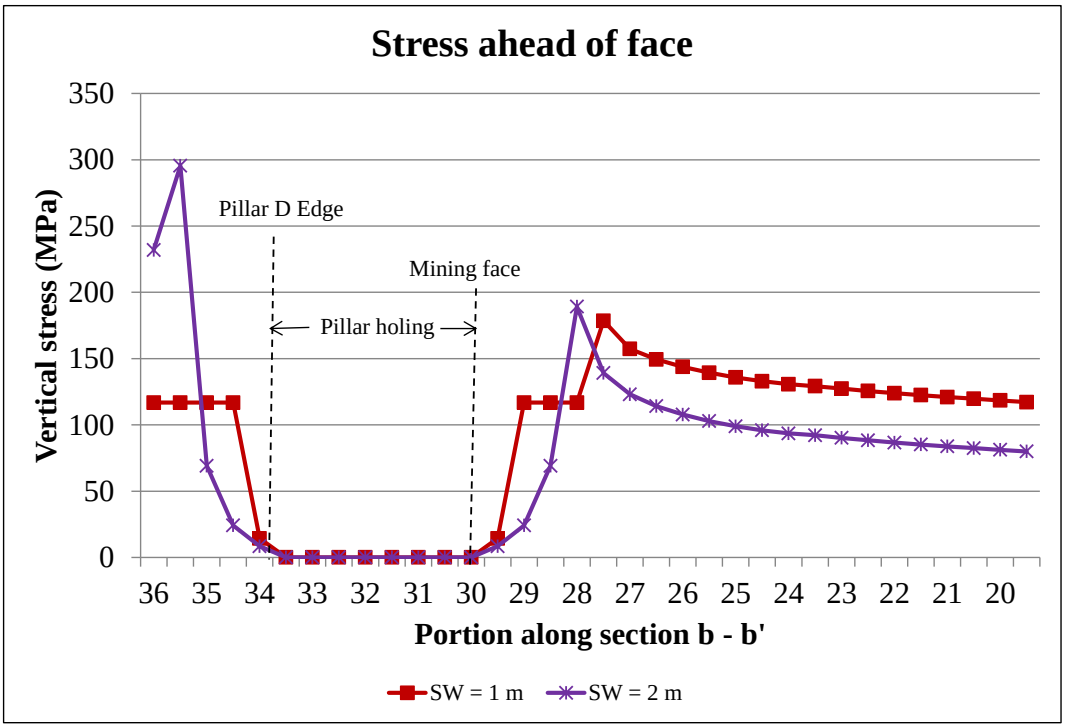

Figure 4.23: Effect of stoping width on pillar behaviour for pillar w:h = 2:1 along section b – b' (mining step 5).

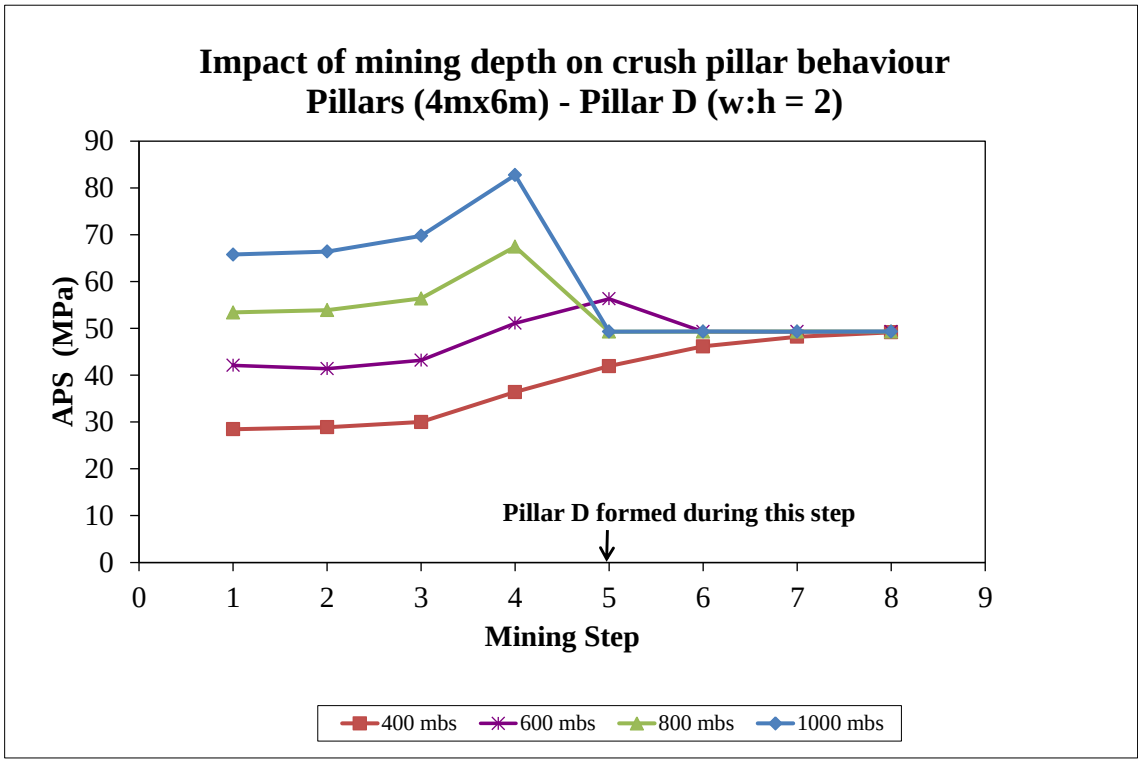

Figure 4.24: Effect of mining depth on behaviour of a 2:1 crush pillar (stoping width = 2 m).

In the previous section (Effect of pillar size) it was demonstrated that a minimum width to height ratio of two is required to ensure that pillar crushing is achieved. Figure 4.19 further illustrates that for pillar crushing to occur at 400 m below surface the pillar width will have to be reduced. Figure 4.25 and Figure 4.26 illustrates that even at increased depths (i.e. 800 m and 1000 m below surface) a minimum width to height ratio of two is required to ensure that pillar crushing is achieved (based on the assumed parameters).

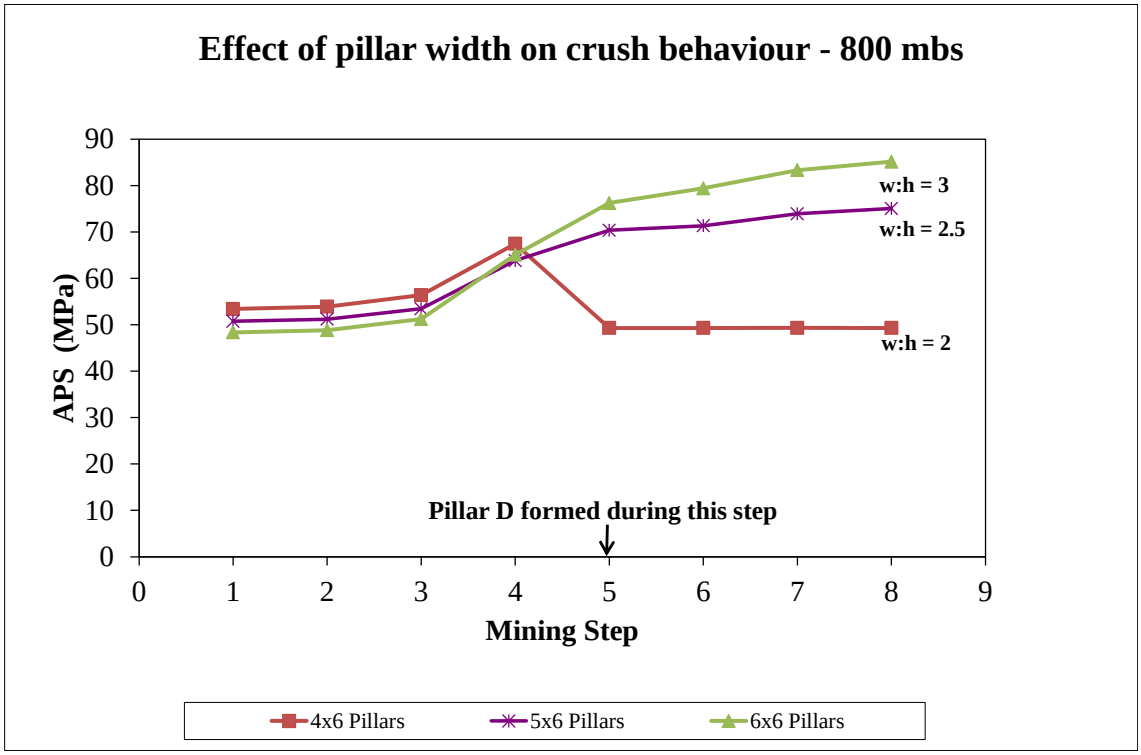

Figure 4.25: Effect of pillar width on pillar behaviour (800 m below surface) - stoping width = 2 m.

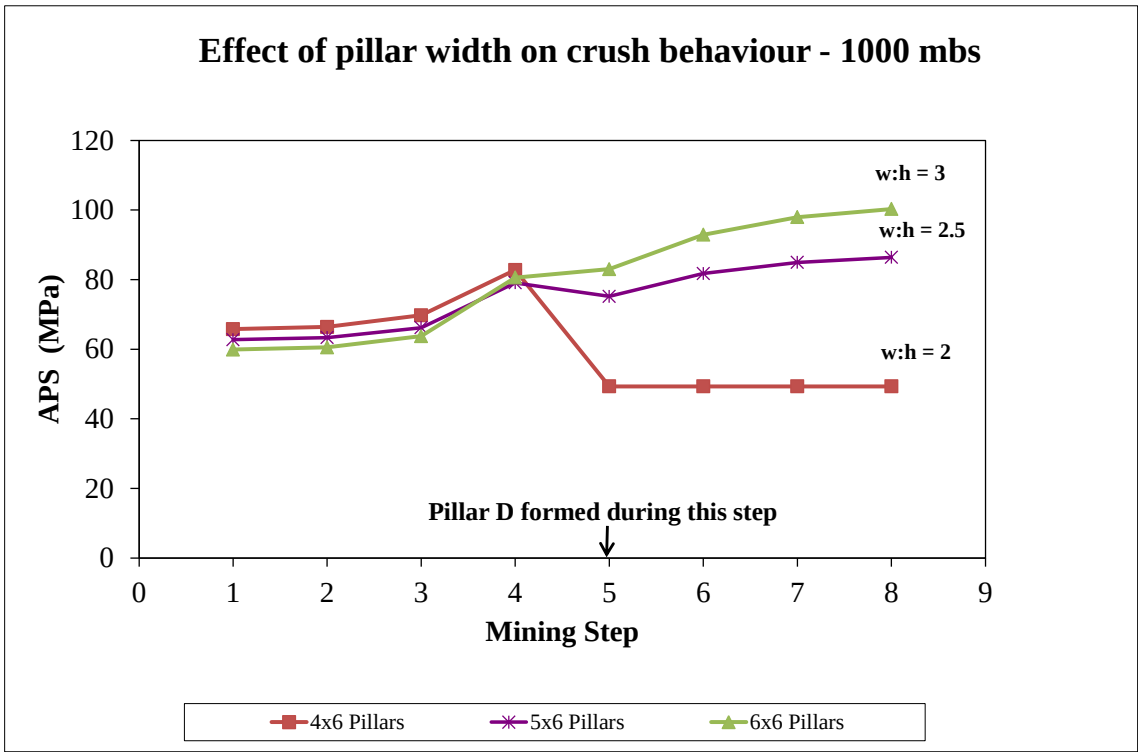

Figure 4.26: Effect of pillar width on pillar behaviour (1000 m below surface) - stoping width = 2 m.

4.2. Summary

In this chapter the behaviour of slender in-stope pillars were evaluated using numerical simulations of an idealised crush pillar layout. The pillar behaviour (crushing) was simulated by a limit equilibrium model which was implemented in the boundary element program TEXAN. The results indicated the ability of the code to simulate crush pillar behaviour. The simulated pillar behaviour indicated that once the peak strength of a pillar is reached, the stress increase can cause complete failure of the core of the pillar and the pillar assumes a residual state. This allowed for the investigation of various parameters influencing the behaviour of crush pillars as found in typical mine layouts. The objective was to use a simple representative model as an investigation tool of the behaviour of crush pillars in a representative layout. The purpose was to understand when pillars will crush, where they will crush relative to the mining face and why some pillars can potentially burst.

A sensitivity analyses was conducted to determine the effect of each input parameter on the behaviour of the model and simulated pillars within the layout. Note that these values were chosen arbitrarily. The intent was to establish trends regarding the pillar behaviour, even though the parameters used may not represent the actual environment. The results indicated that the choice of parameters gave qualitative agreement with observed crush pillar behaviour and previous underground measurements. Calibration of the model, based on the underground trial measurements and laboratory rock testing to establish appropriate rock mass parameters, are required to substantiate the preliminary conclusions.

The effect of oversized pillars was investigated. Oversized pillars, which are typically encountered underground, either do not crush or fail violently in the back area. The study highlighted a key attribute of the limit equilibrium model: The pillar stress of a failed pillar increases in an exponential fashion towards the center of the pillar. This may lead to the formation of unduly high stresses in the core of wide pillars. The simulated results indicated that the core of the oversized pillars were still intact. As the oversized pillars did not crush at the face, these intact pillars move into the back area as the mining face advances. In the back area, the pillar is at a higher stress. The change in stress caused by a mining increment is lower compared to when the pillar is formed at the face. The pillar may therefore either not crush (especially when oversized) or fail violently as the stress on these pillars are much higher and the loading environment has become softer.

Simulations were conducted to determine the effect of both pillar size with regard to width to height ratio and pillar width required to achieve pillar crushing at various depths.

The preliminary results based on the assumed model parameters indicated that:

- A crush pillar system should not be implemented shallower than 600 m below surface.
- A maximum width to height ratio of 2:1 is required to ensure that slender in-stope pillars crush at the face whilst they are being cut.
- If crush pillars are to be implemented at depths shallower than 600 m below surface, the width of the pillars will have to be reduced (e.g. w:h = 1.5 is required at 400 m below surface). This might not be practical to implement as pillar dimensions must also cater for out-of line mining and blast effects. Furthermore the overall behaviour of the pillars could still be effected by the influence of mining losses and geological features which will add to the stability of the rock mass. A minimum practical pillar width of 2 m (1 m stoping with) will only crush at 600 m below surface (w:h = 2:1).
- Pillar length does not appear to have a significant impact on crush pillar behaviour for pillar width to length ratios (w:l) of up to four. Infinitely long pillars were also simulated which indicated that the initial stress level of these long pillars are reduced and that pillar crushing is either delayed or not achieved. In these simulations the pillars had a w:l > 6 (36 m long pillar) which is rather uncommon in an underground scenario.
- Different mining heights require different pillar widths for a constant width to height ratio (w:h = 2). The results from the simulations indicated that the narrower pillars implemented as a result of the lower stoping width (2 m wide pillar, 1 m high stoping width), had higher initial, peak and residual stress levels. At 600 m below surface, the larger pillars (4 m wide pillar, 2 m high stoping width) crushed slightly later as it achieved its peak stress whilst being cut and then only moved to the residual state during the next mining step. In both cases, significantly high face stresses were achieved in the first approximately 2 m ahead of the mining face. This was sufficiently high to initiate early pillar crushing whilst the pillar was being formed at the face. This is, however, not achieved for larger pillars with w:h > 2:1. Lower pillar edge stress is achieved for the pillars with larger w:h ratios.
- This does signify the importance and impact of stoping width on the overall performance of crush pillars. Wider pillars are at a lower initial stress and therefore need more time to crush, even if at the same width to height ratio. When simulated at increased depth, the pillar stress for both scenarios (pillar height of 1 m and 2 m) were sufficient to induce pillar crushing. However, narrower pillars experienced higher pillar stresses.

4.3. References

Canbulat, I., Grodner, N., Lightfoot, N., Ryder, J.A., Essrich, F., Dlokweni, A., Wilkinson, C., Krog, G. and Prohaska, G. (2006). The determination of loading conditions for crush pillars and the performance of crush pillars under dynamic loading. SIMRAC project SIM040302, Johannesburg.

Jager, A.J. and Ryder, J.A. (1999). *A handbook on Rock Engineering Practice for Tabular Hard Rock mines*. SIMRAC, Johannesburg.

Ozbay, M.U. and Roberts, M.K.C. (1988). Yield pillars in stope support. *Proceedings SANGORM Symposium in Africa*, Swaziland, pp. 317-326.

CHAPTER 5

THE EFFECT OF LAYOUT PARAMETERS ON CRUSH PILLAR BEHAVIOUR

Potholes, mining losses and sidings

5. EFFECT OF LAYOUT PARAMATERS ON CRUSH PILLAR BEHAVIOUR

The geological environment should be a key consideration when implementing a crush pillar system as the pillar behaviour is not only determined by depth and rock properties. Factors which affect the pillar stress can influence pillar crushing. Poor mining discipline resulting in unfavourable layouts also impact on the size of pillar cut at the mining face. Although these are common occurrences on most mines using crush pillars, these elements have historically not been identified as factors prohibiting pillar crushing or inducing pillar seismicity. In this chapter, the influence of mining losses (potholes) and the use of sidings will be investigated as possible factors impacting on crush pillar behaviour.

5.1. Mining and geological losses (potholes)

On many operations pillar crushing does not occur. In the previous chapters, many of the contributing factors have been highlighted. One of the most prominent contributors has not been quantified up to now. Underground, non-minable blocks of ground are left *in-situ* where poor ground conditions prevail or geological features are intersected. The geological features could include faults, dykes, Iron Rich Replacement Pegmatite (IRUP), significant undulating reef or potholes. In the Bushveld Complex (BC), potholes, on most operations, make up the largest component of these "mining and geological" losses. Pothole losses can contribute to an extraction loss of between 5 – 25 percent.

A pothole may be described as a circular or elliptical area (Figure 5.1) in which portions of the footwall succession of the Merensky or UG2 Reefs are absent, so that the reef and its hangingwall layers transgress into this area with an inward or centripetal dip (Farquhar, 1986). The pothole depression is normally defined by the bottom contact of the Merensky or UG2 Reefs, which is not at normal elevation, and clearly crosscuts stratigraphic layering in the footwall. Reef that is contiguous and changes dip or thickness significantly, but without this crosscutting field relationship, is termed "rolling" reef (Carr et al, 1994).

Figure 5.1: Photograph of potholing in a UG2 Opencast operation in the Bushveld Complex.

As an example of the extent and impact potholes have on an ore-reserve, a mining area on Lonmin Platinum, which is situated along the Western Limb of the Bushveld Complex, was assessed. The area is known to have an above average pothole density. Potholes at the Lonmin site vary in size from 5 m to 420 m in diameter. From a seismic survey conducted, the geological losses associated with the potholes structures across the K3 decline and K4 resource block (Figure 5.2) were analysed. The area, comprising 1574 potholes, was assessed to determine the size, size distribution and spacing between the potholes. Most of the pothole diameters range from between 20 m and 100 m (Table 5.1). No potholes with diameters less than 12 m were detected by the seismic survey as these may be smaller than the resolution of the survey. The largest pothole is approximately 420 m in diameter. The spans between adjacent potholes were assessed and it was determined that in the majority of cases (93 %), the spans are less than 100 m (Figure 5.3). There are nevertheless some very large spans, the maximum being approximately 260 m.

Potholes have the advantage that they add to the regional stability as the structures are commonly not mined and blocks of ground are left surrounding potholes. The structures can therefore be incorporated as part of the regional stability strategy in the form of regional pillars. Due to the irregular size, shape and unpredictable location of these structures, the potholes are located throughout the mining layout. As a result, the potholes can and will be positioned ahead of mining faces and adjacent to in-stope pillars. These structures or mining losses impact on the behaviour of crush pillars as the pillars either do not crush, delayed crushing is experienced or the pillars fail violently. The impact of these unmined blocks of ground situated within a mining layout has to date not been quantified with regard to the effect on pillar crushing.

Furthermore, where potholes are present, violent pillar failure can be exacerbated by the change in reef lithology. The brittle hangingwall Anorthosite commonly replaces the regular Merensky Reef Pyroxenite in a potholed area as the strata slumps.

Table 5.1: Pothole size distribution.

Potholes size range (m)	Number (%)
0 -10	0
10 - 20	10
20 - 30	23
30 - 40	20
40 - 50	16
50 - 100	24
100 - 200	5
200 - 300	1
300 - 400	0
> 400	1

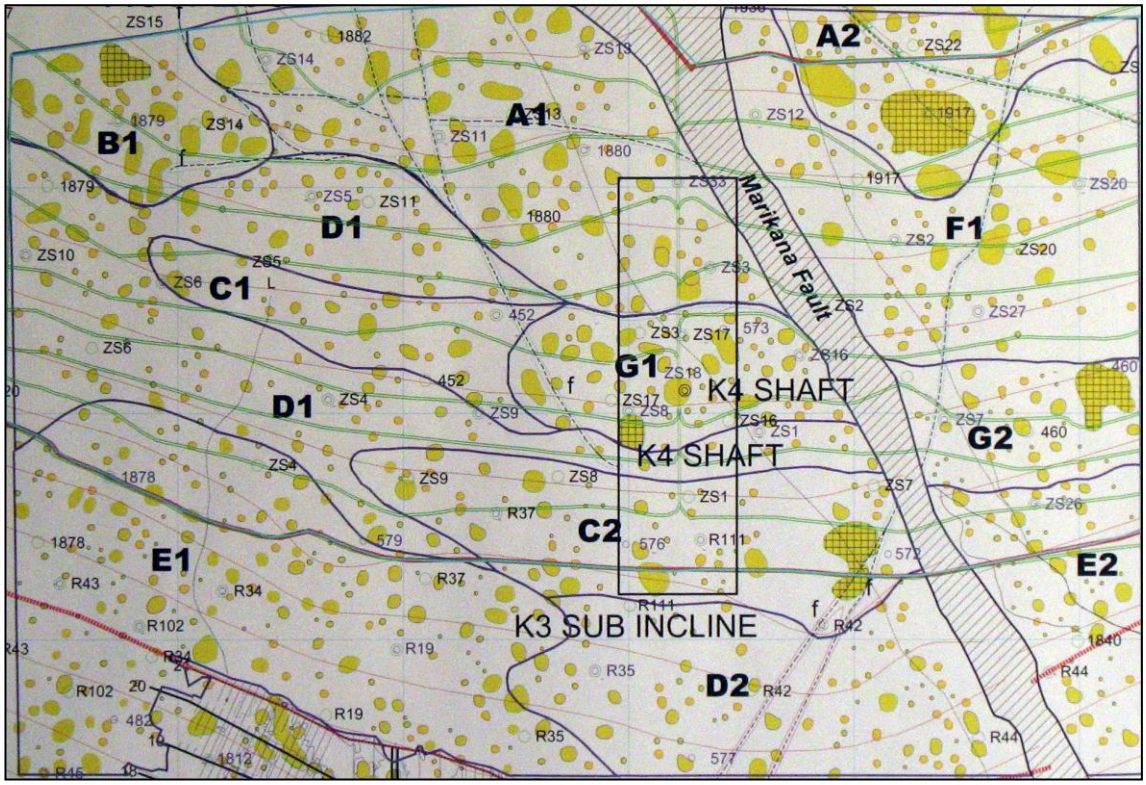

Figure 5.2: Seismic survey indicating density of potholes along the Karee block (area ≈ 6 km x 6 km). The potholes are indicated by the yellow circles.

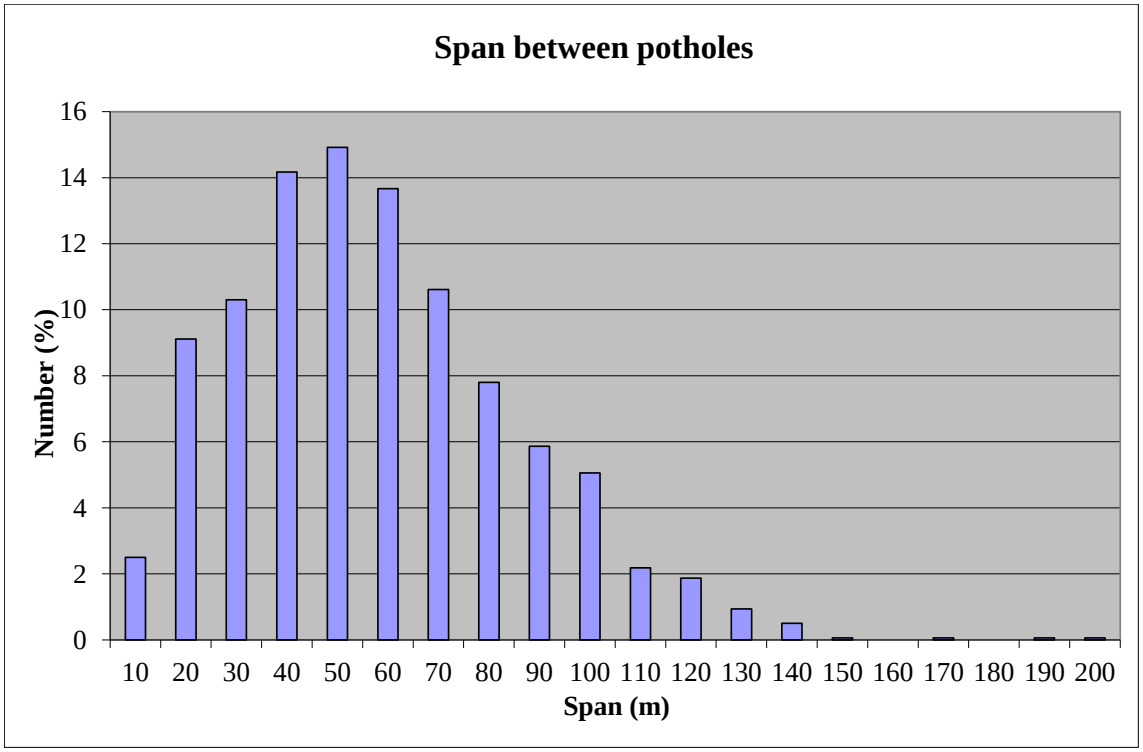

Figure 5.3: Span between potholes.

To quantify the effect of a pothole or mining loss adjacent to a line of crush pillars, the idealised crush pillar layout (Figure 4.1) was adjusted to take these losses into consideration. Various simulations were conducted to determine the effect of an unmined block positioned 5 m from a line of crush pillar. The unmined block was simulated as a square block of which the dimensions [(Xm) x (Ym)] were governed by the percentage extraction locked up by the block (Refer to Figure 5.4). It is therefore a function of the panel size indicated by mining step 1 [*e.g. Pothole area (10m x 10m) versus Step 1 area (30m x 70 m) ≈ 5%*].

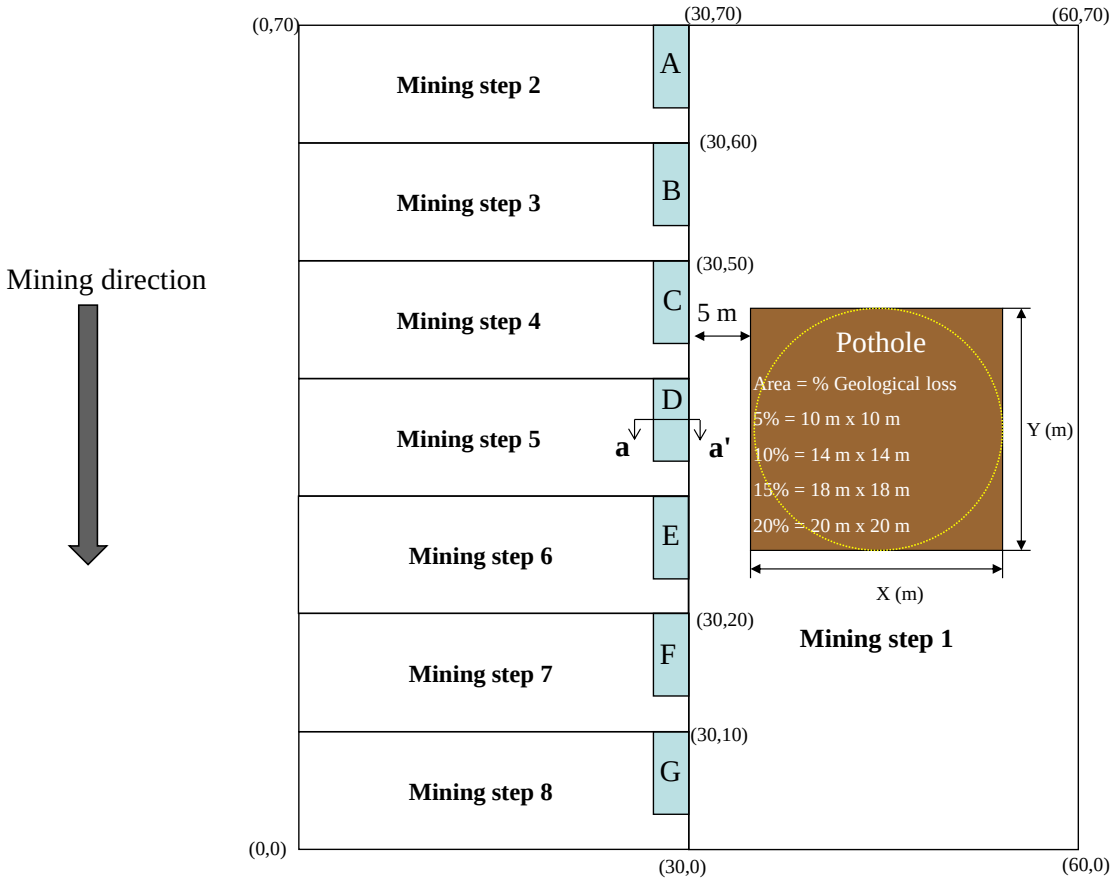

Figure 5.4: Idealised crush pillar layout used to simulate the effect of unmined ground adjacent to a pillar on pillar crushing.

The results summarised in Figure 5.5 highlight the impact of the additional stability added by the pothole on the behaviour of the pillars. For all of the scenarios simulated at 600 m below surface, the pillars did not crush if there is a pothole present 5 m adjacent to the line of crush pillars. To induce pillar crushing, the crush pillar width has to be reduced. Figure 5.6 shows that a width to height ratio of approximately 1.5 is required for the pillars to crush (600 m below surface) when formed at the face when a 10% mining loss is present approximately 5 m from the line of crush pillars. The 5 m distance relates with the distance across a gully and coincides with the width of the gully and sidings cut either side of the gully (adjacent to both the crush pillar and regional pillar or pothole).

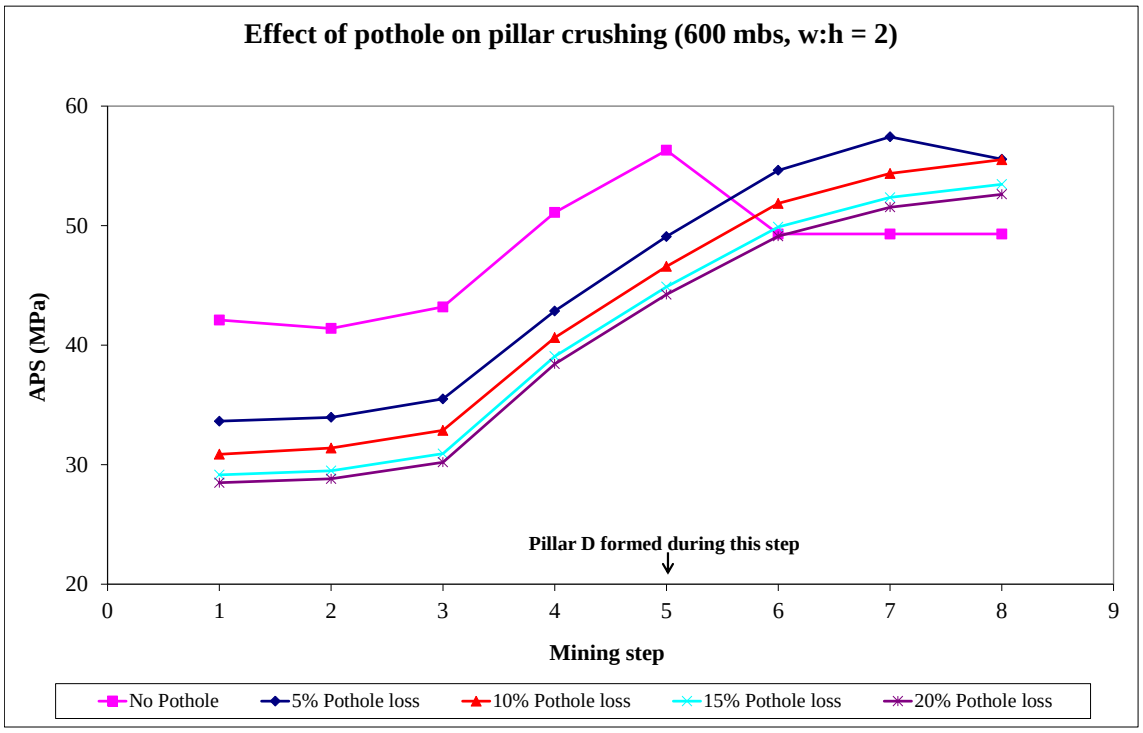

Figure 5.5: Effect of percentage mining loss on pillar crushing at a depth of 600 m below surface (the pothole is positioned 5 m from the pillars).

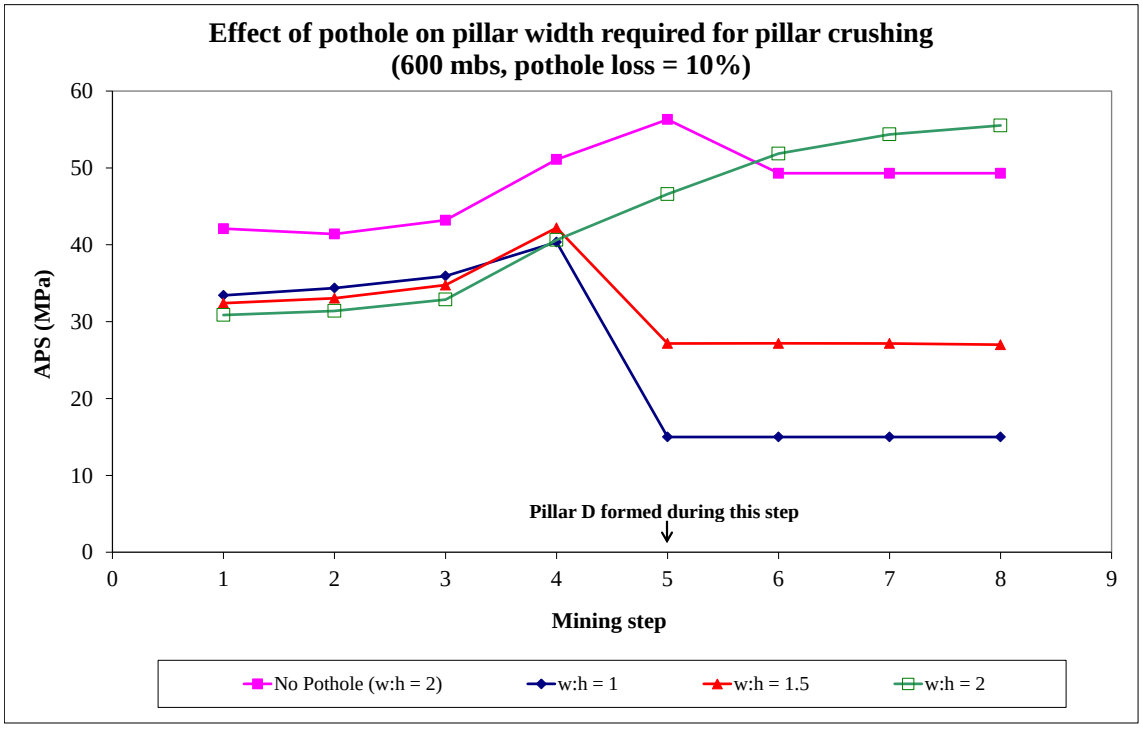

Figure 5.6: Effect of 10% mining loss on pillar crushing at a depth of 600 m below surface (the pothole is positioned 5 m from the pillars).

Further simulations were conducted for increased mining depth (800 m and 1000 m below surface) to determine the impact on the pillar behaviour for the same layout. Figure 5.7 illustrates the effect of higher initial pillar stress as a result of mining depth. All of the pillars achieve a crushed state once formed (mining step 5). For the simulations conducted at 800 m below surface, pillar crushing is reached at the face when either no pothole or a 5% mining loss is present. Delayed pillar crushing is achieved when higher mining losses (>10%) are present. The results from Figure 5.8 indicate that pillars with a width to height ratio of 2 will crush whilst being formed at the face if a 10% mining loss is present 5 m from the line of pillars. A reduced width to height ratio (i.e. w:h < 2) will improve the state of pillar crushing. The results from the simulations conducted for a mining depth of 1000 m below surface indicated that the pillars were all sufficiently stressed to crush for all of the percentage mining loss scenarios simulated (Figure 5.9).

These results highlight the importance of taking the geological environment into consideration when implementing a crush pillar system as the pillar performance is not purely governed by mining depth. The pillar stress is impacted on by the additional stability provided by unmined blocks of ground. This causes a reduction in the pillar stress and prevents effective pillar crushing. To overcome this, smaller pillars will have to be cut, which could be impractical.

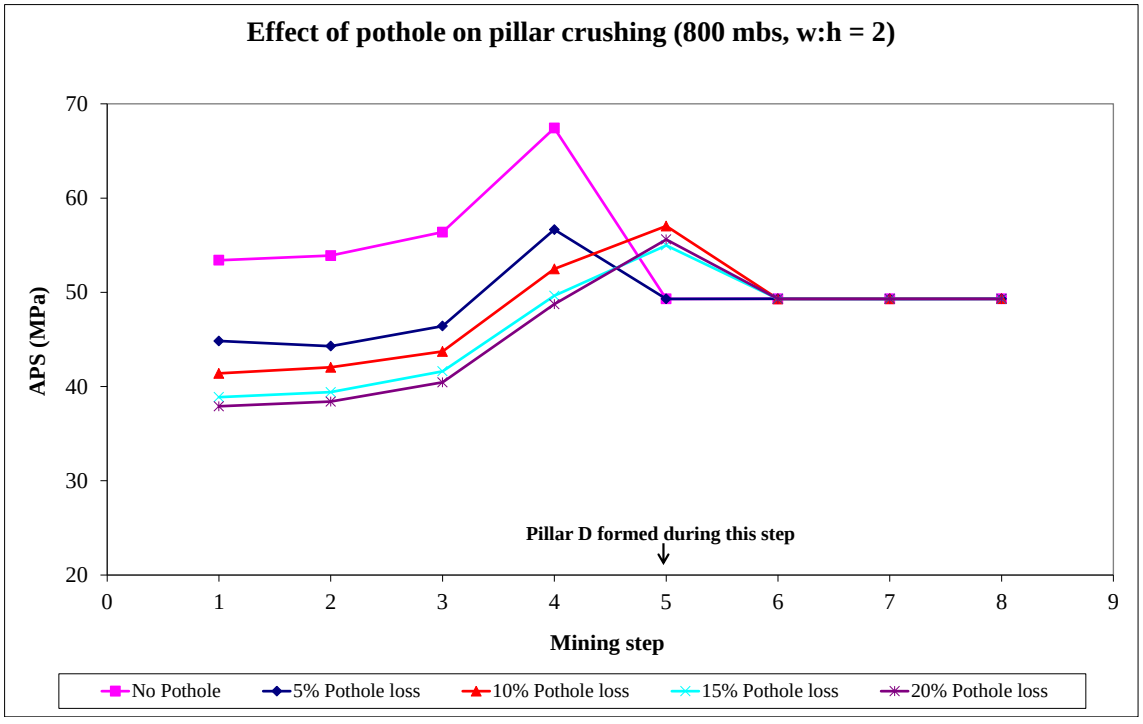

Figure 5.7: Effect of percentage mining loss on pillar crushing at a depth of 800 m below surface (the pothole is positioned 5 m from the pillars).

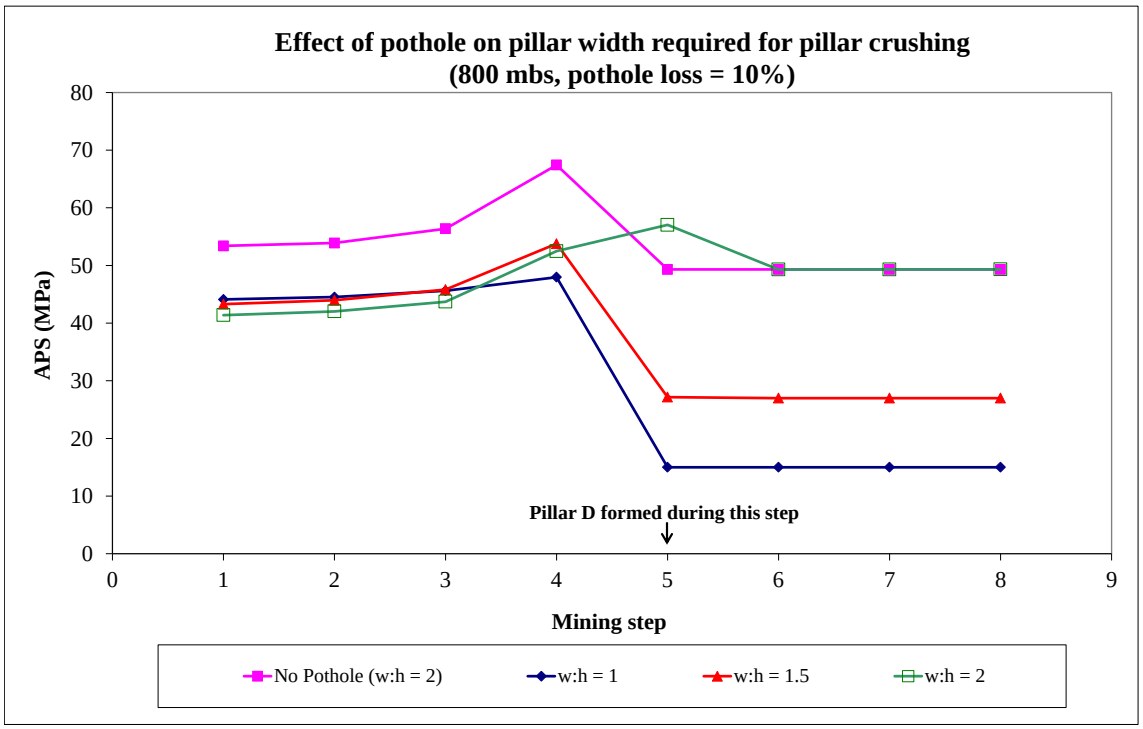

Figure 5.8: Effect of 10% mining loss on pillar crushing at a depth of 800 m below surface (the pothole is positioned 5 m from the pillars).

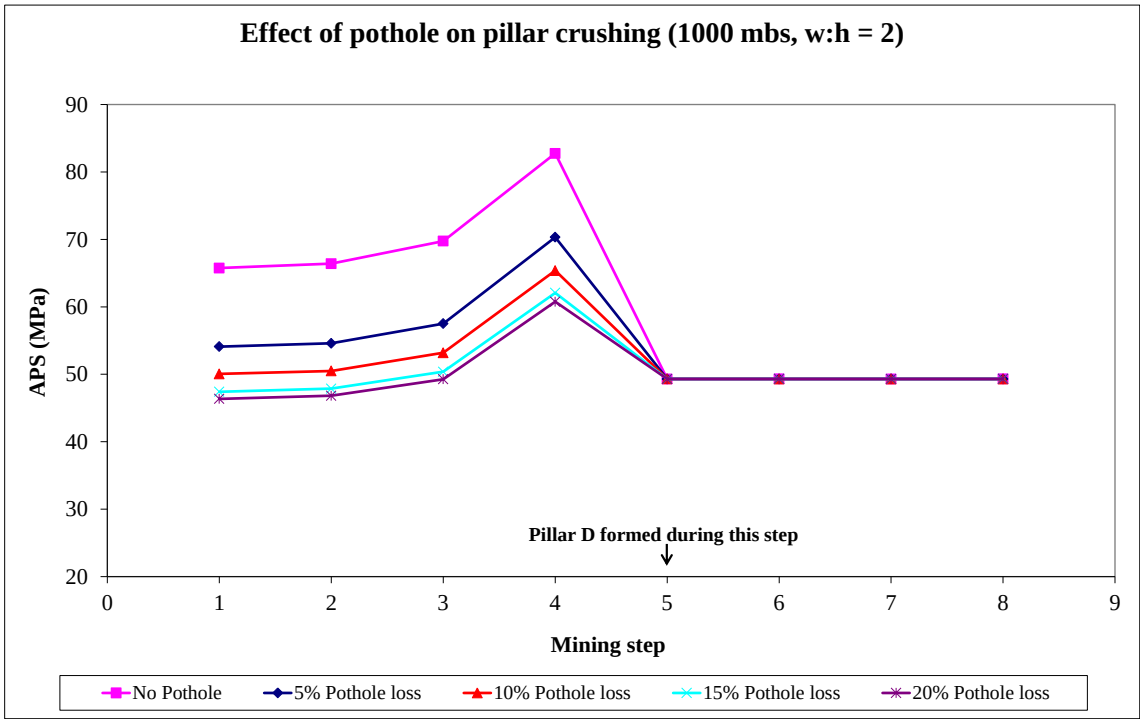

Figure 5.9: Effect of percentage mining loss on pillar crushing at a depth of 1000 m below surface (the pothole is positioned 5 m from the pillars).

Underground, potholes may be present at various positions throughout a panel. Typically a panel is mined until the pothole encompasses approximately two thirds of the face length whereafter the panel is deemed as unpayable and stopped. Situations also arise whereby pillars are left intact within a panel to stabilize the hangingwall where unstable ground conditions exist or where regional pillars are left within a regular grid. To model these scenarios, an unmined block was simulated at various positions from the pillar edge. A pothole dimension of 14 m x 14 m (approximately 10% of the mining area of mining step 1) was chosen to ensure that a situation is simulated whereby a panel will normally not be stopped (Figure 5.10).

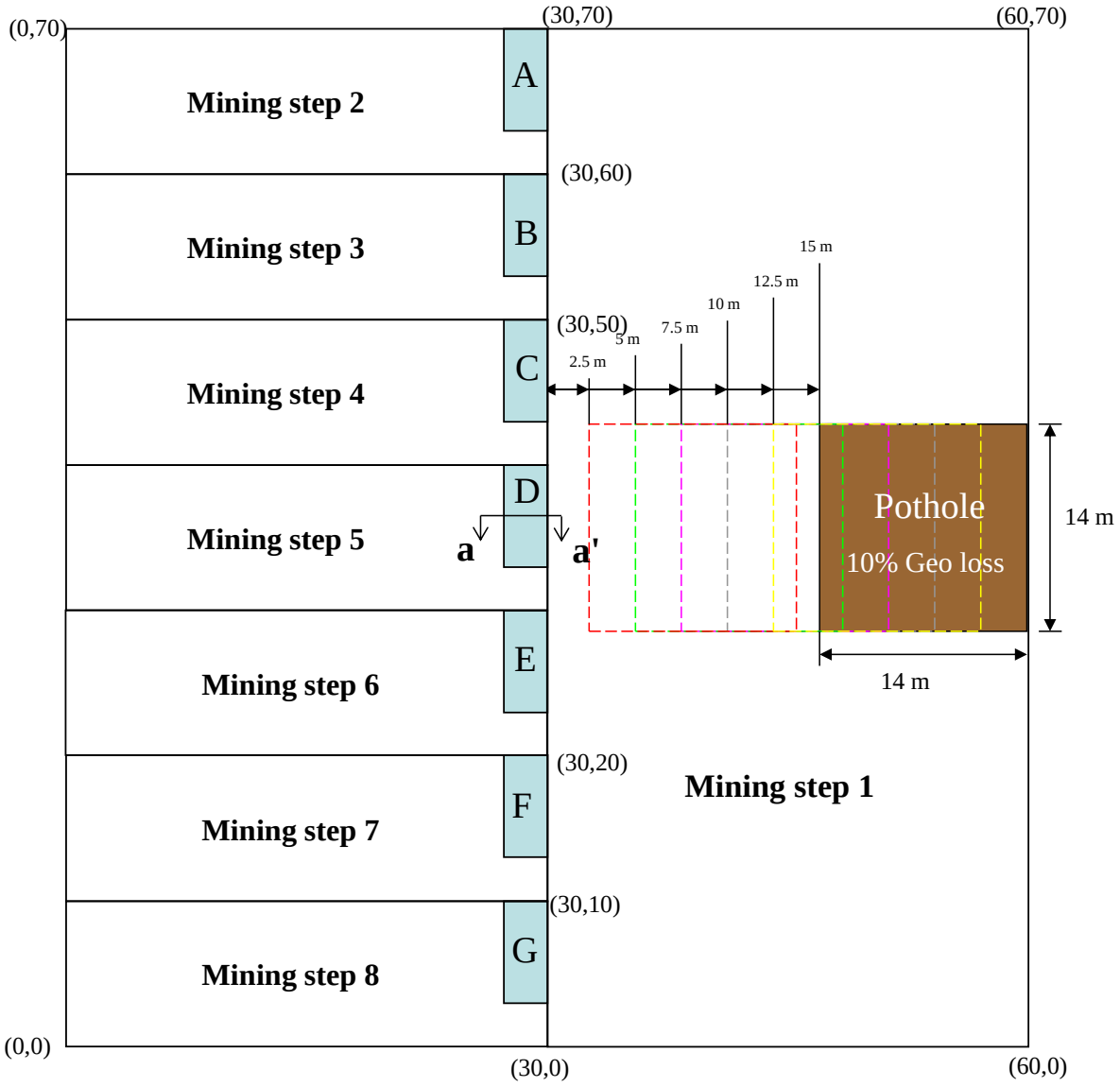

Figure 5.10: Idealised crush pillar layout used to simulate the effect of unmined ground at various positions from the pillar line on crush pillar behaviour.

Figure 5.11 indicates that pillar crushing is only achieved for the simulated layout at 600 m below surface when the pothole is between 12.5 m to 15 m away from the line of crush pillars. Late pillar crushing could nevertheless result due to the impact of the additional stability provided by the unmined block (reduces the initial stress the pillar is subjected to). In reality this will not occur as in this instance the pothole would be less than 3.5 m from the adjacent panel's line of crush pillars. The results also indicated that the presence of the pothole impacts on the pillars which are approximately 20 m ahead or behind the pothole position. The results from the simulations indicated that Pillars E, F and G do not show any sign of crushing for the mining block being positioned 5 m from pillar D's edge.

The same layout was simulated at 800 m and 1000 m below surface. At 800 m below surface (Figure 5.12) the pillars crush in the step when the pillars are formed when the pothole is more than 10 m from the line of crush pillars. When simulated at 1000 m below surface (Figure 5.13), pillar crushing is achieved for all of the scenarios. The simulated pillar behaviour is clearly sensitive to the input parameters as indicated in the previous chapter and will have to be calibrated.

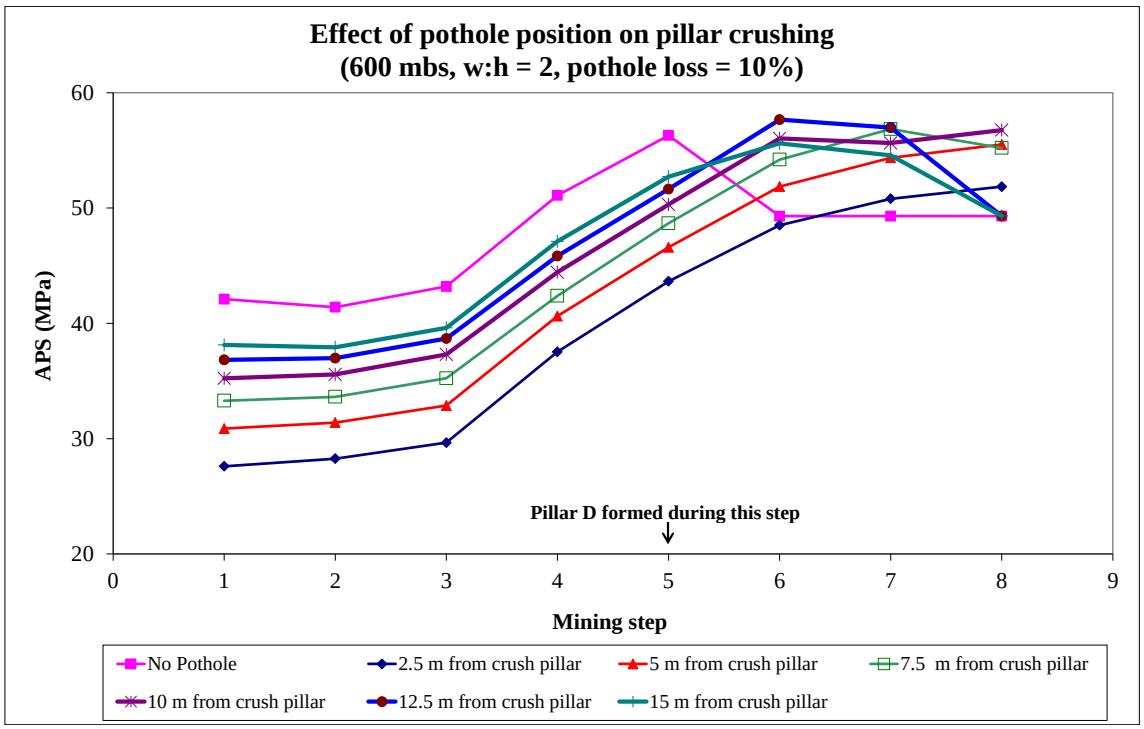

Figure 5.11: Effect of pothole position on pillar crushing for a 10% mining loss at a depth of 600 m below surface.

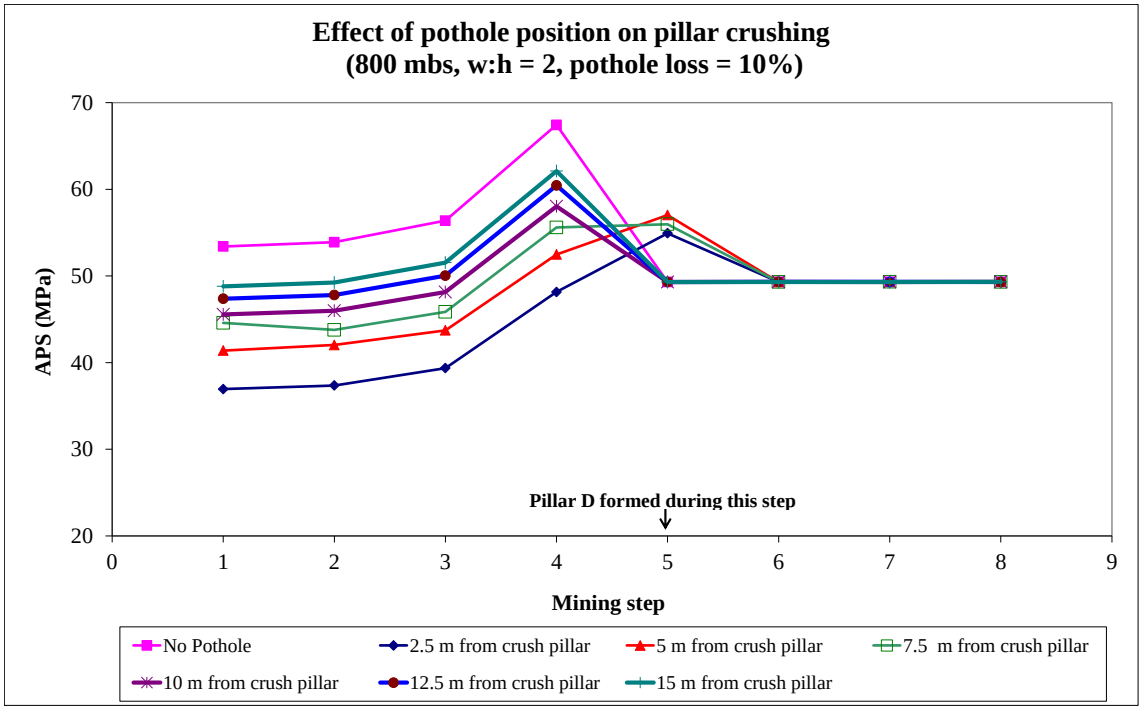

Figure 5.12: Effect of pothole position on pillar crushing for a 10% mining loss at a depth of 800 m below surface.

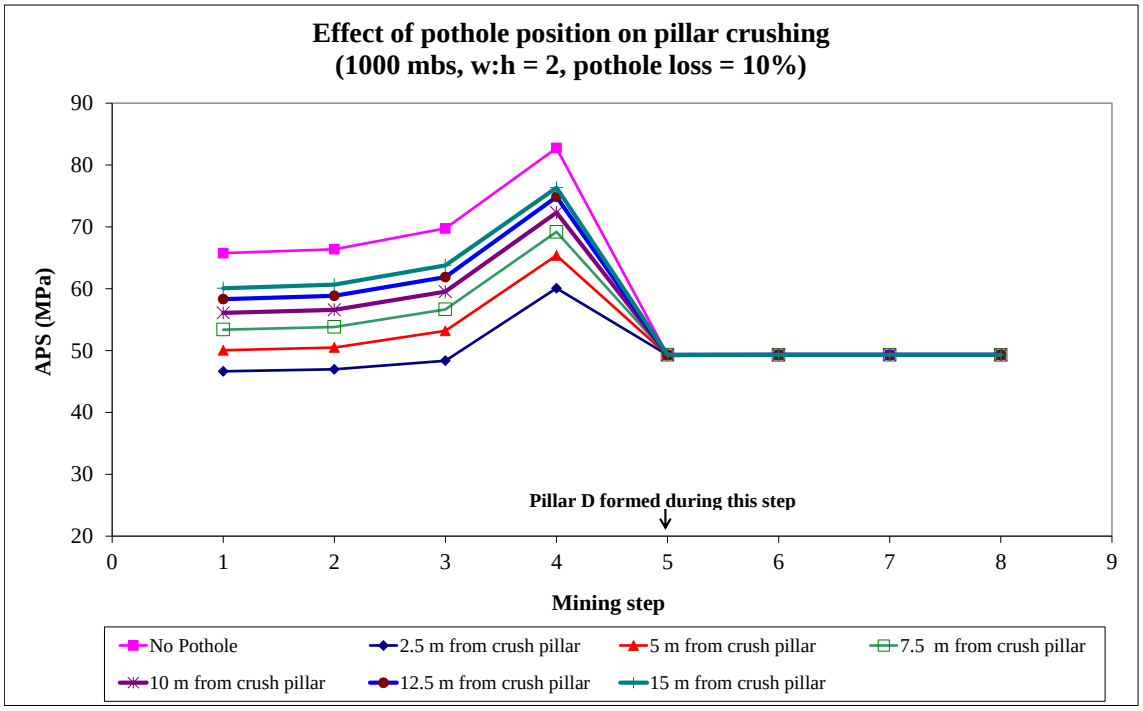

Figure 5.13: Effect of pothole position on pillar crushing for a 10% mining loss at a depth of 1000 m below surface.

5.2. The impact of sidings

A siding is a 1 – 2.5 m wide ledge or heading carried on the one side of an on-reef development end adjacent to the panel being mined (Figure 5.14 and 5.15). The main intent of the siding is to either modify the fracture patterns resulting from high face abutment stress (Figure 5.16) or to move crush pillars away from the travelling way (development end such as a raise or gully) to ensure that failed rock do not fall onto people. In intermediate depth platinum mines sidings fulfil both these functions. Note that Figure 5.16 demonstrates a poor mining configuration to show the impact of the face positions on the fracture orientations.

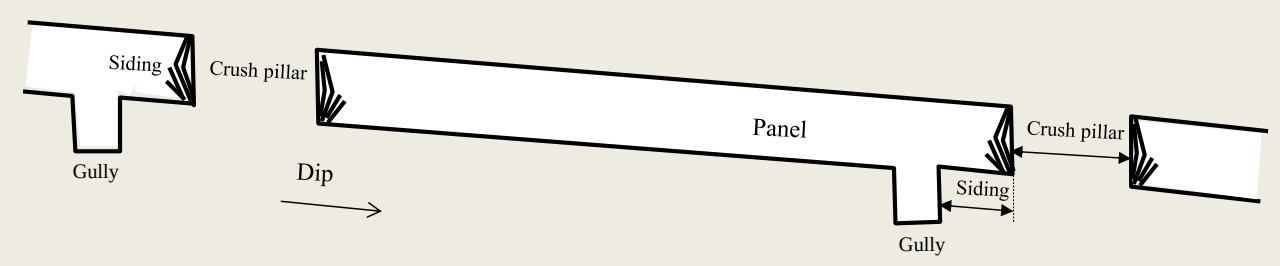

Figure 5.14: Section view of typical intermediate depth mining geometry applied with a crush pillar layout.

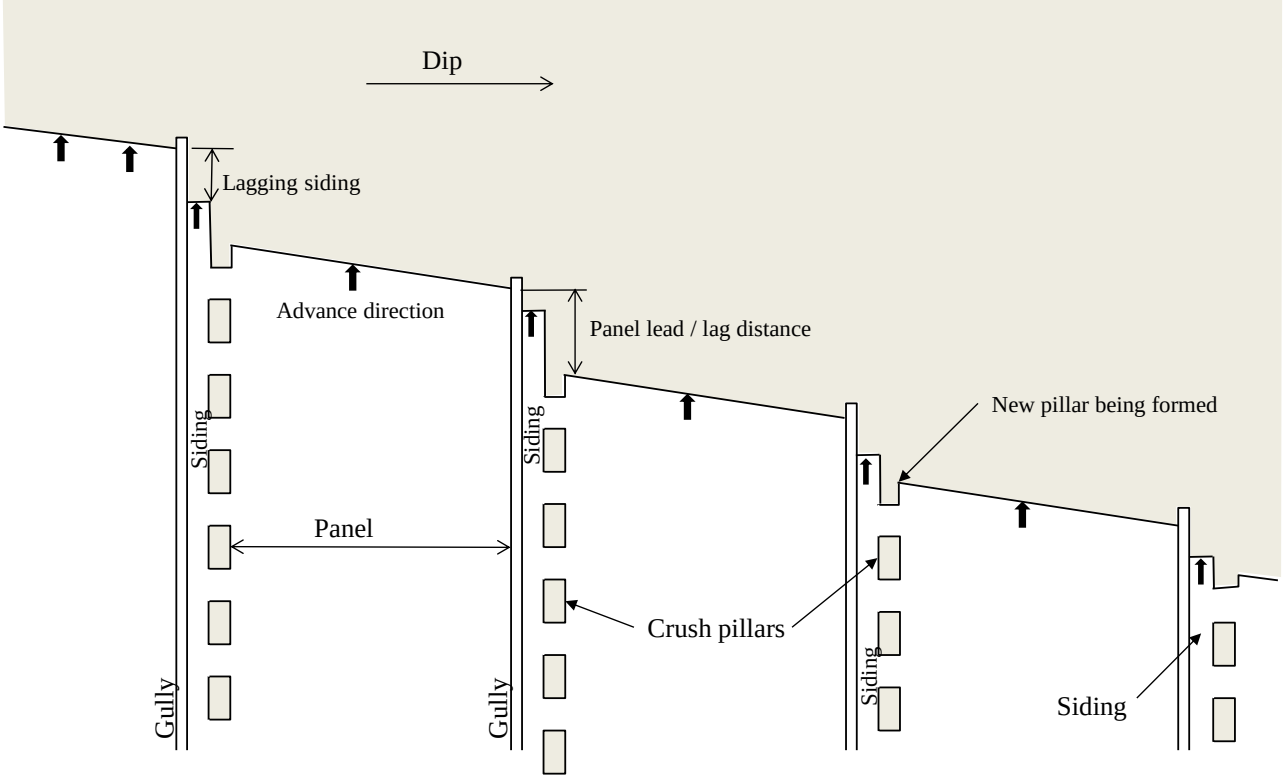

Figure 5.15: Plan view of a typical crush pillar layout (underhand breast layout).

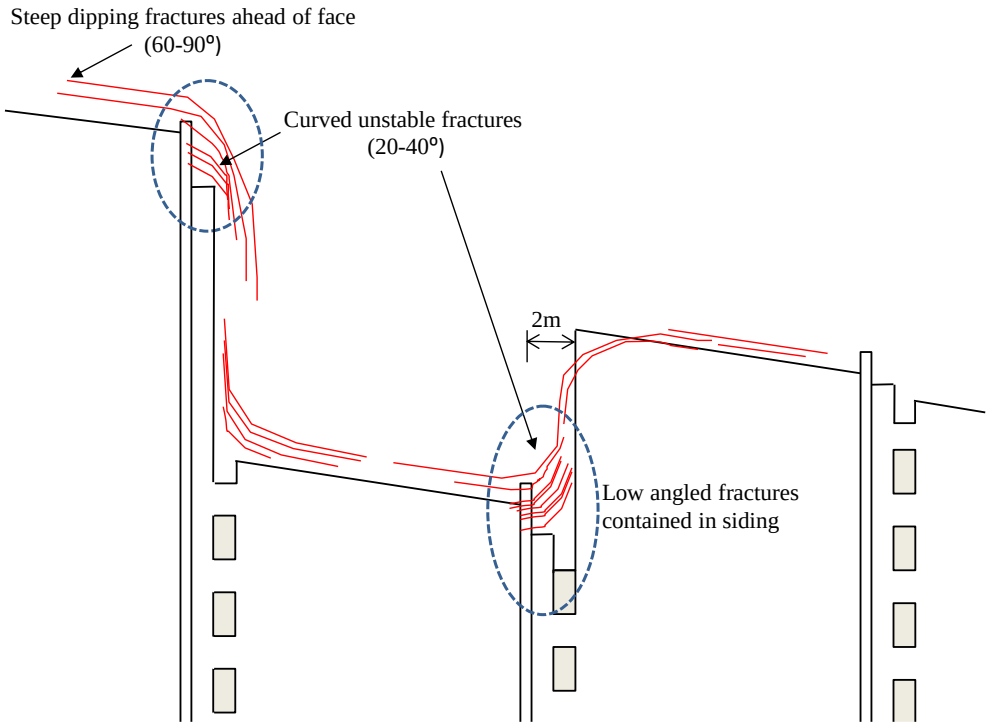

Figure 5.16: Typical fracture patterns around an intermediate to deep mining stope (plan view). Low angled fractures are predominantly found in the siding. Diagram constructed based on the findings after Naidoo et al (2002) and Budavari (1983).

Figure 5.17: Crush pillar directly adjacent to a gully (with no siding) in a Merensky stope at 700 mbs (after Naidoo et al, 2002).

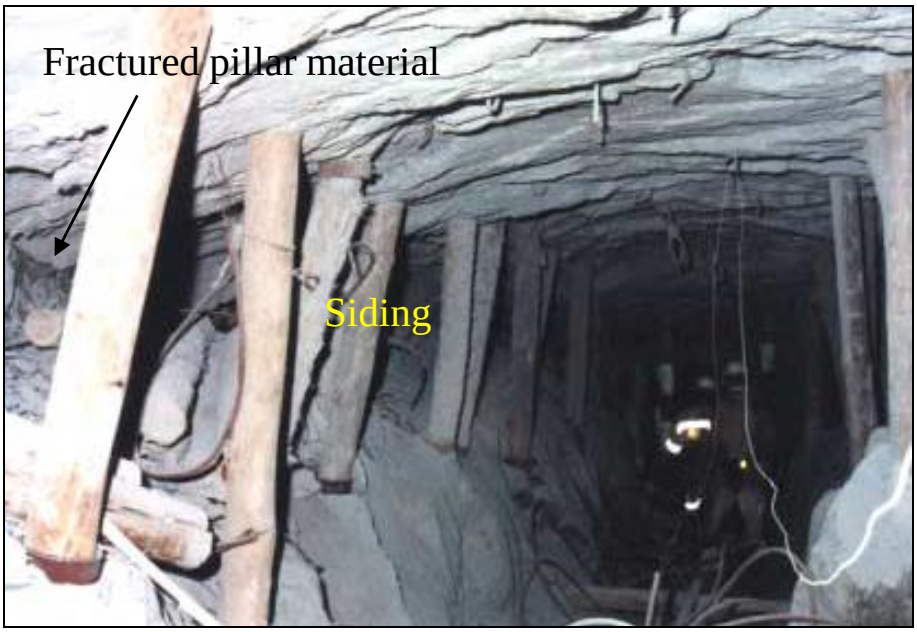

Figure 5.18: Merensky Reef gully with 1 m siding on the left. Fractured pillar material is contained in the siding (after Naidoo et al, 2002).

An optimal lead lag distance between panels is approximately 10 m with the gully leading the panel (for cleaning purposes) by approximately 2 m (Naidoo et al, 2002). Increased lead lag distances creates increased stress concentrations adjacent to the gully causing the hanging-and footwall to become highly fractured along the abutment. This results in the toe of the lag at the bottom of the upper panel becoming badly damaged. A siding should lag a maximum of 3 m behind the face (also prevents damage to support or contamination of the back area as a result of the blast). Naidoo et al (2002) recommended a 2 m-wide siding for a crush pillar environment. This distance will ensure that the pillars (or abutment) will not damage the gully and that the fractured pillar material is contained in the siding. Sidings are therefore important for both gully and pillar stability. An effective siding width will ensure that the pillar width to height ratio is not jeopardised. It also prevents premature foundation failure of the pillar should the siding edge fail.

Sidings are difficult to clean (it must be hand lashed) and support. For this reason sidings are not always cut to the required dimensions (2 m wide), typically lag the panel face (> 3m) or are not cut at all. Owing to mining difficulties and poor mining practices, in some instances sidings are purposely lagged 20 – 30 m behind the advancing face. The entire length of lagging siding is then charged up as a single face and blasted to create the gully shoulder.

A lagging siding impacts on the width of the pillar cut at the mining face. Many variations exist. Two examples are demonstrated in Figure 5.19 and 5.20. All prior research conducted on gullies and sidings were

aimed at determining the ideal gully dimensions (including headings, sidings and depth). This was conducted to ensure that gullies are not impacted by high stress conditions, resulting stress fracturing, panel convergence or crushing pillars. To date, the impact of a lagging siding on the pillar width has not been identified as a contributor to pillar seismicity in a crush pillar environment.

Figure 5.19 indicates the effect of a siding lagging significantly behind the advancing face. In this case, oversized pillars are cut by the advancing lagging panel. Once the lagging siding is mined either sequentially or as a single down-dip blast, the pillars will be reduced to the correct dimension. The pillars will, however, be positioned in the back area of the stope in a soft loading environment. Pillar crushing might therefore not be achieved (e.g. 4 m wide pillar reduced to the required 2 m wide dimension). If up-dip pillar holings, as illustrated in Figure 5.19 are not developed, the situation will be exacerbated.

Figure 5.20 illustrates that when a siding lags behind the bottom lagging panel, oversized pillars will also be cut by the advancing lagging panel face. The pillars will only be reduced in size to the required dimension when the siding catches up. However, at this point the pillar might not be able to crush sufficiently.

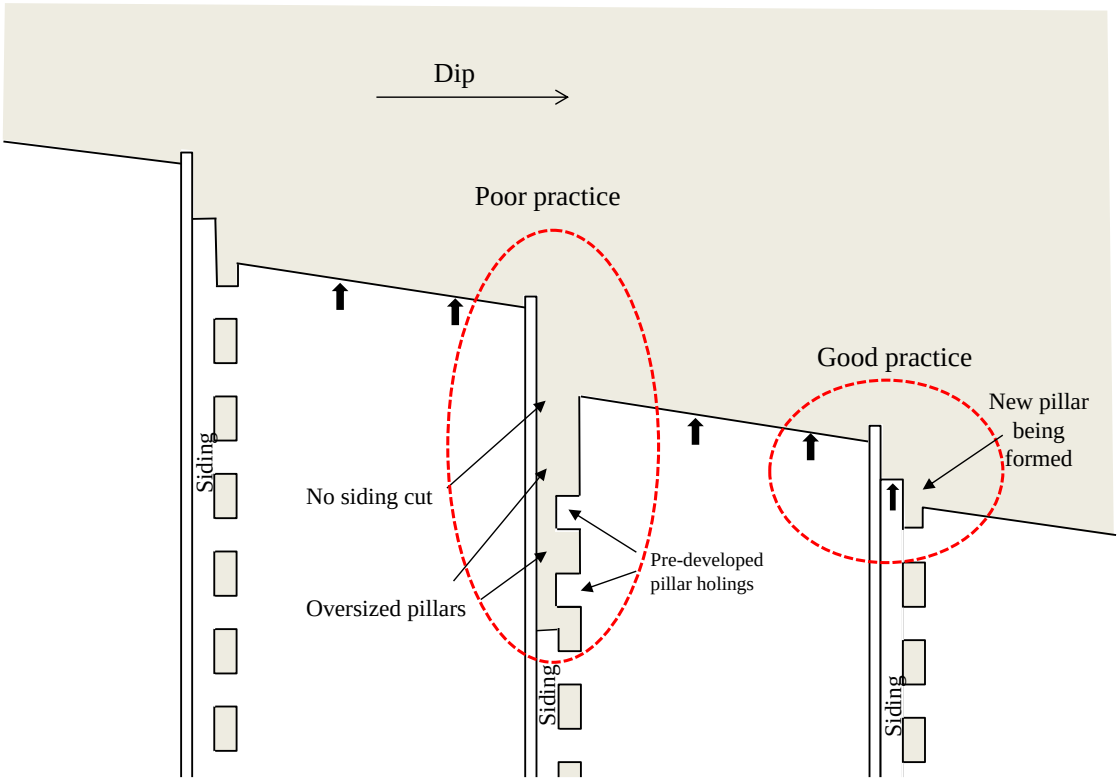

Figure 5.19: The impact of a significantly large lagging siding on crush pillar behaviour (plan view).

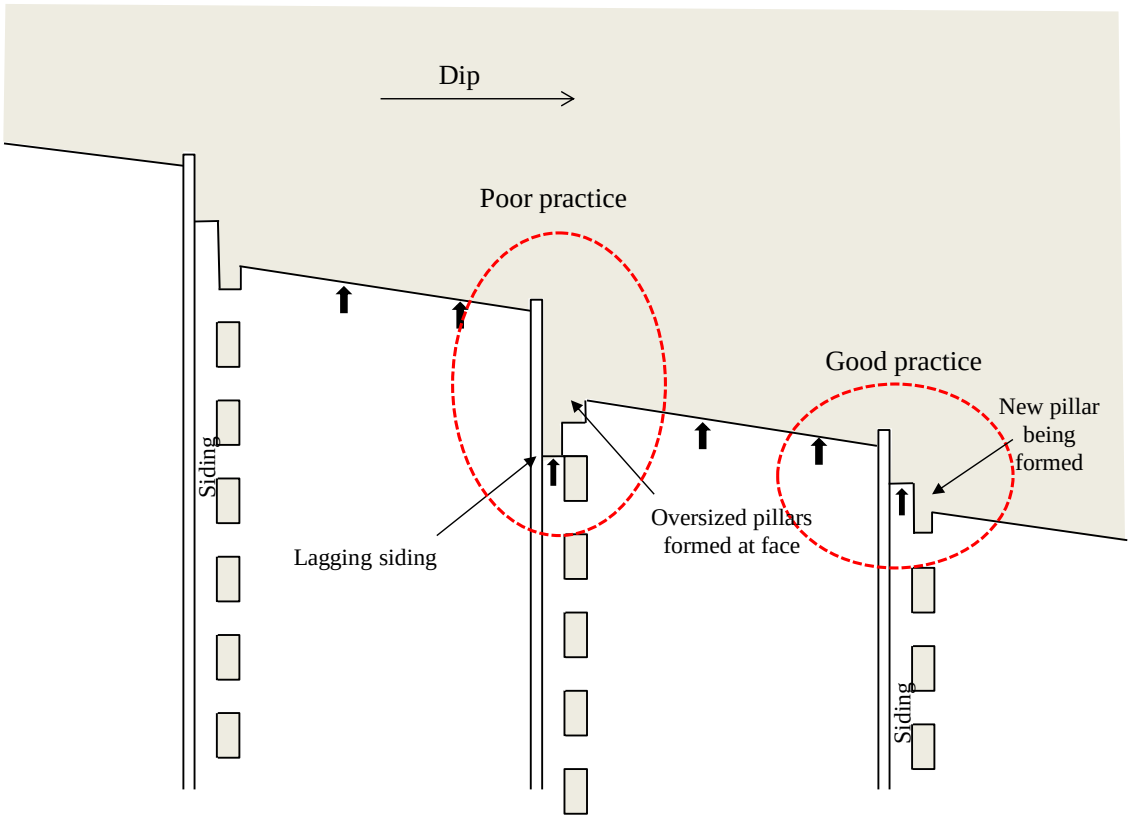

Figure 5.20: Lagging siding creating oversized pillars when cut at the advancing mining face (plan view).

5.2.1. Simulating the impact of a lagging siding on crush pillar behaviour

To investigate the impact of a lagging siding on crush pillar behaviour, the mining sequence of the idealised layout was adjusted. The same layout as Figure 4.1 was used where the pillars are 4 m wide in a 2 m stoping width (w:h = 2:1). A 2 m wide siding was added to the layout by initially making the pillars 6 m wide. The siding is then mined by simulating the additional 2 m portion of pillar as being mined. The length of the oversized pillar resulting from a lagging siding was controlled by the delayed mining of the pillar holings. Initially a 6 m wide by 20 m long pillar is formed. The siding is mined, reducing the pillar width (at the pillar position) to 4 m (w:h = 2:1). At this point the siding is lagging the panel face by 10 m. The face is advanced again and the cycle repeated. The final cut pillar is only created when the pillar holing is developed. This happens when the pillar is 20 m in the back area.

The simulated layout might over-exaggerate the lagging siding, but is representative of actual underground layouts as shown in Figure 5.19 and 5.20 especially so if the pillar holings are not pre-developed. Owing to the manual labour required (the pillar holings are cleaned by hand), this is not something the mining crew wants to do.

Mining sequence followed:

- **Step 1:** Mining of 30 m x 70 m panel
- **Step 2:** Mining adjacent panel (First 10 m face advance) — 6 m wide pillar being formed
- **Step 3:** Another 10 m face advance — 6 m wide x 16 m long pillar
- **S1**: Mine 2 m siding — Pillar A cut to 4 m wide. The pillar has not been holed yet and is still part of the 16 m long pillar (A+B)
- **Step 4**: Another 10 m face advance
- **H2:** Cut holing — Pillar A is formed 20 m in the back area
- **S2:** Mine a 2 m siding — Pillar B cut to 4 m wide. The pillar has not been holed yet and is still part of the 16 m long pillar (B+C)
- **Step 5:** Another 10 m face advance
- **H3:** Cut holing — Pillar B is formed 20 m in the back area
- **Repeat** cycle as per the sequence indicated in Figure 5.21.

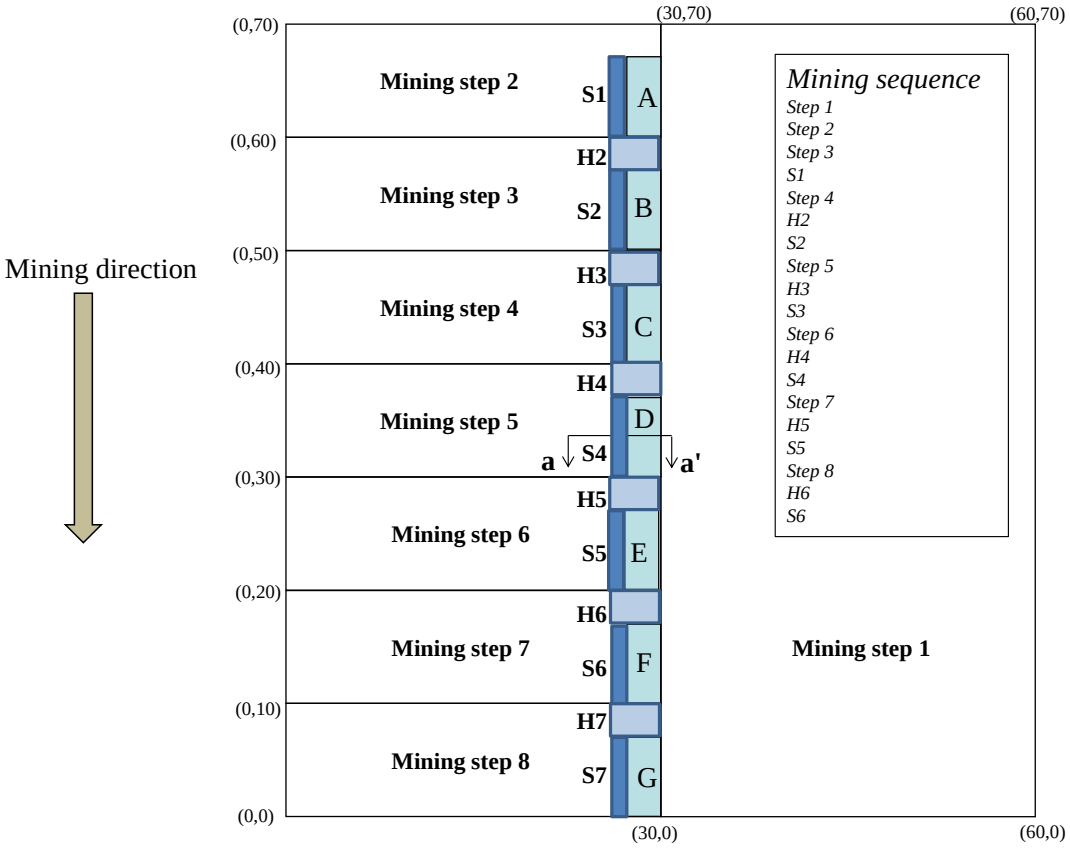

Figure 5.21: Idealised crush pillar layout representing the impact of a lagging siding.

Simulations were conducted at various mining depths. The aim was to determine if pillar crushing would occur if the pillar is only formed in the back area of the stope as a result of a lagging siding. Figure 5.22 demonstrates the impact of every mining step on the average pillar stress for pillar D (simulated at 600 mbs). There is only a significant increase in pillar stress once the pillar is cut along the face during mining step 5 (although oversized and long; 6 m x 26 m). Cutting of the holing in the back area (H3) to form pillar B and the siding (S3) along pillar C has no impact on the average pillar stress of pillar D even though the pillar has been reduced in length (20 m) and width along the pillar C position (4 m wide). As the face advances (Step 6) and pillar D moves into the back area, there is another increase in pillar stress. However, as the pillar is shortened and the siding is cut along pillar D, there is no change in stress condition. Any additional mining has limited impact on the overall behaviour of pillar D.

Due to the final pillar dimension (required dimension) only being achieved in the back area of the stope, the reduction in pillar size (H4 and S4) has a minimal impact on the average pillar stress when the pillar is fully formed (step 7 and H5). As the change in pillar dimension is occurring towards the back area of the stope (10 - 20 m behind the face) when the pillar width is reduced (siding cut; S4) or pillar holings are mined (H4 and H5), the influence of these geometric changes are not significant (compared to when the pillar is formed at the mining face) and will not necessarily cause pillar failure.

The same layout was simulated at increased depths as can be seen in Figure 5.23. All of the results presented are for pillar D. Mining depth does not appear to have any impact on the overall behaviour of the pillar (although the pillar is at a higher stress). These results again illustrate how important it is to achieve pillar crushing whilst the pillar is close to or being formed at the mining face.

The results indicate that a lagging siding could impact on pillar crushing. These pillars, being at a higher stress could therefore be sources of seismicity when situated in the back area of a stope.

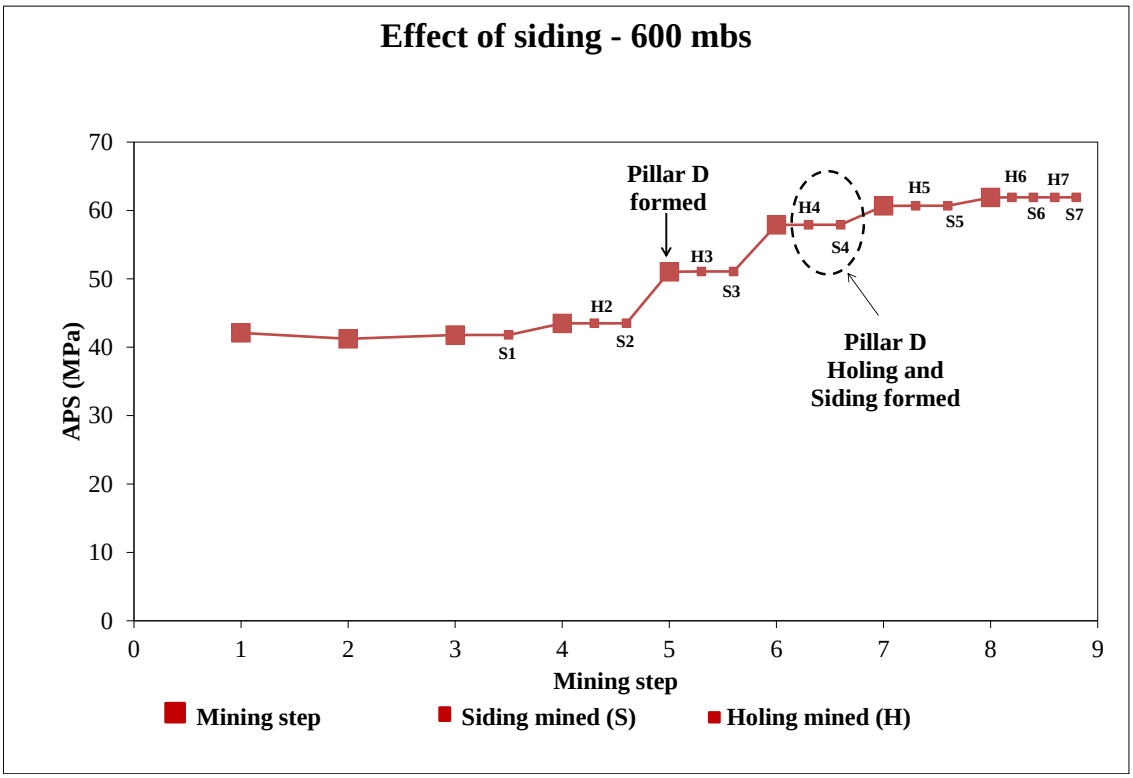

Figure 5.22: The effect of a lagging siding (per mining step) on pillar stress for pillar D (w:h = 2).

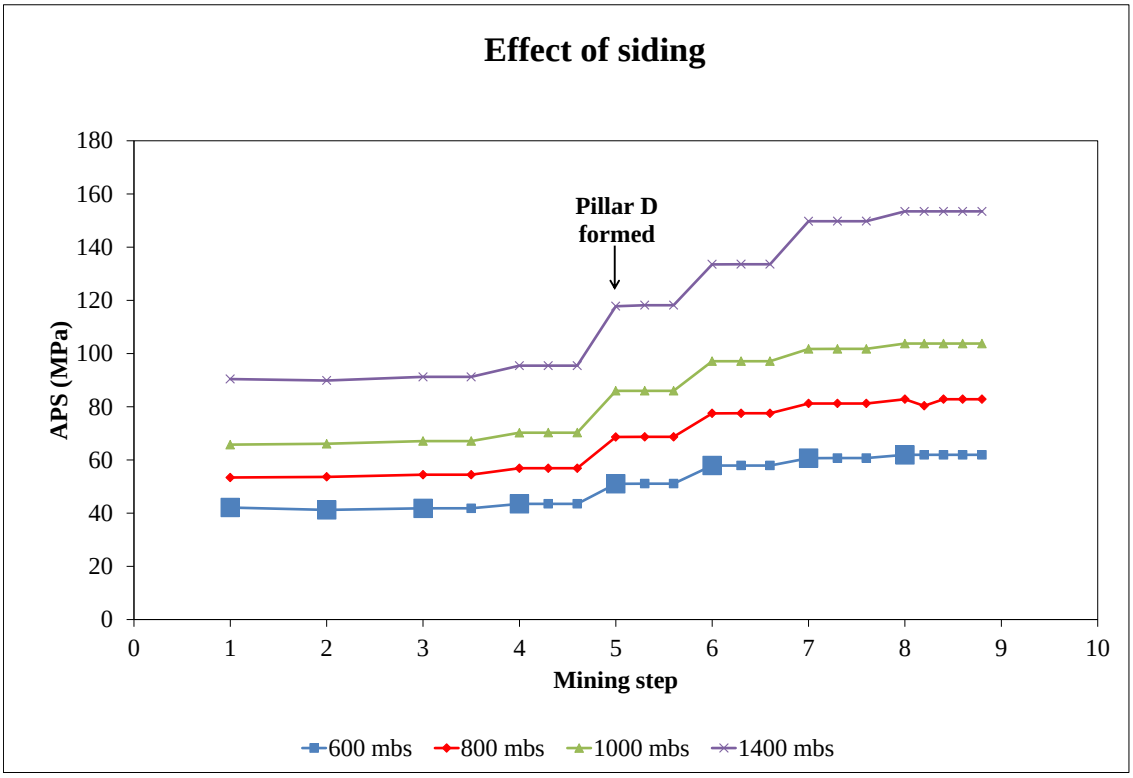

Figure 5.23: The effect of a lagging siding on crush pillar behaviour (pillar D) at various depths (w:h = 2).

5.3. Summary

The presence of unmined blocks of ground (geological or mining losses) in a layout and the impact thereof on the behaviour of crush pillars were investigated. These structures can contribute to a reduced extraction of up to 25% on some operations. The effect of these unmined blocks of ground are considerable and have up to now not been considered in any form of analyses to evaluate crush pillar behaviour.

The preliminary modelling results indicated that the impact of mining losses as a result of geological features such as potholes impact on the pillar behaviour.

- Crush pillars implemented at 600 m below surface with a width to height ratio of two will not crush if a 10% mining loss is situated adjacent to the pillar line. In this case, narrower pillars are required to ensure that pillar crushing is achieved (e.g. w:h = 1.5 is required at 600 m below surface),
- Pillars situated 20 m ahead or behind an unmined block will also be affected, resulting in either partially crushed (core still solid) or intact pillars.
- Crush pillars implemented 800 m and deeper below surface are impacted to a lesser extent when in close proximity to a pothole. Large mining losses (>10%) and potholes situated closer than 10 m from the pillar line can either prevent pillar crushing or induce delayed crushing.
- Crush pillars implemented beyond 1000 m below surface are not affected if a 10% mining loss (pothole) is situated 2.5 m from the line of crush pillars.

The geological environment is therefore a key consideration when implementing a crush pillar system as the pillar behaviour is not purely governed by depth. Factors which affect the pillar stress will influence pillar crushing.

Most of the Merensky Reef crush pillar sites cut a 1 – 2 m wide siding adjacent to the gully. The aim of the siding is to move pillar stress and low angled stress fractures away from the gully. The siding also provides an area where fractured pillar material (in the case of crush pillars) is contained so that it does not fall onto people using the gully as a travelling way. An effective siding width provides an intact foundation for the crush pillar and does not influence the pillar width to height ratio. Inconsistencies in the mining of a layout does determine when and where a pillar is formed relative to the mining face, the size of the pillar when formed and how the pillar will behave as a result. Pillar seismicity is a serious problem in many of the mines using crush pillars. As shown in this and in the previous chapters, possible causes for this are either oversized, uncrushed pillars situated in the back area of a stope, or when the pillar behaviour is affected, by for example the proximity of a pothole. Research has been conducted on gullies with regard to size, position, impact of stress, stress fracture patterns and convergence. Platinum specific research was aimed at determining the ideal siding width, considering fracture patterns and the effect of a siding on the crush pillar width to height ratio. Underground sidings often significantly lag the mining face. The sidings being

approximately 2 m wide are difficult to clean (hand lashed) and support. For this reason, mining of the siding is frequently behind schedule. In some cases, sidings lag the face by 20 – 30 m and are then developed as a single mining face.

A lagging siding impact on the width of the pillar formed at the mining face. Two examples were presented in this chapter, although numerous variations exist. Until now, the impact of a lagging siding on the pillar width has not been identified as a contributor to undesired pillar behaviour or a source of pillar seismicity in a crush pillar environment.

Once the siding of an advancing panel lag behind the adjacent lagging panel face, over-sized pillars are created. The pillars will only be reduced in size to the required dimension when the siding is blasted. At this point the pillar might not be able to crush sufficiently as the pillar is moving to the back area of a stope. The simulations conducted confirmed this effect. The pillars could therefore pose a seismic risk.

5.4. References

Budavari, S. (1983). *Rock Mechanics in Mining Practice*. *South. Afr. Inst. Min. Metall. Monograph series No. 5*. Johannesburg.

Carr, H.W., Groves, D.I. and Crawthorn, R.G. (1994). Magma loading and synmagmatic deformation: A new concept to explain regional and mine scale discontinuities, including Merensky Reef potholes in the Bushveld Complex. *Econ. Geol*. Vol 89, pp. 1398-1410.

Farquhar, J. (1986). The Western Platinum Mine. In: Annhaeusser, C.R. and Maske, S. Ed. *Mineral Deposits of Southern Africa vol. II. Geol. Soc. S. Afr*., pp. 1135-1142.

Naidoo, K., Leach, A.R. and Spencer, D. (2002). Stope gully support and sidings geometry at all depths and at varying dip. SIMRAC final report, GAP 602, SIMRAC, Johannesburg.

CHAPTER 6

ASSESSMENT OF THE DERIVED ANALYTICAL SOLUTION FOR THE PREDICTION OF CRUSH PILLAR RESIDUAL STRESS

A tool to investigate the behaviour of crush pillars

6. ASSESSMENT OF ANALYTICAL SOLUTIONS TO DETERMINE THE RESIDUAL STRESS OF A COMPLETELY FAILED PILLAR

In this chapter, various analytical solutions for the peak and residual strengths of crush pillars will be assessed. The objective is to investigate the application of the derived analytical solution for the APS of a completely crushed pillar. The results were compared to the numerical analyses conducted in the previous chapters, as well as to the actual performance of instrumented underground Merensky pillars (after Watson, 2010).

As described in Chapter 3, the method of slices, (Barron, 1984) is based on the confined core concept developed by Wilson (1972) whereby a pillar is presumed failed when the peripheral fractured zone extends to the pillar centre. The model is based on the concept that a pillar can be represented by a large number of vertical slices for which each slice is analysed and compared to an appropriate failure criterion. If a slice fails, its residual load capacity is calculated. The variance between the initial elastic and residual stress on a slice is then transferred to the remaining unfailed slices. As there is a minimum pillar stress below which fracture cannot initiate, there should be a minimum pillar strength. Barron calculated the vertical stress distribution through a pillar as:

$$S_{yy} = \frac{UCS_b}{2Sin\phi_b}\left\{\left(1+Sin\phi_b\right)\cdot e^{Tan\phi_b\frac{(1+Sin\phi_b)\cdot x}{(1-Sin\phi_b)\cdot h}} - \left(1-Sin\phi_b\right)\right\} \quad (6.1)$$

Where

Syy = Vertical stress acting on the pillar

φ_b = Internal friction angle of the broken rock

UCS_b = Uniaxial compressive strength of the crushed (broken) material; equivalent to C_b

x = Horizontal distance into the pillar

h = Pillar half height

w = Pillar width

C_r = Residual cohesion

With

$$UCS_b = \frac{2\cdot C_r \cdot Cos\phi_b}{1-Sin\phi_b} \quad (6.2)$$

Kuijpers et al (2008) integrated equation 6.1 to obtain the average residual pillar strength. This is represented by equation 6.3.

$$APS_{res} = \frac{h}{w}\left[\frac{UCS_b}{2Sin\phi_b}\left\{\left(\frac{1-Sin\phi_b}{Tan\phi_b}\right)\cdot e^{Tan\phi_b\left(\frac{(1+Sin\phi_b)\cdot x}{(1-Sin\phi_b)\cdot h}\right)} - (1-Sin\phi_b)x\right\}\right] \quad (6.3)$$

Salamon (1992) attempted to overcome some of the shortcomings in the approaches of Wilson and Barron and devised a complex expression to describe the stress distribution in a failed pillar which allows for non-uniform stress distribution in the vertical slices. Salamon made the assumption that if the uniaxial compressive strength of a material should rapidly drop to zero when the pillar edge starts to yield, then violent pillar failure should occur. However, stable behaviour cannot be expected when the strength drop is abrupt. Stable behaviour is only possible if the rate of strain softening is small to moderate. Equations 6.4 and 6.5 give the analytical solution of Salamon for the limit equilibrium approach to represent the stress distribution through a pillar as well as the residual pillar strength.

$$S_{yy} = 3.2\left(0.8\cdot e^{\frac{2.5x}{2h}}\right) \quad (6.4)$$

$$APS_r = \frac{2h\cdot 0.8\dfrac{C_r}{0.5}}{2.5w}\left[e^{2.5\left(\frac{w}{2h}\right)} - 1\right] \quad (6.5)$$

Similarly, equation 6.6 (Malan and Napier, 2006) predicts an exponential increase in the pillar stress away from the edge towards the centre of the pillar (equation 6.6 is a repeat of equation 3.11 although rewritten to use the same notation as above). If the pillar is completely failed, assuming that the stress profile is symmetric about the centre of the pillar, the average stress in the pillar is given by equation 6.8 (equation 3.17 as shown in a previous section with the notation adjusted as described above).

$$S_{yy} = UCS_b\cdot e^{\alpha x} \quad (6.6)$$

With

$$\alpha = 2\mu m/2h \quad (6.7)$$

and

$$APS_r = \frac{UCS_b.2h}{\mu mw}\left[e^{\frac{\mu mw}{2h}} - 1\right] \quad (6.8)$$

Where *m* is a strengthening parameter equal to the slope of the failure envelope.

6.1. Comparison of analytical solutions

In this section the various analytical approaches for the residual pillar strengths, as described in the previous section, will be compared. Watson (2010) compared the results of instrumented pillars with regard to the measured peak and residual pillar stress (Table 6.1) to the expressions derived by Barron, Kuijpers and Salamon. Note that in all instances the measured pillar stresses (Table 6.1) were significantly adjusted upward to be comparable to the back analysed elastic numerical modelling results and the peak pillar strength formula derived based on the results of unfailed pillars at Impala Mine. Similarly, the residual pillar strengths are estimated based on the results of the analytical solution after Salamon.

In addition, punch tests results by Spencer and York (1999) where they replicated pillar foundation behaviour (Table 6.2) were also included by Watson as a comparison to the stress measurement and analytical solution. The results of the punch tests are included in the analyses performed by the author. The application of the limit equilibrium model cannot, however, model foundation failure. Also, Watson's inclusion of the punch test results is not valid as it does not reflect the pillar failure mechanism for the range of small w:h ratio pillars.

Watson (2010) indicated that the analytical solutions were very sensitive to the values of the parameters. He commented that the effect of foundation behaviour is not taken into consideration by the analytical solutions and the residual pillar strength is overestimated at a width to height ratio exceeding approximately three.

Table 6.1: Results from stress measurements of crush pillars (after Watson, 2010).

Site	Depth (mbs)	Siding	Pillar no.	Peak strength measured (MPa)	Residual strength measured (MPa)	Actual w:h
Amandelbult	600	No siding. Gully was filled with ore	P1	320	20	2.3
Amandelbult			P2a	276	14	2.7
Amandelbult			P2b	265	17	2.7
Impala	1100	1.8 m wide	P1	295	32	4.7
Impala			P2a	320	32	2.9
Impala			P2b	327	32	2.9
Impala			P3	263	28	2.1
Impala			S1	353	33	6.7
Union	1400	2 m wide	P1	191	16	2.0

Table 6.2: Average values of laboratory punch tests (after Spencer and York, 1999).

Peak strength (MPa)	Residual strength (MPa)	w:h
471.5	217	5.0
392	29	3.0
248.5	6.9	1.0

Wilson (1972) listed a value for residual cohesion of C_r = 0.00689 MPa (1 lb/in^2) where it was assumed for comparison and related to measurements done at Pye Hill colliery (Shepherd and Kellet, 1969). It was, mentioned that the value of C_r can vary significantly. This will impact on the results of the analytical solution. Salamon (1992) criticized the application of C_r = 0.01 MPa as used by Barron and Wilson. However, after investigation, Salamon could not fault the use of this parameter value when applied in case studies conducted on coal.

Watson et al (2010) investigated various values for the residual cohesion including C_r = 0.011 MPa to find a solution representative of the residual stress measurements and punch tests conducted. Both equations 6.3 and 6.5 were used for the comparison. Figures 6.1 and 6.2 compiled by Watson (2010) represent the solutions by applying various values for the residual cohesion for a constant friction angle (30 degrees). These figures highlight the variability of the results depending on the value of the parameters used. Furthermore, it also indicates the sensitivity of both the Barron and Salamon solutions to specific values, each yielding different results.

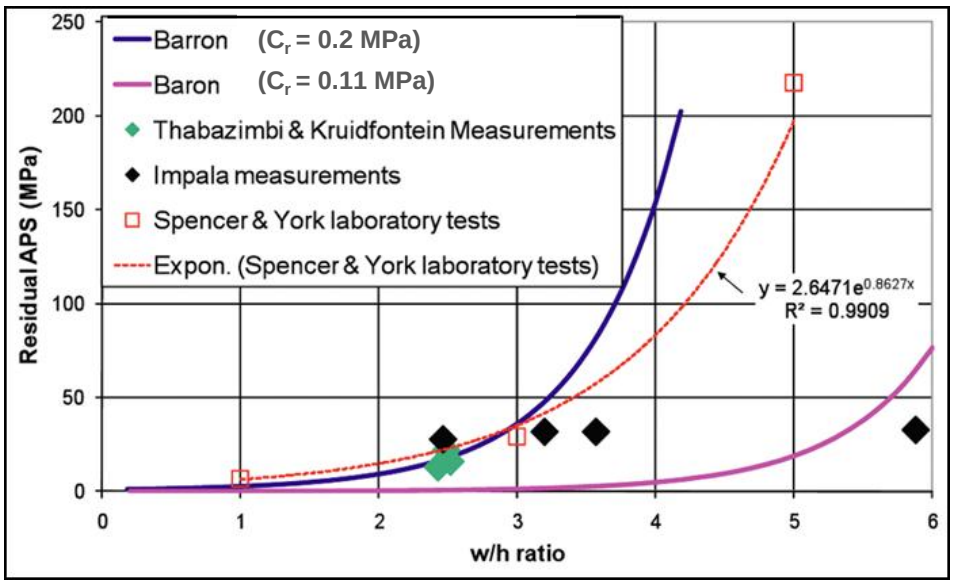

Figure 6.1: Effect of w:h ratio on the residual APS for the Barron solution. (φ=30°). Figure after Watson et al (2010).

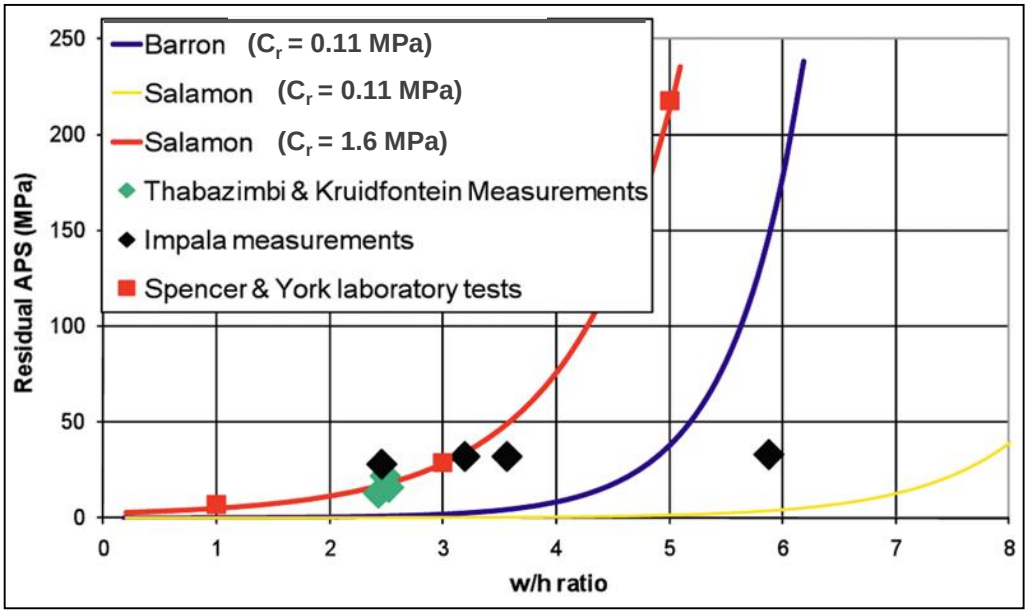

Figure 6.2: Effect of w:h ratio on the residual APS for the Barron and Salamon solutions (φ=30°). Figure after Watson et al (2010).

The results of the residual pillar stress measurements detailed in Figure 6.1 and Figure 6.2 are not plotted against the actual pillar dimensions. Watson took consideration of the effects of pillar dimension (width and length) and position relative to a gully (presence of siding) by adjusting the actual pillar width and pillar height. Both effective pillar height (H_{eff}) and effective pillar width (W_{eff}) were used to depict the width to height ratio of the instrumented pillars in these diagrams. Furthermore, the scale used and point size representing the stress measurements skews the actual effect with regard to best fit or representative curve.

In the previous chapters, the preliminary modeling results highlighted that pillar length does not have a significant impact on crush pillar performance (for a pillar width to length ratio of up to four). The effect of pillar width to length ratio and the influence of an effective pillar width might therefore be less significant when considering crush pillar behaviour. It therefore appears that adjustment to account for rectangular or elongated pillars should only be relevant when considering rigid pillars. This consideration must be further investigated and validated during the underground trial.

Where pillars are situated adjacent to gullies, it could influence the pillar behaviour. In some cases, the pillar could eject the footwall of the gully when loaded, or slabs resulting from pillar fracturing could fall from the pillar edge into the gully. As the pillar height is increased on one side of the pillar, it can be taken into account by adjustments for an effective pillar height. In most cases the instrumented pillars had a siding cut adjacent to the pillar.

The monitoring of the Amandelbult pillars where no sidings were present indicated that the broken ore which was lying in the gully provided sufficient confinement to the crush pillar foundations to prevent premature failure. Most of these pillars, especially oversized pillars only started crushing once the gully was cleaned from excessive ore at the end of the panel's mining cycle. This should therefore also be borne in mind when considering to apply adjustments to actual pillar dimensions.

Figure 6.3 was produced from Watson's data regarding the actual pillar dimensions. As a comparison, the pillar dimension (range of w:h ratios) and "measured" residual stress were also plotted to demonstrate the influence of dimension adjustments on the pillar width to height ratio. The subscripts and application is expanded on below (refer to Figure 6.3 to see this impact).

- **W:** Watson's dimensions with adjustments for pillar height to account for gully height if a siding was not present ($w : h_{eff}$),
- **Wact:** Watsons values used ($w_{eff} : h_{eff}$) as seen in Figure 6.1 and 6.2,
- **Adj:** Pillar sizes adjusted based on interpreted data. Adjustments were made to pillar dimensions. If no siding was present, h_{eff} was used. If the gully was full of ore which restricted pillar foundation mobility, the regular pillar height was used (h),
- **w:h**: Reflects the actual width to height of the pillar and ignores any adjustments.

Figure 6.3 highlights the importance of using a consistent approach (similar or no adjustments) when conducting pillar investigations. The adjustments used by Watson resulted in reduced w:h ratios and the results therefore plotted closer to the analytical solution. All pillar dimensions used from this point forward will refer to the actual width and actual height of the pillars to give a true reflection of the width to height ratio of the pillars.

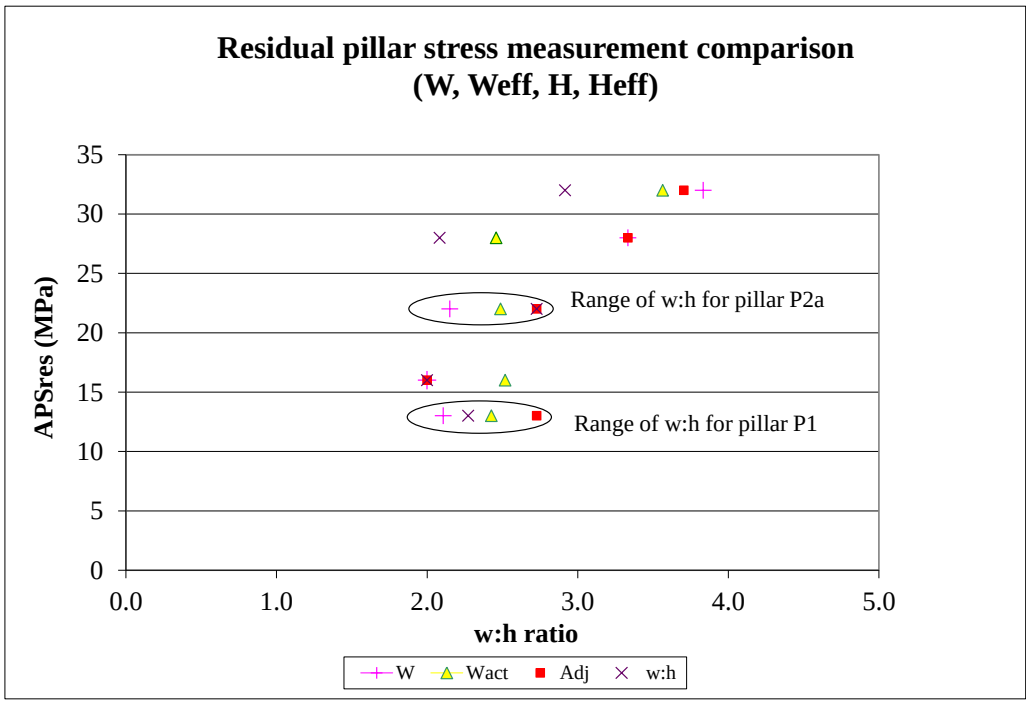

Figure 6.3: Effect of w:h pillar adjustment factors (effect highlighted for pillars P1 and P2a).

Analyses were conducted to establish which of the analytical solutions provided the most appropriate representation of the data. The analytical curves were plotted against the actual width to height ratio and "measured" residual pillar stress (Table 6.1) as well as the punch tests conducted by Spencer (Table 6.2). The input parameters for the" best fit" solutions are summarized in Table 6.3. The "best fit" values and results determined by Watson (2010) were incorporated for the Salamon and Baron solutions.

Figure 6.4 indicates that the simple analytical solution derived by the author for this PhD study provides an equally good fit to the data points compared to both the Salamon and Barron solutions. The results are, however, very sensitive to the selection of the input parameters. The purpose of the analytical solutions would be to provide a first order estimate of crush pillar dimensions. It must therefore provide a good approximation and be based on back analysed behaviour.

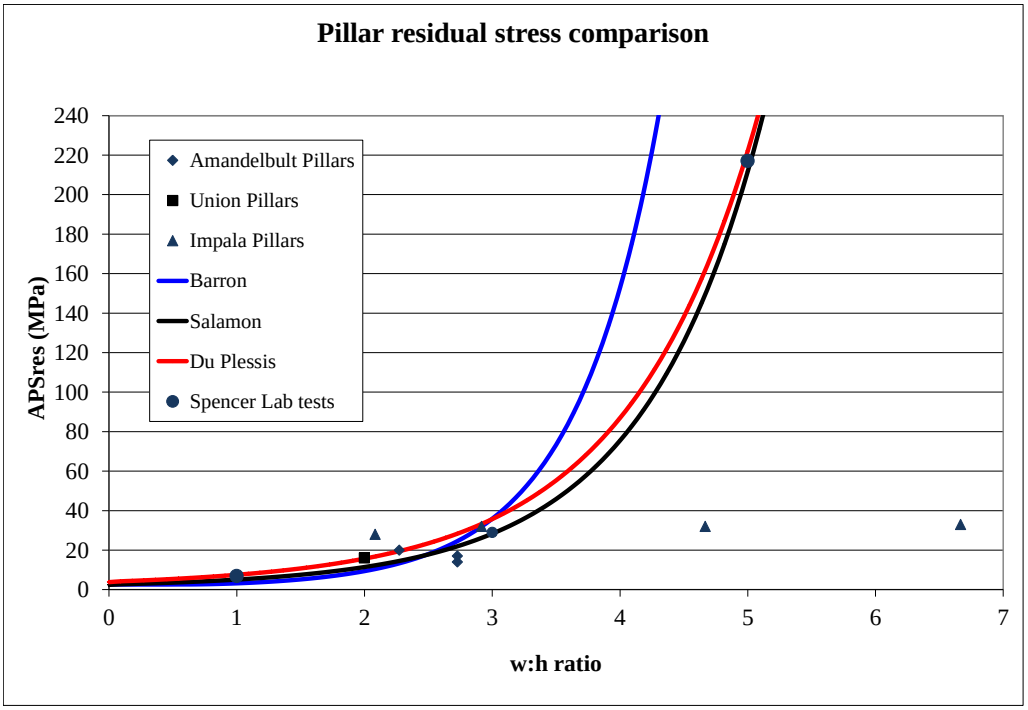

Figure 6.4: Comparison of analytical solutions versus actual residual stress measurements.

The results in Figure 6.4 indicate that the analytical solutions are only accurate to a width to height ratio of approximately three. Although the analytical solution curves intersect the punch tests at w:h = 5, this data point is not relevant. As previously discussed, the analytical solutions do not consider this mode of failure. The condition of the Impala pillars with w:h ratios approaching 5 and 7 are also questionable. Pillars at these w:h ratios will not completely crush.

In the following section the analytical solution derived by the author will be expanded on to test sensitivity, agreement with numerical modeling results and the limitations highlighted above.

Table 6.3: Input parameters used for the analytical solutions displayed in Figure 6.4.

	Pillar height (m)	Friction angle(φ)	Slope Failure envelope m	Residual Cohesion C_r (MPa)	Crushed material strength UCS_b (MPa)
Baron	1.1	30	NA	0.2	NA
Salamon	1.1	30	NA	1.6	NA
Du Plessis	1.1	30	2	NA	4

Watson (2010) plotted the vertical stress distribution across a pillar using equations 6.1 and equation 6.4. This was compared to the stress measurements as determined at various positions above a pillar at the Amandelbult site (P1). As with the results of the residual pillar strength solutions, various values of residual cohesion were used in an attempt to find a solution representative of the underground measurements. Figure 6.5 and 6.6 compiled by Watson (2010) show the results for the Baron and Salamon vertical stress distribution solutions.

As a general comparison equation 6.6 after Malan and Napier (2006) was evaluated by using various values representing the crushed material strength UCS_b and compared it to outputs for both the Baron and Salamon solutions (refer to Figure 6.7). The Salamon solution for vertical stress distribution through a pillar is not influenced by the value of the residual cohesion but is dependent on the width of the pillar. The Salamon result (C_r = 1.6 MPa), which is displayed in Figure 6.6, also compare well to the results using equation 6.6 when the crushed material strength equals 4 MPa (refer to Figure 6.8). Although these parameters are not directly relatable, the results provide good agreement with the underground measurement.

This finding is important as this model is used to simulate crush pillar behaviour within the TEXAN code (refer to Figure 3.6). The result being a close approximation of the underground measurements increases the level of confidence in the model which is used as an appropriate tool to assess crush pillar behaviour on a larger scale. As previously mentioned, the input parameters are critical and means of determining appropriate and applicable values are essential.

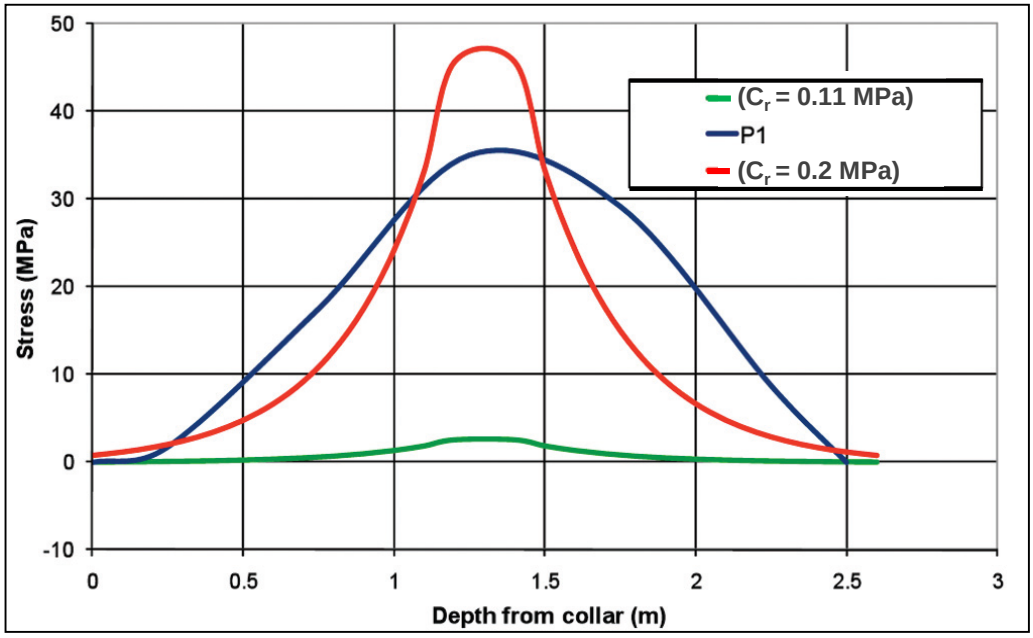

Figure 6.5: Comparison of Barron vertical stress distribution solution and pillar P1 stress profile (φ=30°). Figure after Watson et al (2010).

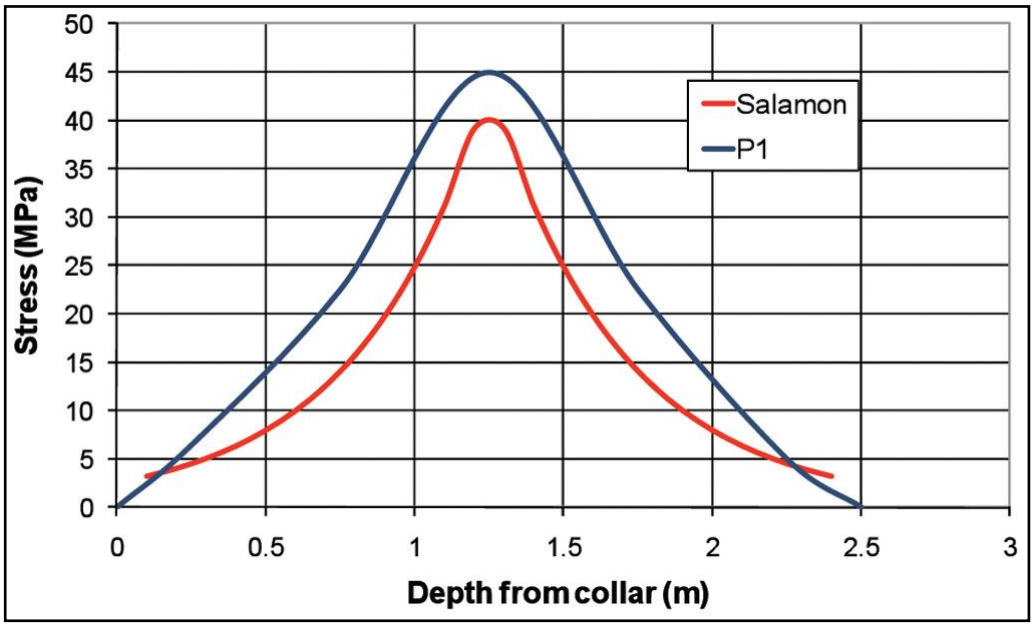

Figure 6.6: Comparison of Salamon's vertical stress distribution solution and pillar P1 stress profile (φ=30° and C_r = 1.6 MPa). Figure after Watson et al, (2010).

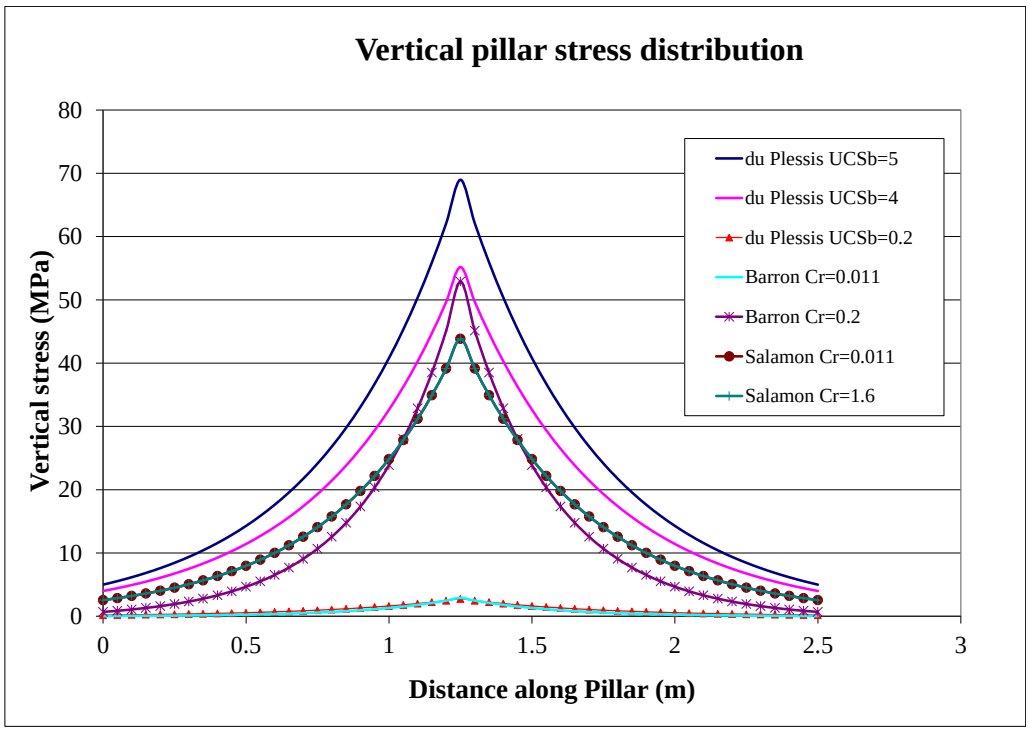

Figure 6.7: Comparison of vertical stress distribution (φ=30°, pillar height = 1.1 m, pillar width = 2.5 m).

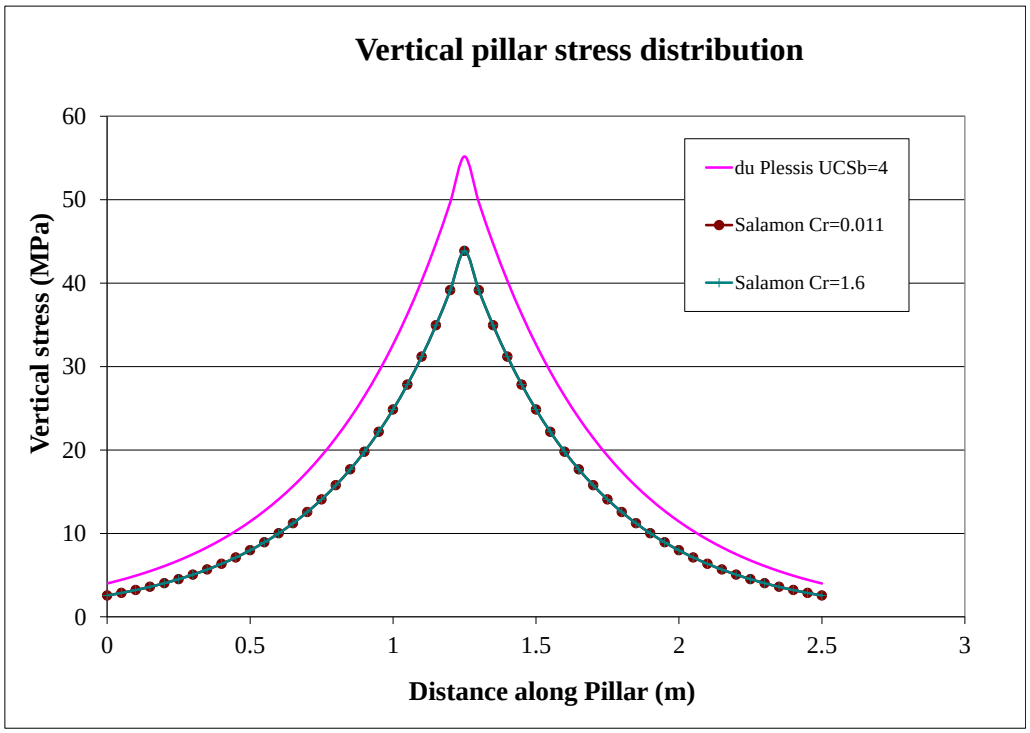

Figure 6.8: Comparison of vertical stress distribution; du Plessis UCS_b=4 and Salamon C_r=1.6 and C_r=0.011.

6.2. Effect of parameter values on the derived residual APS solution

As highlighted in the previous sections, the application of an analytical solution to predict the residual strength of a crush pillar is very dependent on the model parameters. Various analyses were conducted to determine the effect of these parameters. The governing parameters are:

- Fiction angle φ (degrees). Also used to calculate frictional coefficient μ where $\mu = \tan(\varphi)$
- Strengthening parameter m
- Crushed material strength UCS_b (MPa); also equivalent to C_b
- Width to height ratio of the pillar (w:h)
- Average pillar strength (MPa)

The average residual stress of a completely failed pillar is given by equation 6.8 which, for the purpose of the discussion, is repeated below:

$$APS_r = \frac{UCS_b.2h}{\mu mw}\left[e^{\frac{\mu mw}{2h}} - 1\right] \qquad (6.8)$$

The strengthening parameter m and the crushed material strength UCS_b have the most profound effect on the behaviour of the pillars. This is also confirmed by the modeling results as indicated in Figure 4.10 to 4.14. The impact of the residual strength of the crushed material (UCS_b) on the crushed state of a pillar is not fully understood. In the previous section various values were compared. Figure 6.9 shows that the crushed material strength has an effect on overall pillar behaviour. Low values of UCS_b will result in lower average residual pillar strengths. This could imply early pillar crushing as indicated by the numerical modeling results (Figure 4.10).

The results from the numerical analyses (Figure 4.12) indicated that early pillar crushing was achieved for low friction angles (25 degrees) whereas late pillar crushing was achieved for higher friction angles (35 degrees). A higher friction angle therefore requires a higher level of pillar stress to ensure pillar crushing. As friction angle impacts on pillar strength, an increase in pillar w:h ratio exacerbates this effect (Figure 6.10).

The impact of parameters such as the crushed material strength UCS_b and strengthening parameter m needs to be further investigated. Other than the width to height effect on the behaviour of pillars, these two parameters have the greatest impact in estimating the residual strength of a crush pillar. It would be of great value if the magnitude of these parameters could be determined or derived from laboratory test results representing the actual rock mass properties defining these parameters, rather than estimating values aimed at reproducing representative solutions.

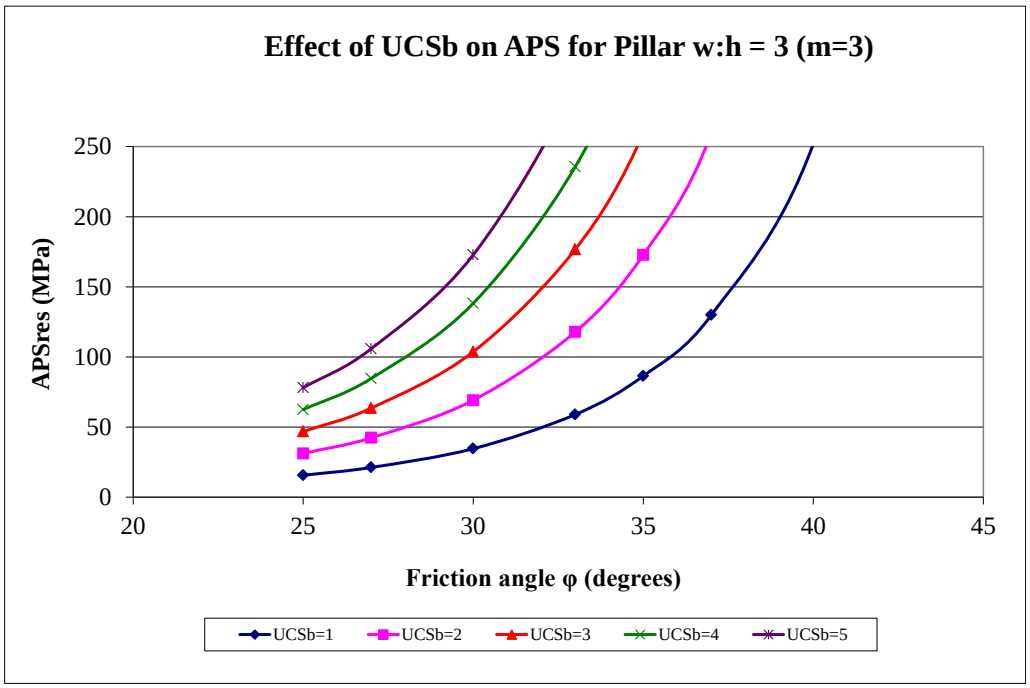

Figure 6.9: Effect of crushed material strength (UCS_b) on pillar performance.

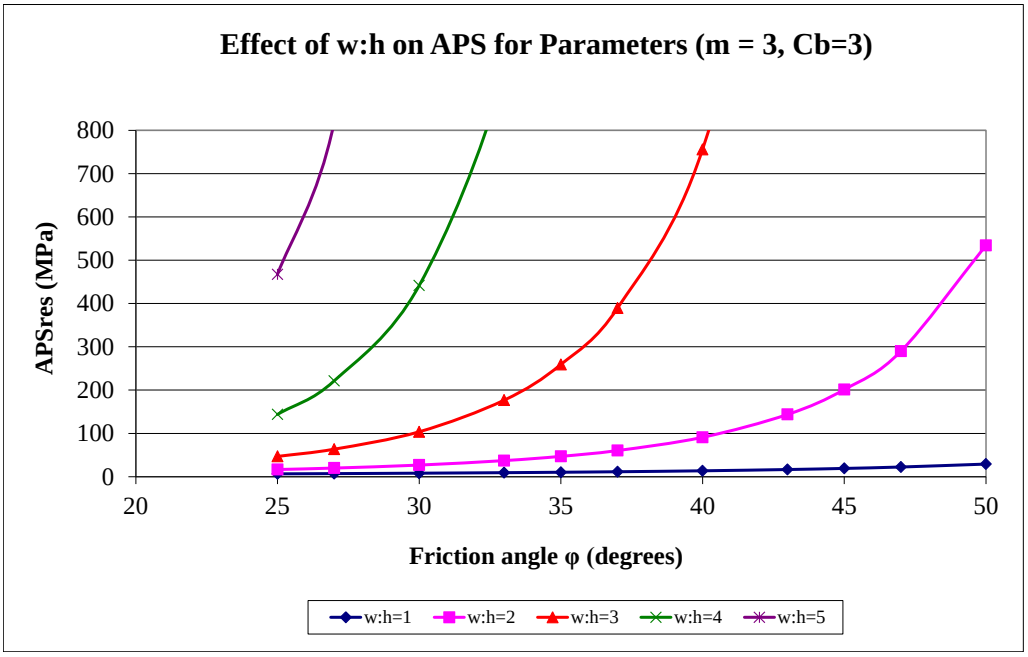

Figure 6.10: Effect of width to height ratio on pillar strength.

6.3. Use of the analytical residual APS solution as a practical tool

As mentioned in the previous section, the analytical solution derived to estimate the residual strength of a failed crush pillar is sensitive to the value of the input parameters. A comparison (Figure 6.11) was compiled using various values for the parameters as well as the values suggested by Watson and Salamon. The various combinations of input parameters are detailed in Table 6.4. The results from the instrumented pillars (Watson, 2010), punch tests (Spencer and York, 1999) and some of the TEXAN simulations from Chapter 4 (for pillar height = 2 m) are included in the figure to investigate the relevance of the solutions and the effect of the various values of input parameters on the solution.

Table 6.4: Input parameters used for the sensitivity analyses.

Output	Crushed material strength UCS_b (MPa)	Friction angle(φ) (Degrees)	Slope Failure envelope m
DUP 1	4	30	2
DUP 2	1.6	40	2
DUP 3	15	40	0.3
DUP 4	0.011	30	5
DUP 5	5	35	3

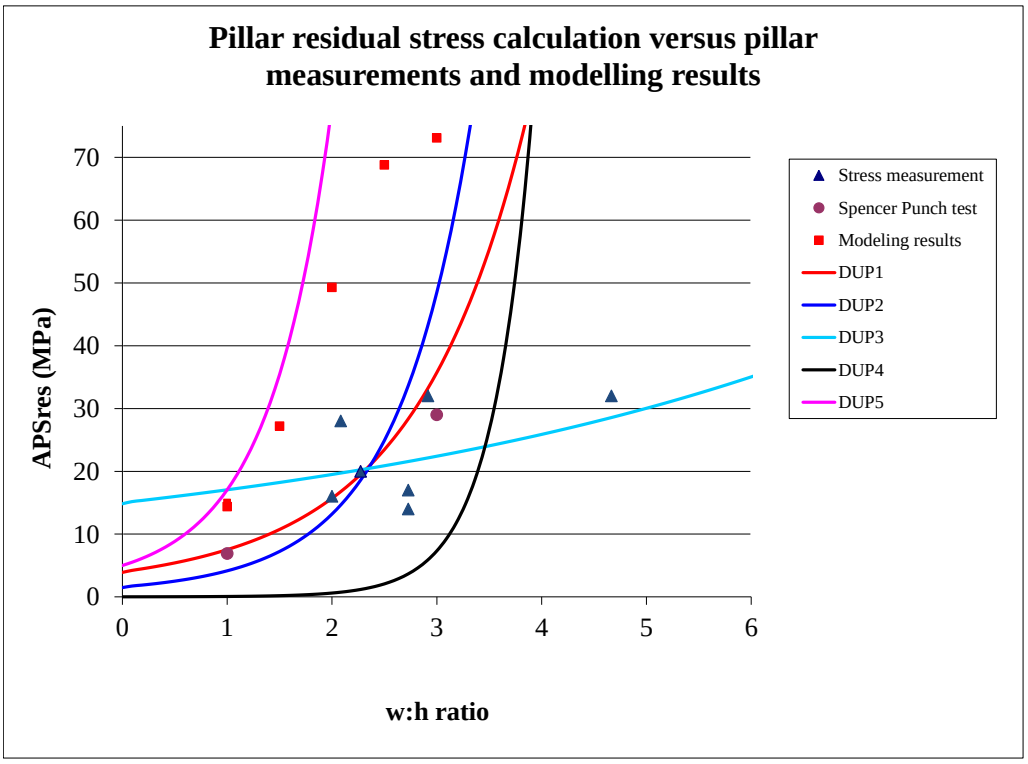

Figure 6.11: Effect of input parameters on residual pillar strength.

Figure 6.11 indicates that the output of an analytical solution can be manipulated to provide a representative solution by the choice of an input parameter such as residual cohesion, friction angle or material strength (i.e. Barron, Salamon, du Plessis). The solution derived by the author nevertheless provides a useful approximation of the underground measured pillar performances (DUP 1 in Figure 6.11).

The results of the TEXAN simulations (Chapter 4) compare well to the analytical solution when the same input parameters were used (as can be seen by comparing DUP5 and the points representing the modeling results for which the same input parameters were used). Note that the smaller simulated pillars included in Figure 6.11 (also in Figure 6.12) were already in crushed state and therefore extend just beyond the analytical curve (DUP 5). The larger simulated pillars with a width to height ratio of 2.5 and 3 were not yet in a crushed state (refer to Figure 6.12 and Figure 4.15).

To assess the numerically simulated performance of pillars with various width to height ratios and to compare it to an analytical solution, Figure 6.12 was compiled. The same input parameters were used for both the analytical solution and numerical simulations. The residual (for smaller w:h range pillars) and peak (for larger w:h range pillars) values obtained from the numerical simulations (Figure 4.15) were used to construct Figure 6.12. Note that the larger w:h range pillars did not reach a residual state and therefore the peak stress of these pillars were used. From Figure 6.12 it can be seen that for pillars within the lower range of width to height ratios the numerically simulated residual stress lies just beyond the analytical solution curve. As the width to height ratio of the pillars increase, so also does the variance in results of the two methods applied.

The preliminary numerical analyses did indicate that the pillars with a width to height ratio exceeding two were not in a crushed state. This figure indicates that the analytical solution may only be representative for pillars with low width to height ratios. Furthermore, the numerical model considered the influence of a much larger area and did not only look at the behaviour of a single pillar. The analytical solution as indicated in Figure 6.12, however, provides a two-dimensional solution (infinitely long pillars) to a three-dimensional problem. If very long pillars are simulated in TEXAN, the residual pillar stress of the failed pillars move closer to the analytical solution (pillars with w:h $\leq$ 2:1) as indicated in Figure 6.13. The residual pillar stress of these failed pillars touches or lies just below the analytical solution curve.

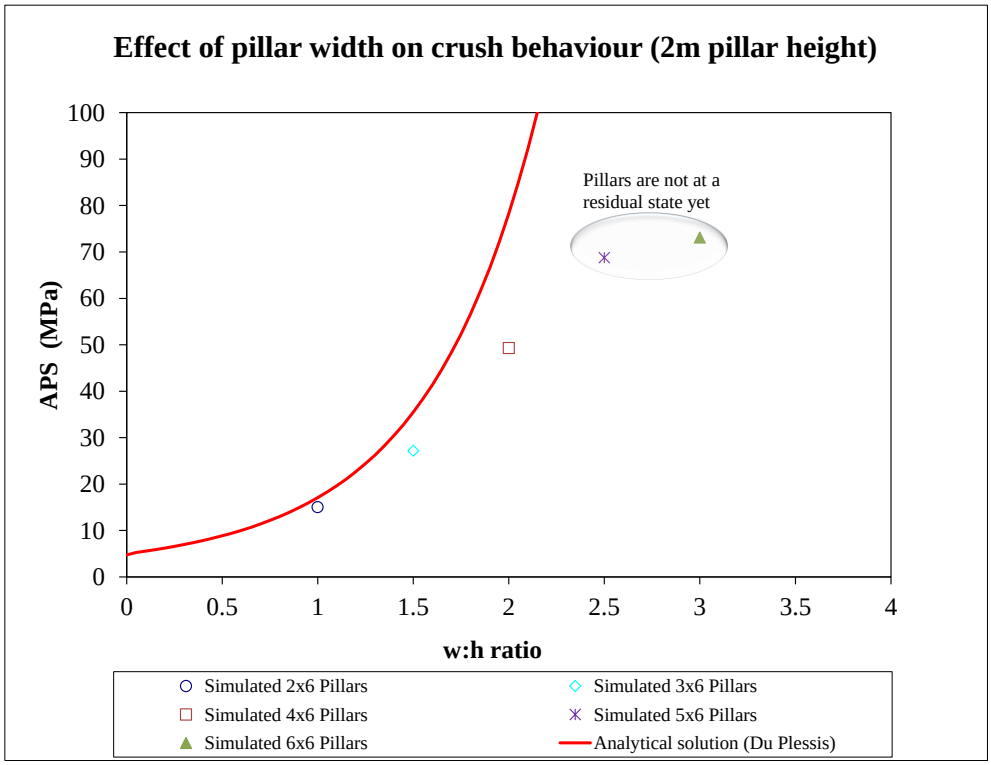

Figure 6.12: Results for the analytical solution of a completely crushed pillar (equation 6.8) and numerical simulation for pillars with various width to height ratios (the same input parameters were used for both methods of analyses).

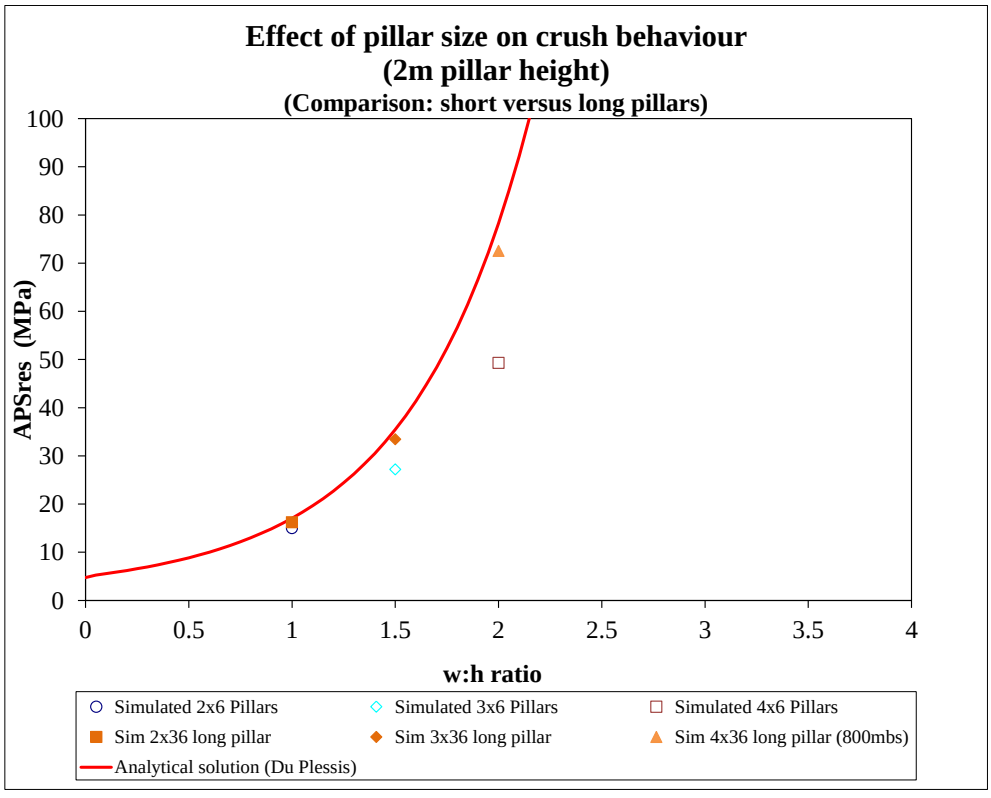

Figure 6.13: Comparison of residual pillar stress for simulated short versus long pillars (600 mbs).

Figure 6.14 combines the results of the numerical simulations and the analytical solution. The figure illustrates how the state of stress of each pillar changes and compares in relation to the analytical solution during the pillar forming stage. The behaviour of each pillar is indicated by the arrows representing the stress evolution as a result of mining. *Numbers (1, 2, 3) are used as an explanatory example for pillar w:h = 1.5*. The range includes the initial state of stress (1. pre-mining), the increase in stress as the pillar is formed (2. towards the maximum) and where applicable the reduction in pillar stress to the residual state (3. pillar crushing). From the figure it is apparent that the stress range of the larger pillars (w:h > 2) are situated far away and below the analytical solution.

Figure 6.15 compares the initial and the peak pillar stress for the various pillars. ***Line A*** represents the initial pillar stress (all pillars) and ***line B*** the peak pillar stress (for the failed pillars only). From the figure it is clear that the pillars with a larger width to height ratio (i.e. w:h > 2) are at a much lower initial stress. The pillars are therefore able to absorb the change in stress as the pillars are formed and mining progresses. The state of peak pillar stress is, however, not reached and pillar crushing is not achieved. In the back area the change in stress per mining increment reduces and the pillar core remains solid. For these pillars to crush a much higher level of initial stress is required. Numerical simulations conducted for pillars with w:h ≥ 2.5 (Figure 4. 26) indicated that the pillars did not crush even at a 1000 m below surface.

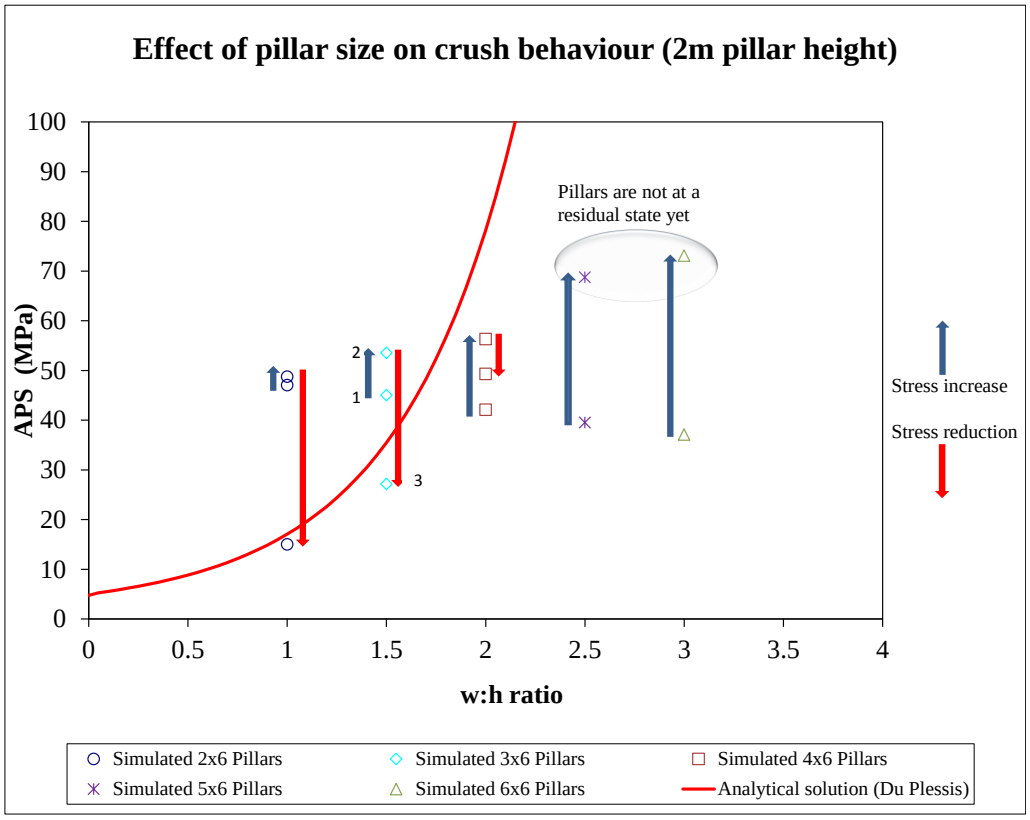

Figure 6.14: Pillar stress relationship for different pillar widths (simulated pillars at 600 mbs). Arrows indicate stress development (numbers are also used for w:h=1.5 as an explanatory example).

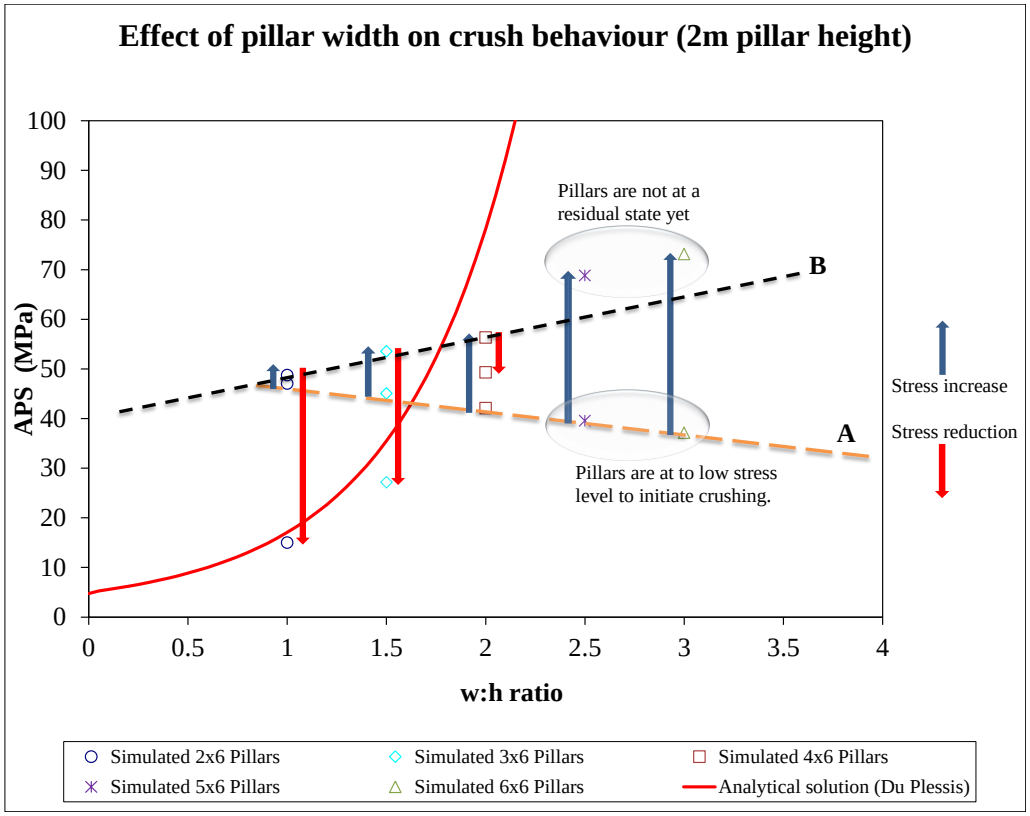

Figure 6.15: Pillar stress trends for different pillar widths (simulated pillars at 600 mbs). Line A: (initial pillar stress); line B: (peak pillar stress for crushed pillars).

6.4. Summary

In this chapter analytical solutions to determine the peak and residual strengths of crush pillars were assessed. Watson (2010) compared the results of instrumented underground pillars as well as laboratory punch tests to the solutions derived by Barron, Kuijpers and Salamon. Watson postulated that the residual pillar strength determined by these analytical solutions was overestimated at a width to height ratio exceeding approximately three. The analytical solutions did also not take consideration of the pillar foundation behaviour experienced at the larger w:h ratio instrumentation sites.

Watson (2010) applied various values for the input parameters of these analytical solutions as well as adjustments to the dimensions of the instrumented pillars. Actual pillar dimensions were adjusted to account for pillar length and sidings or gullies positioned adjacent to the instrumented pillars. The adjustments applied by Watson resulted in reduced w:h ratios. This prevents a clear analyses of what drives the pillar behaviour (i.e. pillar at w:h = 3 might not be in a crushed state yet). Also, the punch tests included in Watson's comparative analyses are not representative of the failure mechanism addressed by the analytical solution. It is very important to apply a constant approach when conducting pillar investigations.

The simple analytical solution derived by the author for this PhD study provided an equally good fit to the underground measured pillar performances compared to both the Salamon and Barron solutions. The results are, however, very sensitive to the selection of the input parameters. The output of an analytical solution can be manipulated to provide a representative solution by the choice of an input parameter such as residual cohesion, friction angle or material strength. The purpose of the analytical solutions would be to provide a first order estimate of crush pillar dimensions. The analytical solution, however, provides a two-dimensional approximation (infinitely long pillars). If very long pillars are simulated in TEXAN, the residual pillar stress of the failed pillars is in better agreement with the analytical solution.

In this chapter the derived analytical solution for the average pillar stress of a completely failed crush pillar was used as a tool to investigate the behaviour of these pillars. The results of the numerical modelling (Chapter 4) were compared to the analytical solution. The results indicated that the stress range of the larger pillars (w:h > 2:1) are situated far away from the analytical solution. These larger pillars are at a much lower initial stress. The pillars are therefore able to absorb the change in stress as the pillars are formed and mining progresses. The state of peak pillar stress is not reached and pillar crushing is not achieved. For these pillars a much higher level of initial stress is required. The peak strength of the pillar must be exceeded whilst the pillar is close to the mining face to cause complete failure of the pillar core. It is for this reason that it is envisaged that the analytical solution may only be of practical use for pillars with low width to height ratios (w:h $\leq$ 2). Numerical simulations conducted for pillars with w:h $\geq$ 2.5 indicated that the pillars did not crush even at a 1000 m below surface. The preliminary modelling results indicated that the initial stress required to ensure the crushing of a 2:1 pillar core is only achieved at mining depths greater than 600 m below surface.

It should be emphasized that all of these results and conclusions are based on the parameters assumed for both the limit equilibrium model and analytical solution. Calibration of the model, based on underground measurements and laboratory rock testing to establish accurate rock mass parameters are required to substantiate the preliminary conclusions highlighted in the chapter.

6.5. References

Barron, K. (1984). An analytical approach to the design of coal pillars. *CIM Bulletin*, vol. 77, no 868, pp. 37–44.

Kuijpers, J.S., Roberts, D.P. and Napier, J.A.L. (2008). Modelling of brittle pillar behaviour, *Proc. 1st South. Hem. Int. Rock Mech. Symp*., Perth, Western Australia, *Australian Centre for Geomechanics*, Vol.1, pp. 391-402.

Malan, D.F. and Napier, J.A.L. (2006). Practical application of the TEXAN code to solve pillar design problems in tabular excavations. *SANIRE 2006 Symposium - Facing the Challenges,* Rustenburg, pp. 55-74.

Salamon, M.D.G. (1992). Strength and stability of coal pillars. *Workshop on coal pillar mechanics and design, US Bureau of the Interior*. US Bureau of Mines, Santa Fe, USA.

Shepherd, R., and Kellet, W.H. (1969). Ribside destressing: tests in and adverse heading at Pye Hill colliery. *Colliery Guard*., 217, March. pp.166-172.

Spencer, D. and York, G. (1999). Back-analysis of yielding pillar system behaviour at Impala Platinum Mine. *Proc. SARES99,* Johannesburg, RSA, pp. 44-52.

Watson, B.P. (2010). Rock behaviour of the Bushveld Merensky Reef and the design of crush pillars. PhD thesis, School of Mining Engineering, University of the Witwatersrand, Johannesburg, South Africa.

Watson, B.P., Kuijpers, J.S. and Stacey, T.R. (2010). Design of Merensky Reef crush pillars. *J. South. Afr. Inst. Min. Metall*. pp. 581–591.

Wilson, A.H. (1972). Research into the determination on pillar size. Part 1: an Hypothesis concerning pillar stability. *The mining Engineer*, Vol. 131, pp. 409-417.

CHAPTER 7

QUANTIFICATION OF ROCK PROPERTIES

Properties of the rock contained in the Merensky Reef crush pillars

7. QUANTIFICATION OF ROCK PROPERTIES

In this chapter the properties of the Merensky Reef obtained from laboratory testing is discussed. The objective of the tests was to determine the elastic and post-peak properties of the rock contained in the pillar and pillar foundations. The results of the tests are used in the subsequent chapters for assessing the underground performance of the pillars. It was observed that the performance of the pillars depends on the composition of the pillars. If the pillar comprises of a larger percentage Anorthosite, the pillar fractures more readily. The presence of Anorthositic rock in a pillar poses a higher seismic risk, however, this is due to the brittle nature of this rock type. Post failure rock testing is typically not conducted on rock specimens from South African hard rock mines. It requires specialised equipment and only two stiff testing machines are available in the country. The equipment is not well maintained and in most cases not readily available for testing due to outstanding maintenance. Almost no historic records of any post failure rock testing on Merensky samples could be found. It is, however, important to have some insight to the post failure properties of the pillar material.

7.1. Sample selection and criteria

Six boreholes were drilled from crosscut 23M68 which is situated approximately 16 m below the Merensky Reef horizon. The spacing between the holes was approximately 1 m. The position of the holes was in close proximity to the underground mining trial. This was done to ensure that the rock samples selected for testing would be representative of the rock contained in the pillar and pillar foundations at the trial site. Although the boreholes were drilled from the crosscut position 16 m below reef and was extended to intersect the top contact of the Bastard Merensky, situated approximately 14 m above the top contact of the Merensky Reef, only about 4.5 m of core from each hole (entire hole length roughly 33 m long) was selected for testing. The area of interest consisted of the Merensky Pyroxenite (1.4 m thick), 1.5 m of the immediate footwall (FW) below the reef consisting of Mottled Anorthosite and 1.5 m of the immediate hangingwall (HW) consisting of Spotted Anorthosite. This is illustrated in Figure 7.1. These zones essentially define the pillar and pillar foundations. Elastic properties of the HW2 Mottled Anorthosite were also obtained from different boreholes drilled to conduct stress measurements (approximately 4 m above the Merensky Reef and away from the immediate fracture zone).

The reason for the boreholes being extended to the top of the Bastard Merensky contact was to determine the height and the condition of the contacts defining the Bastard Merensky Reef. The Bastard Merensky top and bottom contacts are potential weakness planes which must be catered for by the support system when in close proximity to the reef, or by means of in-stope crush pillars capable of providing the support resistance required when these contacts are situated far above the reef. The Bastard Merensky can be situated up to 45 m above the reef in some areas along the Bushveld Complex.

The diameter of the core drilled was approximately 55 mm. The specification from the rock testing service provider was that a minimum core diameter of 47.6 mm is required. Pieces of core selected from each zone of interest had to be at least 150 mm long and free from joints or fractures. This criterion was based on the service provider's requirement that the UCM and UCP tests (uniaxial compressive strength tests for elastic and post-failure deformation measurements respectively) be performed on a core length being 2.5 times the core diameter.

All of the holes drilled for the rock testing were photographed and geotechnically logged. Figure 7.2 shows a photograph of borehole 772. The rock type and jointing is visible from the photograph. Figure 7.3 is an example of the borehole log for the same borehole.

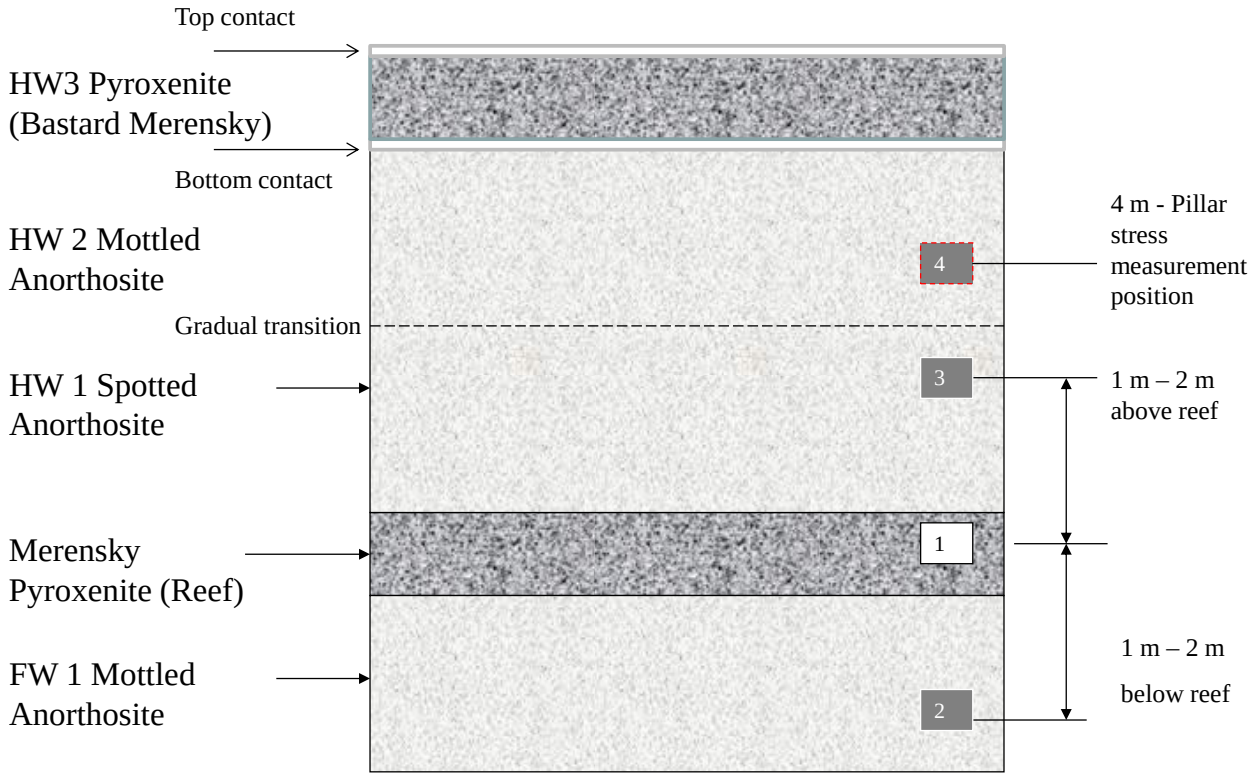

Figure 7.1: Representation of Merensky Reef stratigraphy indicating the area of interest for rock sample selection and testing.

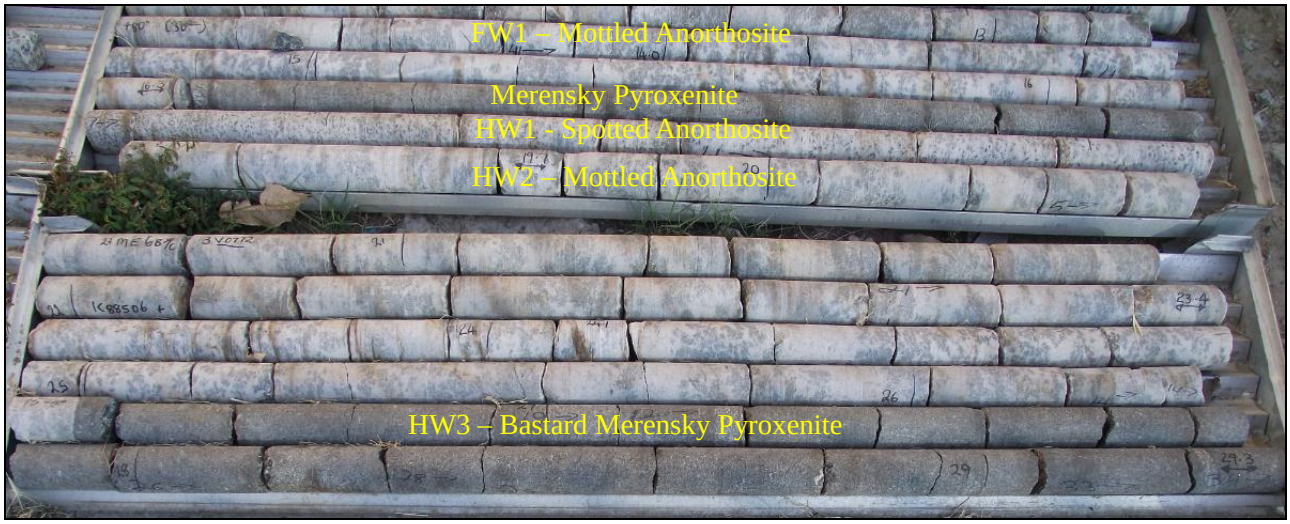

Figure 7.2: Photograph indicating rock types and joint frequency. Note that core is packed in the direction of drilling (footwall to hangingwall). The footwall therefore appears along the top of the photograph. The length of the core tray is 1.5 m.

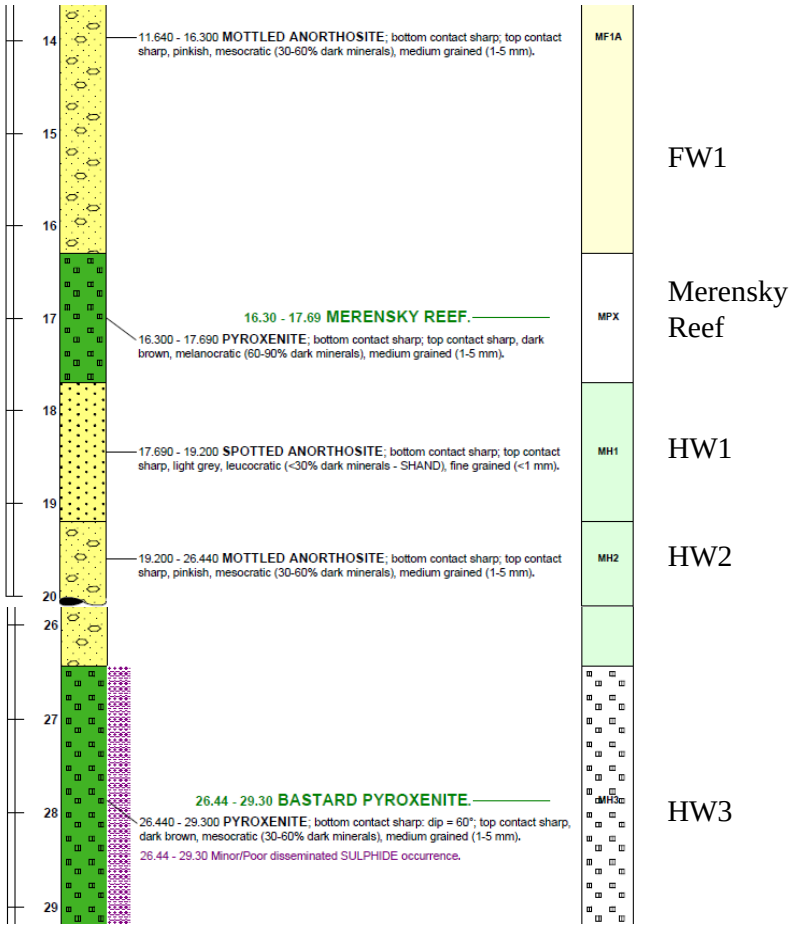

Figure 7.3: Compressed borehole log of hole 772 indicating different rock horizons. Note that the log is in the direction of drilling (footwall to hangingwall). The footwall therefore appears along the top of the log.

7.2. Results

Different rock tests were performed to establish both the elastic and post-failure properties for each zone of interest. The tests performed were:

- Uniaxial compressive strength tests (UCM)
- Triaxial compressive strength tests (TCM)
- Triaxial compressive strength tests with post-failure deformation measurements (TCP)
- Brazilian indirect tensile strength test (UTB)

A summary of the results are tabled below. According to Ryder and Jager (2002), if a near-linear strengthening relationship is found to apply in a σ_1 - σ_3 plot, an acceptable procedure is to simply establish a best-fit straight line. The value of σ_c (failure stress in the unconfined condition defining the UCS) and slope β_0 (σ_3:σ_1 relationship) can be read from the plot (e.g. Figure 7.4). The value of the friction angle (φ) and cohesion (C or C_r) can be calculated using the appropriate equations (equations 7.3 and 7.4).

Table 7.1: Uniaxial compressive and Brazilian indirect tensile strength tests (average values).

	UCM (Uniaxial) and UTB (Brazilian)			
	UCS (MPa)	Youngs modulus (E) - Tangent (GPa)	Poissons ratio (γ) (Tangent)	Brazilian tensile strength (MPa)
Merensky Pyroxenite (Reef)	140.70	108.1	0.29	9.3
Mottled Anorthosite (Footwall)	236.30	79.4	0.38	9.1
Spotted Anorthosite (Hangingwall)	171.80	76.7	0.35	9.4
Mottled Anorthosite (Hangingwall)	158.73	73.9	0.44	

Table 7.2: Triaxial compressive strength tests (average values).

	TCM (Triaxial)					
	UCS (MPa)	Youngs modulus (E) - Tangent (GPa)	Poissons ratio (γ) (Tangent)	Strength factor (Tanβ) *	Cohesion (C) (MPa)	Friction angle (φ) (deg)
Merensky Pyroxenite (Reef)	119.15	109.30	0.28	6.62	23.15	47.53
Mottled Anorthosite (Footwall)	233.25	92.10	0.39	10.67	35.71	55.95
Spotted Anorthosite (Hangingwall)	203.09	86.20	0.32	8.17	35.52	51.45

** Strength factor (Tanβ) is calculated using equation 7.2*

Table 7.3: Triaxial compressive strength tests; Post-failure results (average values).

	TCP (Triaxial - Post failure)					
	UCS (MPa)	Youngs modulus (E) - Tangent (GPa)	Poissons ratio (γ) (Tangent)	Strength factor (Tanβ) *	Cohesion (C_r) (MPa)	Friction angle (φ) (deg)
Merensky Pyroxenite (Reef)	138.00	119.70	0.26	2.76	41.57	27.87
Mottled Anorthosite (Footwall)	231.17	85.17	0.34	4.57	54.05	39.87
Spotted Anorthosite (Hangingwall)	178.32	85.05	0.36	6.26	35.65	46.42

** Strength factor (Tanβ) is calculated using equation 7.2*

The confining stress applied for the triaxial tests were at:

- TCM: 5, 10, 15, 20 and 30 MPa,
- TCP: 8, 20, 35 and 50 MPa.

7.2.1. Strength criteria

There is an increase in triaxial strength with an increase in confining stress (σ_3). However, this does occur with a significant amount of scatter. Figures 7.4 and 7.5 indicate the triaxial results for the three rock types tested. The value of the axial stress at zero confining stress defines the UCS (σ_c) and the initial slope of the $\sigma_1 - \sigma_3$ relationship the strengthening parameter β_0 (Ryder and Jager, 2002). This relationship is indicated in the formula displayed for each linear trendline on each figure where x and y represents σ_1 and σ_3 respectively so that:

$$\sigma_1 = \beta_0 \cdot \sigma_3 + \sigma_c \qquad (7.1)$$

Where

σ_1 = Stress required to cause failure of the rock or flow if the rock is already broken

σ_c = Failure stress in the unconfined condition

σ_3 = Confining pressure (pillar side restraint)

β = Slope of the straight line

β_0 = Tanβ as depicted in equation 7.1 and 7.2.

with

$$Tan\beta = \frac{(1 + Sin\phi)}{(1 - Sin\phi)} \qquad (7.2)$$

$$C = \frac{\sigma_c}{2\sqrt{\beta_0}} \tag{7.3}$$

$$Sin\phi = \frac{(\beta_0 - 1)}{(\beta_0 + 1)} \tag{7.4}$$

The UCS is indicated by the dashed extrapolation of the linear trendlines in Figures 7.4 and 7.5. Figures 7.6 to 7.8 show the results for the reef, footwall (FW) and hangingwall (HW) correspondingly.

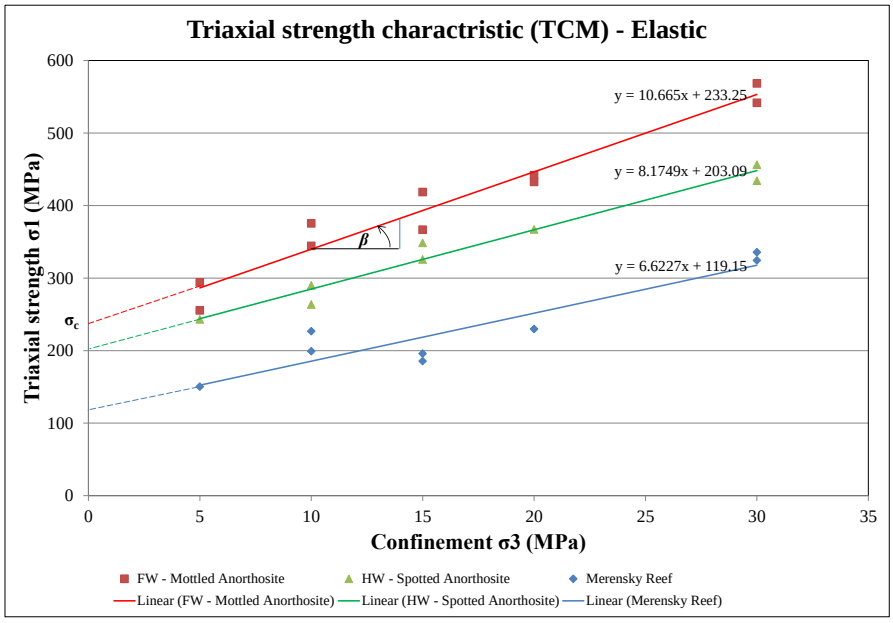

Figure 7.4: Triaxial strength characteristic for the Elastic tests (TCM).

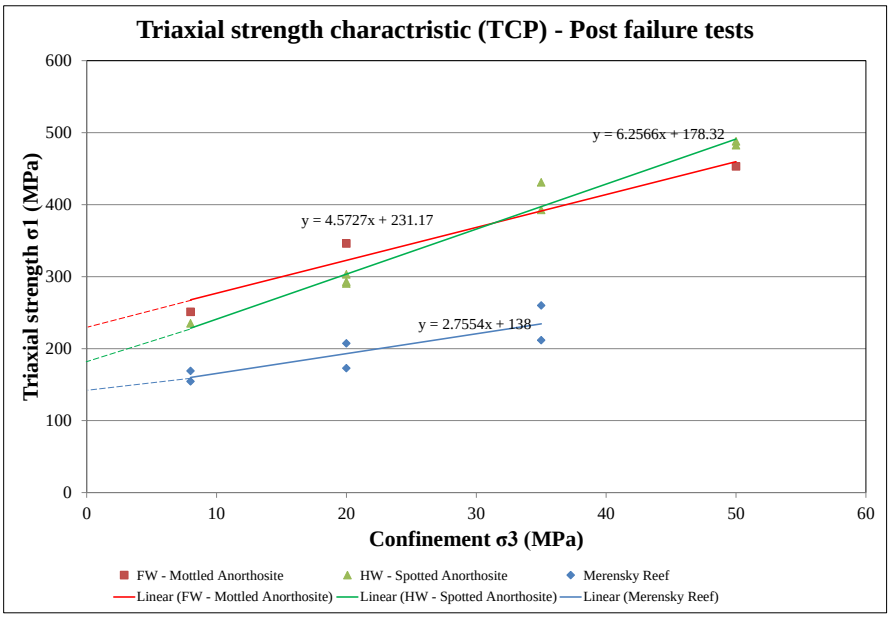

Figure 7.5: Triaxial strength characteristic for the Post-failure tests (TCP).

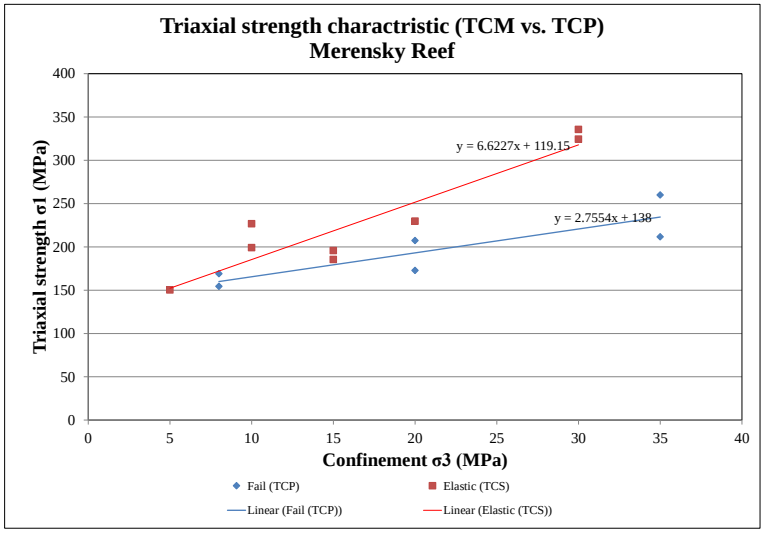

Figure 7.6: Triaxial strength characteristic for the Merensky Pyroxenite.

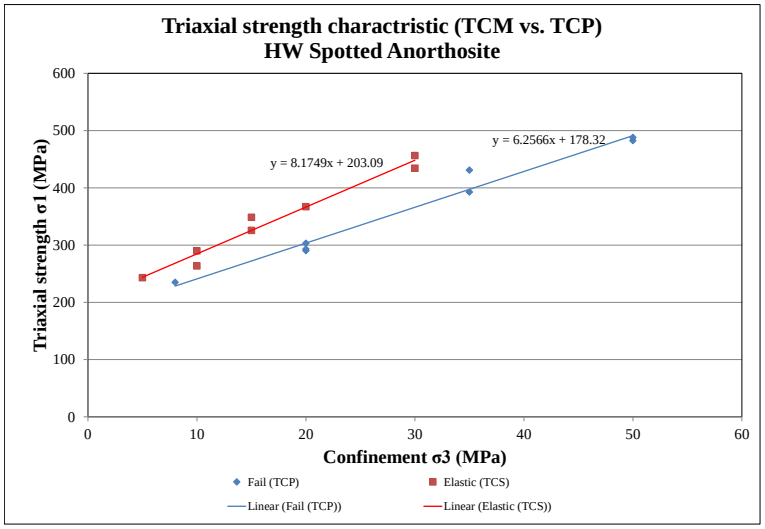

Figure 7.7: Triaxial strength characteristic for the hangingwall Spotted Anorthosite.

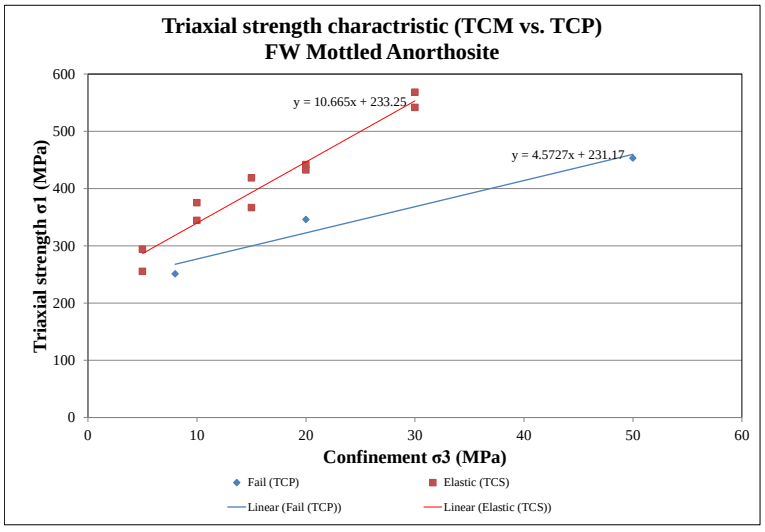

Figure 7.8: Triaxial strength characteristic for the footwall Mottled Anorthosite.

7.3. Summary

The rock testing provided both elastic and post-peak deformation parameters for the three different rock types defining the pillar and pillar foundations. No reliable record could be found of any post failure rock testing on Merensky samples. It was therefore important to gain some insight into the post failure deformation properties of the pillar material. The samples selected were retrieved from boreholes in close proximity to the underground trial mining site to ensure the results would be representative. The derived rock properties are considered in the subsequent chapters for assessing the underground performance of the pillars.

From the evaluation of the results, a strengthening parameter (β_0) could be derived. There is no relationship between the strengthening parameter (β_0) which is a function of the rock's internal properties, and the strengthening parameter (m) of the limit equilibrium model.

The strengthening parameter and friction angles achieved from the post-peak measurements are low and characteristic of what could be anticipated from failed material. The relevance of all the parameters with regard to crush pillars will have to be quantified through further assessment and back analyses. Also, underground the failure mechanism of the pillars might be different from the failure experienced by rock specimens subjected to uniaxial and triaxial loading in a laboratory.

7.4. References

Ryder, J.A. and Jager, A.J. (2002). *A textbook on Rock Mechanics for Tabular Hard Rock mines*. SIMRAC, Johannesburg.

CHAPTER 8

UNDERGROUND TRIAL – PART A

Visual observations and qualitative descriptions

8. UNDERGROUND TRIAL PART A: VISUAL OBSERVATIONS

Chapter 8 and 9 will cover all of the aspects of the underground trial. The two chapters have been compiled to describe:

- Chapter 8: Visual observations and qualitative descriptions,
- Chapter 9: Measurements and quantitative behaviour.

Chapter 8 is structured to describe:

- The trial site,
- The general pillar behaviour observed throughout the trial,
- Some specific pillar behaviours observed whilst individual pillars were being cut during the extraction of the final mining section.

From the observations, the failure mode of the crush pillars could be recorded and interpreted to provide a guide on the behaviour of this type of pillars applied in a specific environment (intermediate depth, shallow dipping hard rock narrow tabular orebody). This has not been systematically recorded for crush pillars before. It was established that the mining sequence influences the stress orientation above a pillar. This in turn initiates fracture development, orientation, slab migration and failure plane interaction. A distinctive failure pattern and sequence was identified in the failed pillars, some of which could be related to failure modes identified in failing pillars in other environments.

The motivation to establish a crush pillar trial site

Lonmin's long term mining strategy entails mining at increased depth, optimising extraction and managing the risk associated with mining at depth. An underground trial mining site was established to investigate the behaviour of crush pillars and the rock mass in an area where the mine stability would be dependent on these pillars. The objective of the trial was to gain a better understanding of the pillar system and the associated risks as highlighted in the previous chapters.

The typical terminology to describe the appearance of rock or pillars as it deforms may not be universally applied and therefore some definitions are provided below:

Definitions

Spalling or scaling pillars refers to the process where slabs of rock defined by fractures close to the surface of a pillar are pushed outward and appears as broken slabs or sheets along the external surface of a pillar. These slabs are typically formed parallel to the surface of a pillar as a result of the formation of stress (tensile) fractures. In most cases the expansion of the fractures are also characterised by the buckling and

rotation of the slabs. In South African platinum mines the term scaling is commonly used to describe the spalling process. This term will be used throughout the document.

Slabbing forms part of the process described above. It is typically observed when the slabs defined by the fracture planes are pushed outward and rotate (no buckling of the slabs).

Baggage is referred to as the fractured zone which shows signs of dilation or bulking. This portion of the pillar is characterised by the observed scaling or slabbing.

Crush: When a pillar is deforming and significant scaling or slabbing is observed along the surface of the pillar. The pillar will be in a in a post-peak or residual state. Vertical extension fractures will extend through the entire width of the pillar.

Semi crushed: Refers to a pillar which is displaying some minor scaling or slabbing along the surface of the pillar. The pillar might have reached a post-peak state, however, the pillar is not fractured throughout and is not at a residual state yet. Can also be referred to as partially crushed pillars.

8.1. Crush pillar trial site

Lonmin Platinum Limited's Marikana operations are located approximately 50 km west of Pretoria on the Western Limb of the Bushveld Complex (refer to Figures 1.5 and 8.1). Both the Merensky and UG2 Reef horizons are exploited for Platinum Group Metals. Mining operations are conducted using opencast and underground mining methods along the approximately 28 km strike length of the mining lease area. An underground crush pillar trial site was established on Lonmin's Karee 3 (K3) shaft. This is currently the deepest Merensky Reef mining section on Lonmin (Figure 8.2).

The trial site was established on 23 level, which is at a depth of approximately 770 mbs. The Merensky Reef was mined using a split down-dip layout mining from 23 to 24 level (800 mbs). The pillars were situated in the middle of a "panel" and away from other excavations (i.e. raise) which could possibly influence the pillar behaviour (Figure 8.3). The pillars were required to be cut 2 m wide and 4 m long with a 2 m pillar holing separating adjacent pillars. Based on this, the anticipated w:h ratio would be approximately 1.4 - 1.7, depending on the actual stoping width at the pillar position. The anticipated stoping width was expected to range between 1.2 m and 1.4 m. The pillar lines were approximately 35 m apart on strike. Level spacings are approximately 180 m apart on dip. The reef dips at approximately 8 degrees.

8.1.1. K3 shaft geological environment pertaining to the Merensky Reef

The shaft geology is described by Pillai (2013). On K3 shaft the Merensky orebody consist of a mineralised Pyroxenite containing one or more visible chromitite layers which are used as reference markers for stoping. Across the K3 Shaft block area the average thickness of the Merensky Pyroxenite is around 1.2 m. However, mining parameters are determined by the Geology and Evaluation departments based on the value distribution in relation to the chromitite layer to ensure economical extraction. The average stoping width can therefore vary.

The strike of both the UG2 and Merensky orebodies at K3 Shaft are typically east-west, dipping towards the north at an average of 10 degrees. The Merensky Reef is separated from the UG2 Reef by a 145 m thick middling of inter-layered Norites and Anorthosites (Merensky Reef situated above the UG2 Reef). The middling to the top of the Bastard Merensky Reef (Hangingwall 3) above the Merensky Reef varies between 10 m and 13 m. Both the top and bottom contacts of the Bastard Merensky are potential planes of separation.

The K3 Shaft block area is bounded by 2 major fault zones striking in a NNW - SSE direction, namely the Marikana fault zone on the eastern boundary and the Spruitfontein fault zone on the western boundary. The Spruitfontein fault zone has an estimated up throw displacement of 4 - 10 metres to the west. The Marikana fault has a down throw displacement to the east of approximately 15 - 20 metres. A trend of minor faulting is present within the K3 Shaft block area. These “mostly” reverse faults strike ESE to WNW and rarely have a displacement of more than 2 m. Jointing is common at K3 Shaft with both open and closed joints present as recorded underground during geological mapping. Sporadic feldspar, pegmatite and calcite veins occur along major joint sets as “infill” resulting in healed or closed joints. Similar to the faults, joints also vary in strike, dip and characteristics. Two major joint sets are recognised. This classification is based on their strike, dip and characteristics. These are:

- J1: NNW-SSE striking joints, approximately vertical: These joints are characterised with high frequency of talc-chlorite-sericite infilling and may be closely spaced, creating blocky ground conditions. The joints also have a similar orientation to the major fault structures.
- J2: ESE-WNW striking joints, dipping 60 - 80 degrees: These are the most prominent joints and are frequently associated with pegmatite infill.

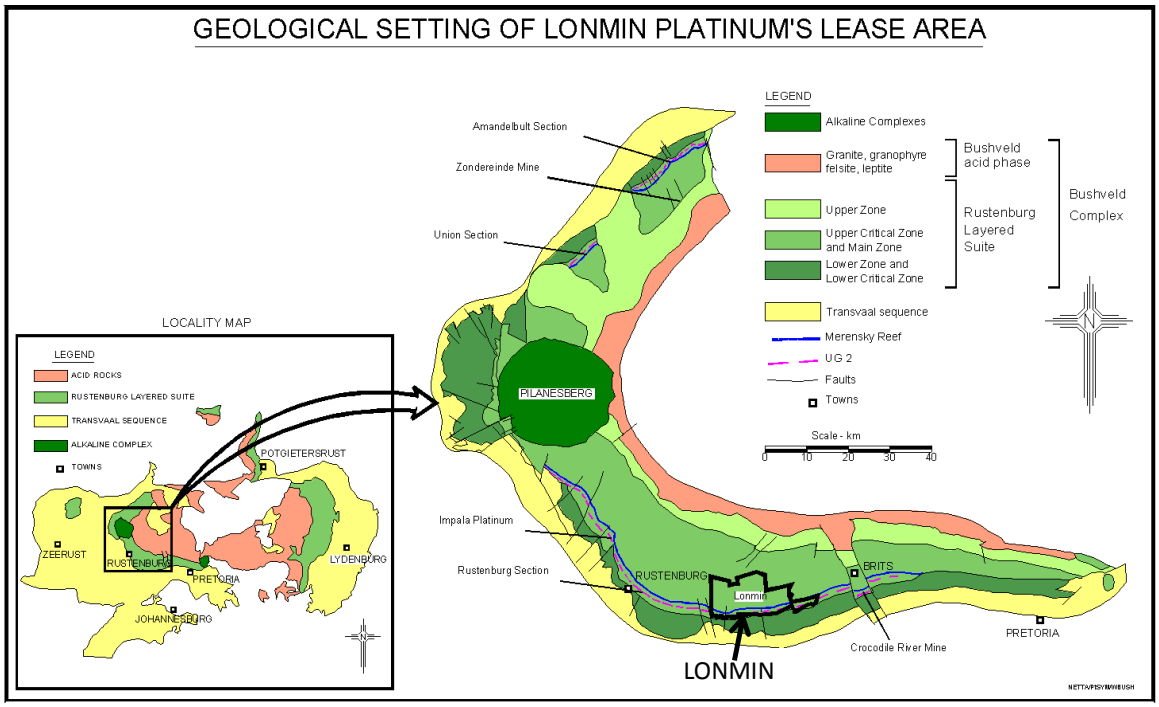

Figure 8.1: Locality of Lonmin Platinum in relation to the Bushveld Complex.

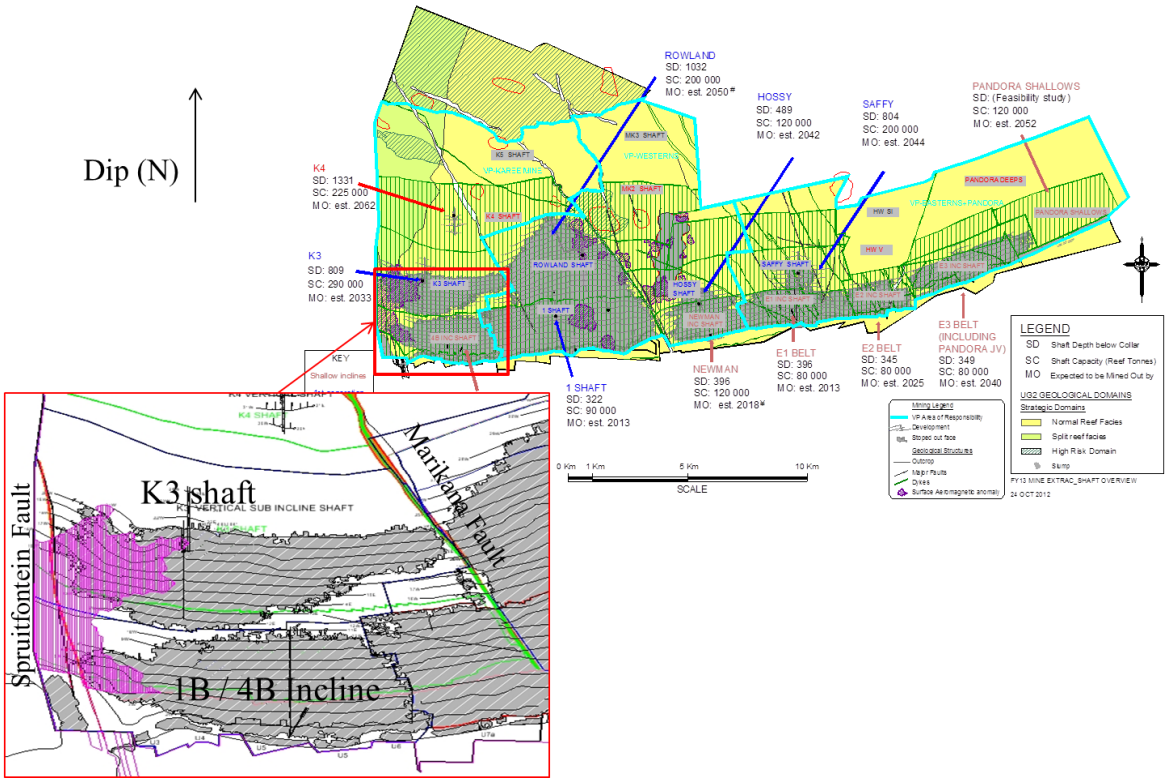

Figure 8.2: Locality of Lonmin's K3 operation.

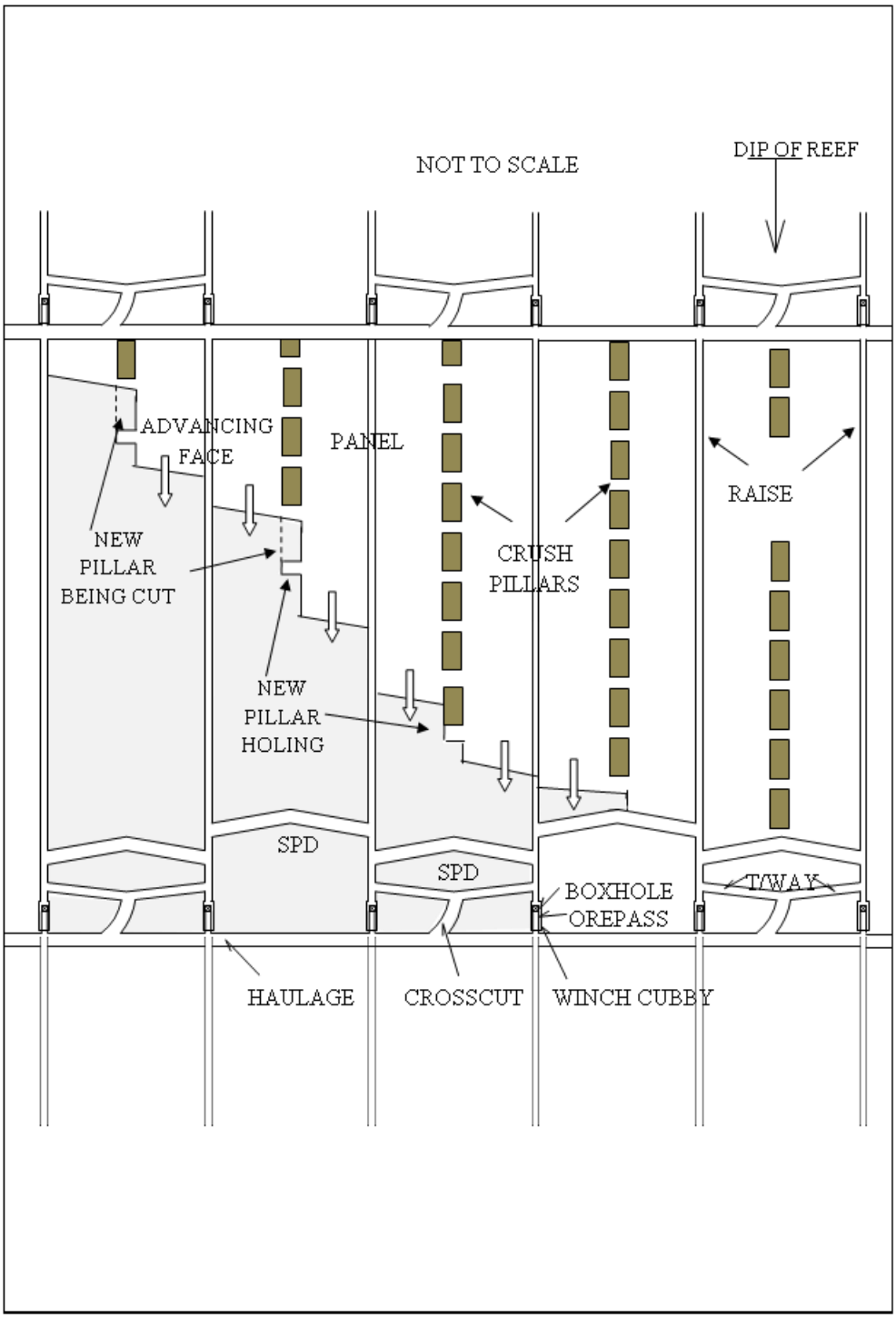

Figure 8.3: Crush pillar down-dip split panel layout as used in the trial section.

8.1.2. Problems experienced with establishing a crush pillar trial site

The initial trial site was planned to be mined from 24 – 25 level. This site was established in May 2012. The site was, however, abandoned in July 2012 when mining intersected a series of faults and potholes. Due to the adverse ground conditions intersected, a significant amount of ground was left unmined and resulted in a poor layout for the pillar monitoring trial site. The first crush pillars on Lonmin were cut in this section. In August 2012, a 6 week long Lonmin strike (10 August – 20 September 2012) occurred. A new trial site was identified in November 2012. All of the findings described in this and the next chapters are based on the pillar behaviour monitored at this site, which mined from 23 - 24 level using crush pillar support. The site consisted of 6 adjacent panels exposing a sufficiently large area in which the pillar and rock mass behaviour could be assessed (Figure 8.4).

Six individual instrumentation sites were initially planned and identified for monitoring. The objective was to record the behaviour of differently sized pillars at these sites to understand the behaviour of these pillars. For all the sites, the pillars were specified to be 2 m wide and 4 m long. However, it was anticipated that this would not necessarily be achieved owing to practical mining difficulties. By April 2013, most of the panels towards the east were mined out, including the initial planned instrumentation sites. The production line management were not very keen to stop production to wait for the installation of instruments, although they were requested to do so. The aim was to have the instruments installed in time to ensure that measurements could be obtained prior to the specific pillar being formed. The scenario was planned whereby a sufficient lead lag distance would be established by the panels mining either side of the “planned” instrumentation site (pillar). This required that these panels had to stop for approximately one week to ensure that the holes for the strain cells, extensometers and borehole camera surveys could be drilled. In a production environment, this kind of stoppage is very hard to enforce and resulted in most of the panels being extensively mined prior to the instrumentation being installed. Furthermore, several problems were experienced with the drilling contractors. This involved a lack of service and supervision resulting in either delays, drilling the wrong diameter holes or pre-mature removal of the drill rig in the case where the hole position and diameter had to be verified or over-coring being required. These holes could therefore not be used and the instrumentation site had to be abandoned.

By June 2013, the focus area of the trial was moved to the pillars between raise lines E2C and E3 where a sufficient lead lag was available.

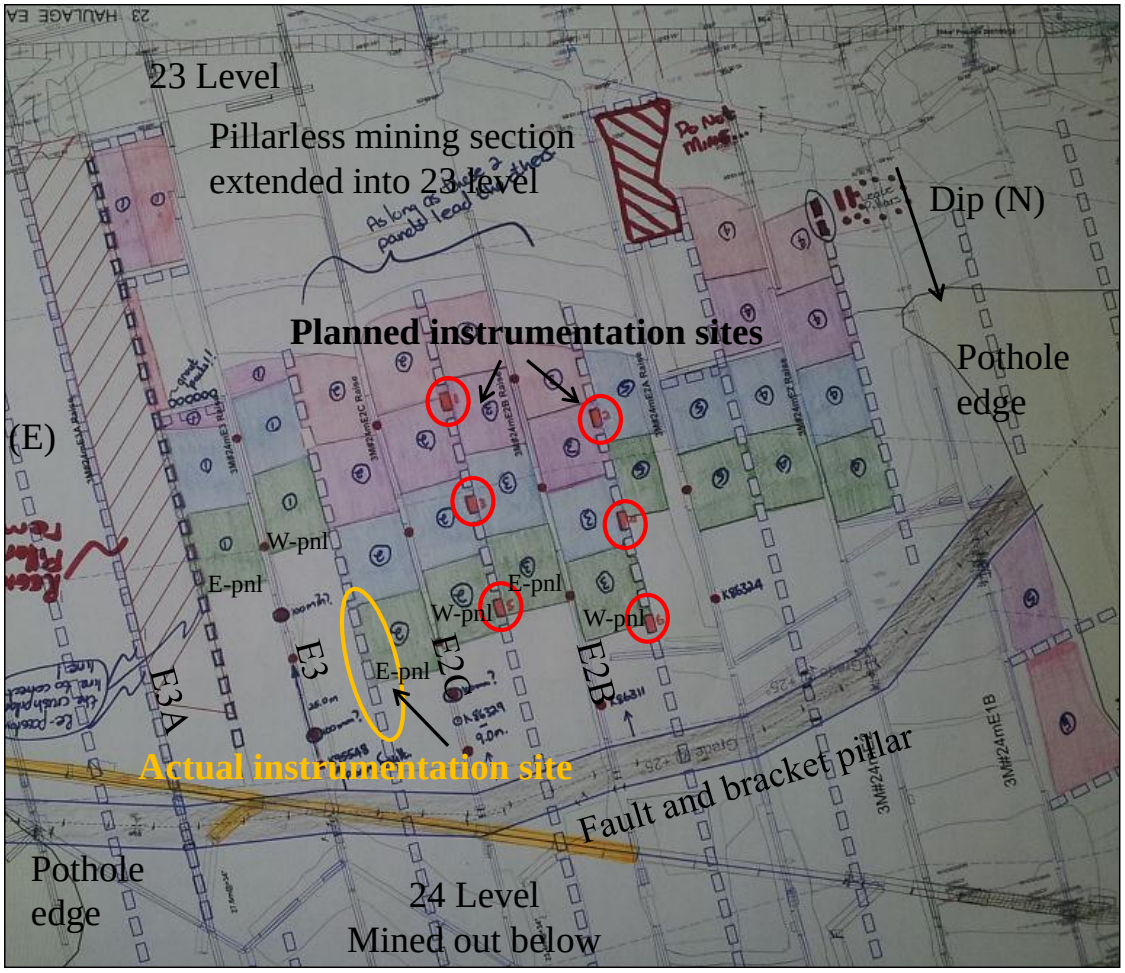

Figure 8.4: Planned mining in the trial section on 23 level (November 2012). Coloured blocks in the panels indicate planned mining related to a subsequent month. Also see the position of the planned instrumentation sites versus the final site as a result of production pressure and mining discipline.

Status at the end of June 2013:

- The first instrumented pillar (P1) was cut in April 2013 with the strain cell only installed on 20 May 2013 (Figure 8.5). This first site (P1) was treated as a "trial and error" site to ensure that the various instrumentation was well understood before monitoring the final pillars.
- Both the east and west panels adjacent to raise line E2C had almost mined to the position of the fault bracket pillar.
- The east panel of raise line E2C, which formed the western boundary of the line of crush pillars which would be instrumented, stopped just short of the bracket pillar. It was anticipated to mine this panel for another 10 m if conditions allowed it.

- The western panel of raise line E3 formed the eastern boundary of the line of crush pillars. The panel only mined until the end of April 2013 and advanced approximately 5 m beyond the first instrumented pillar position (P1).
- The panels towards the east (E3A raise line) were also approximately at the bracket pillar position when all mining was stopped.

An additional 3 pillars were identified for monitoring (P2, P3, P4). The pillars were situated in the same pillar line immediately down-dip of the first instrumented pillar. The final instrumentation sites were therefore situated in the area with limited mining remaining (approximately 25 m of advance) before these panels would also stop against the bracket pillar. It nevertheless created good monitoring sites with large mining spans being created as a result of the surrounding mining. As all mining in the trial section was temporarily stopped, the instrumentation site preparation could be completed.

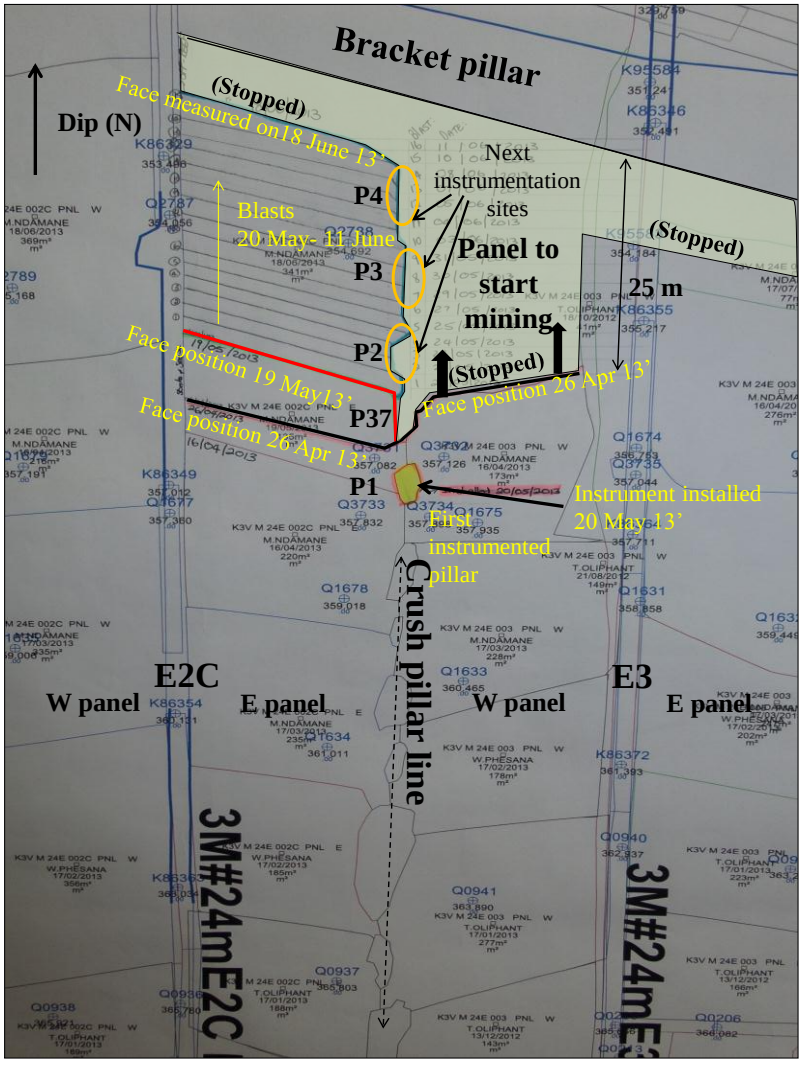

Figure 8.5: Plan of face positions (July 2013) before the final mining started. The highlighted area indicates the remaining area of unmined ground.

Mining of the panels either side of the instrumented pillar line was expected to start in January 2014 after the Christmas break. Unfortunately another strike action started on 23 January 2014 and continued until 25 June 2014. As a result, the crush pillar trial was again put on hold. Mining of panel E3 West started in March 2015. The area was not mined since the end of June 2013.

8.1.3. Overview of the trial layout and parameters

The trial area (Figure 8.6) was mined using conventional drill and blast techniques. Split dip panels (14 m face lengths) were mined either side of a centre-raise, resulting in a maximum inter-pillar span of 31 m between lines of crush pillars. The average stoping width mined in the trial section was approximately 1.3 m. The w:h ratio was therefore approximately 1.5 based on the planned 2 m pillar width. The down-dip panels in the crush pillar site were stopped against a bracket pillar which was left along a 1.5 m strike orientated (E–W) reverse fault. No reef regional pillars were cut in the trial section as two large potholes (off-reef structures) were situated either side of the trial site. The area above the trial site was supported by dip regional pillars which provided the regional stability and partially intersected the top portion of the trial area. Furthermore, there were smaller potholes intersected in the mining area which provided additional regional stability. As previously mentioned, by the end of February 2015, only one active mining panel remained in the trial site along which the final four crush pillars would be formed. Two of these pillars were extensively instrumented.

Table 8.1: Parameters of the trial site.

Depth of mining (mbs)	782 - 800
Reef dip (deg)	8
Crush pillar width - planned (m)	2
Stoping width (m)	1.3
No. of pillars cut	55
Area mined (m^2) arbitrarily chosen to include the entire crush pillar area	22000

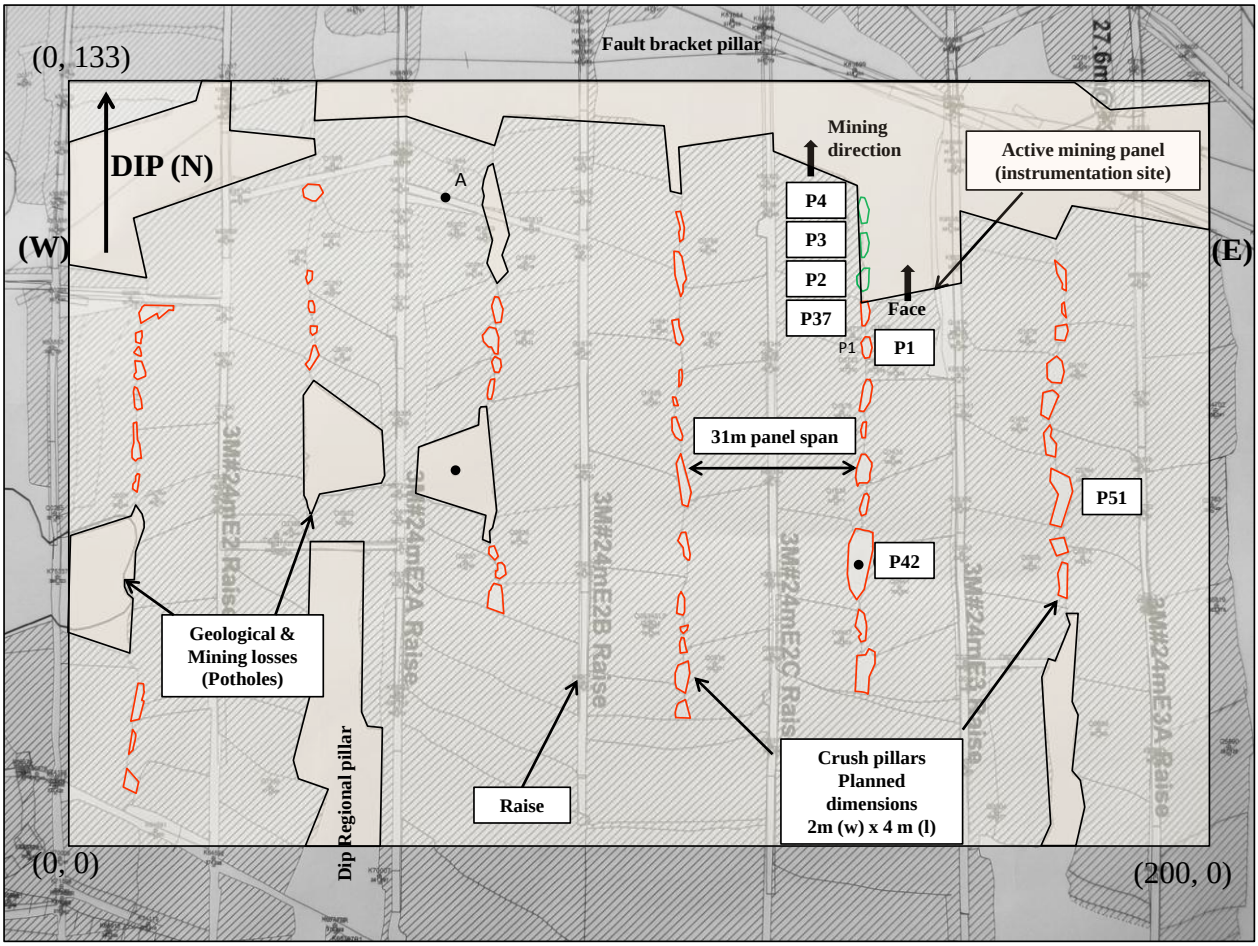

Figure 8.6: Plan view indicating trial area, layout elements and parameters. The existing crush pillars are shown in red and planned pillars (P2, P3, P4) in green. The plan indicate the face positions during February 2015.

Of the 6 panels mined, only 2 panels were extensively instrumented. Continuous strain cells were installed above three pillars to determine the stress change during the pillar formation cycle. Two absolute stress measurements were also conducted to calibrate the continuous stress measurements and the numerical model. Other forms of monitoring conducted included:

- Physical observations,
- Photogrammetry,
- Pillar borehole surveys,
- Pillar dilation measurements,
- Separation of potential partings in the hangingwall,
- Pillar fracturing using micro seismic measurements.

Of the 55 crush pillars cut, a range of actual width to height ratios were achieved (Table 8.2). This was as a result of poor pillar cutting discipline as well as layout restrictions. In the trial area, approximately 22000 m^2 was mined. 87 Percent of the pillars had a w:h ratio of less than 2:1 and only seven pillars had w:h ratios greater than 2:1 with the maximum pillar width being 3.1 m.

Table 8.2: Pillar w:h ratio distribution at the trial site.

w:h ratio	Pillar dimensions
<1	29%
1 - 1.5	36%
1.5 - 2	22%
>2	13%

8.1.4. Geotechnical characterization of the crush pillar site

Stress environment

Stress measurements conducted on K3 shaft (Coetzer, 2003) at a depth of 820 mbs and in close proximity to the crush pillar trial site, indicated that the major principal stress was orientated horizontally (E-W). The results of the stress measurements are illustrated in Table 8.3 and Figure 8.7. The measured virgin vertical stress (23.2 MPa) corresponds well with the calculated virgin vertical stress (24.1 MPa) at the corresponding depth using equation 8.1. The k-ratio (ratio of horizontal : vertical stress) is approximately 1.8. Stress measurements conducted at K4 shaft, immediately down-dip of K3 shaft at a depth of 896 mbs, indicated very similar stress orientations. The magnitudes differed slightly and the major principal stress orientated approximately N-S, aligned with the major fault structures (Figure 8.8). The magnitude of the vertical stress for both measurements were almost identical.

$$\sigma_v = \rho g h \qquad (8.1)$$

With

ρ = Average density of the overburden rock mass (3000 kg/m^3)

g = Gravitational constant (9.81 m/s^2)

h = Depth below surface (m)

Table 8.3: Principal virgin stress magnitudes and orientations measured on K3 shaft.

	σ_1 (E-W)	σ_2 (N-S)	σ_3
Stress magnitude (MPa)	45.1	28.8	25
Bearing (strike) degrees	91	182	277
Dip (degrees)	23	2	-67

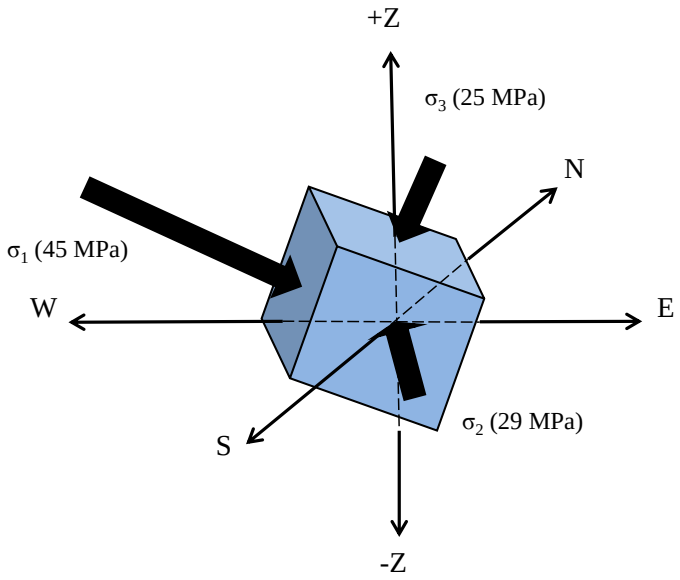

Figure 8.7: Virgin principal stress magnitudes and orientations from stress measurements conducted at K3 shaft.

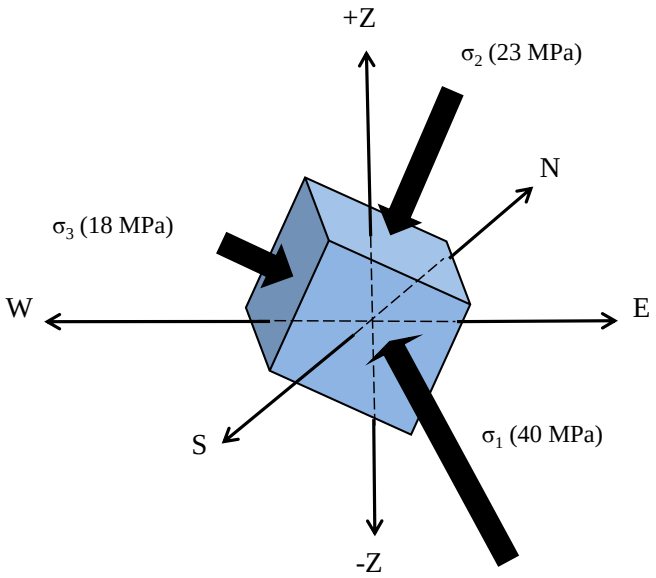

Figure 8.8: Virgin principal stress magnitudes and orientations from stress measurements conducted at K4 shaft.

Rock strength

As indicated in Chapter 7, the strength of the Merensky footwall, reef and hangingwall vary. The footwall Mottled Anorthosite is the strongest (236 MPa) compared to the reef (140 MPa), the hangingwall 1 Spotted Anorthosite (171 MPa) and hangingwall 2, Mottled Anorthosite (158 MPa).

Parting planes

On K3 shaft, the middling to the top of the Bastard Merensky Reef varies between 10 m and 13 m. Occasionally there is an inconsistent parting plane present at approximately 1.5 m in the hangingwall. Results from geotechnical logged drill core indicated good ground conditions to exist in the immediate hangingwall of the Merensky Reef. Exceptions do exist in geologically disturbed areas. Hangingwall instability is predominantly limited to the presence of doming features, low angle joints and shear zones.

The middling layer comprising of the HW1 / HW2 (Spotted / Mottled Anorthosite) series between the Merensky Reef and Bastard Merensky Reef has similar properties to the upper Anorthosite series above the Bastard Merensky (Figure 8.9). The behaviour of the immediate hangingwall (HW1 / HW2) will, however, be dominated by the overlying Bastard Merensky Reef as a result of the parting potential which could exist along the top and bottom contacts. Consequently, the Bastard Merensky Reef will act as deadweight on this middling layer.

In general, the cohesive strength of the bottom Bastard Merensky contact is less than that of the top contact. Separation along the bottom contact will most likely result in separation along the top Bastard Merensky contact due to the reduction in confinement. Figure 8.10 is a photograph of the K3 core used for the rock testing. These contacts are visible in the figure.

The upper Anorthosite series which extends from above the top Bastard Merensky contact to surface, behave to its bulk properties rather than to the shear properties of the inherent joints. As a result this competent zone is not influenced by the behaviour of the immediate hangingwall to the Bastard Merensky Reef. The stability requirements for the immediate hangingwall (HW1, HW2, HW3) and upper Anorthosite series are therefore very different and must be catered for through the application of a crush and regional pillar system respectively.

Figure 8.9: Diagram indicating hangingwall stratigraphy. The crush pillars are indicated by the piles of broken rock.

Figure 8.10: Photograph indicating the condition of the top and bottom contacts of the Bastard Merensky Reef.

8.2. Underground observation of the pillar behaviour in the trial section (excluding the final mining section)

The condition of the pillars was visually assessed during underground site visits. The intent was to determine if the pillars were in a crushed state, if the pillars were crushing when being formed at the face and if blocks of unmined ground (i.e. potholes) have an impact on the pillar behaviour for the pillars in these areas.

Some of the characteristics observed included:

- There appears to be a distinct failure pattern,
- Fracture intensity was more profound on one side of the pillar,
- Buckling of the fractured slabs was either along the top or the bottom of the pillar depending on the mining sequence,
- Fracturing of solid abutments occurred ahead of the mining face, indicating that the stress was sufficiently high to initiate early pillar crushing,
- Pillars were fractured whilst being formed at the mining face (e.g. P37; see Figure 8.11 indicating the pillar position and Figure 8.19 regarding the actual condition),
- The composition of the pillar, including the exposed hangingwall rock, influenced the pillar behaviour.

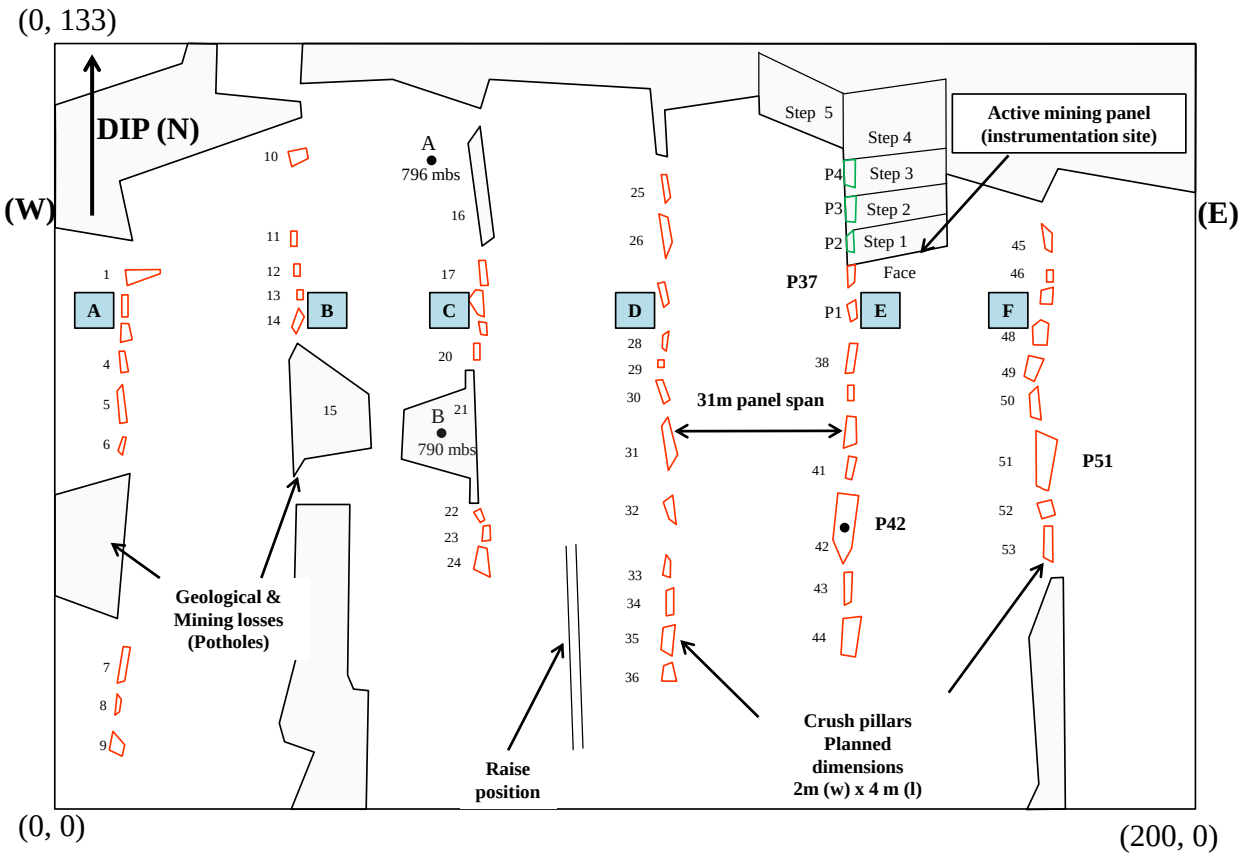

Figure 8.11: Digitized layout of the crush pillar trial section indicating approximated pillar outlines, mining face positions and anticipated future mining (Step 1 – 5). Pillars with green outlines (P2 – P4) will be cut once mining resumes. Position of the blocks numbered A - F relative to the pillar line (east versus west) indicate the side of the pillar which had a greater intensity of fracturing.

Table 8.4: Pillar dimensions.

Pillar number	Pillar width (m)	Pillar length (m)	w:h
1	6	3	2.31
2	1.1	4	0.85
3	2	3.4	1.54
4	1.3	3.4	1.00
5	1.6	7.5	1.23
6	1	3.2	0.77
7	1.6	6.4	1.21
8	0.7	4.3	0.50
9	2.5	2.6	1.93
10	2.8	3.8	2.15
11	0.9	2.4	0.69
12	1.1	2.1	0.85
13	1.3	1.7	1.00
14	1.3	4	1.00
16	2.8	20	2.15
17	1.5	4.6	1.15
18	1.8	4.6	1.38
19	1.4	2.7	1.08
20	0.9	3.5	0.69
22	1.4	2.4	1.08
23	1.4	2.7	1.08
24	2.5	4.7	1.92
25	0.8	5	0.62
26	1.6	8	1.23
27	1.4	4.5	1.08
28	0.45	3.1	0.35
29	0.7	1.3	0.54
30	1.3	4	1.00

Pillar number	Pillar width (m)	Pillar length (m)	w:h
31	1.7	9.2	1.31
32	1.2	4.8	0.92
33	1.3	4	1.00
34	1.1	4.5	0.85
35	2.3	5	1.77
36	2.2	3	1.69
37	1.1	3.4	0.85
P1	1.7	3.6	1.31
P2	2.5	2.6	1.92
P3	2.3	3.1	1.77
P4	2.3	3.3	1.77
38	1.5	5.3	1.15
39	0.8	2.9	0.62
40	2.2	5	1.69
41	1.1	4	0.85
42	3.05	12	2.35
43	1.6	5.4	1.23
44	3.1	6	2.38
45	1.3	4.4	1.00
46	0.9	1.5	0.69
47	2.7	4.2	2.08
48	2.8	4.5	2.15
49	2.3	5	1.77
50	1.9	5.4	1.46
51	2.6	9	2.00
52	2.4	2.8	1.85
53	1.7	6.2	1.31

8.2.1. Fracture patterns

The pillars were more prone to fracturing on the one side of the pillar. The positions (east versus west) relative to the line of pillars are indicated by the blocks numbered (A – F) as shown on Figure 8.11. Investigating the mine plan and mining sequence; the side of the pillar which was more susceptible to the fracturing was mined first. Mining therefore created an open space, exposing the pillar sidewall (abutment). The fractured rock continued to propagate towards the “free face”. However, pillars which fractured towards the west had the slabs defined by the fracture planes buckling closer to the footwall (Figure 8.12a). In contrary, pillars which fractured towards the east had the fractured slabs buckling closer to the hangingwall (Figure 8.12b).

Figure 8.12a: Pillar scaling towards the west. Photograph of the up-dip side of pillar 18.

Figure 8.12b: Pillar scaling towards the east. Photograph of the up-dip side of pillar P1.

Proposed fracture mode

Hangingwall stress fractures were observed to have a low dip angle on the side of the pillar which was exposed first. The fractures propagated from the hangingwall, extended through the pillar and disappeared into the footwall. This observation can be attributed to the pillar initially consisting of a piece of solid unmined ground approximately 16 m wide (2 m wide pillar and 14 m wide panel). The pillar is only exposed on one side by the leading panel creating the "free face". As the pillar abutment along the exposed "free face" is highly stressed, stress fractures form. The stress concentration is the highest along the edges of the solid and dissipates into the solid, away from the "free face". As a result the angles of the fractures steepen away from the edge of the solid. As the lagging panel is mined and the pillar is cut, the pillar continues to fracture as a result of the induced mining stress. As the newly exposed pillar surface was initially part of the solid, the stress fractures along this side of the pillar are much steeper. As the mining face continues to mine and the pillar moves to the back area, the pillar continues to fracture, however, along the existing fracture planes. Figure 8.13 is a representation of this behaviour.

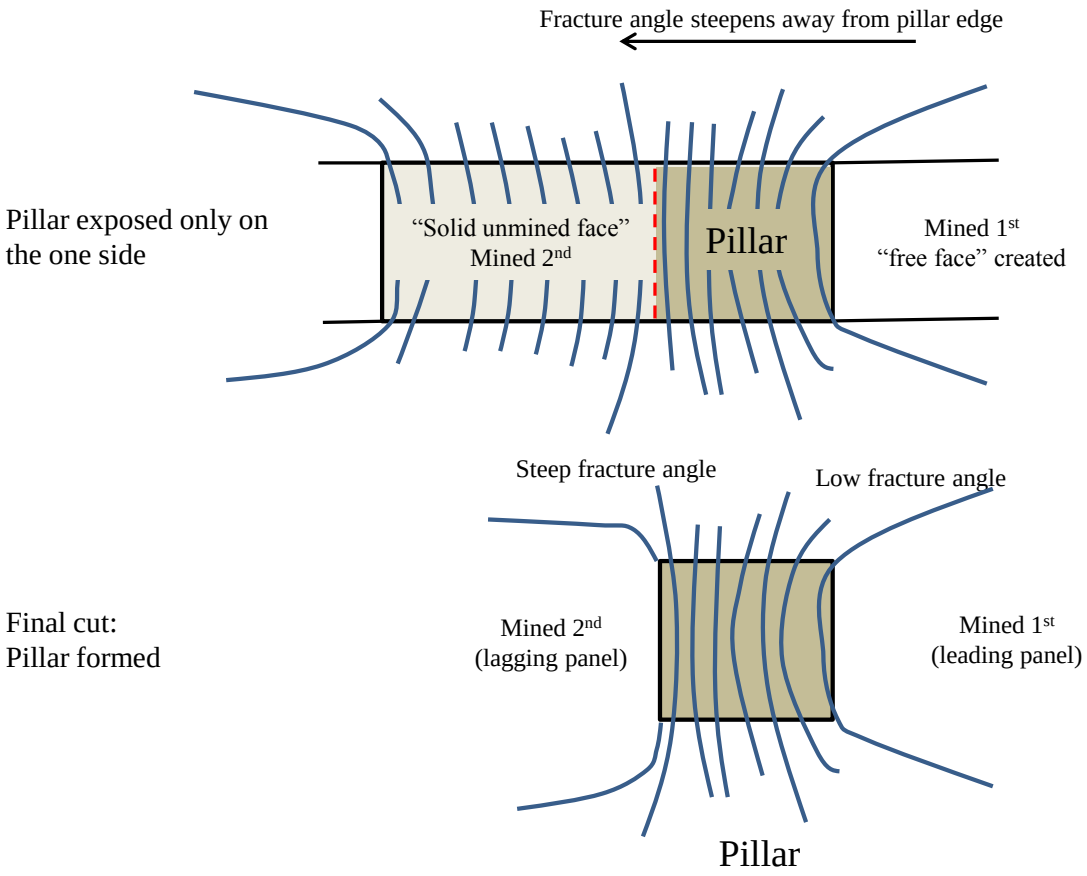

Figure 8.13: Diagram indicating fracture orientation based on underground observations and the mining sequence.

Figures 8.14 and 8.15 are photographs of pillar 46 and pillar 6 respectively. In both cases, the western panel led the eastern panel. The fractures had a low dip angle along the western side of the pillar with increased pillar scaling observed.

As the pillars continued to crush the fractures dilate. As a result, the slabs defined by the fracture planes buckle and are pushed out. Note, however, that the confining stress provided by the failing slabs do contribute to the strength of the pillar (Jager and Ryder, 1999).

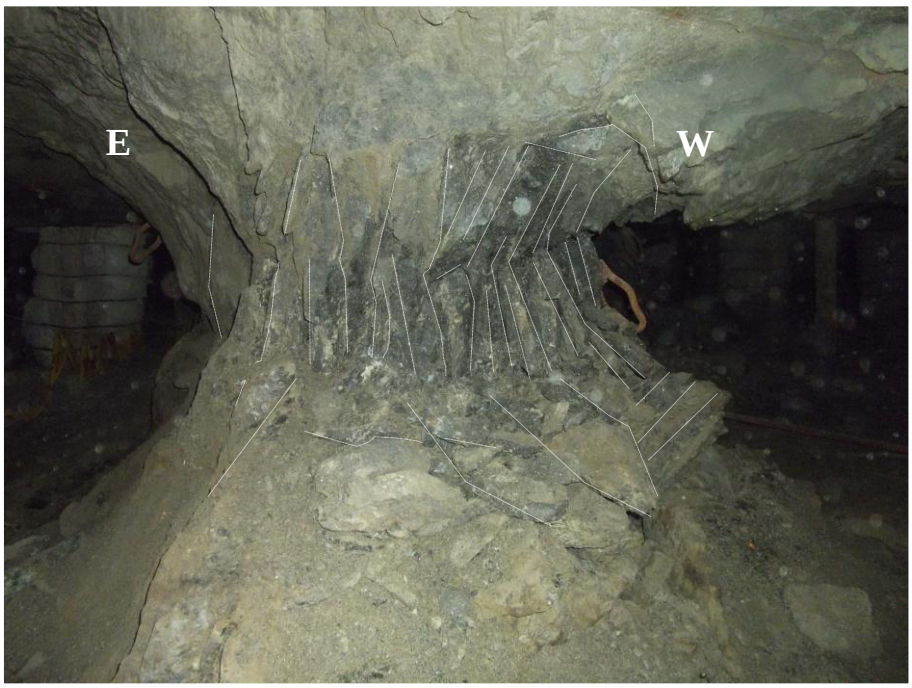

Figure 8.14a: Pillar 46 scaling towards the west. Photograph of the down-dip side of the pillar.

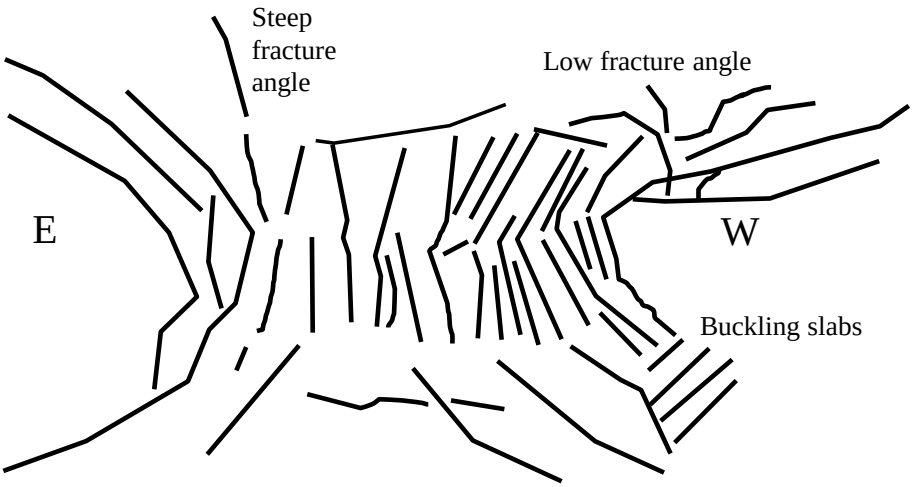

Figure 8.14b: Trace of pillar fractures and orientation.

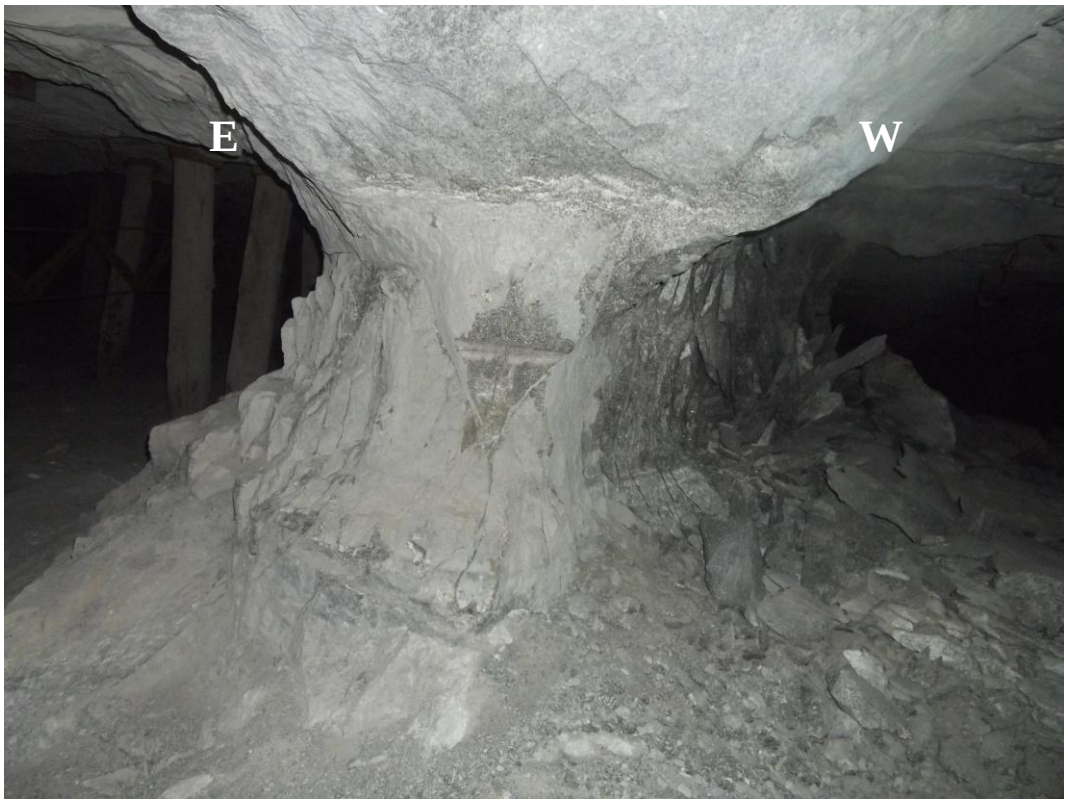

Figure 8.15a: Pillar 6 scaling towards the west. Photograph of the down-dip side of the pillar.

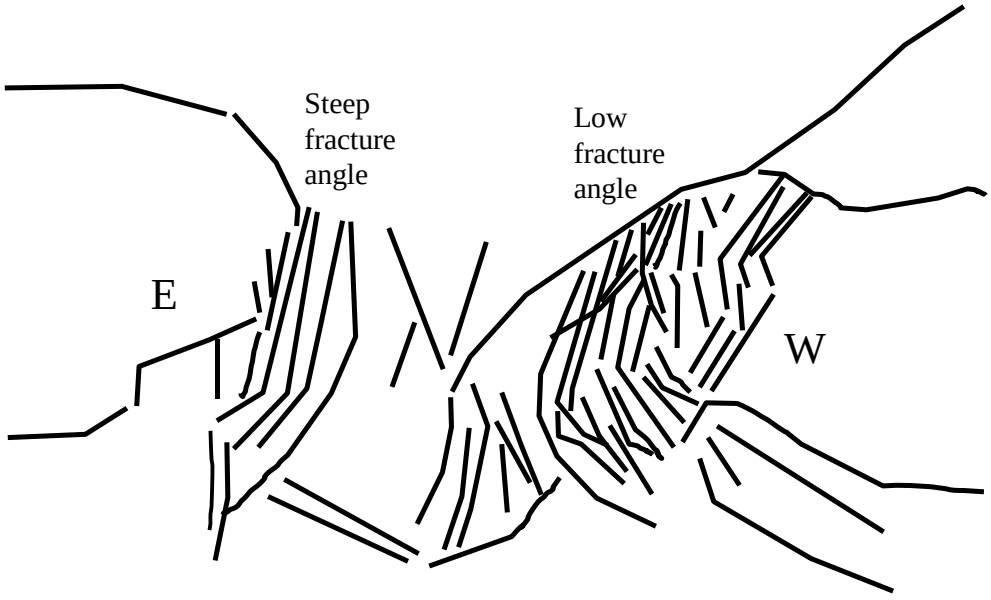

Figure 8.15b: Trace of pillar fractures and orientation.

Stress induced fractures are formed when the absolute stress (virgin and induced stress) exceed the strength of the rock. Martin (1997) indicated that crack growth and extension occurs in the direction of the maximum applied stress at about 30 – 40 percent of the unconfined peak strength of the rock. The stress concentration induced by mining are the largest directly in front of a mining face, and are particularly severe in abutments and pillars (Jager and Ryder, 1999). In the case of crush pillars, these stress induced fractures are extension fractures which extend around a mining face (or edge of a panel) and extend through the pillar. Extension fractures are formed in induced tension, but within an entirely compressive stress field. The fractures develop in the σ_1/σ_2 plane (the plane normal to the minor principal stress σ_3). The phenomenon of the fractured slabs buckling with the scaling concentrated either closer to the footwall (when the west side of the pillar is exposed first) or hangingwall (when the east side of the pillar is exposed first) as shown in Figure 8.12a and 8.12b respectively could be assessed following the results of absolute stress measurement conducted over pillar P1 and the anticipated pillar P2 position. *Note: the details regarding the stress measurements will be discussed in subsequent chapters.*

8.2.2. The impact of rock material on observed pillar behaviour

The pillar lines situated along the west of the trial section were intensely fractured. Fractures extended into the hangingwall with crushed rock fragments observed. This may have occurred as the stress induced fractures formed and propagated. These pillars were situated close to potholes and the hangingwall consisted of Anorthosite (hard, brittle rock). The pillars situated towards the east of the trial site had a Pyroxenite hangingwall. Here the pillar fracturing was less prevalent and the failed slabs appeared to squeeze and dilated outwards. The Pyroxenitic hangingwall allowed for more ductile type behaviour. Figures 8.16 and 8.17 shows the difference in behaviour of the above-mentioned cases.

Figure 8.16a: Pillars consisting of mostly Anorthosite hangingwall (pillar 6). Note the difference in fracture intensity compared to Figure 8.16b below.

Figure 8.16b: Pillar consisting of Pyroxenite hangingwall (pillar 42).

Figure 8.17a: Anorthositic pillar sidewall scaling.

Figure 8.17b: Squeezing Pyroxenitic pillar sidewall.

8.2.3. Early pillar fracturing

When the mining trial was stopped at the end of June 2013, pillar 37 was in the process of being formed. The pillar was initially cut by the east panel. The pillar was never holed via a pillar holing from the west panel due to the east panel being stopped to ensure that a sufficient lead lag distance could be established so that the final instrumentation could be installed. As a result the pillar was still part of the mining face (Figure 8.18).

During the underground investigation, the condition of pillar 37 was investigated. It was observed how the pillar was already in a fractured state although the pillar was still part of the mining face and in the process of being formed (Figure 8.19). Fracturing of the solid abutments also occurred ahead of the mining face indicating that the stress was sufficiently high to initiate early pillar crushing.

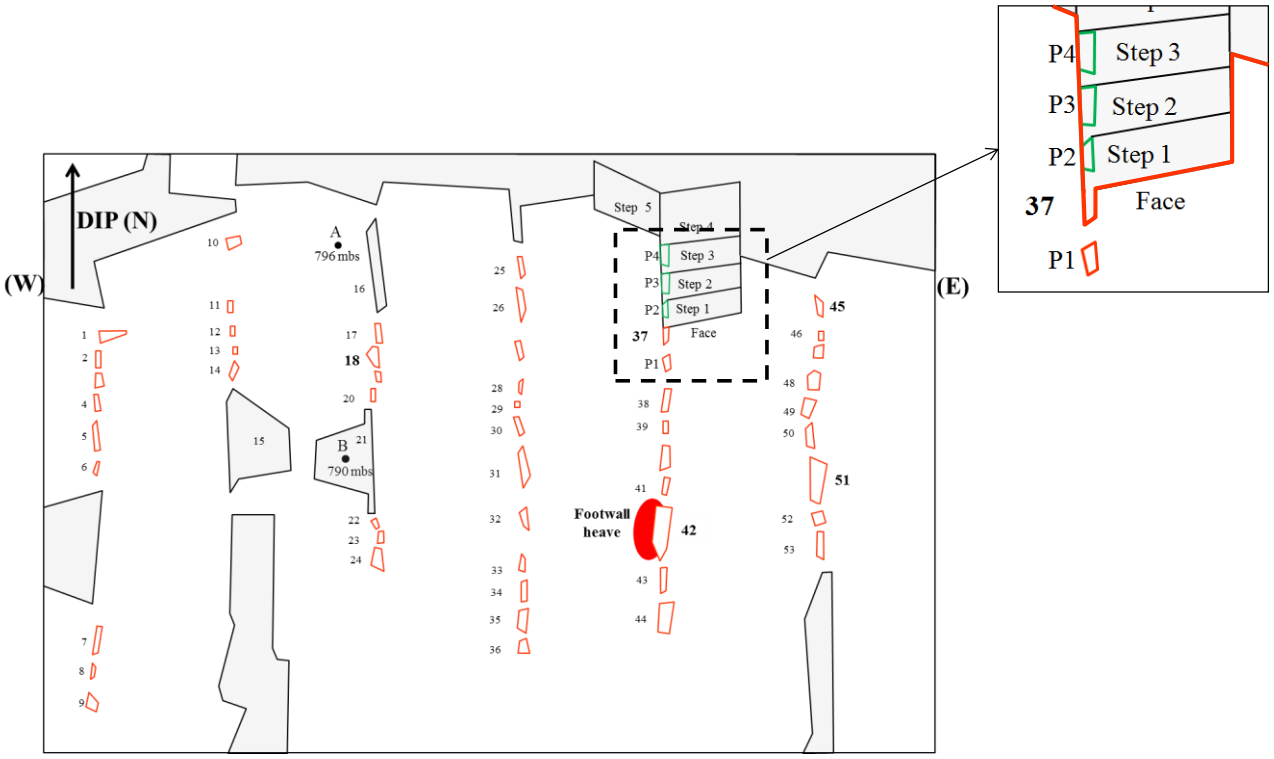

Figure 8.18: Layout of the trial section indicating the position of pillar 37 prior to the re-start of mining the east face. Note that pillar 37 is part of the mining face. Step 1, 2, 3 indicates the anticipated mining in which pillars P2, P3 and P4 will be formed when mining resumes.

Figure 8.19: Condition of pillar 37 whilst still part of the mining face.

8.2.4. Oversized pillar

There was one incident where a large oversized pillar, pillar 42 (3.05 m wide and 12 m long) did not completely crush. Footwall heave was observed adjacent to the west side of this pillar (Figure 8.20). The footwall contained open tension cracks and the support adjacent to the west side of the pillar indicated significant convergence as a result of the up-heave of the footwall. Figure 8.21 indicates the pillar fracture alignment orientated to the east “free face” which was first exposed.

Figure 8.20: Footwall heave experienced adjacent to the west side of pillar 42.

Figure 8.21a: Up-dip view of oversized pillar 42.

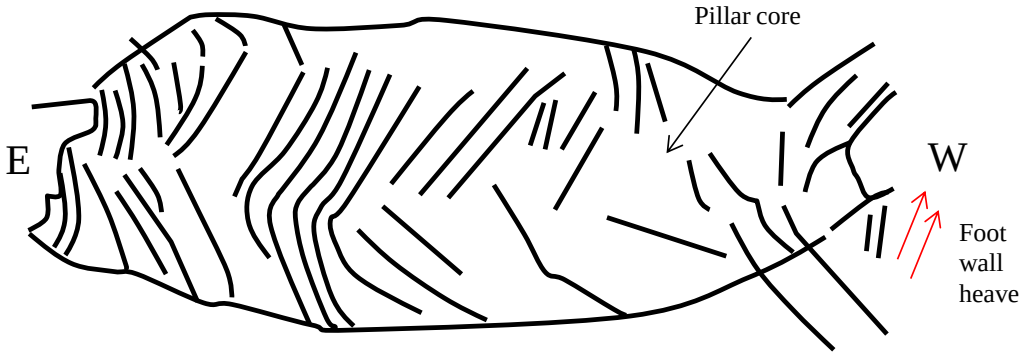

Figure 8.21b: Trace of pillar fractures and orientation.

8.3. Observed pillar behaviour during the extraction of the final mining section

At the end of June 2013 mining in the trial area was stopped to ensure that the required instrumentation could timeously be installed and to ensure that the mining sequence could be controlled. The mining layout at the time is indicated in Figure 8.22. The planned pillar and holing positions are indicated in the figure. Table 8.5 summarises the blasting schedule. An average face advance of 1 m was achieved per blast. The approximately 20 month stoppage was predominantly as a result of strike action in 2013 and 2014. It did, however, provide a window to visually assess the pillar behaviour throughout the trial site and to do all the required preparation for the monitoring of the final mining section.

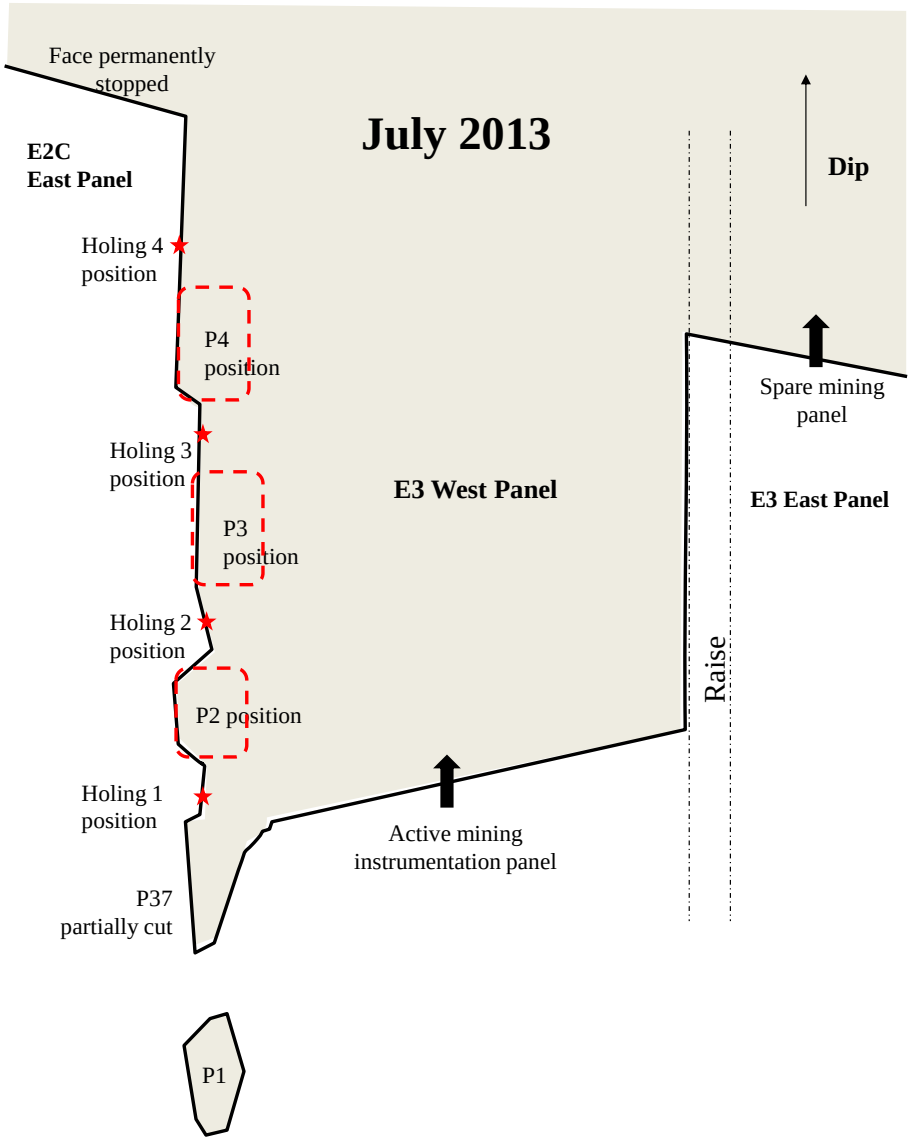

Figure 8.22: Mining layout at the time when the trial site was temporarily stopped (July 2013).

Table 8.5: Blasting schedule during the trial period.

Initial mining			
East 2C E pnl	Holings	E3 W pnl Active mining panel	E3 E pnl Spare mining panel
20-May-13			
21-May-13			
23-May-13			
24-May-13			
25-May-13			
27-May-13			
29-May-13			
30-May-13			
31-May-13			
03-Jun-13			
04-Jun-13			
05-Jun-13			
07-Jun-13			
08-Jun-13			
10-Jun-13			
11-Jun-13			
Panel stopped against fault			
Area stopped			

Final mining - Area started up again				
East 2C E pnl	Holings		E3 W pnl Active mining panel	E3 E pnl Spare mining panel
	28-Feb-15	1,2,3,4		
	02-Mar-15	1,3,4		
	03-Mar-15	2		
	04-Mar-15	3,4		
	09-Mar-15	2		09-Mar-15
			10-Mar-15	10-Mar-15
			11-Mar-15	11-Mar-15
			12-Mar-15	
				14-Mar-15
			16-Mar-15	16-Mar-15
Section 54 (17 - 27 Mar-15)				
Easter break (2 - 6 Apr-15)				
			08-Apr-15	
			09-Apr-15	
			10-Apr-15	
			15-Apr-15	
			16-Apr-15	
			17-Apr-15	
			18-Apr-15	
			20-Apr-15	
			22-Apr-15	
			23-Apr-15	
			24-Apr-15	
			25-Apr-15	
				28-Apr-15
			29-Apr-15	
			07-May-15	
			08-May-15	
			09-May-15	
			11-May-15	
			12-May-15	
			15-May-15	
			16-May-15	
			17-May-15	17-May-15
All mining completed				

Once mining resumed at the end of February 2015, various site visits were conducted to investigate the pillar condition, install instrumentation, download data or conduct other forms of measurement. The following section will provide an overview of the observed pillar behaviour during some of these site visits. This section is structured in a way that the fracturing sequence per pillar will be discussed in a chronological manner corresponding to the pillar forming sequence. It will also be used to cross-reference to other measurements. Pillar P1, P2, P3 and P4 as indicated in the figures refer to the instrumented pillars.

Table 8.6: Observations 28 February 2015 before mining re-started (Figure 8.22).

Pillar No.	Observations
P1	The mining face was approximately 5 m beyond the pillar P1 position. From the up and down dip holings it appeared that the pillar was fractured throughout. The eastern side of the pillar was mined first and all the fracture propagation was towards the eastern side. The western side of the pillar had very little to no surface slabbing or scaling visible. Refer to Figure 8.12b.
P37	The pillar was partially formed although still part of the mining face. The pillar was already in a semi-crushed state. Refer to Figure 8.19.
P2	The pillar was approximately 3 m ahead of the current face position. Pillar holings were being established above and below the pillar (pre-developed 0.5 m in). The pillar surface (exposed western side) contained loose slabs indicating partial outer crushing and slabbing of the pillar edge.
P3	The pillar was approximately 9 m ahead of the current face position. The pillar displayed no scaling. The hangingwall conditions along the exposed western side of the pillar indicated anomalous jointing intersecting the pillar with fallout observed between intersecting joints. This could perhaps speed up the crushing process. Figure 8.39 indicates the mapped geology.
P4	The pillar was approximately 15 m ahead of the current face position. The condition of the pillar was not assessed at the time. Although the mining face west of the pillar (panel E2C East panel) was stopped just short of the bracket pillar, it was anticipated that this panel could potentially be mined a few more metres to determine the impact of an increased overall span on all the pillars.

8.3.1. Mining sequence

As indicated in the blasting schedule, the majority of mining took place in the E3 West panel (active instrumentation panel). It was anticipated that the panel could advance at least another 25 – 30 m before intersecting the fault bracket pillar. Due to the instrumentation installation or measurement requirements, a daily blast could not always be achieved. Panel E3 East was therefore allocated as a spare panel which could also be blasted if there were any unforeseen delays. This assisted in ensuring that the section was still productive although mining at a slow rate. Panel E2C East, was not re-started again as the face winch was already removed and removal of broken ore would therefore not be possible. Most of the delays during the final mining stages were either as a result of planned stoppages (e.g. grout pack installation to ensure additional aerial coverage in areas where dense jointing was intersected), or as a result of unplanned stoppages (e.g. section 54 issued by the mining inspectors resulting in all mining activity on the entire shaft

being suspended or the shaft winder not working). The following figures indicate the face position at a point in time relative to the pillar forming cycle.

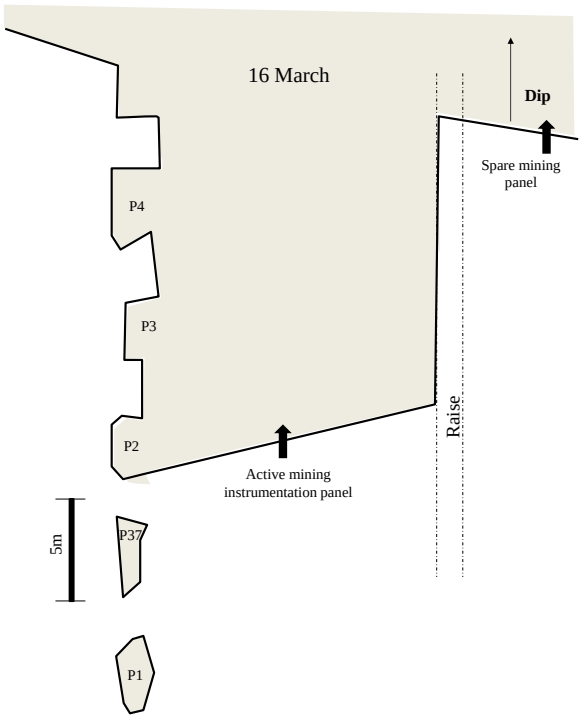

Figure 8.23: Face position on 16 March 2015. Mining face aligned with pillar P2.

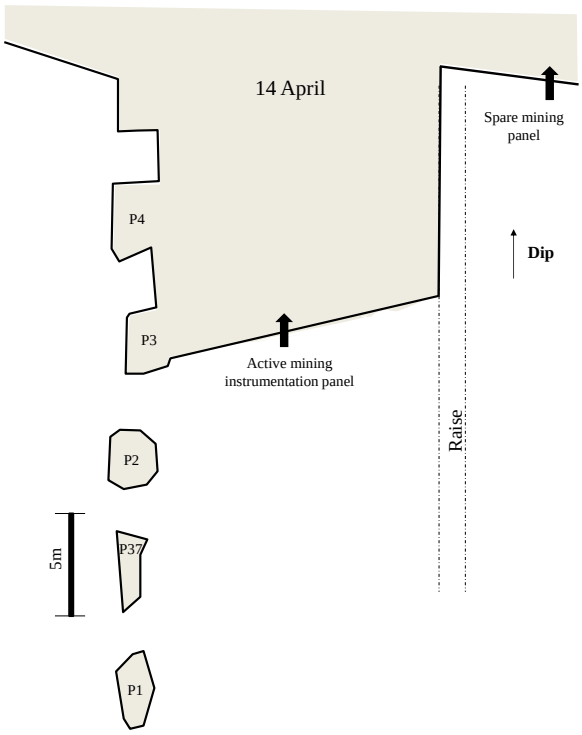

Figure 8.24: Face position on 14 April. Mining face aligned with pillar P3. Pillar P2 was now fully formed.

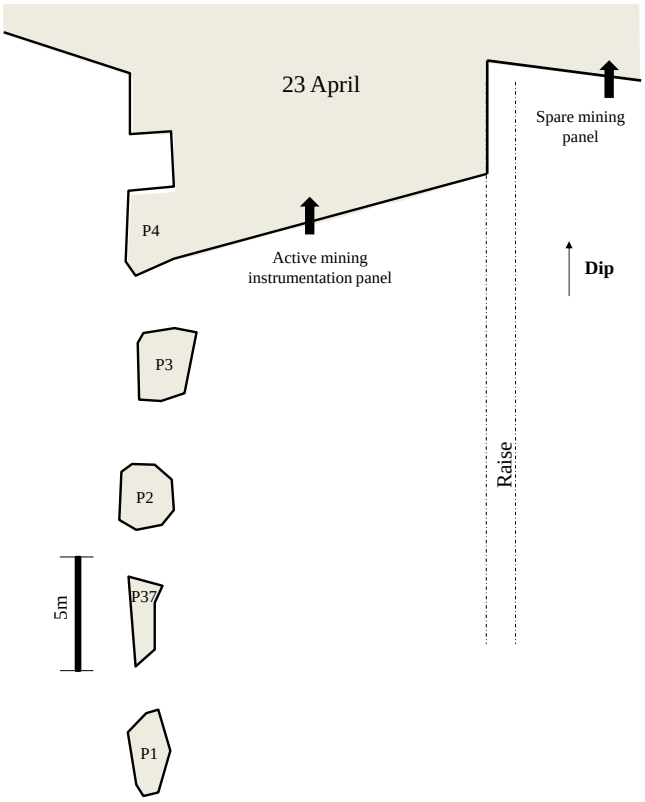

Figure 8.25: Face position on 23 April. Mining face aligned with pillar P4. Pillar P3 was now fully formed.

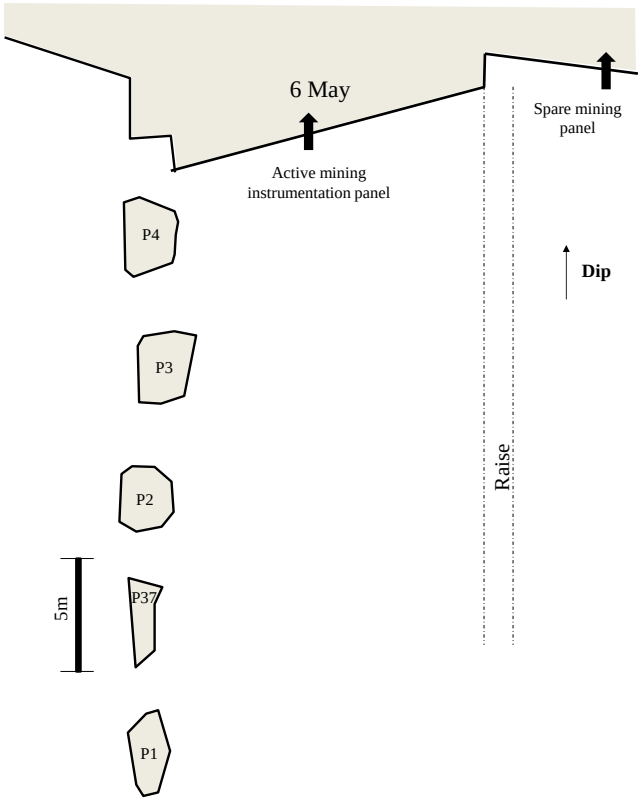

Figure 8.26: Face position on 6 May. Pillar P4 was now fully formed.

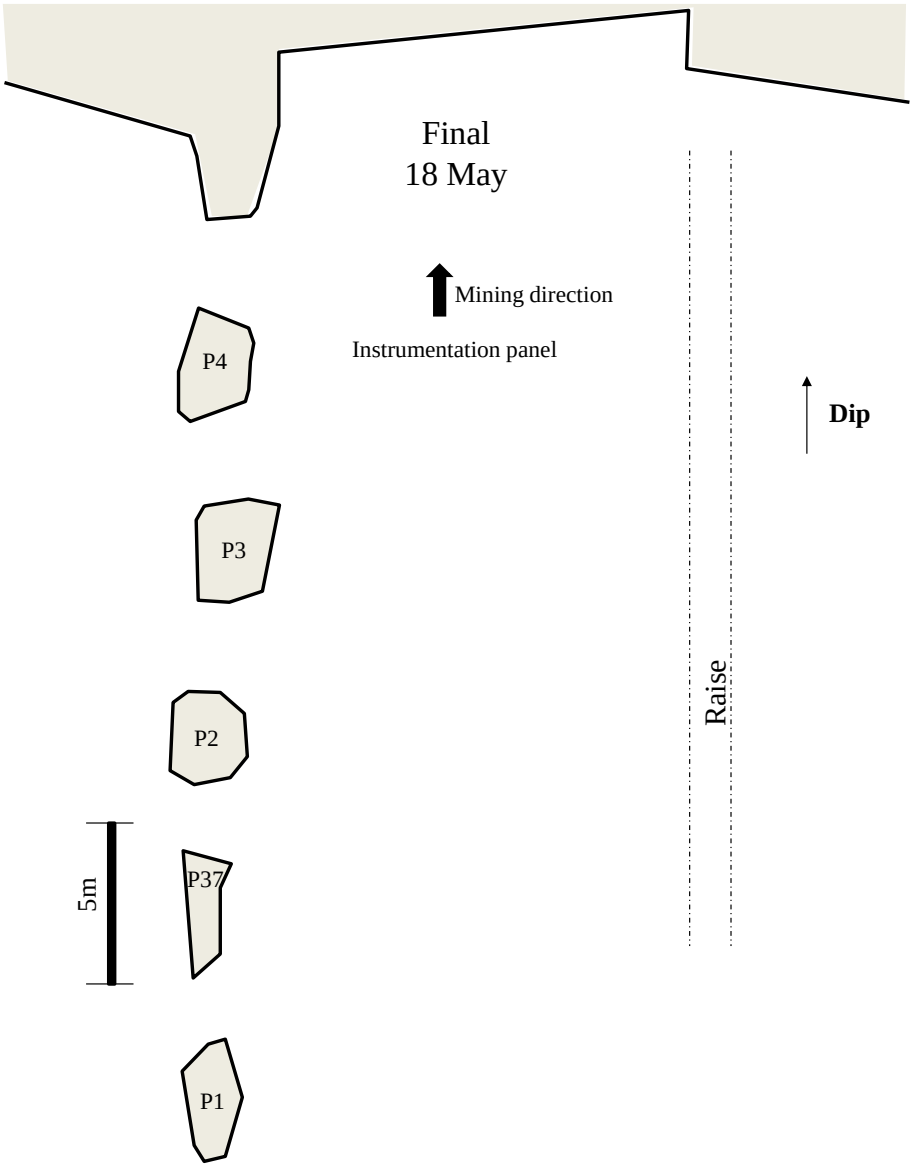

Figure 8.27: Face position on 18 May. All mining stopped.

8.3.2. Behaviour of pillars during the pillar forming cycle

The underground site visits were scheduled in such a manner that the condition of each pillar could be observed prior to being formed, when being formed at the mining face and as the face advanced and the pillar moved to the back area of the stope. The observations for each pillar corresponding to the face position will be expanded on in the sections below.

Pillar P1

The pillar was formed in April 2013 prior to the trial site initially being stopped. This was the first instrumented pillar with most of the instrumentation installed on a trial basis to determine the way forward with regards to the monitoring of the remaining pillars. When the pillar was formed, the panel east of the pillar was leading the west panel by approximately 9 m. The pillar is approximately 1.7 m wide and 3.6 m long (w:h ≈ 1.3). The pillar was completely fractured with fracture planes spaced approximately 30 - 50 mm apart throughout the pillar. Additional movement was visible along these slabs defined by the fracture planes once the pillar was located in the back area. Also, a wedge-like structure was observed along the down-dip side of the pillar where the intersection of fractures occurred approximately halfway through the pillar. There was almost no scaling visible along the western side of the pillar with all the scaling concentrated towards the eastern side of the pillar (side mined first).

Table 8.7: Observations pillar P1.

Date	Pillar position	Observations
16 March	Face at P2. P1: 8m back.	The pillar was fractured throughout. The fracture planes were spaced between 30 - 50 mm apart throughout the pillar. Approximately 0.5 m of the eastern side of the pillar was barred solid prior to mining restarted. The western side of the pillar did not show much slabbing or scaling.
14 Apr	Face at P3. P1: 14 m back.	No visible change.
23 Apr	Face at P4. P1: 20 m back.	There appeared to be some movement along the fracture planes along both the up and down dip sides of the pillar (Figure 8.28 and 8.29). Along the down-dip side of the pillar a wedge-like structure was observed where the fractures intersect (Figure 8.28). Only marginal to no scaling was visible along the western surface of the pillar.
6 May	P4 formed. P1: 24 m back.	No additional visible change.
18 May	Additional 7m advance. P1: 31 m back.	No additional visible change.

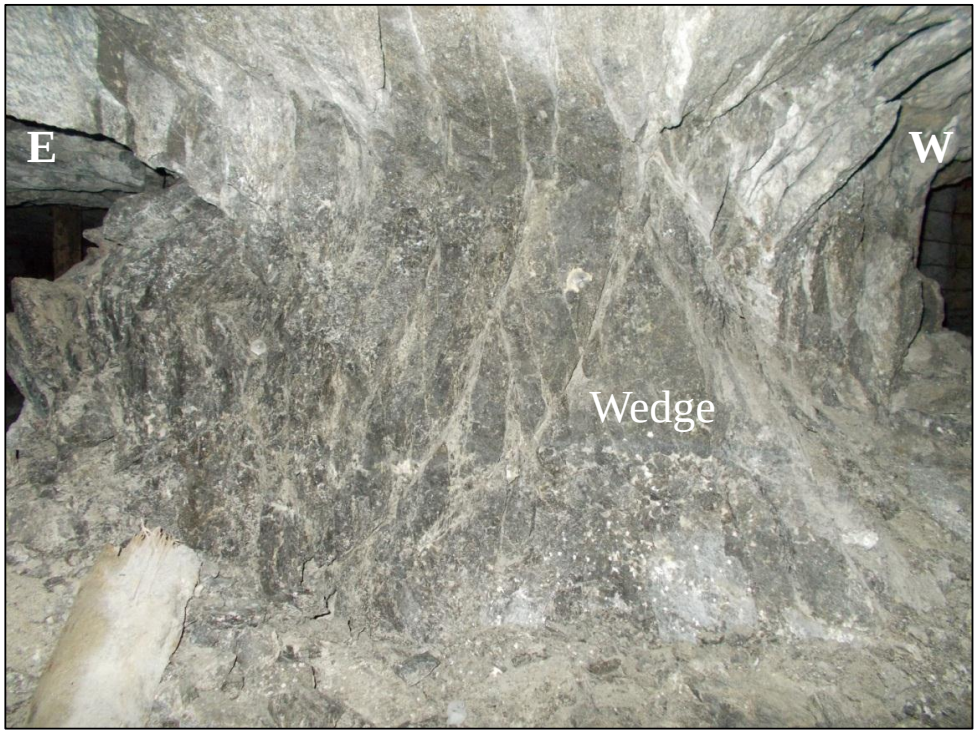

Figure 8.28: Up-dip view of pillar P1. Photograph taken on 23 April. Note the wedge-like structure visible where the fractures intersect. Fractures concentrated predominantly towards the east which was mined first.

Figure 8.29: Down-dip view of pillar P1. Notice the intensity and spacing of the fractures towards the eastern side. Photograph taken on 23 April.

Pillar P37

The pillar was partially formed in April 2013 prior to the trial site initially being stopped. When the pillar was formed, the panel east of the pillar was leading the west panel by approximately 5 m. The east panel was, however, temporarily stopped prior to the pillar being holed. The panel west of the pillar was mined another 23 m to establish a significant lead-lag scenario so that instrumentation (i.e. strain cells) could be installed along the planned pillar positions (P2, P3, P4). The pillar is approximately 1.1 m wide and 3.4 m long (w:h ≈ 0.85). The pillar, being very narrow, showed almost no additional crushing as mining continued.

Table 8.8: Observations pillar P37.

Date	Pillar position	Observations
16 March	Face at P2. P37: 2m back.	The pillar was barred solid and white washed to visually identify any further fracturing. Loose slabs were barred from the pillar reducing the overall pillar width by 0.5 – 1 m prior to mining restarted. The pillar width was therefore significantly reduced.
14 Apr	Face at P3. P37: 8 m back.	No visible change.
23 Apr	Face at P4. P37: 14 m back.	Some minor additional scaling visible.
6 May	P4 formed. P37: 18 m back.	No additional visible change.
18 May	Additional 7m advance. P37: 25 m back.	No additional visible change.

Pillar P2

The pillar is approximately 2.5 m wide and 2.6 m long (w:h ≈ 1.9). The pillar showed early signs of crushing even before being formed. This could be confirmed by means of a borehole camera survey. Unfortunately the holes drilled for the borehole scans quickly closed once mining started as a result of ongoing pillar crushing (movement along fracture planes). The value of the borehole scans, especially with this pillar, was to validate the external appearance of the pillar (visual fractures) to the internal condition observed in the borehole. This pillar predominantly fractured towards the western side of the pillar (the side mined first), with almost no scaling occurring along the eastern side of the pillar. Some minor fractures did form later along the eastern side of the pillar which was visible from the up and down dip holing positions. The pillar did not fracture to the same extent as pillar P1. Pillar P2 was approximately 0.8 m wider.

Table 8.9: Observations pillar P2.

Date	Pillar position	Observations
16 March	Face at P2.	The exposed western side of the pillar had some scaling visible along the pillar surface. From the up-dip holing position it could be observed that the fracturing extended approximately 1 m into the pillar (Figure 8.30). The borehole drilled through the pillar identified numerous visible fractures. The fractures appeared to have moved up or down relative to one another (Figure 8.31). The observed fractures visible from the up-dip holing appeared to agree with the borehole camera log conducted within the pillar (Figure 8.32).
14 Apr	Face at P3. P2: 3 m back.	The pillar now fully formed continued to scale along the western side. The borehole used to conduct the initial borehole camera scans was completely closed as a result of the movement of the slabs defined by the fractures (up or down) relative to one another. The eastern surface of the pillar showed no signs of scaling. The pillar was white-washed to identify any further change.
23 Apr	Face at P4. P2: 9 m back.	Prominent fractures along the up-dip western edge of the pillar were opening. The fractured slabs were pushed outwards as the pillar continued to dilate. New fractures were visible along the eastern down-dip side of the pillar.

6 May	P4 formed. P2: 13 m back.	There was increased fracturing along the western up-dip side of the pillar (Figure 8.33). Very little additional movement was observed on the surface along the western side of the pillar. Additional new fractures were visible along the eastern down-dip side of the pillar. These fractures were spaced approximately 100 mm apart and extend to approximately half the pillar width. There was no fracturing or scaling visible along the eastern surface of the pillar.
18 May	Additional 7m advance. P2: 20 m back.	There was very little additional movement visible along the western side of the pillar. New (small scale) fractures formed along the eastern up-dip edge of the pillar. The fractures formed along the eastern down-dip side of the pillar started to open.

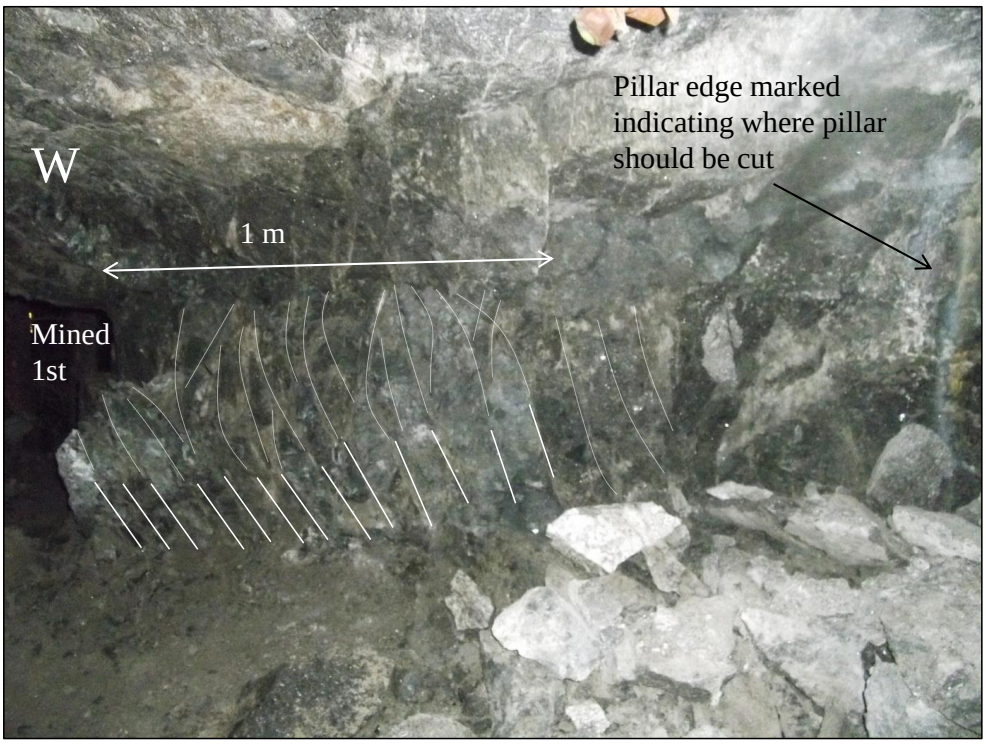

Figure 8.30: Formation of pillar P2 (down-dip view from the holing above the pillar). The face was aligned with the pillar. The fractures are visible along the west side of the pillar (indicated by white traces along the footwall of the pillar). The photograph was taken on 16 March.

Figure 8.31: Photograph of a borehole through pillar P2. Note how the slabs defined by the fracture planes have moved relative to one another. The photograph was taken on 16 March prior to the formation of the pillar.

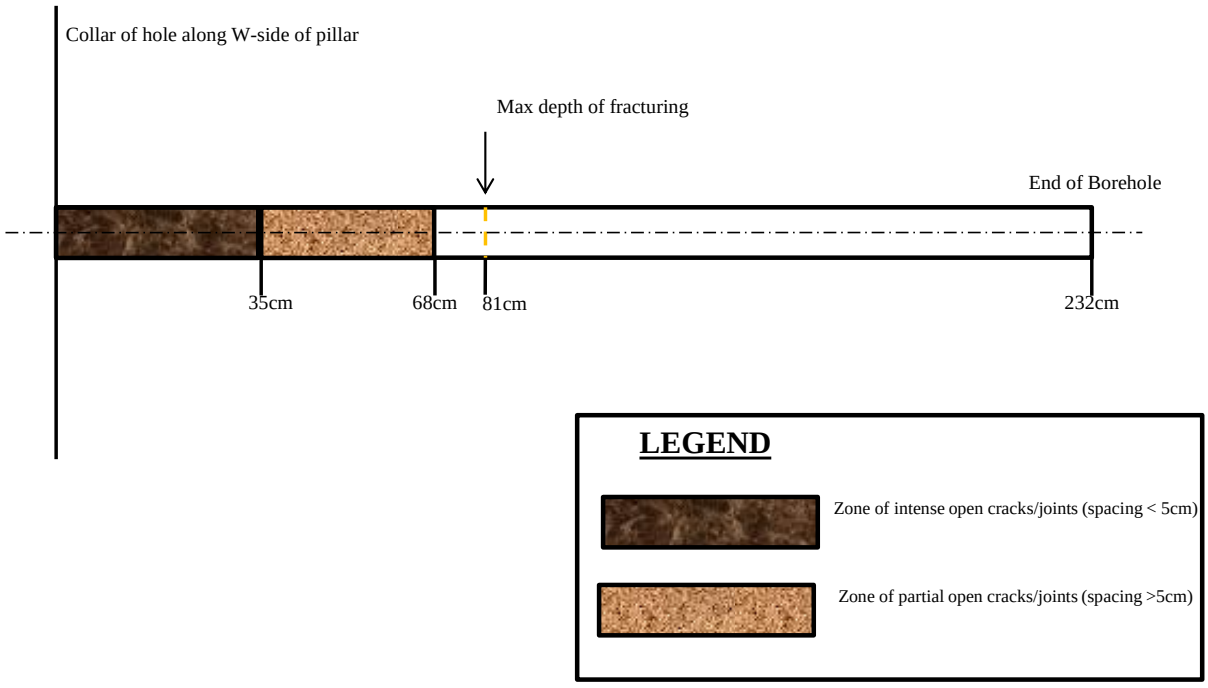

Figure 8.32: Borehole log through pillar P2. Scan conducted on 27 January 2015 (prior to the start of mining). The pillar was still part of the solid face abutment. The hole was drilled approximately 4 m ahead of the face position at the time.

Figure 8.33: Continued scaling and dilation of the western side of pillar P2 (down-dip view from the holing above the pillar). The photograph was taken on 6 May.

Pillar P3

The pillar is approximately 2.3 m wide and 3.1 m long (w:h ≈ 1.8). The pillar only crushed at a late stage. The pillar was intersected by closely spaced joints and minor faulting orientated approximately E-W (Figure 8.39). It appeared as if these structures influenced the fracture process of the pillar. The pillar only started to fracture once fully formed (face at P4 position). It appeared as if all movement were initially along the joints. The fracture intensity and observed scaling was towards the western side of the pillar (mined first). New fractures did eventually form along the eastern down dip side of the pillar (similar to pillar P2) when the pillar was fully formed. Ongoing movement was visible along the fractures in the borehole drilled through the pillar. In this pillar, the initial internal fractures visible in the borehole could not be verified by external fractures visible on the pillar surface as with pillar P2. However, there were additional movement visible along the back of the hole when new fractures formed along the top and bottom of the pillar. There was no fracturing or scaling visible along the exposed eastern side of the pillar. The pillar was not fractured to the same extent as pillar P1. Pillar P3 was, however, 0.6 m wider and intersected by complex geology.

Table 8.10: Observations pillar P3.

Date	Position	Observations
16 March	Face at P2. P3: 6 m ahead.	The pillar showed no signs of scaling along the exposed western side, up dip or down dip holings. Minor movement was visible along the fracture planes inside the borehole used for the borehole camera scans. These fractures were separated 30 – 50 mm apart. There was, however, no sign of scaling on the external surface of the pillar.
14 Apr	Face at P3.	Some additional movement was visible inside the borehole used for the borehole camera scan. There was almost no scaling visible on the surface of the pillar. New fractures were visible along the western up-dip corner of the pillar which extended for the first approximately 40 cm.
23 Apr	Face at P4. P3: 3 m back.	The pillar suddenly started to fracture along the western side. Increased movement was visible along the fracture planes inside the borehole (hole almost closed). Refer to Figure 8.36. The fracture intensity also increased along the western up-dip corner of the pillar and extended to approximately 60 cm (fractures approximately 30 mm apart). Some new fractures were visible along the down-dip side of the pillar (centre of the pillar). These fractures were spaced approximately 100 mm apart. There was no visible scaling along the eastern surface of the pillar.

6 May	P4 formed. P3: 7 m back.	Significant scaling and fracturing occurred along the western side of the pillar. The fractures along the western up-dip corner were opening (approximately 5 - 10 mm apart) and extended for the first metre of the pillar. New fractures formed along the eastern up-dip side of the pillar. These fractures were 30 – 50 mm apart and were opening 3 - 5 mm. New fractures were also visible along the down-dip side of the pillar. These fractures also started opening slightly.
18 May	Additional 7m advance. P3: 14 m back.	Additional scaling was visible along the western surface of the pillar. All of the fracturing and scaling was concentrated predominantly towards the west side of the pillar (mined first) and concentrated along the bottom portion of the pillar. The pillar was intersected by anomalous jointing (Figure 8.35). There appeared to be an interaction between the fracture and joint planes. Along the up-dip side of the pillar, a piece of scaled material parted from an exposed slickensided plane (orientated E-W). Additional movement was observed along the back of the borehole. The fractures visible along the bottom of the pillar continued to open.

Figure 8.34: Down dip view of the top and western side of pillar P3. Bottom insert indicates the degree of fracturing along the top western side of the pillar (see white line traces along the bottom of the pillar). The photograph was taken on 6 May.

Figure 8.35: Dense jointing intersecting pillar P3. Photograph of the bottom down-dip portion along the western side of the pillar.

Figure 8.36: Movement along the borehole drilled through the pillar from the western side. The photograph was taken on 6 May.

Pillar P4

The pillar is approximately 2.3 m wide and 3.3 m long (w:h ≈ 1.8). The western side of the pillar showed early signs of slabbing. This was also visible along the borehole drilled through the pillar. Fractures developed very early along the up-dip western portion of the pillar (visible from the up-dip pillar holing). These fractures increased and started to open as the pillar was being formed. The pillar had a chromitite contact present along the top of the pillar along the hangingwall interface. It appeared as if this contact facilitated the pillar dilation and rotation along the western surface of the pillar. Almost no scaling was visible along the eastern side of the pillar. Although this pillar also showed a high degree of fracturing, it was not fractured to the same extent as pillar P1. It did, however, fracture more than pillars P2 and P3.

Table 8.11: Observations pillar P4.

Date	Position	Observations
16 March	Face at P2. P4: 9 m ahead.	Minor scaling was visible along the exposed western side and down-dip holing of the pillar. There were distinct fractures visible along the up-dip side of the pillar. The fractures appeared to be tightly sealed. Minor movement was visible inside the borehole used for the borehole camera scans.
14 Apr	Face at P3. P4: 6 m ahead.	The fractures visible in the up-dip holing appeared to extend for the first metre of the pillar and were spaced approximately 30 – 70 mm apart. The borehole drilled through the pillar was displaying significant movement (up or down) along the fracture planes. The western surface of the pillar was displaying a significant degree of scaling.
23 Apr	Face at P4.	The fractures along the western up dip edge started to open. The scaling along the western surface of the pillar was increasing and there were increased movement visible along the fractured planes in the front portion of the borehole.

6 May	P4 formed. P4: 1 m back	The outer slabs along the western side of the pillar have buckled, pushed out (dilated) and rotated to such an extent (Figure 8.38) that the borehole was completely shut-off. A prominent chromitite contact was present along the top of the pillar which seemed to have facilitated the movement of the fractured slabs. The fractures along the top western portion (80 cm) continued to open. An oblique fracture was visible along the up-dip centre of the pillar. New fractures have formed along the bottom of the pillar. These fractures extended for the first approximately 1 m from the western edge.
18 May	Additional 7m advance. P4: 8 m back.	The western side of the pillar continued to buckle. New fractures were visible along the bottom eastern side of the pillar spaced approximately 15 cm apart. The top portion of the eastern surface of the pillar was fractured. This extended approximately 1 m down the eastern surface of the pillar.

Figure 8.37: Fracturing along the top western side of pillar P4. The photographs were taken from the up-dip holing. Also note the diagonal fracture in the photograph labeled 6 May.

Figure 8.38: Fracturing along the bottom west and western surface of pillar P4. The photograph was taken from the holing below the pillar on 6 May. The pillar extensometer is also visible in the photograph (steel pipe casing protruding from pillar).

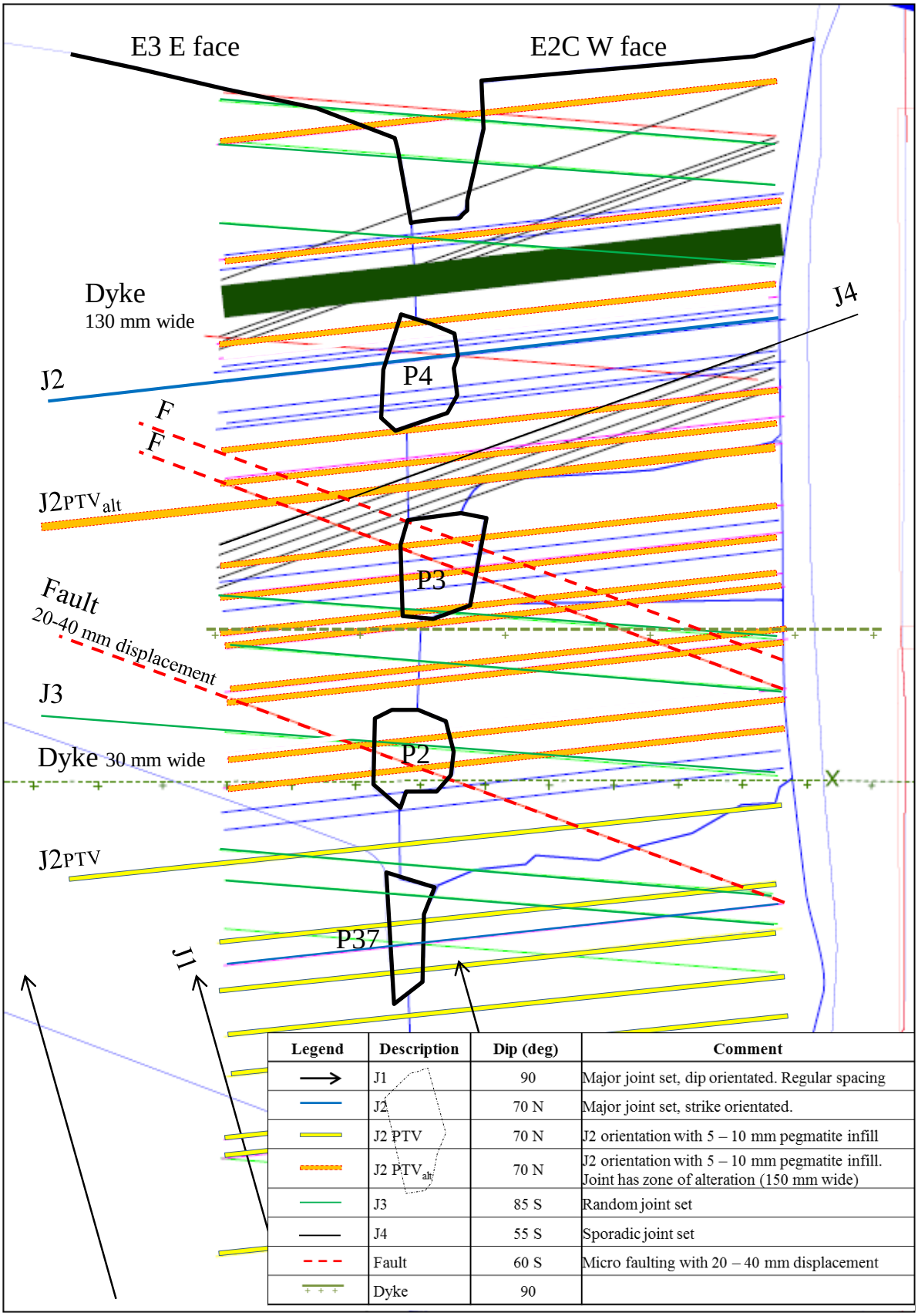

Legend	Description	Dip (deg)	Comment
→	J1	90	Major joint set, dip orientated. Regular spacing
	J2	70 N	Major joint set, strike orientated.
	J2 PTV	70 N	J2 orientation with 5 – 10 mm pegmatite infill
	J2 PTV$_{alt}$	70 N	J2 orientation with 5 – 10 mm pegmatite infill. Joint has zone of alteration (150 mm wide)
	J3	85 S	Random joint set
	J4	55 S	Sporadic joint set
	Fault	60 S	Micro faulting with 20 – 40 mm displacement
	Dyke	90	

Figure 8.39: Representation of the mapped geological structures which intersected the pillars during the extraction of the final mining section.

Borehole camera scans

Borehole camera scans were conducted prior to mining the final mining section. The intent was to determine how the fracture intensity increased during the pillar forming cycle. At the time of the scans, boreholes were drilled at the anticipated pillar positions. The borehole positions were approximately:

- P2: 4 m ahead of the face,
- P3: 11 m ahead of the face,
- P4: 17 m ahead of the face.

Grodner and Canbulat (2005) proposed a pillar fracturing index (PFI) as a quantitative method to determine the condition of a pillar (refer to Chapter 2 Section 2.2.3). PFI is simply an adaption of RQD (Rock quality designation) where the ratio of factures spaced more than 10 cm apart is compared to the overall length of the hole and expressed as a percentage; equation 2.13. The method entails conducting repetitive scans in the same hole over a period of time or having to drill a new hole every time a subsequent scan is required. When the pillar is in a crushed state, the pillar should have a PFI less than 45.

Unfortunately, the holes drilled for the scans could only be used during the initial scans conducted on 27 January 2015. Thereafter the borehole camera could not be used as the holes became partially closed (slabs moved up or down relative to one another or rotated) as mining advanced. Drilling of these holes required specialised drilling to ensure that drill core disking does not occur and that the correct diameter hole could be drilled (rotary diamond drilling). It was therefore not possible to mobilise another rig and drill new holes for subsequent scans. The results of the scans are shown in Figure 8.40. As previously mentioned, the value of these initial scans was to confirm if the external appearance of the pillar could be validated through internal observations. Pillar P2 showed a good correlation. However, at the time of the scans, the pillars were not formed yet and the degree of scaling diminished along the axis of the hole. Figure 8.40 does show that fracture intensity and depth of fracturing decreases ahead of the face.

Also, it was established from the external observations that a crush pillar does not fracture uniformly along the width of the pillar. Fractures form along the side of the pillar which was exposed first. The fracturing extends to approximately mid-way through the pillar. New fractures do form, but only once the pillar is approximately 3 - 7 m in the back area. In most cases these new fractures were spaced more than 100 mm apart and would not contribute to the PFI. Unfortunately the internal condition of the pillar could not be visually assessed to confirm all the external observations. A follow up site visit conducted at the end of September 2015 confirmed that there was no sign of time dependent deterioration of the pillars once mining stopped.

PFI does therefore not appear to be a valid or appropriate tool to establish the extent to which a pillar is yielding (PFI: 45 - 90) or crushing (PFI < 45). Also drilling of holes in a production crush pillar environment (stoping with ≈ 1 – 1.5 m) will almost be impossible (specialised and costly drilling process). Furthermore the information takes time to process (post underground scan) and requires a trained eye.

The stress change measurements conducted above pillar P2 and P3 indicated that the pillars moved to a residual state by the time the pillar was fully formed (face at next pillar position). This was also inferred by the micro seismic analyses of the seismic velocity change measurements conducted across pillars P2 and P3 indicating that there was a high degree of fracturing, even through the core of the pillar.

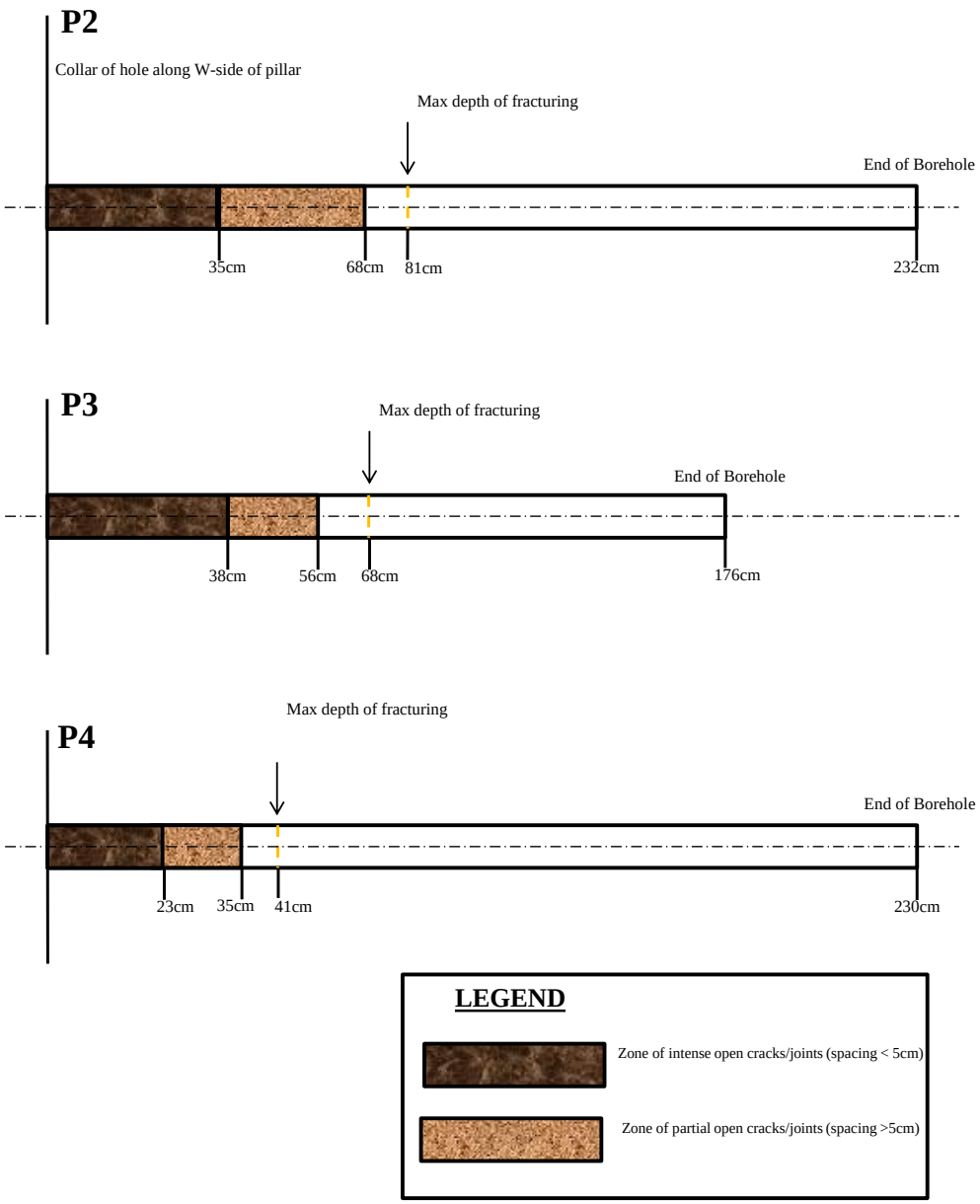

Figure 8.40: Borehole camera scans through pillars P2, P3, P4. Scans conducted prior to mining the final section (27 February 2015).

8.4. Pillar fracturing mechanism from observed behaviour

Although the application of a crush pillar system is rather unique to the intermediate depth gold and platinum mines of South Africa, crushing of pillars or failing pillars have been identified in other underground environments across the world. The following subsection describes these pillars. The findings were compared to the observations of the crush pillars in the underground trial site to obtain a better understanding regarding the failure process of a crush pillar.

8.4.1. Literature review on failing pillars

Brady and Brown (1985) described five modes of pillar behaviour. Three of these modes occur when the pillar stress approaches the rock mass strength whilst the other two are structurally driven. These failure modes are represented in Figure 8.41 and consist of:

1. Spalling (scaling) of pillar edges into the mine opening (Figure 8.41a),
2. The formation of an inclined failure plane which develops within the core of a pillar (Figure 8.41b),
3. Axial splitting as a result of movement along soft top and bottom pillar contacts (Figure 8.41c),
4. Movement along geological structures intersecting a pillar (Figure 8.41d),
5. Buckling along vertically defined planes of weakness (Figure 8.41e).

The failure mode experienced by the majority of the crush pillars in the trial site displayed a combination of these behaviours namely spalling ***(a)***, formation of an inclined failure plane or wedge ***(b)*** and buckling along vertically defined planes of weakness or fracture planes ***(e)***. However, pillar P3 displayed late crushing and it is therefore presumed that most of the movement was absorbed by the geological structure which intersected the pillar ***(d)***. Also, pillar P4 had a chromitite contact present along the top of the pillar. The pillar displayed very early signs of slabbing which is presumed to coincide with possible mobilisation of the slabs defined by the fracture planes along this contact ***(c)***. The last two scenarios mentioned ***(d and c)*** was not common of the general behaviour and will therefore not be included as the predominant failure mode (although it could contribute to the degree of fracturing observed or experienced by a pillar).

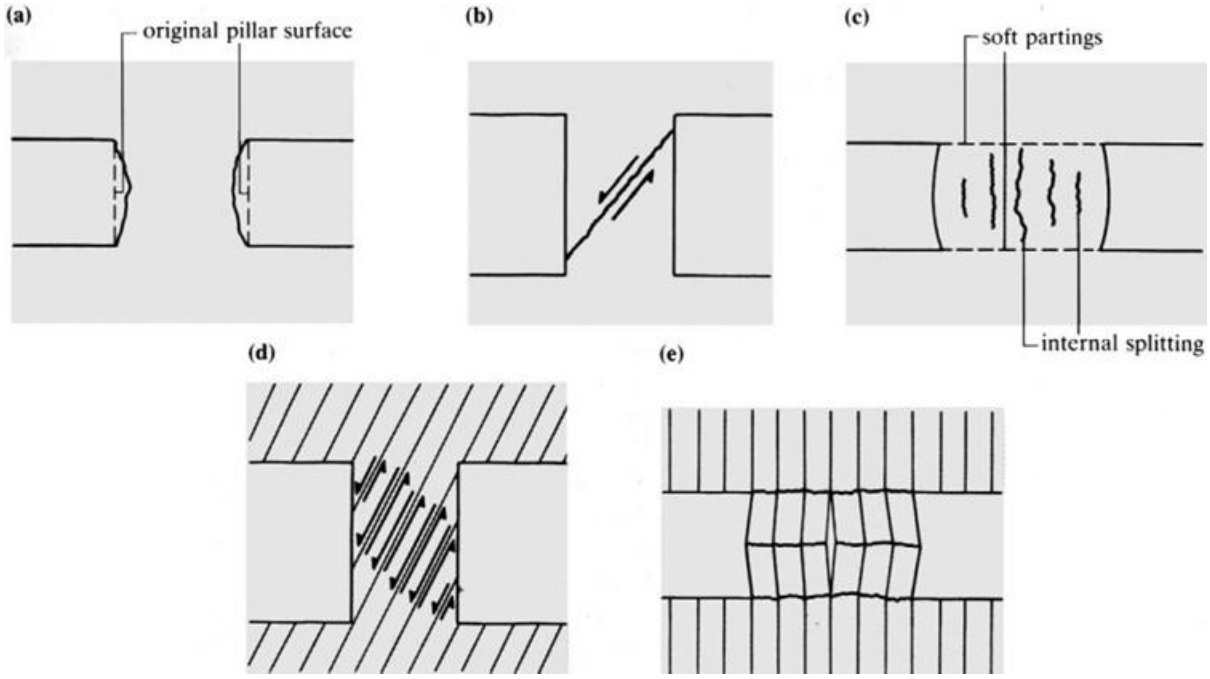

Figure 8.41: Principal modes of pillar deformation behaviour (after Brady and Brown, 1985).

Lunder (1994) presented a pillar stability classification based upon the methodology after Krauland and Soder (1987) and the observed pillar condition at H-W mine situated on Vancouver Island (massive sulphide pillars with pillar heights of between 4 and 5 m; w:h ≈ 0.9 – 3). Similarly, Roberts et al (1998) applied a condition rating based on the visual appearance of lead pillars at Doe Run mine in Missouri, USA (pillar height approximately 20 m). Both of these approaches were based on various stages of deformation for pillars subjected to stress states satisfying the condition for fracture initiation and damage (refer to Figure 8.42 and Table 8.12 as an example of Lunder's classification).

Although the observed behaviour of both case studies (Lunder and Roberts et al) have various similarities with one another and some of the observed pillar behaviour at the Lonmin crush pillar trial site, it must be noted that these pillars had a considerably greater pillar height (4 – 20 m) versus 1.3 m. However, the w:h range was, for all cases, below three and the pillars failed as a result of the interaction of the network of extension fractures intersecting the pillars.

What is of importance is that the condition of the pillars is well understood. If the mode of failure is studied and recorded, the anticipated behaviour for the type of pillar in a particular environment can be predicted.

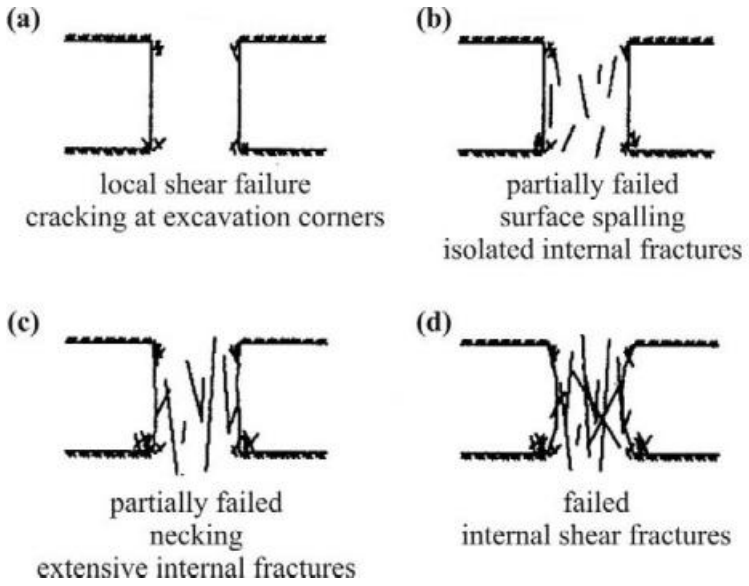

Figure 8.42: Pillar stability condition classification indicating the evolution of fractures and failure (after Lunder, 1994).

Table 8.12: Pillar stability classification method (after Lunder, 1994).

Pillar stability classification	Observed pillar condition
a	Corner breaking up only
b	Fracturing in pillar walls Fractures < 1/2 pillar height in length Fracture aperture < 5 mm
c	Fractures > 1/2 pillar height in length Fracture aperture > 5 mm, < 10 mm
d	Disintegration of pillar Blocks falling out Fracture aperture > 10 mm Fracture through pillar core

Diedrichs (2002) indicated that extension cracking and growth is the primary form of damage, even under compression. At low confinement, crack extension leads to the observed scaling (spalling) seen along the external surface of a pillar. In a low confinement environment crack propagation dominates, resulting in premature crack interaction and yield. The yield envelope collapses to the initiation threshold (Figure 8.43). However, Diedrichs commented that crack growth and crack opening removes the possibility for frictional interaction between the crack surfaces. As a result, cohesive strength is lost before the frictional strength can be mobilised. With on-going damage, the frictional strength can be restored as the crack surfaces are re-mated. This results in the brittle post-yield behaviour characterised by the formation of surface parallel

discontinuities or fractures. At much higher confining stress the dilation of cracks can be suppressed. The frictional strength is re-mobilised simultaneously with cohesion loss resulting in continuous yield behaviour and damage (also possible seismic potential).

The observed damage, however, corresponds to a lower bound threshold (Figure 8.43) equivalent to approximately $0.5\sigma_c$ (unconfined peak strength). Lunder (1994) determined this transition to occur at between $0.3 – 0.5\sigma_c$ which he defined as the average "rock mass strength size factor". Kaiser et al (1996) indicated that for stress-induced progressive failure to occur (scaling), the pillar stress must exceed the pillar strength; occurs at approximately $0.3 – 0.5\sigma_c$. The findings summarised in Figure 8.43 is based on the microscopic and mesoscopic damage processes and subsequently, on a macro scale based on the pillar performance in highly variable conditions at depth at Brunswick mine (zinc mine in Canada). The case study at the mine revealed interesting findings regarding the overall pillar behaviour when related to the failure envelope, namely:

- Sidewall scaling initiates at the crack ***initiation*** threshold,
- Scaling changes the pillar geometry and therefore the confinement within the pillar core,
- As the initial damage begins to ***accumulate***, the internal core stresses deviate from the applied stresses,
- The core yields when the actual local stress state reaches the yield envelope defined by crack ***interaction*** (failure slope),
- The load bearing capacity of the pillar is only changed when this failure limit is reached.

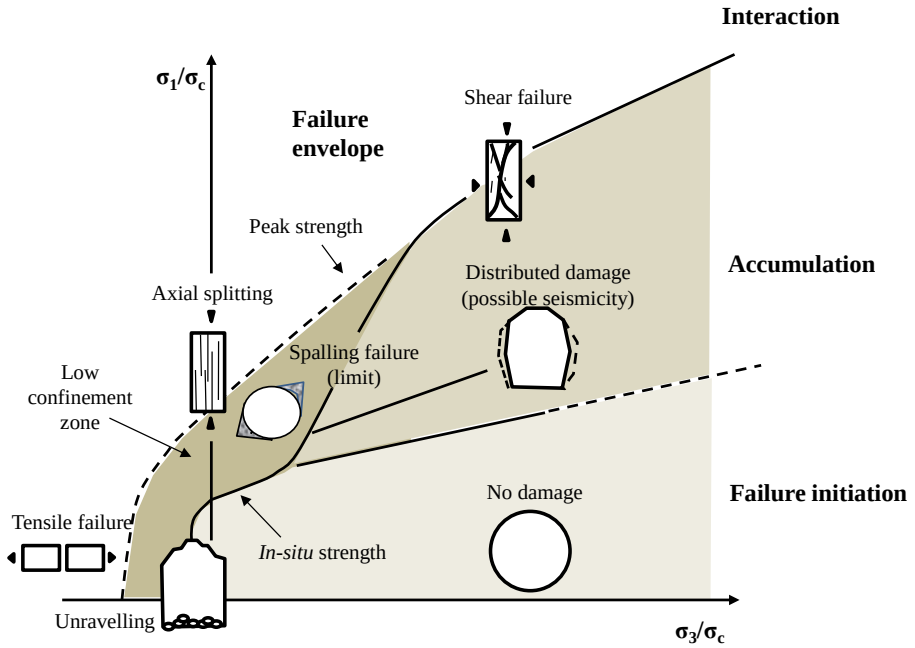

Figure 8.43: Resultant *in-situ* failure envelope for hard rock (Lac du Bonnet Granite). Figure re-constructed based on the findings of Diedrichs (2002).

Martin (1997), based on experimental work on Lac du Bonnet Granite, indicated that the ***initiation*** of damage as a result of crack growth in the direction of the maximum applied stress occurs at about $0.3 - 0.4\sigma_c$. The transition from stable to unstable cracking (sliding as friction is mobilised) occurs when the deviatoric compressive stress reaches about $0.7\sigma_c$. If a sample is subjected to a loading process which causes damage, the strength of the sample is significantly reduced and the cohesion loss could result in 50 percent or more of the initial cohesion of the sample.

Maybee (2000) describes typical hour-glassing observed in failed pillars as a progressive spalling mode of failure. As the skin of an excavation is subjected to no confinement and high tangential stresses, cracks and slabs form parallel to the direction of the major principal stress. As scaling occurs, stresses flowing through the pillar are redistributed to the intact pillar core. The loss of fractured slabs reduces core confinement and further damage occurs to the newly exposed pillar walls. If the progressive failure propagates too far, the pillar can reach a critical cross sectional area and fail.

Stress induced fractures propagate from stress raisers (concentration) at the corner of an excavations forming semi-circular fracture patterns (Kaiser et al, 1996). These fractures connect areas of high stress. This is also commonly referred to as observed onion skinning which has the tendency to dilate or bulk. Kaiser et al referred to this tensile fractured zone as “baggage”. Figure 8.44 indicates the baggage principle. The extent of baggage for a non-circular opening where w > 2h can be determined by:

$$\Delta_{max} = \frac{h}{4}\left(1 - 2\frac{w}{h} + \sqrt{1 + 4\left(\frac{w}{h}\right)^2}\right) \qquad (8.2)$$

or assuming the angle α is equal to 45 degrees (2α = 90);

$$\Delta = \frac{h}{2\sin\alpha}\left(\sqrt{2} - 1\right) \qquad (8.3)$$

Where

Δ = Depth of “baggage” (m). Approximately 20% of excavation height or width

h = Excavation height (m)

w = Excavation width (m)

a = Radius of circle defining baggage depth (m). Could also depend on the *in-situ* stress ratio

2α = Angle between radii defining excavation corners (stress raisers) – degrees

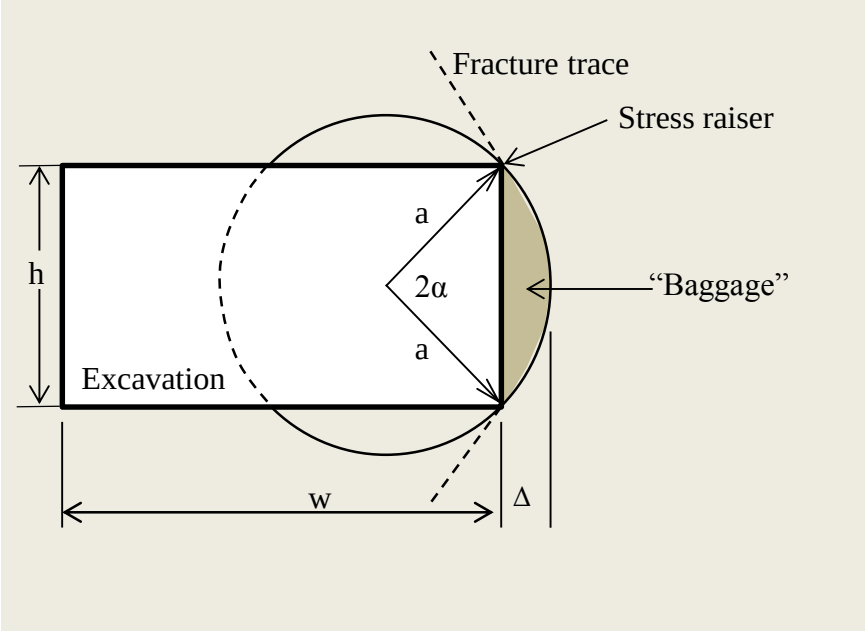

Figure 8.44: Fractured zone around excavation ("baggage principle"). Figure reconstructed after Kaiser et al (1996).

Maybee (2000) suggested the application of the concept presented by Kaiser et al (1996) where the total amount of fracturing experienced around a circular opening be applied to pillars to determine the total amount of progressive failure ("baggage" plus the additional failure). A pillar typically consists of rectangular excavations either side.

Kaiser et al (1996) proposed the depth of additional failure d_f (beyond the "baggage") could be approximated by equation 8.4. The concept is presented in Figure 8.45.

$$\frac{d_f}{a} = 1.34\frac{\sigma_{\max}}{\sigma_c} - 0.57(\pm 0.05) \qquad (8.4)$$

With

$$a = \frac{h}{\sqrt{2}} \text{ or approximately } 0.7h \qquad (8.5)$$

$$\sigma_{\max} = (\sigma_{\max})_{circle} + \left(\frac{w}{h} - 1\right) \qquad (8.6)$$

$$(\sigma_{max})_{circle} = 3\sigma_1 - \sigma_3 \quad (8.7)$$

Where

d_f = Depth of additional failure (m)

σ_{max} = Tangential stress (MPa)

σ_c = Unconfined peak strength of rock (pillar material) - MPa

σ_1 = Maximum principal stress (MPa)

σ_3 = Minimum principal stress (MPa)

The total thickness of failed rock therefore comprises of the fractured zone Δ ("baggage") and the potential depth of additional failure d_f.

This concept needs to be tested against the various forms of measurement conducted in the crush pillar trial site. Table 8.13 summarises the results by applying the approach described above and incorporating the parameters of the Merensky crush pillar trial mining site.

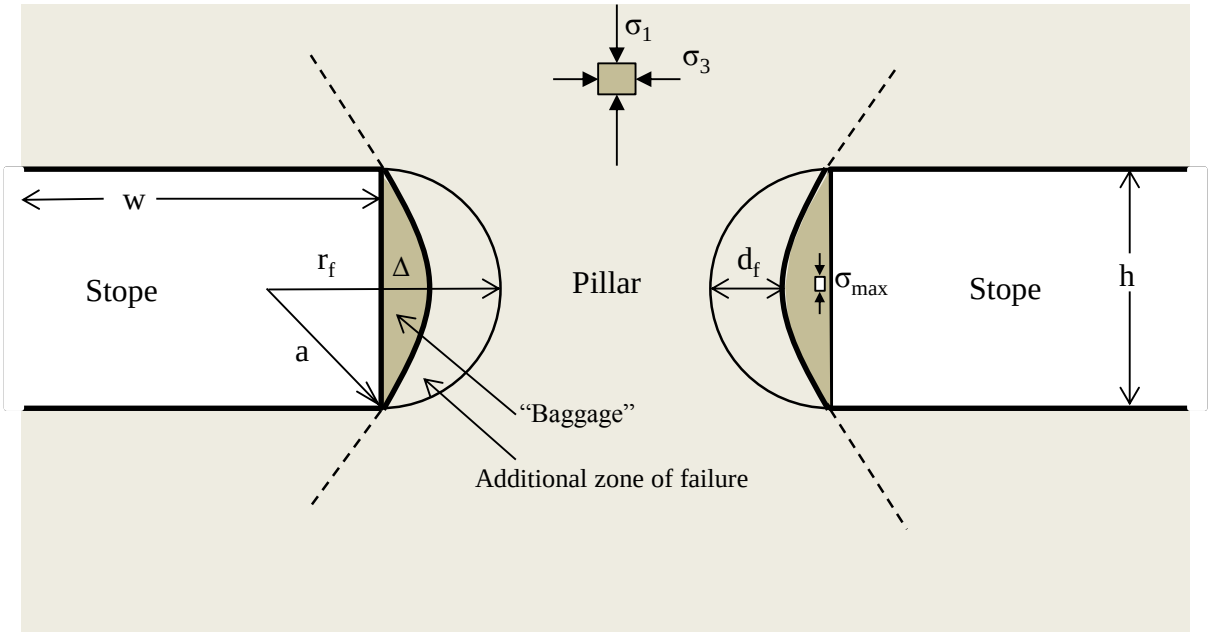

Figure 8.45: Depth of stress induced failure. Figure reconstructed after Kaiser et al (1996) to represent the influence on a pillar.

Table 8.13: Depth of predicted failure on either side of the crush pillars.

w (m)	14
h (m)	1.3
σ_c (MPa)	140
σ_1 (MPa)	45.1
σ_3 (MPa)	25

Circular	Rectangular	Radius	Additional fracturing	Baggage	Total failure zone
σ_{max} (MPa)	σ_{max} (MPa)	a (deg)	d_f (m)	Δ (m)	(m)
110.30	120.07	0.92	0.59	0.33	0.92

The result essentially suggests that the outer 30 cm of the pillar is lost as a result of scaling (baggage). The amount of scaling visible along pillar P2 (prior to formation) Figure 8.30 and (after formation) Figure 8.33 indicate approximate scaling to this extent. However, as observed from the crush pillars in the underground trial section, scaling was in all instances only found to occur predominantly on the one side of the pillar (the side exposed first). It is therefore not a symmetrical characteristic, unless both sides are perhaps exposed simultaneously (which would be rather uncommon). The additional 59 cm of failure was typically observed along all pillars. In essence, the result suggest that pillars with a width of 1.51 – 1.84 m or less should be fractured throughout (0.33 baggage + 59 cm additional fracturing one side +59 cm additional fracturing from the other side + 0 - 33 cm baggage from the other side).

8.4.2. Crush pillar fracturing mechanism

Section 8.3 provided an improved understanding of the fracturing sequence of the crush pillars during various stages of the pillar forming cycle. The results agreed well with the observed behaviour as described in Section 8.2.1. Cutting of pillars P2, P3 and P4 confirmed that the side of the pillar which was exposed first created a "free face". Fractures form parallel to this "free-face" and propagate towards this "free-face".

The literature review on failing pillars (Section 8.4.1) indicated that there are many similarities between pillars designed to fail (crush pillars) and pillars failing as a result of their size (even though at increased mining heights). Three modes of failure could be identified as being common to the crush pillars (refer to Figure 8.41). These are (in order of sequence):

a) Spalling,
e) Buckling along failure or fracture planes,
b) Formation of an incline failure plane.

Kaiser et al (1996) suggested a model to determine the amount of progressive failure. This concept, applied to the crush pillar scenario indicated that pillars at a width of less than the range 1.51 – 1.84 m should be completely fractured.

A prominent observation from many pillars in the crush pillar trial site was the formation of a wedge-like structure or failure plane which formed where fractures meet in approximately the centre of the pillar. This is apparent in Figures 8.15a (pillar 6), 8.28 (pillar P1) and also in Figure 8.46 and 8.47 below. Pillar P4 also had an oblique fracture forming along the up-dip side of the pillar. This fracture formed approximately in the centre of the pillar (refer to Figure 8.37 dated 6 May). Figure 8.48 and 8.49 shows the combination of failure modes typically experienced as referred to above. These observations were essential in establishing the failure mode of the crush pillars.

Figure 8.46: Wedge like formation along the down dip side of pillar 4 where the fractures intersect.

Figure 8.47: Wedge like formation in the centre of a pillar (pillar 43 up-dip view).

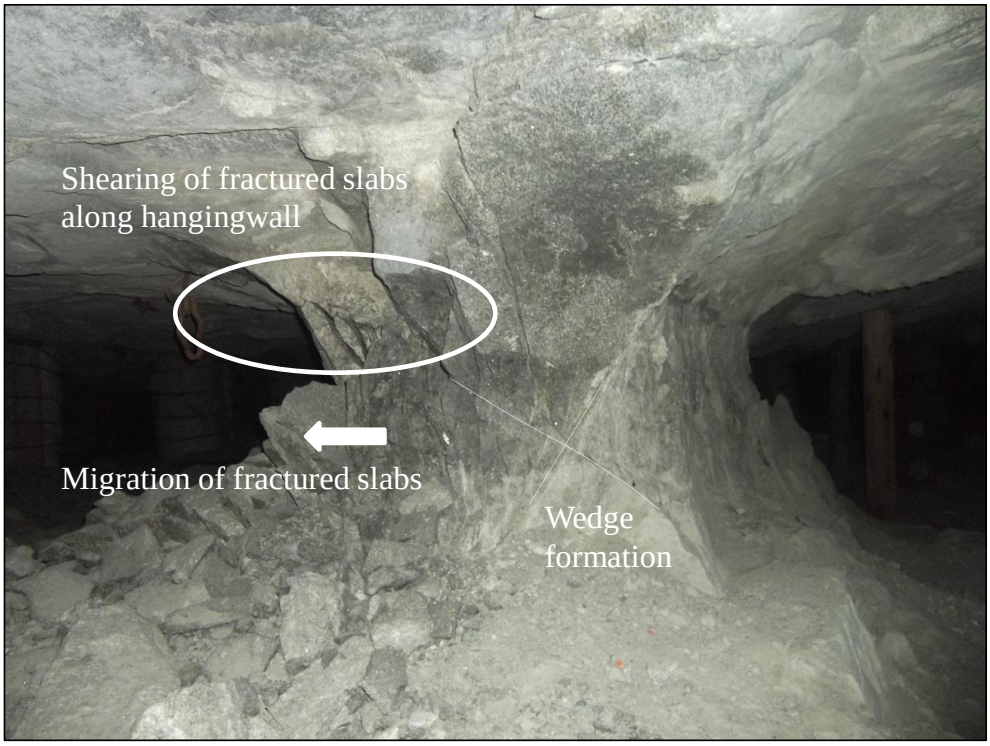

Figure 8.48: Shearing of fractured slabs along the hangingwall and wedge formation (up-dip side of pillar 6).

Figure 8.49: Shearing of fractured slabs along low angled extension fracture (down-dip side of pillar 5).

Inferred failure mode:

- As a pillar is being cut, a “free face” is formed along the long axis of the pillar.
- The pillar abutment along this “free face” is highly stressed.
- Extension fractures form parallel to the exposed surface “free-face” and extend into the hanging-and footwall.
- As mining continues and the pillar is formed, these fractures continue to develop parallel to the long axis of the pillar.
- As new fractures form, previously formed fractures start to dilate.
- The fracture concentration is intensified towards the side of the pillar which was exposed first.
- Fractured slabs defined by fracture planes continue to form. These fractured slabs buckle at approximately mid-height as the slabs are pushed outward. This is observed as increased scaling towards the initially exposed side of the pillar.
- The slabs defined by the fracture planes move up-or down relative to one-another as the slabs rotate outwards while the pillar continues to deform.
- The fractured, buckled slabs, in some instances shear off along the hangingwall or along low angled extension fractures.
- As extension fractures continue to open and fractured slabs migrate outwards, the confinement it provided to the core of the pillar is reduced.
- As a result more extension fractures are formed.
- Where the extension fractures meet at approximately the centre of the pillar, the fractures and failure surfaces interact and form a wedge-like structure.

The diagrams in Figure 8.50 and 8.51 illustrate this process. Similarly, should the panel to the left be mined first the fracturing sequence will be concentrated towards the left side of the pillar (see photograph of pillar 38 in Figure 8.52).

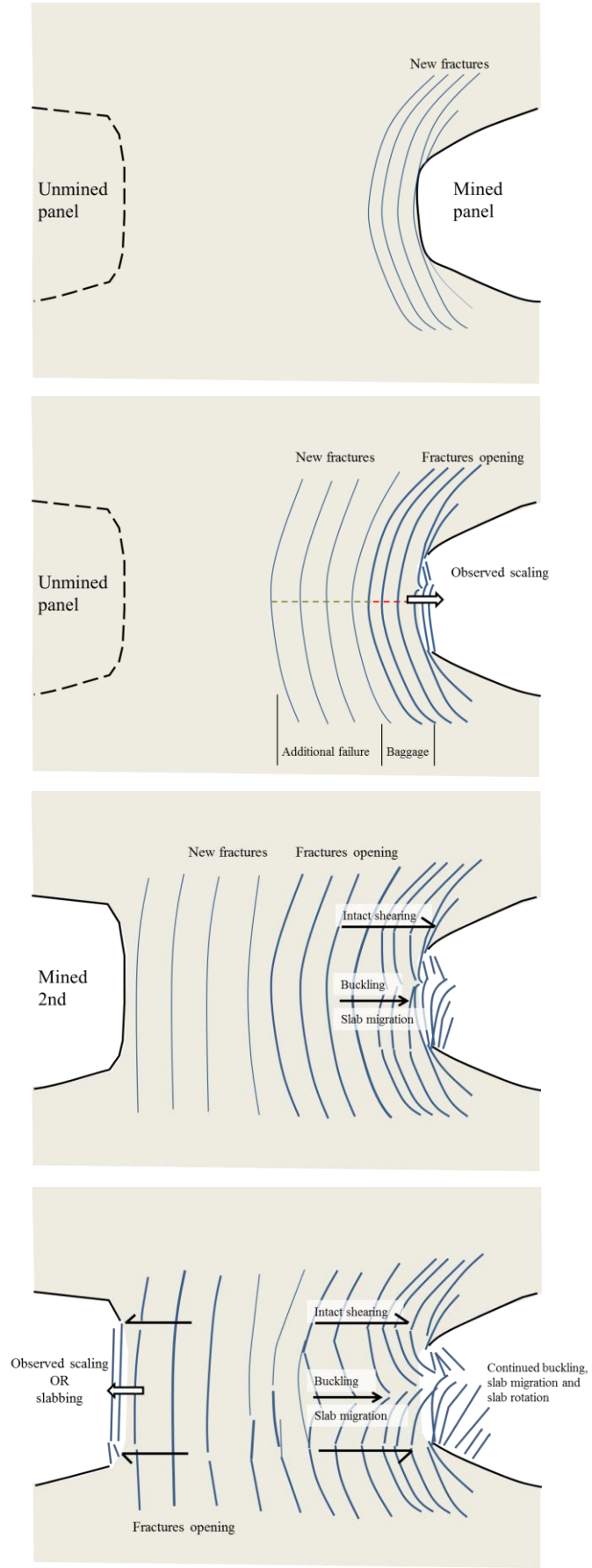

Figure 8.50: Crush pillar fracturing sequence observed in the underground mining trial.

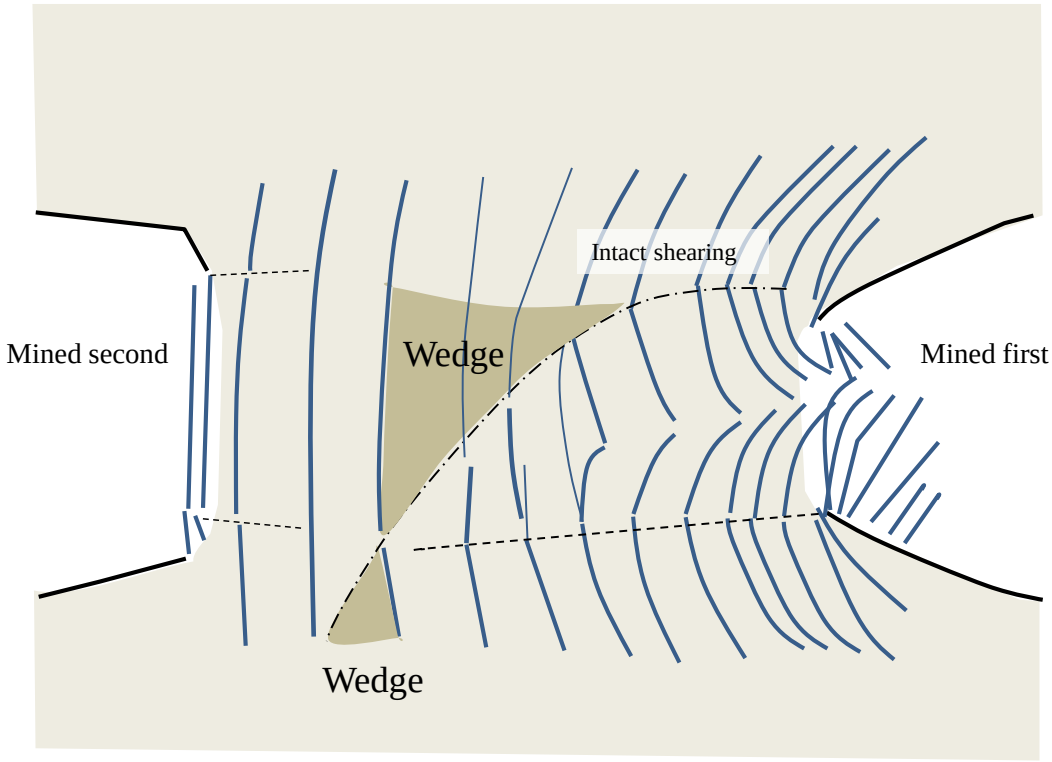

Figure 8.51: Crush pillar fracture pattern observed in failed pillars.

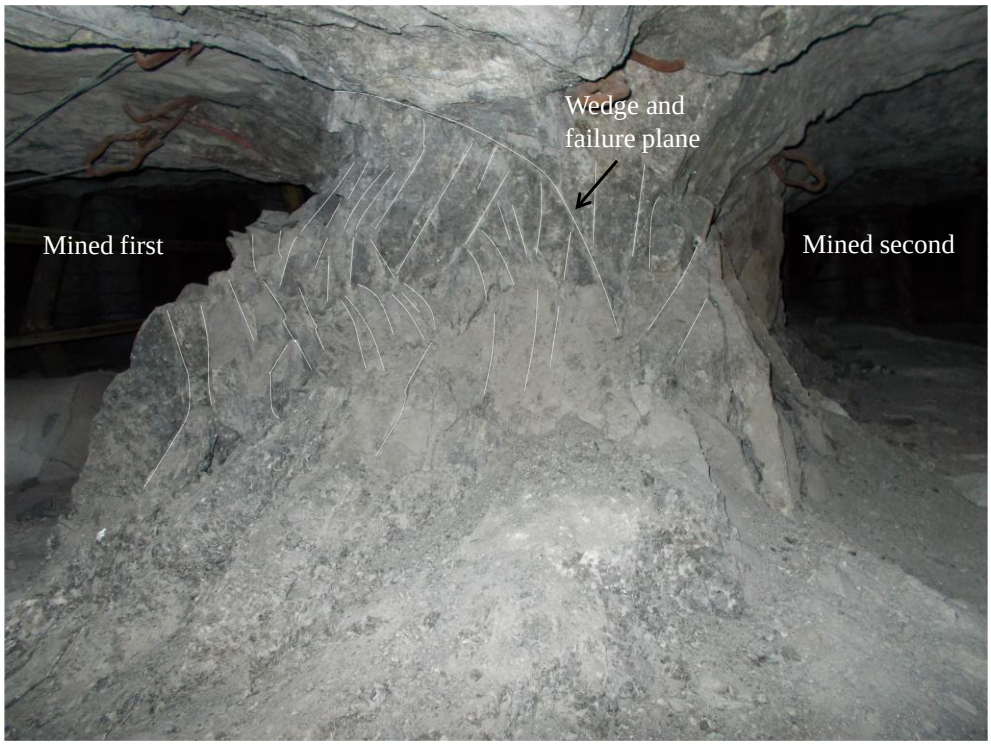

Figure 8.52: Failure patterns observed along the down-dip side of pillar 38 (1.5 m wide) validating the representation in Figure 8.51.

Abnormal behaviour

There was only one other mode of failure identified. This was along pillar P4. The pillar had a prominent chromitite contact present along the top of the pillar close to the hangingwall. As mentioned, this pillar displayed early signs of slabbing, and a lot of scaling focussed towards the west of the pillar (Figure 8.38). An inclined failure plane was observed along the up-dip side of the pillar, dipping towards the east. However, along the down-dip portion of the pillar a circular failure plane was observed close to the centre of the pillar. The failure plane defined the edge of the fractured zone along the western side of the pillar (Figure 8.53).

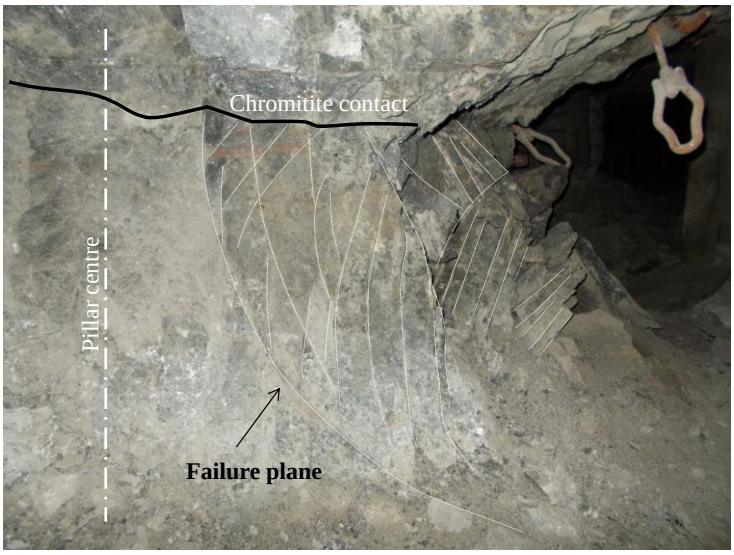

Figure 8.53: Circular failure plane observed along the down-dip side of pillar P4. This was abnormal behaviour. The pillar had a chromitite contact present along the top of the pillar.

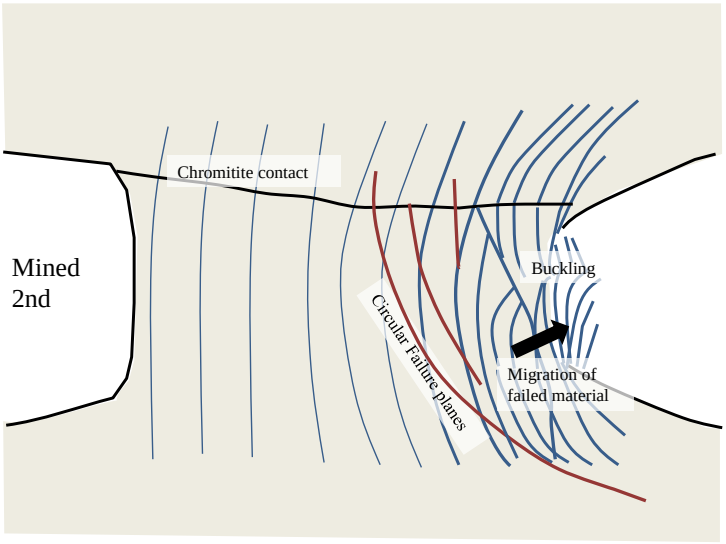

Figure 8.54: Representation of regular fracturing and failure mode observed along the down-dip side of pillar P4.

Simplified model to describe the pillar behaviour

A generalised representation of the pillar behaviour is illustrated in Figure 8.55. Assuming that both sides of the pillar are exposed simultaneously the fracturing process will start concurrently from the outer edges of the pillar. As the vertical fractures dilate the slabs defined by the fracture planes will start to migrate outward. This is accompanied by the intact shearing of the rock along the hanging-and footwall boundaries of the pillar. Continued pillar dilation result in buckling of these slabs. A failed slab will result in a reduction in the overall pillar strength. As the failed slabs migrate outward, the confinement of the pillar core is reduced. New fractures form and the process repeats. At some point, the fractures from both sides of the pillar will interact. This will result in the formation of a wedge-like structure cutting through the pillar core. At this point the pillar strength will be reduced to a residual value as the pillar has reached complete failure.

In wide pillars there will be no interaction of the fractures formed from either side of the outer pillar. The failed slabs could also provide a sufficient amount of confinement to stop the formation of new fracture planes. As the pillar is fully formed and becomes highly stressed in the back area of a stope, new fractures can again form. At some point there could be an instantaneous rupture of the core along an inclined failure plane when fracture planes interact resulting in violent pillar failure. This analogy is also supplemented by the findings of Diedrichs (2002) in that the dilation of cracks are suppressed at higher confining stress resulting in yield and potential damage once the frictional strength is once again mobilised whilst suffering a simultaneous cohesion loss.

The limit equilibrium model described in Chapter 3 approximates the behaviour of the crush pillars observed in the trial site. In the model, the pillar is divided in thin material slices, similar to the slabs defined by the fracture planes. Each slice is loaded to failure, transferring its load to the adjacent unfailed slices which results in the gradual crushing from the outside to the inside of the pillar. As with the model, a pillar is presumed failed when the peripheral fractured zone extends to the pillar centre. The formation of a wedge-like structure or inclined failure plane cannot be represented by the model. However, the failure mechanism remains the same. Interacting fracture planes are represented by the complete failure of all the material slices. The surface of a pillar provides a horizontal clamping stress (although marginal). As the fractured slabs migrate outwards, the clamping stress (equal to p) is overcome. Failure of the pillar (slabs) is described by equations 3.10 and 3.11 which are strongly influenced by the outward migration of the failing slabs, resisted by friction along the pillar hanging-and footwall interfaces. The overall impact hereof is accounted for by the residual strength of the pillar as described by equation 3.15.

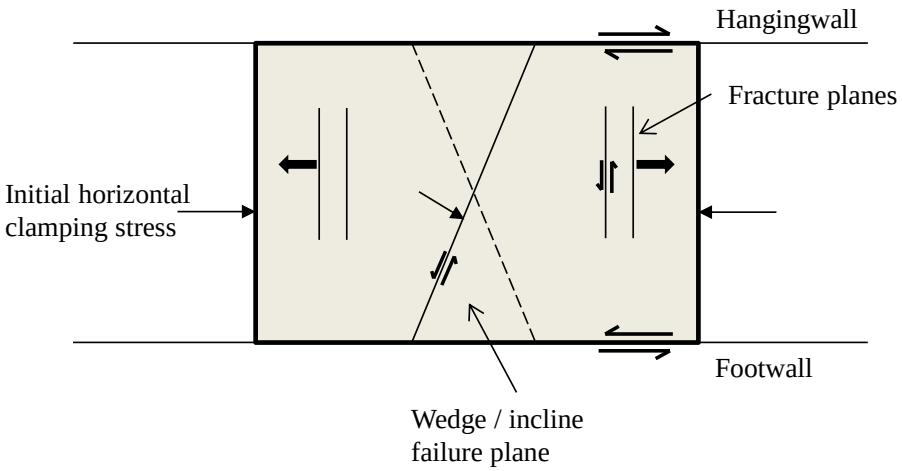

Figure 8.55: Simplified crush pillar model representing mode of failure.

8.5. Summary

An underground crush pillar trial site was established towards the end of 2012 on Lonmin's K3 shaft at a depth of approximately 782 mbs. The Merensky Reef, dipping at approximately 8 degrees was mined at an average mining height of approximately 1.3 m using conventional drill and blast techniques. The trial area comprised an area of approximately 22000 m^2. During the trial, 55 crush pillars were cut with 87 percent of the pillars having a w:h ratio of less than 2:1 and only seven pillars with a w:h ratios greater than 2:1. The objective of the trial was to obtain a better understanding of the pillar system and the associated risks.

The most prominent findings from the underground observations were:

- The composition of the pillar, including the exposed hangingwall rock, influenced the pillar behaviour.
- The fracture intensity was more profound on the side of the pillar which was mined first.
- Pillars were observed to be partially fractured whilst being formed at the mining face. This indicated that the stress was sufficiently high to initiate early pillar crushing.
- Fractures were observed to form approximately 9 m ahead of the lagging face position. These fractures would increase as the lagging face advanced. By the time the face was aligned with the pillar, the fracture planes were spaced approximately 30 - 50 mm apart along the outer metre of the pillar. These fractures would start to open (5 – 10 mm) as the pillar was being formed and would continue to dilate until the pillar was approximately 14 m in the back area. Little to no scaling or slabbing was visible along the side of the pillar which was exposed by the advance of the lagging face. New fractures did form along this side of the pillar, only when the pillar was 3 – 7 m in the back area. In most cases these new fractures were spaced more than 100 mm apart and extended to approximately half the pillar width. These fractures did start to dilate when the pillar was approximately 10 m in the back area. It did not result in any observed scaling or slabbing of the pillar surface along this side of the pillar.
- Pillars that were completely fractured throughout comprised of fracture planes spaced approximately 30 - 50 mm apart.
- Buckling of the fractured slabs was either along the top or the bottom of the pillar depending on the mining sequence. Pillars which fractured towards the west had the fractured slabs buckling closer to the footwall. In contrary, pillars which fractured towards the east had the fractured slabs buckling closer to the hangingwall.
- A wedge-like structure or failure plane was observed where fractures intersected each other approximately halfway through the pillar.

The observed behaviour of the crush pillars in the underground trial site identified many similarities between pillars designed to fail (crush pillars) and failing pillars. Three modes of failure could be identified as being common:

- Spalling (scaling),
- Buckling along failure or fracture planes,
- Formation of an incline failure plane (wedge-like structure).

From the observations a sequence and mode of failure was formulated which explicitly described the behaviour of the crush pillars in the trial section. The findings were incorporated in a simplified model representing the generalised crush pillar behaviour. Upon comparison, it was found that the limit equilibrium model presented in Chapter 3 closely approximated this model and mode of failure.

8.6. References

Brady, B.H.G. and Brown, E.T. (1985). *Rock Mechanics for Underground Mining*. 1st ed. London: Allen and Unwin.

Coetzer, S.J. (2003). Measurement of rock stress at Lonmin Platinum mines. CSIR consultancy report issued by CSIR Miningtek, Johannesburg.

Diederichs, M. S. (2002). Stress induced damage accumulation and implications for hard rock engineering. Mining and tunnelling innovation and opportunity. *Proc. 5th North Am. Rock Mech. Symp. and 17th Tunn. Assn. Can. Conf.*, Toronto, Canada.

Grodner, M.W. and Canbulat, I. (2005). A Methodology for quantification of hard rock pillar behaviour. *3rd Southern African Rock Engineering Symposium*. South African Institute of Mining and Metallurgy Symposium Series 41, pp. 121–130.

Jager, A.J. and Ryder, J.A. (1999). *A handbook on Rock Engineering Practice for Tabular Hard Rock mines*. SIMRAC, Johannesburg.

Lunder, P.J. (1994). Hard Rock Pillar Strength Estimate an Applied Empirical Approach. Masters thesis, University of British Columbia, Canada.

Kaiser, P.K., McCreath, D.R. and Tannant, D.D. (1996). *Rockburst Research Handbook.* Mining research directorate, Canada.

Krauland, N. and Soder, P. (1987). Determining pillar strength from pillar failure observations. E&MJ. pp. 33-40.

Martin, C.D. (1997). The effect of cohesion loss and stress path on brittle rock strength. *Seventeenth Canadian Geotechnical Colloquium.* Can. Geotechnical Journal 34. pp. 698 - 725.

Maybee, W.G. (2000). Pillar Design in Hard Brittle Rocks. Masters thesis at Laurentian University, Sudbury, Ontario Canada.

Pillai. S. (2013). Lonmin Platinum Mines Ltd Marikana Operations K3 shaft Geological environment. *Internal Lonmin document.*

Roberts, D. P., Lane, W. L. and Yanske, T. R. (1998). Pillar extraction at the Doe Run Company. *Minefill '98, Proc. 6th Int. Symp. Mining with Backfill*, Brisbane, Australia. pp. 27–33.

CHAPTER 9

UNDERGROUND TRIAL – PART B

Measurements and quantitative behaviour

9. UNDERGROUND TRIAL PART B: MEASUREMENT RESULTS

The objective of this chapter is to describe the measurements of the pillar behaviour in the trial section. It will also relate the measured performance to the pillar condition as observed during the pillar forming cycle (Chapter 8).

The instrumentation confirmed that a pillar reaches a residual state once the pillar is completely formed (holed). However, the pillars also experienced secondary reductions in stress when new pillars were formed. This phenomenon is believed to be associated with the transfer of stress to the newly formed pillars. This unloading phase, has in the past, typically only been referred to as continued strain softening behaviour. However, it was found that at some point the pillars experienced no further reduction in stress whilst the pillars continued to dilate. This observation was also verified by the convergence measurements. After all mining stopped, continued convergence was measured.

9.1. Overview of significant monitoring conducted at other crush pillar sites

In the past a significant effort was made to gain an improved understanding of crush pillar behaviour. This was done mostly through back analysing historic collapses or the underground pillar behaviour. More recently (past 20 years), instrumentation was used to measure the crush pillar response to mining. The research focussed mostly at determining the most critical factors believed to be the source of instability. The investigations varied and predominantly assessed the elements as listed below:

- Backbreaks, York et al (1998), Roberts et al (2005a).
- Pillar bursts sites, Watson et al (2007), Watson (2010).
- Seismic databases in mines using crush pillars, Haile and Jager (1995).
- Micro-seismic activity around crush pillars, York et al (1998).
- Horizontal stress change in crush pillar stopes, York et al (1998), Watson (2010).
- Pillar stress measurements, Lougher (1994), York et al (1998), Roberts et al (2005a), Watson (2010).
- Convergence monitoring in crush pillar sites, Lougher (1994), Piper and Flanagan (2005), York et al (1998), Roberts et al (2006), Canbulat et al (2006), Watson (2010).
- Inelastic hanging-and footwall behaviour around crush pillars, York et al (1998), Watson (2010).
- Fracture mapping in pillars, the surrounding hanging-and footwall, Lougher (1994), Piper and Flanagan (2005), York et al (1998), Canbulat et al (2006), Watson (2010).
- Rockmass properties, Canbulat et al (2006), Watson (2010).
- Numerical modelling, back analyses or desktop studies, Lougher (1994), Piper and Flanagan (2005), York et al (1998), Roberts et al (2002), Canbulat et al (2006), Watson et al (2007), Watson (2010).

In most cases the stress measurement results were adjusted based on numerical back analyses of the instrumented sites. Estimated pillar strengths were obtain by applying adjustments or estimated rock properties. Crush pillar peak strengths were determined from elastic models and analytical equations. Questionable residual strength measurements were calibrated against elastic numerical models. The researchers were, in most cases, satisfied once the results for the residual pillar strength was aligned with values predicted by previous researchers, i.e. (Ozbay and Roberts, 1988) or (Ryder and Ozbay, 1990) which was in the region of 13 - 20 MPa. These predictions came from back analysing stope collapses and not from measuring the actual pillar stress.

From a review of the various crush pillar studies it is clear that very few considered measuring both pillar stress and the resulting convergence. The majority of the measurements were aimed at relating convergence measured using closure stations (pegs) to either pillar fracturing, or hangingwall and / or footwall fracturing through the use of a borehole camera (or petroscope) or extensometer readings. Stress measurements were mostly focussed on determining the horizontal stress above a crush pillar panel.

9.1.1. Results obtained from attempted stress measurements

Pillar stress measurements are in general difficult to perform, especially if the complete stress-strain behaviour of a crush pillar is the desired outcome. The intent of the measurement needs to be weighed up against the technology available and the restrictions of a particular instrument. Pillar stress should ideally be measured in the centre of the pillar or directly below the pillar. It is, however, anticipated that these small crush pillars are subjected to very high initial loads followed by a significant stress reduction. The pillar geometry will also continuously change as a result of the pillar fracturing process. Therefore, pillar stress or stress change should be measured some distance above or below the pillar to ensure that it is not influenced by the zone of failure. In a narrow stoping width, this necessitates specialised drilling and drilling accuracy which entails high cost and high risk. In some applications it was found that the footwall and immediate hangingwall was not the best locations to conduct the pillar stress measurements. Oversized pillars undergo significant footwall deformation. Also, there appears to be a considerable zone of stress induced hangingwall fracturing (up to 4 m and even 6 m above the pillars) that can influence the measurements. The experimental site is, in most cases not free of complex geology and although pillars are aimed to be of a certain dimension, precise pillar cutting (due to mining practices and discipline) is difficult to achieve. Isolating pillars to conduct stress change measurements involve creating mining layouts whereby sufficient leads and lags are established so that instruments can be installed at the future pillar position. Once mining starts, the stress change can be measured as the pillar is formed. However, ground conditions, mining practices or unforeseen stoppages could impact on the actual face advance and pillar cutting. In most cases the pillar is not cut at the correct position, to the correct dimension or within the anticipated timeframe. Consequently the final pillar dimension is not what was required and the behaviour of the pillar is therefore not driven by the pillar size (i.e. w:h ratio) but by the rock type, geology intersecting the pillar, or mining sequence.

Attempts have been made to measure the upper (peak) and lower (residual) stress limits of crush pillars. The documented case studies are summarised below:

- Lougher (1994) presented a case study with regards to the stress-strain behaviour of the Impala yield pillars. Pillar stress was measured using a vibrating wire stress meter to measure the stress change resulting from ongoing mining. Strain was measured using closure pegs installed approximately 4 m from the pillar. The convergence was unfortunately only measured at the one position with the convergence pegs installed up-dip of the planned pillar position in the adjacent mined-out panel (could only measure change in convergence and not the total convergence). The initial stress prior to the installation of the vibrating wire stress meter was estimated using elastic modelling. The results therefore provide an estimated stress-strain profile for the Impala yield pillars.
- York et al (1998) attempted to determine the residual strength of a crush pillar at Amandelbult Mine using various stress measuring instruments available at the time. These included permanent and overcored CSIR doorstoppers (measures two-dimensional stress state), vibrating wire strain meter (measures one-dimensional stress change), hard inclusion strain cells, Glotz load cell and flat jacks (one-dimensional stress change). Unfortunately most of the equipment was installed directly in or just above-or below the pillar and was not ideally suited as the pillar would start to scale during the load shedding process. Most of the instruments therefore failed and connecting wires were cut by failing pillar slabs. The pillar was also situated in Iron Rich Replacement Pegmatite (IRUP) making it very hard. Eventually the pillar suffered a pillar burst and no meaningful information could be obtained.
- Roberts et al (2005a) measured the two-dimensional stress using a CSIR doorstopper above a 2:1 pillar presumed to already be at a residual state. The pillar was situated in the back area of a mined-out stope. The residual stress measured approximately 1 m above the pillar was estimated at 19 MPa. This was similar to predictions made by Ryder and Ozbay (1990) and therefore presumed to be correct.
- Watson (2010) conducted various stress and deformation measurements on Impala, Union and Amandelbult Mines. In all instances the measured pillar stresses (using either CSIRO stress cells or CSIR doorstoppers) were adjusted based on numerical modelling results using elastic models or pillar strength formula derived from stable unfailed pillar case studies. Watson measured convergence using closure stations installed either directly adjacent to the pillar (approximately 4 m away) or a line of stations along the panel face installed perpendicular to the pillar. Unfortunately this only provided good information for one pillar and at the point of measurement. The measurement results were modified by applying adjustments and this resulted in agreement with the modelling predictions, as well as the peak pillar strength and residual strength estimates provided by analytical solutions.

The Lonmin instrumentation site presented its own challenges. Fortunately, towards the end of the trial, mining was controlled by the author which simplified matters. Still, the cost of instruments and specialised drilling was difficult to motivate on a mine which was focussed on producing target outputs in challenging times. An extensive monitoring programme was planned incorporating new generation instruments and new technologies available.

9.2. Monitoring at the Lonmin crush pillar trial site

The objective of the monitoring was to provide answers to the following areas as well as to validate the observations described in Chapter 8:

- When does a pillar start to crush (post-peak state)?
- When has a pillar reached a residual state?
- What is the peak and residual pillar strengths?
- Does the pillar crush all the way through the core?
- Do the measurements substantiate the observed behaviour?
- How much convergence occurs at the crush pillar site?
- Is the convergence purely elastic?
- Is compression experienced by the pillar?
- Is there a relation between pillar dilation (fracturing or slabbing) and convergence?
- Can a failure pattern or mechanism be established from the measurements?
- Can a design criterion be established (w:h ratio or other)?

Various types of instruments were used to achieve the desired objectives. Table 9.1 provides a summary of the instruments used (number in brackets refers to the number of instruments used). Figure 9.8 represents the instrumentation layout. A brief description of the convergence and stress monitoring instrumentation used is provided below.

Table 9.1: Summary of the parameters measured and the equipment used.

Measurement	Equipment
Pillar stress	CSIRO HI cell (3) and CCBO stress measurements (2)
Elastic convergence in the panel	Continuous closure loggers (20), closure ride stations (33) and visual observations (impact on support)
Elastic convergence next to the pillar to measure possible pillar deformation	Closure loggers and closure ride stations
Closure as a result of potential hangingwall separation along partings	Hangingwall extensometers (5)
Pillar dilation	Pillar extensometers (3), borehole camera surveys (3), pillar off-sets via pegs
Pillar fracturing	Borehole camera surveys, micro seismic probing (3 pillars), photogrammetry, visual observations

Hangingwall separation was measured with tape extensometers installed along raise line E3. The extensometers were anchored at 14 m (above the Bastard Merensky top contact), 9 m (below the Bastard Merensky bottom contact) and at 3 m. However, no movement was measured during the trial. The majority of the convergence experienced in stope was therefore purely elastic (with the exception of pillar 42 where footwall heave was observed). The crush pillars seemed to have prevented any potential separation which could have occurred along the Bastard Merensky top and bottom contacts. The results of the extensometer measurements will not be further expanded on.

Methods and equipment used to perform stress measurements

HI cell and top loggers: The CSIRO hollow inclusion (HI) strain cell has twelve strain gauges that are configured in such a manner that the full three-dimensional state of stress can be obtained. Only six of the twelve strain gauges are required to determine the three-dimensional stress and therefore provides reliable data should there be factors influencing the bonding of some strain gauges. A statistical analysis of the measured strain change provides a measure of the level of confidence in the results and also to determine errors if there were any poorly bonded gauges. The cell is connected to a data logger which records continuously from the cell at set intervals. Any change in strain is therefore recorded as it occurs and can be related to mining activity or other events. Analysis of the strain change is undertaken using an elastic, isotropic solution technique. This, combined with the uniaxial laboratory tests, provides information on whether or not the measurements are reasonable based on the induced strain changes.

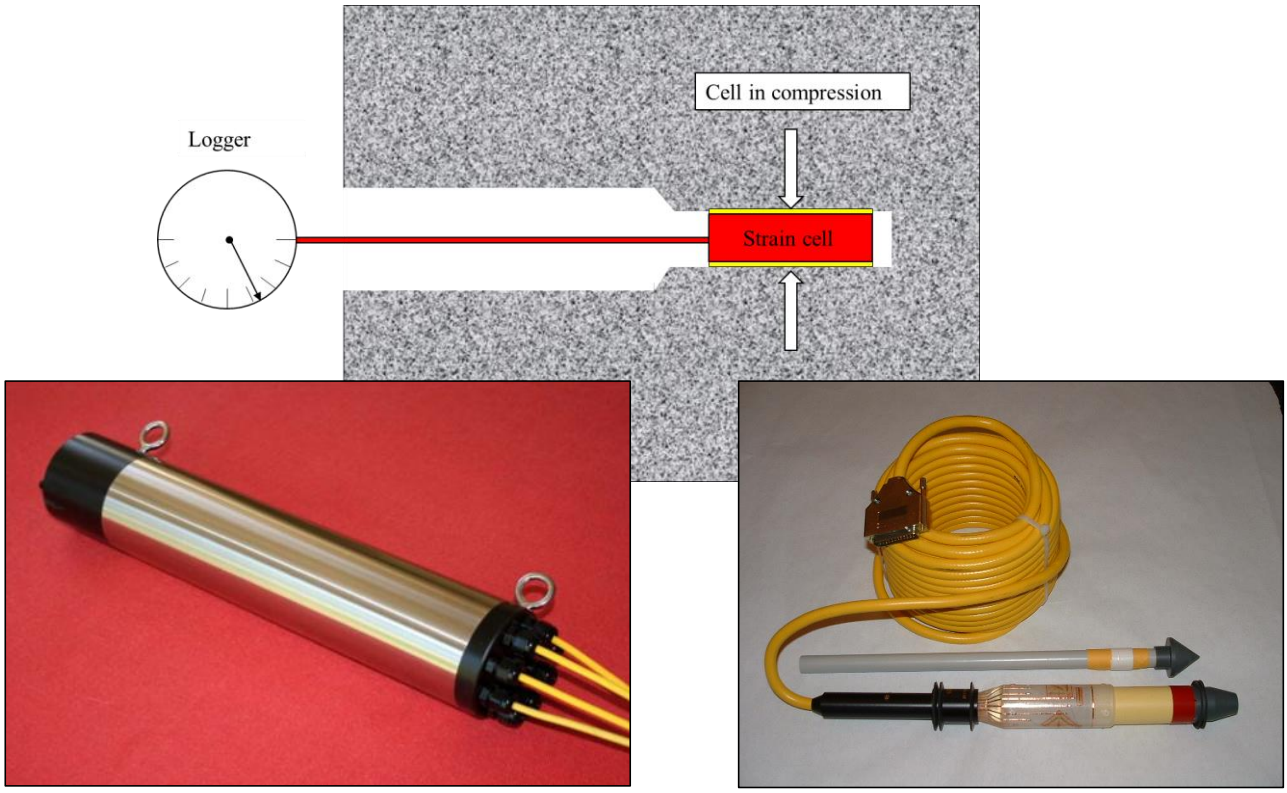

Figure 9.1: Stress measurement method using a CSIRO 12-gauge Hollow Inclusion stress cell (right) connected to a CSIRO stress cell data logger (left).

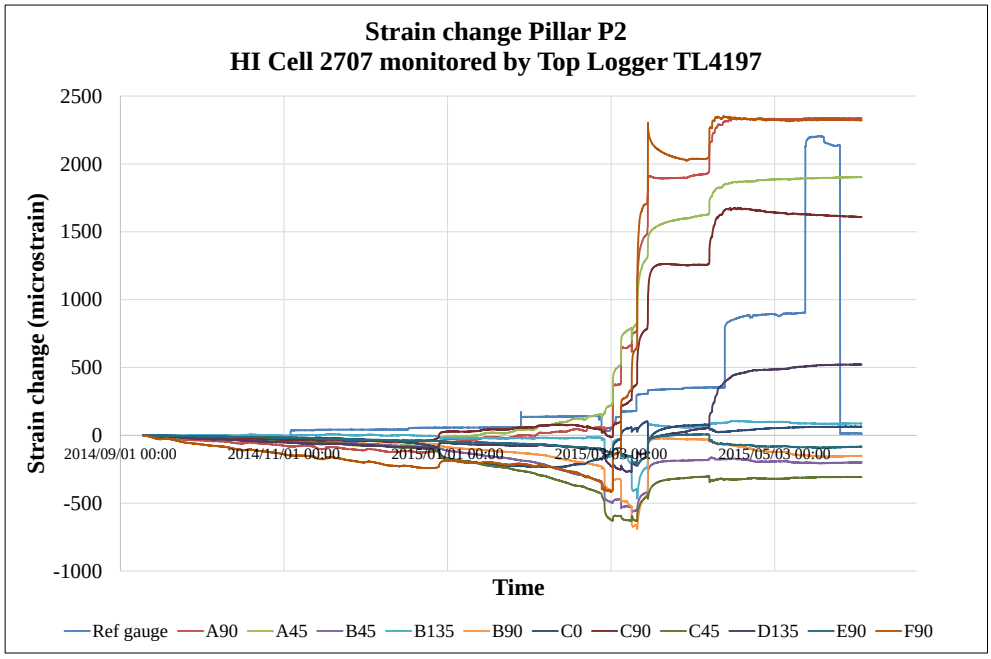

Figure 9.2: Strain change recorded by the CSIRO data logger during the formation of pillar P2.

CCBO Overcoring method: Determining the *in-situ* stress involves measuring the change in strain when a section of stressed rock is relieved of its stresses by detaching it from the surrounding rock. The stress relief is done by overcoring the strain cell while it is glued to the surrounding rock. The Young's modulus and Poisson's ratio of the host rock are determined using a uniaxial test and are used to back-calculate the stresses from the strain change data.

The compact conical-ended borehole overcoring technique (CCBO) allows for overcoring to be done in a hole with the same size as that created by drilling the pilot hole (Ogasawara et al, 2012). The hole size required is small (60 or 76 mm) and can be drilled with a regular pneumatic AQ or BQ machine commonly used to drill underground exploration holes. At the trial site, 60 mm diameter holes (BX size) were used. Once the hole is drilled to the required depth, the borehole end is conically shaped with a conical bit. A 16 element strain cell is glued to the borehole end. The cell is overcored using the same diameter bit used to drill the pilot hole. Only approximately 10 cm of overcoring is required which increases the chance of achieving a successful overcore in heavily fractured conditions. The hole is then extended and the same procedure can be repeated in the same hole within the same shift if time allows.

Figure 9.3: A 16 element BX-size strain cell. Compare the size of the cell to the HI cell shown in Figure 9.1.

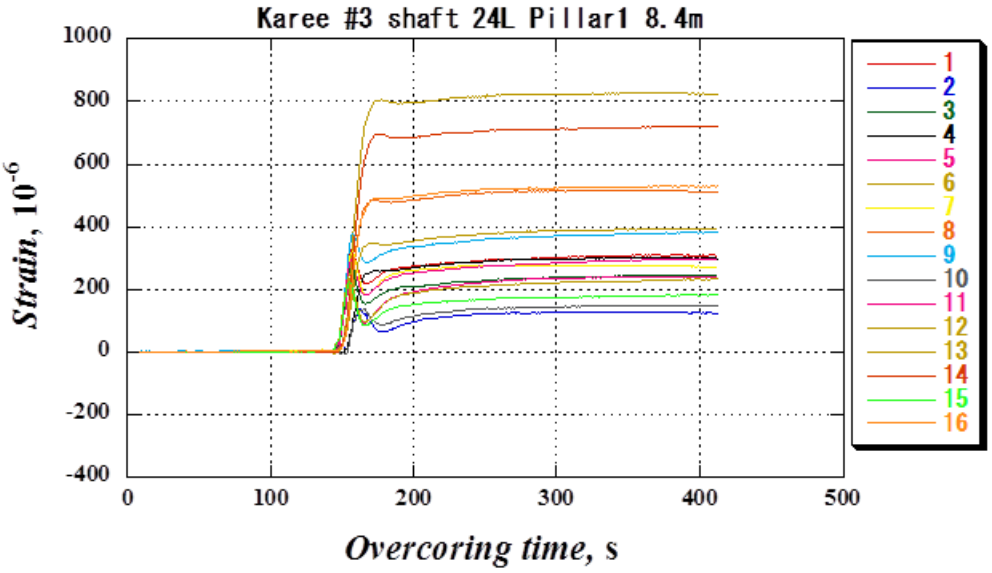

Figure 9.4: Strains recorded during the successful overcoring above pillar P1 using the CCBO method.

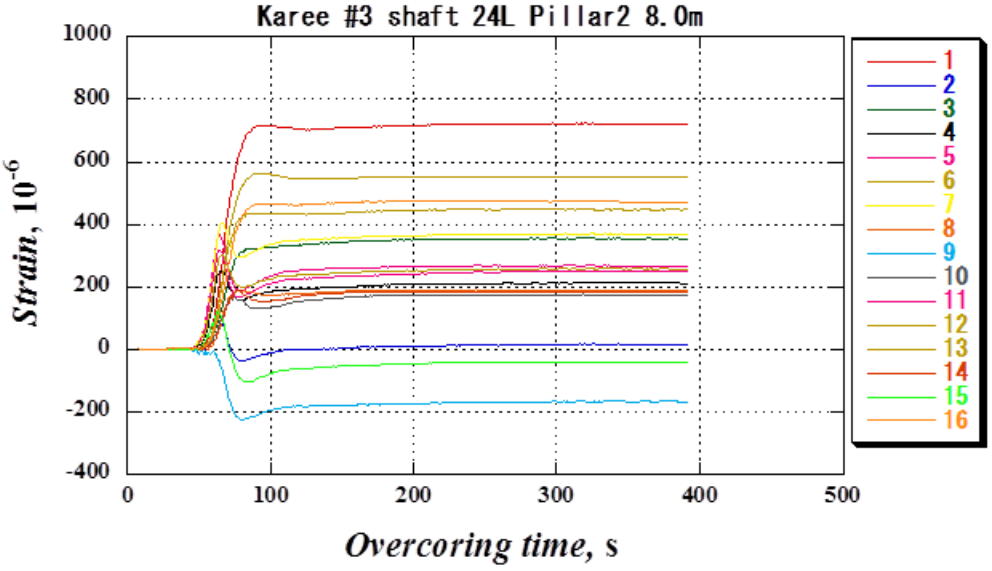

Figure 9.5: Strains recorded during the successful overcoring above pillar P2 using the CCBO method.

Methods and instruments used to measure convergence

Closure stations: The closure-stations installed utilised the newly designed Dist-o-Rock measurement system. This provided improved quality and repeatability of the measurements. The Dist-o-Rock uses a distomat to determine the absolute distance between closure pegs installed in the hangingwall and footwall. At each closure-station two closure pegs were installed in the hangingwall and two in the footwall. This allows for 4 readings to be taken at a site which provides accurate results. Also, the additional pegs ensure that convergence can continue to be measured at a particular site should a peg be damaged.

Figure 9.6: Convergence measurement at a closure station using a Dist-o-Rock measuring device.

Closure logger: Once the instrument is installed, convergence is recorded in a continuous fashion. Any hanging-or footwall movement is recoded at a point in time by electronic data loggers. Time-dependent convergence can be quantified using this type of monitoring. The closure logger also has a measuring tape glued to the bottom part of the instrument so that recorded measurements can be verified and manual measurements can also be obtained during successive site visits.

Figure 9.7: A closure logger measuring continuous convergence in the trial site.

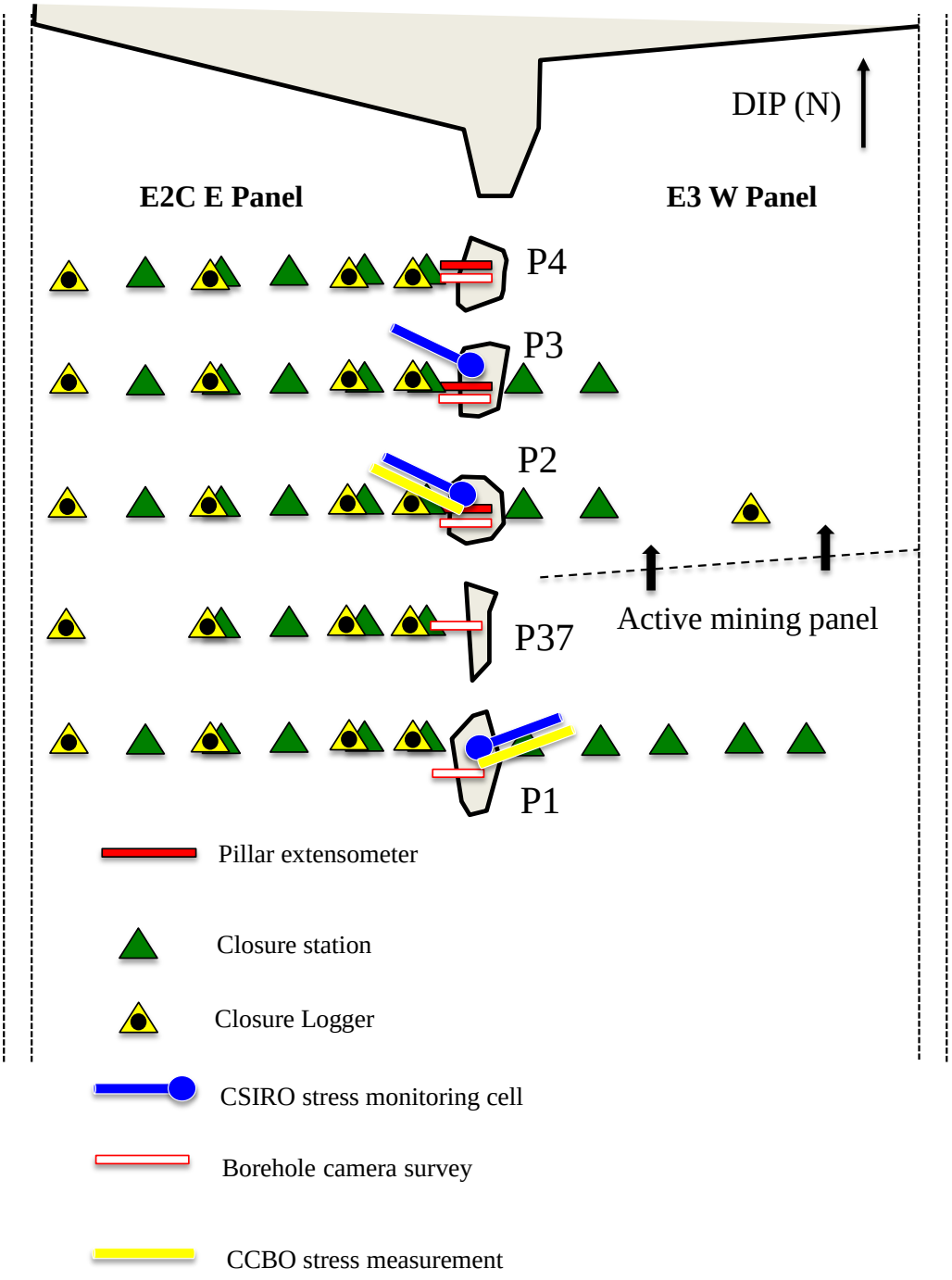

Figure 9.8: Plan of actual instrumentation installed at the trial site.

9.2.1. Pillar stress

The objective of the stress measurements was to determine the peak and residual pillar stresses for the identified pillars. Furthermore the intent was to determine possible trends during the pillar forming cycle. Two types of stress measurements were conducted.

1. Absolute stress measurements to determine the absolute stress (virgin and induced) at a location at a point in time using the CCBO overcoring method. This was done to determine the stress above a pillar before the pillar was formed and would form the starting point (baseline) for further measurements.
2. Stress change measurements using CSIRO HI cells connected to data loggers.

Figure 9.9 indicates the instrument positions for the continuous measurements at the trial site. The absolute measurements were conducted at the same locations. In both cases the boreholes were drilled from the leading panel and intended to stop at a height of approximately 4 m above the centre of the planned pillar position. The 4 m height was based on recommendations by Watson (2012) to ensure that the strain cells were not positioned in significantly damaged or fractured rock.

The absolute stress measurements were conducted above pillars P1and P2 in November 2014 before mining the final section (Figure 8.22). The HI cells and top loggers were installed at the same time to monitor how the stress above the pillars (P1, P2, and P3) would change once mining started.

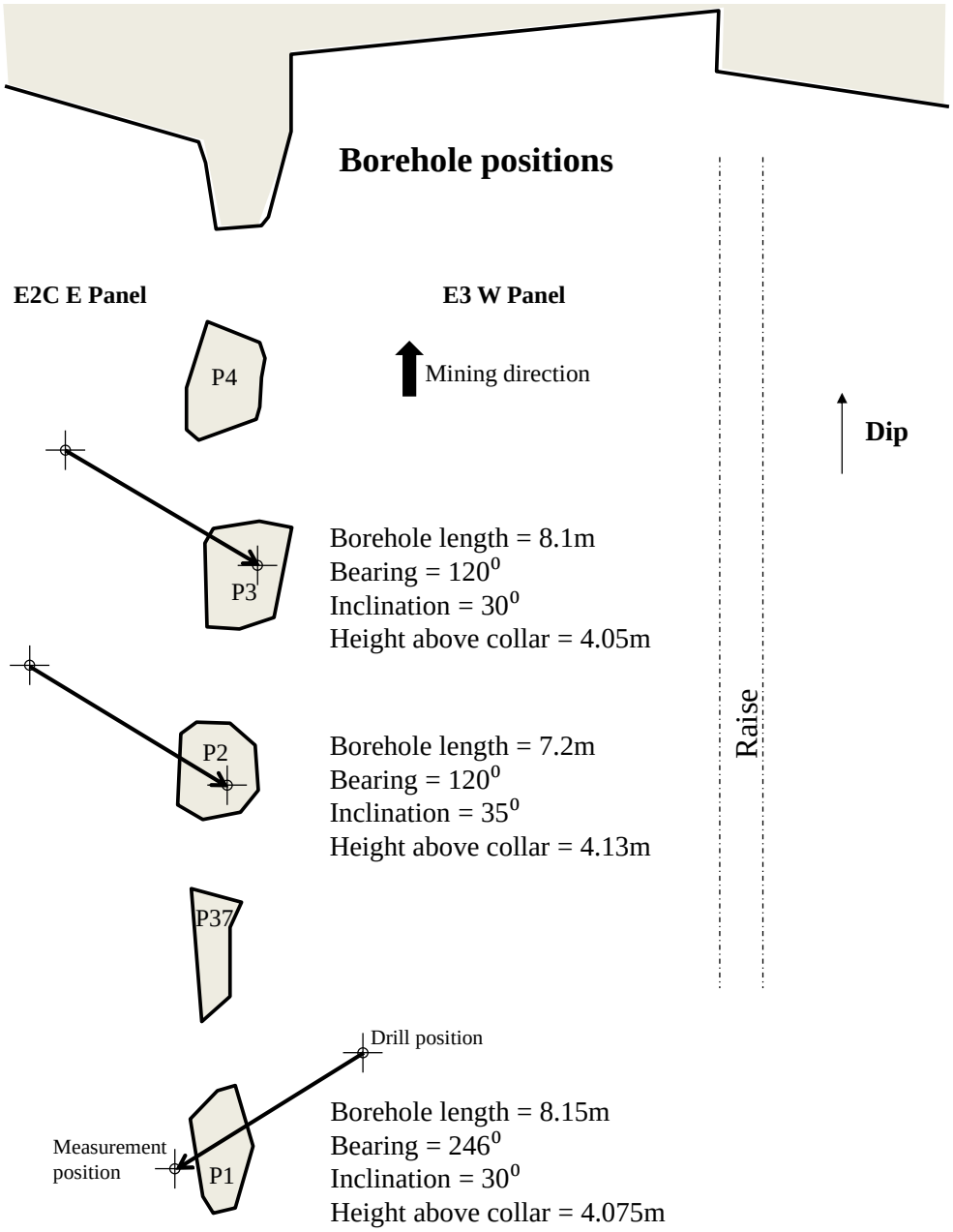

Figure 9.9: Borehole positions for continuous stress measurements.

Results

Absolute measurements: Two CCBO measurements were conducted above pillar P1 and two measurements above pillar P2. Unfortunately one test in each hole was unsuccessful as both of the overcores broke into pieces during the drilling process. The measurements above pillar P1 was conducted at a hole length of 7.9 m and 8.4 m (successful measurement) and above pillar P2 at 8 m (successful measurement) and 8.3 m. It is speculated that the unsuccessful measurements could be as a result of high stress at these locations (relative to the strength of the rock) as there were signs of core disking in some of the recovered core.

It is possible that the *in-situ* rock stresses can vary significantly between each of the three pillars and from point-to-point above the pillars themselves. There was a difference in the measured stresses from the two successful overcoring tests carried out above pillars P1 and P2 (Tables 9.2 and 9.3). The major difference was in the magnitude of σ_1 (27.1 MPa versus 40.3 MPa). Although the measured directions were almost identical between the two measurements, there was a 43 degree difference in the dip angle of σ_1. As indicated in Figures 9.10 and 9.11, σ1 was orientated towards the side of the pillar which was exposed first, arching over the solid unmined abutment. When these measurements were conducted, pillar P1 was completely formed. When the pillar was formed, the east face relative to the pillar was mined first. σ_1 was dipping towards this panel. The measurement above pillar P2 was conducted prior to the pillar being formed. Only the west panel relative to the line of pillars had been mined. The pillar was approximately 3 m ahead of the east face position. In this case, σ_1 was orientated towards the west face mined first (refer to Figure 8.22).

The measured vertical stresses above both pillars (17.1 MPa and 18.2 MPa) were lower than the theoretical magnitude of approximately 23 MPa calculated using equation 8.1 and the measured virgin vertical stress of 24.1 MPa as indicated in Section 8.1.4. However, the measurements were conducted above partially-to fully crushed pillars which could significantly impact on the induced stress state experienced.

Rock property values of 60 GPa for the Young's modulus and 0.25 for Poisson's ratio were used to determine the stress values from the measured strains. These average secant values were based on the uniaxial tests (UCM) conducted on the hangingwall Mottled Anorthosite core extracted at the point of measurement.

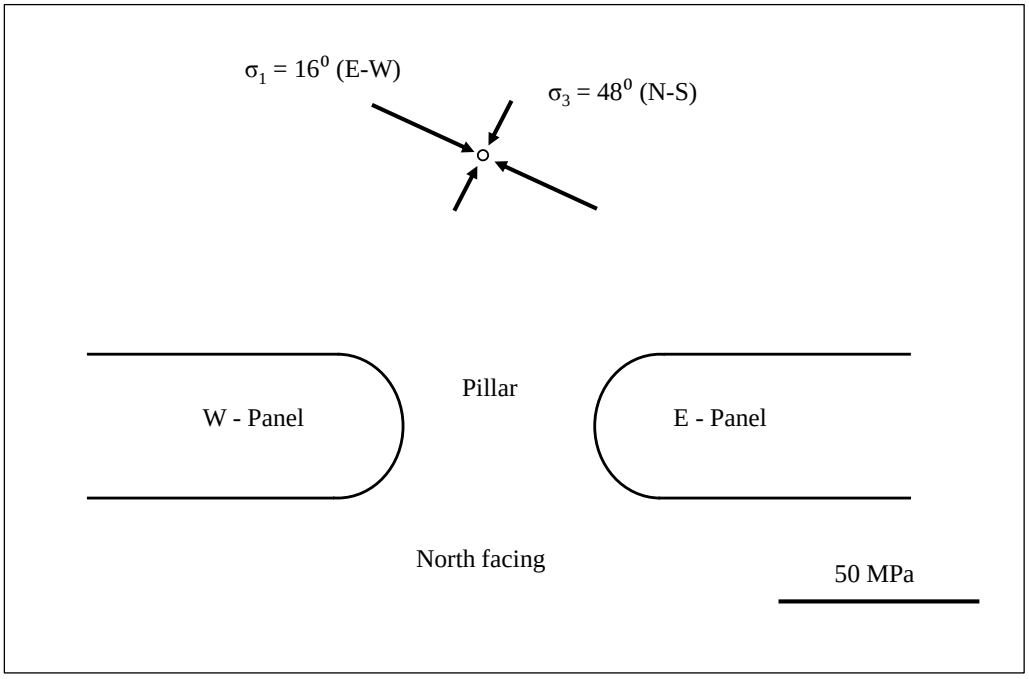

Figure 9.10: Absolute stress measurement conducted 4 m above pillar P1. The eastern panel was mined first (section view).

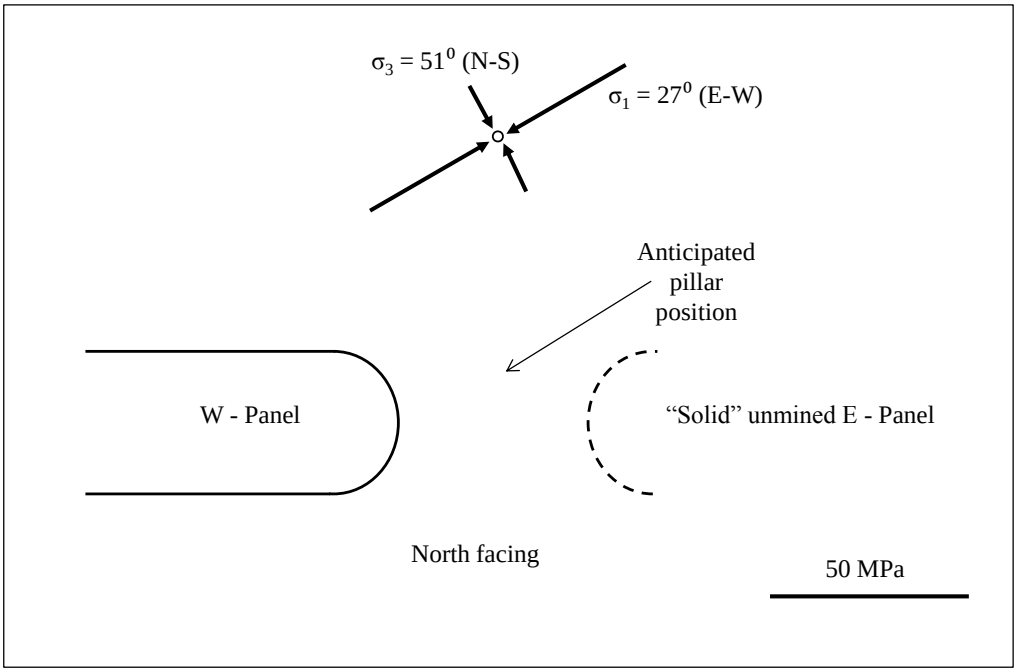

Figure 9.11: Absolute stress measurement conducted 4 m above the anticipated pillar P2 position. Only the western panel was mined at the time. The pillar was not formed yet (section view).

Table 9.2: Absolute stress magnitudes and orientation measured above pillar P1 (November 2014).

	Pillar P1					
	σ_1	σ_2	σ_3	σ_{Vert}	$\sigma_{(E-W)}$	$\sigma_{(N-S)}$
	approx. (E-W)	approx. (N-S)				
Stress magnitude (MPa)	27.1	22.6	11.8	17.1	25.5	19.1
Bearing (strike) degrees	101	359	210			
Dip (degrees)	16	38	48			

Table 9.3: Absolute stress magnitudes and orientation measured above pillar P2 (November 2014).

	Pillar P2					
	σ_1	σ_2	σ_3	σ_{Vert}	$\sigma_{(E-W)}$	$\sigma_{(N-S)}$
	approx. (E-W)	approx. (N-S)				
Stress magnitude (MPa)	40.3	19	10.4	18.2	34.6	17
Bearing (strike) degrees	282	26	154			
Dip (degrees)	27	26	51			

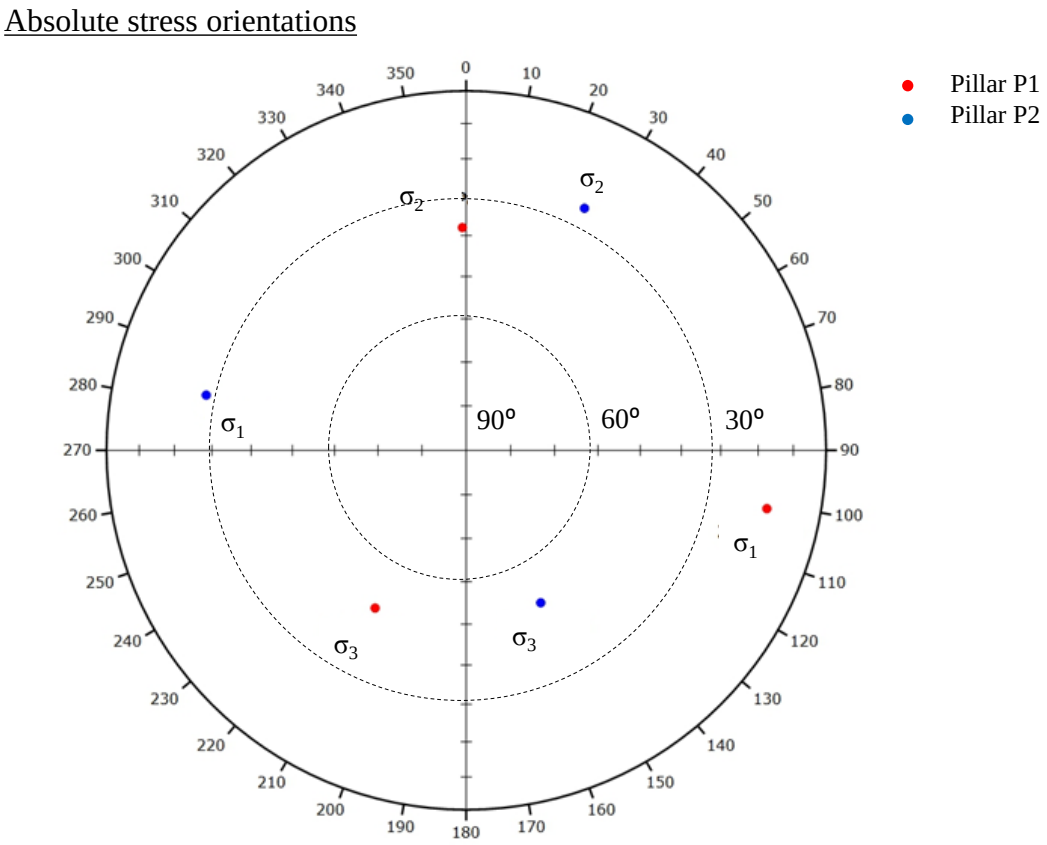

Figure 9.12: The lower hemisphere projection of the principal stress directions measured above pillars P1 and P2 (November 2014) before mining the final section.

Stress change measurements: The stress change measurements for all three pillars (P1, P2, P3) were referenced to the absolute stress measurement carried out above pillars P1 and P2. These stresses were used as the baseline *in-situ* stress condition from which all stress change were calculated. The stress change calculations for the measurements conducted above pillar P3 assumed the P2 baseline stress condition. The absolute measurements only reflect a specific measured point which can be influenced by various factors and can therefore differ from point to point or site to site.

Stress change occurrences were determined from events shown in strain change versus time graphs for each pillar (refer to Figures 9.2, 9.4 and 9.5 as examples). In some instances, these events occurred at the same time for different pillars. The largest total tensile strain change measured by any of the strain gauges of the HI cell installed above pillar P1 was approximately 700 microstrain *(με).* The largest total tensile strain change measured by any of the strain gauges of the HI cell installed above pillar P2 was approximately 3000 *με*. These values are in line with what would be expected should these have been overcoring tests.

The stress change measured above each pillar was analysed by comparing changes in magnitude and orientation to events corresponding to each pillar forming cycle. Similar trends were identified to exist between the three pillars. The detail of the results and the interpretation thereof is included in the following subsections. The most prominent findings were:

- As the advancing face approaches a future pillar, at the point where it is aligned with the new pillar position, the pillar has already experienced a significant reduction in vertical stress (23% - 64%).
- Whilst the pillar is being formed and until it is holed by the advancing face, the pillar experiences another reduction in vertical stress (28% - 41%). At this point the pillar has reached its true residual state (14.8 – 23.74 MPa).
- As mining continues and new pillars are formed, the instrumented pillars continued to experience a reduction in vertical stress (38% - 41%). This secondary reduction resulted in residual pillar stresses of 10.16 – 17.4 MPa.
- The underground observations at specific intervals of the pillar forming cycle could be compared to the measured behaviour.
- The pillars were observed to experience continued deformation up to the point where the pillars were approximately 14 m in the back area. The measured change in vertical stress as a result of the secondary stress reductions occurred within 6 m of additional face advance (after the pillar had been formed). The pillars therefore continued to deform even though there was no further change in stress recorded above the pillars.
- Once pillar P4 was completely formed, there was no further change in vertical stress experienced by the instrumented pillars.

Stress orientation: Figures 9.13 – 9.15 indicate the change in direction and dip angle of each stress tensor measured 4 m above pillars P1, P2 and P3. The change in the stress orientation is indicated by the coloured legend which links to a specific event when there was a substantial change in the stress orientation. The changes are also shown by the arrows and numbering (i.e. 1, 2, 3, f) which display the start (1), path and end orientation (f).

The starting position (point 1) for the stress orientations are based on the absolute stress orientations measured above pillar P1 and P2. The results for pillar P2 indicate that this was most likely different for the position where the absolute measurement was conducted versus where the change measurement was conducted. It is suspected that the eastern face which was approximately 3 m behind the pillar P2 position had a noteworthy impact on the initial stress orientation and perhaps also the magnitude. However, the trends identified are regardless of the exact starting point (baseline position) as the stress orientation would still have migrated in the same manner as a result of the pillar forming cycle.

The most significant findings regarding the stress orientations were:

- The range of stress orientation change (direction and / or dip) is less for the completely formed pillar than compared to pillars P2 and P3 which were only formed when the eastern mining face advanced.
- There was a substantial change in the orientation of σ_1, σ_2 and σ_3 when the face was aligned with the pillar being formed.
- σ_3 became more vertical as new pillars were formed.

Pillar P1

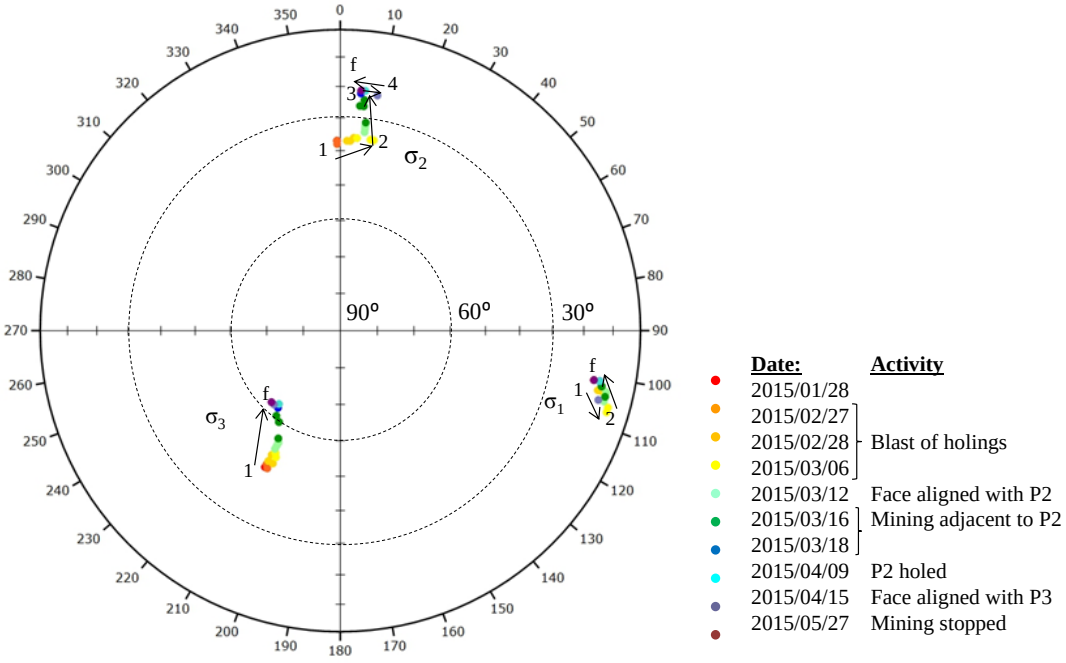

Figure 9.13: The lower hemisphere projection of the stress change data (bearing and dip) measured above pillar P1.

Pillar P2

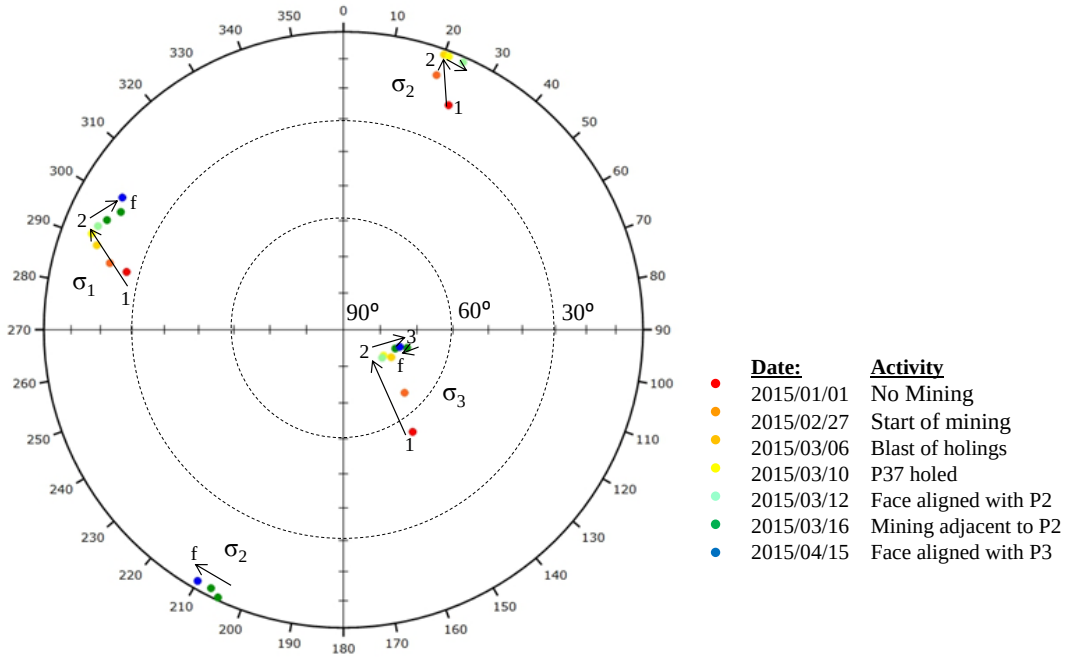

Figure 9.14: The lower hemisphere projection of the stress change data (bearing and dip) measured above pillar P2.

Pillar P3

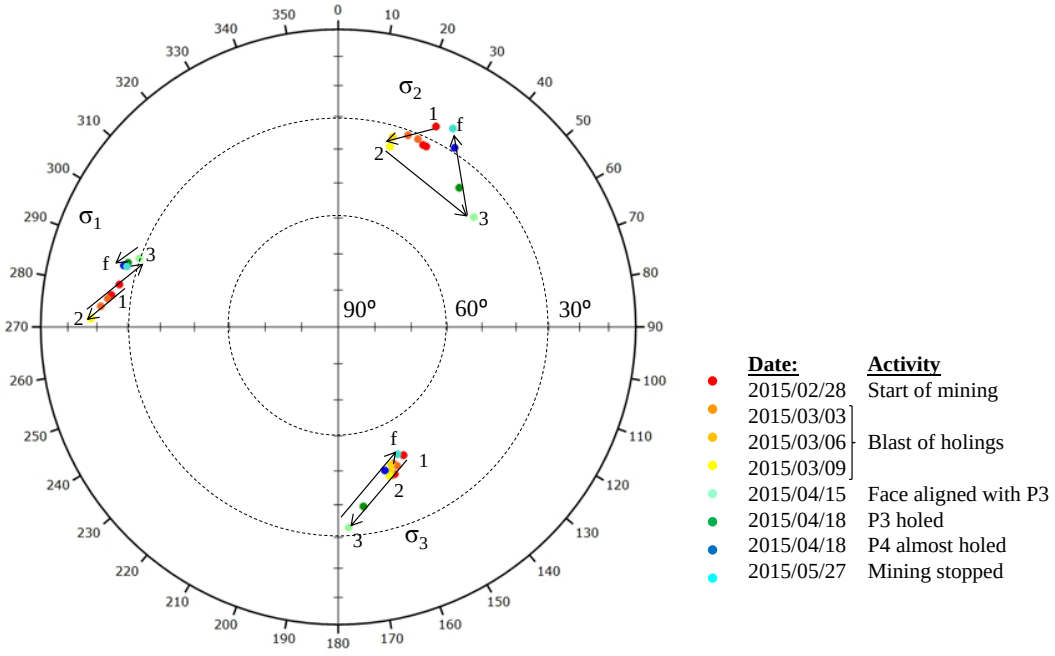

Figure 9.15: The lower hemisphere projection of the stress change data (bearing and dip) measured above pillar P3.

Stress magnitudes: The objective of the stress measurements were to determine when a pillar reaches its peak and residual stress states and to relate these magnitudes to events within the pillar forming cycle. Pillars P1, P2 and P3 behaved differently based on underground observations. However, the stress data revealed many similarities.

The stress change data confirmed that the baseline result obtained above pillar P2 (18.2 MPa) was only relevant to the exact point of measurement. Pillar P2 measured a reduction in vertical stress of 59.84 MPa, while pillar P3 measured an overall reduction of 22.75 MPa. The numerical model used to back analyse the behaviour of the pillars in the trial section was used to provide a more appropriate prediction of the baseline value at the point of measurement above each pillar. Although the detail of the back analysis will only be described in the next chapter, the relevant data is included in this section to understand and substantiate the data obtained from the measurements. It was also used to validate the results obtained for pillar P1.

While the baseline stress measurement result obtained above pillar P2 was questionable, the stress change data did provide meaningful trends corresponding to observations and specifics around the pillar forming sequence. Once mining stopped at the end of May 2015, there was no further change measured in stress magnitude at any of the instrumented sites. The results obtained for each pillar was investigated separately. The purpose was to study the sequence of events experienced by each pillar and to compare it to the stress results.

Pillar P1:

The pillar was formed in April 2013 with panel E3 West (east panel relative to the pillar line) stopping approximately 5 m ahead of the pillar position. The new pillar (pillar 37) positioned immediately down-dip (ahead) of pillar P1 was partially formed although still part of the face. The CSIRO strain cell was installed on 20 May 2013. The east and west face either side of pillar 37 was aligned at the time. Mining of E2C East panel (west panel relative to the pillar line) to create the lead lag scenario to install all further instruments resulted in a 12.5 MPa stress increase. At the time there was no baseline stress recording and therefore only the stress change was recorded between 21 May and 5 June 2013 in which panel E3 west advanced approximately 20 m.

The absolute stress measurement conducted in November 2014 indicated a vertical stress of 17.1 MPa. Underground, the pillar appeared to be in a crushed state (Figure 8.12b). Also, pillar 37 appeared to be partially crushed with some degree of scaling observed along the eastern side of the pillar (Figure 8.19). However, when mining resumed in February 2015 up until mining stopped at the end of May 2015, there was another 10.58 MPa reduction in vertical stress. The most significant

reductions appeared to coincided with the formation of new pillars (refer to Figure 9.16). The red dots highlighted on the figure correspond to specific events when new pillars were formed.

- P37 was fully formed on 10 March 2015,
- P2 was formed between 12 March – 9 April 2015,
- P3 was formed between 15 April – 18 April 2015.

The pillar was also barred solid (all loose fractured and scaled material removed from the pillar surface) along the eastern side around 10 – 12 March 2015 which could have caused a reduction in pillar strength due to a loss in confinement. The portion barred consisted of approximately 0.5 m of failed pillar material.

From the data it can be inferred that as new pillars are formed, stress is transferred to the new pillars and abutments resulting in a reduction in vertical stress experienced by the instrumented pillar. However, during the period in which pillar P2 was formed, the pillar was barred, which could have reduced the pillar strength. This resulted in a vertical stress reduction of approximately 5.7 MPa. It is therefore not clear if the reduction in vertical stress experienced by the pillar was as a result of further pillar crushing or as a result of the transfer of stress, thus reducing the overall load experienced by the pillar. The upper limit of the range of residual pillar stress experienced by the pillar (6.52 – 17.1 MPa) does relate to the predictions from past research (13 - 20 MPa). The lower limit might not be a function of the residual strength of the pillar, but rather a function of the load experienced by the pillar. The formation of pillar P4 towards the end of April did not seem to have any further effect on the overall stress state experienced by the pillar.

Figure 9.17 indicates the result of the numerical back analysis (see Chapter 10) of the anticipated vertical stress along a section of pillar P1 at the approximate absolute stress measurement position. The model indicated a vertical stress of approximately 15 MPa for the layout which existed at the time of the measurement. This compared well with the measured 17.1 MPa.

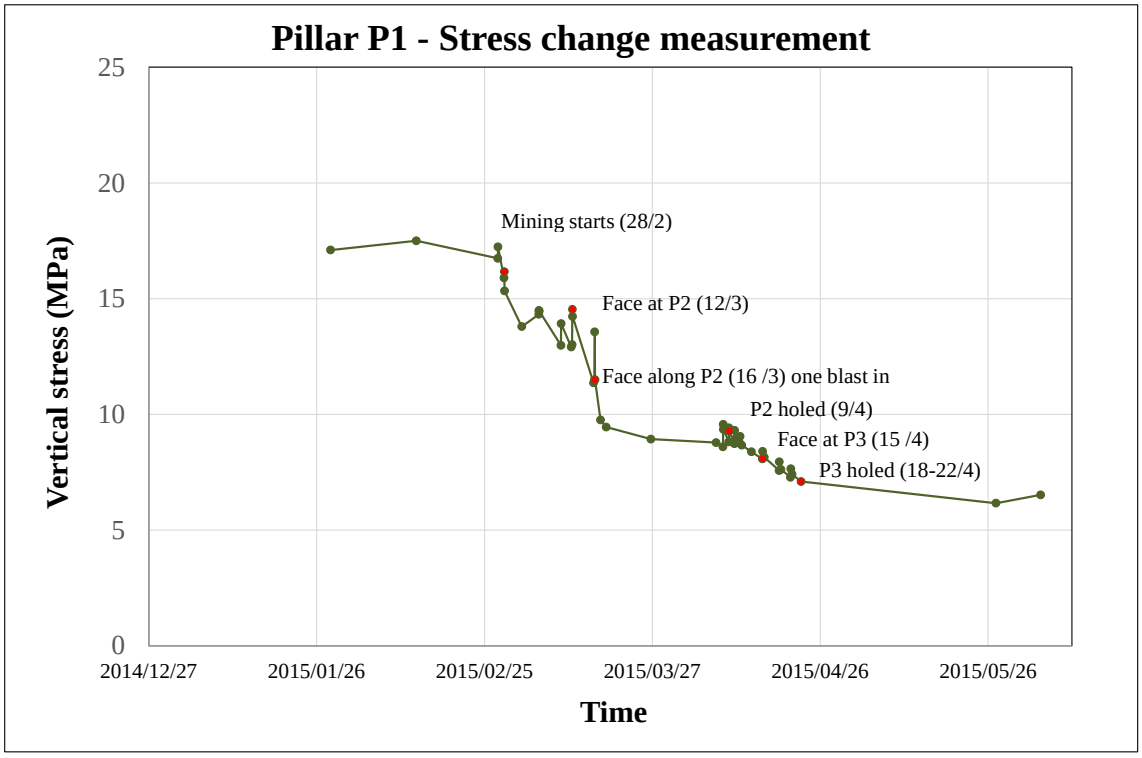

Figure 9.16: Pillar P1 stress change versus time.

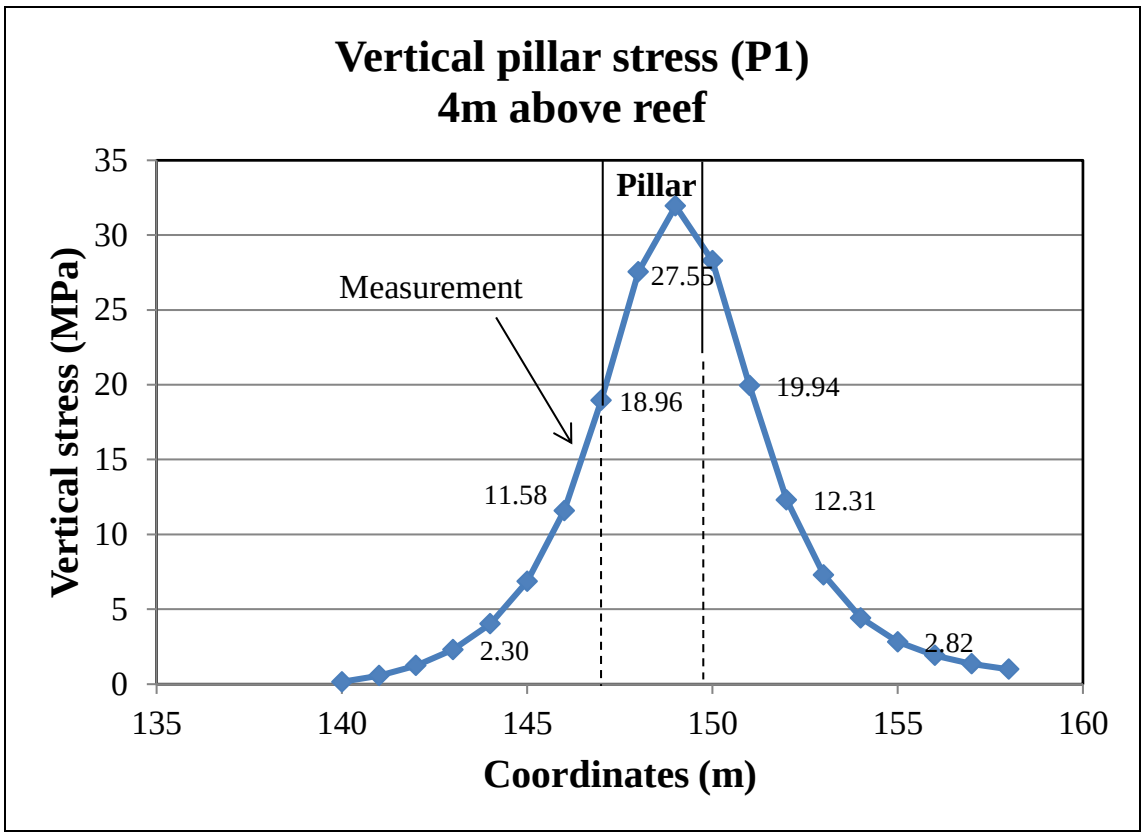

Figure 9.17: Predicted vertical stress profile through a section of pillar P1 at the approximate absolute stress measurement position conducted 4 m above the reef.

Pillar P2:

The absolute stress measurement above pillar P2 indicated a vertical stress of 18.2 MPa. The stress reduction measured from November 2014, when the absolute stress measurement was conducted, until the end of May 2015, when all mining stopped, was 59.82 MPa. The measurement of 18.2 MPa does therefore not reflect the actual baseline value. The numerical back analysis indicated that the anticipated baseline vertical stress at the measurement position should have been approximately 52 - 55 MPa (Figure 9.19).

Figure 9.18 indicates the measured stress change data based on the measured baseline value (18.2 MPa). Also indicated in the figure is the suggested adjustment to the data taking cognisance of the vertical stress reduction. Based on this the baseline value should have been around 70 MPa. As a result, the vertical stress experienced by the pillar was approximately 10 MPa when mining stopped.

As with pillar P1 there were specific events which led to significant stress changes experienced by the pillar (refer to notes on figure corresponding to the red dots). When mining resumed at the end of February 2015, pillar P2 was approximately 3 m ahead of panel E3 West. As the face advanced, pillar 37 was formed. Mining alongside the approximately 3 m wide pillar holing, until the face was aligned with pillar P2 (refer to Figure 8.23) resulted in a vertical stress reduction of 41.91 MPa. At the time it was observed that the outer approximately 1 m of the pillar towards the west contained various closely spaced fracture planes (refer to Figure 8.30). The pillar therefore appeared to be in a partially crushed state.

Pillar P2 was formed from 16 March to 8 April. This caused another reduction in vertical stress of 9.11 MPa. The entire stress reduction at this point could only be a result of pillar crushing as pillar P2 was now fully formed. The pillar has therefore reached a residual state. Mining of the face alongside the down-dip holing position until the face was aligned with pillar P3 (15 April) led to a further stress reduction of 4.64 MPa. The underground observations made at this time indicated continued pillar scaling along the western side of the pillar. This stress reduction experienced could therefore be a function of the pillar presumably unloading as stress is transferred to the solid ahead of the pillar. The pillar continued to deform until the pillar was approximately 13 m in the back area (refer to Table 8.9). Pillar P3 also experienced load regeneration during the same period. This could be coincidental and could be attributed to either stress transfer to pillar P3 as pillar P2 was unloading or friction lock-up along failure planes within pillar P3.

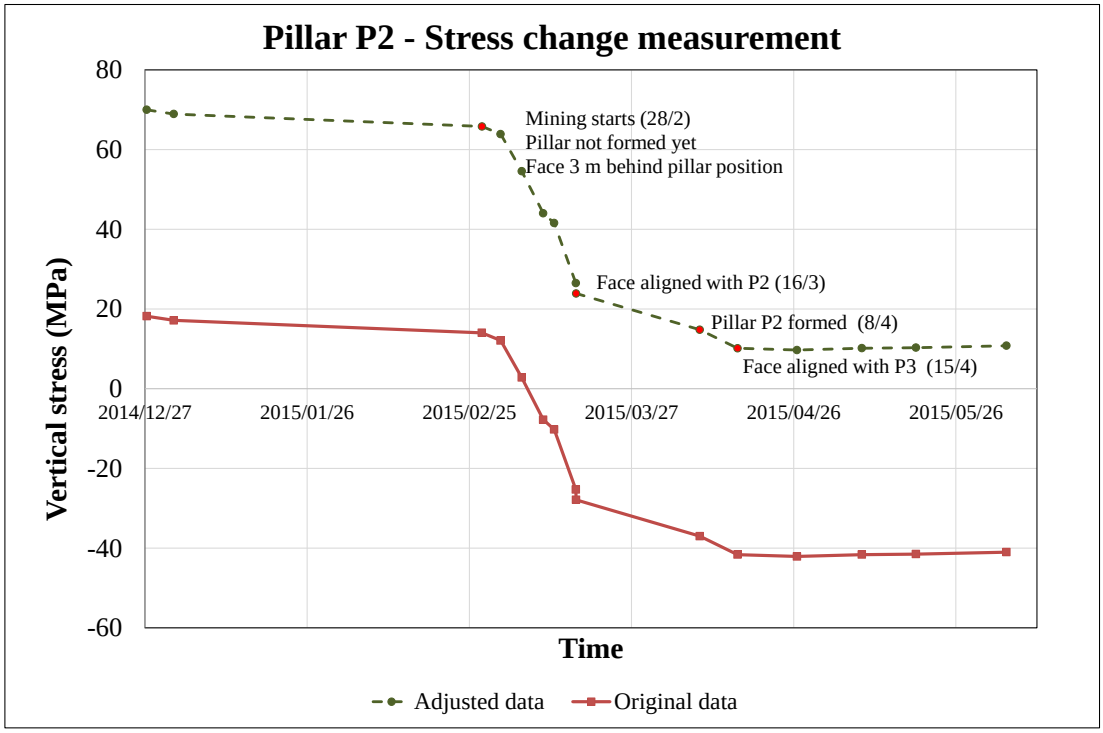

Figure 9.18: Pillar P2 stress change versus time. Adjusted data incorporates the total reduction in vertical stress.

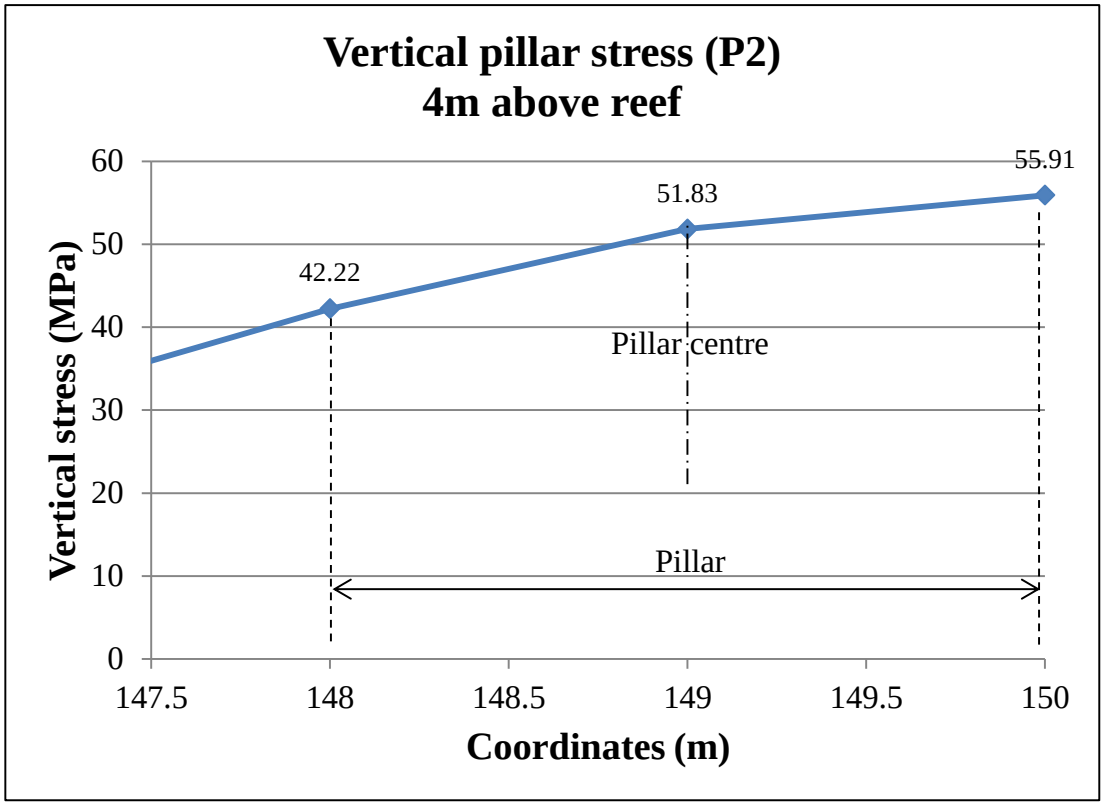

Figure 9.19: Simulated vertical stress profile through a section of pillar P2 at the approximate absolute stress measurement position conducted 4 m above the reef.

Pillar P3:

The baseline measurement for pillar P3 was assumed to be the same as measured above pillar P2. However, the stress change data for pillar P3 (Figure 9.20) also indicated that this measurement (18.2 MPa) was not relevant. When initially planning the absolute stress measurements, it was anticipated that the stress condition 4 m above the reef alongside the abutment (pillar line) would be similar. As the result of the numerical back analysis indicate, the anticipated baseline vertical stress above pillar P3 at the point of measurement was approximately 42 - 44 MPa (Figure 9.21). The magnitude of the predicted vertical stress is lower than predicted above pillar P2, however, pillar P2 also had the influence of the face in close proximity. Similar trends could be identified from the behaviour of pillar P3 when compared to pillars P1 and P2. There were significant events leading to the measured stress change.

Pillar 37 which was fully formed on 10 March 2015 resulted in a stress reduction of 9.82 MPa. The stress cell data logger did not record any events between 10 March and 15 April as the batteries were depleted. The mine was standing as a result of an unplanned stoppage and the Easter break during most of this period. The data pertaining to the formation of pillar P2 was lost (pillar P2 was formed from 16 March to 8 April). It is suspected that the stress reduction could have been more significant as a result of pillar P2 being formed. Of significance is the stress increase as the face was aligned with pillar P3. In contrast to the other pillars, pillar P3 displayed late pillar crushing and was intersected by anomalous jointing. When mining resumed at the end of February 2015, the pillar was approximately 9 m ahead of the face. The pillar first started displaying some minor fracturing along the up-dip western corner of the pillar and along the borehole drilled through the pillar when the face was aligned with the pillar. Only when the pillar was holed and the face was aligned with pillar P4 did the pillar display significant fracturing along the western side and did new fractures form along the down-dip side of the pillar. It is therefore anticipated that the initial stress reduction experienced by the pillar was associated with movement along existing joint planes rather than the formation of fracture planes. It appears that the pillar regenerated some of the initial stress reduction prior to formation. This could be as a result of friction lock-up along either joint or fracture planes. The pillar did not experience any deformation at this time (no scaling) and therefore this analogy could be plausible. Alternatively it could be a function of pillar P2 unloading and stress being transferred to pillar P3. It could also be a combination of both of these influences.

As the pillar was being formed between 15 and 18 April, the pillar experienced a stress reduction of 16.54 MPa. Most of this was accompanied by observed pillar fracturing and scaling. Another stress reduction of 6.34 MPa occurred during the formation of pillar P4. As with pillars P1 and P2, it is suspected that this secondary reduction in stress is as a result of stress transfer as a new pillar is formed. The pillar, however, continued to deform even until the pillar was approximately 14 m in

the back area (refer to Table 8.10). Although stress was monitored after the formation of pillar P4, essentially no change in stress was experienced. This is most likely due to no additional pillars being formed. The adjusted data indicated in Figure 9.20 is based on the back analysed baseline vertical stress magnitude.

The mining configuration relative to pillar P3 on 29 April corresponded to the initial configuration relative to pillar P1 before mining resumed on 28 February. Of relevance is that the magnitude of the residual pillar stress of pillar P3 was similar to the measured absolute magnitude of pillar P1 at the time (17.1 MPa). This could serve as an indication that the adjustment applied is appropriate.

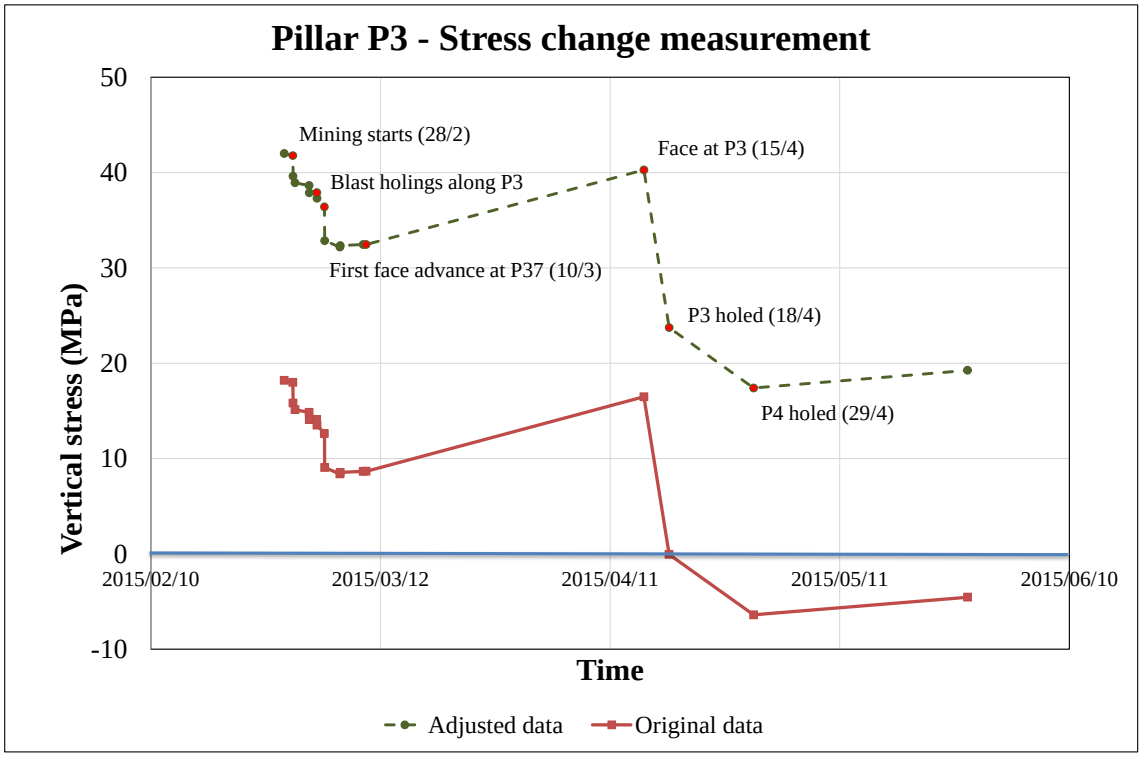

Figure 9.20: Pillar P3 stress change versus time.

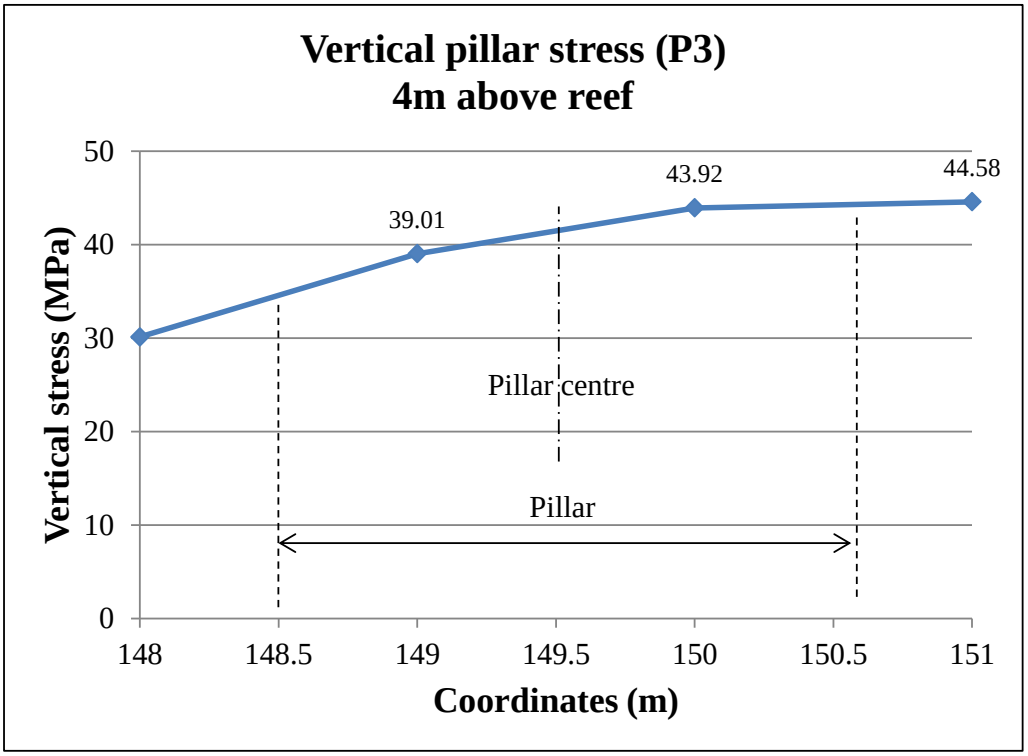

Figure 9.21: Simulated vertical stress profile through a section of pillar P3 at the approximate stress measurement position conducted 4 m above the reef.

General behaviour: A reduction in stress of 9.11 MPa and 16.54 MPa was measured during the formation of pillars P2 and P3 respectively. The pillars also experienced an overall reduction in stress as a result of events which occurred prior to complete pillar formation. Crush pillars are expected to fail whilst being formed at the mining face. Watson (2010) also measured stress change at various Merensky crush pillar sites. However, when comparing the results it is obvious that the pillars being larger in size compared to the pillars at the Lonmin trial site, different behaviour was obtained. Some of Watson's findings included:

- Measuring a 45 MPa stress change at a site on Union Mine at 600 mbs. The pillar had a w:h ratio of 2.7. The pillar reached a residual state within 10 of the pillar being formed. Underground observations indicated that the pillar appeared to fail 3 to 6 m behind the face after the pillar was formed. Scaling was observed along the intact abutment approximately 16 m ahead of the face.
- Measuring an approximate 100 MPa stress change at an Impala site situated at 1100 mbs for a pillar with a w:h ratio of 3. As the pillar was being formed, the stress level increased with approximately 27 MPa in the 10 m prior to the pillar being cut. As the pillar was formed and the face advanced another 10 m, the pillar experienced a stress reduction of 73 MPa. The pillar having a w:h ratio of 3 would be anticipated to be at a relatively high stress. The pillar did experience footwall heave confirming this. Once the pillar was 10 m in the back area almost no further change in stress was

measured. The residual performance of the pillar was, however, attributed to the behaviour of the crushed foundation.

Although the exact behaviour of the pillars monitored by Watson were dissimilar to the pillars monitored at the Lonmin trial site, in all instances the pillars reached a residual state within 10 m of being formed. The Lonmin findings also confirmed that crush pillars should start to crush before the pillars are formed. The majority of the pillars monitored by Watson had w:h ratios greater than two, started failing after the pillar was formed and should therefore have been classified as "yielding" pillars.

An interesting observation in the stress change data for pillars P1, P2 and P3 was the reduction in stress experienced by a pillar when new pillars were formed. This characteristic can only be attributed to the pillar either experiencing a stress reduction as the pillar continued to fail, or load being transferred to the abutments and new pillars being formed. However, the stress change data as well as the micro seismic pillar profiling indicated that once the pillars were formed, internally the pillars were already completely fractured even though it was not visible along the external surfaces of a pillar. Therefore, the load transfer model does appear to be a more attractive model. What this characteristic does point out is that interpretations of stress data by previous researchers might have been obscured as they have assumed the pillars to be in a residual state during the time of measurement. In many instances the residual state of a pillar was measured post pillar formation; e.g. (Roberts, 2005a) and only by conducting an absolute stress measurement. The stress change data of pillar P1 clearly illustrates secondary stress reductions which occurred after pillar formation and coincided with the formation of new pillars (Figure 9.16). The pillar experienced a reduction of 10.58 MPa after the pillar was already formed and visually appeared to be fractured throughout. Unloading of pillars is not commonly studied and as a result there is limited information available.

Although the vertical stress in a crush pillar is the main contributor to the pillar behaviour, horizontal stress change above crush pillars or crush pillar stopes have been measured by York et al (1998) and Watson (2010). This was done for two reasons:

1. Significant falls of ground incidents were experienced as a result of presumably low clamping forces in the hangingwall. The stress condition above a panel was measured. The results indicated that there was an increase in horizontal stress just prior to the face undermining the instrument position (installed in the hangingwall). The horizontal stress then returned to almost the initial magnitude as the face continued to advance. Of significance was the change in vertical stress experienced. Once the face undermined the instrument position, there was a significant reduction in vertical stress with the stress becoming tensile. This explained the falls of ground experienced and therefore the low clamping forces expected.
2. It was anticipated that the dilation experienced by the crush pillars as well as possible mobilisation along fracture or joint planes could extend into the hangingwall above a pillar. It was believed that

this could introduce additional horizontal stress into the hangingwall above a stope which could then break possible hangingwall beams and result in increased fall of ground instances. However, the results did indicate an increase in horizontal stress up to the point when the pillar was formed, followed by a decrease in horizontal stress as the face continued to advance. This beam buckling theory is therefore not deemed plausible.

The results for the horizontal stress change measurements conducted above pillars P1, P2 and P3 are shown in Figures 9.22 – 9.24. The absolute stress measurements conducted above pillar P1 and P2 were used as the baseline values for pillar P1 as well as pillars P2 and P3 respectively. Significant events contributing to stress changes are highlighted in the various diagrams. Note that the baseline value for pillars P2 and P3 are considered to be too low as highlighted in the previous subsections. Nevertheless, the general trend remains unchanged although the actual magnitudes might be different.

The results indicate that the horizontal stresses in both directions reach a peak value prior to the pillar being formed. The majority of the observed scaling was along the long axis of the pillar orientated approximately north-south. Pillar dilation was therefore in the E-W direction. Once a pillar was completely formed, the pillar experienced secondary stress reductions, similar to that identified in the other stress measurement results. Pillar P3, experienced an increase in horizontal stress in the E-W direction (different from the other pillars) prior to pillar formation which only reduced as the pillar was being formed. The pillar did experience late pillar crushing. It is suspected that the pillar experienced friction lock-up along joint or fracture planes. Once the pillar was completely formed the fracture planes which formed along the long axis of the pillar started to dilate as the pillar was crushing.

The general trends obtained from the horizontal stress change measurements above the pillars in the trial site agreed well with the results obtained by Watson (2010). However, the instrumented pillars in the trial area experienced a reduction in horizontal stress prior to the pillars being formed. The pillars instrumented by Watson only experienced a reduction in horizontal stress after a pillar was formed.

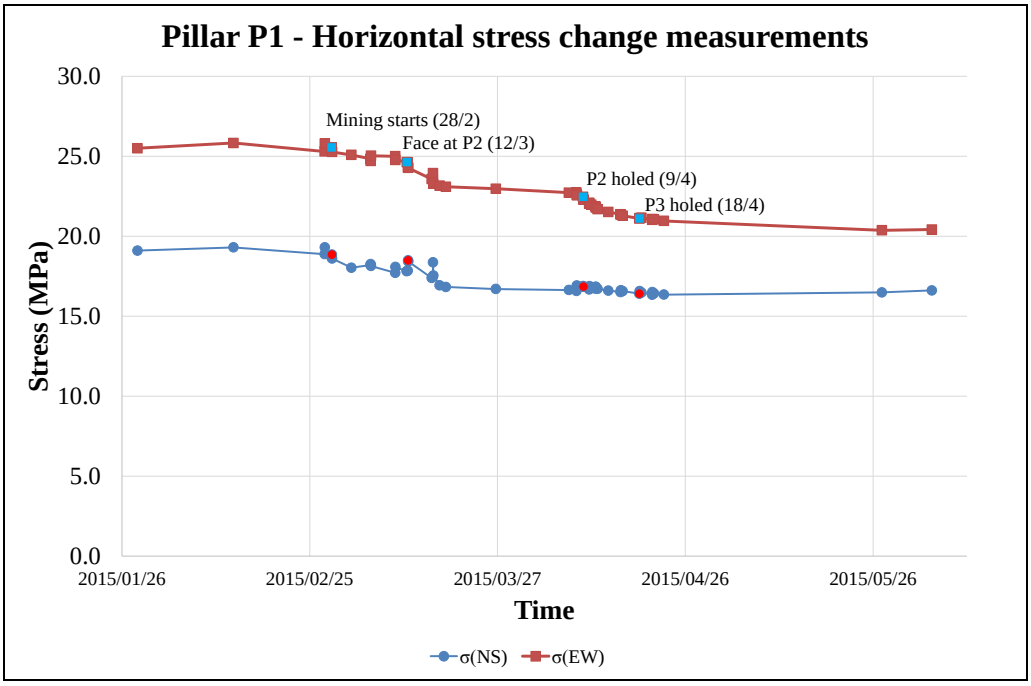

Figure 9.22: Horizontal stress change measured above pillar P1.

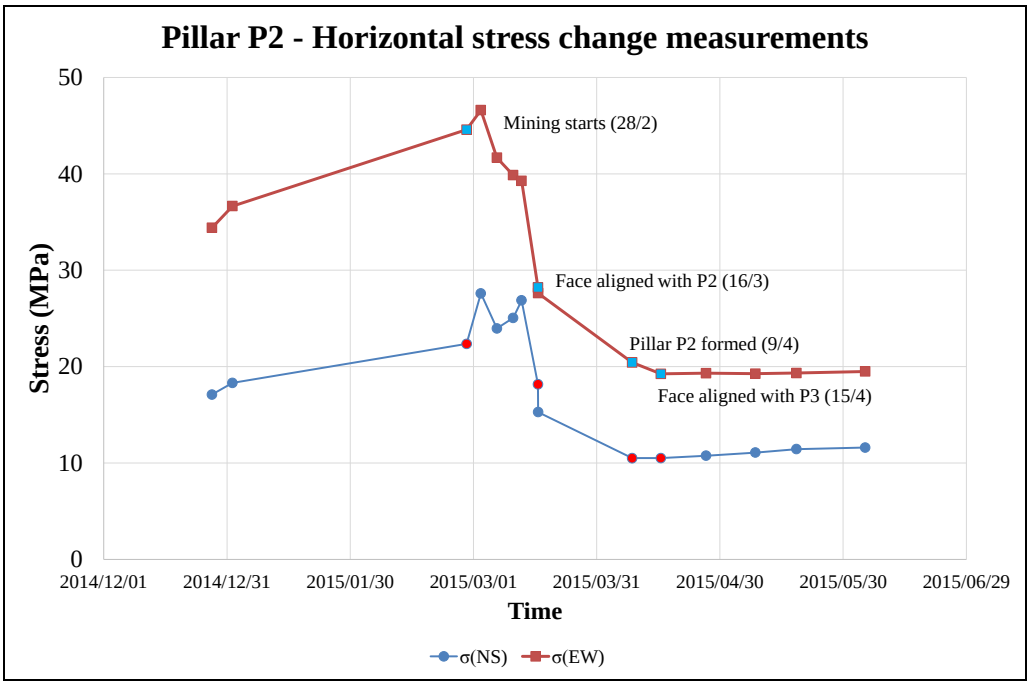

Figure 9.23: Horizontal stress change measured above pillar P2.

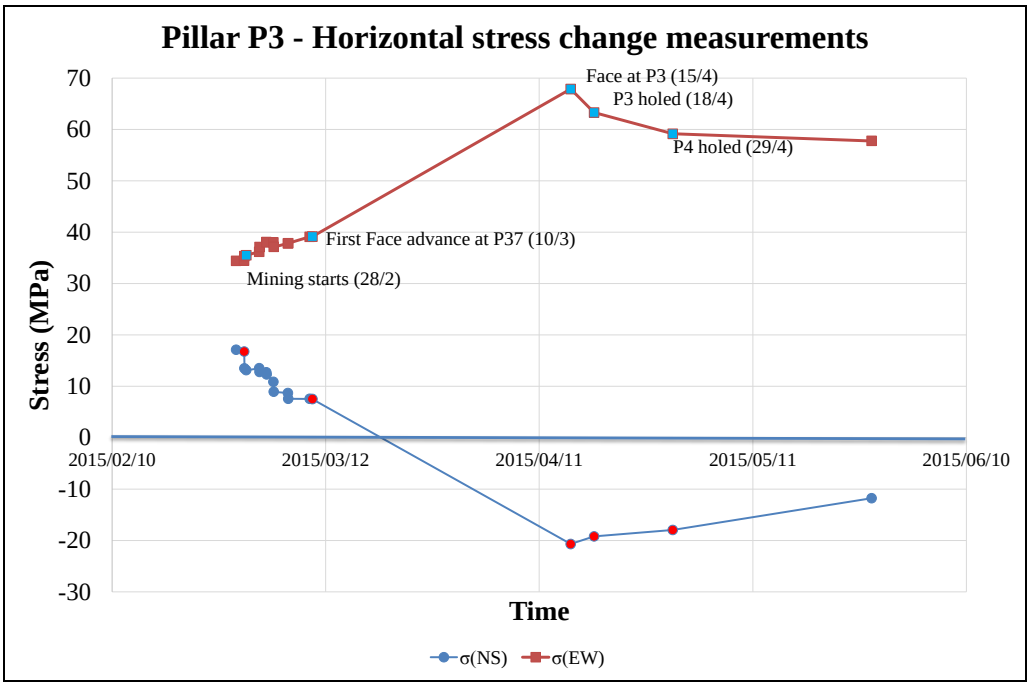

Figure 9.24: Horizontal stress change measured above pillar P3.

9.2.2. Pillar fracturing

Visually a pillar is considered failed when the outer surfaces of a pillar bulges as failed fractured material dilates outward (scaling). It is also occasionally assumed that even if the surrounding outer layers of a pillar are heavily fractured and the pillar may have reached a residual state, the core of a pillar is still solid. In the past this could only be investigated through the examination of holes drilled through a pillar. However, as indicated in Section 8.3.2, these holes quickly close up once a pillar starts to fail. Also, new holes cannot be drilled through the fractured scaled material. The inner portion of a pillar can therefore not be investigated.

A new seismic velocity process was developed by the company IMS (Institute of Mine Seismology) and tested on the crush pillars in the trial site to determine the internal condition of the pillars. The process involves installing sensors and hitting points around the perimeter of a pillar at mid height, examining a two-dimensional horizontal plane passing through the entire pillar (Figure 9.25a).

The hitting points (pegs) are repeatedly struck with a hammer that has a seismic sensor attached. The impact of the hammer generates a seismic vibration that travels through the pillar and is measured by sensors installed on the pillar perimeter. The hitting process is repeated for all pegs installed around the pillar. For each hitting point, a set of straight rays are drawn between the hitting point and the different pillar sensors (Figure 9.25b). A source and sensor distance is calculated from the seismic waves. The recorded seismograms are used to determine a seismic travel time measured between the source and the respective sensors. Technically it is not correct to assume a straight ray signal path when considering crush pillars as this will assume a homogenous medium. For this reason, multiple hitting points were used to establish over-lapping ray paths to calculate an average path (Figure 9.25c).

A two-dimensional velocity grid is overlain over the pillar cross-section. The pillar outline is established using the surveyed co-ordinates of the installed pegs. If the arrangement of sensors and hitting positions are good, then ray-path distributions throughout the grid should cover most of the cells (Figure 9.25d). Cells that are not covered by ray-paths are still adjusted when profile smoothing is applied. The velocity in each of these cells is adjusted based on the velocity calculated for that ray. The process is repeated for all the different ray-paths for all sensor and hitting point combinations. The result is displayed in the outputs for each respective pillar presented in the subsequent figures.

Profiling was done for pillar P1, P2 and P3. Pillar P1 was, however, used as the trial pillar to test the technique with the results not providing a tangible outcome. It was nevertheless used to develop the methodology for pillars P2 and P3.

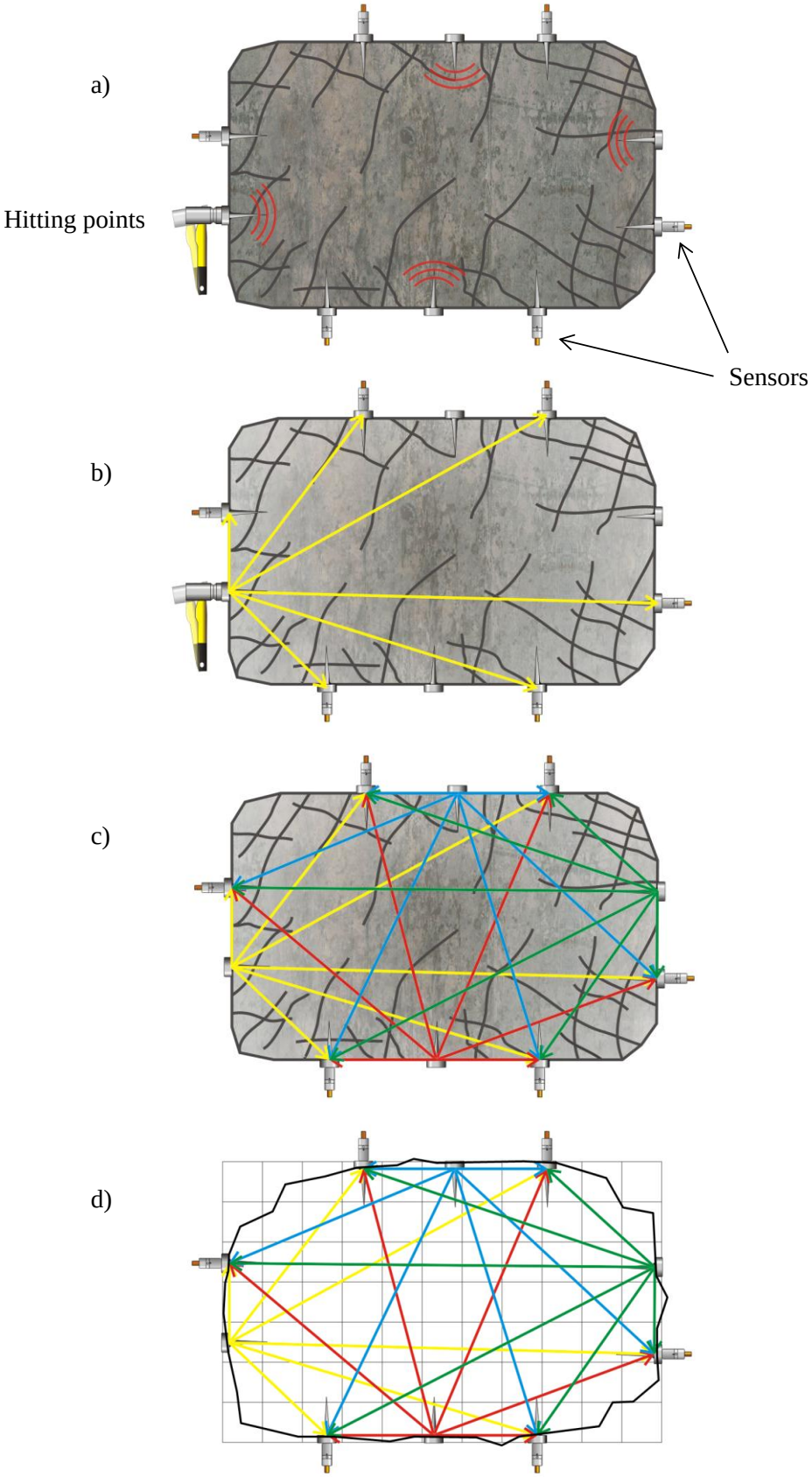

Figure 9.25: Pillar micro seismic profiling method to determine the degree of fracturing experienced by a crush pillar (plan view).

Results and interpretation

The objective of the seismic scans was to see how the pillars fracture during the pillar forming cycle. The intervals of the scans were therefore set out to determine:

- Fracture profile of the pillar before the pillar was formed (Stage 1). A zero base profile is conducted when the face was aligned with the pillar.
- Fracture profile of the pillar when it has just been formed (Stage 2). The face was aligned with the next pillar position and the scanned pillar was standing on its own.
- Fracture profile of the pillar when it is in the back area (Stage 3).

In order to conduct the base reading, the pillar holings had to be pre-developed around each proposed pillar position so that the pillar could be exposed as much as possible. This allowed for the installation of hitting points and sensors almost around the entire pillar prior to the pillar being formed by the advancing face.

The results indicated that the pillars experienced a significant overall reduction in seismic velocity once the pillars were formed (Stage 2). This compared well with the underground observations which showed a significant change in the pillar appearance at these times. Subsequent scans indicated that the pillars were already reasonably fractured during the pillar forming stage and that the advancing face did cause some damage to the eastern side of the pillar, although not visible along the exposed surface. Underground the pillars continued to deform, although this was not necessarily evident in the subsequent scans. The stress change measurements confirmed that the pillars were already at a residual state when the pillars were completely formed (Stage 2). The pillars, however, experience an unloading phase as new pillars are formed and load is transferred to the newly formed pillars. During this unloading phase the pillars continue to deform. The scans (Stage 3) therefore do not illustrate any substantial change in seismic velocity as the fracture or weakness planes already exist along which dilation is taking place as the pillar unloads.

The detail of the results obtained for each pillar will be expanded on in the following sub-sections. High seismic velocities indicate zones of little or no fracturing. In contrast, low seismic velocities indicate zones of high fracturing. Fracture profiles were also constructed to indicate the zones where recent fracturing has taken place.

Pillar P2: The initial profile indicated high velocities for the intact abutment (Figure 9.26). Underground observations indicated that the exposed western side of the pillar had experienced some degree of scaling. The borehole drilled through the bottom section of the pillar did indicate many visible fractures which have also moved relative to one another. This agrees well with the low velocities indicated along this region. However, the fracturing observed along the up-dip holing (Figure 8.30) is not evident in the profile. With the initial scan the overall ray coverage was reported to be low. This was significantly improved with the second scan. Figure 9.27 shows a profile with much lower velocities implying a higher degree of fracturing throughout the pillar. There was a large drop in velocity along the western side of the pillar. A slightly higher velocity region formed along the newly exposed pillar surface (S5 and S6). This would suggest that the pillar has higher rock competence closest to recently exposed pillar surface. The underground observations indicated that the newly exposed eastern side of the pillar did not display any signs of scaling (Table 8.9). The western side of the pillar, however, continued to scale. The stress measurements conducted indicated that the pillar had, at this point (15 April), reached a residual state with no further change recorded thereafter (Figure 9.18).

The change in seismic velocity experienced by the pillar (Figure 9.29) at this stage indicated that there was a significant overall drop implying a high degree of fracturing after the pillar was fully formed. The largest change calculated occurred along the upper western corner (S1). This could possibly be as a result of the poor data coverage experienced during the initial survey. However, this was the area where the most change was observed underground.

The third scan (Stage 3) did not indicate any significant change from the second scan conducted. A fairly low uniform drop in the overall change experienced, implied a low degree of crush of the already fractured pillar. The underground observations nevertheless indicated that fractures along the up-dip western side of the pillar were opening and that new fractures had formed along the eastern down-dip side of the pillar. This process was observed to continue to approximately 6 May (Figure 8.33). The fact that the scans did not indicate any significant additional change could therefore indicate that all the fractures were already formed. As the pillar was already at a residual state and started to unload as new pillars were formed (load transfer to newly formed pillars), the formed fractures continued to dilate.

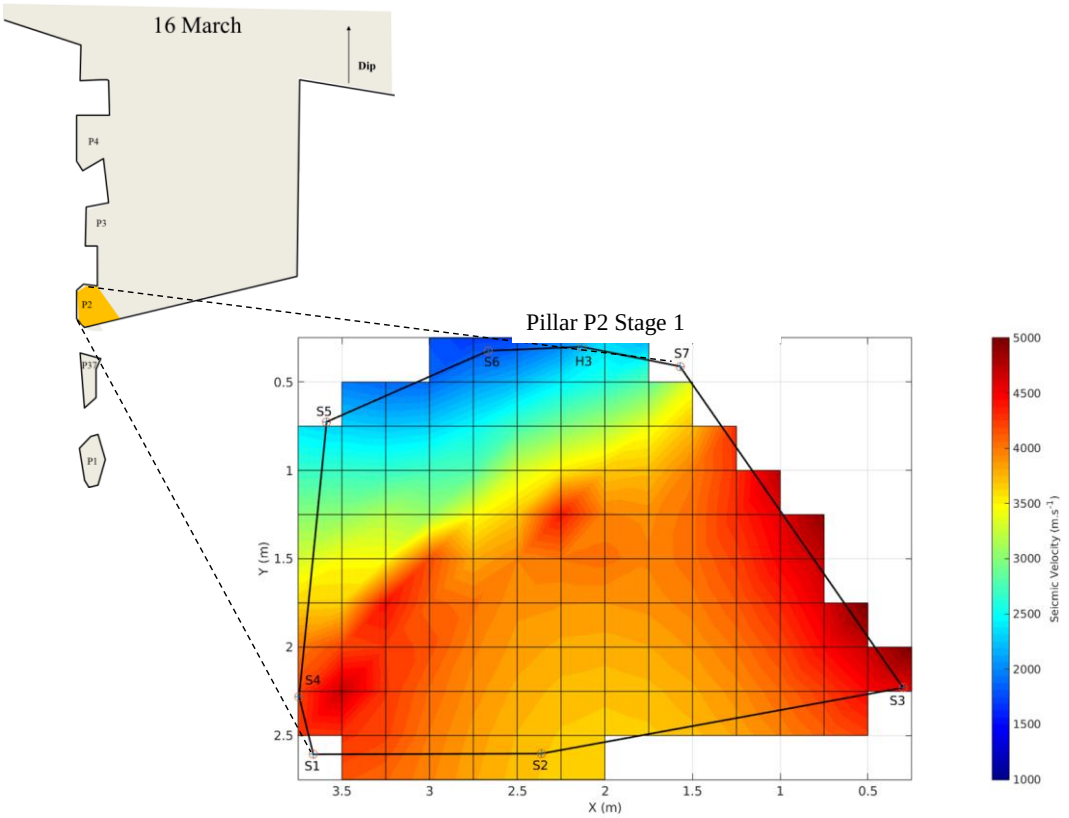

Figure 9.26: Pillar P2 scan 1; pillar parallel with the face.

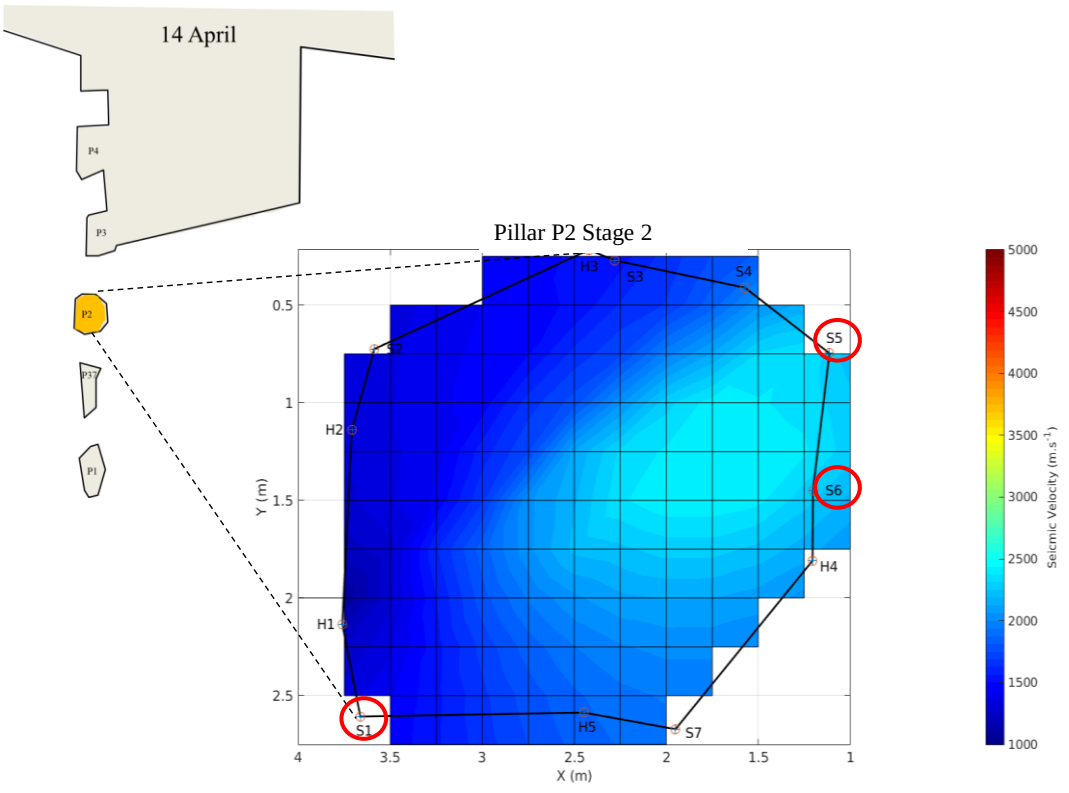

Figure 9.27: Pillar P2 scan 2; pillar formed. The pillar is 3 m behind the face position.

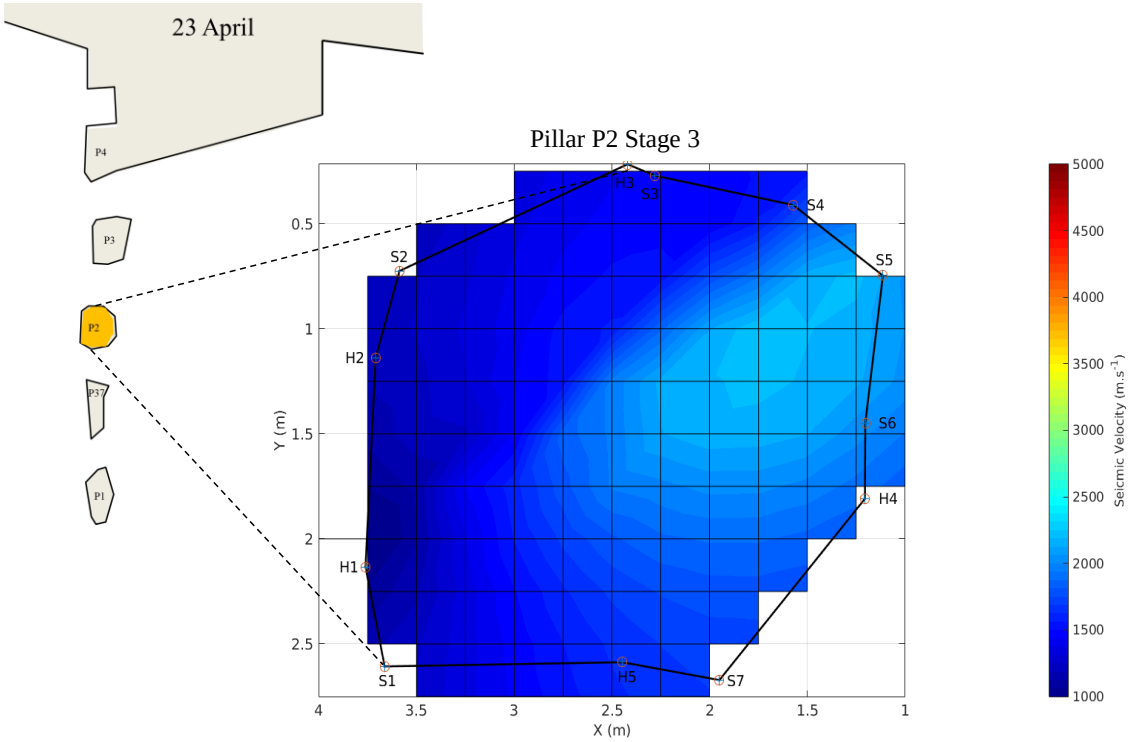

Figure 9.28: Pillar P2 scan 3. The pillar is 9 m behind the face position.

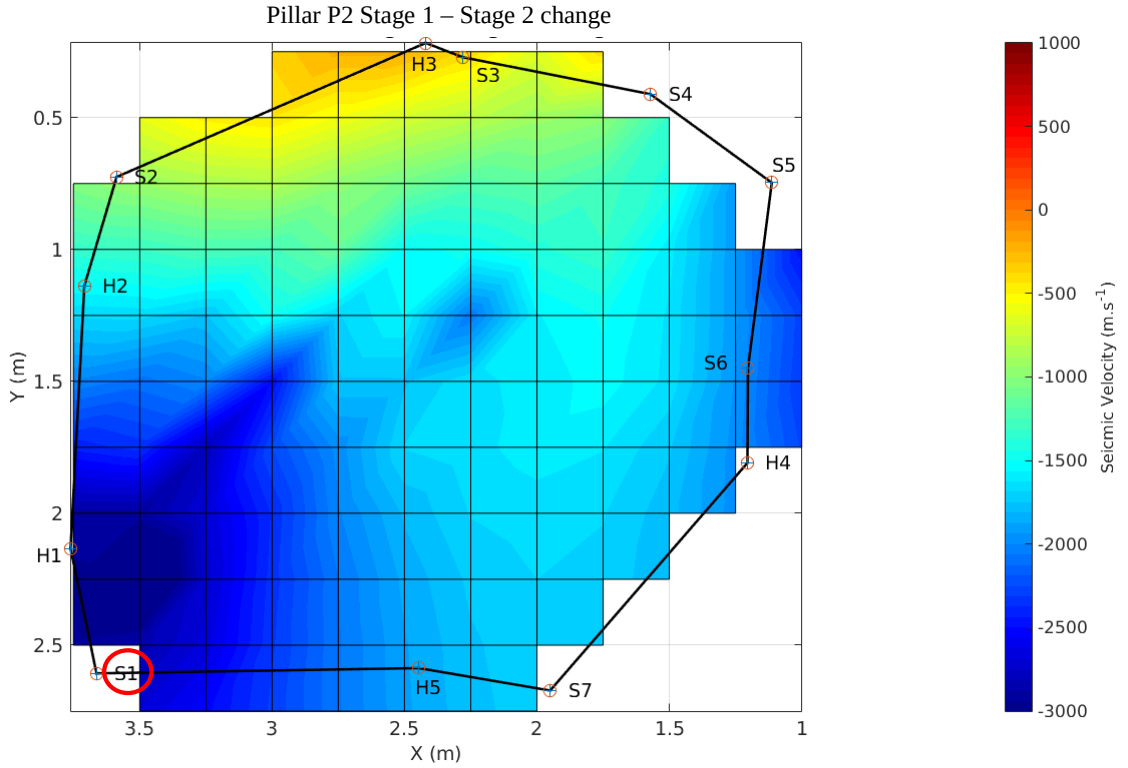

Figure 9.29: Pillar P2 change in seismic velocity measured between scans 1 and 2.

Pillar P3: As with pillar P2, the velocities were high along the intact eastern abutment. The first scan (Stage 1) did have good ray coverage and indicated low velocities along the exposed pillar edges (Figure 9.30). The underground observations indicated almost no signs of any visible scaling along the exposed surfaces of the pillar. There were some movement visible inside the borehole drilled through the pillar and there were new fractures visible along the western up-dip corner. However, the outer appearance does not seem to relate with the profile obtained from the internal pillar scan. The stress change measurements (Figure 9.20) did indicate that there was some stress regeneration prior to this event. The pillar, intersected by anomalous jointing could have been in a friction lock-up phase and therefore, although the pillar was internally fractured, did not experience any form of dilation.

After the pillar was formed (Stage 2) the profile indicated low seismic velocity regions along the perimeter of the pillar and a small medium velocity region between sensors S61 and S51 (Figure 9.31). This suggests the pillar had higher rock competency closer to the newly exposed pillar surface, similar to results obtained for pillar P2. The underground observations seemed to agree well with this profile obtained. Once the pillar was formed, the pillar suddenly started to fracture along the western side, western up-dip holing and along the centre of the down-dip side of the pillar. There was still no visible scaling along the newly exposed eastern side of the pillar. The change in seismic velocity between scans 1 and 2 indicated that there was a significant drop around the S61 to S41 sensor positions (Figure 9.33). This implied that the advancing panel caused significant fracturing along this side of the newly formed pillar when compared to its former intact state. The stress change measurements indicated a significant change in stress to the point when the pillar was fully formed. Any potential friction lock-up between joint or fracture planes were most likely again mobilized resulting in the observed behaviour. As the pillar was experiencing an unloading phase it could have resulted in the observed dilation along the fracture planes. The areas along the existing edges of the pillar showed lower degrees of change and therefore imply that these portions of the pillar were already in a partially fractured state, although not visible.

The third scan (Stage 3) conducted indicated similar data to that of the second survey, with an overall drop in seismic velocity experienced. The largest drop were experienced in the region between sensors S32 and S21 (down-dip side) and S61 and S51 (eastern side). Refer to Figure 9.34. The drop between sensors S61 and S51 suggests crushing of the relatively intact region along which the face was mined. Underground observations indicated that the western side of the pillar was experiencing significant scaling. New fractures formed along the eastern up-dip side of the pillar and along the down-dip side of the pillar. These observations appear to agree well with the fracture profiling conducted. Also, the pillar continued to deform until 18 May. The continued deformation of the pillar therefore also seemed to relate with an unloading phase the pillar was subjected to.

The calculated change in seismic velocity for pillar P3 was fairly similar to the change calculated for pillar P2. There was a slightly larger overall drop in velocity experienced by pillar P3.

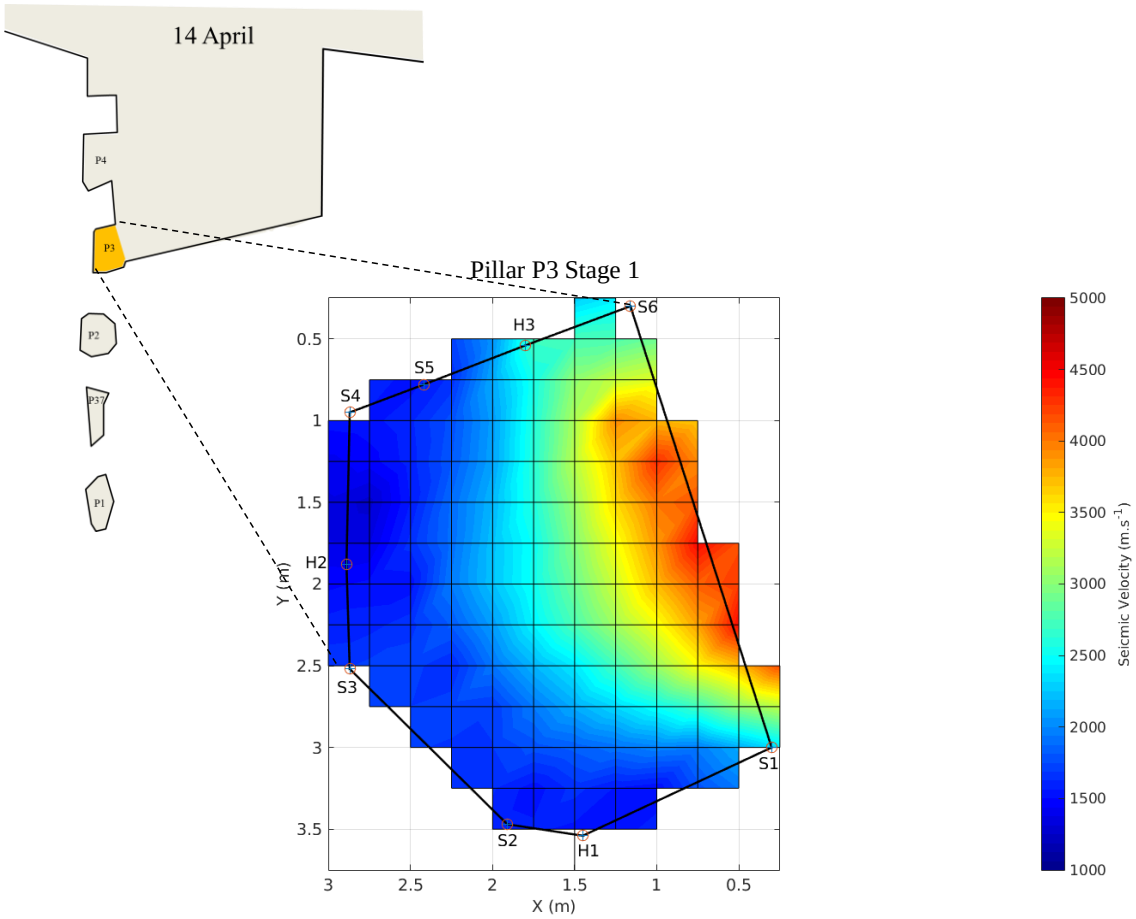

Figure 9.30: Pillar P3 scan 1; pillar parallel with the face.

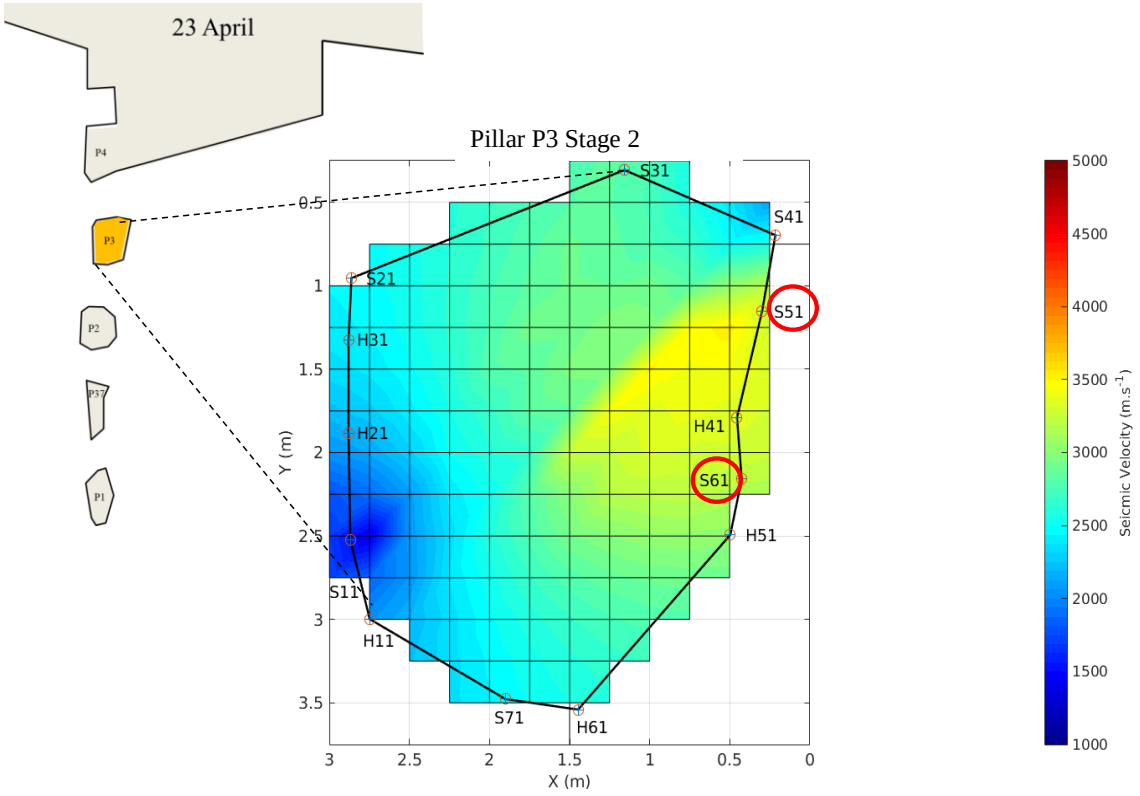

Figure 9.31: Pillar P3 scan 2; pillar formed. The pillar is 3 m behind the face position.

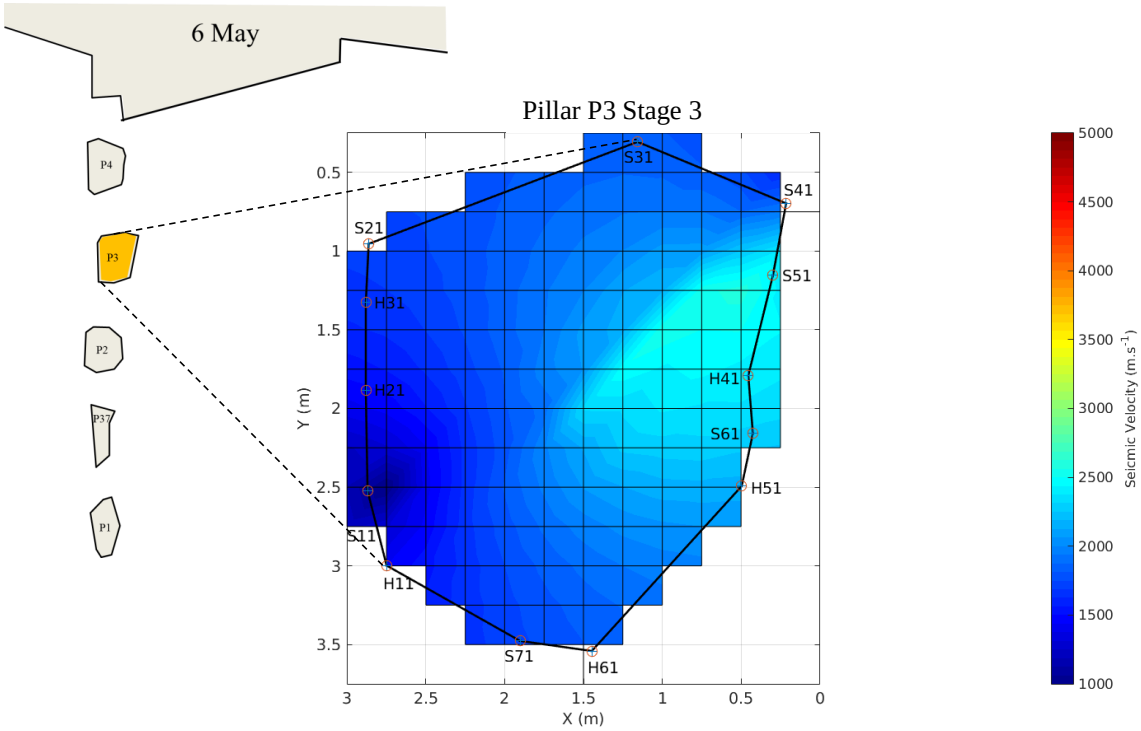

Figure 9.32: Pillar P3 scan 3. The pillar is 7 m behind the face position.

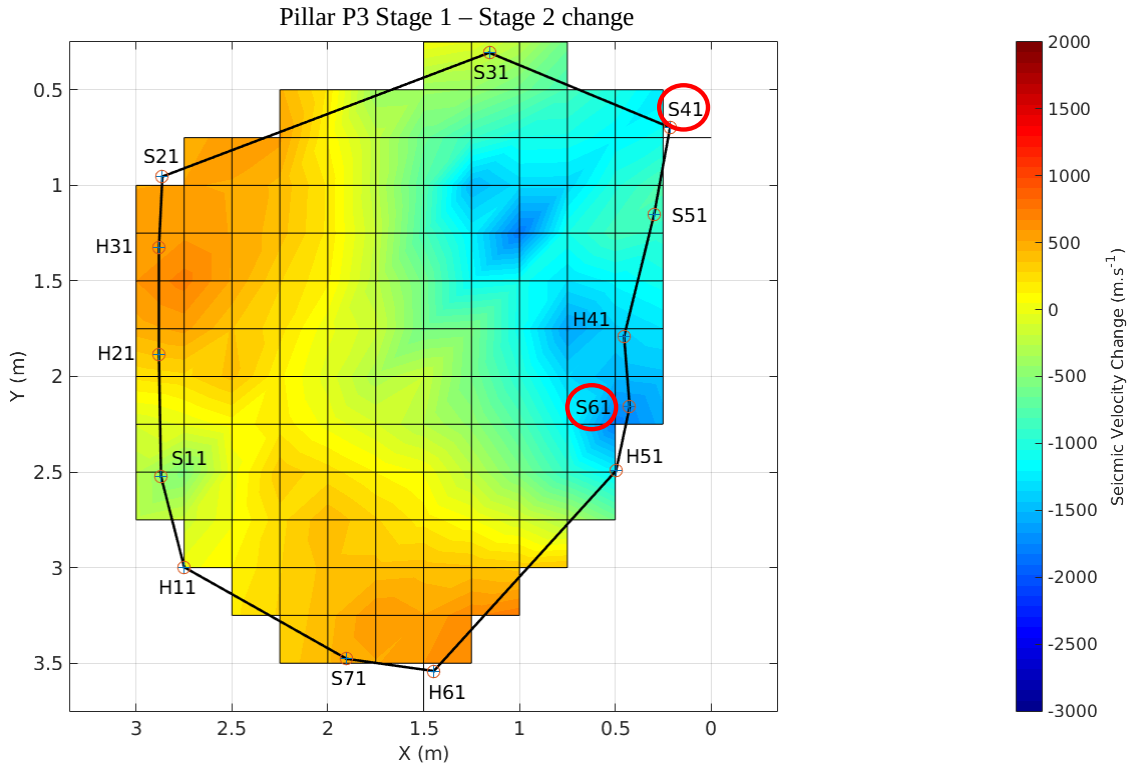

Figure 9.33: Pillar P3 change in seismic velocity measured between scans 1 and 2.

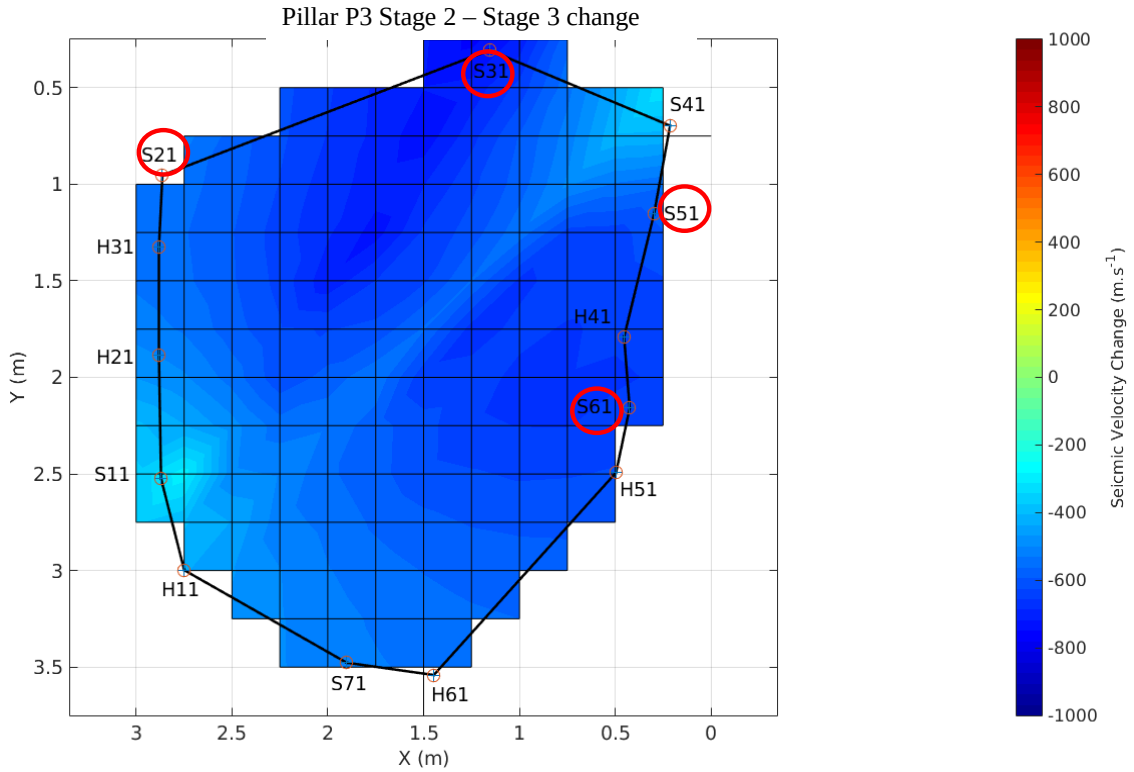

Figure 9.34: Pillar P3 change in seismic velocity measured between scans 2 and 3.

9.2.3. Pillar dilation

Tape extensometers were installed in horizontal boreholes drilled into the pillars and anchored approximately halfway through the pillar. The outer portions of the holes were cased with steel pipes to ensure that the tapes were not cut-off by the scaled pillar material. The results of the extensometer readings for the holes which were still accessible are tabled below. The maximum amount of pillar dilation measured was along pillar P4 (100 mm). Although this does not seem to agree with the observed bulking experienced as a result of the scaled material alongside the pillar, the measurement does seem to be valid. Figure 8.38 shows the tape and casing visible along the western side of pillar P4 which experienced significant fracturing and scaling. However, if one considers that the outer metre of a fully fractured pillar comprises of fractured slabs spaced approximately 50 mm apart and these slabs were opening approximately 5 mm relative to one another; the amount of dilation experienced along the surface of the pillar would then be approximately 100 mm. Watson (2010) reported pillar dilation as much as 37 cm at a crush pillar site at Union Mine. Canbulat et al (2006) determined that the pillar dilation is equal to approximately twice the amount of convergence. This finding appears to be supported by the results of the convergence measurements in the trial section (30 – 55 mm).

Figure 9.35: Photograph of tape extensometer installed in horizontal borehole through pillar P2.

Table 9.4: Pillar dilation measured from extensometers anchored along the centre of the pillars.

	P2	P3	P4
Date	**Pillar dilation (cm)**		
2015/02/28	0	0	0
2015/04/14	4.8	7.4	4.8
2015/06/04	7.8	NA	10.4

9.2.4. Convergence

Convergence was monitored with both closure stations and closure loggers. The intent was to have fixed closure stations installed throughout the trial site as it provides a reference point where measurements can repeatedly be conducted (long term). Convergence could therefore be measured on a larger scale. The loggers, on the other hand are easy to install and easy to move to new locations. Continuous convergence could therefore be measured close to the face and data could be compared to reflect events in the mining or pillar forming cycle. The instruments provided the means to determine the large scale convergence experienced throughout the section as well as the time-dependent convergence in the active mining area.

Underground observations identified the need to understand how the panel was deforming from the pillar to the panel mid-span. The footwall heave experienced adjacent to pillar 42 could be identified and observed from the loading on the installed support units in the panel. Extensive convergence instrumentation was installed in the final mining section to understand the rock mass deformation and pillar behaviour as a function of mining (face advance) and pillar crushing. Figure 9.36 is an indication of the approximate position of the closure stations. Each instrument site was referenced to a row and position. Each site reference was measured with respect to distance behind the face (dip) and distance from a pillar (strike) at a specific time (e.g. on 28 February 2015 closure station F2 was 7.7 m behind the face of panel E3 West and installed 7 m from pillar P1). Also, at most sites both closure loggers and closure stations were installed to verify the results obtained. Figure 9.37 is an example of the output generated by a closure logger installed at site A2. Also overlain on the continuous convergence output is the convergence measured by the closure station as well as the closure logger ruler reading. Therefore the information could be triple verified. The formation of pillars P2, P3 and P4 are also highlighted in the figure. A pillar and the holing ahead of the pillar can be formed in 6 blasts (i.e. pillar P3 was formed with daily blast intervals). Any stoppage does obscure the results (i.e. pillar P2 was formed over the period when the shaft was stopped due to a section 54 and for the Easter break) as the convergence experienced in the panel is related to the mining events and therefore pillar formation and crushing. The closure station sites in panel E2C East could be installed prior to the commencement of mining the final mining section. The new closure stations sites in panel E3 West was installed as the face was advanced (i.e. rows G, H, I).

The rate of convergence discussed in the results is referenced as mm / m of advance. This was used to easily compare the results obtained at the various sites. Various interruptions were experienced resulting in significant delays in the mining cycle. Geometric convergence rates (mm / m of face advance) are generally greater than the steady-state convergence rates expressed as mm / day at crush pillar sites (Roberts et al, 2006).

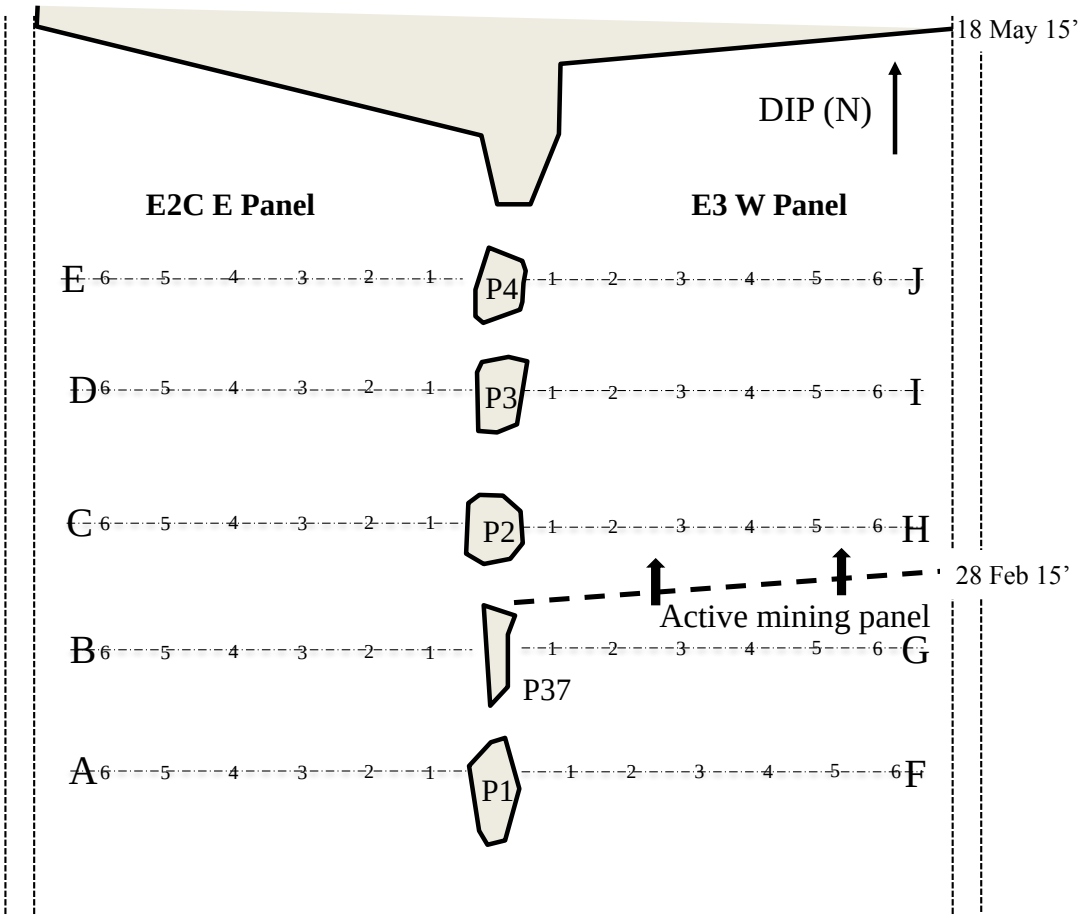

Figure 9.36: Layout of the closure stations in the final mining section.

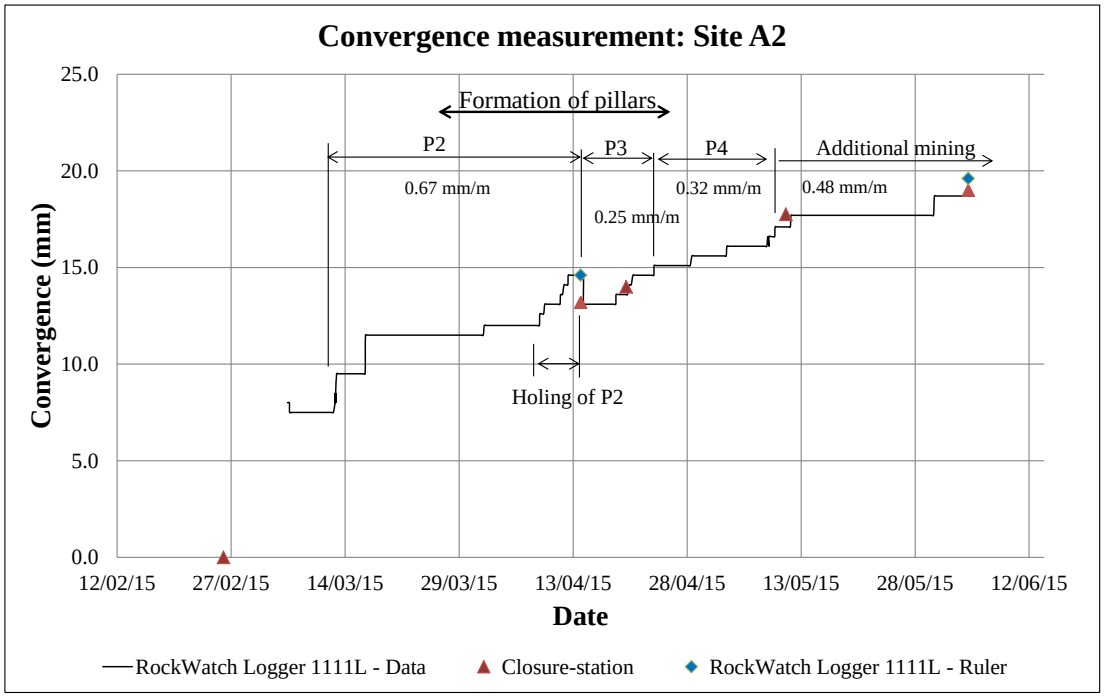

Figure 9.37: Convergence measured at site A2.

Results

The key objective was to understand how the pillars were behaving. The dates indicated in the figures correspond to dates in which data was obtained from underground. The dataset could therefore be validated.

Some important events:

- Mining of the final mining section resumed on 28 February. This is used as the baseline readings.
- P2 formation: 14 March – 8 April. Advance past down-dip holing 9 – 14 April.
- P3 formation: 15 – 18 April. Advance past down-dip holing 19 – 22 April.
- P4 formation: 23 – 29 April. Advance past down-dip holing 3 – 8 May.
- Additional face advance: 9 – 18 May. Mining stopped.

Figure 9.38 indicates the convergence measured adjacent to the completely formed pillar P1. The convergence in the panel east of the pillar (row F) was higher than the convergence measured in the west panel (row A). The pillar was initially formed with the east panel (E3 West) leading. The majority of the scaling observed along the pillar was also to the east side of the pillar. The figure indicates that the convergence measured was the highest directly adjacent to the pillar. However, the figure does not demonstrate the convergence at the panel mid-span which took place as both the east and west panels were initially mined (A5 and F5). Panel E2C East would have experienced most of the convergence at mid span as the panel already advanced to the bracket pillar situated 30 m down dip of the closure stations (row A). The east panel does show some of this effect as panel E3 West was started up again. The closure stations (row F) were 7.7 m behind the face position when mining of panel E3 West resumed. The figure therefore indicates the additional convergence measured post pillar formation. The west panel experienced additional convergence predominantly as a result of pillar crushing (refer to A1 and A2 versus A4 and A5). The east panel experienced additional convergence as the face, situated 5 m ahead of pillar P1 advanced. The convergence experienced is therefore due to the elastic response of the hangingwall (refer to F3 – F5) as well as pillar crushing (refer to F1 and F2).

Once mining resumed, most of the convergence took place during the formation of pillar P2 (refer to 14/04 dataset). This is illustrated by the closure logger data represented in Figure 9.37. The stress change data (Figure 9.16) confirms that the majority of the secondary vertical stress reduction was experienced during the formation of pillar P2. The formation of pillar P3 has minimal impact on the additional convergence experienced (refer to dataset 20/04 in Figure 9.38). The stress change data supports this finding.

The underground observations indicated that there were some additional movement along the fracture planes along the top and bottom of pillar P1 when the face was aligned with pillar P4. At this time a wedge-like structure was observed along the down-dip side of the pillar (Figure 8.28). This appears to relate with the

increased convergence experienced at the closure station along row A (refer to dataset 11/05). It can therefore be assumed that the pillar, at this point was completely crushed. Any additional convergence experienced may be as a result of ongoing pillar deformation.

The convergence measured in the west panel (E2C East) along pillar 37 (row B) agreed well with the results measured along row A adjacent to pillar P1. The two rows of closure stations were approximately 5.5 m apart on dip. The additional convergence experienced alongside pillar 37 (Figure 9.39) was slightly higher (8.5 - 10.3 mm) compared to pillar P1 as the pillar was only partially formed when mining resumed at the end of February. The variance can therefore be attributed to the pillar completely crushing as the face advanced and the pillar was formed.

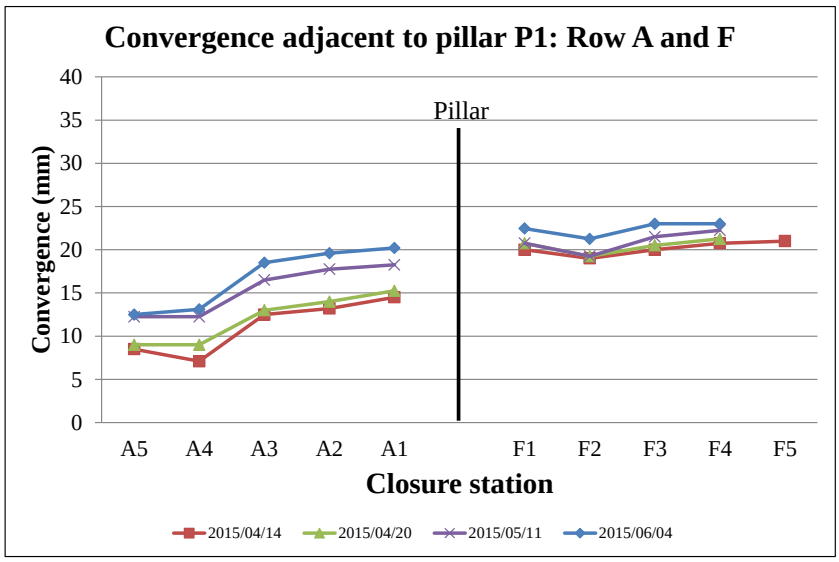

Figure 9.38: Convergence measured adjacent to pillar P1 along closure stations, rows A and F. The baseline readings were taken on 28 February 2015.

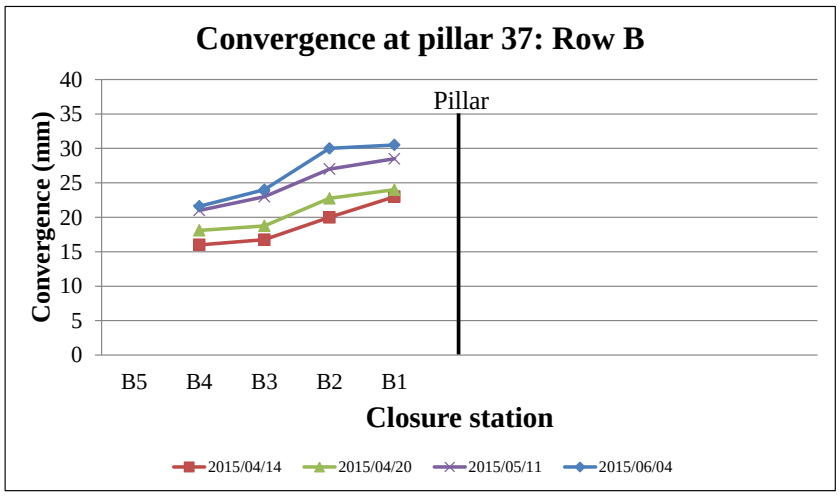

Figure 9.39: Convergence measured west of pillar 37 along closure stations, row B.

Figure 9.40 indicates the convergence measured either side of pillar P2. The pillar was initially exposed by the leading western panel (E2C East). The pillar predominantly scaled towards the western side. The measurements show that the majority of the convergence occurred adjacent to the western side of the pillar during the time in which pillar P2 was formed (refer to dataset 14/4). The closure stations in the eastern panel (row H) were only installed on 23 April after pillar P3 had been formed. The underground observations indicated that pillar P2 continued to fracture along the western side. However, the pillar was significantly deforming from around 23 April with the fractures along the western side of the pillar opening and new fractures forming along the eastern down-dip side. During this period pillar P3 was formed. Pillar P3 only started deforming when the face was aligned with pillar P4 (23 April). The increase in convergence measured (6.25 – 7 mm) adjacent to pillar P2 occurring between datasets 14/4 and 11/5 is therefore related to the late pillar crushing of pillar P3 and also the formation of pillar P4. At the time additional fracturing was observed along the western side of the pillar and additional fractures have formed along the eastern down-dip side. Hereafter the pillar continued to deform as these fractures continued to dilate. This is reflected in the increased convergence at station H1 (dataset 04/06).

The stress change measurements conducted above pillar P2 (Figure 9.18) indicated that most of the reduction in vertical stress occurred prior to the formation of pillar P2 and continued until the pillar was completely holed (15 April). No secondary stress reductions were experienced by the pillar.

The additional convergence measured in the panel was less than measured next to the pillar as the panel hangingwall would have already converged during the initial mining of panel E2C East. Nevertheless, the events contributing to the convergence still remain the same. Figure 9.41 indicates the convergence recorded by the closure logger at site C4 (also highlighted in Figure 9.40). The formation of pillar P2 and P4 caused an increase in additional convergence of 6 mm and 3.5 mm respectively at this site. Similarly, the additional pillar deformation which continued to occur at this site once all the pillars were formed caused another 3.5 mm of additional convergence resulting in a geometric rate of convergence of 0.34 mm / m (when mining stopped) to 0.68 mm / m (when the logger was removed).

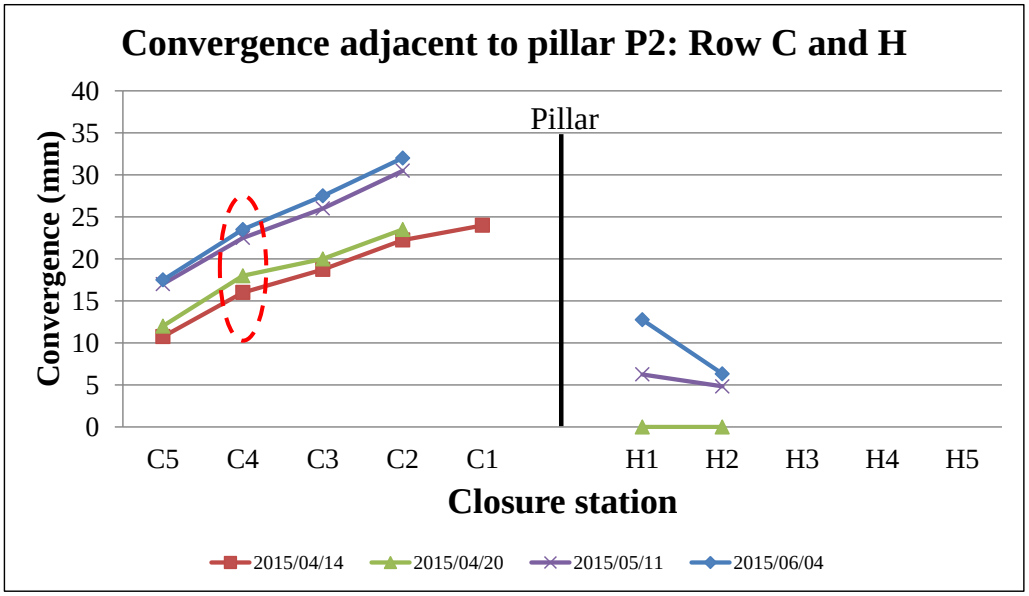

Figure 9.40: Convergence measured adjacent to pillar P2 along closure stations, row C and H.

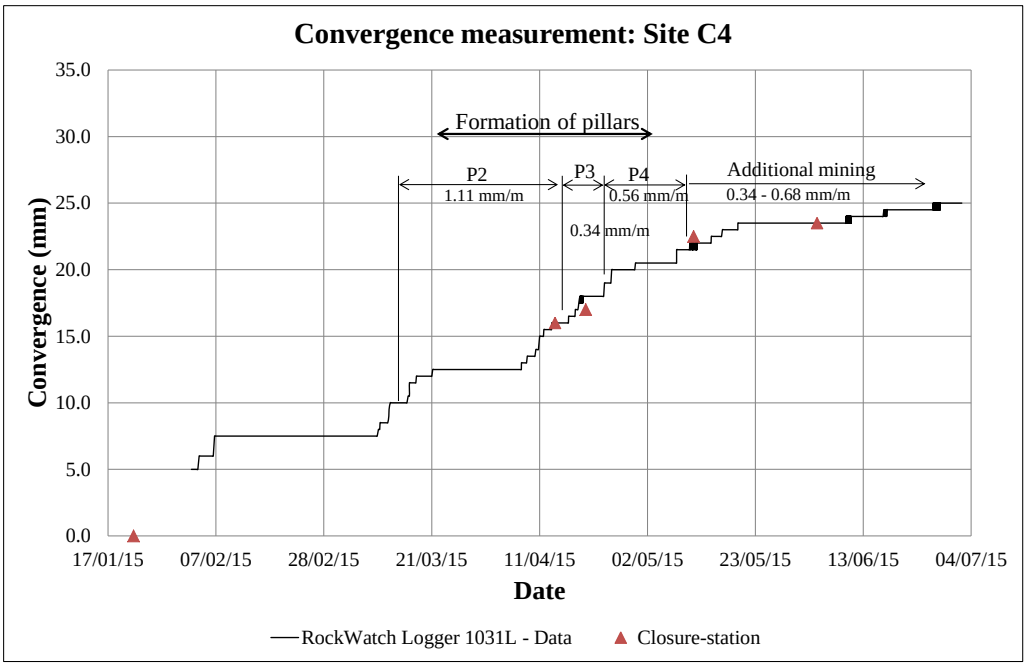

Figure 9.41: Convergence measured at site C4.

Pillar P3 experienced late pillar crushing. Most of the additional convergence measured was adjacent to the pillar and along the side of the pillar which was exposed first (west). Dataset 27/4 in Figure 9.42 indicates that there was an increase in convergence corresponding to the observed deformation of the pillar which occurred when the face was aligned with pillar P4. As the face advanced the pillar continued to deform with existing fractures opening and new fractures forming along the eastern up-and down-dip sides of the pillar.

Figure 9.43 indicates that the rate of convergence was rather low during the formation of pillar P3 compared to the formation of the other pillars (pillar P2 was 1.25 mm / m measured adjacent to pillar P2).

The closure station in the eastern panel was installed after the formation of pillar P4. The convergence indicated at site I1 is therefore most likely as a result of ongoing pillar deformation experienced by pillar P3.

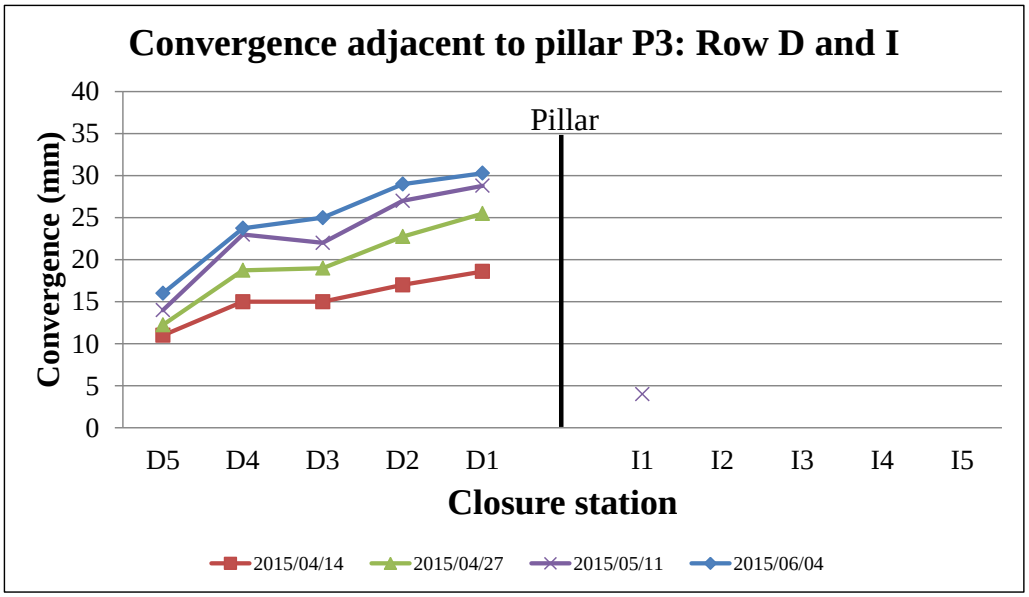

Figure 9.42: Convergence measured adjacent to pillar P3 along closure stations, row D and I.

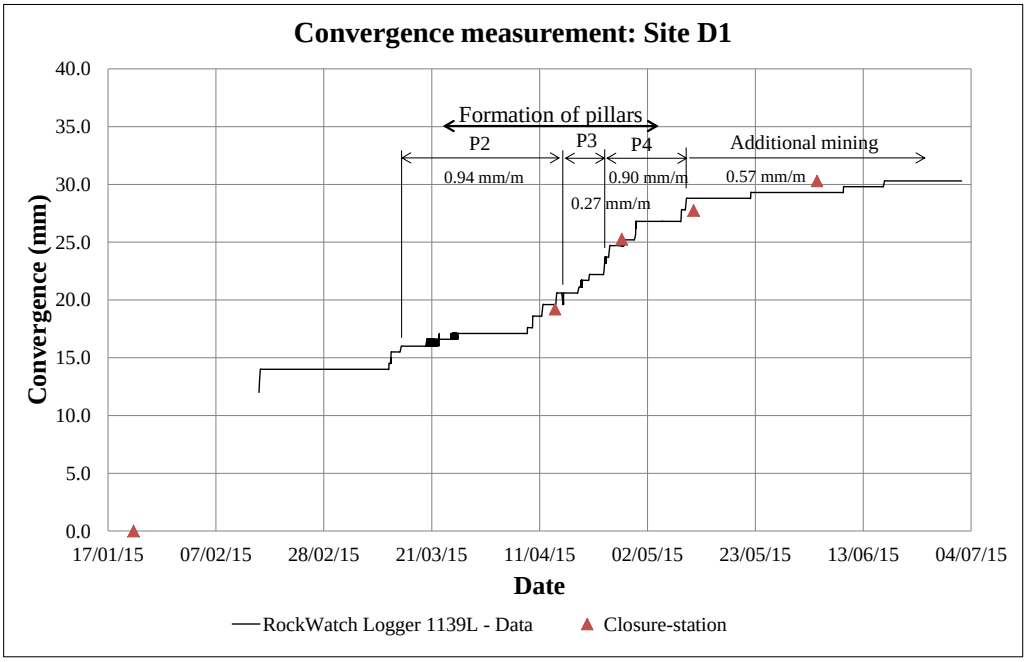

Figure 9.43: Convergence measured at site D1.

The convergence measured adjacent to pillar P4 (row E) indicated that the observed crushing along the western side of the pillar which occurred prior to the formation of the pillar (before 23 April) contributed significantly to the convergence measured by the closure stations along row E. The closure stations installed 6.6 m behind the stopped face abutment of panel E2C East measured an increase in the additional convergence experienced in the panel (towards the centre) compared to the other closure station sites situated further back (e.g. row D). The ongoing deformation of pillar P4 therefore contributed to the continued convergence experienced close to the stiff face abutment. This demonstrates that pillar crushing does contribute to the convergence experienced close to the face.

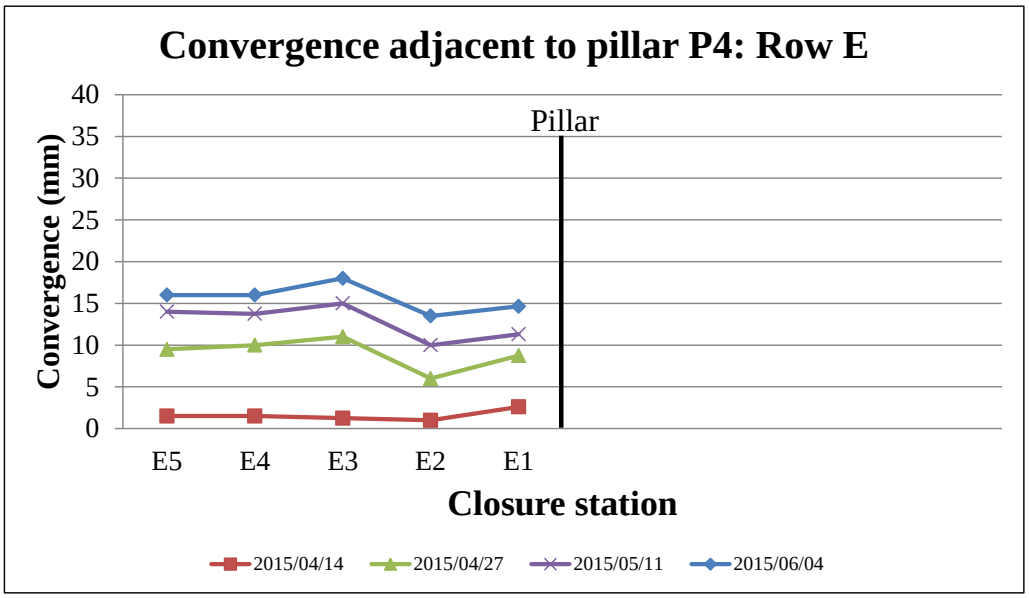

Figure 9.44: Convergence measured adjacent to pillar P4 along closure stations, row E.

The convergence measured adjacent to newly formed pillars (e.g. pillar P2) was approximately 10 mm higher than adjacent to completely formed pillars (e.g. pillar P1). This finding is also visible in Figures 9.47 and 9.48. The convergence and convergence rates measured adjacent to the pillars were higher compared to the centre of the panel. This is illustrated in Figures 9.45 and 9.46. There were closure loggers which recorded ongoing convergence after all mining stopped (45 days later). There does therefore appear to be an agreement between ongoing pillar deformation and convergence even after a pillar has reached its minimum vertical stress. This is also indicated in the two figures as “additional” and indicates the rate of convergence based on the total amount of convergence experienced as a result of the extra mining advance after pillar P4 was formed and the additional convergence measured after all mining stopped. Figures 9.45 and 9.46 indicate that the rate of convergence is the highest closest to the pillars. Also, the formation of pillar P3 did not have a tremendous impact on the overall convergence experienced at the various closure station sites. This is most likely due to the late pillar crushing experienced by the pillar.

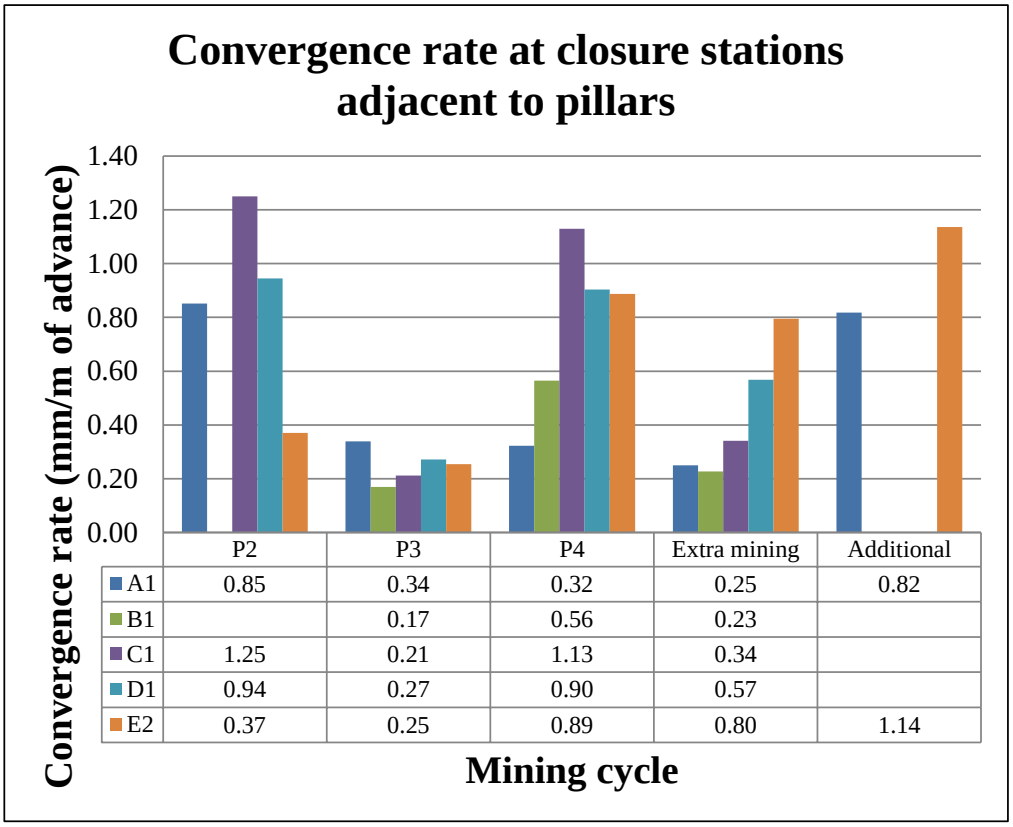

	P2	P3	P4	Extra mining	Additional
A1	0.85	0.34	0.32	0.25	0.82
B1		0.17	0.56	0.23	
C1	1.25	0.21	1.13	0.34	
D1	0.94	0.27	0.90	0.57	
E2	0.37	0.25	0.89	0.80	1.14

Figure 9.45: Convergence rate measured along closure stations adjacent to the pillars (line 1 and 2).

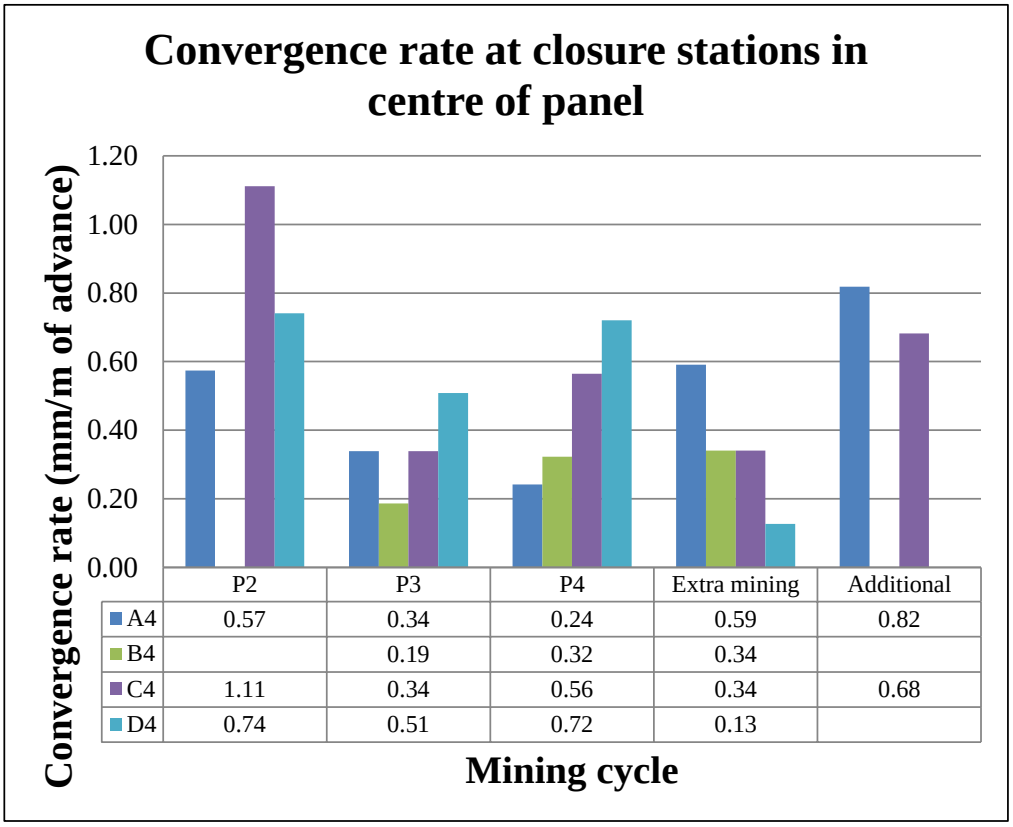

	P2	P3	P4	Extra mining	Additional
A4	0.57	0.34	0.24	0.59	0.82
B4		0.19	0.32	0.34	
C4	1.11	0.34	0.56	0.34	0.68
D4	0.74	0.51	0.72	0.13	

Figure 9.46: Convergence rate measured towards the centre of the panel (line 4).

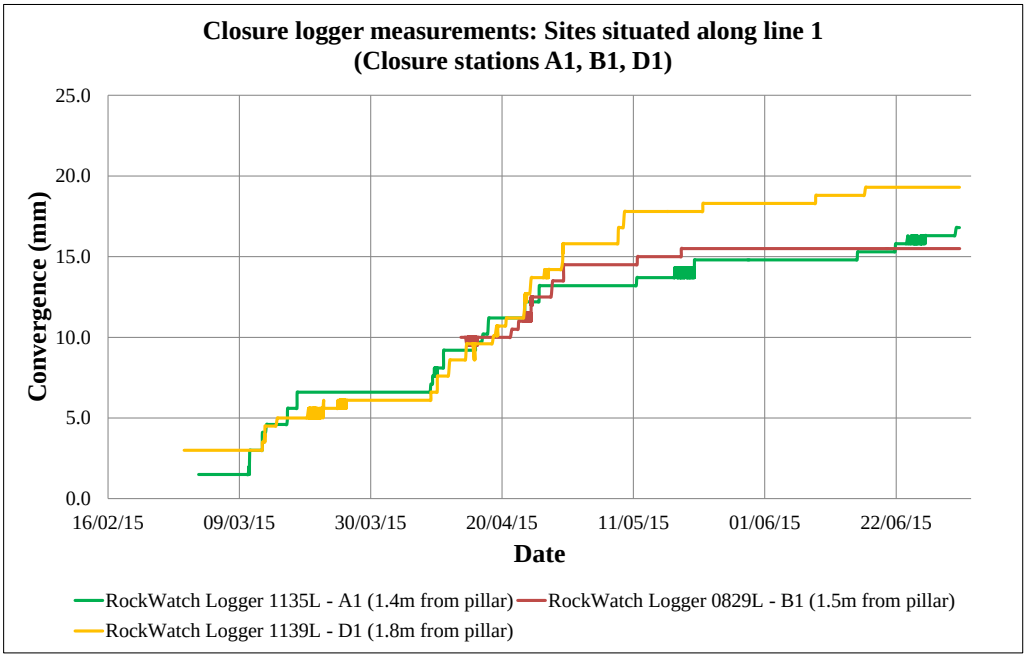

Figure 9.47: Closure logger measurements along closure stations situated adjacent to the pillars (line 1).

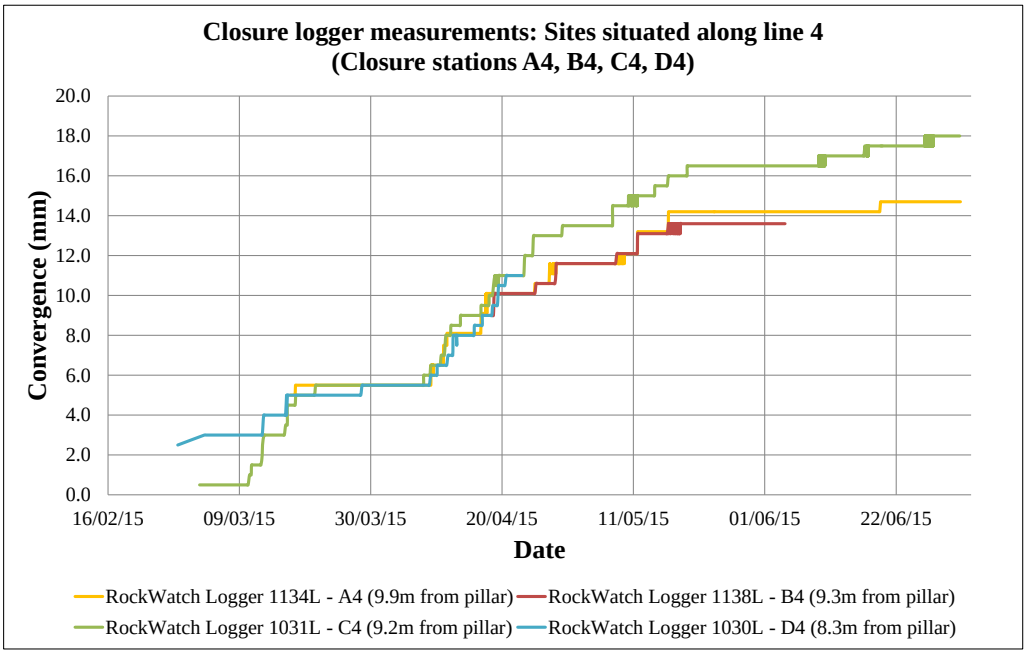

Figure 9.48: Closure logger measurements along closure stations situated in the centre of the panels (line 4).

The results of the closure stations installed either side of instrumented pillars indicated that the side of the pillar which was exposed first experienced the most convergence. Pillar P1 which was completely formed prior to the extraction of the final mining section had a full range of data which showed the agreement between the pillar behaviour and the convergence experienced as a result. Underground observations also identified that the side of the pillar exposed first would experience the most fracturing and scaling. Two closure stations installed during the initial mining (May 2013) either side of pillar 39 (w:h = 0.62) were assessed to verify this finding. At the time the panel east relative to the line of crush pillars (E3 West) was leading the west panel (E2C East) by approximately 10 m. The underground observations identified the east side of the pillars to be fractured (refer to Figure 8.52 which is a photograph of pillar 38; w:h = 1.15 situated immediately down-dip of the closure stations). Stations 1 and 2 were installed on 22 May 2013. Figure 9.50 indicates the layout and sequence of events. The stations therefore recorded the final mining which took place in panel E2C East (22 May – 11 June 2013) before the panel was stopped against the bracket pillar. Convergence measurements were taken weekly (July 2013), thereafter monthly (August to January 2014) and randomly thereafter. Figure 9.49 indicates the convergence which took place as a result of the initial mining. The convergence measured was higher in the leading panel (station 1). However, the convergence did not stop when mining stopped. There were two events as highlighted in the figure which significantly contributed to the amount of convergence experienced at these two sites. Additional convergence of 6 mm and 13 mm (first event) and 3 mm and 5 mm (second event) were measured at station 2 and 1 respectively. The exact cause of these events is unknown. The results do, however, confirm important characteristics regarding crush pillar behaviour namely;

- After a pillar has reached a completely residual state, ongoing pillar deformation contributes to an increase in convergence experienced at a site.
- The side of the pillar which was exposed first will experience the highest convergence (related to pillar fracturing sequence).

Unfortunately, very few closure loggers or stations were installed close to the advancing mining face. The majority of the convergence measured therefore reflect the change in convergence (additional convergence) in the back area (20 m behind the face) and not in the immediate face area (first 5 - 10 m). The measured convergence at the closure stations (row F) adjacent to pillar P1 measured the convergence as the face advanced (panel E3 West). These closure stations were installed 7.7 m behind the face. The convergence measured (23 mm) is indicated in Figure 9.51. However, some initial convergence would have taken place when panel E2C East was originally mined to the bracket pillar. Underground observations also identified early pillar crushing which would have contributed to the convergence experienced at the site.

The convergence measured in the stopped face area (panel E2C East) at the closure stations installed along row E adjacent to pillar P4 indicated approximately 10 - 15 mm of additional convergence (Figure 9.44) during the advance of panel E3 West. Based on these results, the convergence experienced in the face area

adjacent to pillar P1 should be adjusted by approximately 10 - 15 mm. The total amount of convergence experienced at this site (e.g. F4) should be approximately 33 - 38 mm. The amount of convergence is similar to what was experienced along the west side of pillars 37, P2 and P3 considering that some initial convergence have also taken place prior to measurement. However, the effect of the face abutment in close proximity could also have a significant impact on the total amount of convergence experienced at the site.

Figure 9.51 indicates that most of the convergence experienced in the stope takes place in the first 15 m behind the face. The underground observations of pillars P2 and P3 revealed that fractures along these pillars would continue to dilate until the pillars were approximately 14 m in the back area.

Malan et al (2005) indicated that with regular blasting, time dependent convergence rates at an instrumented crush pillar site at a distance of 15 m - 20 m from the face was found to be approximately 2 mm / day. They estimated that the steady-state convergence rates varied between 2.2 mm / day and 0.14 mm / day. Similar results were obtained from convergence measured in the trial area by means of closure loggers. The average rate of geometric convergence was 0.4 – 0.6 mm / m of advance. This will differ from site to site and will also be influenced by mining depth and regional stability (will impact on rock mass stiffness).

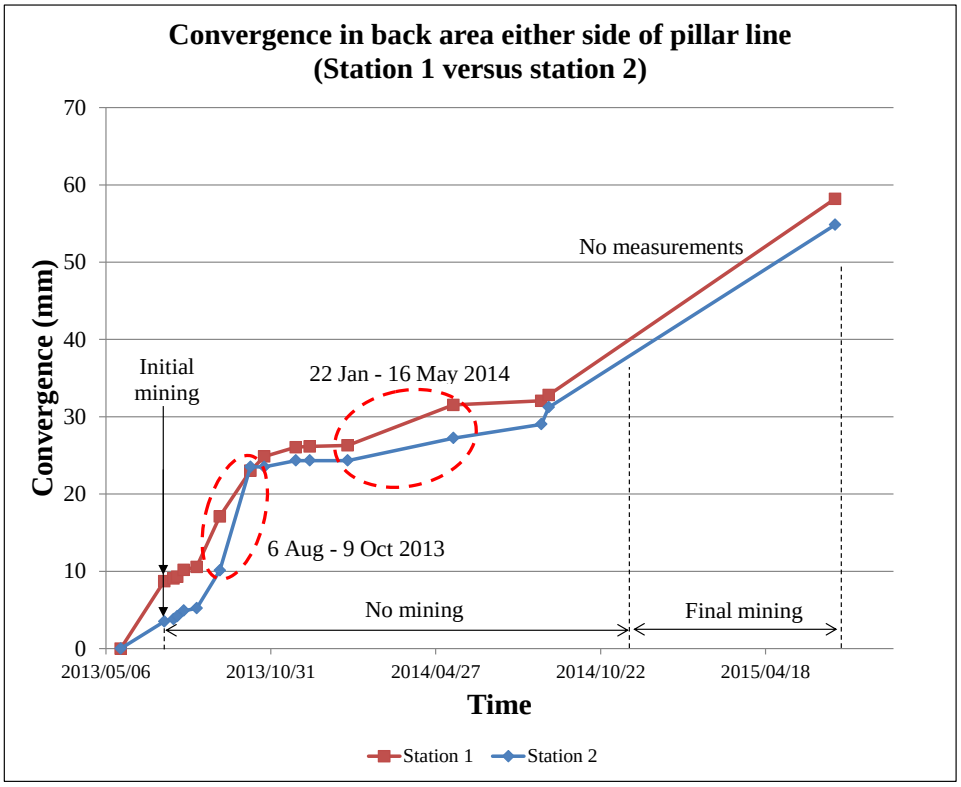

Figure 9.49: Convergence comparison measured at closure stations 1 and 2 installed either side of the pillar line. The closure stations were installed before mining stopped in 2013. The panel east of the crush pillars (E3 West) was leading the west panel by approximately 10 m.

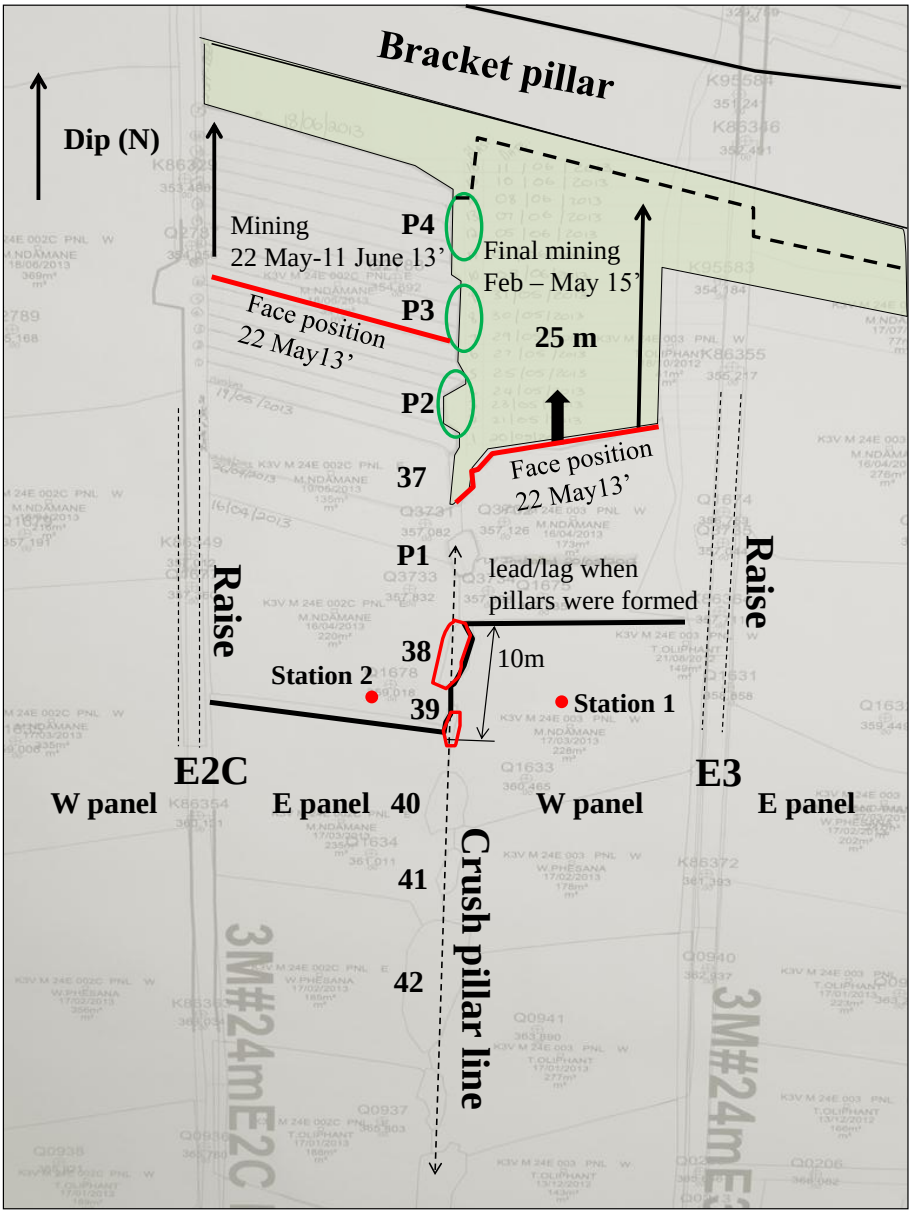

Figure 9.50: Position of closure stations 1 and 2. The diagram also shows the sequence of events including face positions and mining activity.

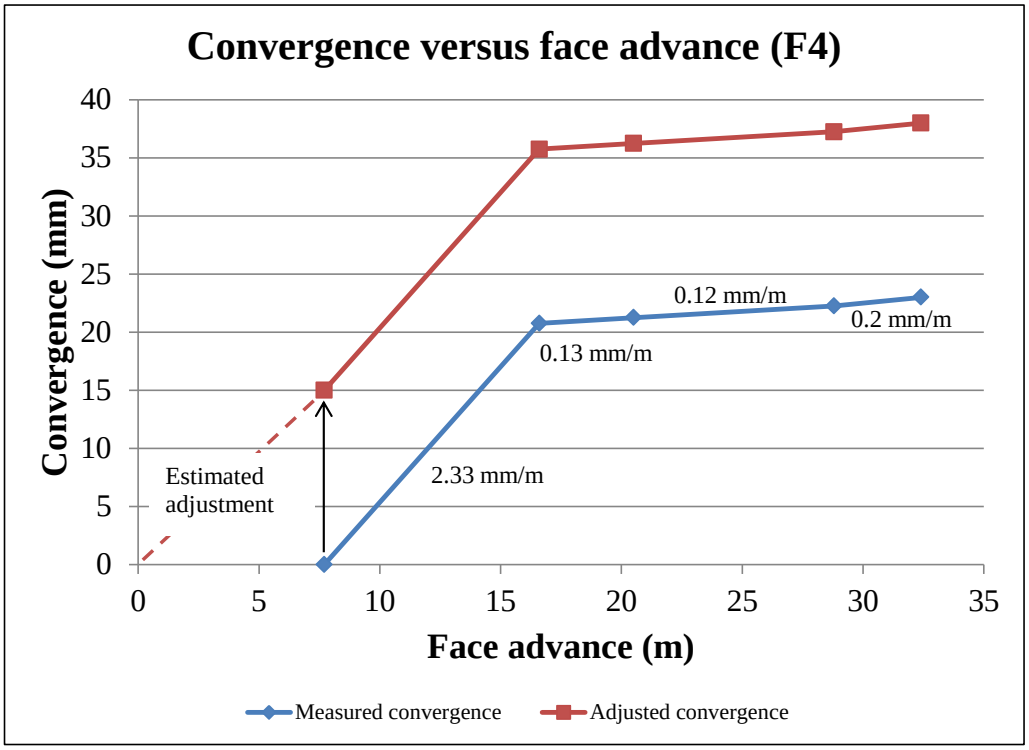

Figure 9.51: Convergence measured as a function of face advance at site F4 installed adjacent to pillar P1. The rate of convergence is also included on the figure.

9.3. Summary

The instrumentation programme during the trial was one of the most comprehensive monitoring exercises ever conducted at a crush pillar site in South Africa. The results have revealed new information regarding the behaviour of crush pillars. The instrumentation confirmed that a pillar reaches a residual state once the pillar is completely formed (holed). However, the pillars also experienced secondary reductions in stress when new pillars were formed closer to the face. This phenomenon is believed to be associated with the transfer of stress to the newly formed pillars. This unloading phase, has in the past, typically only been referred to as continued strain softening behaviour. However, it was found that at some point the pillars experienced no further reduction in stress whilst the pillars continued to deform. This observation was also verified by the convergence measurements. After all mining stopped, continued convergence was measured.

The objective of the stress measurements was to determine the peak and residual pillar stresses for the identified pillars as well as trends in relation to the pillar forming cycle. Both absolute and stress change measurements were conducted. This was conducted to determine the stress above a pillar before the pillar was formed (baseline measurement) and how the stress would change as pillars are formed (continuous measurements). The stress change data illustrated that the baseline values obtained above pillar P2 (18.2 MPa) was probably only relevant to the exact point of measurement. Pillar P2 demonstrated a reduction in vertical stress of 59.84 MPa, while pillar P3 experienced an overall reduction of 22.75 MPa. The numerical model used to back analyse the behaviour of the pillars in the trial section was used to provide a more appropriate baseline value above pillars P2 and P3. The model indicated a vertical stress of approximately 15 MPa above pillar P1 for the layout which existed at the time of the measurement. This agreed well with the measured 17.1 MPa. However, the baseline vertical stress magnitudes of pillar P2 and pillar P3 should have been approximately 70 MPa and 42 MPa respectively. The magnitude of the predicted vertical stress for pillar P3 was lower than predicted above pillar P2; however, pillar P2 also had the influence of the face in close proximity.

The stress change measured above each pillar was analysed by comparing changes in magnitude and orientation to events corresponding to each pillar forming cycle. Similar trends were identified for the three pillars. The key findings were:

- As the advancing face is approaching a pillar to the point where it is aligned with the new pillar position, the pillar has already experienced a significant reduction in vertical stress (23% - 64%).
- Whilst the pillar is being formed and until it is holed by the advancing face, the pillar experiences another reduction in vertical stress (28% - 41%). At this point the pillar has reached its true residual state (14.8 – 23.74 MPa).

- As mining continues and new pillars are formed, the instrumented pillars continued to experience a reduction in vertical stress (38% - 41%). This secondary reduction resulted in residual pillar stresses of 10.16 – 17.4 MPa.
- The underground observations at specific intervals of the pillar forming cycle could be related to the measured behaviour.
- The pillars were observed to experience continued deformation up to the point where the pillars were approximately 14 m in the back area. The measured change in vertical stress as a result of the secondary stress reductions occurred within 6 m of additional face advance (after the pillar had been formed). The pillars therefore continued to deform even though there was no further change in stress recorded above the pillars.
- Once pillar P4 was completely formed, there was no further change in vertical stress experienced by the instrumented pillars.

An interesting observation in the stress change data for pillars P1, P2 and P3 was the reduction in stress experienced by a pillar when new pillars were formed. This characteristic is attributed to load being transferred as new pillars are being formed. During this unloading phase the pillars continued to deform. The stress change data as well as the micro seismic pillar profiling indicated that once the pillars were formed, internally the pillars were already completely fractured even though it did not appear that way along the external surfaces of a pillar.

The maximum amount of pillar dilation measured was along pillar P4 (100 mm). The results of the pillar dilation and convergence measurements in the trial section (30 – 55 mm) appears to support the finding of Canbulat et al (2006); Pillar dilation is equal to approximately twice the amount of convergence.

Convergence was monitored with both closure stations and closure loggers. The instruments provided the means to determine the convergence experienced throughout the section as well as the time-dependent convergence in the active mining area. All of the continuous convergence measurements conducted had a similar profile. The events leading to changes in convergence could be compared to events in the mining cycle (pillar formation). The formation of pillars P2 and P4 caused an increase in the rate of convergence experienced at the various sites. The late pillar crushing experienced by pillar P3 was also evident in the measurements. Additional convergence was measured after all mining had stopped. There does therefore appear to be agreement between ongoing pillar deformation observed underground and the convergence experienced, even after a pillar has reached its minimum vertical stress. The most prominent findings were:

- Very few closure loggers or stations were installed close to the advancing mining face. The majority of the convergence measured reflect the change in convergence (additional convergence) in the back area (20 m behind the face) and not in the immediate face area (first 5 – 10 m).

- Measurements conducted at the closure stations installed 7.7 m behind panel E3 West indicated that most of the convergence experienced in the stope takes place in the first 15 m behind the face. The underground observations revealed that fractures along newly formed crush pillars would continue to dilate until the pillars were approximately 14 m in the back area.
- Ongoing deformation of pillar P4 contributed to the continued convergence experienced at the closure stations installed close to the face abutment (6.6 m behind the face). This demonstrates that pillar crushing does contribute to the convergence experienced close to the face.
- The convergence measured adjacent to newly formed pillars (e.g. pillar P2) was approximately 10 mm higher than adjacent to completely formed pillars (e.g. pillar P1).
- The convergence and convergence rates measured adjacent to the pillars were higher compared to the centre of the panel. Watson (2010) measured a similar response. He attributed it to footwall heave experienced adjacent to the larger pillars. The additional convergence measured at the Lonmin trial site did not account for the initial convergence experienced which took place prior to the installation of the instruments. The convergence along the first 10 m behind the face was estimated to be approximately 15 mm. This is based on the results of the measurements conducted close to the mining face.
- The maximum amount of additional convergence measured was 32 mm. This was adjacent to the west side of pillar P2.
- The results of the closure stations installed either side of instrumented pillars indicated that the side of the pillar which was exposed first experienced the most convergence. Underground observations also identified that the side of the pillar exposed first would experience the most fracturing and scaling. This was confirmed by measurements conducted at closure stations installed in the back area of the trial site where the lead lag layout first exposed the east side of the pillar as opposed to the west side as in the final mining section.
- The closure stations in the back area of the trial site indicated events contributing to increased convergence (10 mm) during a period when no mining was taking place. This can only be attributed to ongoing deformation processes within the adjacent pillars.
- The average rate of convergence was 0.4 – 0.6 mm / m of advance. This could differ from other crush pillar sites and will be influenced by mining depth and regional stability (impact on rock mass stiffness).

9.4. References

Canbulat, I., Grodner, N., Lightfoot, N., Ryder, J.A., Essrich, F., Dlokweni, A., Wilkinson, C., Krog, and G. Prohaska, G. (2006). The determination of loading conditions for crush pillars and the performance of crush pillars under dynamic loading. SIMRAC project SIM040302, Johannesburg.

Haile, A.T. and Jager, A.J. (1995). Rock mass condition, behaviour and seismicity in mines of the Bushveld Ignious Complex. SIMRAC final project report 027, CSIR, Johannesburg.

Lougher, D.R. (1994). An *in-situ* Investigation into the Behaviour of the Surrounding Rock Mass in a Hard Rock Pillar Mining Environment. M.Sc theses, University of the Witwatersrand, Johannesburg.

Malan, D.F., Janse van Rensburg, A.L. and D.P. Roberts (2005). Closure monitoring as a design and risk assessment tool in platinum mines. *3rd Southern African Rock Engineering Symposium*. South African Institute of Mining and Metallurgy Symposium Series 41. pp. 231–243.

Piper, P.S. and Flanagan, F.W. (2005). The *in-situ* performance of yielding pillars at Impala 12 shaft. *3rd Southern African Rock Engineering Symposium*. South African Institute of Mining and Metallurgy Symposium Series 41.

Roberts, D.P., Canbulat, I. and Jager, J.A. (2002). Design parameters for mine pillars: strength of pillars adjacent to gullies; design of stable pillars with w:h ratio greater than 6; optimum depth for crush pillars. SIMRAC final report, GAP617, SIMRAC, Johannesburg.

Roberts, D.P., Roberts, M.K.C. and Jager, A.J. (2005a). Alternative support systems for mechanised stopes. PlatMine project report 2004-0189, CSIR, Division of Miningtek, Johannesburg.

Roberts, D.P., Malan, D.F., Janse van Rensburg, A.L., Grodner, M.W., and Handley, R. (2006). Closure profiles of the UG2 and Merensky Reef horizons at various depths using different pillar types in the Bushveld Complex. Final project report, SIM 040207, SIMRAC, Johannesburg.

Ryder, J.A. and Özbay, M.U. (1990). A methodology for designing pillar layouts for shallow mining. *ISRM Symp: Static and Dynamic Considerations in Rock Engineering*, Swaziland.

Ogasawara, H., Katao, H., Hofmann, G. and de Bruin, P. (2012). Trial of the conical ended borehole overcoring stress measurement technique. *Proceedings SHIRMS 2012*, Perth, Australia.

Özbay, M.U. and Roberts, M.K.C. (1988). Yield pillars in stope support. *Proc. Rock Mechanics in South Africa*, SANGORM.

Watson, B.P., Ryder, J.A., Kataka, M.O., Kuijpers, J.S. and Leteane, F.P. (2007). Merensky and UG2 pillar strengths back-analyses. PlatMine report 1.2, CSIR, Johannesburg.

Watson, B.P. (2010). Rock Behaviour of the Bushveld Merensky Reef and the Design of Crush Pillars. PhD thesis, School of Mining Engineering, University of the Witwatersrand, Johannesburg, South Africa.

Watson, B.P. (2012). Personal communication.

York, G., Canbulat, I., Kabeya, K.K., Le Bron, K., Watson, B.P. and Wiliams, S.B. (1998). Develop guidelines for the design of pillar systems for shallow and intermediate depth tabular hard rock mines and provide a methodology and support requirements for the panels between pillars. SIMRAC final report, GAP334, SIMRAC, Johannesburg.

CHAPTER 10

BACK ANALYSIS OF THE UNDERGROUND TRIAL

10. BACK ANALYSIS OF THE UNDERGROUND TRIAL

The objective of this chapter is to determine if the observed and measured behaviour of the crush pillars in the trial site can be replicated by the limit equilibrium numerical model. In Chapters 4 and 5, a limit equilibrium model implemented in the TEXAN code was used to investigate the influence of various layout and rock mass parameters for an idealised crush pillar layout. The underground trial site, however, comprised of approximately 22000 m^2 of mined area, 55 crush pillars, as well as two regional dip pillars and four potholes. It is therefore a far more complex geometry that had to be simulated.

To date, no numerical modelling of a mine-wide tabular layout, which explicitly included a large number of crush pillars, has been done in South Africa. Simulating the observed and measured behaviour experienced in the trial site was therefore a significant challenge and this work is considered a major novel contribution of this PhD. The concept, initially tested by the author to determine the appropriateness of the method, proved successful (Du Plessis and Malan, 2011). Although there was a good correlation between the observed and measured behaviour of the crush pillars in the trial site, some of the results achieved, as highlighted in the previous chapters were questionable and had to be verified. Once calibrated, the application of the numerical model was useful to predict and verify the behaviour of the pillars. The model was especially valuable in evaluating the stress condition measured above the pillars, as well as the total amount of convergence experienced adjacent to the pillars and at the panel mid-spans.

10.1. Numerical model

The displacement discontinuity boundary element method (DDM) is a numerical technique that is very well suited to the analysis of large-scale tabular layout problems in which the plan projection of the mined area may cover several square kilometres. This technique has been successfully used for many years to simulate the deep tabular layouts of the South African gold mines. The DDM technique is not commonly applied to crush pillar layouts. While local failure and deformation mechanisms may be analysed using non-linear continuum plasticity finite element or finite difference models, these methods are difficult to apply and are not suited to the large-scale analysis of tabular stopes which include a large number of small pillars. An approach previously used was to approximate the effect of the crush pillars by a “backfill soup” (Kotze, 2005). This is not satisfactory as the effect of potholes for example cannot be simulated.

For early implementations of the DDM type of analysis in South Africa, the plan outline of a mined area was typically tessellated by square shaped elements that were superimposed on the mining and pillar outlines. Although this approach worked well for simulating the gold mine layouts with large stabilizing pillars, it is generally restrictive when considering the analysis of irregular layouts with very small pillars. At the edges of the pillars, this leads to “partially” mined elements that require special treatment. When very small crush

pillars are simulated, it requires very small element sizes which make the simulation of a large-scale layout impractical.

The DDM code developed by Napier (Napier and Malan, 2007), used in this study overcomes this problem by allowing the use of triangular shaped elements. The limit equilibrium model (Malan and Napier, 2006) implemented in the TEXAN code (as described in Chapter 3) was used to represent the behaviour of the reef material in the crush pillars. The model was able to approximate the behaviour of the crush pillars observed in the underground trial section by simulating the gradual crushing of the outside of the pillar and the transfer of stress to the intact core.

10.1.1. Modelling layout and parameters

The layout of the trial section comprising an area, 200 m on strike and 133 m on dip, as indicated in Figure 10.1 was digitised. The pillar and mining outlines were approximated using straight line polygons to enable the area to be easily discretised using triangular elements. The layout with the face positions (pre 2015) was simulated as step 0. Once mining resumed at the end of February 2015 four more pillars were cut by the advancing face of panel E3 West. Two of these pillars were instrumented. These pillars were included in the analysis through the addition of further mining steps. Pillars P2, P3 and P4 are formed in mining step 1, 2, and 3 respectively (each with approximately 6 m of advance). Mining step 4 (8 m advance) and 5 (14 m advance) represent the additional mining conducted to the final stopped face positions.

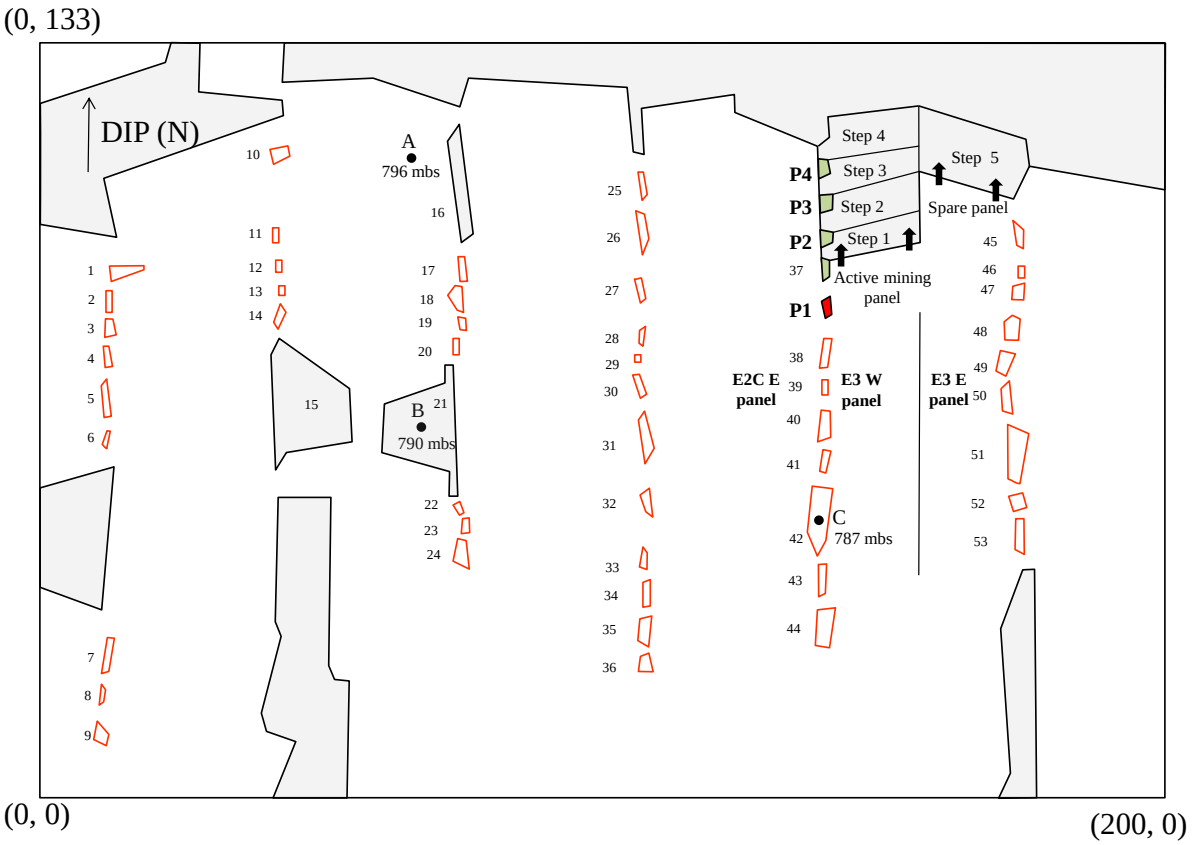

Figure 10.1: Modelling layout of the trial area. The crush pillars are shown in red. The newly formed pillars (P2, P3, P4) are shown in green. Mining steps 1 – 5 show the extraction of the final mining section.

The element sizes selected for the mining steps were approximately 1 m and the pillars were approximately 0.5 m. Various values were tested as inputs to the modelling parameters. The key outputs which had to be achieved by the model to replicate the underground behaviour were:

- Crushing of the pillars throughout the trial site,
- Pillar 37 was partially crushed whilst still part of the mining face,
- P42, an oversized pillar was not completely crushed and experienced footwall heave,
- Pillars located close to the down-dip bracket pillar was not crushed yet (i.e. pillar 45),

Table 10.1 shows the limit equilibrium modelling parameters. Due to the dip of the reef being flat (8 degrees), a dip of zero degrees was included in the model to simplify the analysis. Also, the horizontal stress was assumed to be the same in both directions. Initially, it was attempted to use the actual rock properties obtained from the rock specimen testing as detailed in Chapter 7 as the input parameters representing the pillar material (or rock material where the stress measurements were conducted). However,

it is difficult to relate laboratory values to the limit equilibrium model. Through successive cycles of parameter testing, the parameters as detailed in Table 10.1 presented a close approximation of the underground pillar behaviour. The results are shown in Figures 10.3 - 10.7 which satisfied the above-mentioned criteria. The figures indicate the average pillar stress (average of all collocation points within the pillar) for the respective pillar for each mining step.

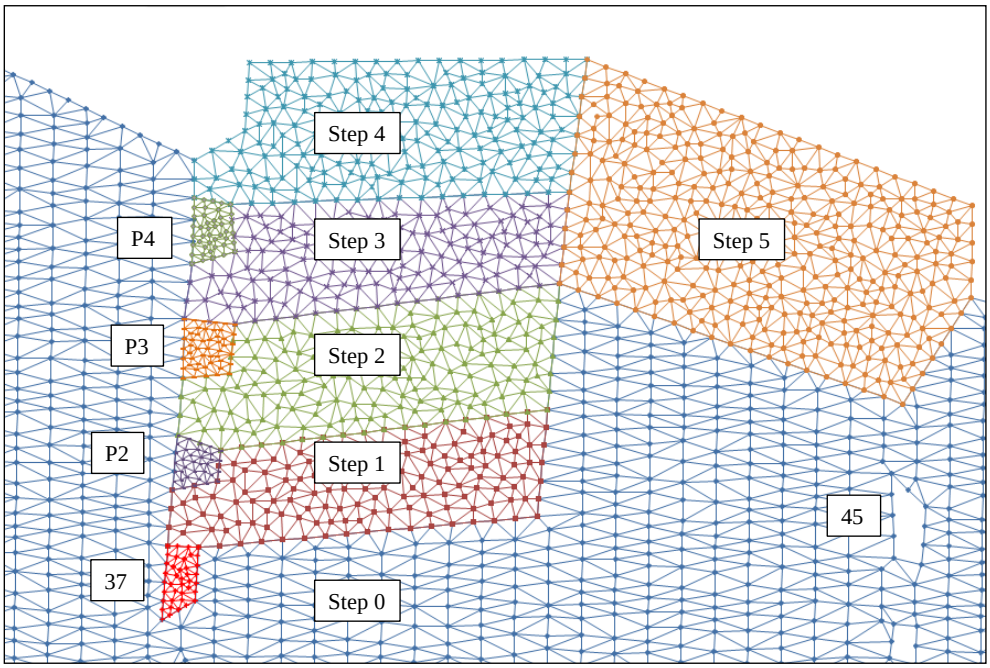

Figure 10.2: Part of the meshing of the mined area, mining steps and pillars of interest.

Table 10.1: Modelling parameters used for the limit equilibrium model.

Parameter	Value
Young's Modulus (MPa)	70 000
Poisson's ratio	0.25
Seam stiffness (MPa / m)	1 000 000
Dip (deg)	0
Mining depth (mbs)	782
Pillar height (m)	1.3
Vertical stress (MPa)	23.5
k-ratio	1.8
Intact material strength C_0 (MPa)	630
Crushed material strength C_b (MPa)	20
Intact slope (m_0)	8
Residual slope (m_b)	1
Friction angle (deg)	50

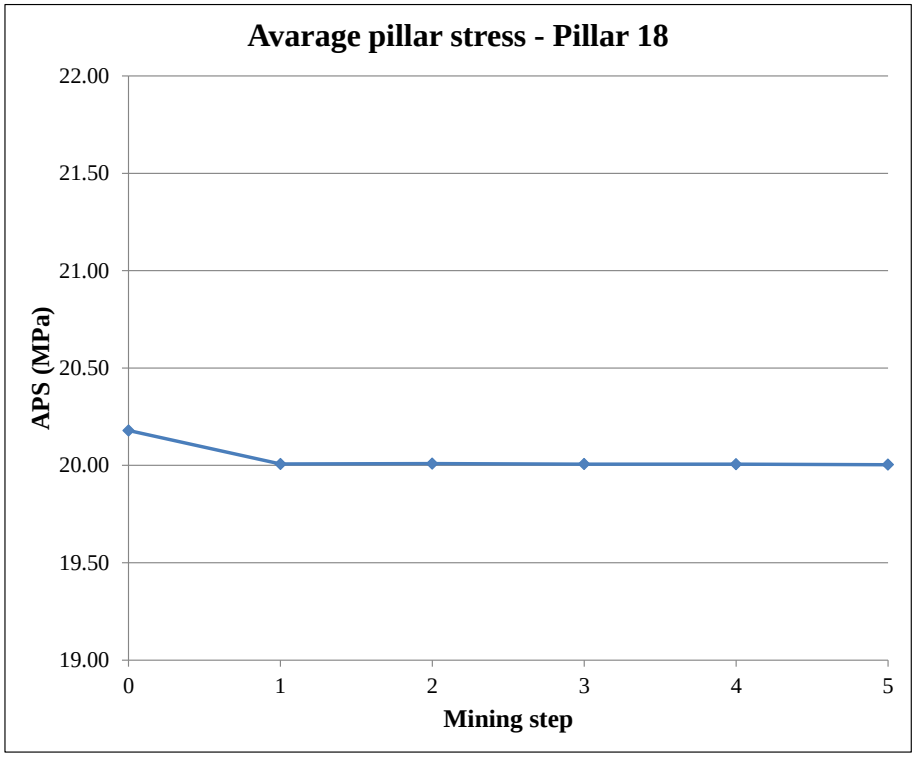

Figure 10.3: Example of a crush pillar at a residual state in the back area (pillar 18). Refer to Figure 8.12a for a photograph of this pillar. The pillar had a w:h = 1.38.

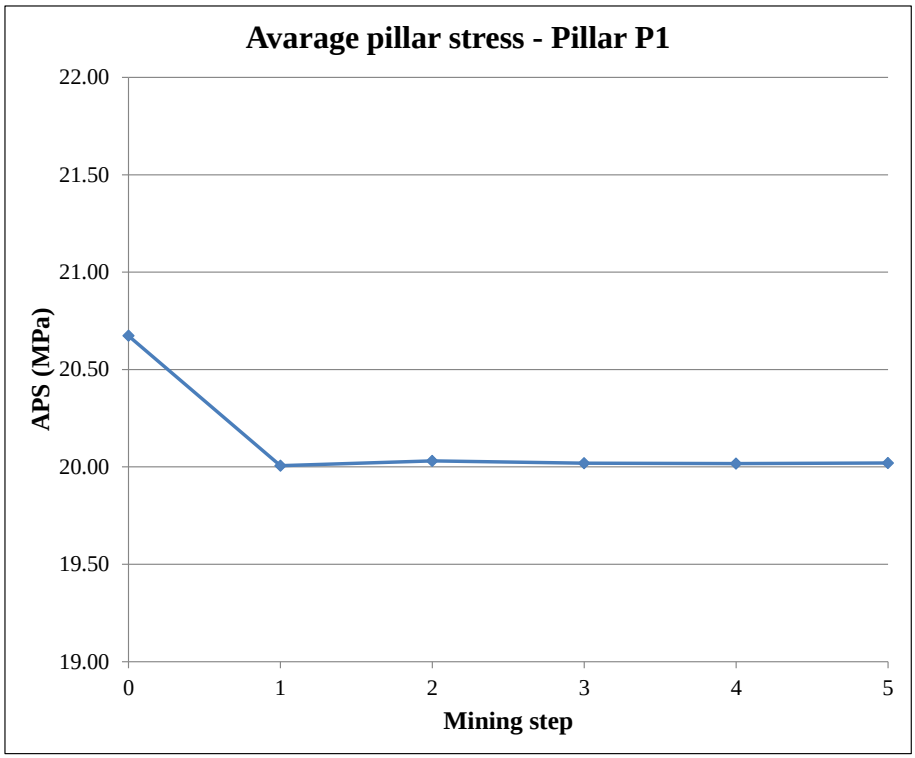

Figure 10.4: Pillar P1 already at a residual state. The pillar is situated 5 m behind the face position (step 0). Refer to Figure 8.12b for a photograph of the pillar.

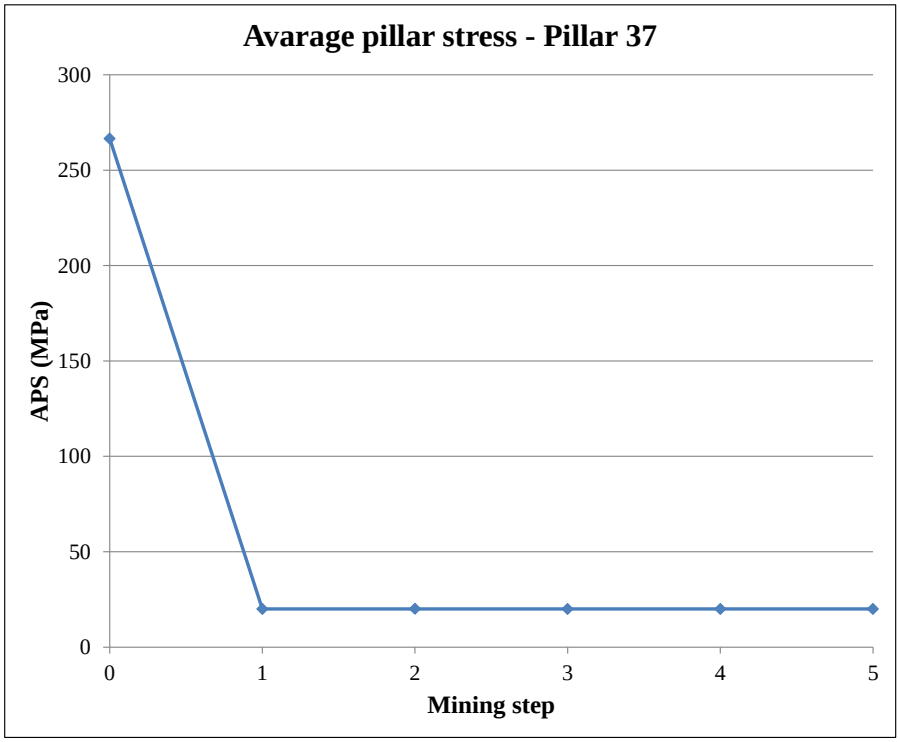

Figure 10.5: Pillar 37 is at a high initial state of stress whilst part of the mining face. The pillar completely fails in mining step 1 when the pillar is holed. Refer to Figure 8.19 for a photograph of the pillar.

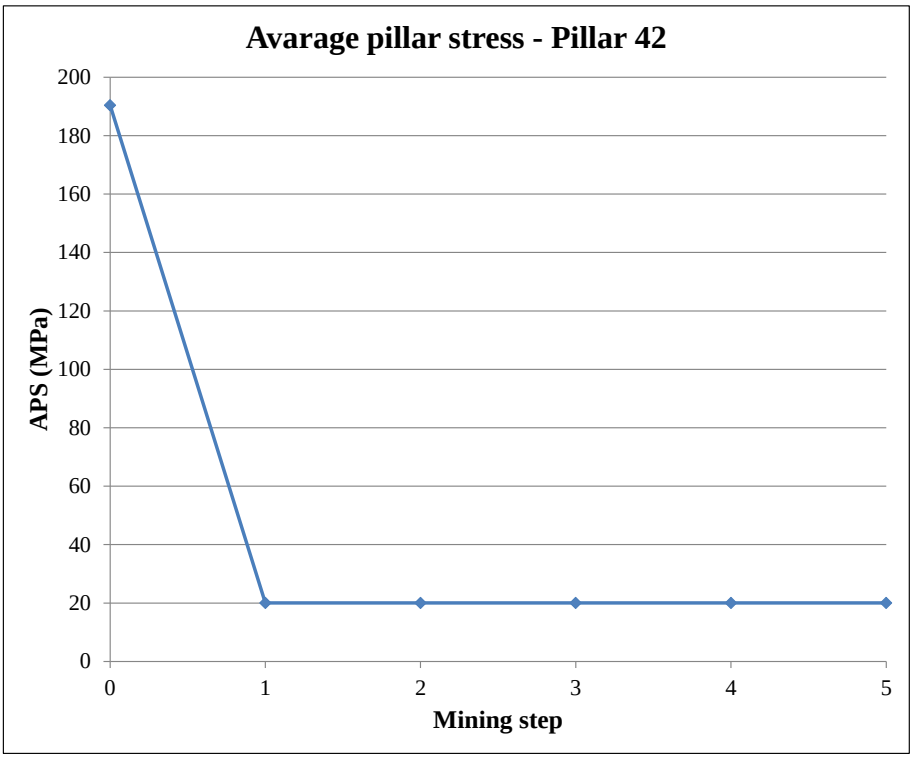

Figure 10.6: Pillar 42 at a high state of stress in the back area (w:h = 2.35). The pillar completely crushes as the mining face advanced. Refer to Figures 8.20 and 8.21 for photographs of the pillar.

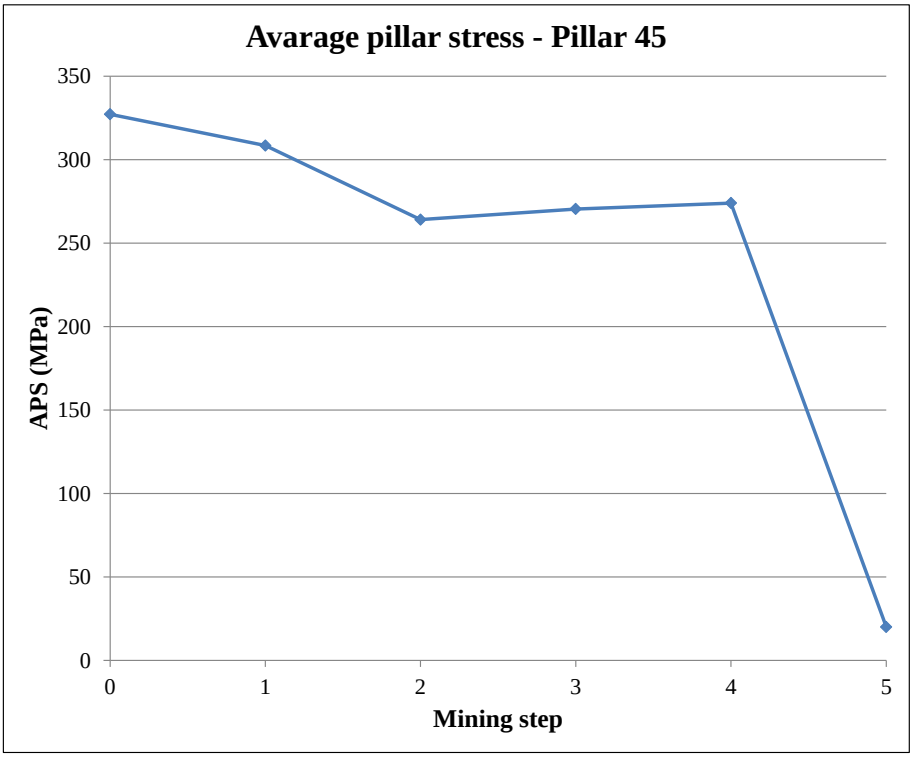

Figure 10.7: Pillar 45 situated close to the down-dip bracket pillar (4 m away) only crushes when the spare mining panel advanced (step 5) increasing the mining span.

Figures 10.3 – 10.7 illustrate the ability of the limit equilibrium model implemented in the TEXAN code to simulate the underground observed behaviour. Although the intact material strength selected was very high (630 MPa) it allowed the pillars to initiate pillar failure as experienced underground. The crushed material residual strength (20 MPa) controlled the residual stress achieved by the pillar once the pillar was in a completely failed state.

10.1.2. Pillar behaviour

As a comparison, two constitutive models were used to simulate the reef material. The first simulation was for an elastic rock mass where the pillars were simulated as a “rigid” material that did not allow any failure or deformation. For the second simulation, the limit equilibrium constitutive model was used. This model allowed failure and load shedding of the pillars.

The average pillar stress (APS) simulated by the elastic model is very high. The purpose of this analysis was to determine if pillar crushing would occur at the face and how the pillar stress would evolve once the pillar is formed and mining advances. Figure 10.8 compares the elastic model (rigid pillars) to the limit equilibrium model (crush pillars). Pillar P2 was selected to illustrate the evolution of pillar stress during the pillar forming process. P2 was initially part of the solid mining face abutment (Figure 10.1). The pillar is

partially formed during mining step 1 although still part of the mining face. The pillar is separated from the mining face during step 2. Figure 10.8 indicates the average pillar stress (average of all collocation points within the pillar) for pillar P2 for each mining step for both the elastic and limit equilibrium model.

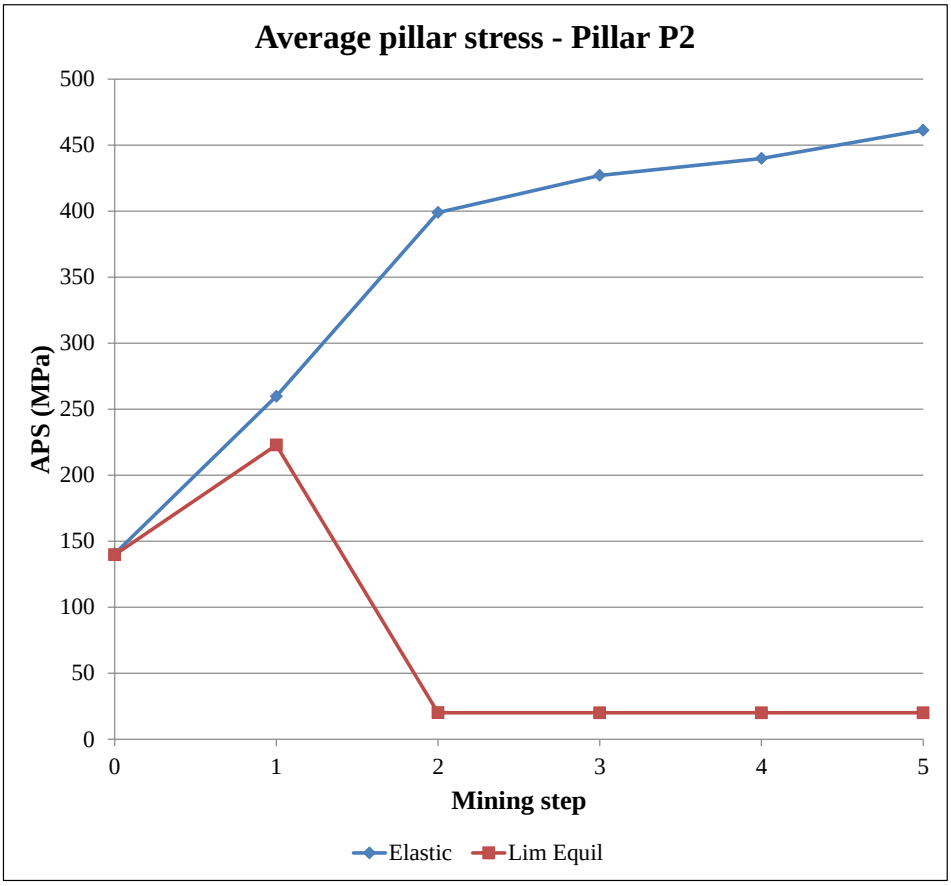

Figure 10.8: Average pillar stress for pillar P2; Elastic versus limit equilibrium model.

The non-linear profile of the curve for the elastic model is caused by the geometric effect of the pillar moving away from the mining face in each successive mining step. The stress starts off at a relatively low value when the pillar is still part of the face abutment. This stress rapidly rises after the mining step in which the pillar is formed. If the pillar is far away from the face, the change in stress caused by a mining increment is less compared to a pillar in close proximity to the face. This highlights a very important principle regarding crush pillar behaviour, namely, that it should be designed to crush in the face area. If the pillar does not crush and moves into the back area, the change in stress becomes less and the pillar may therefore never crush, especially if it is significantly oversized. Alternatively, pillar failure in the back area may occur violently as the stresses on the pillars are much higher and the loading environment has become much softer.

The limit equilibrium model illustrates that the pillar reaches a peak value when the pillar is formed during mining step 1 and then reduces to a residual state during step 2 as the pillar is separated from the mining face. The findings in Chapter 6 indicated that pillars require a sufficiently high initial stress level to ensure that the pillar can fail completely and move to a residual state. The peak strength of the pillar must be exceeded whilst the pillar is close to the mining face to cause complete failure of the core.

The behaviour simulated by pillar P2 (step 1) is qualitatively similar to what was observed underground for pillar 37 which was in a partially crushed state whilst still part of the mining face. The pillar has therefore reached or exceeded its peak strength.

Figure 10.10 considers a section a - a' through pillar P2 (as indicated in Figure 10.9) and shows the evolution of pillar stress during each mining step using the limit equilibrium model to simulate the crush pillar behaviour. Step 0 considers the stress through the 2 m solid abutment at the pillar position. Step 1 indicates the stress through the pillar whist the pillar is formed at the mining face and Step 2, when the mining face advances and the pillar moves 6 m in to the back area.

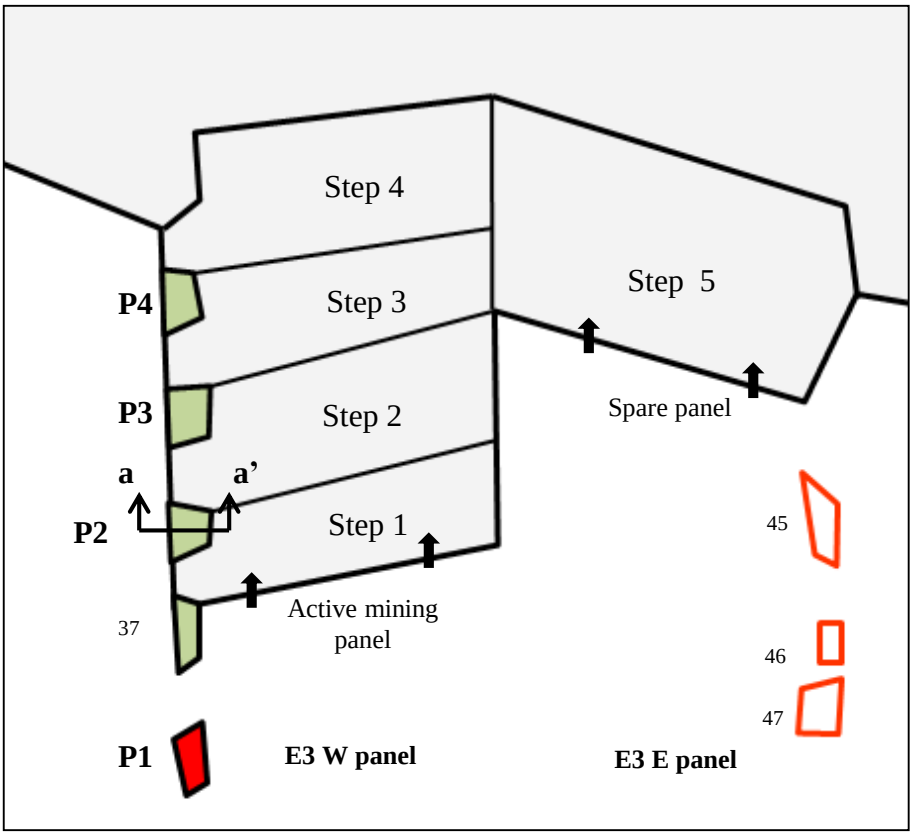

Figure 10.9: Area indicating final mining section extracted by mining steps 1 – 5.

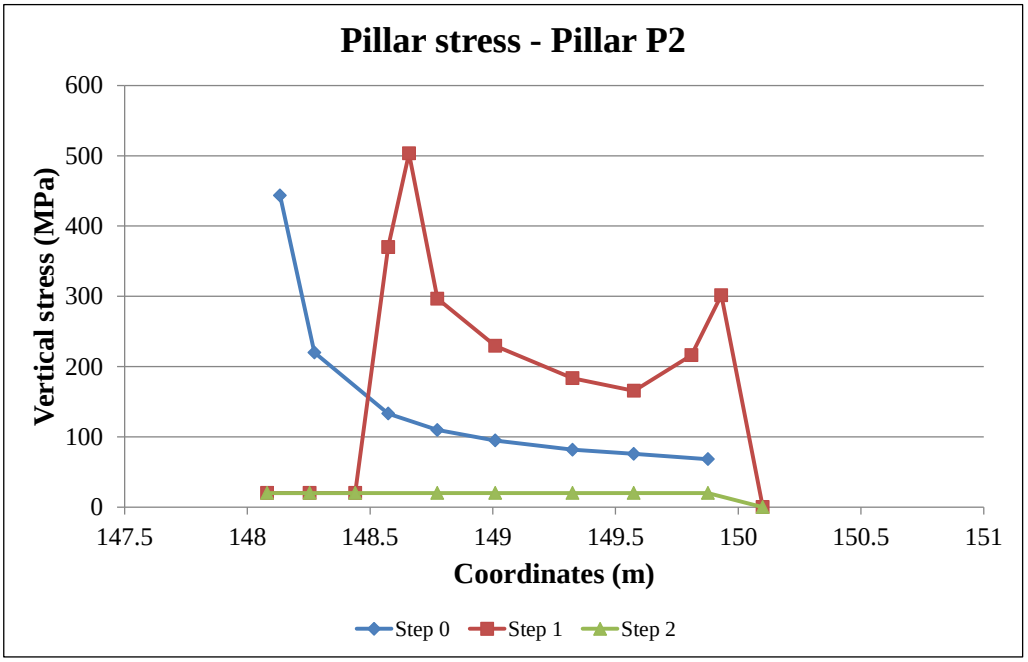

Figure 10.10: Development of pillar stress during the pillar formation cycle (pillar P2); section a – a' in Figure 10.9.

The results indicate:

- Step 0: High abutment stress along the exposed edge of the pillar. The stress is dissipated into the solid unmined ground ahead of the face.
- Step 1: Complete crushing of the outer 35 cm along the western side of the pillar. The pillar stress increases from the outer edges towards the centre of the pillar resulting in the high peaks indicated (57 cm from the western pillar edge). The core of the pillar, still presumably intact or in a partially crushed state is at a lower stress.
- Step 2: Complete failure of the pillar resulting in the residual state.

Similar stress profiles were obtained for pillar P3 and P4 as well. Pillar P3 failed during mining step 3 and pillar P4 failed during mining step 4; once the pillars were holed. Of interest is that the profile obtained for pillar P2 after mining step 1 indicates two potential zones of crushing. The outer 35 cm (at a residual stress) and the position of the peak stress at 57 cm (measured from the western pillar edge). This closely resembles the findings of the borehole camera log conducted through the pillar (refer to Figure 8.32).

The behaviour predicted by the model for pillar P2 also coincides with the continuous stress measurement and pillar fracturing profile for this pillar. In both cases, the results indicated that the pillar was at a residual or failed state once the pillar was fully formed. The model therefore appears to be useful to simulate the pillar behaviour.

Two noticeable underground observations prior to the extraction of the final mining section were the partially crushed condition of pillar 37 whilst still part of the face and the footwall heave experienced adjacent to pillar 42. Figures 10.5 and 10.6 indicate the modelled APS for these pillars (for all colocation points) for each successive mining step. As experienced underground, the pillars did continue to crush as the face advanced. The vertical stress profile for sections (similar to section a - a' through pillar P2) through pillar 37 and 42, prior to the extraction of the final mining section (step 0) are shown in Figures 10.11 and 10.12. The results indicate that pillar 37 was already experiencing some degree of crushing along the outer edges of the pillar.

Pillar 42 (3.05 m wide) was not completely crushed with the outer edges of the pillars failing, although the core of the pillar still appeared to be intact. This result agreed with the underground observations (refer to the photograph taken at the time; Figure 8.21a). The pillar being oversized (w:h = 2.35) situated approximately 40 m in the back area was behaving as a yield pillar. The unfailed pillar core, being at an elevated stress level, fractured the footwall rock. The failed foundation was observed as footwall heave adjacent to the pillar.

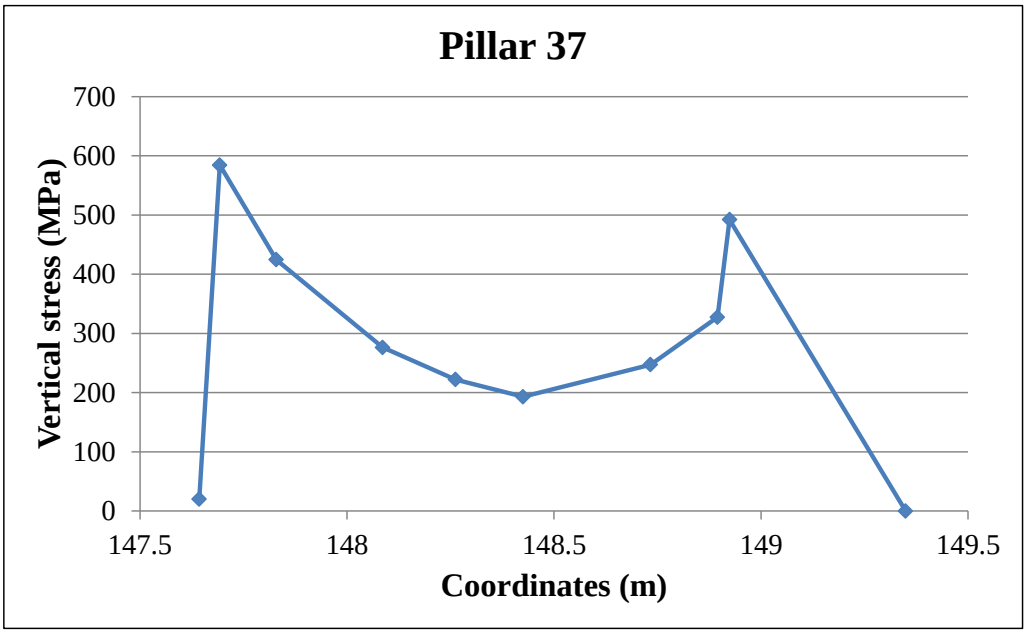

Figure 10.11: Vertical stress profile through the centre of pillar 37 (Step 0).

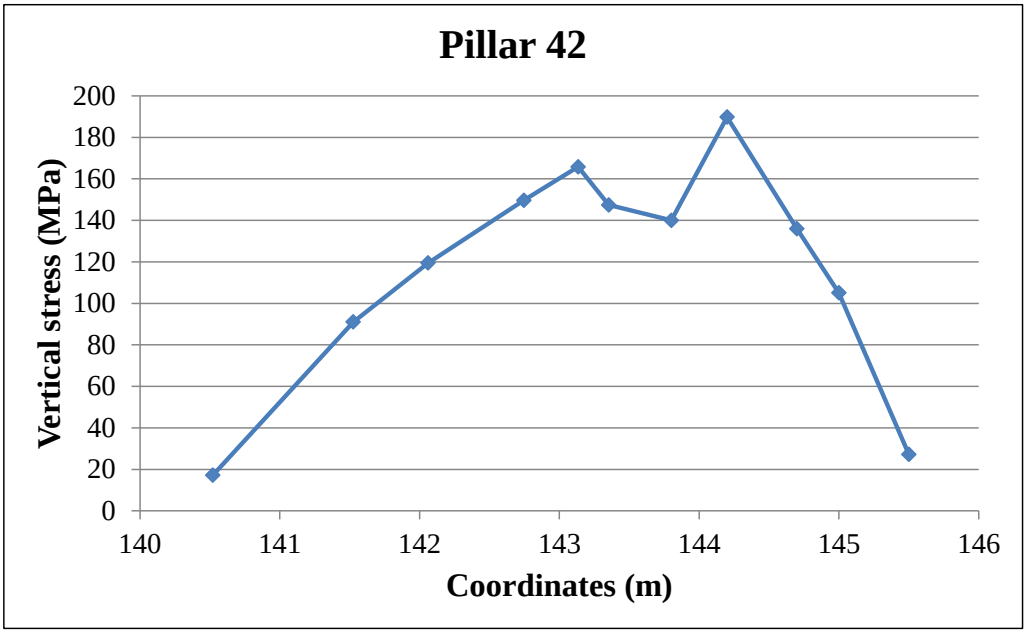

Figure 10.12: Vertical stress profile through the centre of pillar 42 (Step 0).

10.1.3. Measured versus modelled pillar stress

Stress measurements were conducted 4 m above the crush pillar positions. To simulate the stress state at the point of measurement, a horizontal plane was included 4 m above the reef. Figure 10.13 shows the result of the vertical stress along this plane across the entire trial area for mining step 0. The figure indicates that most of the pillars have zones of high stress along the centre of the pillars, even though the pillars are presumed to be fully crushed. This is an effect of the limit equilibrium model. The scale of the output generated does not show the exact detail per pillar and therefore sections are included in the subsequent figures to investigate the stress above particular pillars of interest. Note that even at 4 m above the reef there are still zones of tensile stress above the panels. If a comparative model is run and the crushed material strength is set to 8 MPa, this tensile zone slightly increases.

Figures 10.14 and 10.15 shows the modelling results for pillars P2 and P3 where stress change was simulated above each pillar. Pillar P2 was 3 m ahead of the mining face at step 0. As the face advanced (step 1) with the pillar still being part of the face, there is a slight reduction in vertical stress. This also coincides with the partial crushing of the pillar observed underground. As the pillar is fully formed (step 2), the vertical stress reduces to the residual level. Pillar P3 behaves similarly although the pillar is only completely formed in mining step 3. There is an increase in vertical stress between mining steps 0 and 1 as the mining face approaches the pillar. In the next mining step (step 2) the pillar being part of the face also experienced a reduction in vertical stress (partial pillar crushing). Once the pillar is fully formed (step 3) the vertical stress reduces to a residual level. The model indicated a stress drop of approximately 44 MPa above

each pillar. The measured stress change for pillar P2 was 59 MPa and pillar P3, 22 MPa. Pillar P3 was subjected to an increase in stress of approximately 8 MPa from when mining started to the point when the face was parallel with the pillar. The model also indicated this behaviour (step 0 – step 1) resulting in a vertical stress increase of about 5 MPa above the pillar position.

The modelling results, agreed well with the measured and observed behaviour and it appears that the limit equilibrium model is useful to simulate crush pillar behaviour.

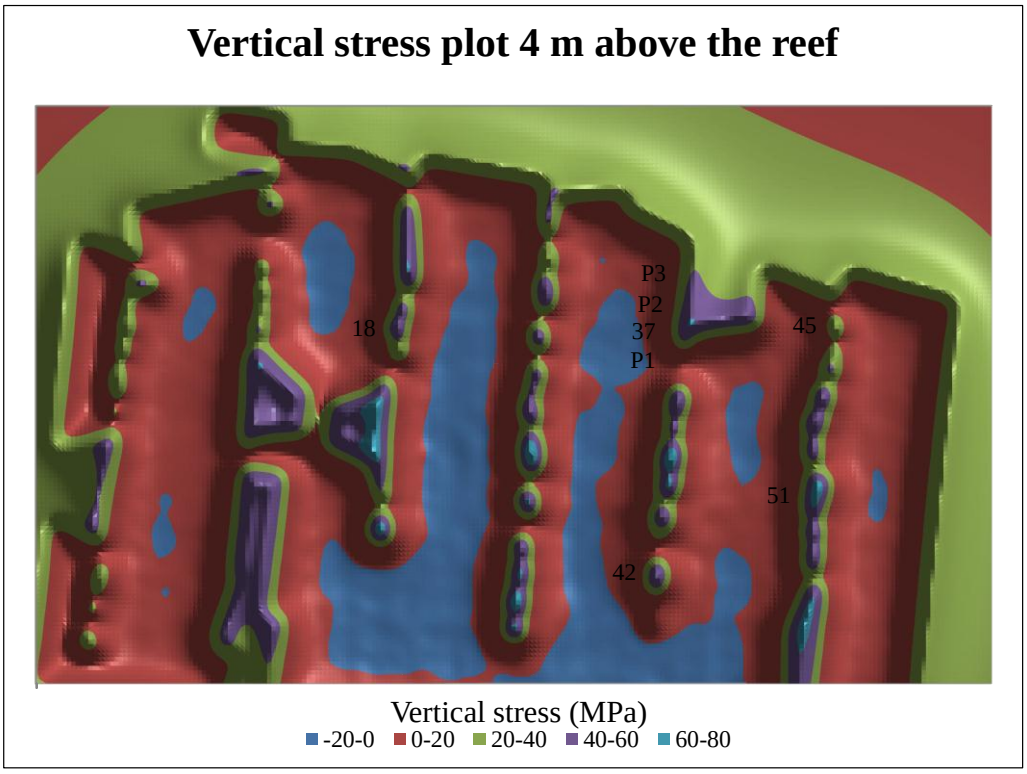

Figure 10.13: Vertical stress plot 4 m above the reef for mining step 0.

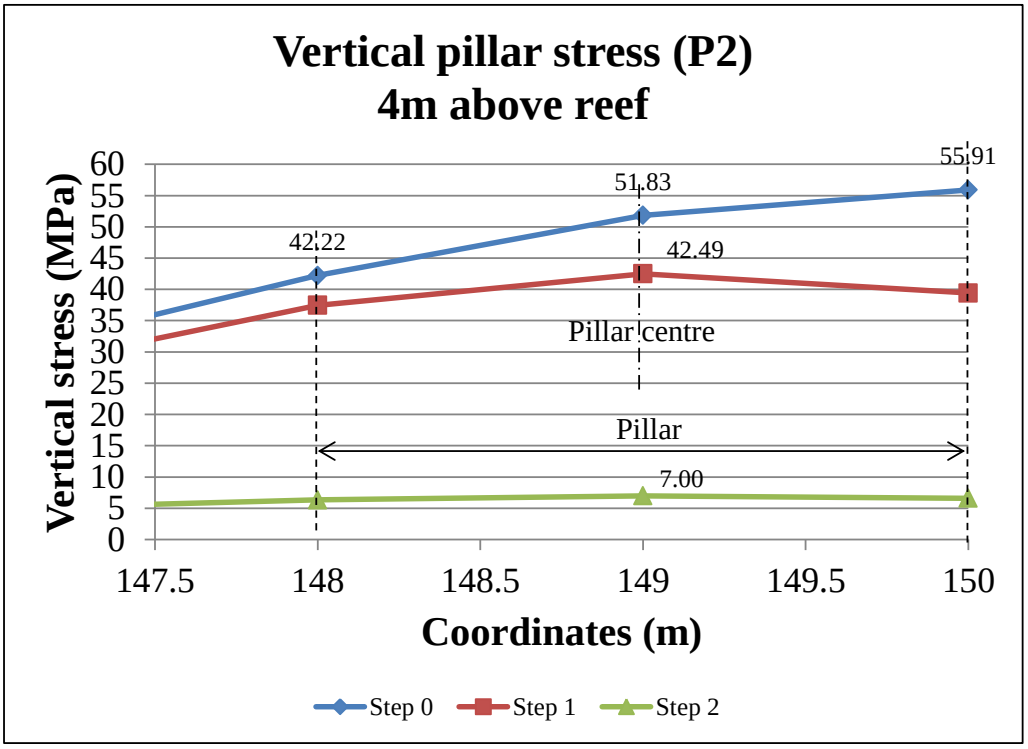

Figure 10.14: Vertical stress above pillar P2 per mining step.

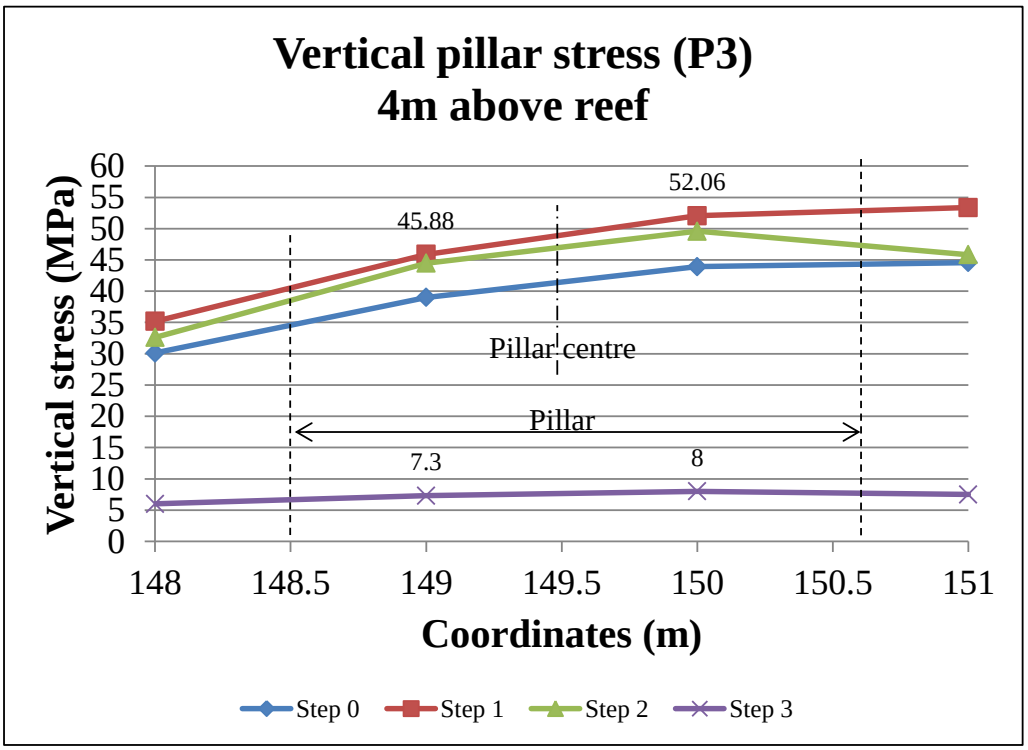

Figure 10.15: Vertical stress above pillar P3 per mining step.

10.1.4. Convergence

The convergence profiles for both the constitutive models (average of all the collocation points in the mining region) were similar (magnitude difference of 0.36 mm – 1.1 mm between models). Refer to Figure 10.16. The average convergence as predicted by the limit equilibrium model for mining step 0 was 17.5 mm. Figure 10.17 compares the convergence profile of the block defining mining step 1 (approximately 100 m^2 of mining). As can be seen from the figure, the incremental convergence resulting from mining is the highest closest to the face. As the mining face advances, the rate of convergence reduces. Table 10.2 normalises the convergence per meter mined. From approximately 18 m behind the face, the increase in convergence decreases substantially. The model used for the study did not have the capability to simulate the time dependent rate of convergence.

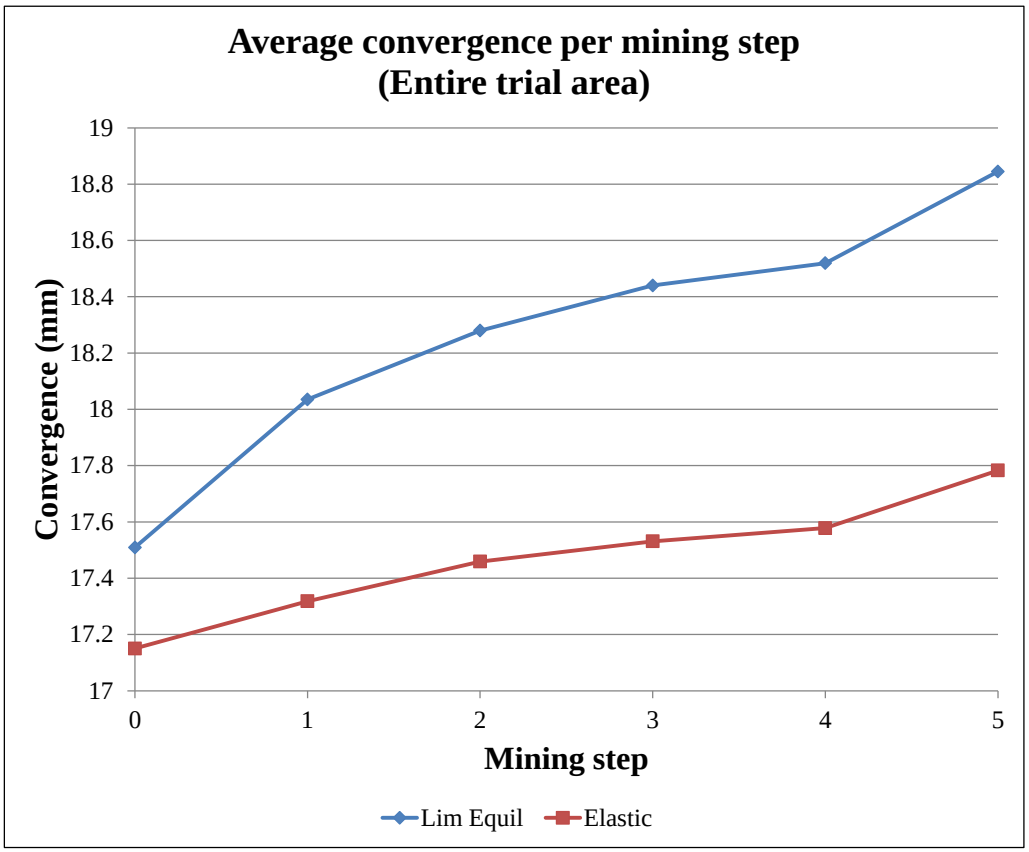

Figure 10.16: Convergence profile for the trial area. Limit equilibrium versus elastic model.

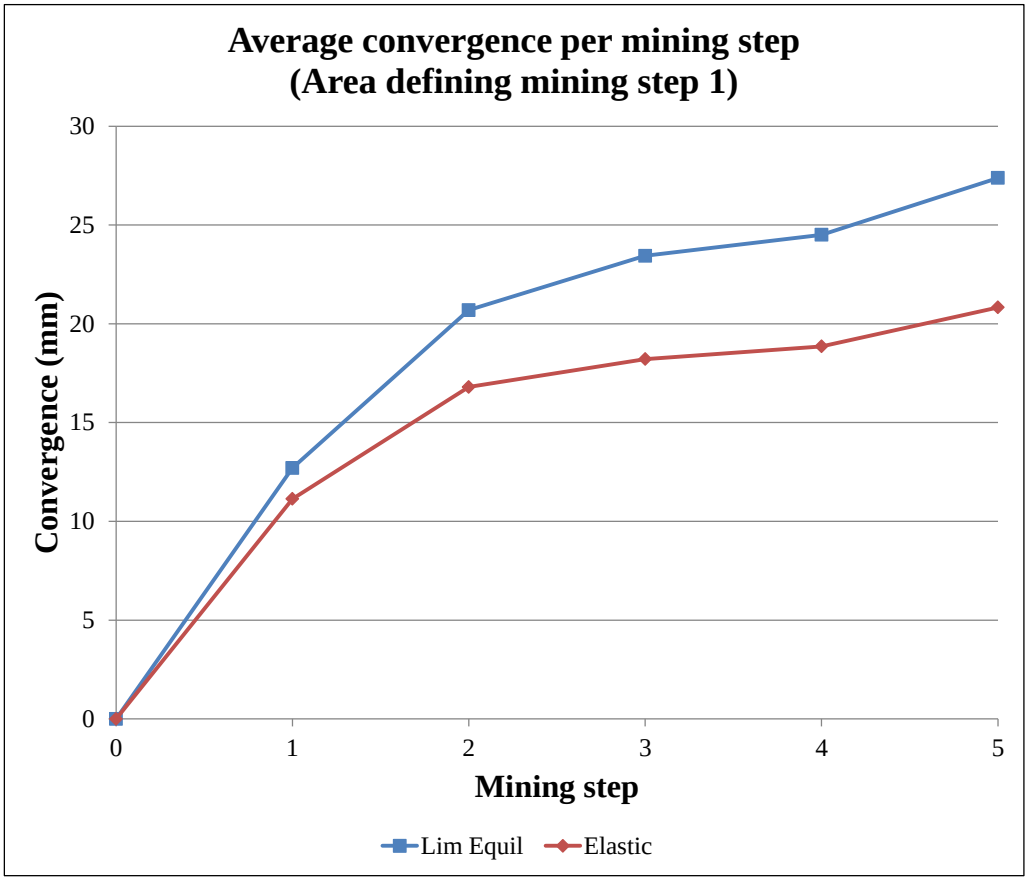

Figure 10.17: Convergence profile for the area defining mining step 1; Limit equilibrium versus elastic model.

Table 10.2: Geometric convergence rate for the limit equilibrium model as experienced in the block defining step 1.

Face advance (m)	Convergence rate (mm / m)
Step 1 (0-6)	1.86
Step 2 (6-12)	0.94
Step 3 (12-18)	0.24
Step 4 (18-26)	0.08

Section 9.2.4 presented the results of the actual underground convergence measurements. Refer to Figure 10.18 for the positions of the closure stations discussed below. Figure 9.51 illustrated the convergence which took place at site F4 (situated 7.7 m behind the face of panel E3 West) as a function of the advance of panel E3 West when mining resumed. However, the amount of initial convergence experienced prior to the installation of the closure stations (first 7.7 m) as well as the total amount of convergence experienced at this location were estimated based on the convergence results achieved along the closure stations (row E) which were installed close (6.6 m) to the stopped face abutment of panel E2C

East. The model was used to simulate the convergence at this location. The objective was to replicate the underground measurements and to understand what the "complete" convergence profile should look like considering the initial and measured convergence which occurred at a site.

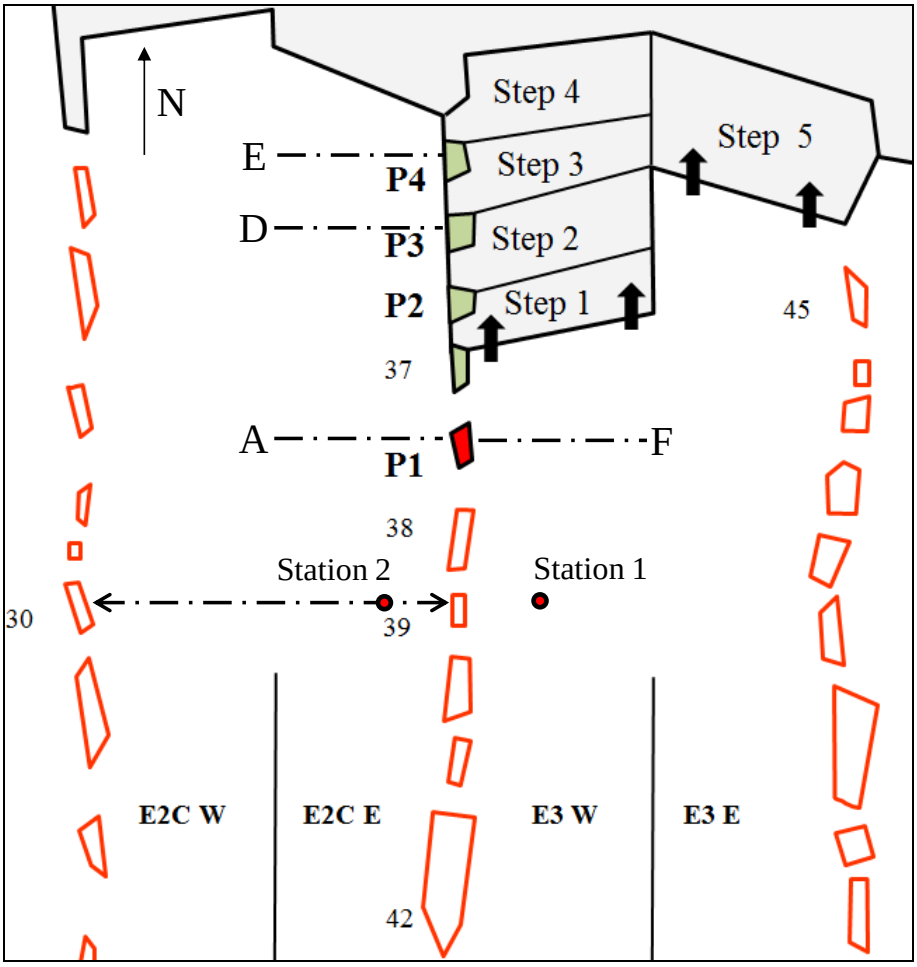

Figure 10.18: Layout indicating approximate position of the closure stations referred to in the modelling results.

The results of the measured versus modelled convergence profiles were compiled for closure station sites F4 and E4. Figure 10.19 indicates that the convergence profiles for the measured and modelled convergence at site F4 are similar. However, the model indicated that most of the convergence was occurring very close to the face. Figure 10.20 illustrates the simulated convergence profile from the face to the back area for panel E3 West at site F4, step 0. The figure indicates that the majority of the convergence is taking place along the 2 m immediately behind the face (14.45 mm). This is most likely a function of the limit equilibrium model which will also cause partial crushing of the face abutment. Increased convergence is therefore experienced. The measured convergence adjustment (15 mm) established from measurement at site E4 (refer to Figure 9.51) is slightly lower than the convergence indicated by the model to occur in the face area (20 mm).

Figure 10.21 indicates the simulated convergence profile per mining step at closure station E4. The convergence predicted by the model (step 0) at the site (13.95 mm) agrees well with the adjustment derived from the measurements (15 mm).

The measured and modelled convergence profile for site A2 situated 7.1 m west of pillar P1 in the mined out panel E2C is presented in Figure 10.22. The results illustrate that a significant amount of convergence occurred prior to the installation of the closure logger. The average variance between the measured and modelled results is 14 mm. It therefore agrees well with the adjustments predicted by the analyses of the other sites. Figure 10.23 compares the profile for the measured and modelled convergence at site D1 adjacent to pillar P3. The results are almost identical indicating that the convergence experienced adjacent to a newly formed pillar do not need adjustment as the majority of the convergence is as a result of the pillar crushing.

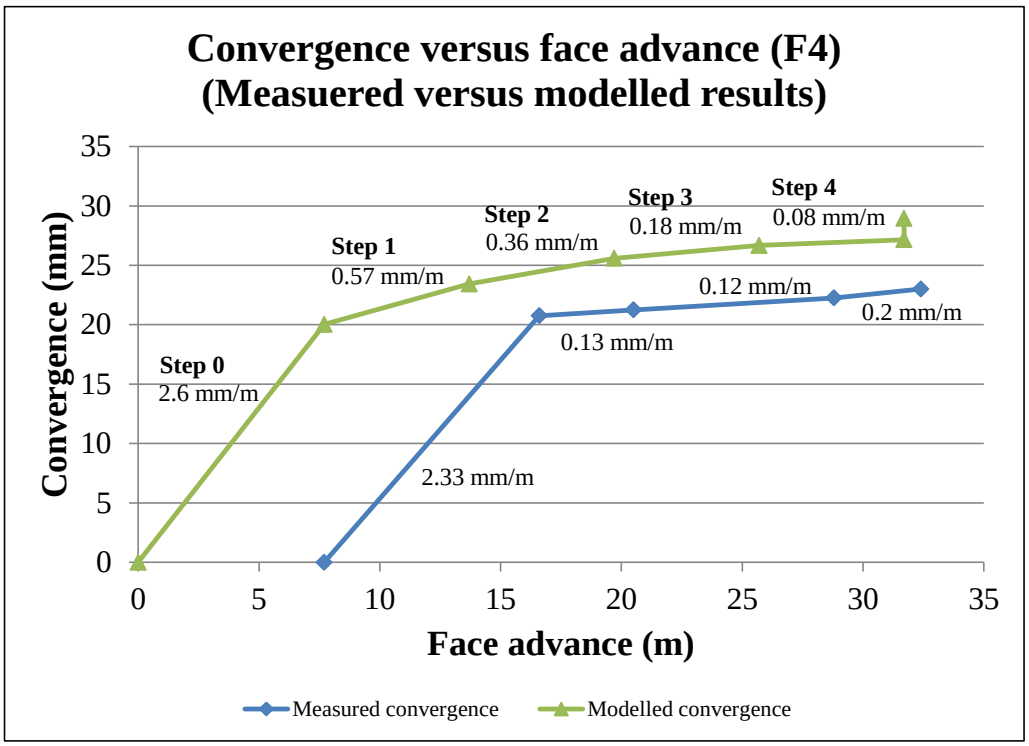

Figure 10.19: Measured versus simulated convergence measured at site F4. The closure station was aligned with pillar P1 and was installed 7.7 m behind the face (panel E3 West), prior to mining the final section.

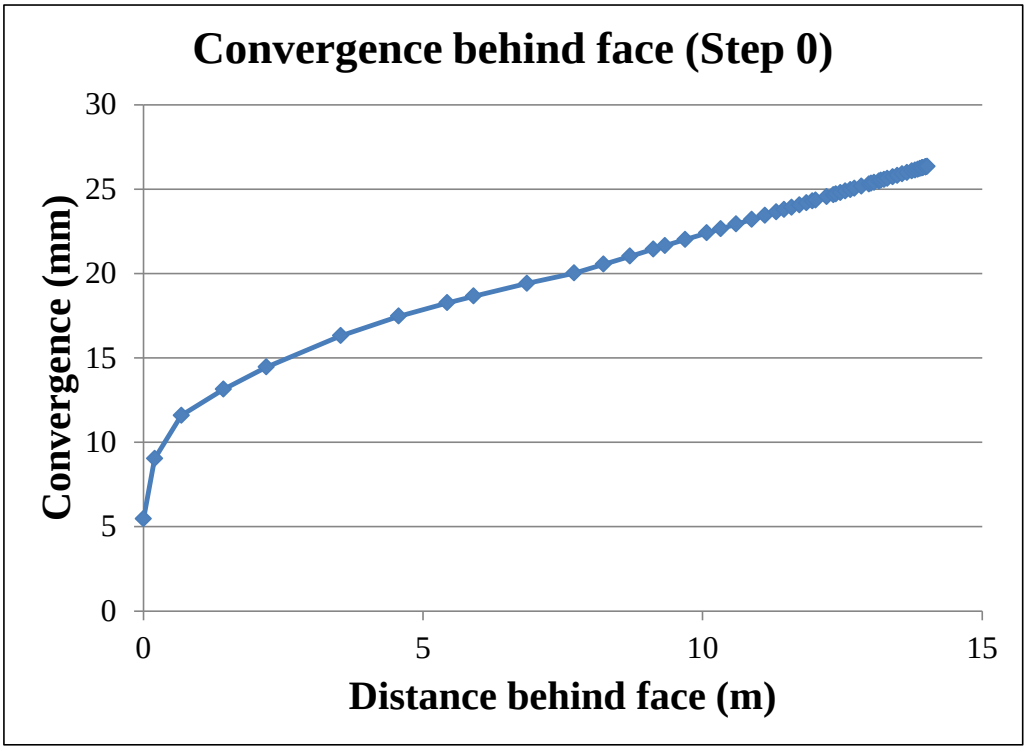

Figure 10.20: Simulated convergence behind the face of panel E3 West at site F4 prior to extracting the final mining section (step 0).

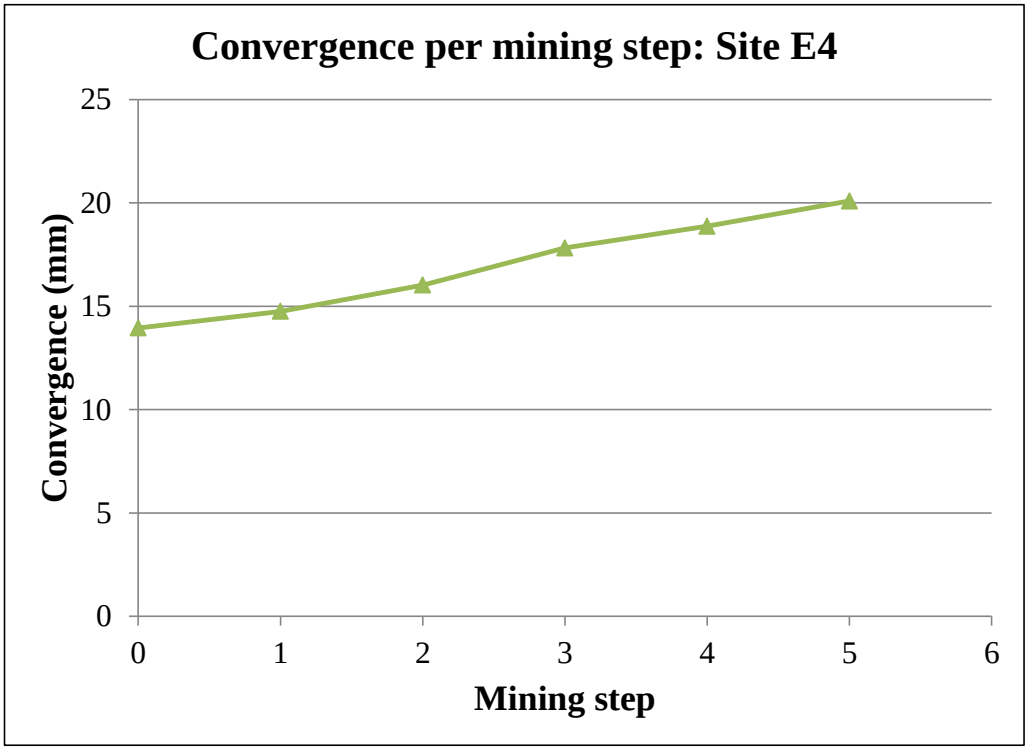

Figure 10.21: Simulated convergence profile at closure station E4, installed 6.6 m behind the face of stopped panel E2C East.

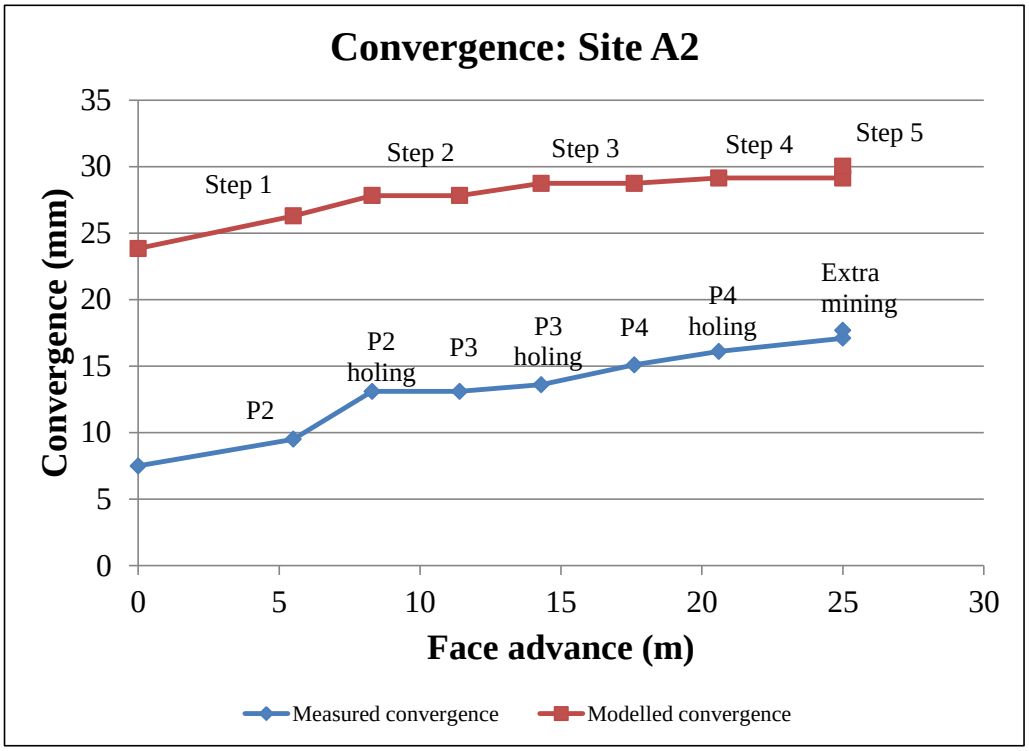

Figure 10.22: Measured versus modelled convergence at site A2 situated 7.1 m west of pillar P1 in the mined out panel E2C East. The average variance between the two profiles is 14 mm. The formation of the pillars as well as the corresponding mining steps is also included in the figure.

Figure 10.23 illustrates how the model approximates the measured convergence at site D1 adjacent to pillar P3. There is an increase in the measured convergence after pillar P4 is completely formed. As panel E3 West is advanced another 7 m, the convergence measured adjacent to the pillar continued to increase above the rate predicted by the model. The underground observations identified continued pillar deformation occurring in the back area of the stope. The measured convergence at the various sites also indicated continued convergence occurring after mining has stopped. The majority of the additional convergence experienced underground can therefore be attributed to continued pillar deformation.

Figure 10.24 illustrates the modelled convergence profiles in the panels either side of pillar P3. The pillar is partially formed in mining step 2 and holed in mining step 3. Once the pillar is completely formed the convergence adjacent to the pillar significantly increases (step 3). Steps 3 – 5 indicate convergence occurring across the pillar. Watson (2010) attempted to measure deformation taking place above and below a pillar by anchoring extensometers 4.2 m above and immediately below the pillar in a hole drilled through the pillar from a footwall drive below. The hangingwall measurement indicated 4.7 mm of compression to the point when the pillar was formed. As the face advanced and the pillar moved to the back area, the hole sheared,

resulting in additional compression measured (between 4 and 12 mm). Similarly, the measurement conducted below the pillar indicated a compression of approximately 6 mm occurring to the point when the pillar was formed. This hole also sheared as the face advanced. These results therefore indicate that the pillar can undergo approximately 10 mm of compression prior to the pillar being completely formed. As the pillar is formed and the face advances, internally the pillar continues to deform. This was also observed in the boreholes drilled through the pillars (refer to Figures 8.31 and 8.36) where the fractured slabs moved up or down relative to one-another. Observations at pillar P3 indicated some additional movement detected at the back of the borehole during the final mining (18 May). Additional movement will therefore be experienced post pillar formation. The value indicated by the model (23 mm) may therefore be appropriate. The mechanism contributing to additional compression or shearing is unfortunately not evident.

The convergence profiles, east versus west of pillar P3 shown in Figure 10.24 illustrate the difference in convergence experienced by the leading and lagging panel respectively. Once the pillar is completely formed and the pillar moves to the back area, sufficient mining span will result in the convergence experienced in both panels to be almost similar. However, as the underground measurements indicated, the side of the pillar exposed first will experience the most convergence. This is also illustrated in Figure 10.24.

Figure 10.25 shows the convergence profile across panel E2C between pillars 38 and 39. The maximum total convergence across the panel indicated by the model is 30.9 mm.

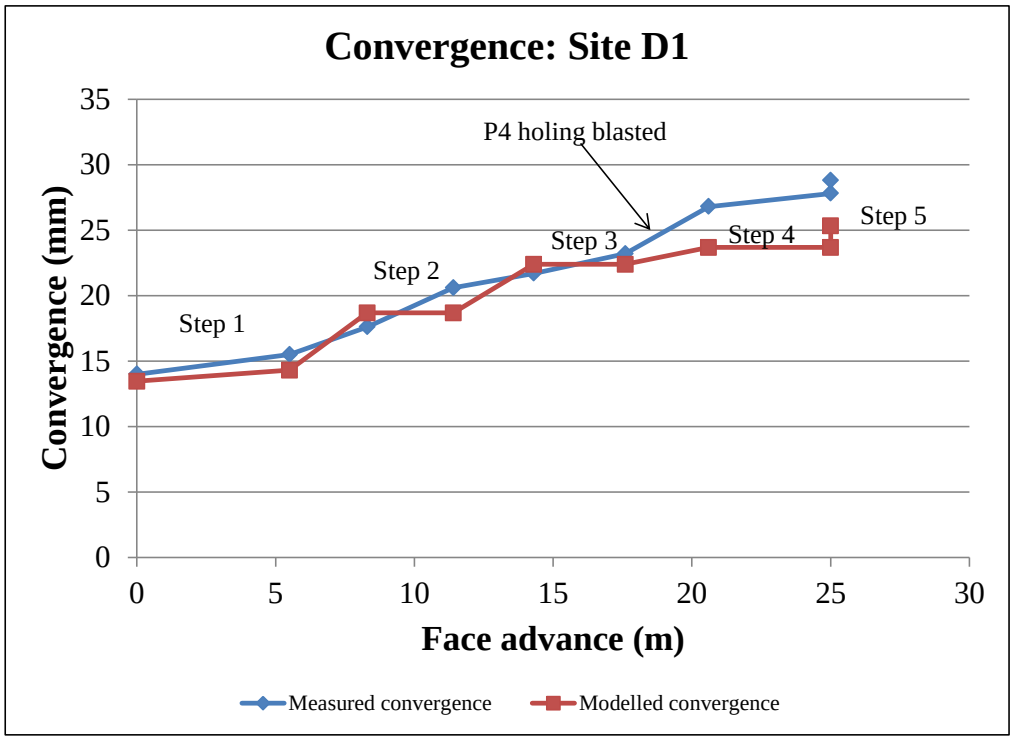

Figure 10.23: Measured versus modelled convergence measured at site D1 adjacent to pillar P3. The pillar is formed in mining step 2 and holed in mining step 3.

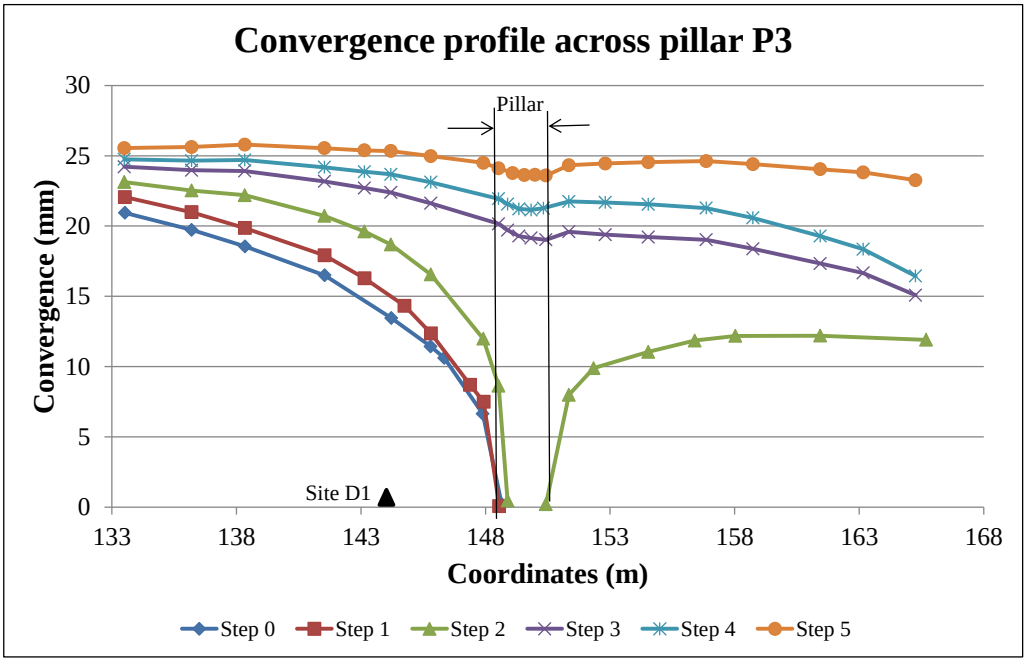

Figure 10.24: Modelled convergence across the panels either side of pillar P3. Pillar P3 is formed in mining step 2 and holed in mining step 3.

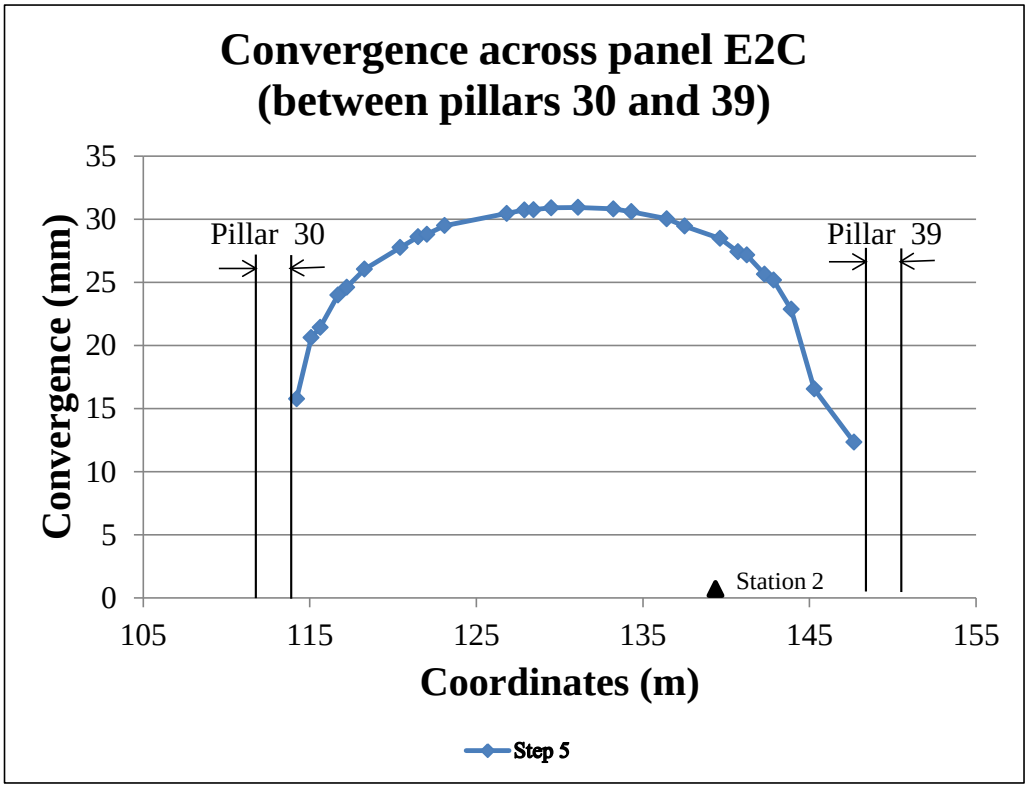

Figure 10.25: Convergence profile across panel E2C between pillars 38 and 39.

10.2. Summary

The results presented in this chapter validate the use of the limit equilibrium model implemented in the TEXAN code to simulate the behaviour of crush pillars on a large scale. To date, no numerical modelling of a mine-wide tabular layout, which explicitly included a large number of crush pillars, had been reported in South Africa. After a trial and error calibration of the model, both the observed and measured behaviour of the crush pillars in the trial site could be replicated. This was especially useful in evaluating the stress condition measured above the pillars as well as the total amount of convergence experienced adjacent to the pillars and at the panel mid-spans. It is nevertheless clear that calibration of this model will never be easy as a large number of parameters are involved. Future work will have to address this calibration issue.

The limit equilibrium model illustrated how pillars reach a high APS while being formed and then reduces to a residual state once the pillar was separated from the mining face. This agreed well with the findings of the continuous stress measurements and the pillar fracturing profiles for the instrumented pillars. In both cases, the results indicated that the pillar was at a residual or failed state once the pillar was fully formed.

The model indicated that the crush pillars were failing at an APS of between 220 – 270 MPa. Although this value is dependent on the choice of input parameters and the size of the pillar, it is also effected by the displacement discontinuity solution method where the stresses along the edges of the pillar will be infinitely high. The stress analysis indicated that there are portions of a pillar which may be subjected to much higher vertical stresses (above 500 MPa).

The model indicated a stress drop of approximately 44 MPa above newly formed pillars. The measured stress change for pillar P2 was 59 MPa and pillar P3 22 MPa. Pillar P3 also measured an increase in stress of approximately 8 MPa from when mining started to the point when the face was parallel with the pillar. The model also indicated this behaviour.

The modelled convergence profiles indicated that the majority of the convergence was occurring along the 2 m immediately behind the face (14.45 mm). The limit equilibrium model causing partial crushing of the face abutment contributed to this. The model indicated approximately 20 mm of convergence to take place in the face area. The model's predicted convergence profile adjacent to a pillar agreed well with the measured behaviour.

The model was used to back analyse the initial convergence which occurred at a closure station site in close proximity to the face prior to the measurements being conducted. The convergence predicted by the model at the site (13.95 mm) agreed well with the estimated adjustment derived from the measurements (15 mm). The model predicted a maximum convergence at the panel mid-spans of approximately 31 mm.

The convergence profiles, east versus west of a pillar illustrated the difference in convergence experienced by the leading and lagging panel respectively. Once a pillar is completely formed and the pillar moves to the back area, sufficient mining span will result in the convergence experienced in both panels to be almost similar. However, the underground measurements indicated, the side of the pillar exposed first will experience the most convergence (function of pillar fracturing).

10.3. References

Du Plessis, M. and Malan, D.F. (2011). A new approach to simulate crush pillar behaviour in a tabular layout. *Proc. 12th ISRM congress*, Beijing, China.

Kotze, T.J. (2005). A critical assessment of backfill as a means of representing the support resistance of panel pillars in MINSIM. Comments by T.J. Kotze on the initial assessment of the Impala yield pillars using a backfill soup to represent the pillar behaviour, as well as the various limmitations.

Malan, D.F. and Napier, J.A.L. (2006). Practical application of the TEXAN code to solve pillar design problems in tabular excavations. *SANIRE 2006 Symposium - Facing the Challenges*, Rustenburg, pp. 55-74.

Napier, J.A.L. and Malan, D.F. (2007). The computational analysis of shallow depth tabular mining problems. *J. South. Afr. Inst. Min. Metall.*, vol. 107, Nov 2007, pp. 725-742.

Watson, B.P. (2010). Rock Behaviour of the Bushveld Merensky Reef and the Design of Crush Pillars. PhD thesis, School of Mining Engineering, University of the Witwatersrand, Johannesburg, South Africa.

CHAPTER 11

CONCLUSION

11. CONCLUSION

The key objective of this PhD study was to improve our understanding of crush pillar behaviour. Past research was mainly focussed at determining the most critical factors believed to be the source of pillar instability. Merensky crush pillar sites are still nevertheless subjected to unpredictable pillar behaviour.

A major challenge in the design of crush pillar layouts is to integrate an appropriate representation of the pillar failure behaviour with the overall analysis of the tabular mining stress distribution. In this study, a limit equilibrium model was investigated as a representation of the reef material in crush pillars. Crushing of the outer portions of a pillar and the stress transfer to the pillar core can be replicated by this model. The objective was to use a simple representative model as an investigation tool of the behaviour of crush pillars. The limit equilibrium model implemented in the TEXAN displacement discontinuity boundary element code (DDM) provided a numerical modelling approach that could fulfil these requirements. A simple idealised crush pillar layout was used as a starting point to investigate the effect of various parameters on crush pillar behaviour. The impact of the rock and pillar properties, layout parameters, mining sequence and the effect of off-reef structures in a layout could be investigated. The purpose was to understand when pillars will crush, where they will crush relative to the mining face and why some pillars can potentially burst. The results indicated the ability of the code to simulate crush pillar behaviour.

An analytical solution derived by the author for this study to estimate the average pillar stress of a completely failed crush pillar was useful to approximate the behaviour of these pillars. The value of this analytical solution would be to provide a first order estimate of crush pillar dimensions. However, the predictions derived from the analytical solution is very dependent on the choice of input parameters such as material strength and friction angle. The results indicated that, in most cases, there is no relationship to actual laboratory defined rock properties if residual pillar stress measurements are to be approximated by the analytical solutions. The results of the numerical modelling were also compared to the analytical solution. Good agreement was obtained for the smaller w:h range pillars. The results indicated that the stress range of the larger pillars (w:h > 2:1) are not in agreement with the analytical solution. It is envisaged that the analytical solution may only be of use for pillars with low width to height ratios (w:h $\leq$ 2).

An underground crush pillar trial site was established on Lonmin's K3 shaft at a depth of approximately 782 mbs. The Merensky Reef, dipping at approximately 8 degrees was mined at an average mining height of approximately 1.3 m using conventional drill and blast techniques. The trial comprised an area of approximately 22000 m^2. During the trial, 55 crush pillars were cut with 87 percent of the pillars having a w:h ratio of less than 2:1 and only seven pillars with a w:h ratios greater than 2:1. The objective of the trial was to obtain a better understanding of the entire pillar system and the associated risks. The instrumentation

programme during the trial was one of the most comprehensive monitoring exercises ever conducted at a crush pillar site in South Africa. The monitoring included stress measurements, physical observations, photogrammetry, pillar borehole surveys, pillar dilation measurements, separation of potential partings in the hangingwall and pillar fracturing using micro seismic measurements. The measured behaviour was also related to the pillar condition as observed during the pillar forming cycle. The results have revealed new information regarding the behaviour of crush pillars. A distinctive failure pattern and sequence was identified in the failed pillars, some of which could be related to failure modes identified in failing pillars in other environments. Three modes of failure could be identified as being common namely, spalling (scaling), buckling along failure or fracture planes and the formation of conjugate failure planes (wedge-like structure).

The stress change measured above each pillar was analysed by comparing changes in magnitude to events corresponding to each pillar forming cycle. Similar trends were identified to exist between the three instrumented pillars. The instrumentation confirmed that a pillar reaches a residual state once the pillar is completely formed (holed). However, the pillars also experienced secondary reductions in stress when new pillars were formed. This phenomenon is believed to be associated with the transfer of stress to the newly formed pillars. This unloading phase, has in the past, typically only been referred to as continued strain softening behaviour. The stress change data as well as the micro seismic pillar profiling indicated that once the pillars were completely formed (holed), internally the pillars were already completely fractured even though it did not appear that way along the external surfaces of a pillar. However, it was found that at some point the pillars experienced no further reduction in stress whilst the pillars continued to deform. This observation was also verified by the convergence measurements. After all mining stopped, continued convergence was measured. The closure stations in the back area of the trial site indicated events contributing to increased convergence (10 mm) during a prolonged period when no mining was taking place. This can only be attributed to ongoing deformation processes within the adjacent pillars.

The back analysis of the underground trial site validated the use of the limit equilibrium model implemented in the TEXAN code to simulate the behaviour of crush pillars on a large scale. To date, no numerical modelling of a mine-wide tabular layout, which explicitly included a large number of crush pillars, had been reported in South Africa. Initially, it was attempted to use the actual rock properties obtained from the laboratory testing as the input parameters representing the pillar material. However, the intact and crushed material residual strength are mostly responsible for the onset of pillar failure and the residual stress state achieved by the model. Through successive cycles of parameter testing, the modelling parameters selected provided simulated results which closely resembled the observed underground pillar behaviour. After this trial and error calibration of the model, both the observed and measured behaviour of the crush pillars in the trial site could be replicated. This was especially useful in evaluating the stress condition measured above the pillars as well as the total amount of convergence experienced adjacent to the pillars and at the panel

mid-spans. The limit equilibrium model illustrated how pillars reach a high APS while being formed and then reduces to a residual state once the pillar was separated from the mining face. This agreed well with the findings of the continuous stress measurements and the pillar fracturing profiles for the instrumented pillars.

Observed and measured behaviour of crush pillars

The observed and measured behaviour of the crush pillars in the trial site provide parameters to benchmark the performance of the pillar system against. It can therefore be used as a guide to understand how to identify acceptable pillar behaviour.

During the extraction of the final mining section, three additional pillars were formed. Two of these pillars were extensively instrumented. The objective was to relate the observed pillar condition at specific intervals of the pillar forming cycle to the measured behaviour. The most prominent observations during the formation of the pillars were that fractures were observed to form parallel to the surface of the exposed abutment approximately 9 m ahead of the lagging face position. These fractures would increase as the lagging face advanced. By the time the face was aligned with the pillar, the fracture planes were spaced approximately 30 – 50 mm apart along the outer metre of the pillar (from the exposed surface of the pillar). These fractures would start to open (5 - 10 mm) as the pillar was being formed. Little to no scaling or slabbing was visible along the side of the pillar which was exposed by the advance of the lagging face. New fractures did form along this side of the pillar, only when the pillar was 3 - 7 m in the back area. In most cases these new fractures were spaced more than 100 mm apart and extended to approximately half the pillar width. These fractures started to dilate when the pillar was approximately 10 m in the back area. It did not result in any observed scaling or slabbing of the pillar surface along this side of the pillar. Continued pillar deformation was observed until the pillar was approximately 14 m in the back area. The underground observations at specific intervals of the pillar forming cycle could be compared to the measured behaviour.

The observations throughout the trial site identified similar patterns regarding the general pillar behaviour, namely:

- The composition of the pillar, including the exposed hangingwall rock, influenced the pillar behaviour.
- The fracture intensity was more profound on the side of the pillar which was mined first.
- Buckling of the fractured slabs were either along the top or the bottom of the pillar depending on the mining sequence. Pillars which fractured towards the west had the fractured slabs buckling closer to the footwall. In contrary, pillars which fractured towards the east had the fractured slabs buckling closer to the hangingwall.
- Pillars were observed to be partially fractured whilst being formed at the mining face. This indicated that the stress was sufficiently high to initiate early pillar crushing.

- Pillars that were completely fractured throughout comprised of fracture planes spaced approximately 30 - 50 mm apart.
- A wedge-like structure or failure plane was observed where fractures intersected each other approximately halfway through the pillar.

The continuous stress measurements indicated that as the advancing face approaches a pillar to the point where it is aligned with the new pillar position, the pillar has already experienced a significant reduction in vertical stress (23% - 64%). Whilst the pillar is being formed and until it is holed by the advancing face the pillar experiences another reduction in vertical stress (28% - 41%). At this point the pillar has reached its true residual state (14.8 – 23.74 MPa). As mining continues and new pillars are formed, the instrumented pillars continued to experience a reduction in vertical stress (38% - 41%). This secondary reduction resulted in residual pillar stresses of 10.16 – 17.4 MPa. The measured change in vertical stress as a result of the secondary stress reductions occurred within 6 m of additional face advance (after the pillar had been formed). Once the final pillar had been formed (pillar P4), there was no further change in vertical stress experienced by the instrumented pillars. The pillars nevertheless continued to deform even though there was no further change in stress recorded above the pillars.

Both absolute and stress change measurements were conducted approximately 4 m above the three instrumented pillars. This was done to determine the stress above a pillar before the pillar was formed (baseline measurement) and how the stress would change as pillars are formed (continuous measurements). Pillar P2 measured a reduction in vertical stress of 59.84 MPa, while pillar P3 measured an overall reduction of 22.75 MPa. The objective of the stress measurements was to determine the peak and residual pillar stresses for the identified pillars. The numerical model was used to validate the baseline value at the point of measurement above each pillar. The model indicated a vertical stress of approximately 15 MPa above pillar P1 (completely formed) for the layout which existed at the time of the measurement. This agreed well with the measured 17.1 MPa. The stress change data confirmed that the baseline magnitude obtained above the anticipated position of pillar P2 (18.2 MPa) was only relevant to the exact point of measurement. The model and stress change measurements indicated that the baseline vertical stress magnitudes of pillar P2 and pillar P3 should have been approximately 70 MPa and 42 MPa respectively.

All of the continuous convergence measurements conducted had a similar profile. The events leading to changes in convergence could be related to events in the mining cycle (pillar formation). Measurements conducted at the closure stations installed 7.7 m behind panel E3 West indicated that a significant part of the convergence experienced in the stope occurred in the first 15 m behind the face. The underground observations revealed that fractures along newly formed crush pillars would continue to dilate until the pillars were approximately 14 m in the back area. In some cases, closure loggers or stations could not be installed close to the advancing mining face. Then, the majority of the convergence measured at these sites

reflect the change in convergence (additional convergence) in the back area (20 m behind the face) and not in the immediate face area (first 5 - 10 m). The convergence anticipated to take place along the first 10 m behind the face was estimated to be approximately 15 mm. This is based on the results of the measurements conducted close to the mining face. The convergence predicted by the model at the site (13.95 mm) agreed well with the estimated adjustment derived from the measurements.

The convergence and convergence rates measured adjacent to the pillars were higher compared to the centre of the panel. The additional convergence measured did not account for the initial convergence which occurred prior to the measurements being conducted. The model's predicted convergence profile adjacent to a pillar agreed well with the measured behaviour. This indicated that convergence alongside the pillars only started to occur once the pillars started to crush. The convergence measured adjacent to newly formed pillars (e.g. pillar P2) was approximately 10 mm higher than adjacent to completely formed pillars (e.g. pillar P1).

Ongoing deformation of pillar P4 contributed to the continued convergence experienced at the closure stations installed close to the face abutment (6.6 m) of panel E2C East. This does demonstrate that pillar crushing contributes to the convergence experienced close to the face. Furthermore, the results of the closure stations installed either side of instrumented pillars indicated that the side of the pillar which was exposed first experienced the most convergence (related to fracturing sequence). This was confirmed by measurements conducted at closure stations installed in the back area of the trial site where the lead lag scenario firstly exposed the east side of the pillar as opposed to the west side as in the final mining section. The underground observations identified that the side of the pillar exposed first experience the most fracturing and scaling. Therefore, an amount of convergence experienced at a crush pillar site appears to be related to the pillar fracturing process. The maximum amount of additional convergence measured was 32 mm. This was adjacent to the west side of pillar P2.

The model predicted a maximum convergence at the panel mid-spans of approximately 31 mm. Although the model's predicted total amount of convergence is lower than the measurement at the two closure stations situated in the back area of the trial site (approximately 55 mm), the impact of pillar crushing or continued pillar deformation cannot be ruled out as contributors to the additional convergence experienced. This is demonstrated by the ongoing convergence measured when no mining was taking place. The model used in the study did not take the continued time dependent deformation into account and therefore potentially underestimates the total amount of convergence experienced in the back areas.

The average rate of geometric convergence measured was 0.4 – 0.6 mm / m of advance. This could differ in other crush pillar sites and will be influenced by mining depth and regional stability (impact on rock mass stiffness).

In addition to the parameters derived from the observed and measured pillar behaviour, a set of criteria was required to give guidance on the implementation of a crush pillar system. The behaviour of the pillar system is influenced by various factors (i.e. mining depth). The numerical model, being able to replicate the behaviour of the crush pillars in the trial site validated the use of the limit equilibrium model implemented in the TEXAN code to simulate the pillar behaviour. The simulation of the macro layout verified some of the preliminary results and conclusions identified when simulating the idealised crush pillar layout. This included:

- Pillars being partially crushed when formed at the mining face,
- The behaviour of a large "oversized" pillar (w:h = 2.3) which did not completely crush; Footwall heave was observed adjacent to the pillar,
- A pillar, in close proximity to a block of unmined ground not being in a crushed state.

The simulation of an idealised layout has a lot more merit compared to a large scale underground layout. It is easy to set up and with little effort, trends can be established through consecutive runs by simply varying a parameter. This is not possible with large scale layouts even if the model is based on actual measurements. It is very difficult to replicate large scale layouts as there are many variables which can influence the overall behaviour. It can furthermore not be used as a simple tool to investigate trends.

The idealised layout provided the means to investigate parameters influencing crush pillar behavior. The design guidelines derived were based on the values assumed for the model parameters. A sensitivity analysis was conducted to determine the effect of each input parameter on the behaviour of the model and simulated pillars within the idealised layout. The results indicated that the choice of parameters gave qualitative agreement with observed crush pillar behaviour and underground measurements. The findings therefore confirm the preliminary results below.

Design guidelines derived from the preliminary analyses using an idealised crush pillar layout

The study was conducted to determine the effect of both pillar size with regard to width to height ratio and pillar width required to achieve pillar crushing at various depths. The preliminary results based on the assumed model parameters indicated that:

- A crush pillar system should not be implemented shallower than 600 m below surface.
- A maximum width to height ratio of 2:1 is required to ensure that the slender in-stope pillars crush at the face whilst they are being cut.
- If crush pillars are to be implemented at depths shallower than 600 m below surface, the width of the pillars will have to be reduced (e.g. w:h = 1.5 is required at 400 m below surface). This might not be practical to implement as pillar dimensions must also cater for out of line mining and blast effects. Furthermore the overall behaviour of the pillars could still be effected by the influence of mining

losses and geological features which will add to the stability of the rock mass. A minimum practical pillar width of 2 m (1 m stoping with) will only crush at 600 m below surface (w:h = 2:1).

- Pillar length does not appear to have a significant impact on crush pillar behaviour for pillar width to length ratios (w:l) of up to four.
- Different mining heights require different pillar widths for a constant width to height ratio (w:h = 2). The results from the simulations indicated that the narrower pillars implemented as a result of the smaller stoping width (2 m wide pillar, 1 m high stoping width), had higher initial, peak and residual stress levels. At 600 m below surface, the larger pillars (4 m wide pillar, 2 m high stoping width) crushed slightly later as it achieved its peak stress whilst being cut and then only moved to the residual state during the next mining step. In both cases, significantly high face stresses were achieved in the first approximately 2 m ahead of the mining face. This was sufficiently high to initiate early pillar crushing whilst the pillar was being formed at the face. This is, however, not achieved for larger pillars with w:h > 2:1. Lower pillar edge stress is achieved for the pillars with larger w:h ratios.
- This does signify the importance and impact of stoping width on the overall performance of crush pillars. Wider pillars are at a lower initial stress and therefore need more time to crush, even if at the same width to height ratio. When simulated at increased depth (>600 mbs), the pillar stress for both scenarios (pillar height of 1 m and 2 m) were sufficient to induce pillar crushing. However, narrower pillars experienced higher pillar stresses.

The effect of oversized pillars was investigated. Oversized pillars, which are typically encountered underground, either do not crush or fail violently in the back area. The study highlighted a key attribute of the limit equilibrium model: The pillar stress of a failed pillar increase in an exponential fashion towards the center of the pillar. This may lead to the formation of unduly high stresses in the core of wide pillars. The simulated results indicated that the core of the oversized pillars were still intact. As the oversized pillars did not crush at the face, these intact pillars move into the back area as the mining face advances. In the back area, the pillar is at a higher stress. The change in stress caused by a mining increment is lower compared to when the pillar is formed at the face. The pillar may therefore either not crush (especially when oversized) or fail violently as the stress on these pillars are much higher and the loading environment has become softer.

The effect of unmined blocks of ground or geological losses such as potholes on crush pillar behaviour, have up to now, not been considered as factors prohibiting pillar crushing or inducing pillar seismicity. For this reason it was included in the numerical analyses. The preliminary modelling results indicated that:

- Crush pillars implemented at 600 m below surface with a width to height ratio of two will not crush if a 10% mining loss is situated adjacent to the pillar line. In this case, narrower pillars are required to ensure that pillar crushing is achieved (e.g. w:h = 1.5 is required at 600 m below surface).

- Pillars situated 20 m ahead or behind an unmined block will also be affected, resulting in either partially crushed (core still solid) or intact pillars.
- Crush pillars implemented 800 m and deeper below surface are impacted to a lesser extent when in close proximity to a pothole. Large mining losses (>10%) and potholes situated closer than 10 m from the pillar line can either prevent pillar crushing or induce delayed crushing.
- Crush pillars implemented beyond 1000 m below surface are not affected if a 10% mining loss (pothole) is situated 2.5 m from the line of crush pillars.

Poor mining discipline resulting in unfavourable layouts also impact on the size of pillar cut at the mining face. Although these are common occurrences on most mines using crush pillars, these elements have historically not been identified as factors prohibiting pillar crushing or inducing pillar seismicity.

Underground sidings often significantly lag the mining face. The main function of the siding is to either modify the fracture patterns resulting from high face abutment stress or to move crush pillars away from the travelling way to ensure that failed rock do not fall onto people. The sidings being approximately 2 m wide are difficult to clean (hand lashed) and support. For this reason, mining of the siding is frequently behind schedule. In some cases, sidings lag the face by 20 – 30 m and are then developed as a single mining face. A lagging siding impact on the width of the pillar formed at the mining face. Until now, the impact of a lagging siding on the pillar width has not been identified as a contributor to undesired pillar behaviour or a source of pillar seismicity in a crush pillar environment. Once the siding of an advancing panel lag behind the adjacent lagging panel face, over-sized pillars are created. The pillars will only be reduced in size to the required dimension when the siding is blasted. At this point the pillar might not be able to crush sufficiently as the pillar is moving to the back area of a stope. The simulations conducted confirmed this effect. The pillars could therefore pose a seismic risk.

In summary, the findings compared to the original objectives of the study are:

Effect of pillar width: The impact of pillar width and width to height ratio must be determined to establish the affect it has on the overall performance of the pillar system. This will assist in determining if pillar dimensions can be standardised (width to height ratio or standard pillar width).

The results indicated that crush pillars should have a w:h ≤ 2:1. Narrower pillars are preferred as these pillars will fracture throughout and whilst being formed at the mining face. A pillar width of 2 m is recommended for all Merensky crush pillar sites. This will cater for all stoping widths (up to 2 m) and will ensure pillar crushing. The 2 m pillar width will accommodate poor mining practice and should not result in significantly oversized pillars which could induce seismicity. Pillar robbing and increased mining heights will promote pillar crushing. Pillar lengths should not exceed a w:l ratio of 4.

The impact of mining depth on pillar crushing: Guidelines are required regarding the implementation of crush pillars at different depths to ensure pillar crushing can be achieved safely.

Crush pillars should not be implemented shallower than 600 mbs. If the mine where the crush pillar system is being implemented has a combined mining and geological loss of 10 percent or more, the crush pillar system should only be implemented from approximately 800 mbs.

Determining the peak crush pillar strength: The peak pillar strength is unknown, however, accurate measurements will provide great insight with respect to the behaviour of the pillar system relating to the complete stress cycle. This could also provide detail regarding when and where relative to the mining face the peak and residual states are reached.

Due to the stress measurements being conducted 4 m above the pillars, the peak on-reef pillar stress could not be measured. The results nevertheless indicated that the crush pillars exceeded their peak strength prior to being formed at the mining face. The numerical back analysis indicated that the crush pillars were failing at an APS of between 220 – 270 MPa.

Determining the residual crush pillar strength: Although the residual crush pillar strength has previously been estimated, accurate measurements will confirm this and provide insight into the behaviour of the pillar system.

The stress measurements and micro seismic fracture profiling indicated that a crush pillar reaches a residual state once the pillar is fully formed. The residual stress at this point varied between 15 and 24 MPa. The pillars experienced a reduction in residual stress as new pillars were formed. The upper limit of the range of residual pillar stress experienced by the pillars (6.52 – 17.1 MPa) does agree with predictions from past research (13 - 20 MPa). The lower limit might not be a function of the residual strength of the pillar but rather a function of the load being experienced by the pillar.

Determining if and how convergence is related to pillar crushing: Various factors can affect the amount of convergence experienced at a pillar position at different distances from the face. The behaviour of the pillar and the relation to the convergence experienced at the site should be investigated. Also, the effect of elastic convergence experienced in a panel on pillar crushing should be investigated.

The convergence measurements and numerical modelling indicated that the convergence experienced adjacent to a crush pillar was directly related to the pillar crushing. Also, any change in convergence measured in a panel could be related to the formation and crushing of new pillars ahead of the instrumented site. As a result, a large amount of convergence is experienced in the first 15 m of face advance. The convergence measurements indicated that the side of the pillar which was exposed first experienced the most convergence. The measurements support the observations and micro seismic pillar fracture profiling which confirmed that this side of the pillar was fractured more intensely.

The effect of oversized pillars: On many operations pillar crushing is not achieved as a result of pillars being cut oversize. These pillars typically do not crush when formed at the face and can be a major source of seismicity in the back areas.

Both the underground observations and preliminary numerical modelling indicated that oversized pillars do not completely crush when formed (intact core). These pillars, when situated in the back area of a stope are at a higher stress. In the back area the loading environment has become much softer. These pillars could fail violently or induce different behaviour (i.e. footwall punching). Prior research at other Merensky sites indicated that pillars with w:h ratios exceeding 2 only reached their peak strength 3 – 6 m after being formed. The stress change experienced above these pillars was approximately 100 MPa confirming the high loads on these large pillars. Also, in most cases the residual behaviour of the pillars was controlled by the failure of the foundations and not as a result of pillar crushing. Consequently, these larger pillars can induce seismicity. Poor mining discipline resulting in unfavourable layouts also impact on the size of pillar cut at the mining face. A contributor to the formation of oversized pillars is lagging sidings. Should a siding of an advancing panel lag behind the adjacent lagging panel face, an over-sized pillar is created.

The impact of geological losses (e.g. potholes) and mining losses on pillar crushing: On many operations, pillar crushing is not achieved as a result of unmined blocks of ground left *in-situ*. Although these unmined blocks provide regional stability, it influences the behaviour of the pillars in the area surrounding them.

The underground observations and preliminary numerical modelling confirmed that pillar crushing was impacted when pillars are positioned in close proximity to these unmined blocks of ground. Guidelines were derived from the numerical analyses guiding on the implementation of a crush pillar system in areas where large mining or geological losses exist.

The following additional work needs to be conducted:

1. **Calibration of the limit equilibrium method:** Although the method appears very useful to simulate crush pillar behaviour, a more thorough calibration of all the parameters is required.

2. **The pillar fracture development process and sequence:** Although the numerical model was able to simulate the stress state of the pillars, explicit failure patterns or modes of failure as identified in the underground trial, has to be investigated by means of finite element or finite different methods.

3. **A prominent underground observation was the wedge-like failure plane identified where fractures intersected each other approximately halfway through a completely crushed pillar.** The formation of this failure plane and the impact it has on the behaviour of the pillar should be investigated with finite element methods.

4. **The extent of fracture development in the hanging-and footwall and the impact on crush pillar behaviour.** Fractures are observed to propagate from the hangingwall, through the pillar and into the footwall. The extent of the entire fracture zone and the zone impacting on the deformation experienced by a pillar has not been adequately researched. Stress measurements and borehole investigations indicate that these fractures can extend significantly into the hangingwall. The limit equilibrium method restricts the failure to the reef plane only.

5. **Pillar compression and constitutive behaviour.** Previous deformation measurements above and below a crush pillar indicated that a crush pillar undergo compression prior to being formed and during the pillar forming cycle. The convergence measurements indicated ongoing deformation processes after mining has stopped. Also, pillar deformation was observed to occur after the pillar has reached a residual state. Researchers have always believed that at some point a pillar undergoes sufficient compression to exhibit strain hardening behaviour. This concept has to date not been measured at any of the crush pillar sites. This behaviour needs to be investigated further.

6. **Pillar peak stress.** This is still an unknown parameter. A method is required to measure the on reef stress in or immediately below a pillar. This might be an irrelevant parameter as the pillar design is reliant on pillar failure. However, it can define a design limit which can contribute to design methodology.

7. **Regional and local stiffness and the impact on pillar behaviour.** This has been researched in the 1960's - 1980's. These parameters impact on the ability of pillars to crush in a controlled manner or to pose a seismic risk in the back area of a stope. Very little has been done to understand the impact of these parameters on the behaviour of pillars on the Merensky Reef where one of the main risks is

bursting pillars. Regional pillars as well as mining and geological losses (potholes) impact on the regional behaviour of the rock mass. The interaction of these, as well as the design of regional pillars on platinum mines has not been adequately defined.